Universidade do Minho
I3Bs - Instituto de Investigação em Biomateriais,
Biodegradáveis e Biomiméticos

Joana Margarida Mota Gomes

Biocompatible ionic liquids as processing tools forbiomaterials to be applied as novel therapeutic platforms

Outubro de 2022

Biocompatible ionic liquids as processing tools for biomaterials to be applied as novel therapeutic platforms
Joana Margarida Mota Gomes
UMinho | 2022

Universidade do Minho

I3Bs - Instituto de Investigação em Biomateriais, Biodegradáveis e Biomiméticos

Joana Margarida Mota Gomes

Biocompatible ionic liquids as processing tools for biomaterials to be applied as novel therapeutic platforms

Tese de Doutoramento

Doutoramento em Engenharia de Tecidos, Medicina Regenerativa e Células Estaminais

Trabalho efetuado sob a orientação do

Doutora Simone dos Santos Silva

Professor Doutor Rui Luís Gonçalves dos Reis

Outubro de 2022

DIREITOS DE AUTOR E CONDIÇÕES DE UTILIZAÇÃO DO TRABALHO POR TERCEIROS

Este é um trabalho académico que pode ser utilizado por terceiros desde que respeitadas as regras e boas práticas internacionalmente aceites, no que concerne aos direitos de autor e direitos conexos.

Assim, o presente trabalho pode ser utilizado nos termos previstos na licença abaixo indicada.

Caso o utilizador necessite de permissão para poder fazer um uso do trabalho em condições não previstas no licenciamento indicado, deverá contactar o autor, através do RepositóriUM da Universidade do Minho.

Licença concedida aos utilizadores deste trabalho



Atribuição-NãoComercial-SemDerivações

CC BY-NC-ND

https://creativecommons.org/licenses/by-nc-nd/4.0/

ACKNOWLEDGMENTS

This PhD has been a journey that would have never been possible without the support and guidance of several people. This is the time to acknowledge them.

First of all, I would like to acknowledge the financial support of the "Fundação para a Ciência e Tecnologia – FCT" that allowed me to conduct the experimental studies.

I would like to express my gratitude to Dra. Simone S. Silva for both her scientific and personal support. Simone always believed in me, my vision, and my potential. When I look back on this journey, I see that I am not the same inexperienced and unconfident person I was. This was mostly owned to her support, guidance and our long, honest, personal, and scientific conversations. In the first day we met, she said, "I'm not only your supervisor, I'm your friend". She was/is.

I would also like to acknowledge Prof. Rui L. Reis, not only for the unique opportunity of developing my PhD project in such a prestigious Research Group as i3Bs, but also for his guidance and trust. Our meetings and conversations were always so rich, and always brought great value to my work. I thank him for his availability and all the shared knowledge.

I would like to acknowledge Dra. Luísa C. Rodrigues for her scientific guidance but, most of all, for her support. Whenever there was a crisis, she was always there to "put out the fire".

To all my co-authors. All of you have been essential for producing the scientific outcomes of this thesis, and I would like to acknowledge you for help, support and scientific contribution, in the laboratory and/or in the review of the papers herein presented.

To the friends that I made at 3Bs. I would never be able to put into words how important you were and are to me. Thank you for always being there for a conversation, a shared moment of silence, or beer. You are truly amazing and beautiful people. To my long-time friends. I want to thank you for always being my "safe harbor" and my escape.

To my Filipe, for his support and love. You caught me in the middle of this journey and made everything feel better and brighter. Thank you for your warm hug, which always feels like home. Everything is better with you.

Last, but not least, to my parents. The most important people in my life. I could never thank them enough. Their unconditional love and support make this thesis also them.

STATEMENT OF INTEGRITY

I hereby declare having conducted this academic work with integrity. I confirm that I have not used plagiarism or any form of undue use of information or falsification of results along the process leading to its elaboration.

I further declare that I have fully acknowledged the Code of Ethical Conduct of the University of Minho.

ABSTRACT

Biocompatible ionic liquids (Bio-ILs) are versatile compounds, and their exploitation to produce Bio-IL/biopolymer systems offers unlimited potential for developing innovative biomedical solutions. However, the use of Bio-ILs in the biomedical field is still modest when considering their fully unexploited potential (Chapter I). Therefore, the main focus of this thesis is to demonstrate the potential of Bio-ILs for creating therapeutic platforms through their ability to process natural polymers as bioactive materials.

Envisioning to explore the potential of Bio-ILs to dissolve and process α-chitin into sponges, cholinium acetate, a commercial Bio-IL was used. This study revealed the harmless biological effect of Bio-ILs when kept in the final constructs (Chapter III). Considering this, antioxidant and anti-inflammatory Bio-ILs were synthesized, cholinium gallate (Ch[Gallate]) and cholinium caffeate (Ch[caffeate]). These Bio-ILs were dissolved into silk fibroin solutions, allowing to produce sponges with additional antioxidant and anti-inflammatory features, and the ability to support human adipose stem cell growth (Chapter IV). Motivated by these outcomes, the architectures were explored to address the main osteoarthritis (OA) treatment targets: inflammation, oxidative stress, and cartilage damage. In addition, the antimicrobial properties of the Bio-ILs and the sponges were confirmed against clinically relevant bacteria. These matrices sustain the primary human chondrocyte growth, reducing reactive oxygen species generation while downregulating the pro-inflammatory gene expression in osteoarthritic human chondrocytes (HC-OA) (Chapter V). To explore the Bio-IL platform as an innovative drug delivery system for OA, alginate/acemannan/Ch[Caffeate] beads were produced. The beads promoted great drug encapsulation, allowing the sustainable release of Ch[Caffeate]. In addition, these beads provided a suitable environment for ATDC5 chondrocyte-like cell growth, and cartilage-like extracellular matrix formation, and blocked the secretion of pro-inflammatory cytokines from differentiated THP-1 (Chapter VI). The versatility of alginate/acemannan/Ch[Caffeate] led us to explore this system as a bioactive ink with encapsulated ATDC5 cells. The establishment of co-culture systems using cell-laden constructs and macrophages allowed us to mimic the inflammation events in OA (Chapter VII).

Overall, this thesis contributed for developing advanced technologies comprising Bio-ILs, natural polymers, and relevant cells that may have greater implications in the biomedical field as promising solutions to address cartilage pathologies, including OA.

Keywords: Biocompatible ionic liquids, natural polymers, cartilage regeneration, osteoarthritis

RESUMO

Os líquidos iónicos biocompatíveis (Bio-ILs) são compostos versáteis. A sua exploração para o desenvolvimento de sistemas Bio-IL/polímero tem potencial ilimitado no desenvolvimento de soluções biomédicas inovadoras. O uso de Bio-ILs na área biomédica é, no entanto, escasso (Capítulo I). Neste sentido, o principal foco desta tese é demonstrar o potencial dos Bio-ILs para o desenvolvimento de plataformas terapêuticas, através da sua capacidade de processamento de polímeros naturais como materiais bioativos.

Visando explorar o potencial dos Bio-ILs na dissolução e processamento de α-quitina em esponjas, um Bio-IL comercial, colina acetato, foi usado. Este estudo permitiu-nos validar o carácter não tóxico dos Bio-ILs, quando mantidos nos materiais (Capítulo III). Considerando isto, Bio-ILs com propriedades antioxidantes e anti-inflamatórias foram sintetizados, colina *gallate* (Ch[Gallate]) e colina *caffeate* (Ch[Caffeate]). Os Bio-ILs foram dissolvidos em soluções de fibroína de seda, usadas para produzir esponjas com propriedades antioxidantes e anti-inflamatórias, e suportando o crescimento de células estaminais do tecido adiposo (Capítulo IV). Motivado por esses resultados, estes biomateriais foram explorados para o tratamento dos principais sintomas da osteoartrite (OA): inflamação, stress oxidativo e degeneração da cartilagem. As propriedades antimicrobianas dos biomateriais contra bactérias clinicamente relevantes foram também confirmadas. As esponjas suportaram o crescimento de condrócitos humanos (HC), reduziram o stress oxidativo e a expressão de genes associados à inflamação em condrócitos humanos osteoartríticos (HC-OA) (Capítulo V). Para explorar os Bio-ILs como plataformas de entrega de fármacos para o tratamento da OA, o sistema alginato/acemanana/Ch[Caffeate] foi usado para produzir *beads*. As *beads*, permitiram encapsular e libertar Ch[Caffeate] de forma eficiente e sustentável. Além disso, promoveram crescimento da linha celular condrogénica ATDC5, a formação de matriz extracelular cartilaginosa, bloqueando a libertação de citocinas pro-inflamatórias em macrófagos THP-1 (Capítulo VI). A versatilidade do sistema mencionado levou-nos a explorá-lo para o desenvolvimento de uma *bioink,* encapsulando células ATDC5. A criação de sistemas em co-cultura, usando hidrogéis com células ATDC5 encapsuladas e macrófagos, permitiu reproduzir os eventos de inflamação encontrados na OA e estudá-los (Capítulo VII).

No geral, esta tese contribuiu para o desenvolvimento de tecnologias avançadas englobando Bio-ILs, polímeros naturais e células relevantes que podem ter implicações significativas no campo biomédico como soluções promissoras para tratamento de patologias da cartilagem, incluindo a OA.

Palavras-chave: líquidos iónicos biocompatíveis, polímeros naturais, regeneração da cartilagem, osteoartrite

TABLE OF CONTENTS

ACKNOWLEDGMENTS III

STATEMENT OF INTEGRITY IV

ABSTRACT V

RESUMO VI

LIST OF ABBREVIATIONS XIV

LIST OF FIGURES XVIII

LIST OF SCHEMES XXI

LIST OF SUPPLEMENTARY FIGURES XXII

LIST OF TABLES XXII

LIST OF SUPPLEMENTARY TABLES XXIII

LIST OF EQUATIONS XXIII

SHORT *CURRICULUM VITAE* XXV

LIST OF PUBLICATIONS XXVI

INTRODUCTION TO THE THESIS FORMAT XXX

SECTION 1 GENERAL INTRODUCTION 1

CHAPTER I BIOCOMPATIBLE IONIC LIQUIDS: FUNDAMENTAL BEHAVIOURS AND APPLICATIONS 2

Abstract 3

I-1. Graphical abstract 4

I-2. Introduction 4

I-3. Ionic liquids – A remarkable class of chemical compounds 5

I-4. Biocompatible Ionic Liquids – A family in the expansion 7

I-4.1. Cholinium as the Bio-ILs cationic moiety 10

I-4.2. Glycine Betaine-based ILs as alternatives to the cholinium family 11

I-5. Synthesis of Biocompatible Ionic Liquids- the path 12

I-5.1. Synthesis of Choline- based Ionic liquids 13

I-5.2. The post-synthesis: physico-chemical characterization 17

I-5.3. Recovery and reuse of the Bio-ILs 18

I-6. Toxicity: the environmental and biological impact 20

I-6.1. Biodegradation 21

I-6.2. (Eco)-toxicity 23

I-6.3. Cytotoxicity and Biological Activity 29

I-6.4. Toxicity: cautions, predictions, and trends 31

I-7. Applications of Biocompatible Ionic Liquids 32

I-8. Conclusions and future trends 37

I-9. References 38

SECTION 2 EXPERIMENTAL DESIGN 52

CHAPTER II MATERIALS & METHODS 53

Overview 54

II-1. Materials 56

II-1.1. Chitin 56

II-1.2. Silk Fibroin (SF) 57

II-1.3. Alginate (ALG) 58

II-1.4. Acemannan (ACE) 59

II-2. Methods 60

II-2.1. Biocompatible ionic liquids (Bio-ILs) synthesis and characterization 60

II-2.2. Biomaterials processing 61

II-2.3. Biomaterials' characterization 67

II-2.4. Evaluation of the antimicrobial properties of the fabricated constructs 76

II-2.5. Biological assessment assays 78

II-2.6. Statistical Analysis 91

II-3. References 92

SECTION 3 EXPERIMENTAL STUDIES 105

CHAPTER III EXPLORING THE USE OF CHOLINE ACETATE ON SUSTAINABLE DEVELOPMENT OF α-CHITIN-BASED SPONGES 106

Abstract 107

III-1. Graphical abstract 108

III-2. Introduction 108

III-3. Materials and methods 110

III-3.1. Materials 110

III-3.2. Preparation on the α-chitin/Bio-IL -based structures 110

III-3.3. Preparation of CACE-A and CACE-B based sponges. 111

III-3.4. Physico-chemical characterization 111

III-3.5. Cell culture studies 114

III-3.6. Statistical analysis 116

III-4. Results and discussion 117

III-4.1. Processing of α-chitin using Ch[ACE] and morphological features of the resultant structures. 117

III-4.2. Effect of the presence/absence of Bio-IL into the architectures 121

III-4.3. Cell culture studies 126

III-5. CONCLUSION 128

III-6. Supplementary material 129

III-7. References 130

CHAPTER IV SILK FIBROIN/CHOLINIUM GALLATE-BASED ARCHITECTURES AS THERAPEUTIC TOOLS 135

Abstract 136

IV-1. Graphical abstract 137

IV-2. Introduction 137

IV-3. Materials and methods 139

IV-3.1. Materials 139

IV-3.2. Synthesis of Choline-Gallate (Ch[Gallate]) 139
IV-3.3. Preparation of the SF/Ch[Gallate] sponges 140
IV-3.4. Physico-chemical and morphological characterization of the SS and SChGallate sponges 142
IV-3.5. Cell Culture Studies 145
IV-3.6. Hemolytic properties 148
IV-3.7. Statistical analysis 149
IV-4. Results and discussion 149
IV-4.1. SCh[Gallate] loaded sponges production and physico-chemical characterization 149
IV-4.2. Cell Culture Studies 162
IV-4.3. Hemocompatibility 169
IV-5. Conclusions 170
Acknowledgments 171
IV-6. Supplementary material 172
IV-7. References 174
CHAPTER V UNRAVELING THE POTENTIAL OF BIOCOMPATIBLE IONIC LIQUID-BASED SPONGES FOR OSTEOARTHRITIS THERAPY BY REDUCING INFLAMMATION AND OXIDATIVE STRESS 181
Abstract 182
V-1. Graphical abstract 183
V-2. Introduction 183
V-3. Materials and methods 185
V-3.1. Materials 185
V-3.2. Synthesis of Cholinium-Gallate (Ch[Gallate]) and Cholinium-Caffeate (Ch[Caffeate]) 185
V-3.3. Preparation of the SF/Bio-IL sponges 186
V-3.4. Physico-chemical characterization 188
V-3.5. Antimicrobial properties 192
V-3.6. *In vitro* studies 193
V-3.7. Statistical analysis 197

V-4. Results and discussion 197

V-4.1. SF/Bio-IL-based sponges' preparation and characterization 197

V-4.2. SF/Bio-IL-based/acetaminophen (ACT) loaded sponges - physico-chemical and *in vitro* assessment of the designed constructs 203

V-4.3. *In vitro* studies 211

V-4.4. Assessment of the anti-inflammatory potential of the developed sponges 211

V-5. Conclusions 218

V-6. Supplementary material 220

V-6.1. Supplementary methods 220

V-6.2. Supplementary figures and tables 221

V-7. References 222

CHAPTER VI ALGINATE/ACEMANNAN DERIVED BEADS LOADED WITH A BIOCOMPATIBLE IONIC LIQUID AS A BIOACTIVE DELIVERY SYSTEM 231

Abstract 232

VI-1. Graphical abstract 233

VI-2. Introduction 233

VI-3. Materials and methods 235

VI-3.1. Materials 235

VI-3.2. Synthesis of Cholinium Caffeate (Ch[Caffeate]) 235

VI-3.3. Preparation of the ALG/ACE-Ch[Caffeate] beads 236

VI-3.4. Physico-chemical and morphological characterization of the ALG/ACE-Ch[Caffeate] beads 237

VI-3.5. Cell Culture Studies 239

VI-3.6. Statistical analysis 242

VI-4. Results and discussion 242

VI-4.1. Physico-chemical and morphological characterization of the ALG/ACE-Ch[Caffeate] beads 243

VI-4.2. Cell culture studies 253

VI-5. Conclusion 259

VI-6. Supplementary material 260

VI-7. References 261

CHAPTER VII 3D BIOACTIVE IONIC LIQUID-BASED CONSTRUCTS: AN ANTI-INFLAMMATORY APPROACH FOR EARLY-STAGE OSTEOARTHRITIS 268

Abstract 269

VII-1. Graphical abstract 270

VII-2. Introduction 270

VII-3. Materials and methods 272

VII-3.1. Materials 272

VII-3.2. Synthesis of Choline-Caffeate (Ch[Caffeate]) 272

VII-3.3. ALG/ACE/Ch[Caffeate]ink preparation and characterization 273

VII-3.4. 3D printing methodology 275

VII-3.5. 3D Printed hydrogels characterization 275

VII-3.6. Cyto-compatibility and *in vitro* assessment of the 3D bioprinted constructs 277

VII-3.7. Statistical analysis 280

VII-4. Results and discussion 280

VII-4.1. Bioink production and physico-chemical characterization of the produced 3D constructs 280

VII-4.2. Cyto-compatibility and *in vitro* assessment the 3D bioprinted constructs 287

VII-4.3. Early-stage OA mimicking and therapeutic effect 290

VII-5. Conclusions 294

VII-6. Supplementary material 295

VII-7. References 295

SECTION 5 303

GENERAL CONCLUSIONS 303

CHAPTER VIII GENERAL CONCLUSIONS AND FUTURE PERSPECTIVES 304

VIII-1. General conclusions _____ **305**

VIII-2. Future perspectives _____ **308**

LIST OF ABBREVIATIONS

#

°C – Degrees Celsius

3D – 3-Dimensional
2D – 2-Dimensional

% - Percentage

µL – Microliter

µm – Micrometer

µg mL^{-1} – Microgram per milliliter

%wt. – Percentage of weight

λ – Wavelength

α – Alpha
β - Beta

A

AA – Amino acids

AA(%) – Radical scavenging activity

A/A – Antibiotic/antimycotic

Abs – Absorbance

ABS – Aqueous biphasic systems

ACE – Acemannan

ACT – Acetaminophen

Ala – Alanine

ALG - Alginate

ANOVA – Analysis of variance

APC – Allophycocyanin

APIs - active pharmaceutical ingredients

APIs-Bio-IL - active pharmaceutical ingredients in biocompatible ionic liquids systems

APIs-IL - active pharmaceutical ingredients in ionic liquids systems

APPACDM - Portuguese Association of Parents and Friends of Mentally Disabled Citizens

ATDC5 - Mouse chondrogenic-like cell line

ATR – Attenuated total reflectance

B

Ba- Barium

$BaCl_2$- Barium chloride
BES - N,N-bis(2-hydroxyethyl)-2 aminoethanesulfonic acid
Bio-IL – Biocompatible ionic liquid

[bmim][Ac] - 1-butyl-3-imidazolium acetate

C

C - Carbon

Ca - Calcium

Calcein-AM – Calcein-Acetoxymethyl

$CaCl_2$ – Calcium chloride

CAPS - 3-(cyclohexyla-mino)-1-propanesulfonic acid

cDNA – Complementary DNA

[Ch][AA] – Choline amino acid-based ionic liquids

Ch[ACE] - Cholinium acetate

[Ch][Ala] – Choline alanine

Ch[Caffeate] – Cholinium caffeate

CHES - N-Cyclohexyl-2-aminoethanesulfonic acid

[Ch]Cl - Choline chloride

Ch[Gallate] – Cholinium gallate

[Ch][Gly] – Choline Glycinate

[Ch][HCO_3^-] - Choline bicarbonate

[Ch][Hist] – Choline histidine

Ch[ILs] - Cholinium-based ionic liquids

Ch[OH] - Choline hydroxide

[Ch][Phe] – Choline phenylalanine

[Ch][Sac] - Choline sacarinate

CLSM - confocal laser scanning microscope

Cm – Centimeter

CO_2 – Carbon dioxide

COL2A1 – Collagen type II, alpha 1

COX-2 – Cyclooxygenase-2

[Ch][Threonine] – Choline threonine

CTRL – Control

Cyt-c Cytochrome C

D

D_2O – Deuterium oxide

Da - Dalton

DAPI – 4',6-diamidino-2-phenylindole

DD% - Deacetylation degree

DES - Deep eutectic solvents

DIPSO - 3-(N,N-bis[2-hydroxy-ethyl]amino)-2-hydroxypropanesulfonic acid

DMB – Dimethylmethylene blue

DMEM – Dulbecco's modified eagle medium

DMSO – Dimethylsulfoxide

DNA - Deoxyribonucleic acid

dsDNA - Double-stranded DNA

DPPH - 2,2- diphenyl-1 picrylhydrazyl

DSC - Differential scanning calorimetry

E

EC_{50}- Half maximum effective concentration

ECM – Extracellular matrix

EDTA - Ethylenediaminetetraacetic acid

E. coli - Escherichia coli

EDS – energy dispersive spectrometer

ELISA – Enzyme-linked immunosorbent assay

$EtMeim^+$ - methylimidazolium cations

eV – Electron volt

EWC – Equilibrium water content

F

FBS – Fetal bovine serum

FE – Fold expression

FSD – Fourier self-deconvolution

FTIR – Fourier-transform infrared spectroscopy

G

g – g force

G - L-guluronic acid

G′ – Storage modulus

G″ – Loss modulus

GAGs – Glycosaminoglycans

GB - Good's buffers

GelMA - Gelatin methacryloyl

GlcNAc - N-acetylglucosamine

Gly – Glycine

GM-CSF - Granulocyte-macrophage colony-stimulating factor

H

h – Hours

H – Hydrogen

H_2O – Water

H_2O_2 – Hydrogen peroxide

HaCat - Human epidermal keratinocyte cell line

hASCs – Human adipose stem cells

hB2M - Human Beta-2 microglobulin

HBSS - Hank's Balanced Salt Solution

HCl – Hydrochloric acid

HC – Human chondrocytes

HC-OA – Human chondrocytes osteoarthritis

HEPES - 4-(2-Hydroxyethyl) piperazine-1-ethanesulfonic acid

Hz – Hertz

I

IL – Ionic liquids

IL-6 – Interleukin 6

IL-10 – Interleukin 10

iNOS-2 – Inducible nitric oxide synthase 2

IPC-81 - Leukemia Rat Cell Line

K

K - Kelvin

kDa – kilodalton

L

L929 – Mouse fibroblast-like cells

LB – Luria-Bertani

LC_{50} – Half lethal concentration

LiBr – Lithium bromide

LPS – Lipopolysaccharide

LVER – Linear viscoelastic region

M

M - D-mannuronic acid

MCF-7 - Human breast cancer cell line

MEM – Minimum essential medium

MES - 4-(2 hydroxyethyl)-1-piperazinepropanesulfonic acid

MIC - Minimal inhibitory concentrations

Micro-CT – Micro-computed tomography

mm – Millimeter

mM - Millimolar

Min – Minute

MFC – Minimal fungicidal concentrations

MHz – Megahertz

ml/min – Milliliter per minute

MMPs - Matrix metalloproteinases

MOPS - 3-(N-morpholino)propanesulfonic acid

MOPSO - b-hydroxy-4-morpholi- nepropanesulfonic acid

mRNA – Messenger RNA

MRSA - methicillin-resistant Staphylococcus aureus

MTS – 3-(4,5-dimethylthiazol-2-yl)-5-(3-carboxyme-thoxyphenyl)-2-(4 sulfophenyl)-2H Tetrazolium

MWCO – Molecular weight cut off

N

N – Newton

N_2 - Nitrogen

N/A – Not applicable, Not available

Na - Sodium

NaCl – Sodium chloride

Na_2CO_3 – Sodium carbonate

NAL - nalidixic acid

NAS - National Academy of Sciences

NF-kB - Nuclear factor-kB

NH_2 – Amine group

NIF - Niflumic acid

Nm - nanometer

nM – Nanomolar

NMR – Nuclear magnetic resonance

NO – Nitric oxide

NSAIDs - Non-steroidal anti-inflammatory drugs

O

O - Oxygen

OA – Osteoarthritis

OECD - Organization of Economic Co-Operation and Development

P

PAS - 4- amino-salicylic acid

PBS – Phosphate buffer saline solution

PE - Polymer electrolyte

PGE_2 –Prostaglandin E2

Ph - Phalloidin

PI – Propidium iodide

PIC - Picolinic acid

PMA - Phorbol 12-myristate-13 acetate

PPM – Parts per million

PYR - Pyrazinoic acid

R

RNA – Ribonucleic acid

ROS – Reactive oxygen species

rpm – Rotations per minute

RT – Room temperature

RT-PCR – Real-time polymerase chain reaction

RTILs - room temperature ionic liquids

S

SD – Standard deviation

SEM – Scanning electron microscopy

Ser - Serina

SF – Silk fibroin

SK-MEL-28 - Melanoma cell line

Sr^{2+}- Strontium

SVF – Stromal vascular fraction

T

TAPSO - 2-hydroxy-3-[tris(hydroxymethyl)methylamino]-1-propanesulfonic acid

TBS - Tris-HCl-buffer

TE – Tissue engineering

TERM – Tissue engineering and regenerative medicine

TES -2-[(2-Hydroxy-1,1 bis(hydroxymethyl)ethyl)amino]ethanesulfonic acid

TGF-β1 – Transforming growth factor-beta 1

THP-1 – Human monocyte cell line

TNF-α –Tumor necrosis factor alpha

TNMD – Tenomodulin

Tricine - N-[Tris(hydroxymethyl)methyl]glycine

TSILs - task-specific ionic liquids

Tyr – Tyrosine

U

UV – Ultraviolet

(v/v) – Percentage of volume/volume

V

Val – Valine

VRSA - vancomycin-resistant *Staphylococcus aureus*

LIST OF FIGURES

Figure I-1- The ILs evolution. 7

Figure I-2 - Schematic representation of the strategy used for the synthesis of lignin- and hemicellulose derived ILs. 9

Figure I-3 - Synthetic pathways towards bio-based ILs. 12

Figure I-4 - Schematic illustration of the purification of Bio-ILs after the metathesis reaction by ion-exchange chromatography. 14

Figure I-5 – (A) The synthetic pathway for the [Ch][AA] and (B) Synthesis of the choline carboxylate Bio-ILs and chemical structures of the anions used. 15

Figure I-6 – (A) Model neutralization reaction (B) The synthetic pathway for [Ch][CHES]. 17

Figure I-7 – Synthetic pathway of Glycine betaine-based ILs. 17

Figure I-8 – Different Ecosystems affected by ILs as potential chemical pollutants. 21

Figure I-9 - Viability of HeLa cells. 30

Figure I-10 . Schematic representation of the intensity of research regarding the use of Bio-ILs in a selected range of areas. 32

Figure I-11 - Schematic configuration and optical image of a cross-sectional view of the integrated biopolymer electrolyte-thin and compact magnesium-air Battery. 36

Figure I-12 - *In vivo* biodegradation and biocompatibility tests of a GelMA/Bio-IL composite hydrogel using a rat subcutaneous model. 37

Figure II-1 – Schematic overview representation of the natural macromolecules used, the synthetized biocompatible ionic liquids. 55

Figure II-2 – Chitin structure. 57

Figure II-3 - Silk fibroin primary structure. 58

Figure II-4 – Alginate. 59

Figure II-5 – Bio-ILs synthesis experimental set-up 61

Figure III-1 - Structural representation of the choline acetate (Ch[ACE]) and the polymer chitin. 110

Figure III-2 - Light microscope images of the 1 % wt chitin in Ch[ACE]. 118

Figure III-3 - Stereomicroscope photos of the gels. 119

Figure III-4 - SEM cross-section images of the CACE-based sponges. 120

Figure III-5 - Conductivity measurements on the aliquots of methanol obtained after immersion of the structures . 121

Figure III-6 - Micro-CT images of the CACE-based sponges (scale bar 500μm) 122

Figure III-7 - Storage modulus (G') and loss modulus (G'') of the CACE-based sponges. 123

Figure III-8 - Swelling profile for CACE sponges immersed in PBS. 125

Figure III-9 - MTS results of L929 seeded both on the CACE-A and CACE-B structures. 126

Figure III-10 - MTS results (a) and dsDNA content, (b) of hASCS seeded both on the CACE-A and CACE-B structures up to 7 days of culture. 128

Figure IV-1 - Antioxidant activity of gallic acid, Ch[Gallate] ,SS, SChGal1 and SChGal3 in a solution of DPPH in Methanol. 152

Figure IV-2 - (A) FTIR spectra of SS, SChGal, and Ch[Gallate]; (B) Percentage of β-sheet, random coil, and turn conformations. 154

Figure IV-3- ^{13}C-CPMAS spectra of solid samples. 156

Figure IV-4 – SEM images of the SS and SChGallate-based sponges' cross sections. 158

Figure IV-5 - Mechanical behavior of the sponge materials under compression load. (A) Compressive modulus. 160

Figure IV-6 – Water uptake (A), weight loss (B) of the SS, SChGal1, and SChGal3 in PBS 161

Figure IV-7 - (A) Metabolic activity and (B) DNA content of hASCs seeded on the SS, SChGal1, and SChGal3 sponges. 164

Figure IV-8 - *In vitro* ROS measurement using DCF-DA fluorescence assay. 165

Figure IV-9 - (A) TNF-α, (B) IL-6 and (C) IL-10 amounts in the different conditions. 168

Figure IV-10 - (A) Representative images of the hemolysis assay and (B) Percentage of hemolysis induced by the controls . 170

Figure V-1 - ^{13}C-CPMAS spectra of solid sponges. 199

Figure V-2 - Mechanical behavior of the sponge materials under compression load. 201

Figure V-3 - (A) Live/dead images, (B) live/dead quantification by excess bacterial percentage, and (C) SEM images of the bacteria fixed on the sponges. 203

Figure V-4 - Percentage of β-sheet, random coil, and turn conformations. 205

Figure V-5 - (A) SEM cross-sectional images of the developed sponges; (B) Mean pore sizes and (C) distribution. 206

Figure V-6 - Water uptake (A) and weight loss (B) of the SS, SS-A, SCG, SCG-A, and SCC-A. 209

Figure V-7 - Antioxidant activity of the sponges formulations by DPPH method. 210

Figure V-8 - Cytokines quantification. 213

Figure V-9 - Cytocompatibility and antioxidant effect of SS, SS-A, SCG, SCC, SCG-A and SCC-A over HC stimulated with H_2O_2. 214

Figure V-10 - (A) Metabolic activity, (B) and DNA content, (C) Microscope projection image of the live/dead assay of HC seeded in the SS, SCG, and SCG-A sponges. 216

Figure V-11 - Gene expression of TNF-α, IL-6, iNOS, COX-2 and TGF-β. 218

Figure VI-1 - Cholinium Caffeate (Ch[Caffeate]) chemical structure. 236

Figure VI-2 - NMR spectra of Ch[Caffeate], ACE, and the different ACE/Ch[Caffeate] mixtures, used for the beads preparation. 244

Figure VI-3 (A) SEM images of the ALA and ALAC beads surfaces and cross-sections; (B) mean pore sizes; and (C) pore size distribution. 245

Figure VI-4 - Summary of XPS results. 248

Figure VI-5 - Antioxidant activity of Caffeate acid, Ch[Cafeic], and the developed ALA and ALAC beads. 250

Figure VI-6 - (A) Water uptake, (B) stability in PBS of the developed ALA and ALAC beads. 252

Figure VI-7 (A) Metabolic activity and (B) DNA content of ATDC5 cells after contacting with ALA and ALAC beads, up to 21 days. 255

Figure VI-8 -. (A) GAGs quantification assay of ATDC5 cells and (B) Chondrocyte marker analysis on ATDC5 cells by histochemical staining of the proteoglycan's synthesis. 256

Figure VI-9 - Quantification of the TNF-α and IL-6 content in the medium in LPS and non-LPS stimulated cells, betamethasone treated cells, and in contact with the different ALA and ALAC beads. 258

Figure VII-1 - Cholinium Caffeate (Ch[Caffeate]) chemical structure. _____ 273

Figure VII-2 - (a) Injection force profile of the prepared inks; (b) macroscopic printability evaluation using different 3D models, and (c) photos of the hydrogels right after the printing process. _____ 282

Figure VII-3 - (a) Macroscopic appearance of the 3D printed constructs after freeze drying; (b) SEM images of the printed hydrogels and (c) values of mean thickness, pore size, porosity, and interconnectivity obtained using μ-CT analysis._____284

Figure VII-4 - (a) equilibrium water content, (b) weight loss and (c) cumulative Ch[Caffeate] release of the hydrogels in TBS, up to 14 days._____287

Figure VII-5 - Biological performance of the bioprinted hydrogels._____290

Figure VII-6 - (a) Metabolic activity and (b) dsDNA content of the ATDC5 cells encapsulated in the 3D bioprinted hydrogels in an inflammatory environment after 1 and 7 days of culture._____ 293

LIST OF SCHEMES

Scheme III-1 - Scheme used for the production of the CACE sponges _____ 111

Scheme IV-1 - Schematic representation for the preparation of the SChGallate sponges. _____ 141

Scheme V-1 - Schematic representation of the SS-A, SCG. SCC, SCG-A and SCC-A sponges' preparation_____ 187

Scheme VI-1 - (A) Alginate and acemannan chemical structure and (B) Schematic representation of the ALA and ALAC-based beads preparation._____ 237

Scheme VI-2 - Schematic representation of the beads components in the mixture and their distribution over the structure of the beads following immersion in the $BaCl_2$ bath and freeze-drying process._____ 246

Scheme VII-1 - Schematic representation of the 3D bioprinting process and macroscopic image of the printed constructs. _____ 274

Scheme VII-2 - Schematic representation of the experimental culture conditions of the developed direct transmembrane co-culture system. _____ 279

Scheme VII-3 - Interactions between the bioink components_____ 285

LIST OF SUPPLEMENTARY FIGURES

Supplementary Figure III-1 – FTIR spectra of the CACE-based sponges and α-chitin. 129

Supplementary Figure III-2 - Representative live/dead images from hASCs seeded both on the A and B structures up to 7 days of culture. 130

Supplementary Figure IV-1 - ^{1}H of pure Ch[Gallate]. 172

Supplementary Figure IV-2 - Micro-CT data of silk sponges at different % (w/v) - micro-CT 3D images and morphometric parameters. Scale bar 250nm. 173

Supplementary Figure IV-3 - Confocal microscope projection image of the live/dead assay after 7 days of culture. 173

Supplementary Figure IV-4 - Confocal microscope image of the SS – Green channel (488nm). 174

Supplementary Figure V-1 - Metabolic activity of L929 and ATDC5 cell line after 24, 48 and 72h of culture with ACT extracts. 221

Supplementary Figure V-2 - Disc diffusion assay results with A) 0.5% (w/v), B) 1% (w/v) and C) B) 3% (w/v) Bio-IL solution. 221

Supplementary Figure VI-1 ^{1}H of pure Ch[Caffeate]. 260

Supplementary Figure VI-2 - Confocal microscope projection image of the live/dead assay of ATDC 5 cells after contact with ChAL and ChAL-Ch[Caffeate] beads, up to 21 days. 260

Supplementary Figure VII-1 - ^{1}H of pure Ch[Caffeate]. 295

LIST OF TABLES

Table I-1– Toxicity of [Ch]ILs towards different levels of aquatic biological systems including bacteria, algae, vertebrate, and invertebrate. 25

Table II-1 - Sample identification used throughout the Chapter VI 64

Table II-2 – Sequence of the primers used for real-time quantitative RT-PCR analysis 89

Table III-1 - Observations obtained from the stability assay. 120

Table III-2 - Values of interconnectivity, pore size, and porosity for CACE-based sponges obtained using micro-CT analysis. 122

Table IV-1 - Sample identification used throughout the paper _____ 141

Table IV-2 - The ratio of cytokines in THP-1 activated macrophages. _____ 169

Table V-1 - Sample identification used throughout the paper. _____ 188

Table VI-1 - Identification of the samples. _____ 236

Table VII-1 - Sample identification used throughout the paper _____ 273

LIST OF SUPPLEMENTARY TABLES

Supplementary Table V-1 - Primers used for real-time quantitative RT-PCR analysis _____ 222

LIST OF EQUATIONS

Equation II-1 _____ 62

Equation II-2 _____ 68

Equation II-3 _____ 73

Equation II-4 _____ 74

Equation II-5 _____ 74

Equation II-6 _____ 75

Equation II-7 _____ 75

Equation II-8 _____ 89

Equation II-9 _____ 91

Equation III-1 _____ 112

Equation III-2 _____ 113

Equation IV-1 _____ 140

Equation IV-2 _____ 142

Equation IV-3 _____ 144

Equation IV-4 _____ 144

Equation IV-5 _____145

Equation IV- 6_____149

Equation V-1_____186

Equation V-2_____190

Equation V-3_____190

Equation V-4_____191

Equation V-5_____191

Equation VI-1 _____238

Equation VI-2 _____239

Equation VI-3 _____239

Equation VII-1_____276

Equation VII-2_____276

SHORT *CURRICULUM VITAE*

Joana Gomes is currently a Ph.D. student at 3 B's Research Group - I3Bs, Research Institute on Biomaterials, Biodegradables and Biomimetics, at the University of Minho, Headquarters of the European Institute of Excellence on Tissue Engineering and Regenerative Medicine at Avepark, under the supervision of Dr. Simone S. Silva and Professor Rui L. Reis.

She graduated in 2013 and received her Master's degree in 2015, both in Biochemistry, from the University of Aveiro, Portugal, with a final grade of 16 (0-20). Joana Gomes' MSc project focused on the development of extraction and purification platforms for biomolecules and other added-value compounds from biological matrices using ionic liquids (ILs). During 2016, Joana developed research at the University of Aveiro and most of her studies aimed to continue her previous work, directed to the use of ILs for developing efficient separation and extraction strategies.

From January to August of 2017, Joana worked as a Research Assistant, at King's College London, in the Department of Infectious Diseases. Her main project aimed to identify, produce and purify human proteins that interacted with HIV, inhibiting the infectivity of this virus.

In September 2017, she started pursuing her PhD at 3B's Research Group in the PhD program in Tissue Engineering, Regenerative Medicine and Stem Cells (TERM&SC) at the University of Minho. Her research focuses on biocompatible ionic liquids for the processing of natural molecules and their application as therapeutic platforms.

As a result of her research work, she is the author or co-author of 14 peer-reviewed papers in international journals and 2 book chapters. In addition, she attended several important conferences in tissue engineering and regenerative medicine (10 communications, oral and poster).

LIST OF PUBLICATIONS

The work performed during the Ph.D. period resulted in the publications listed below.

Papers in international scientific journals with referees (as first author)

1. **Gomes J. M.**, Silva S. S. and Reis R. L. "Biocompatible Ionic Liquids: Fundamental behaviors and applications"; Chemical Society Reviews, 2019, 48, 4317-43352019. doi: 10.1039/C9CS00016J
2. **Gomes J. M.**, Silva S. S. and Reis R. L. "Exploring the Use of Choline Acetate on the Sustainable Development of α-Chitin-Based Sponges"; ACS Sustainable Chem. Eng. 2020, 8, 35, 13507–1351. doi: 10.1021/acssuschemeng.0c05076
3. **Gomes J. M.,** Silva S. S., Fernandes E. M., Lobo F. C. M. Martín-Pasto M., Taboada and Reis R. L "Silk fibroin/cholinium gallate-based architectures: bio-based tools for inflammatory diseases treatment"; Acta Biomaterialia 2022, 147, 168-184, doi: /10.1016/j.actbio.2022.05.020
4. **Gomes J. M.,** Silva S. S, Rodrigues L. C., Franco A. R., Fernandes E. M., Leonor I. B., Lobo F. C. M. Martín-Pasto M., Taboada, and Reis L. R. "Unraveling the potential of biocompatible ionic liquid-based sponges for osteoarthritis therapy by reducing inflammation and oxidative stress", Submitted, 2022.
5. **Gomes J.M.,** Silva S. S., Rodrigues, L. C. and Reis, R. L. "Alginate/acemannan derived beads loaded with a biocompatible ionic liquid as a bioactive delivery system", Carbohydrate Polymers 2022, under review.
6. **Gomes J.M.,** Marques C. F., Rodrigues, L. C., Silva T. H., Silva S. S., and Reis, R. L. " 3D bioactive ionic liquid-based architectures: An anti-inflammatory approach for early-stage osteoarthritis", submitted, 2022.

Papers in international scientific journals with referees (as co-author)

1. Goncalves C., Silva S. S., **Gomes J. M.**, Oliveira I. M., Canadas, R. F., Maia F. R., Radhouani H., Reis R. L., Oliveira, J. M., "Ionic liquid-mediated processing of SAIB-Chitin scaffolds". ACS Sustainable Chemistry & Engineering, 2020, 8(9): 3986-3994. doi: 10.1021/acssuschemeng.0c00385.

2. Silva S. S., **Gomes J. M.**, Vale A C., Lu S., Reis R. L., and Kundu S. C., "Green Pathway for Processing Non-mulberry Antheraea pernyi Silk Fibroin/Chitin-Based Sponges: Biophysical and Biochemical Characterization", Front. Mater 2020, 7, 135. doi: 10.3389/fmats.2020.00135

3. Silva S. S., **Gomes J.M.**, Rodrigues L.C., Reis R. L., "Marine-Derived Polymers in Ionic Liquids: Architectures Development and Biomedical Applications.", Marine Drugs 2020, 18, 346. doi: 10.3390/md18070346

4. Silva S. S, Rodrigues L. C., Fernandes E. M., Lobo F. C. M., **Gomes J. M**., Vilas-Boas A., and Reis R. L., "Approach on chitosan/virgin coconut oil-based emulsion matrices as a platform to design superabsorbent materials", Carbohydrate polymers, 2020 249, 116839. doi: 10.1016/j.carbpol.2020.116839

5. Silva S. S., **Gomes J. M.**, Reis R. L., and Kundu S. C., "Green Solvents Combined with Bioactive Compounds as Delivery Systems: Present Status and Future Trends", ACS Applied Bio Materials, 2021, 4, 5, 4000-4013. doi: 10.1021/acsabm.1c00013

6. Goncalves C., **Gomes J. M.**, Maia F.R., Radhouani H., Silva S. S., Reis R. L., and Oliveira J. M., "Fabrication of biocompatible porous SAIB/silk fibroin scaffolds using ionic liquids", Materials Chemistry Frontiers, 2021, 5, 17, 6582 – 6591, doi: 10.1039/D1QM00583A

7. Piaia L, Silva S. S., **Gomes J. M.**, Franco A. R Fernandes E. M., Lobo F. C. M., Rodrigues L. C., Leonor I. B., Fredel M. C., and Salmoria G. V., Hotza D. and Reis R. L., "Chitosan/β-TCP composites scaffolds coated with silk fibroin: a bone tissue engineering approach", Biomed. Mater., 2021 17 015003. doi: 10.1088/1748-605X/ac355a

8. Silva S. S, Rodrigues L. C., Fernandes E. M., Lobo F. C. M., **Gomes J. M**., and Reis R. L. "Tailoring Natural-Based Oleogels Combining Ethylcellulose and Virgin Coconut Oil", Polymers, 2022, 14, 2473-2481. doi: 10.3390/polym14122473

Book Chapters

1. Silva S. S, Rodrigues L. C., **Gomes J. M.,** and Reis R. L., "Marine-Derived Polymers in Ionic Liquids: Architectures Development and Biomedical Applications", Marine Drugs, 18, 7, 246, doi: 10.3390/md18070346

2. Silva S. S, Rodrigues L. C., **Gomes J. M.,** and Reis R. L., "Biomedical exploitation of chitin and chitosan-based matrices via ionic liquid processing". Handbook of Chitin and Chitosan, Sreerag G., Sabu T., Anitha P. (Eds.), Elsevier, 2020, 3, 471-497. doi: 10.1016/B978-0-12-817966-6.00015-7

Oral presentations

1. **Gomes J. M.**, Silva S. S. and Reis R. L; "Processing of α-chitin into 3D structures using biocompatible ionic liquids". 1st Discoveries Forum on Regenerative and Precision Medicine, Porto, Portugal, September, 2019.

Conference posters

1. **Gomes J. M.**, Silva S. S and Reis R. L., "Design of the biocompatible ionic liquids for biomaterials processing". Chem2Nature, Porto, Portugal, June 2018.
2. **Gomes J. M.**, Silva S. S, Lu S., Kundu S. C. and Reis R. L., "Ionic liquids: a processing approach to fabricate Antheraea pernyi silk-based sponges". Chem2Nature, Guimarães, Portugal, October 2018.
3. **Gomes J. M.**, Silva S. S. and Reis R. L., "Biocompatible ionic liquids as platforms for the processing of α-chitin". First Aquilles Conference, Porto, Portugal, July 2019.
4. Rodrigues L. C., Costa, R. R., **Gomes J. M.**, Vilas-Boas A., Herrero-Gutiérrez M., Rodriguez-Cabello J. C., Silva S. S. and Reis R. L., "Engineered tubular structures based on Natural origin blended polymers for tissue engineering applications", First Aquilles Conference, Porto, Portugal, July 2019
5. Goncalves C., Silva S. S., **Gomes J. M.**, Radhouani H., Reis R. L. and Oliveira I. M., "Ionicl liquid-assisted processing of SAIB/SF scaffolds", , First Aquilles Conference, Porto, Portugal, July 2019
6. **Gomes J. M.**, Silva S. S. and Reis R. L., "Chitin-based 3D structures processed with Biocompatible ionic liquids". First Aquilles Conference, Braga, Portugal, November 2019.
7. **Gomes J. M.**, Silva S. S. and Reis R. L., "Engineering silk fibroin/cholinium gallate based sponges envisioning inflammatory diseases treatment". FoReCaST Final Conference, Porto, Portugal, October 2021.

8. **Gomes J. M.**, Silva S. S. and Reis R. L., "Acemannan/alginate/biocompatible ionic liquid-based beads as a sustainable therapeutic approach", SFB 2022 Annual Meeting, Baltimore, MD, USA, April 2022.
9. **Gomes J. M.**, Silva S. S., Rodrigues L. C. and Reis R. L., "Acemannan/alginate-based beads loaded with a biocompatible ionic liquid", Workshop MicSeaOnMed, Guimarães, Portugal, May 2022

Awarded grants

1. FCT scholarship (PD/BD/135247/2017) financed by the PhD programme in Advanced Therapies for Health (PATH) (PD/00169/2013).

International Mentorship Program

Mentee on the International Mentor Program (IMP) at IMFAHE Foundation (2019/2020)

INTRODUCTION TO THE THESIS FORMAT

The work performed under the scope of this PhD is divided into four main sections (**Section 1** to **Section 4**) containing eight chapters (**Chapter I** to **Chapter VIII**). The defined structure allows for an organized follow-up to the thesis content, subdivided according to the subject and aim of each work.

Section 1 (Chapter I) includes a general introduction mainly focused on the state-of-the-art of biocompatible ionic liquids (Bio-ILs), their evolution, and their use in several fields, including the biomedical one.

Section 2 (Chapter II) presents a detailed description of the materials, experimental procedures, and protocols used in this thesis.

Section 3 (**Chapter III** to **Chapter VII**) is based on a series of papers published or submitted for publication in international journals. Thus, each chapter is presented as an adapted version of the published or submitted manuscript, keeping its contents, i.e., abstract, introduction, experimental section, results, discussion, conclusion, and acknowledgments. The specific publication is identified on the front page of each chapter, and a list of relevant references is also presented at the end of the chapter.

Section 4 (**Chapter VIII**) contains the summarization and general conclusions of work developed in the scope of this thesis, as well as future perspectives.

Section 1 – General introduction

Chapter I – Biocompatible ionic liquids: Fundamental behaviors and applications: This chapter provides an overview of the Bio-ILs origin, the main strategies used for their synthesis, their progress toward their impact, and their use in a broad range of fields. Moreover, the use of these compounds in the biomedical and tissue engineering (TE) field is discussed, emphasizing the future directions for their widespread use.

Section 2 – Experimental design and detailed description of experimental materials and methodologies

Chapter II – Materials and Methods: This chapter provides a detailed description of the materials used throughout this thesis, the processing techniques, the strategies used for Bio-ILs synthesis, and biomaterials' development. Moreover, the techniques employed for their physico-chemical

characterization, and the description of the performed biological assays on the developed architectures are also provided.

Section 3 – Experimental studies

Chapter III – Exploring the use of choline acetate in the sustainable development of α-chitin-based sponges: This chapter describes the use of a commercially available Bio-IL, Cholinium acetate (Ch[ACE]) for the dissolution and processing of the natural polymer α-chitin, into 3D sponges. The physico-chemical characterization of the produced Ch[ACE]/α-chitin-based sponges and their biological characterization were performed. The main goal of this work was to determine and understand the impact of keeping the Bio-IL, Ch[ACE] into the final constructs.

Chapter IV - Silk fibroin/cholinium gallate-based architectures as therapeutic tools: In this chapter, cholinium gallate (Ch[Gallate]), a phenolic-based Bio-IL, with intrinsic bioactivity including anti-inflammatory and antioxidant features, was synthetized. Ch[Gallate] was dissolved into silk fibroin (SF) solutions, and the resulting sponges were further physico-chemical characterized. Moreover, the biological behavior of the developed sponges, and their anti-inflammatory potential were studied.

Chapter V - Unraveling the potential of biocompatible ionic liquid-based sponges for osteoarthritis therapy by reducing inflammation and oxidative stress: In this chapter, cholinium gallate (Ch[Gallate]) and cholinium caffeate (Ch[Caffeate]), were synthesized, combined with the model analgesic drug acetaminophen (ACT), and added into SF solutions to produce bioactive SF/Bio-IL-based sponges. The physico-chemical characterization of the sponges was performed, and the antimicrobial properties of the Bio-ILs, and the Bio-IL/SF-based sponges was assessed against clinically relevant bacteria. In addition, the influence of the sponges containing Ch[Gallate], Ch[Caffeic], and ACT on the intracellular ROS scavenging in primary human chondrocytes (HC) was studied. Moreover, the ability of the sponges containing Ch[Gallate] and ACT in their matrix to support HC growth and proliferation was evaluated, and their influence on the expression of primary human osteoarthritic chondrocytes (HC-OA) was explored.

Chapter VI - Alginate/acemannan derived beads loaded with a biocompatible ionic liquid as a bioactive delivery system: In this chapter, the synthesized cholinium caffeate (Ch[Caffeate]) was entrapped into alginate (ALG)/acemannan (ACE) based beads, using the extrusion dipping method. The physico-chemical characterization of the beads was performed, and their ability to promote ATDC5

chondrocyte-like cell growth and proliferation for up to 21 days, was evaluated. Moreover, the capacity of the produced beads to block the release of pro-inflammatory cytokines was evaluated.

Chapter VII - 3D bioactive ionic liquid-based architectures: An anti-inflammatory approach for early-stage osteoarthritis: Herein, ALG, ACE, and Ch[Caffeic] were combined to produce printable inks. The ink preparation and bioprinting process was optimized, and the versatility of the developed strategy was evaluated by printing different architectures. The physico-chemical characterization of the fabricated constructs was performed, and ATDC5 chondrocyte-like cells were encapsulated in the bioinks. Further, the cellular viability and proliferation were assessed, and a co-culture system using THP-1 activated macrophages and the encapsulated ADTC5 chondrocyte-like cells was established, envisioning to evaluate the potential of the developed system in the management of the early-stage OA inflammatory events.

Section 4 – Concluding remarks

Chapter VIII – General Conclusions and Future Perspectives: The main conclusions of each chapter, the limitations, and potential benefits found during the thesis development are herein detailed and discussed. The future perspectives of the work developed in this thesis and the research lines to be followed were also presented.

"*Foi o tempo que dedicaste à tua rosa que tornou a tua rosa tão importante.*"

Antoine de Saint-Exupéry

SECTION 1

GENERAL INTRODUCTION

Chapter I

Biocompatible Ionic Liquids: Fundamental behaviours and applications

Chapter I[1]

Biocompatible Ionic Liquids: Fundamental behaviours and applications

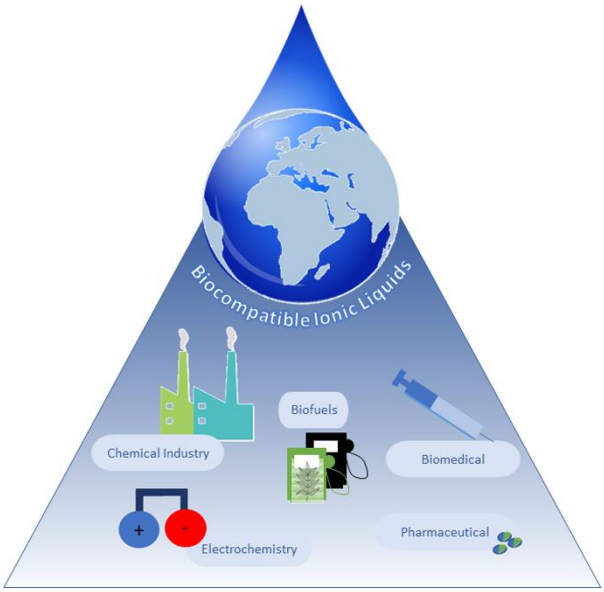
ABSTRACT

Biocompatible ionic liquids (Bio-ILs) represent an eco- and bio-friendly family of ionic liquids (ILs) useful for applications ranging from the electrochemical to the biomedical fields. The most promising strategies for their synthesis, consist of the use of molecules from bio-renewable sources as a basis for both anionic and cationic counterparts of the Bio-ILs structure. Several studies have been carried out on Bio-ILs properties, including their impact on the environment and health safety. Herein, we review the progress and the strategies towards the synthesis of Bio-ILs and address their ecotoxicological and biological impact. Moreover, it is approached the impact of using these compounds in a diverse range of applications, with some insights into their use for the development of improved technologies.

[1] This chapter is based on the following publications:

Gomes J. M., Silva S. S. and Reis R. L. "Biocompatible Ionic Liquids: Fundamental beahviours and applications"; Chemical Society Reviews, 2019, 48, 4317-43352019. doi: 10.1039/C9CS00016J

I-1. GRAPHICAL ABSTRACT



I-2. INTRODUCTION

Globalization increased the consumption of a wide range of products including, food, medical, and other essential materials, leading to higher demand for chemicals and solvents by the worldwide growing industry [1]. This has been the driving force for the continuous growth of the research on the development of compounds with enhanced environmental and health features. On that way; the scientific and industrial evolutions have been boosting the emergence of novel ionic liquids (ILs), one of the most important classes of green media that can act as solvent and reaction media [2,3]. The evolution in this field was driven by the implicit green character of this family of compounds, which is a direct consequence of their features, including the non-flammability and negligible vapor pressure [4]. However, in recent years, it has emerged that the commonly used ILs are not as environmental and biologically friendly as though, mostly due to their non-biodegradability and toxicity towards the environment, as well as the ecosystems [5,6]. In this context, the development of biocompatible ILs (Bio-ILs) has been a focus of intense research, resulting in the emergence of novel compounds, with enhanced toxicological profiles and adequate biodegradable features. The synthesis of Ls using biocompatible moieties such as amino acids (AA) [7–11], non-nutritive sweeteners [12], glucose [13], and carboxylic acids [14] has demonstrated

a crescent growth. Particularly, the use of choline, a biodegradable, inexpensive, and water-soluble organic salt, has been commonly employed as the cationic counterpart of the Bio-ILs [9,14–16]. The use of this molecule opened up the doors towards a more accessible and cost-effective synthesis of Bio-ILs, resulting in compounds with low toxicity and high biocompatibility [6].

This review addresses the progress and strategies towards the synthesis, ecotoxicity, and biological impact of the Bio-ILs. Furthermore, exploits an overview of the Bio-ILs applications, which goes from the electrochemical to the biomedical field. In this context, the present review provides a tool to obliterate the gap between the most commonly used ILs, and the biocompatible classes of compounds from this family.

I-3. IONIC LIQUIDS – A REMARKABLE CLASS OF CHEMICAL COMPOUNDS

ILs are stable salts composed of organic cations and inorganic anions, with melting temperatures below 100 °C [15,17–20]. According to the 12 principles of Green Chemistry, ILs represent the best alternative as a green solvent to be used in chemical reactions, constituting theoretically "greener" alternatives to the commonly used organic solvents [21,22]. The ILs striking characteristics include their low vapor pressure, high chemical and thermal stabilities, and nonflammability [1,23,24]. The possibility of different cation and anion combinations promotes a vast range of available ILs, allowing to tune their intrinsic characteristics such as conductivity, density, viscosity, melting point, polarity, solvation power, hydrophilicity/hydrophobicity, and acid/base character [23,25,26]. Then, it is possible to tune a suitable candidate for a specific application, and for that reason, ILs are called "designer" solvents [27]. Their specificity and selectivity allowed to use them as selective recovery solvents, as in carbon dioxide capture [28–30]. In general, ILs present a high solvation power concerning either organic/inorganic compounds and natural polymers, encouraging their use as drug delivery systems, plasticizers, catalysts and to produce and process polymeric materials [31–38]. Moreover, their wide electrochemical window, a consequence of their ionic nature, makes them an excellent pathway to improve the conductivity of various materials, enabling its use as electrolytes in different applications from photovoltaic to electrochemical actuators [39].

The massive expansion in the field of ILs happened in the 70s and 80s decades, when a set of compounds with unique features, including non- or very low volatility, thermal stability, and large

liquid ranges emerged, establishing the so-called 1st Generation of ILs. [40] At that time, due to those ILs' interesting properties, they were recognized as the ideal solvents and media to be used in both the electrochemical field and in the still emerging field of Green Chemistry [41,42].

Figure I-1 depicts a schematic representation of the ILs evolution and the main characteristics of each generation. The 2nd Generation of ILs arose years later to overcome the need to develop compounds with tunable and targeted physical and chemical properties. The first IL from this generation was introduced in 1992 [43], and the main goal of this preliminary work was to reduce the inert character of the ILs, making feasible to work with them under ambient conditions. The authors were able to widespread the use of these compounds by the introduction of selected anions (e.g., NO3-, NO2-, BF4- and MeCO2-), in some known methylimidazolium cations (EtMeim+) [43]. From this moment on, it was possible to tune the design of new functional materials, modifying independently the properties of both the cation and the anion, while retaining the core desired features of an IL. At the beginning of the 21st century, the investigation on ILs turn its attention towards their toxic, chemical, and biological feature and the focus was no longer exclusive on the physical properties of these compounds. [41] As a result, the 3rd Generation of ILs emerged, and ILs with targeted and selected biological properties were produced, rising the concept of task-specific ionic liquids (TSILs) [41,44]. TSILs allowed the scientists to develop compounds with antifungal and antibacterial activities, as well as to use ILs with biologically active ions, enhancing their use into the biomedical and pharmaceutical fields [25,45]. Recently, MacFarlane and co-workers [42] have proposed a 4th evolution for ILs, based on the fact that ILs can offer unique and unpredictable properties when in solutions/mixtures with molecular liquids. According to the authors, these properties are not ruled by the simple mixing rules and are not those from the salt-in-solvent solutions. The uniqueness of these mixtures is dependent on the balance of interactions between the ions and the solvent making the ILs field a much broader one, offering a more widespread application of these compounds.

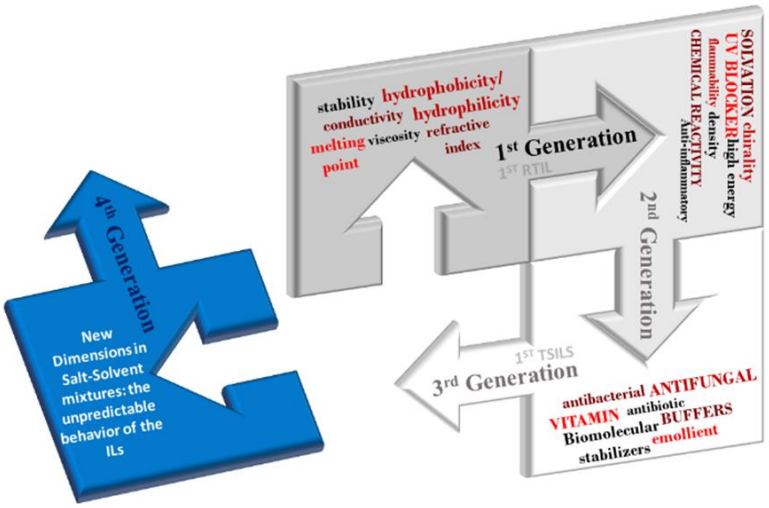


Figure I-1- The ILs evolution.

ILs' task-specific character, along with the fact that they constitute an innovative approach to sustainable chemistry, have strongly encouraged their wide use and extended their application into a broader range of fields [25,41,46–50]. Though, there are some worries concerning their high prices when compared with commonly used organic solvents. The recycling nature of ILs is frequently used as an argument to devalue the associated high costs. However, the recovering of these compounds can sometimes compromise their inherent characteristics such as, purity and reactivity, which are essential features for some applications [51]. Additionally, in most cases, their ionic nature does not infer an absolute non-toxic character to the compound. There are some well-known toxicological risks both for the environment and for humans, which may result in a restriction concerning the large-scale application of the ILs [52–56]. Aiming to surpass these drawbacks and to increase the life quality of the global population, the scientific community has taken advantage of the current superior knowledge on the synthesis of ILs to develop novel and safer synthetic strategies, which result in "greener" families of compounds.

I-4. BIOCOMPATIBLE IONIC LIQUIDS – A FAMILY IN THE EXPANSION

Face to the "dubious" green nature of commonly used ILs, the synthesis of biocompatible ILs (Bio-ILs) is in expansion. The ideal strategy to synthesize Bio-ILs is the use of both anionic and

cationic counterparts derived from biocompatible materials [15] such us AA [7–11], non-nutritive sweeteners [12], glucose [13], and carboxylic acids [14]. As a first approach to the development of more sustainable synthetic routes and aiming the synthesis of more benign compounds, the stated biomacromolecules may be used either as the cation or the anion in the ILs structure. The use of these bio-renewable and natural compounds constitutes a promising approach for the synthesis of novel ILs considering both the environmental and economic concerns, strongly associated with the conventional methods. Still, in some cases, the resulting compounds, are not considered Bio-ILs entirely [10,57,58].

The bulk research on the use of bio-renewable compounds for the ILs synthesis has been focused on protein-derived AA cations and anion [7,11,22,50,59]. AA are nontoxic, biodegradable, and biocompatible compounds derived from protein hydrolysis and subsequent purification [7,10,22]. These molecules are abundant and economical, which boosts its use as feedstocks for the ILs synthesis [60]. The first room temperature ILs (RTILs) derived from AA reports to the year 2005 [10]. Fukumoto et al. were the pioneers in describing the successful synthesis of RTILs by coupling the imidazolium cation with twenty different natural AA. The use of different AA [10] as the anionic counterpart of the ILs allows the developing TSILs with various characteristics, considering the value of the functional groups on AA structure. In the same year, Tao et al. described the synthesis of AA-based ILs using the AA as the ILs' cationic moiety, which has rarely been done until then [7]. In this work, the authors were able to synthesize more than one hundred ILs directly derived either from natural α- AA and α - AA ester salts. The produced compounds were able to maintain the chirality of the original α- AA, an interesting feature considering chemical and biological applications.

In addition to protein and AA-derived ILs, also has been done the synthesis of ILs using natural compounds derived from sugars, obtained either by the depolymerization or direct refining of polysaccharides. In this case, the available data is mainly focused on the sugar-based IL cations. [22] Handy and his group [58] were pioneers in the synthesis of ILs derived from naturally occurring sugars. They used the D-fructose monomer and transformed it into monosubstituted imidazole compounds. Several works followed using fructose derivatives as ILs precursors, such as isomannide [61], glucose [13,62], and glucose derivatives namely arabinose and isosorbide [63], the last resulting in compounds with chiral moieties. It is also noteworthy that the first RTILs containing a polysaccharide were synthesized in 2007 [57]. The authors prepared RTILs by

combining carboxymethylated chitosan and 1-ethyl-3-methylimidazolium hydroxide. In another study, aldehydes from lignin and hemicellulose were explored as target molecules to the synthesis of ILs, of which the reaction is depicted Figure I-2- [64]. The outcomes of this study gave some insights into the performance of a "closed-loop" process in the lignocellulosic biorefineries; contributing to a more economical and green process, allowing to replace the current used ILs for those from renewable resources.

As previously mentioned, despite the efforts and advances described above, the development of fully benign and bio-friendly compounds remains a challenge and calls for new strategies. The Bio-ILs persist as a very restricted and exclusive family of compounds. The use of the cholinium as the cationic moiety in the structure of the Bio-ILs has emerged as the most effective approach towards the development of "greener" compounds and being therefore of primary relevance to this review. Nevertheless, the perseverance of the scientific community has been leading to the development of novel compounds, such as some ammonium- and glycine betaine-based ILs, a subject further discussed.

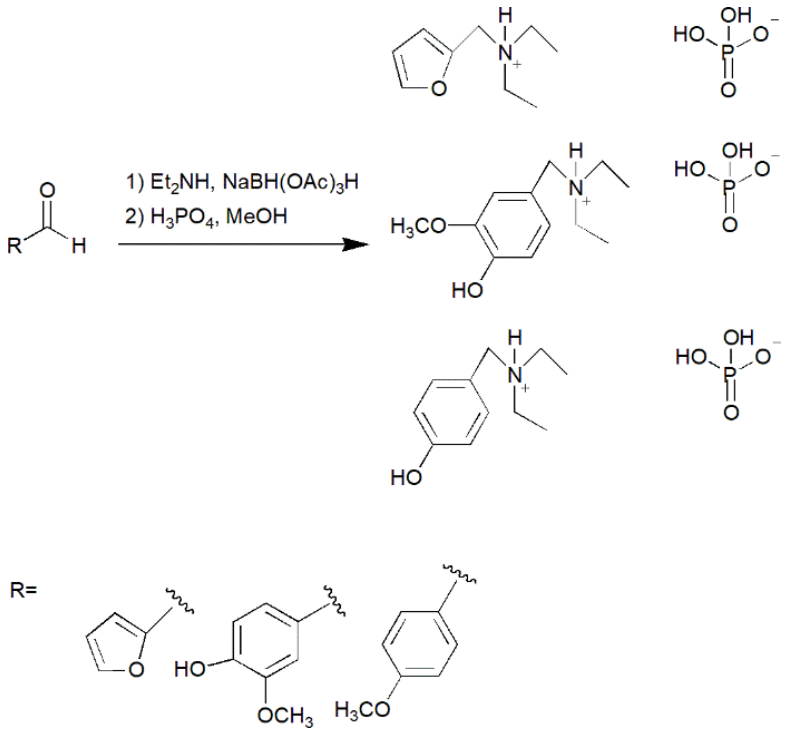


Figure I-2 - Schematic representation of the strategy used for the synthesis of lignin- and hemicellulose derived ILs. Adapted from ref. [64] with permission from the National Academy of Sciences, Copyright (2014)

I-4.1. Cholinium as the Bio-ILs cationic moiety

In the past decades, a remarkable number of studies have shown that the use of choline as a cation in the Bio-ILs structure, provides them biodegradability and low toxicity [5,27,65,66]. This molecule can be obtained from natural sources and is usually combined with B-complex vitamins [67]. In 1998, choline (vitamin B) was added to the list of human vitamins by the National Academy of Sciences (NAS). Moreover, choline is involved in many functions including memory and muscle control due to its function as a precursor for the neurotransmitter acetylcholine. [6] Cholinium cation also integrates the head groups of two classes of cell membrane-abundant phospholipids: phosphatidylcholine and sphingomyelin [67].

Since the early 2000s, the number of works reporting the use of cholinium as the cation, and a variety of other compounds, including AA, artificial sweeteners, and carboxylic acids, as the anion have been significantly increased [6,12,60,66,68,69]. The use of active pharmaceutical ingredients (APIs) in IL systems (APIs-IL) has been explored motivated by the ILs tuning potential, along with their biological activity [25]. The cholinium cation properties have been investigated in combination with the ones from different APIs such as phenytoin [70] , ampicillin [71], nalidixic acid (NAL), niflumic acid (NIF), 4- amino-salicylic acid (PAS), pyrazinoic acid (PYR) and picolinic acid (PIC). [72] The developed APIs-Bio-ILs systems allowed to improve of the solubility of the APIs, as well as to increase their potential to penetrate the cell membrane, offering possibilities for the development of novel and improved treatment platforms.

Good's buffers (GB) have also been explored as a different anionic counterpart to prepare other classes of Bio-ILs. [73] GB are zwitterionic AA derivatives suitable for use as biological hydrogen ion buffers between pH 6 and 8. They possess a wide set of advantages in biological research, mainly due to their buffering capacity, as well as their low toxicity [20,73,74]. Following the background knowledge regarding the use of GB in the synthesis of other classes of ILs, as well as the known advantages of using the cholinium as a Bio-IL counter cation, in 2014, Matias and co-workers presented the synthesis of novel cholinium-sulfonate Bio-ILs with buffering properties [69]. The results obtained in this study showed the potential of the synthesized compounds in the cytochrome c (cyt-c) dissolution and reduction. These findings have a strong biological impact considering the cyt-c function as an electron-carrying mitochondrial protein, playing a central role

in cellular oxidations in plants and animals. In the following years, some works emerged, reporting the synthesis of new sets of Bio-ILs from the same class [20,74,75].

I-4.2. Glycine Betaine-based ILs as alternatives to the cholinium family

It is clear the dominance of the cholinium-based ILs (Ch[ILs]) when the topic is the Bio-ILs family. However, despite the well-earned merit, as a consequence of the intensive research in this field, some biocompatible alternatives to the cholinium as the cationic building block for the Bio-ILs synthesis have gained attention. Researchers have recently turned their attention to glycine betaine for the Bio-ILs synthesis. Glycine Betaine is an abundant natural raw material that represents 27% of molasses of sugar in beet in weight [76]. It is obtained after the extraction of saccharose, and its structure is characterized by a trimethylalkylammonium moiety and a carboxylate function, which is useful for the synthesis of Bio-ILs [76,77]. In 2015 a novel set of Bio-ILs with glycine betaine esters as cationic moiety was synthesized [76]. The effects of changing the alkyl side chain length and the nature of the anions were evaluated, and the authors concluded that the length increase in the alkyl chain improves the thermal stability of the compounds and that the organic or inorganic nature of the anions strongly influences their thermal and viscosity properties. The interfacial properties studies allowed to evaluate the self-assembly ability of the compounds, and the results suggested the possibility of using these Bio-ILs for solvent-based applications or in extraction processes. This ability was tested in a later study from the same group [78]. The authors used the ion pair Centrifugal Partition Extraction technique and Bio-ILs from this family for the removal of pesticides from wastewater. Moreover, glycine betaine has recently been combined with other compounds to form deep eutectic solvents (DES), widely used for biopolymers dissolution and processing [79]. DES, also known as deep eutectic mixtures or low melting mixtures, were introduced by Abbott et al. [80] in the year 2003, as alternatives to ILs [81,82].

Several studies have been carried out, checking the toxicity of Bio-ILs against the environment and humans [83–85]. These studies proved their improved benign character when comparing them with the commonly used ILs [16,85–88].

I-5. SYNTHESIS OF BIOCOMPATIBLE IONIC LIQUIDS- THE PATH

Several synthetic strategies have been developed involving the use of non-toxic moieties such as carbohydrates or AA [7] for the cationic species and compounds such as lactates [89,90], acesulfamates [12,91], levulinate [92], carbohydrate derivatives [58] or AA [10,60] as the anion counterparts. The use of anionic and cationic counterparts both derived from natural sources, would be an ideal and sustainable approach to developing a new generation of Bio-ILs [15,22]. In a critical review, Joris and co-workers [22] discussed the practical aspects of the synthesis of ILs from AA, carbohydrates, lignin, and other renewable sources. They described the major synthetic pathways involved in these ILs synthesis as well as some application possibilities such as in the biopolymers processing, as catalysts and reaction media, and as platforms for selective extraction of compounds [22]. Also, they illustrate, in a clear and succinct way, the research emphasis on each of the classes of ILs, using a translation of the number of the publication, as depicted in Figure I- 3.

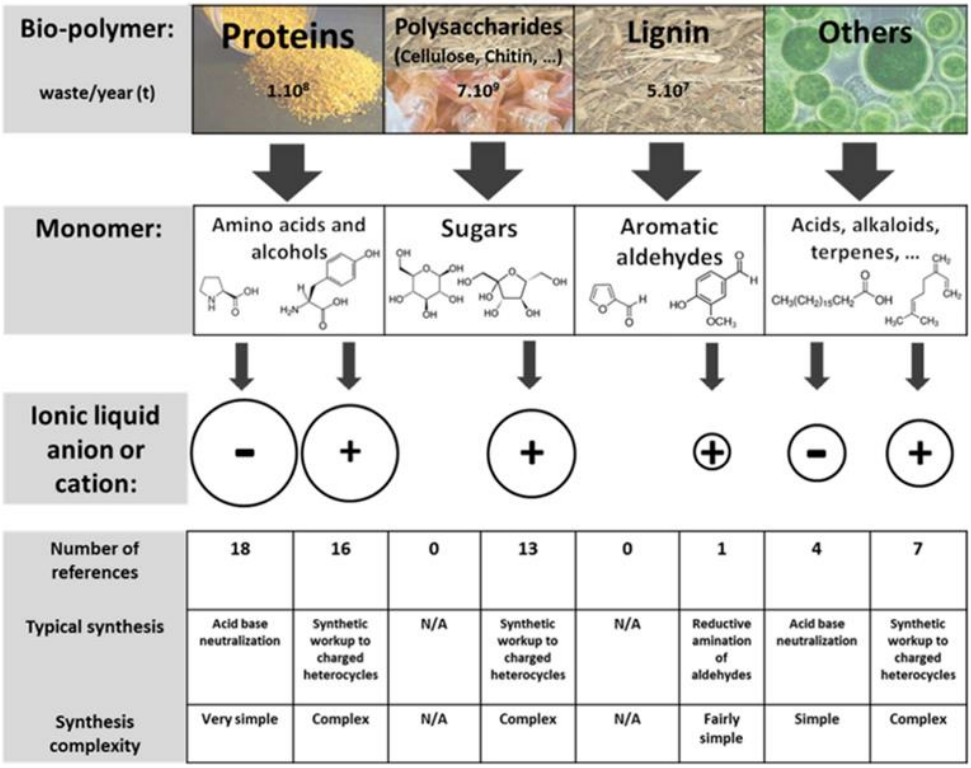


Figure I-3 - Synthetic pathways towards bio-based ILs. For each renewable resource class, typically derived monomers are depicted. The intensity of research (i.e., number of published papers) on converting these monomers to IL anions

or cations is represented by the radius of the circle around the '-' or '+' sign, respectively. Typical synthetic routes and their complexity are mentioned. Reprinted from [22] Copyright © 2016, American Chemical Society.

The conventional technique to prepare RTILs [93] is by the anion exchange of halide salts with metals, though this method seems to be unsuitable for the synthesis of some pure ILs. The inorganic contamination characteristics of the halide salts represent a major drawback for the alkaline salt metathesis synthetic route and also, there is a limited variety of commercially available metal salts [10,72]. These drawbacks can be avoided by the direct use of acids instead of salts. [72] Nonetheless, in some cases, the anion exchange by weaker acids cannot be efficiently performed, demanding alternative techniques [72,94]. The widely used technique adopted for the preparation of RTILs is a two-step anion exchange procedure described by Ohno et al. [10]. Briefly, the first step involves the passage of the halide solution through an anion exchange resin in the OH form, followed by neutralization of the acid of interest using the resultant hydroxide solution. This makes it possible for several types of natural molecules to be converted into ILs through relatively green and straightforward methods such as simple ion exchange chromatography or a direct acid-base reaction [52].

I-5.1. Synthesis of Choline- based Ionic liquids

As suggested before, the use of the cholinium cation has emerged as a major strategy to target the development of Bio-ILs [65,94]. Several works reported the synthesis of [Ch]ILs using the salt choline chloride ([Ch]Cl) [12,95–97]. In 2001, Abbott and his group synthesized [Ch]ILs by mixing choline chloride with hydrated transition metal salts, or with anhydrous zinc-(II) chloride or tin(II) chloride [95,96]. Herein, the authors were able to produce new moisture-stable Bio-ILs, which helped to overcome some of the low tolerance to the moisture of some imidazolium-based ILs. Furthermore, years later, Nockemann and co-workers [12] synthesized two hydrophilic Bio-ILs derived from artificial sweeteners, saccharinate and acesulfamate performing an anion exchange of the same halide salt, [Ch]Cl, followed by the purification of the Bio-IL by ion-exchange chromatography (see the schematic representation in Figure I-4. [12] The depicted methodology allowed the production of hydrophilic Bio-ILs with very low toxicity when compared with other families of ILs, including the imidazolium-based ones.

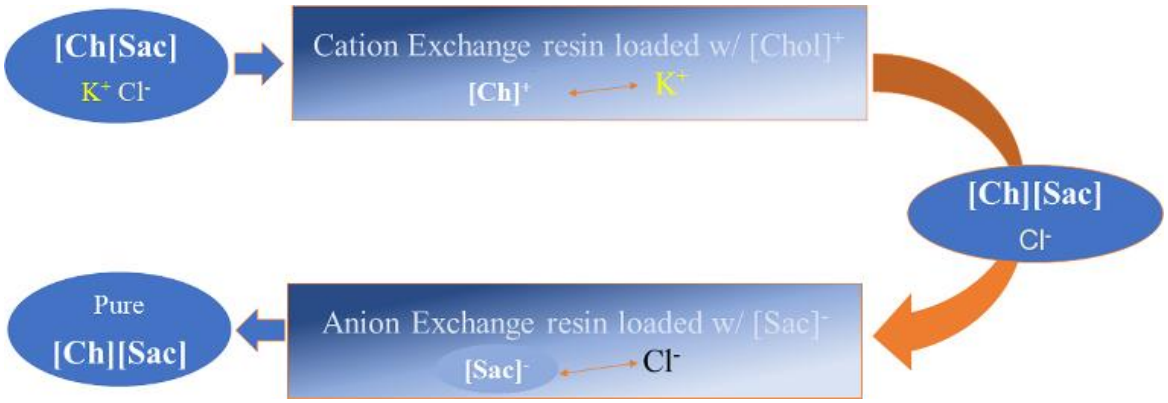


Figure I-4 - Schematic illustration of the purification of Bio-ILs after the metathesis reaction by ion-exchange chromatography. The given example is for the purification of choline saccharinate. Reprinted from [12] Copyright © 2007, American Chemical Society

Alternatively, [Ch]ILs can be synthesized by using [Ch]Cl (as well as other choline halide solutions such as iodide, as the source of the cation, for the preparation of choline hydroxide (Ch[OH]). In the first synthetic step, Ch[OH] solutions may be prepared from a metathesis of [Ch]Cl with a metal oxide, followed by purification and filtration of the final product, Ch[OH] [9]. In another alternative, an anion exchange resin in the OH form may be used to prepare the hydroxide solution from the cholinium halide solution [72,94]. However, these synthetic procedures using cholinium halide solution are usually time-consuming and laborious, requiring additional purification steps. Nowadays, the most common and straight forward procedure for the [Ch]ILs synthesis is carried out by a neutralization reaction between Ch[OH] or choline bicarbonate ([Ch][HCO_3]) solutions (both commercially available), and a slightly equimolar excess of the desired acid [53]. In the most common procedure, the reaction involves mixing between 12h-24h, at room temperature, and then purification using an organic solvent aqueous solution (to precipitate the acid excess) followed by filtration. The crude product is further dried under high vacuum. Representative detailed examples of [Ch]ILs synthetic processes, using both Ch[OH] and [Ch][HCO-3] solutions are shown in Figure I-5A and FigureI- 5B respectively.

The cost-effective and green synthetic pathways characteristics of the preparation of Bio-ILs from renewable materials, along with low toxicity and biodegradability of the resultant compounds, gave rise to a series of works focused on the production of [Ch][AA], as well as in the study of their

physico-chemical characteristics and exploitation of their applications [5,9,60]. In a pioneer work, Calvino-Casilda et al. [8] developed five new choline-AA based Bio-ILs ([Ch][AA]) ILs ([Ch][Gly] [Ch][Ala] [Ch][Phe] [Ch][Threonine] and [Ch][Hist]) (see Figure I- 5A) using the presented green route in which the only by-product is water. The produced Bio-ILs were also successfully tested as catalysts for the Knoevenagel condensation between benzaldehyde and three different active methylene compounds [8].

Petkovic et al. [65] were the pioneers in the synthesis of the carboxylate Bio-ILs, another predominant Bio-IL family. In their work, nine new carboxylates [Ch]ILs were synthesized by dropwise addition of the corresponding acid to an aqueous solution of [Ch][HCO_3^-]. The reaction involved in this synthesis is depicted in Figure I-5B. By using different anions, the authors were able to understand their influence on the characteristics of the final compounds, including their toxicity, while proving once again that the designable character of the Bio-ILs is a powerful tool for its development. Different Bio-ILs from the carboxylate [Ch]ILs family were further synthesized following similar strategies, using either aqueous solutions of [Ch][HCO_3^-] or Ch[OH] [14,88].

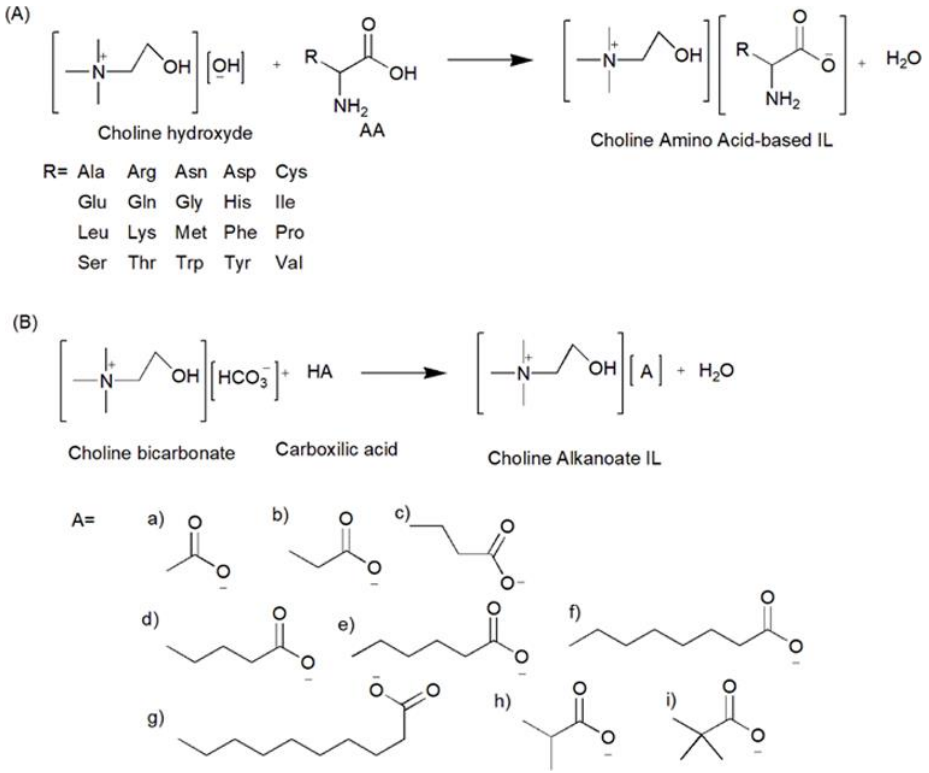


Figure I-5 – (A) The synthetic pathway for the [Ch][AA] and (B) Synthesis of the choline carboxylate Bio-ILs and chemical structures of the anions used: a) ethanoate, b) propanoate, c) butanoate, d) pentanoate, e) hexanoate, f) octanoate,

g) decanoate, h) 2-methylpropanoate, i) 2,2-dimethylpropanoate. Adapted from ref. 8, with permission from Elsevier Copyright © 2010. Adapted from ref. 65, with permission from The Royal Society of Chemistry, Copyright © 2010.

In 2014, Matias and co-workers [69] used the Good's buffers N,N-bis(2-hydroxyethyl)-2-aminoethanesulfonic acid (BES), 3-(cyclohexyla- mino)-1-propanesulfonic acid (CAPS), 3-(N,N-bis[2-hydroxy- ethyl]amino)-2-hydroxypropanesulfonic acid (DIPSO), 2-(N-morpholino)ethanesulfonic acid (EPPS), 4-(2 hydroxyethyl)-1-piperazinepropanesulfonic acid (MES), b-hydroxy-4-morpholi- nepropanesulfonic acid (MOPSO) and 2-hydroxy-3-[tris(hydroxymethyl)methylamino]-1-propanesulfonic acid (TAPSO) to produce a novel family of [Ch]ILs, with buffering ability following three different synthetic procedures. Still, all of them involved the common pre-step above described to obtain Ch[OH], in which a [Ch]Cl solution, dissolved in methanol, was passed through the resin column in the OH form. The resultant choline hydroxide was then collected into a flask containing the desired acid. Following, one of two different purification methods was used: (i) method A, the removal of the unreacted acid was carried out by applying the methanolic solution through a specific column; (ii) method B, the unreacted acid is removed by precipitation with methanol, or methanol–acetonitrile solution, in the case of CAPS. Both methods were followed by solvent removal. The synthesized compounds presented excellent yields (79–94%) and high purities, regardless of the method, which should be tailored according to the desired final Bio-IL. Later, Taha and his group synthesized and characterized a set of the same family of Bio-ILs via neutralization of Ch[OH] (Figure I-6A) with GB [20,75]. Using the same rational novel set of ILs were synthesized using the GBs MES, N-[Tris(hydroxymethyl)methyl]glycine (Tricine), 2-[(2-Hydroxy-1,1-bis(hydroxymethyl)ethyl)amino]ethanesulfonic acid (TES), 4-(2-Hydroxyethyl)piperazine-1-ethanesulfonic acid (HEPES), and N-Cyclohexyl-2-aminoethanesulfonic acid (CHES) on the neutralization reaction which is depicted in Figure I-6B, with a specific example given for the GB anion CHES. The changes in the anions resulted in a wide buffer window between pH 5.33 and pH 11.82 for all the synthesized compounds, offering a novel and broader set of Bio-ILs with buffering properties, with a strong interest in biological applications.

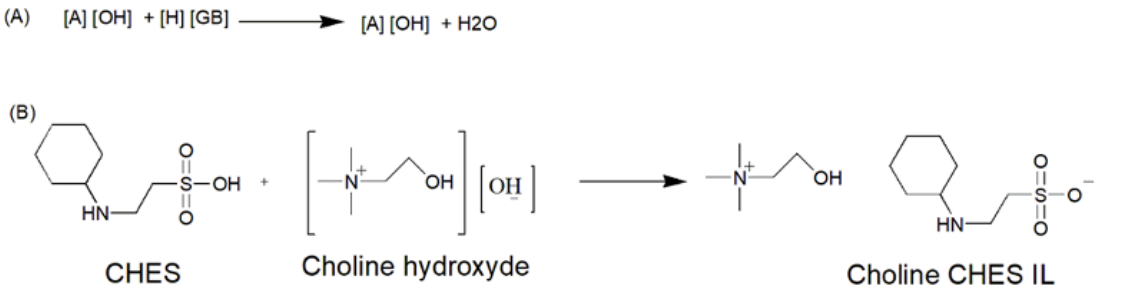


Figure I-6 – (A) Model neutralization reaction (B) The synthetic pathway for [Ch][CHES]. Adapted from 73 with permission from The Royal Society of Chemistry, Copyright © 2014. Adapted with permission from 74 Copyright (2016) American Chemical Society.

I-5.1.1. Glycine betaine-based ILs synthesis

Glycine betaine-based ILs appeared recently, as a potentially more economical alternative to the [Ch]ILs, and their synthetic strategy is here described. These compounds are usually synthesized by the addition of an excess of n-alcohol to a suspension of glycine betaine, and the general reaction is depicted in Figure I-7B. The following step involves the removal of the water formed during the esterification reaction, achieved by the gradual heating of the solution, followed by purification and recrystallization steps [76]. The synthesis of GB-based ILs is a green and cost-effective process, and the resultant compounds have a wide range of promising applications from the removal of pesticides to their use as phase-forming components in aqueous biphasic systems (ABS) [77,78,98].

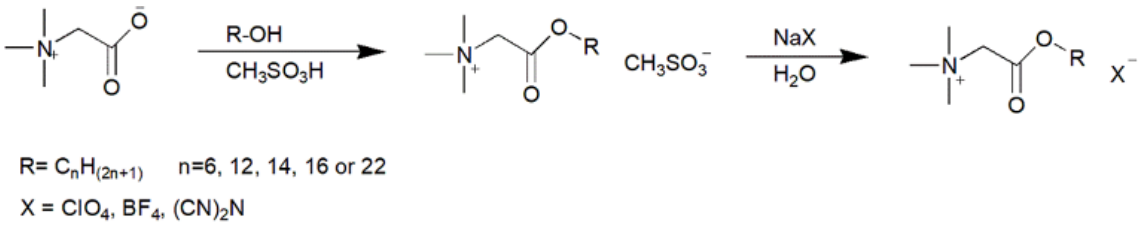


Figure I-7 – Synthetic pathway of Glycine betaine-based ILs. Adapted from [76], Copyright (2016) with permission from Elsevier.

I-5.2. The post-synthesis: physico-chemical characterization

The specific physico-chemical properties of ILs can be easily tuned, making them a class of solvents that can address a wide range of targeted finalities [99]. In that way, the characterization of the newly synthesized Bio-ILs is a necessary step. The first requirement after synthesis is the

confirmation of the newly produced compound structure by RMN, along with the determination of their water content, typically carried out by a Karl–Fischer titration [9,14,100]. Furthermore, one of the most relevant fields of study in the ILs area involves the study of their thermophysical properties. A lack of knowledge in that field limits the development of certain industrial processes, preventing the large-scale application of the compounds [68]. Density, viscosity, and refractive indexes are the most relevant criteria in this field, ending with the melting point and the decomposition temperatures, which determine the liquid range of the fluids. The latter is one of the most relevant properties for Bio-ILs when considering their application as solvents.

The structure of the cation, including the length and the symmetry of the substituent groups, as well as the structure and extent of charge delocalization of the anion, are crucial to determine the Bio-ILs specific physico-chemical and biological characteristics. These properties usually depend on interionic interactions, such as Coulomb forces, hydrogen bonding, and van der Walls interactions [99]. Moreover, considering the potential widespread use of these classes of compounds in both industrial and laboratory practices, it is urgent the evaluation of their toxic profiles. Although the growing use Bio-ILs, the number of works focusing on their environmental impact and cytotoxicity is very reduced and limited when compared with the more common classes of ILs. Moreover, the increasing and variable number of new ILs structures, including the ones from the [Ch]ILs family, have been turning the experimental assessments of the toxicity unfeasible, due to the high time consumption and the associated costs. Therefore, the application of mathematical models which can correlate the chemical structure variation of the compounds with their biological activity appears as an alternative to predict their biodegradation and toxicological profile [101,102]. Mathematical prediction models can also be useful tools to design Bio-ILs concerning not only their toxic behavior but also their potential application [101].

I-5.3. Recovery and reuse of the Bio-ILs

Depending on the desired application, the presence of Bio-ILs in the final product is often vital. For example, in the case of API-ILs and energy storage systems, with applicability as diagnostic devices and biocompatible batteries, the presence of the Bio-IL is imperative for the efficacy of the application [47,55,103–105]. In other situations, such as the biomass pre-treatment and selective purification system, the recovery and reuse of the Bio-ILs contribute to increase the sustainability of the processes and to boost the opportunity for their large-scale application [106–108]. The main

strategies used for the recycling of Bio-ILs include the precipitation of both the compounds of interest, and the contaminants, and the filtration and evaporation of the resultant Bio-ILs' solutions [106–108].

Bio-ILs are regularly used for the pretreatment of biomass [106,109–114]. In a work from 2015, the authors were able to recovery and reuse the Bio-IL choline arginine, through a very simple and straightforward process [109]. After the pretreatment and fractionation of various lignocellulose, the obtained filtrate containing Bio-IL, sodium chloride (NaCl), hydrochloric acid (HCl), and short-chain carbohydrates was neutralized with NaCl, followed by the removal of water under high vacuum by evaporation. The NaCl and short-chain carbohydrates were precipitated as insoluble solids by the addition of anhydrous methanol to the residue and removed by filtration. Methanol was finally removed by evaporation, and the recovered Bio-IL was dried and reused over 8 cycles, without losing the delignification capacity. Several works also report the recovery and reuse of the Bio-IL choline acetate (Ch[ACE]) after its application for biomass pre-treatment [106,110,111,114]. Briefly, after the Bio-IL-assisted pretreatment and the fractionation steps, a Bio-IL aqueous solution was obtained, the water was removed under vacuum and the resulting residue was dried [106]. This strategy allowed a recovery ratio of the Bio-IL around 95%, and its pretreatment capability was kept during 5 cycles of recycling. Moreover, in a study from 2017, the authors used an amino-functionalized Bio-IL, choline taurinate, as a catalyst, and proved that the Bio-IL could be recovered and recycled for several runs using a simple process while retaining significant activity [107]. The process started with the addition of water to the reaction vessel and the mixture was left to stand for several hours; the precipitated crude product was collected by filtration, and the filtrate was distilled to remove ethanol and water. Finally, the recovered Bio-IL was washed with ethyl acetate and dried in a vacuum before reuse.

As mentioned, Bio-ILs are often used as phase-forming components of ABS for the selective separation and purification of added valuable compounds [108,115–117]. Santos and Co-workers suggested the recover and reused of the Bio-ILs-rich phase after its use for the extraction of capsaicin from Capsicum frutescens in an ABS consisting of acetonitrile and Bio-ILs [115]. The recycling of both phases of the ABS was achieved by the evaporation of acetonitrile and its further reuse in the extraction process. The capsaicin was then precipitated, by the washing of the [Ch]Cl with water, and the phenolic compounds by acidification. Following the removal of the contaminants and capsaicin, the Bio-IL-rich phase was neutralized with a base and reintroduced in

the ABS purification system. Following the same rationale, in 2017 Lee and colleagues recycled both phase-forming components of an ABS composed by [Ch][BES] and polyethylene glycol, and they verified that were no significant differences in the purification results with the use of recycled components compared to the initial ABS [116]. In very recent works, the authors used some Good's buffers [Ch]ILs and [Ch][AA], for the successful extraction and preservation of the ribonucleic acid (RNA) molecule [108,117]. They were able to successfully recover the RNA molecule with high-integrity from the Bio-IL aqueous solutions by precipitation with ethanol. The recovered Bio-ILs were reused as preservation media for RNA, with only a maximum loss of 3 (w/w) % of Bio-IL in each cycle of IL recovery/reuse [117]. With this in mind, the same authors developed an integrated RNA extraction system using [Ch]AA and polypropylene glycol as phase-forming components [108]. Following the above described the precipitation of the RNA molecule from the Bio-IL-rich phase was achieved using alcohol, the phase-forming components were dried under vacuum and efficiently used for the formation of new ABS for RNA extraction and preservation.

The possibility of recovering Bio-ILs allows increasing the sustainability of several processes, not only by using more benign compounds but also by the possibility of their reuse [66,108,118]. From an economic point of view, it also constitutes a clear less expensive strategy, allowing to reduce the economic burdens and contributing to overcoming one of the main obstacles for the large-scale application of the processes. However, some improvements should be made in this field, mostly concerning the stability of the final products, which influences the efficacy of the reused Bio-ILs across the cycles.

I-6. TOXICITY: THE ENVIRONMENTAL AND BIOLOGICAL IMPACT

In the last years, several works have been published providing extensive data sets on biodegradation, ecotoxicity, and cytotoxicity, aiming to understand the behavior and the interaction of the ILs with the surrounding systems [19,25,84]. ILs have been proved to influence all levels of life, as depicted in Figure I-(, and for that reason, their toxicity has been studied in different models of bacteria, fungi, crustaceans, algae, plants, cell lines, and animals. Still, most of the available studies are focused on the commonly used ILs, such as imidazolium, pyridinium, and pyrrolidinium ones [18,85,119]. Similarly, to the other ILs families, most of the Bio-ILs have significant water solubility. Thus they present environmental impact in particular in the event of accidental release

[19,25]. The use of these compounds as alternative solvents allows to considerably reduce the workers exposure to inhalation and almost removes the risk of fast exothermic oxidations, due to their low volatility [4]. Besides, the properties as, e.g. their high stability, that make them the target solvent of interest for the scientific and industrial communities, may be the ones that impose problems when their degradation products persist [18,25].

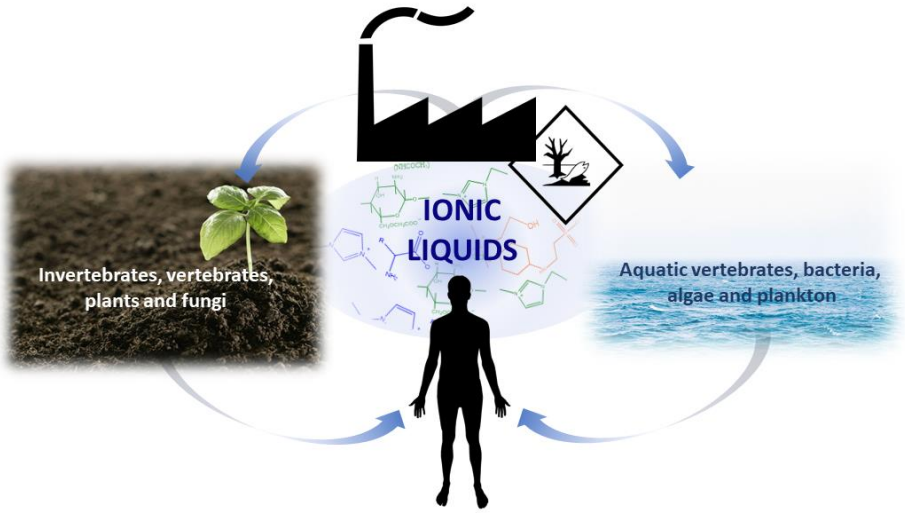


Figure I-8 – Different Ecosystems affected by ILs as potential chemical pollutants.

I-6.1. Biodegradation

The biodegradation profile is usually evaluated following some standardized tests defined by the Organisation of Economic Co-Operation and Development (OECD) and the International Organisation for Standardisation (ISO) [120]. The list of supported tests includes the following: fresh water, inherent biodegradation, aerobic sewage, seawater, soil sediment and water, and anaerobic biodegradation tests. The biodegradation research results may be categorized into primary degradation, inherently biodegradable, readily biodegradable, and mineralization, according to the outcomes of the test. The OECD proposes an evaluation strategy that consists of an evaluation of aerobic biodegradation, to assess the readily biodegradable profile of a compound. Once a chemical fails the first test, other simulation tests are performed, in other to determine its biodegradability. As a final approach, the potential biodegradability may be determined under anaerobic conditions.

Concerning the biodegradation of Bio-ILs, parameters such as the structure and cation and anion nature play a critical role in the degradation profile of the compound [5,102,121]. According to an earlier published critical review [102], almost 50% of the biodegradable ILs synthesized to date contain cholinium as cation and an organic acid as the anion. It is well known that the use of the cholinium as the cation highly improves the biodegradability of the resultant compounds [5,121]. Stolte and his group [87] evaluated the biodegradability of Bio-ILs containing the cholinium and the pyrrolidinium cations, combined with methylsulphate and methylsulphonate anions. The results revealed the ready biodegradation profile of the [Ch]ILs when combined with the methylsulphate anion, while the ILs from the pyrrolidinium family were classified as not readily biodegradable. As expected, the variation of the cationic moiety in the ILs structure proved to have a strong impact on their degradation profile; and using the cholinium as the cation proved once again to be a great strategy to synthesize Bio-ILs with reasonable biodegradability rates [122]. In general, combining a cation with a biodegradable anion, such as AA, sugar acids, and organic acids originates Bio-ILs with ready biodegradable features [5,12,121,123]. The biodegradation and toxicological profile of a new group of Bio-ILs, which combined the already known as readily biodegradable, cholinium cation, with anions from organic acids were evaluated, and their ready biodegradable profile was verified [65]. Concerning the [Ch]AA-based Bio-ILs, several works [5,121] were able to prove the ready biodegradable profile of this Bio-IL family. These results are own to the use of cholinium as the cation and the characteristic structural carboxyl and primary amino groups present in the anions.

In another study and aiming to understand the influence of the side chain length on the biodegradation behavior of the Bio-ILs, Marija et al. [65] incubated carboxylate Bio-ILs in P. corylophilum cultures for four weeks. The authors verified that anions with longer and linear alkyl chains such as butanoate, pentanoate, hexanoate, and octanoate presented reasonable degradation rates, with the opposite being observed for the anions with shorter chains. Keeping the cholinium as the cationic moiety, Yazdani and co-workers [121] verified that the biodegradability of [Ch]AA once again improved as the size of the anion increased, as well as the alkyl side chain length. Similar results were previously obtained by Hou and co-workers [5].

I-6.2. (Eco)-toxicity

A strong effort was made to understand the toxicological effects of Bio-ILs into different life systems by performing (eco)toxicity, phytotoxicity, antimicrobial, and antibacterial activities tests [101,124]. Most of the studies are carried out using marine microorganisms such as aquatic crustaceous, water fleas, algae, and marine bacteria, since, as mentioned, the Bio-ILs solubility makes the water the most likely medium for accidental discharge. The enzyme inhibition test, commonly performed with the acetylcholinesterase, is also a widely used biological marker in (eco)toxicology, allowing to evaluate the influence of toxicants on the central nervous system of organisms [5]. The [Ch]ILs have expected low toxicities, although the Bio-ILs specific data are dependent on the type of the microorganism used for the study. Some representative results obtained for the family of [Ch]ILs are presented in Table I- 1 and discussed below.

According to Passino and Smith [125] toxicity ranking, if a compound has EC50 values between 100-1000 mg L-1 it is considered practically harmless; 10-100 m gL-1 moderately toxic; 1-10 mg L-1 slightly toxic and 0.1-1 mg L-1 as highly toxic. From a general overview over Table 1 is possible to conclude that most of the represented [Ch]ILs can be considered as “practically harmless,” regarding the above-stated toxicity models used. However, looking more closely, it is possible to notice some intriguing points. As seen in the biodegradation rate studies, the anion provides a specific influence over the toxicity profile [65,101,121]. Petkovic and his group [65] evaluated the toxicity of a group of [Ch]ILs, using different alkanoates as anions (information not available in the table). In general, their results of minimal inhibitory and fungicidal concentrations (MIC and MFC, respectively), obtained by tests performed in four fungal isolates, revealed that as longer the anion side chain, the higher the hydrophobicity and higher the toxic character of the Bio-ILs towards the microorganisms. Moreover, similar trends were observed when using different AA combined with the same cation, with different results towards different bacterial species [5,121]. In general, the use of smaller anion-size molecules such as alanine and serine, improves the toxicity, while bigger anion molecules, namely the AA tyrosine and tryptophan, are revealed to be more toxic [121]. Surprisingly, Rantämaki et al. [126] evaluated the toxicity of novel [Ch]ILs towards, using the luminescent marine bacteria Vibrio fischeri model, and concluded that while the increase of the alkyl chain length leads to an increase in the toxicity, its branching contributes to its decrease. Several authors have been using the marine bacteria Vibrio fischeri test to define the eco-toxic profile of different families of [Ch]ILs and [Ch]ILs derivatives all revealing similar results,

with most of the tested compounds being classified as "practically harmless" [20,87,101,124,126,127]. On the other hand, Ventura and her group [101] used the same test and proved that, despite generally known as non-toxic, some of the [Ch]ILs and salts tested could not be considered harmless. Considering the results, the authors concluded that [Ch]Dihydrogenocitrate and [Ch]Bitartrate are classified as "harmful," and, once again, it was proved that the anion plays a key role in the overall toxicity of the compound. Similar results were obtained in a very recent study, where a series of [Ch]ILs were classified as "practically harmless" to "harmless", with the anions being stated as the major contributors to toxicity [128].

Several studies allowed to verify that Gram-positive bacteria such as, B. subtilis, Bacillus licheniformis, and Staphylococcus aureus, were more susceptible to various Bio-ILs solutions than Gram-negative bacteria, namely Escherichia Coli, Pseudomonas aeruginosa and Vibrio cholerae, which revealed higher EC50 values [16,121]. Furthermore, the determination of the inhibition zones of the same [Ch]ILs towards the Gram-positive B. subtilis and Gram-negative E. coli, corroborated these results, with the latter not being affected even by the higher Bio-IL concentration solutions [16]. The structural nature of the gram-negative bacteria, namely the presence of an outer peptidoglycan layer adjuvant to the cytoplasmic membrane, is thought to be responsible for these results, by decreasing the permeability of the cell membranes to the Bio-ILs [121].

The studies using both marine invertebrates and vertebrates allow confirming that in general [Ch]ILs may be considered practically harmless. However, once again, it is important to remark that the use of different microorganisms, in addition to the different Bio-ILs structures, may provide different results. Though, there is an evident gap regarding the number of works using invertebrates and vertebrate models to determine the toxicity of the [Ch]ILs, which calls for more studies in that area.

Table I-1– Toxicity of [Ch]ILs towards different levels of aquatic biological systems including bacteria, algae, vertebrate, and invertebrate.

IL	ENZYME	BACTERIA							INVERTEBRATES			VERTEBRATES	REF
	Acetylcholinesterase	*B. subtilis*	*E. coli*		*S. aureus*			*B. licheniormis*	*V. fischeri*	*Pseudokirchn. riella subcapitata* (lower limit-upper limit)	*Daphnia magna* (lower limit-upper limit)	*Selenastrum capricornutum*	*Danio rerio* (Zebra Fish)	
	EC_{50} (mg/L^{-1})	**Inhibition halo (cm)**	**MIC (mgL^{-1})**	**MBC (mgL^{-1})**	**EC_{50} (mgL^{-1})** (lower limit-upper limit)	**MIC (mgL^{-1})**	**MB (mgL^{-1})**	**EC_{50}(mgL^{-1})** (lower limit-upper limit)		**EC_{50}(mgL^{-1})**				
[Ch]Chloride	441.20 ± 12.57		>750	>750		>750	>750		469.34 (383.76-554.91)					[5,101]
[Ch] bis(trifluoromethanesulfonyl)imide	>100								>100		>100	>100		[87]
[Ch] Alanine	643.26 ± 19.32		9060	18119	547 (218-1375)	36316	96585	474 (345-652)						[5,16,121]
[Ch]Arginine	1020.88 ± 19.47		13046	26092	212 (167-268)	26092	34771	298 (190-485)						[5,16,121]
[Ch]Glutamine	878.10 ± 40.03	1.00 ± 0.00	31271	47032		31271	47032							[5,16]
[Ch]Glutamate	934.35 ± 17.58		125585	188378	231 (171-310)	188378	188378	366 (300-478)						[5,16,121]

[Ch]Glycine	686.22 ± 30.46	1.05 ± 0.21	22396	44793		44793	89585		[5,16]
[Ch]Methionine	792.42 ± 35.44	0.90 ± 0.07	7924	15823	610 (371-998)	31646	63293	417 (371-998)	[5,16,121]
[Ch]Phenylalanine	737.53 ± 43.07	095 ± 0.05	8425	12624	251 (194-326)	16823	25248	217 (186-260)	[5,16,121]
[Ch]Valine	676.78 ± 26.54		10373	13823		20746	27646		[5]
[Ch]Leucine	790.17 ± 11.76		11029	14698		22059	29396		[5]
[Ch]Isoleucine	881.89 ± 16.46		11029	14698		22059	29396		[5]
[Ch]Serine	744.65 ± 31.38		6547	13073	716 (554-925)	26146	52293	395 (355-466)	[5,16,121]
[Ch]Threonine	769.94 ± 33.48		6985	13948		27896	55793		[5]
[Ch]Aspartate	903.62 ± 21.35		118585	177878	882 (446-1979)	177878	177878	588 (309-695)	[5,16,121]
[Ch]Asparagine	930.04 ± 11.80		22142	29506		44378	59013		[5]
[Ch]Lysine	870.59 ± 32.52		7830	11733		15636	23466		[5]
[Ch]Histidine	940.79 ± 18.14		12155	16198	633 (323-1242)	24310	32396	290 (233-372)	[5,16,121]
[Ch]Proline	738.60 ± 35.07		10279	13698		20558	27396		[5]
[Ch]Tryptophan	755.02 ± 6.16		7211	9646	203 (141-291)	14453	19261	194 (170-224)	[5,16,121]
[Ch]Tyrosine					323 (225-464)			160 (144-183)	[121]

Ch[ACE]		500	750							[5]
[Ch]Isosterate[b]					28.69 ± 7.75					[126]
[Ch]Decanoate[b]					27.54 ± 5.51					[126]
[Ch]Neodecanoate[b]					143.22 ± 16.5					[126]
[Ch]Saccharinate							1219 (1109 - 1340)			[12]
[Ch]Acesulfamate							1378 (1288 - 1480)			[12]
[Ch][PF_6]						37.74 (34.65-39.57)	>100		>100	[129]
[Ch]methylsulphate	>100				>100		>100	>100		[87]
[Ch] methylsulphonate	>100				>100		>100	>100		[87]
[Ch] Dihydrogenocitrate					37.23 (28.60-45.85)					[101]
[Ch]Bicarbonate					–					[101]
[Ch]Bitartrate					37.90 (37.73-43.08)					[101]
[Ch]Dihydrogenophosphate					572.72 (487.50-657.94)					[101]

[Ch]Salicylate	236.11 (137.41-334.80)	[101]
[Ch]Propanoate	487.90 (351.53-624.27)	[101]
[Ch] Butanoate	884.10 (670.60-1097.27)	[101]
[Ch] HEPES	19584×10^3	[20]
[Ch] CHES	208.65×10^3	[20]
[Ch] MES	9789×10^3	[20]
[Ch] Tricine	4588×10^3	[20]
[BzCh]Cl	1498.75	[101]

EC_{50}- Half maximum effective concentration: The concentration of a chemical at which 50% of its maximum response is observed

LC_{50} – Half lethal concentration: The concentration of a chemical at which 50% mortality from toxicity is observed

MIC - minimal inhibitory concentrations

MBC - minimum biocidal concentrations

a - No growth inhibition

b - EC_{50} values using *V. fisheri* with15min incubation; the other values for *V. fisheri* were determined after 30min incubation

I-6.3. Cytotoxicity and Biological Activity

The performance of toxicity tests is crucial to promote and boost the utilization of [Ch]ILs in many other areas, in order to assess, for instance, their skin irritation potential [130]. The cytotoxicity of Bio-ILs is not only dependent on their structure, but also in some external factors, namely the cell types [25]. These facts, together with the different and growing number of applications of Bio-ILs, have been encouraging the performance of tests using different cell lines.

Santos de Almeida et al. [85] evaluated and compared the potential of either cholinium- and imidazolium-based ILs for being used in topical drug formulations, with cytotoxicity tests being performed on human keratinocytes (HaCat cells). The results revealed that the [Ch]ILs presented superior results regarding drug solubility and lower cytotoxicity when compared with the other formulations. Moreover, in previous work, Gouveia et al. [16], evaluated the possible damage of human cells due to direct contact with the ILs by studying the toxicity of 14 ILs from the imidazolium-, pyridinium- and cholinium- families, against the HeLa cell line. The results revealed a decrease in cell viability with an increase in the ILs concentration. Despite the impossibility in the determination of the IC50 values (necessary concentration to inhibit cell proliferation by 50%, compared to the control viability), their results showed that the Bio-ILs having the cholinium as the cationic moiety were at least an order of magnitude less toxic than the imidazolium- and pyridinium-based ones, sharing the same anion, as depicted in Figure I-9. Generally, studies in which was evaluated the cytotoxicity of ILs with either the cholinium cation or other amine derivatives as the cationic counterparts, presented superior results when compared with other classes of ILs, by comparison with other formulations [87,131,132].

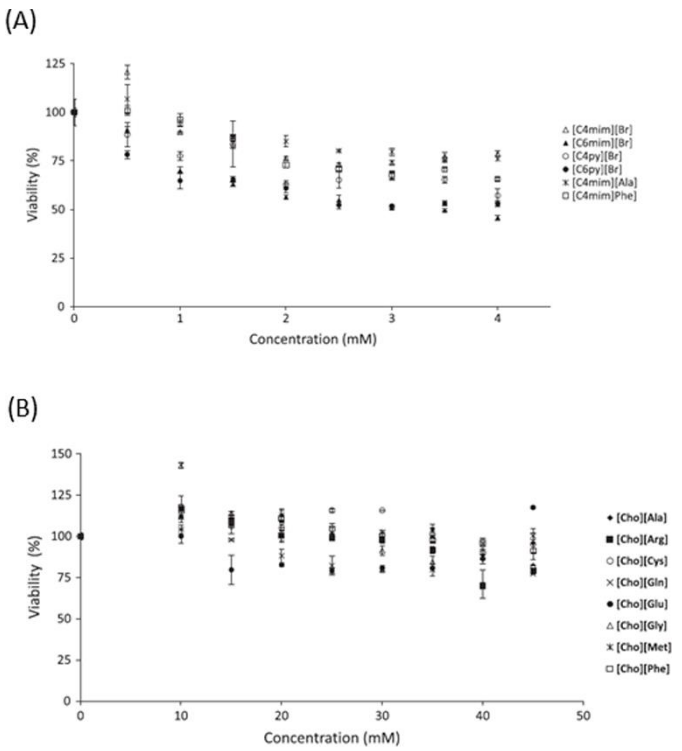


Figure I-9 - Viability of HeLa cells exposed to (A) imidazolium and pyridinium-based ILs and (B) [Ch]ILs. Reprinted from [16] Copyright (2014), with permission from Elsevier.

From a different perspective, several studies have reported results, in which the anion is determinant for the overall toxicity of the compound, with the cholinium cation showing none or little influence over the cytotoxicity [14,88,130,132,133]. In 2012, Muhammad and co-workers [14], have found some exciting results when evaluating the cytotoxicity of a series of [Ch]ILs with different carboxylate anions, toward the human breast cancer cell line, MCF-7. In general, and as expected, the results revealed that the studied Bio-ILs are much less toxic than standard imidazolium-based ILs and it was observed a curious increase in the toxicity with an increase in the carboxylate chain length. The increase in the side chain of the ILs may increase the interactions of the compounds with the phospholipidic layers in the membranes leading to its disruption and cell death [134]. In previous work, Rengstl and his group [130] evaluated the cytotoxicity of a series of carboxylate [Ch]ILs on HeLa and SK-MEL-28 cells, aiming to study the possibility of using these Bio-ILs in pharmaceutical formulations or other applications. In the studied cell lines, the cytotoxicity increases with an increase in the alkyl chain length, but not in a linear way. The noticeable discontinuity in the toxicity results, i.e., a lack of a consistent trend, makes some of the results to be in concordance with the results from Muhammad his group [14], while others follow the opposite trend seen in other works. [83] Though, in general, [Ch]ILs with different carboxylate anions are only

slightly toxic, the cytotoxicity often depends on the considered system and on the cell line that is used for toxicity studies, making it difficult to characterize the toxicity of the compounds and to generalize the conclusions [130].

In general, some Bio-ILs, namely the [Ch]ILs, have been proven to have lower biological activity rates when compared with the imidazolium and pyridinium ILs, which due to their high biological activity and cytotoxicity values, have been intensively studied as potential anticancer agents [25,84,135]. Thus, the ILs biological activity is often seen as an advantage, depending on the desired application, such as their use as API-ILs or the exploitation of their antimicrobial activity [45,70].

I-6.4. Toxicity: cautions, predictions, and trends

It is critical to acknowledge the complexity of the ecosystems and to bear in mind that the results of one test cannot be generalized over the effect of a compound in the environment as a whole system. For instance, Stolte and co-workers [87], in a very comprehensive and complete study, above referred in this review, have used the marine bacteria *Vibrio fischeri*, the water fleas *Daphnia Magna* and the green algae *Selenastrum capricornutum*, to access the ecotoxicity of ammonium- and pyrrolidinium-based ILs. The biological activity of the same ILs was accessed using the enzyme acetylcholinesterase and isolated leukemia cells from rats (IPC-81). Moreover, the biodegradability of the studied compounds was accessed following the OECD test procedures 301 B and 301 F [87]. The results revealed nonexistence or just little effect of all the studied ILs into the tested biological system, since compounds with EC50 values >100 mg L-1 can be classified as “practically harmless” and ‘‘not harmful to aquatic organisms”. The full evaluation of the toxicological profile allowed the authors to conclude that the [Ch]ILs are compounds with low acute toxicity and excellent biodegradability, revealing the best results. Nevertheless, despite the large number of organisms studied, the lack of animal (fish) toxicity tests was considered by the authors as a gap in the evaluation. Thus, a flexible (eco)toxicological test battery considering aquatic and terrestrial compartments, as well as different trophic levels, as previously described by the same group, were thought to test the effect of using different anions into the imidazolium base-ILs structures [136].

The idea of developing tools capable of helping to predict the toxicity of the compounds, as well as supporting its sustainable design, is a fascinating idea. However, many factors are contributing to this equation such as the, already mentioned, variability either in the ILs structures, as well in the toxicity

models used for the evaluation [65]. The mechanisms involved in the ILs toxicities are not entirely understood, and it is thought that membrane disruption is the main occurring event [134]. Though, it is vital to work toward the understanding of the mechanisms behind the toxicity of the compounds and, consequently in the enhancement of the toxicological databases.

I-7. APPLICATIONS OF BIOCOMPATIBLE IONIC LIQUIDS

To understand the current focus of research on the applications of Bio-ILs, a search in different fields of applications was made using the engine Scopus. Figure I-10 shows the outcomes of this search. It was noted that most of the works are focused on using the Bio-ILs as solvents and is also clear the extensive exploitation of their potential into electrochemistry and catalysis, as well as in the pharmaceutical and medical fields. The exploitation of the Bio-ILs potential in areas such as the biomass pre-treatment and food industry is still very restricted, compared to the fields mentioned above, being interesting to emphasize the apparent gap in its use into the tissue engineering field.

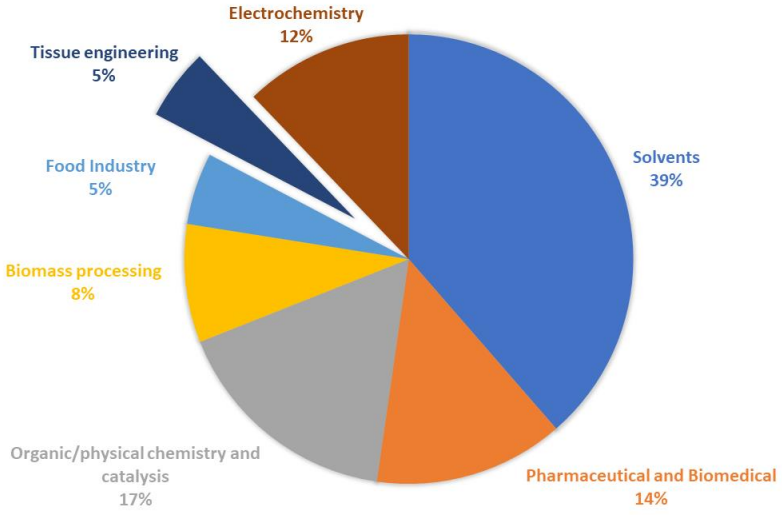


Figure I-10 . Schematic representation of the intensity of research regarding the use of Bio-ILs in a selected range of areas.

Unquestionably, the Bio-ILs family has been studied to a great extent either as solvents or as catalytic agents for biomass processing. The Bio-ILs properties, namely their ability to disrupt strong intermolecular hydrogen bonding networks and to interact with the hydroxyl groups in the structure of the compounds, associated with their low toxicity make them attractive solvents when dealing with poor soluble biopolymers [56,137]. Some [Ch]ILs belonging to the alkanoates family, were effective in the selective

dissolution of the suberin domains, from refined cork, which is insoluble in many solvents. [56] The dissolution of feather keratin, using the Bio-IL choline thioglycolate was also successfully achieved, without the addition of any other chemicals [137]. [Ch]ILs have been reported as effective platforms for the selective dissolution of lignin from biomass, leaving the cellulose-rich residue behind, which is easily digested by enzymes to release fermentable sugars [8,52,53,138–140]. Recent works showed the development of integrated processes for biofuel production, by combining the pre-treatment of either lignocellulosic or switchgrass biomass with Bio-ILs, enzymatic hydrolysis, and microbial fermentation [141,142]. The developed integrated strategies provided a significant decrease in the costs and complexity of the processes. Moreover, due to algae's fast multiplication rates and high lipid contents, they are often considered sustainable platforms for biodiesel production [143]. Once again, when compared with the traditionally used methods, Bio-ILs revealed clear superior results, allowing to dissolve the lipids, which may be further extracted with hexane, leaving behind a carbohydrate-rich solid, subjected to hydrolysis. It is important to mention that [Ch]ILs-derived solvents, namely DES, have been successfully used for the decrystallization of cellulose and the cationic polymer functionalization, a process with considerable industrial importance, particularly in the removal of acidic dyes from aqueous effluent produced by the textile industry [54,144]. Furthermore, in another study, the choline formate was used as an efficient self-polymerizing agent, being able to produce gels at room temperature, without light, heat, or addition of an initiator [145].

In addition to the exploitation of Bio-ILs as solvents and catalysts, they have been extensively used as additives, to provide some materials with enhanced and desired properties. In particular, the ability of the ILs to form strong hydrogen bonds makes them an attractive non-volatile plasticizer for natural biopolymers, namely starch [146]. Bio-ILs can offer efficient, cost-effective, and environmentally friendlier ionic plasticizer platforms [146,147]. In a recent study, the authors compared a typical plasticizer (glycerol) with choline salt, choline chloride, and two [Ch]ILs. The ionic plasticizers revealed more effective results in both of the studied processes (compression molding and extrusion processes) [147]. These compounds were able to provide the final materials with enhanced thermochemical properties and proved to be highly effective either during the destructuration stage of native starch and as glass transition depressors in the final plasticized starch material [146]. The use of Bio-ILs, namely a group from the [Ch]ILs family, proved to be an efficient strategy in the plasticization of starch by film casting [146]. The

thermo(hygro)mechanical and recrystallization behavior of the final materials were strongly influenced by the anion [146,147]. Also, choline chloride-based DES have been explored to a greater extent, and various efficient plasticizers have already been designed. In that case, the hydrogen donor plays a key role in the final material properties [148]. Along with the enhanced thermomechanical properties, cost-effectiveness, low toxicity, and good biodegradability, the use of these ionic plasticizers often provides the materials with intrinsic and improved conductive features [146]. Some [Ch]ILs were previously prepared as proton-conducting ionic plastic crystals, exhibiting proton conductivity, and having potential application as proton-conducting fuel cells [149,150]. Moreover, Bio-ILs have been extensively used in ion gel formulations, which may find application in electrochemistry, as sensors and modulators, or even in the biomedical field [151].

In the pharmaceutics and biomedical fields, Bio-ILs are straightforwardly used as stabilizer agents for biomolecules, as solvents, or as part of drug carrier systems for poorly soluble drugs, such as in API-ILs systems [20,70,156,157,71,72,75,131,152–155]. The use of API-ILs emerged as an excellent tool to help solve the current problems related to, not only the solubility but also the polymorphism, delivery, release rates, handling, the efficacy of the therapeutic and adverse reactions during the administration [25,105,158]. Recent works have shown very promising results concerning the development of formulations for transdermal drug delivery using Bio-ILs, which is often a challenge due to the impermeability of the outer layer of skin [103,159]. In another work, Banerjee and co-workers [104] utilized [Ch]ILs to develop a highly effective oral insulin formulation. The results revealed a considerable improvement in the oral bioavailability of insulin with outstanding oral efficacy, biocompatibility, and long-term stability, indicating that the use of Ch[ILs] is a promising strategy for the development of oral delivery vehicles. Moreover, the Bio-ILs charge disruptions and hydrogen bonding ability have been evaluated for their antimicrobial and antifungal properties for transdermal drug delivery and pathogen neutralization [45,160].

The potential of the Bio-ILs doped materials has been intensively explored into many fields, with a great extent in electrochemistry, leading to the development of superior novel stimulus-responsive systems for biomedical applications [47,55]. Chitosan hydrogels incorporated with [Ch]Cl and choline dihydrogen phosphate, have proved their potential as Bio-ILs-based multi-responsive drug delivery systems, with improved electrical and pH sensitivities [55]. In a work from 2014, the authors developed a thin-film polymer gel electrolyte, composed of chitosan and the Bio-IL choline nitrate, which schematic configuration is shown in Figure I-11A. The produced battery revealed to have robust mechanical

properties and high ionic conductivity directing its application toward implantable medical devices such as cardiac pacemakers or biomonitoring systems [47]. In a later work, the same authors developed a biodegradable thin film magnesium battery, using the naturally occurring polymer silk fibroin to immobilize a Bio-IL, following the scheme depicted in Figure I-11B [161]. The produced polymer electrolyte harnessed the biological activity of the silk fibroin and the ionic conductivity of the Bio-IL, constituting a great tunable platform to the development of new implantable medical devices. The use of Bio-ILs for the design of portable diagnostic devices is a topic with huge potential that from our point of view calls for a more intense investigation. Ideally, these platforms may be able to degrade in a controlled and non-harmful manner while being able to influence the biological processes controllably [161]. They should also be operational without any external or wireless power source. The basic components of a biosensor include a recognition element, a physical transducer, and a signal-processing device. Considering that, along with the Bio-ILs features, it is obvious the drive to use them as components of bio-based sensing devices [26]. Additionally, their known ability to promote the stability of biomolecules may be helpful and beneficial in the case of their use in biosensing devices [50,162,163].

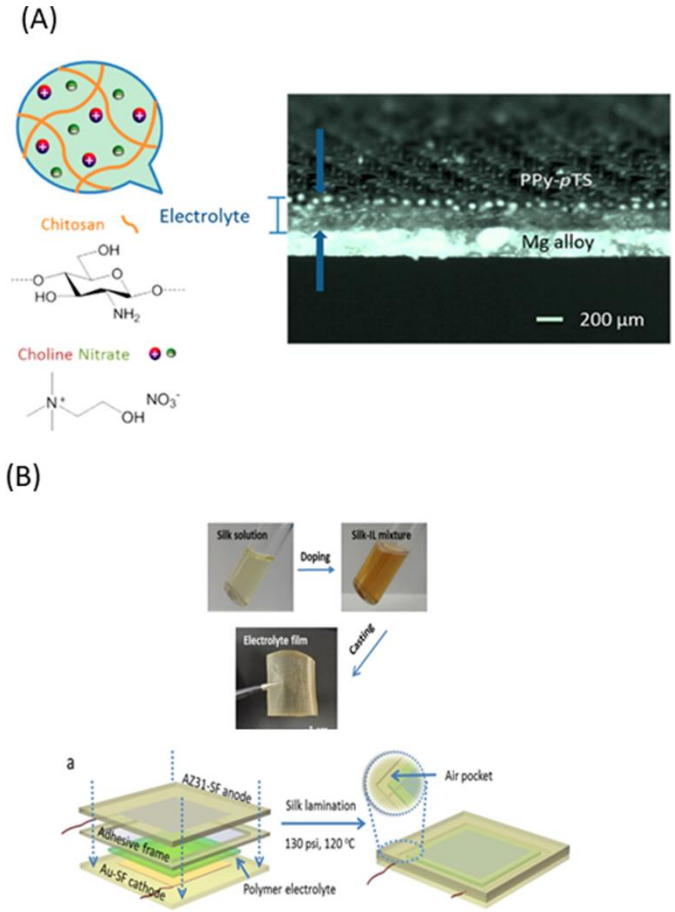


Figure I-11 - Schematic configuration and optical image of a cross-sectional view of the integrated biopolymer electrolyte-thin and compact magnesium-air Battery. Adapted from [47] (B) Fabrication procedures of a polymer electrolyte (PE) film (SF:[Ch][NO3], with a weight ratio of 1:3) and a schematic representation of an encapsulated battery. Adapted from [161]. Copyright © 2017 American Chemical Society

The intense research in this area led the scientists to explore the possibility of using Bio-ILs-based bio-responsive systems as artificial muscles or organs or scaffolds for tissue engineering since transient implantable medical bionics are gaining ground when the matter is tissue regeneration [161]. Recently, a conductive bio-poly(ionic-liquid) hydrogel, with the potential to find application into cardiac tissue repair was developed [164]. This innovative electroconductive gelatin methacryloyl (GelMA)/Bio-IL-based hydrogel presented tunable mechanical properties and conductivity. Moreover, it revealed to be efficiently biodegraded and to possess low immunogenicity when implanted subcutaneously in rats as depicted in Figure I-12. The development of biocompatible poly(ionic liquids) based platforms is, without any doubt, a field with strong potential for future research in many areas [164,165]. In a work from 2013 [165], the authors developed for the first time ion gels entirely composed of biocompatible liquids. For that, [Ch]ILs-based methacrylic monomers with the halides lactate and acetate counter-anions were produced and

polymerized by using free radical polymerization. The features of the developed cholinium-based poly(ionic liquid)s suggest their potential use into a wide range of fields.

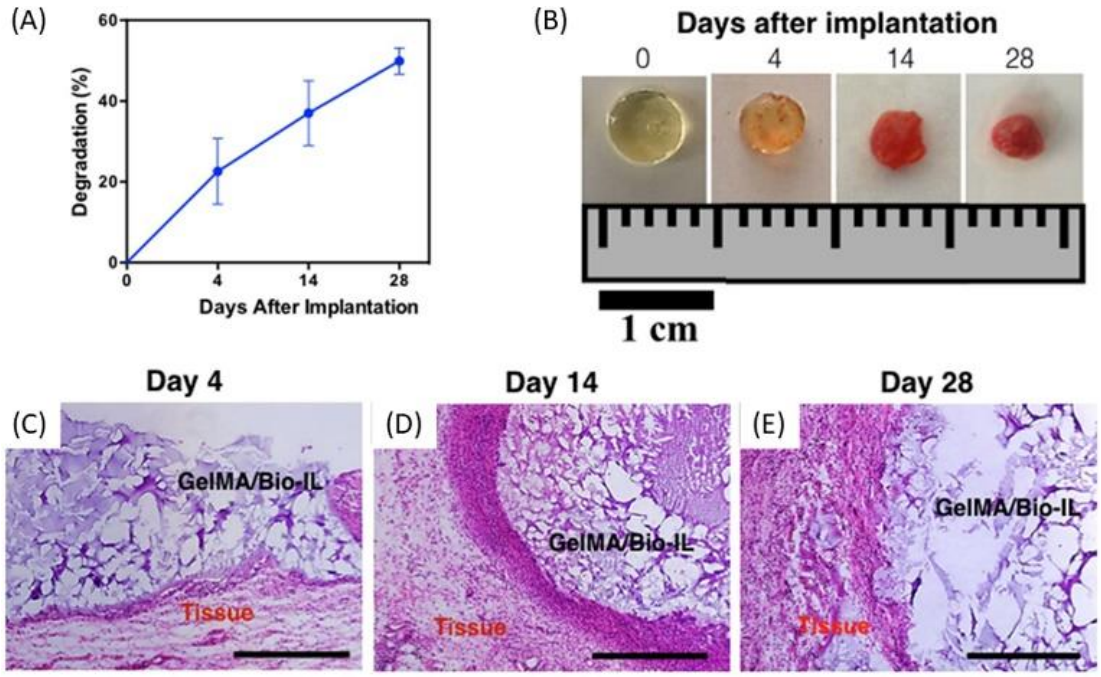


Figure I-12 - *In vivo* biodegradation and biocompatibility tests of a GelMA/Bio-IL composite hydrogel using a rat subcutaneous model (A) i*n vivo* degradation of GelMA/Bio-IL hydrogel based on weight loss of the implants on days 0, 4, 14 and 28 post-implantation, (B) Images of the GelMA/Bio-IL composite hydrogels after implantation at the defined time points and (C to E) Hematoxylin and eosin (H&E) staining of GelMA/Bio-IL sections after (C) 4, (D) 14, and (E) 28 days of implantation showing a negligible amount of inflammatory cells. Adapted from [164], with permission from Springer Nature, Copyright (2017).

I-8. CONCLUSIONS AND FUTURE TRENDS

Despite the large volume of research in the ILs field, the growth in the family of Bio-ILs happened only in recent years. The current exhaustive research in this field was boosted by the emergent need for "greener", safer, and less harmful compounds, as well as more benign and sustainable synthetic routes. As a result, new synthetic strategies appeared, along with new non-toxic and biodegradable Bio-ILs, and, unexpectedly, new classes of compounds also arose. The ability of these compounds to keep the features from the commonly used ILs such as their tunability, ionic character, and solvation ability, while improving their toxic character and biological activity, encourages the scientific and industrial communities to expand and intensify their use in a broader range of fields. Currently, it is observed a daily evolution in the Bio-

ILs-based materials and platforms. Their straightforward use as solvent platforms for poorly soluble compounds, is by far the most explored application, covering a wide range of fields from biomass processing and biofuel production to biomedical and pharmaceutical fields. At the same time, the use of Bio-ILs often results in the improvement of the overall properties of the products while keeping their low-toxic and biodegradability features. The most recent literature data shows an evident growth in the development of API-ILs systems and novel therapeutic strategies based on the use of Bio-ILs. Also, the Bio-ILs catalytic ability, along with their utility in the development of Bio-IL-based composites, dramatically supports the production of sensitive, selective, and reproducible electrodes. The potential of the stated platforms in the biomedical, diagnostic, and tissue engineering fields is unquestionable but still requires more research and investment. Some new outcomes in this field have been significantly boosting the possibility of developing integrated biocompatible batteries, into one single and continuous unit, without the need for packaging [47,55,161]. Recent outcomes offered the basis for the development of energy storage systems in a single chip. The designed platforms ideally possess the enhanced required elements and features to boost their application as regenerative medicine platforms, or as wearable and portable diagnostic devices. However, the Bio-ILs potential is far from being entirely explored, and it must be taken advantage of the currently available information as a resource to produce not only more knowledge but also to boost the development of improved technologies.

I-9. REFERENCES

[1] R.L. Vekariya, A review of ionic liquids: Applications towards catalytic organic transformations, J. Mol. Liq. 227 (2017) 44–60. https://doi.org/10.1016/j.molliq.2016.11.123.

[2] M. Petkovic, K.R. Seddon, L.P.N. Rebelo, C.S. Pereira, Ionic liquids: a pathway to environmental acceptability, Chem. Soc. Rev. 40 (2011) 1383–1403. https://doi.org/10.1039/C004968A.

[3] S.P.F. Costa, A.M.O. Azevedo, P.C.A.G. Pinto, M.L.M.F.S. Saraiva, Environmental Impact of Ionic Liquids: Recent Advances in (Eco)toxicology and (Bio)degradability, ChemSusChem. 10 (2017) 2321–2347. https://doi.org/10.1002/cssc.201700261.

[4] J. Ranke, S. Stolte, R. Sto, J. Arning, B. Jastorff, Design of Sustainable Chemical Products - The Example of Ionic Liquids, Chem.Rev. 107 (2007) 2183–2206. https://doi.org/10.1021/cr050942s.

[5] X.-D. Hou, Q.P. Liu, T.J. Smith, N. Li, M.H. Zong, Evaluation of Toxicity and Biodegradability of Cholinium Amino Acids Ionic Liquids, PLoS One. 8 (2013) e59145. https://doi.org/10.1371/journal.pone.0059145.

[6] B.L. Gadilohar, G.S. Shankarling, Choline based ionic liquids and their applications in organic transformation, J. Mol. Liq. 227 (2017) 234–261. https://doi.org/10.1016/j.molliq.2016.11.136.

[7] G. Tao, L. He, N. Sun, Y. Kou, New generation ionic liquids: cations derived from amino acids, Chem. Commun. 0 (2005) 3562–3564. https://doi.org/10.1039/b504256a.

[8] P. Moriel, E.J. García-Suárez, M. Martínez, A.B. García, M.A. Montes-Morán, V. Calvino-Casilda, M.A. Bañares, Synthesis, characterization, and catalytic activity of ionic liquids based on biosources, Tetrahedron Lett. 51 (2010) 4877–4881. https://doi.org/10.1016/j.tetlet.2010.07.060.

[9] D.J. Tao, Z. Cheng, F.F. Chen, Z.M. Li, N. Hu, X.S. Chen, Synthesis and thermophysical properties of biocompatible cholinium-based amino acid ionic liquids, J. Chem. Eng. Data. 58 (2013) 1542–1548. https://doi.org/10.1021/je301103d.

[10] K. Fukumoto, M. Yoshizawa, H. Ohno, Room temperature ionic liquids from 20 natural amino acids, J. Am. Chem. Soc. 127 (2005) 2398–2399. https://doi.org/10.1021/ja043451i.

[11] S. Kirchhecker, D. Esposito, Amino acid based ionic liquids: A green and sustainable perspective, Curr. Opin. Green Sustain. Chem. 2 (2016) 28–33. https://doi.org/10.1016/j.cogsc.2016.09.001.

[12] P. Nockemann, B. Thijs, K. Driesen, C.R. Janssen, K. Van Hecke, L. Van Meervelt, S. Kossmann, B. Kirchner, K. Binnemans, Choline Saccharinate and Choline Acesulfamate : Ionic Liquids with Low Toxicities, J. Phys. Chem. B. 111 (2007) 5254–5263. https://doi.org/10.1021/jp068446a.

[13] L. Poletti, C. Chiappe, L. Lay, D. Pieraccini, G. Russo, Glucose-derived ionic liquids : exploring low-cost sources for novel chiral solvents, Green Chem. 9 (2007) 337–341. https://doi.org/10.1039/b615650a.

[14] N. Muhammad, M.I. Hossain, Z. Man, M. El-harbawi, M.A. Bustam, Y.A. Noaman, N. Banu, M. Alitheen, M.K. Ng, G. Hefter, C. Yin, Synthesis and Physical Properties of Choline Carboxylate Ionic Liquids, J. Chem. Eng. Data. 57 (2012) 2191–2196. https://doi.org/10.1021/je300086w.

[15] F. Pena-Pereira, A. Kloskowski, J. Namieśnik, Perspectives on the replacement of harmful organic solvents in analytical methodologies: a framework toward the implementation of a generation of eco-friendly alternatives, Green Chem. 17 (2015) 3687–3705. https://doi.org/10.1039/C5GC00611B.

[16] W. Gouveia, T.F. Jorge, S. Martins, M. Meireles, M. Carolino, C. Cruz, T. V. Almeida, M.E.M. Araújo, Toxicity of ionic liquids prepared from biomaterials, Chemosphere. 104 (2014) 51–56. https://doi.org/10.1016/j.chemosphere.2013.10.055.

[17] S.S. Silva, T.C. Santos, M.T. Cerqueira, A.P. Marques, L.L. Reys, T.H. Silva, S.G. Caridade, J.F. Mano, R.L. Reis, The use of ionic liquids in the processing of chitosan / silk hydrogels for biomedical applications, Green Chem. 14 (2012) 1463–1470. https://doi.org/10.1039/c2gc16535j.

[18] T.P. Thuy Pham, C.W. Cho, Y.S. Yun, Environmental fate and toxicity of ionic liquids: A review, Water Res. 44 (2010) 352–372. https://doi.org/10.1016/j.watres.2009.09.030.

[19] M. Amde, J.F. Liu, L. Pang, Environmental Application, Fate, Effects, and Concerns of Ionic Liquids: A Review, Environ. Sci. Technol. 49 (2015) 12611–12627. https://doi.org/10.1021/acs.est.5b03123.

[20] M. Taha, M.R. Almeida, F.A. e. Silva, P. Domingues, S.P.M. Ventura, J.A.P. Coutinho, M.G. Freire, Novel biocompatible and self-buffering ionic liquids for biopharmaceutical applications, Chem. - A Eur. J. 21 (2015) 4781–4788. https://doi.org/10.1002/chem.201405693.Novel.

[21] P.T. Anastas, M.M. Kirchhoff, Origins, current status, and future challenges of green chemistry, Acc. Chem. Res. 35 (2002) 686–694. https://doi.org/10.1021/ar010065m.

[22] J. Hulsbosch, D.E. De Vos, B. Koen, R. Ameloot, Bio-based ionic liquids : solvents for a green processing industry?, ACS Sustain. Chem. Eng. 4 (2016) 2917–2931. https://doi.org/10.1021/acssuschemeng.6b00553.

[23] R. Shi, Y. Wang, Dual Ionic and Organic Nature of Ionic Liquids, Sci. Rep. 6 (2016) 1–12. https://doi.org/10.1038/srep19644.

[24] M. Smiglak, J.M.M. Pringle, X. Lu, L. Han, S. Zhang, H. Gao, D.R.R. MacFarlane, R.D. Rogers, Ionic liquids for energy, materials, and medicine, Chem. Commun. 50 (2014) 9228–9250. https://doi.org/10.1039/C4CC02021A.

[25] K.S. Egorova, E.G. Gordeev, V.P. Ananikov, Biological Activity of Ionic Liquids and Their Application in Pharmaceutics and Medicine, Chem. Rev. 117 (2017) 7132–7189. https://doi.org/10.1021/acs.chemrev.6b00562.

[26] F. Ghorbanizamani, S. Timur, Ionic Liquids from Biocompatibility and Electrochemical Aspects toward Applying in Biosensing Devices, Anal. Chem. 90 (2018) 640–648. https://doi.org/10.1021/acs.analchem.7b03596.

[27] J.I. Santos, A.M.M. Gonçalves, J.L. Pereira, B.F.H.T. Figueiredo, F.A. e Silva, J.A.P. Coutinho, S.P.M. Ventura, F.J.M. Gonçalves, Environmental safety of cholinium-based ionic liquids: assessing structure–ecotoxicity relationships, Green Chem. 17 (2015) 4657–4668. https://doi.org/10.1039/C5GC01129A.

[28] A.E. Visser, R.P. Swatloski, W.M. Reichert, R. Mayton, S. Sheff, A. Wierzbicki, J.H. Davis, R.D. Rogers, Task-specific ionic liquids for the extraction of metal ions from aqueous solutions, Chem. Commun. 0 (2001) 135–136. https://doi.org/10.1039/b008041l.

[29] E.D. Bates, R.D. Mayton, I. Ntai, J.H. Davis, CO2 Capture by a Task-Specific Ionic Liquid, J. Am. Chem. Soc. 124 (2002) 926–927. https://doi.org/10.1021/ja017593d.

[30] G. Latini, M. Signorile, V. Crocellà, S. Bocchini, C.F. Pirri, S. Bordiga, Unraveling the CO2 reaction mechanism in bio-based amino-acid ionic liquids by operando ATR-IR spectroscopy, Catal. Today. (2019) 0–1. https://doi.org/10.1016/j.cattod.2018.12.050.

[31] R.P. Swatloski, S.K. Spear, J.D. Holbrey, R.D. Rogers, Dissolution of cellulose with ionic liquids, J. Am. Chem. Soc. 124 (2002) 4974–4975. https://doi.org/ja025790m [pii].

[32] S.H. Lee, T. V. Doherty, R.J. Linhardt, J.S. Dordick, Ionic Liquid-Mediated Selective Extraction of Lignin From Wood Leading to Enhanced Enzymatic Cellulose Hydrolysis, Biotechnol. Bioeng. 102 (2009) 1368–1376. https://doi.org/10.1002/bit.22179.

[33] S.S.Y.Y. Tan, D.R. Macfarlane, J. Upfal, L.A. Edye, W.O.S.S. Doherty, A.F. Patti, M. Pringle, J.L. Scott, J.M. Pringle, J.L. Scott, Extraction of lignin from lignocellulose at atmospheric pressure using alkylbenzenesulfonate ionic liquid, Green Chem. 11 (2009) 339–345. https://doi.org/10.1039/b815310h.

[34] D. Fu, G. Mazza, Y. Tamaki, Lignin Extraction from Straw by Ionic Liquids and Enzymatic Hydrolysis of the Cellulosic Residues, J. Agric. Food Chem. 58 (2010) 2915–2922. https://doi.org/10.1021/jf903616y.

[35] A. Pinkert, D.F. Goeke, K.N. Marsh, S. Pang, Extracting wood lignin without dissolving or degrading cellulose: investigations on the use of food additive-derived ionic liquids, Green Chem. 13 (2011) 3124–3136. https://doi.org/10.1039/c1gc15671c.

[36] T. Welton, Room-Temperature Ionic Liquids . Solvents for Synthesis and Catalysis, Chem. Rev. 99 (1999) 2071–2084. https://doi.org/10.1021/cr980032t.

[37] R. Sheldon, Catalytic reactions in ionic liquids, Chem. Commun. 0 (2001) 2399–2407. https://doi.org/10.1039/b107270f.

[38] T. Welton, Ionic liquids in catalysis, Coord. Chem. Rev. 248 (2004) 2459–2477. https://doi.org/10.1016/j.ccr.2004.04.015.

[39] M. Yoshizawa, M. Hirao, K. Ito-akita, H. Ohno, Ion conduction in zwitterionic-type molten salts and their polymers, J. Mater. Chem. 11 (2001) 1057–1062. https://doi.org/10.1039/b101079o.

[40] J.S. Wilkes, J.A. Levisky, R.A. Wilson, C.L. Hussey, Dialkylimidazolium Chloroaluminate Melts: A new Class of Room-Temperature Ionic Liquids for Electrochemistry, Spectroscopy and Synthesis., Inorg. Chem. 237 (1982) 1263–1264.

[41] R.P. Swatloski, W.L. Hough, M. Smiglak, S.K. Spear, D.T. Daly, J. Pernak, J.E. Grisel, R.D. Carliss, M.D. Soutullo, J.H. Davis, R.D. Rogers, The third evolution of ionic liquids : active pharmaceutical ingredients, RCS Adv. 31 (2007) 1429–1436. https://doi.org/10.1039/b706677p.

[42] D. MacFarlane, A.L. Chong, M. Forsyth, M. Kar, V. Ranganathan, A. Somers, J.M. Pringle, New Dimensions in Salt-Solvent mixtures: A 4th Evolution of Ionic Liquids, Faraday Discuss. 206 (2018) 9–28. https://doi.org/10.1039/C7FD00189D.

[43] J.S. Wilkes, M.J. Zaworotko, Air and Water Stable l-Ethyl-3-methylimidazolium Based Ionic Liquids, Chem. Commun. 0 (1992) 965–967. https://doi.org/10.1039/C39920000965.

[44] J.H. Davis, K.J. Forrester, Thiazolium-ion based organic ionic liquids (OILs).1,2 Novel OILs which promote the benzoin condensation, Tetrahedron Lett. 40 (1999) 1621–1622.

[45] M. Zakrewsky, K.S. Lovejoy, T.L. Kern, T.E. Miller, V. Le, A. Nagy, Ionic liquids as a class of materials for transdermal delivery and pathogen neutralization, PNAS. 111 (2014) 13313–13318. https://doi.org/10.1073/pnas.1403995111.

[46] M. Armand, F. Endres, D.R. MacFarlane, H. Ohno, B. Scrosati, Ionic-liquid materials for the electrochemical challenges of the future, Nat. Mater. 8 (2009) 621–629. https://doi.org/10.1038/nmat2448.

[47] X. Jia, Y. Yang, C. Wang, C. Zhao, V. Ranganathan, D.R. MacFarlane, M. Forsyth, G.G. Wallace, Biocompatible ionic liquid-biopolymer electrolyte enabled thin and compact magnesium air batteries, ACS Appl. Mater. Interfaces. 6 (2014) 21110–21117. https://doi.org/10.1021/am505985z.

[48] M.A. Brenckle, H. Cheng, S. Hwang, H. Tao, M. Paquette, D.L. Kaplan, J.A. Rogers, Y. Huang, F.G. Omenetto, Modulated degradation of transient electronic devices through multilayer silk

fibroin pockets, ACS Appl. Mater. Interfaces. 7 (2015) 19870–19875. https://doi.org/10.1021/acsami.5b06059.

[49] T. Itoh, Ionic Liquids as Tool to Improve Enzymatic Organic Synthesis, Chemimcal Rev. 117 (2017) 10567–10607. https://doi.org/10.1021/acs.chemrev.7b00158.

[50] A. Kumar, M. Bisht, P. Venkatesu, Exploring the structure and stability of amino acids and glycine peptides in biocompatible ionic liquids, RSC Adv. 6 (2016) 18763–18777. https://doi.org/10.1039/C5RA26690D.

[51] O. Kuzmina, J. Hallett, eds., Application, Purification, and Recovery of Ionic Liquids, 1st ed., Elsevier, 2016.

[52] S. Hu, T. Jiang, Z. Zhang, A. Zhu, B. Han, Functional ionic liquid from biorenewable materials : synthesis and application as a catalyst in direct aldol reactions, Tetrahedron Lett. 48 (2007) 5613–5617. https://doi.org/10.1016/j.tetlet.2007.06.051.

[53] Q. Liu, X.-D. Hou, M. Zong, Ionic liquids from renewable biomaterials : synthesis , characterization and application in the pretreatment of biomass †, Green Chem. 14 (2012) 304–307. https://doi.org/10.1039/c2gc16128a.

[54] Q. Zhang, M. Benoit, K.D.O. Vigier, J. Barrault, Green and Inexpensive Choline-Derived Solvents for Cellulose Decrystallization, Chem. Eur. J. 18 (2012) 1043–1046. https://doi.org/10.1002/chem.201103271.

[55] A.M.A. Dias, A.R. Cortez, M.M. Barsan, J.B. Santos, C.M.A. Brett, H.C. De Sousa, Development of greener multi-responsive chitosan biomaterials doped with biocompatible ammonium ionic liquids, ACS Sustain. Chem. Eng. 1 (2013) 1480–1492. https://doi.org/10.1021/sc4002577.

[56] H. Garcia, R. Ferreira, M. Petkovic, J.L. Ferguson, M.C. Leitão, H.Q.N. Gunaratne, K.R. Seddon, L.P.N. Rebelo, C. Silva Pereira, M.C. Leit, H.Q.N. Gunaratne, K.R. Seddon, P.N. Rebelo, C. Silva, Dissolution of cork biopolymers in biocompatible ionic liquids, Green Chem. 9262 (2010) 3–6. https://doi.org/10.1039/b922553f.

[57] L. Huang, M. Zhai, J. Peng, L. Xu, J. Li, G. Wei, Synthesis of room temperature ionic liquids from carboxymethylated chitosan, Carbohydr. Polym. 71 (2008) 690–693. https://doi.org/10.1016/j.carbpol.2007.06.020.

[58] S.T. Handy, M. Okello, G. Dickenson, Solvents from Biorenewable Sources: Ionic Liquids Based on Fructose, Org. Lett. 5 (2003) 1–3. https://doi.org/10.1021/ol034778b.

[59] L. González, B. Altava, M. Bolte, M.I. Burguete, E. García-verdugo, S. V Luis, Synthesis of Chiral Room Temperature Ionic Liquids from Amino Acids – Application in Chiral Molecular Recognition, Eur. J. Org. Chem. 2012 (2012) 1–15. https://doi.org/10.1002/ejoc.201200607.

[60] S. De Santis, G. Masci, F. Casciotta, R. Caminiti, E. Scarpellini, M. Campetella, L. Gontrani, Cholinium-amino acid based ionic liquids: a new method of synthesis and physico-chemical characterization, Phys. Chem. Chem. Phys. 17 (2015) 20687–20698. https://doi.org/10.1039/C5CP01612F.

[61] V. Kumar, C. Pei, C.E. Olsen, S.J.C. Scha, Novel carbohydrate-based chiral ammonium ionic liquids derived from isomannide, Tetrahedron: Asummetry. 19 (2008) 664–671. https://doi.org/10.1016/j.tetasy.2008.02.009.

[62] A.K. Jha, N. Jain, Synthesis of glucose-tagged triazolium ionic liquids and their application as solvent and ligand for copper (I) catalyzed amination, Tetrahedron Lett. 54 (2013) 4738–4741. https://doi.org/10.1016/j.tetlet.2013.06.114.

[63] C. Chiappe, A. Marra, A. Mele, Synthesis and Applications of Ionic Liquids Derived from Natural Sugars, Top Curr Chem. 295 (2010) 177–195. https://doi.org/10.1007/128.

[64] A.M. Socha, R. Parthasarathi, J. Shi, S. Pattathil, D. Whyte, M. Bergeron, A. George, K. Tran, V. Stavila, S. Venkatachalam, M.G. Hahn, B.A. Simmons, S. Singh, Efficient biomass pretreatment using ionic liquids derived from lignin and hemicellulose, Proc. Natl. Acad. Sci. 111 (2014) E3587–E3595. https://doi.org/10.1073/pnas.1405685111.

[65] M. Petkovic, J.L. Ferguson, H.Q.N. Gunaratne, R. Ferreira, M.C. Leit, K.R. Seddon, N. Rebelo, C. Silva, Novel biocompatible cholinium-based ionic liquids — toxicity and biodegradability †, Green Chem. 12 (2010) 643–649. https://doi.org/10.1039/b922247b.

[66] A. Foulet, O. Ben Ghanem, M. El-Harbawi, J.M. Lévêque, M.I.A. Mutalib, C.Y. Yin, Understanding the physical properties, toxicities and anti-microbial activities of choline-amino acid-based salts: Low-toxic variants of ionic liquids, J. Mol. Liq. 221 (2016) 133–138. https://doi.org/10.1016/j.molliq.2016.05.046.

[67] S.H. Zeisel, A brief history of choline, Ann. Nutr. Metab. 61 (2012) 254–258. https://doi.org/10.1159/000343120.

[68] D. Constantinescu, K. Schaber, F. Agel, M.H. Klingele, T.J.S. Schubert, Viscosities , Vapor Pressures , and Excess Enthalpies of Choline Lactate + Water , Choline Glycolate + Water , and Choline Methanesulfonate + Water Systems, J. Chem. Eng. Data. 52 (2007) 1280–1285. https://doi.org/10.1021/je7000232.

[69] S.C. Matias, Â. Rocha, R. Teixeira, L.J.P.P. Fonseca, N.M.T. Lourenço, Synthesis of choline sulfonate buffers and their effect on cytochrome c dissolution and oxidation state†, RSC Adv. 4 (2014) 15597–15601. https://doi.org/10.1039/c4ra00913d.

[70] P.M. Dean, J. Turanjanin, M. Yoshizawa-Fujita, D.R. MacFarlane, J.L. Scott, Exploring an anti-crystal engineering approach to the preparation of pharmaceutically active ionic liquids, Cryst. Growth Des. 9 (2009) 1137–1145. https://doi.org/10.1021/cg8009496.

[71] R. Ferraz, L.C. Branco, I.M. Marrucho, J.M.M. Araújo, L.P.N. Rebelo, M.N. da Ponte, C. Prudêncio, J.P. Noronha, Ž. Petrovski, Development of novel ionic liquids based on ampicillin, Medchemcomm. 3 (2012) 494–497. https://doi.org/10.1039/c2md00269h.

[72] C. Florindo, A.B. Pereiro, N.S.M. Vieira, A.A. Matias, C.M.M. Duarte, P.N. Rebelo, I.M. Marrucho, Cholinium-based ionic liquids with pharmaceutically active anions †, RSC Adv. 4 (2014) 28126–28132. https://doi.org/10.1039/c3ra47615d.

[73] M. Taha, F.A. e Silva, M. V. Quental, S.P.M. Ventura, M.G. Freire, J.A.P. Coutinho, Good's buffers as a basis for developing self-buffering and biocompatible ionic liquids for biological research, Green Chem. 16 (2014) 3149–3159. https://doi.org/10.1039/c4gc00328d.

[74] S.Y. Lee, F.A. Vicente, J.A.P. Coutinho, I. Khoiroh, P.L. Show, S.P.M. Ventura, Densities, Viscosities, and Refractive Indexes of Good's Buffer Ionic Liquids, J. Chem. Eng. Data. 61 (2016) 2260–2268. https://doi.org/10.1021/acs.jced.5b00936.

[75] M. Taha, M. V. Quental, I. Correia, M.G. Freire, J.A.P. Coutinho, Extraction and stability of bovine serum albumin (BSA) using cholinium-based Good's buffers ionic liquids, Process Biochem. 50 (2015) 1158–1166. https://doi.org/10.1016/j.procbio.2015.03.020.

[76] Y. De Gaetano, A. Mohamadou, S. Boudesocque, J. Hubert, R. Plantier-Royon, L. Dupont, Ionic liquids derived from esters of Glycine Betaine: Synthesis and characterization, J. Mol. Liq. 207 (2015) 60–66. https://doi.org/10.1016/j.molliq.2015.03.016.

[77] M.M. Pereira, M.R. Almeida, J. Gomes, A.F.C.S. Rufino, Glycine-betaine ionic liquid analogues as novel phase-forming components of aqueous biphasic systems, Biotechnol. Prog. 34 (2018) 1205–1212. https://doi.org/10.1002/btpr.2685.

[78] Y. De Gaetano, J. Hubert, A. Mohamadou, S. Boudesocque, R. Plantier-Royon, J.H. Renault, L. Dupont, Removal of pesticides from wastewater by ion pair Centrifugal Partition Extraction using betaine-derived ionic liquids as extractants, Chem. Eng. J. 285 (2016) 596–604. https://doi.org/10.1016/j.cej.2015.10.012.

[79] M. Sharma, C. Muskesh, D. Mondal, K. Prasad, Dissolution of α-chitin in deep eutectic solvents, RCS Adv. 3 (2013) 18149–18155. https://doi.org/10.1039/c3ra43404d.

[80] A.P. Abbott, G. Capper, D.L. Davies, R.K. Rasheed, V. Tambyrajah, Novel solvent properties of choline chloride / urea mixtures †, Chem. Commun. 0 (2003) 70–71. https://doi.org/10.1039/b210714g.

[81] P. Liu, J.-W. Hao, L.-P. Mo, Z.-H. Zhang, Recent advances in the application of deep eutectic solvents as sustainable media as well as catalysts in organic reactions, RSC Adv. 5 (2015) 48675–48704. https://doi.org/10.1039/C5RA05746A.

[82] A. Paiva, R. Craveiro, I. Aroso, M. Martins, R.L. Reis, A.R.C. Duarte, Natural Deep Eutectic Solvents – Solvents for the 21st Century, ACS Sustain. Chem. Eng. 2 (2014) 1063–1071.

[83] X. Wang, C. Andre, Q. Lu, Z. Fei, P.J. Dyson, Cytotoxicity of ionic liquids and precursor compounds towards human cell line HeLa, Green Chem. 9 (2007) 1191–1197. https://doi.org/10.1039/b704503d.

[84] K.S. Egorova, V.P. Ananikov, Toxicity of ionic liquids: Eco(cyto)activity as complicated, but unavoidable parameter for task-specific optimization, ChemSusChem. 7 (2014) 336–360. https://doi.org/10.1002/cssc.201300459.

[85] T. Santos de Almeida, A. Júlio, N. Saraiva, A.S. Fernandes, M.E.M. Araújo, A.R. Baby, C. Rosado, J.P. Mota, Choline- versus imidazole-based ionic liquids as functional ingredients in topical delivery systems: cytotoxicity, solubility, and skin permeation studies, Drug Dev. Ind. Pharm. 43 (2017) 1858–1865. https://doi.org/10.1080/03639045.2017.1349788.

[86] D.J. Couling, R.J. Bernot, K.M. Docherty, J.K. Dixon, E.J. Maginn, Assessing the factors responsible for ionic liquid toxicity to aquatic organisms via quantitative structure–property relationship modeling, Green Chem. 8 (2006) 82–90. https://doi.org/10.1039/B511333D.

[87] S. Stolte, S. Steudte, O. Areitioaurtena, F. Pagano, J. Thöming, P. Stepnowski, A. Igartua, Ionic liquids as lubricants or lubrication additives: An ecotoxicity and biodegradability assessment, Chemosphere. 89 (2012) 1135–1141. https://doi.org/10.1016/j.chemosphere.2012.05.102.

[88] D.J.S. Patinha, L.C. Tomé, C. Isabel, S. Florindo, H. Soares, A.S. Coroadinha, I.M. Marrucho, New low-toxicity cholinium-based ionic liquids with perfluoroalkanoate anions for ABS implementation, ACS Sustain. Chem. Eng. 4 (2016) 2670–2679. https://doi.org/10.1021/acssuschemeng.6b00171.

[89] M. J. Earle, P. B. McCormac, K. R. Seddon, Diels-Alder reactions in ionic liquids. A safe recyclable alternative to lithium perchlorate-diethyl ether mixtures, Green Chem. 1 (1999) 23–25. https://doi.org/10.1039/A808052F.

[90] J. Pernak, I. Goc, I. Mirska, Anti-microbial activities of protic ionic liquids with lactate anion, Green Chem. 6 (2004) 323–329. https://doi.org/10.1039/b404625k.

[91] E.B. Carter, S.L. Culver, P. a Fox, R.D. Goode, I. Ntai, M.D. Tickell, R.K. Traylor, N.W. Hoffman, J.H. Davis, Sweet success: Ionic liquids derived from non-nutritive sweeteners., Chem. Commun. 0 (2004) 630–631. https://doi.org/10.1039/b313068a.

[92] S. Shahriari, L.C. Tomé, J.M.M. Araújo, L.P.N. Rebelo, J.A.P. Coutinho, I.M. Marrucho, M.G. Freire, Aqueous biphasic systems: a benign route using cholinium-based ionic liquids, RSC Adv. 3 (2013) 1835–1843. https://doi.org/10.1039/C2RA22972B.

[93] D.R. MacFarlane, S.A. Forsyth, J. Golding, G.B. Deacon, Ionic liquids based on imidazolium, ammonium and pyrrolidinium salts of the dicyanamide anion, Green Chem. 4 (2002) 444–448. https://doi.org/10.1039/b205641k.

[94] Y. Fukaya, Y. Iizuka, K. Sekikawa, H. Ohno, Bio ionic liquids : room temperature ionic liquids composed wholly of biomaterials, Green Chem. 9 (2007) 1155–1157. https://doi.org/10.1039/b706571j.

[95] A.P. Abbott, G. Capper, D.L. Davies, H.L. Munro, R.K. Rasheed, V. Tambyrajah, Preparation of novel, moisture-stable, Lewis-acidic ionic liquids containing quaternary ammonium salts with functional side chains, Chem. Commun. 0 (2001) 2010–2011. https://doi.org/10.1039/b106357j.

[96] A.P. Abbott, G. Capper, D.L. Davies, R. Rasheed, Ionic Liquids Based upon Metal Halide-Substituted Quaternary Ammonium Salt Mixtures, Inorg Chem. 43 (2004) 3447–3452. https://doi.org/10.1021/ic049931s.

[97] B.L. Gadilohar, H.S. Kumbhar, G.S. Shankarling, Choline Peroxydisulfate : Environmentally Friendly Biodegradable Oxidizing TSIL for Selective and Rapid Oxidation of Alcohols, Ind. Eng. Chem. Res. 53 (2014) 19010–19018. https://doi.org/10.1021/ie5032919.

[98] N. Pedro, J. Gomes, A.P. Coutinho, M.G. Freire, A. Mohamadou, P.M. Ventura, Synthesis and characterization of analogues of glycine-betaine ionic liquids and their use in the formation of aqueous biphasic systems, Fluid Phase Equilibria J. 494 (2019) 239–245. https://doi.org/10.1016/j.fluid.2019.05.001.

[99] H. Mahmood, M. Moniruzzaman, S. Yusup, T. Welton, Ionic liquids assisted processing of renewable resources for the fabrication of biodegradable composite materials, Green Chem. 19 (2017) 2051–2075. https://doi.org/10.1039/C7GC00318H.

[100] A. Bhattacharjee, J.A. Lopes-da-Silva, M.G. Freire, J.A.P. Coutinho, P.J. Carvalho, Thermophysical properties of phosphonium-based ionic liquids, Fluid Phase Equilib. 400 (2015) 103–113. https://doi.org/10.1016/j.fluid.2015.05.009.

[101] S.P.M. Ventura, F.A. e Silva, A.M.M. Gonçalves, J.L. Pereira, F. Gonçalves, J.A.P. Coutinho, Ecotoxicity analysis of cholinium-based ionic liquids to Vibrio fischeri marine bacteria, Ecotoxicol. Environ. Saf. 102 (2014) 48–54. https://doi.org/10.1016/j.ecoenv.2014.01.003.

[102] A. Jordan, N. Gathergood, Biodegradation of ionic liquids – a critical review, Chem. Soc. Rev. 44 (2015) 8200–8237. https://doi.org/10.1039/C5CS00444F.

[103] E.E.L. Tanner, K.N. Ibsen, S. Mitragotri, Transdermal insulin delivery using choline-based ionic liquids (CAGE), J. Control. Release. 286 (2018) 137–144. https://doi.org/10.1016/j.jconrel.2018.07.029.

[104] A. Banerjee, K. Ibsen, T. Brown, R. Chen, C. Agatemor, S. Mitragotri, Ionic liquids for oral insulin delivery, 115 (2018) 1–6. https://doi.org/10.1073/pnas.1722338115.

[105] M.R. Chowdhury, R.M. Moshikur, R. Wakabayashi, Y. Tahara, N. Kamiya, M. Moniruzzaman, M. Goto, *In vivo* biocompatibility, pharmacokinetics, antitumor efficacy, and hypersensitivity evaluation of ionic liquid-mediated paclitaxel formulations, Int. J. Pharm. 565 (2019) 219–226. https://doi.org/10.1016/j.ijpharm.2019.05.020.

[106] K. Ninomiya, K. Inoue, Y. Aomori, A. Ohnishi, C. Ogino, N. Shimizu, K. Takahashi, Characterization of fractionated biomass component and recovered ionic liquid during repeated process of cholinium ionic liquid-assisted pretreatment and fractionation, Chem. Eng. J. 259 (2015) 323–329. https://doi.org/10.1016/j.cej.2014.07.122.

[107] W. Deng, L. Liu, Y. Peng, Choline taurinate:a new biocompatible amino- functionalized ionic liquid as basic catalyst and extraction solvent, Green Process Synth. 7 (2018) 191–197. https://doi.org/10.1515/gps-2017-0009.

[108] M.J. Quental, A. Pedro, P. Pereira, M. Sharma, J.A. Queiroz, J.A.P. Coutinho, F. Sousa, M.G. Freire, Integrated extraction-preservation strategies for RNA using bio-based ionic liquids, ACS Sustain. Chem. Eng. 7 (2019) 9439–9448. https://doi.org/10.1021/acssuschemeng.9b00688.

[109] Y. An, M. Zong, H. Wu, N. Li, Pretreatment of lignocellulosic biomass with renewable cholinium ionic liquids : Biomass fractionation, enzymatic digestion and ionic liquid reuse, Bioresour. Technol. 192 (2015) 165–171. https://doi.org/10.1016/j.biortech.2015.05.064.

[110] K. Ninomiya, S. Omote, C. Ogino, K. Kuroda, M. Noguchi, T. Endo, Saccharification and ethanol fermentation from cholinium ionic liquid-pretreated bagasse with a different number of post-pretreatment washings, Bioresour. Technol. 189 (2015) 203–209. https://doi.org/10.1016/j.biortech.2015.04.022.

[111] K. Ninomiya, A. Kohori, M. Tatsumi, K. Osawa, T. Endo, R. Kakuchi, Ionic liquid/ultrasound pretreatment and in situ enzymatic saccharification of bagasse using biocompatible cholinium ionic liquid, Bioresour. Technol. 176 (2015) 169–174. https://doi.org/10.1016/j.biortech.2014.11.038.

[112] A.A. Elgharbawy, Z. Alam, M. Moniruzzaman, M. Goto, Ionic liquid pretreatment as emerging approaches for enhanced enzymatic hydrolysis of lignocellulosic biomass, Biochem. Eng. J. 109 (2016) 252–267. https://doi.org/10.1016/j.bej.2016.01.021.

[113] T.C. Pin, P.Y.S. Nakasu, S. Mattedi, S.C. Rabelo, A.C. Costa, Screening of protic ionic liquids for sugarcane bagasse pretreatment, Fuel. 235 (2019) 1506–1514. https://doi.org/10.1016/j.fuel.2018.08.122.

[114] K. Ninomiya, A. Rohsari, I. Utami, Y. Tsuge, K. Kuroda, C. Ogino, T. Taima, J. Saito, M. Kimizu, K. Takahashi, Pretreatment of bagasse with a minimum amount of cholinium ionic liquid for subsequent saccharification at high loading and co-fermentation for ethanol production, Chem. Eng. J. 334 (2018) 657–663. https://doi.org/10.1016/j.cej.2017.10.113.

[115] P. Lima, L. Naiadhy, S. Santos, S. Patrícia, M. Ventura, R. Lucena, D. Souza, J. Araújo, P. Coutinho, C. Mara, F. Soares, Á. Silva, Recovery of capsaicin from Capsicum frutescens by applying aqueous two-phase systems based on acetonitrile and cholinium-based ionic liquids, Chem. Eng. Res. Des. 112 (2016) 103–112. https://doi.org/10.1016/j.cherd.2016.02.031.

[116] S. Ying, I. Khoiroh, T. Chuan, P. Loke, Enhanced recovery of lipase derived from Burkholderia cepacia from fermentation broth using recyclable ionic liquid / polymer-based aqueous two-phase systems, Sep. Purif. Technol. 179 (2017) 152–160. https://doi.org/10.1016/j.seppur.2017.01.047.

[117] A. Pedro, P. Pereira, M. V Quental, A. Carvalho, S.M. Santos, J.A. Queiroz, F. Sousa, M.G. Freire, Cholinium-based Good's buffers ionic liquids as remarkable stabilizers and recyclable preservation media for recombinant small RNAs, ACS Sustain. Chem. Eng. 6 (2018) 16645–16656. https://doi.org/10.1021/acssuschemeng.8b03900.

[118] M.A.R. Martins, C.M.S.S. Neves, K.A. Kurnia, P.J. Carvalho, M.A.A. Rocha, L.M.N.B.F. Santos, S.P. Pinho, M.G. Freire, Densities , viscosities and derived thermophysical properties of water-saturated imidazolium-based ionic liquids, Fluid Phase Equilib. 407 (2016) 188–196. https://doi.org/10.1016/j.fluid.2015.05.023.

[119] M. Cvjetko Bubalo, K. Radošević, I. Radojčić Redovniković, J. Halambek, V. Gaurina Srček, A brief overview of the potential environmental hazards of ionic liquids, Ecotoxicol. Environ. Saf. 99 (2014) 1–12. https://doi.org/10.1016/j.ecoenv.2013.10.019.

[120] OECD Guideline for Testing of Chemicals, (2017) Organisation for Economic Co-operation and Develop. http://www.oecd.org/chemicalsafety/testing/oecdguidelinesforthetestingofchemicals.htm (accessed December 10, 2018).

[121] A. Yazdani, M. Sivapragasam, J.-M. Levêque, M. Moniruzzaman, J.M. Leveque, M. Moniruzzaman, Microbial Biocompatibility and Biodegradability of Choline-Amino Acid Based Ionic Liquids, J. Microb. Biochem. Technol. Microb. 8 (2016) 415–421. https://doi.org/10.4172/1948-5948.1000318.

[122] R.S. Boethling, E. Sommer, D. Difiore, Designing Small Molecules for Biodegradability, Chem. Rev. 107 (2007) 2207–2227. https://doi.org/10.1021/cr050952t.

[123] B. Peric, J. Sierra, E. Martí, R. Cruañas, M.A. Garau, J. Arning, U. Bottin-Weber, S. Stolte, (Eco)toxicity and biodegradability of selected protic and aprotic ionic liquids, J. Hazard. Mater. 261 (2013) 99–105. https://doi.org/10.1016/j.jhazmat.2013.06.070.

[124] S.P.M. Ventura, C.S. Marques, A.A. Rosatella, C.A.M. Afonso, F. Gonçalves, J.A.P. Coutinho, Toxicity assessment of various ionic liquid families towards Vibrio fischeri marine bacteria, Ecotoxicol. Environ. Saf. 76 (2012) 162–168. https://doi.org/10.1016/j.ecoenv.2011.10.006.

[125] D.R.M. Passino, S.B. Smith, Acute bioassays and hazard evaluation of representative contaminants detected in great lakes fish, Environ. Toxicol. Chem. 6 (1987) 901–907. https://doi.org/10.1002/etc.5620061111.

[126] A.H. Rantamäki, S.K. Ruokonen, E. Sklavounos, L. Kyllönen, A.W.T. King, S.K. Wiedmer, Impact of surface- active guanidinium-, tetramethylguanidinium-, and cholinium-based ionic liquids on vibrio Fischeri cells and dipalmitoylphosphatidylcholine liposomes, Sci. Rep. 7 (2017) 1–12. https://doi.org/10.1038/srep46673.

[127] F.A. e Silva, F. Siopa, B.F.H.T. Figueiredo, A.M.M. Gonçalves, J.L. Pereira, F. Gonçalves, J.A.P. Coutinho, C.A.M. Afonso, S.P.M. Ventura, Sustainable design for environment-friendly mono and dicationic cholinium-based ionic liquids, Ecotoxicol. Environ. Saf. 108 (2014) 302–310. https://doi.org/10.1016/j.ecoenv.2014.07.003.

[128] M. Sivapragasam, J. Raj, J. Levêque, M. Moniruzzaman, M.I.A. Mutalib, Microbial biocompatibility of phosphonium- and ammonium-based ionic liquids, J. Mol. Liq. 273 (2019) 107–115. https://doi.org/10.1016/j.molliq.2018.10.022.

[129] C. Pretti, C. Chiappe, I. Baldetti, S. Brunini, G. Monni, L. Intorre, Acute toxicity of ionic liquids for three freshwater organisms: Pseudokirchneriella subcapitata, Daphnia magna and Danio rerio, Ecotoxicol. Environ. Saf. 72 (2009) 1170–1176. https://doi.org/10.1016/j.ecoenv.2008.09.010.

[130] D. Rengstl, B. Kraus, M. Van Vorst, G.D. Elliott, W. Kunz, Effect of choline carboxylate ionic liquids on biological membranes, Colloids Surfaces B Biointerfaces. 123 (2014) 575–581. https://doi.org/10.1016/j.colsurfb.2014.09.057.

[131] K.D. Weaver, H.J. Kim, J. Sun, D.R. MacFarlane, G.D. Elliott, Cyto-toxicity and biocompatibility of a family of choline phosphate ionic liquids designed for pharmaceutical applications, Green Chem. 12 (2010) 507–513. https://doi.org/10.1039/b918726j.

[132] R.F.M. Frade, S. Simeonov, A.A. Rosatella, F. Siopa, C.A.M. Afonso, Toxicological evaluation of magnetic ionic liquids in human cell lines, Chemosphere. 92 (2013) 100–105. https://doi.org/10.1016/j.chemosphere.2013.02.047.

[133] A.M.O. Azevedo, S.P.F. Costa, A.F.V. Dias, A.H.O. Marques, P.C.A.G. Pinto, K. Bica, A.K. Ressmann, M.L.C. Passos, A.R.T.S. Araújo, S. Reis, M.L.M.F.S. Saraiva, Anti-inflammatory choline based ionic liquids: Insights into their lipophilicity , solubility and toxicity parameters, J. Mol. Liq. 232 (2017) 20–26. https://doi.org/10.1016/j.molliq.2017.02.027.

[134] T. Review, J. Chen, F. Xie, X. Li, L. Chen, Ionic liquids for the preparation of biopolymer materials for drug/gene delivery: a review, Green Chem. 20 (2018) 4169–4200. https://doi.org/10.1039/c8gc01120f.

[135] K.S. Egorova, M.M. Seitkalieva, A. V. Posvyatenko, V.P. Ananikov, An unexpected increase of toxicity of amino acid-containing ionic liquids, Toxicol. Res. 4 (2015) 152–159. https://doi.org/10.1039/c4tx00079j.

[136] M. Matzke, S. Stolte, K. Thiele, T. Juffernholz, J. Ranke, The influence of anion species on the toxicity of 1-alkyl-3- methylimidazolium ionic liquids observed in an (eco) toxicological test battery †, Green Chem. 9 (2007) 1198–1207. https://doi.org/10.1039/b705795d.

[137] A. Idris, R. Vijayaraghavan, U.A. Rana, D. Fredericks, A.F. Patti, D.R. Macfarlane, Dissolution of feather keratin in ionic liquids†, Green Chem. 15 (2013) 525–534. https://doi.org/10.1039/c2gc36556a.

[138] X.-D. Hou, T.J. Smith, N. Li, M. Zong, Novel Renewable Ionic Liquids as Highly Effective Solvents for Pretreatment of Rice Straw Biomass by Selective Removal of Lignin, Biotechnol. Bioeng. 109 (2012) 2484–2493. https://doi.org/10.1002/bit.24522.

[139] F. Liu, Q. Liu, A. Wang, T. Zhang, Direct Catalytic Hydrogenolysis of Kraft Lignin to Phenols in Choline- Derived Ionic Liquids, ACS Sustain. Chem. Eng. 4 (2016) 3850–3856. https://doi.org/10.1021/acssuschemeng.6b00620.

[140] D. Outeiriño, I. Costa-trigo, A. Paz, F.J. Deive, A. Rodríguez, J. Manuel, Biorefining brewery spent grain polysaccharides through biotuning of ionic liquids, Carbohydr. Polym. 203 (2019) 265–274. https://doi.org/10.1016/j.carbpol.2018.09.042.

[141] J. Sun, N.V.S.N.M. Konda, J. Shi, R. Parthasarathi, T. Dutta, F. Xu, C.D. Scown, A. Simmons, S. Singh, CO2 enabled process integration for the production of cellulosic ethanol using bionic liquids †, Energy Environ. Sci. 9 (2016) 2822–2834. https://doi.org/10.1039/C6EE00913A.

[142] J. Sun, N.V.S.N.M. Konda, R. Parthasarathi, T. Dutta, M. Valiev, F. Xu, B.A. Simmons, S. Singh, One-pot integrated biofuel production using low-cost biocompatible protic ionic liquids, Green Chem. 19 (2017) 3152–3163. https://doi.org/10.1039/c7gc01179b.

[143] T.Q. To, K. Procter, B.A. Simmons, S. Subashchandrabose, R. Atkin, Low cost ionic liquid – water mixtures for effective extraction of carbohydrate and lipid from algae, Faraday Discuss. 206 (2017) 93–112. https://doi.org/10.1039/C7FD00158D.

[144] A.P. Abbott, T.J. Bell, B. Stoddart, Cationic functionalisation of cellulose using a choline based ionic liquid analogue †, Green Chem. 8 (2006) 784–786. https://doi.org/10.1039/b605258d.

[145] O. Winther-Jensen, R. Vijayaraghavan, J. Sun, B. Winther-Jensen, D.R. MacFarlane, Self polymerising ionic liquid gel, Chem. Commun. 0 (2009) 3041–3042. https://doi.org/10.1039/b822905h.

[146] G. Colomines, P. Decaen, D. Lourdin, E. Leroy, Biofriendly ionic liquids for starch plasticization: a screening approach, RSC Adv. 6 (2016) 90331–90337. https://doi.org/10.1039/C6RA16573G.

[147] S. Guilois, V. Jury, N. Allanic, E. Leroy, Choline Chloride vs Choline Ionic liquids for starch thermoplasticization, Carbohydr. Polym. 117 (2017) 424–432. https://doi.org/10.1016/j.carbpol.2017.09.012.

[148] D. Lourdin, W.R. Wise, Glycol based plasticisers for salt modified starch, RSC Adv. 4 (2014) 40421–40427. https://doi.org/10.1039/C4RA06220E.

[149] M. Yoshizawa-fujita, K. Fujita, M. Forsyth, D.R. Macfarlane, A new class of proton-conducting ionic plastic crystals based on organic cations and dihydrogen phosphate, Electrochem. Commun. 9. 9 (2007) 1202–1205. https://doi.org/10.1016/j.elecom.2007.01.024.

[150] U.A. Rana, P.M. Bayley, R. Vijayaraghavan, P. Howlett, D.R. Macfarlane, M. Forsyth, Proton transport in choline dihydrogen phosphate/H3PO4 mixtures, PCCP. 12 (2010) 11291–11298. https://doi.org/10.1039/c0cp00156b.

[151] M. Sharma, D. Mondal, C. Mukesh, K. Prasad, Preparation of tamarind gum based soft ion gels having thixotropic properties, Carbohydr. Polym. 102 (2014) 467–471. https://doi.org/10.1016/j.carbpol.2013.11.063.

[152] S. Sundar, D. Kumar, S. Mahadevan, R. Vijayaraghavan, A. Baran, D.R. Macfarlane, Curcumin loaded poly (2-hydroxyethyl methacrylate) nanoparticles from gelled ionic liquid – *In vitro* cytotoxicity and anti-cancer activity in, Eur. J. Pharm. Sci. 51 (2014) 34–44. https://doi.org/10.1016/j.ejps.2013.08.036.

[153] C. Mukesh, D. Mondal, M. Sharma, K. Prasad, Rapid dissolution of DNA in a novel bio-based ionic liquid with long-term structural and chemical stability: successful recycling of the ionic liquid for reuse in the process†, Chem. Commun. 48 (2013) 6849–6851. https://doi.org/10.1039/c3cc42829j.

[154] R. Moshikur, R. Chowdhury, R. Wakabayashi, Y. Tahara, Characterization and cytotoxicity evaluation of biocompatible amino acid esters used to convert salicylic acid into ionic liquids, Int. J. Pharm. 546 (2018) 31–38. https://doi.org/10.1016/j.ijpharm.2018.05.021.

[155] A.R. Jesus, M.R.C. Soromenho, L.R. Raposo, J.M.S.S. Esperança, P. V Baptista, A.R. Fernandes, P.M. Reis, Enhancement of water solubility of poorly water-soluble drugs by new biocompatible N -acetyl amino acid N -alkyl cholinium-based ionic liquids, Eur. J. Pharm. Biopharm. 137 (2019) 227–232. https://doi.org/10.1016/j.ejpb.2019.03.004.

[156] X. Lin, Y. Yang, S. Li, Y. Song, G. Ma, Z. Su, S. Zhang, Unique stabilizing mechanism provided by biocompatible choline-based ionic liquids for inhibiting dissociation of inactivated foot-and-mouth disease virus particles, RCS Adv. (2019) 13933–13939. https://doi.org/10.1039/c9ra02722j.

[157] R. Moshikur, R. Chowdhury, R. Wakabayashi, Y. Tahara, Ionic liquids with methotrexate moieties as a potential anticancer prodrug : Synthesis , characterization and solubility evaluation, J. Mol. Liq. 278 (2019) 226–233. https://doi.org/10.1016/j.molliq.2019.01.063.

[158] R. Chowdhury, R. Moshikur, R. Wakabayashi, Y. Tahara, N. Kamiya, M. Moniruzzaman, M. Goto, Ionic-Liquid-Based Paclitaxel Preparation: A New Potential Formulation for Cancer Treatment, Mol. Pharm. 15 (2018) 2484–2488. https://doi.org/10.1021/acs.molpharmaceut.8b00305.

[159] X. Wu, Z. Chen, Y. Li, Q. Yu, Y. Lu, Q. Zhu, Y. Li, D. An, J. Gi, W. Wu, Improving dermal delivery of hydrophilic macromolecules by biocompatible ionic liquid based on choline and malic acid, Int. J. Pharm. 558 (2019) 380–387. https://doi.org/10.1016/j.ijpharm.2019.01.021.

[160] J. Pernak, A. Syguda, I. Mirska, A. Pernak, J. Nawrot, Choline-Derivative-Based Ionic Liquids, Chemistry. 13 (2007) 6817–6827. https://doi.org/10.1002/chem.200700285.

[161] X. Jia, C. Wang, V. Ranganathan, B. Napier, C. Yu, Y. Chao, M. Forsyth, F.G. Omenetto, D.R. MacFarlane, G.G. Wallace, A Biodegradable Thin-Film Magnesium Primary Battery Using Silk Fibroin–Ionic Liquid Polymer Electrolyte, ACS Energy Lett. 2 (2017) 831–836. https://doi.org/10.1021/acsenergylett.7b00012.

[162] V. Ranganathan, D.R. Macfarlane, F. Benito-lopez, Probing the specific ion effects of biocompatible hydrated choline ionic liquids on lactate oxidase biofunctionality in sensor applications, PCCP. 16 (2014) 1841–1849. https://doi.org/10.1039/c3cp52845f.

[163] M. Reslan, V. Kayser, Ionic liquids as biocompatible stabilizers of proteins, Biophys. Reviwes. 10 (2018) 781–793.

[164] I. Noshadi, B.W. Walker, R. Portillo-lara, E.S. Sani, Engineering Biodegradable and Biocompatible Bio-ionic Liquid Conjugated Hydrogels with Tunable Conductivity and Mechanical Properties, Nature. 7 (2017) 1–18. https://doi.org/10.1038/s41598-017-04280-w.

[165] M. Isik, R. Gracia, L.C. Kollnus, L.C. Tomé, I.M. Marrucho, D. Mecerreyes, Cholinium-Based Poly(ionic liquid)s: Synthesis, Characterization, and Application as Biocompatible Ion Gels and Cellulose Coatings, ACS Macro Lett. 2 (2013) 975–979.

SECTION 2

EXPERIMENTAL DESIGN

Chapter II

Materials & Methods

Chapter II

Materials and Methods

OVERVIEW

This chapter provides a detailed description of the materials and experimental procedures that were used transversal throughout this thesis, being complementary to the "Materials and Methods" of Chapters III to VII. It starts with describing the materials used, namely the natural polymers, including chitin, silk fibroin (SF), alginate, and acemannan, and the rationale for their selection. Moreover, the methodology used for the biocompatible ionic liquids (Bio-ILs) synthesis will be detailed, and the different techniques used for the physicochemical characterization of the Bio-ILs, as well as the fabricated biomaterials, will be addressed. Finally, the methodologies used to access the biological performance, as well as therapeutic efficacy, of the developed biomaterials will be briefly explained. Figure II- 1 depicts a schematic overview of the materials, the processing strategies, and the characterization methods used.

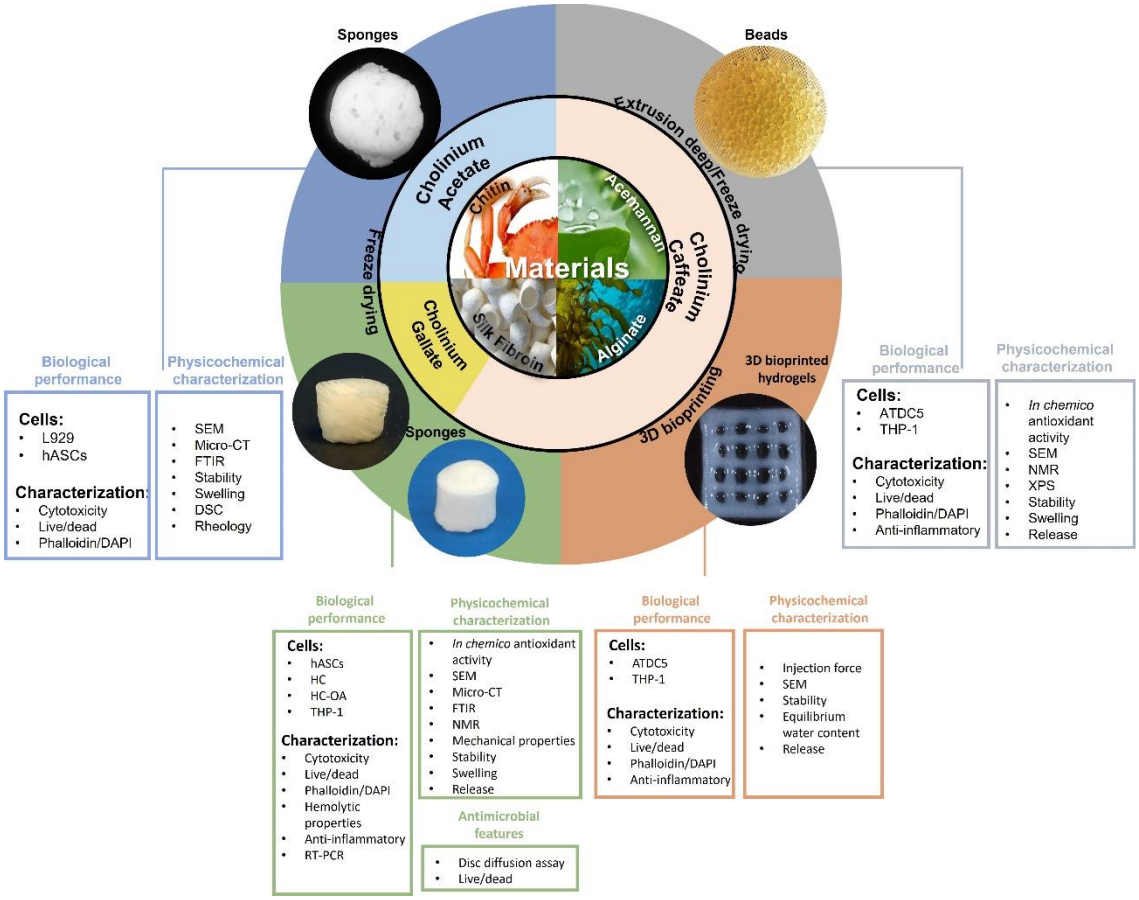


Figure II-1 – Schematic overview representation of the natural macromolecules used, the synthetized biocompatible ionic liquids (Cholinium gallate and Cholinium caffeic) and the processing and characterization methodologies used. (Legend alphabetic order: ATDC5 – mouse chondrogenic-like cell line, DSC - differential scanning calorimetry, FTIR – Fourier-transform infrared spectroscopy, hASCs – human adipose stem cells, HC – human chondrocytes, HC-OA – human chondrocytes osteoarthritis, L929- fibroblast-like cells, Micro-CT- Micro-Computed tomography, NMR – nuclear magnetic resonance, RT-PCR- real-time reverse transcription–polymerase chain reaction, SEM – scanning electron microscopy, SF – silk fibroin, THP-1 – human monocyte cell line, XPS - x-ray photoelectron spectroscopy).

II-1. MATERIALS

The materials used in this thesis and the description of their main features are herein described, aiming to clarify the rationale behind their selection for further experimental studies.

II-1.1. Chitin

Chitin is a well-known natural biomacromolecule and the second most abundant polymer in nature [1]. This polymer can be found in various biomass, including the shell of crustaceans, the cuticles of insects, and the cell walls of fungi, and counts with an estimated annual production of 10^{11}– 10^{14} tons [1,2]. Structurally, chitin is made up of β (1→4)-linked primary units of N-acetyl D-glucosamine (monomer units of 2-acetamido- 2-deoxy-b-d- glucose) (Figure II-2). Despite chitin's abundancy and inherent striking features, such as nontoxicity and biocompatibility, as well as the ability to accelerate wound healing and tumour cell growth suppression, its wide use is limited by the obstacles concerning its processability [3,4]. Chitin chains are bonded by strong inter- and intramolecular hydrogen bonds, which restricts their solubility in water and organic solvents, thus, limiting its processability [1]. Depending on the nature of the hydrogen bounds, chitin exists in three crystalline polymorphic forms designated as α, β, and γ chitin, despite the controversy around the existence of γ chitin [1]. The different arrangements in the chitin structure lead to differences in molecular packing and polarity, which promotes distinct physicochemical properties [1,5]. Overall, the strength of the intermolecular forces in the β-chitin molecule are much weaker than in α-chitin, resulting in a more soluble and reactive character of the β-chitin. Thus, α-chitin is the most stable form of this natural polymer [5].

Recent studies have been proving the ability of the commonly used ionic liquids (ILs) to dissolve and extract chitin from biomass [6–9]. However, due to their doubtful green nature, the synthesis and use of biocompatible ionic liquids (Bio-ILs) for this purpose is growing. Therefore, the use of greener and biofriendly compounds for the processing of α-chitin, is mandatory, particularly when envisioning the application of the fabricated constructs in the biomedical field [1]. Considering that, and aiming to expand the use of this attractive natural polymer into broader fields, in **Chapter III,** α-chitin was processed using cholinium acetate (Ch[ACE]), a commercial Bio-IL., overcoming its insolubility.

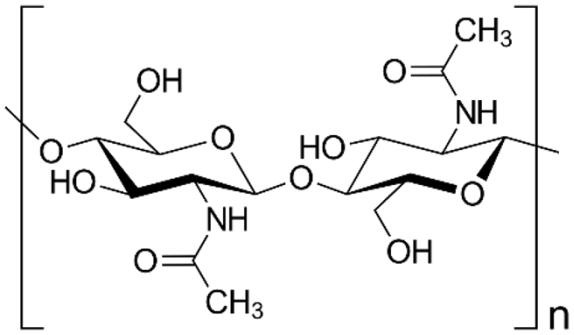


Figure II-2 – Chitin structure.

II-1.2. Silk Fibroin (SF)

Silk is a natural macromolecular protein produced by specialized glands and further spun into fibers [10], that may be obtained from silkworms (e.g., *Bombyx mori*) and orb-weaving spiders (e.g., *Nephila clavipes*), either for textile or biomedical applications [11]. The spun fiber is composed of two proteins: fibroin (72-81%), the central protein, and sericin (19-28%), a soluble glue like-protein that coats fibroin, acting as an adhesive binder to preserve its structural integrity. Sericin free silk fibroin (SF) is composed of β-sheet structures, a consequence of the dominance of hydrophobic domains involving short-side chain amino acids in the primary sequence [12,13]. SF is composed of polypeptide chains with a molecular weight ranging between 200-350 kDa. Its primary structure comprises hydrophilic light chains (L-chain, M_w = 27.7 kDa) with terminal C and N groups and repetitive blocks of hydrophobic heavy chains (H-chain, Mw = 391.6 kDa), both linked by disulfate bonds [13]. The H-chain comprises 5242 amino acids, while the L-chain has 246. The L-chain domain contains amino acid sequences of Alanine (Ala), Serine (Ser), Glycine (Gly), and acetylated N-terminal Ser residues, while the H-chain contains Gly, Ala, Ser, Tyrosine (Tyr), and Valine (Val) [14,15]. The amino acid sequence of H-fibroin can be defined as (–Gly–Ser–Gly–Ala–Gly–Ala–), as depicted in Figure II-3. The H-fibroin chains contain repetitive hydrophobic domains interspersed between non-repetitive hydrophilic domains, which are responsible for fostering the assembly of the silk fibers, providing them with strength [12].

SF is a highly insoluble fibrous protein with unique degradability and biocompatibility features, adequate mechanical properties, and excellent processability [11].

SF-based materials, including films, hydrogels, and scaffolds, can be processed using regenerated SF solutions prepared by traditional solvents, e.g., $CaCl_2$/ethanol/water solution, 1,1,1,3,3,3-Hexafluoro-2-propanol (HFIP) and concentrated formic acid. However, some of those solvents are highly toxic and volatile, causing severe environmental pollution [16], which limits its application as viable tissue

engineering strategies. Different studies have already reported the use of ionic liquids (ILs) as an avenue for the processability and application of SF [17]. However, the toxicity and biodegradability of ILs require their removal from the SF-based matrices before their biomedical use. Therefore, Bio-ILs emerge as an eco-friendly family of ILs due to their biocompatibility, avoiding its removal and improving the biomaterial biological performance. Thus, in the **Chapter IV** and **Chapter V** of this thesis, SF from *Bombyx Mori* cocoons were processed and used in a combinatorial approach with Bio-ILs to produce active sponges with intrinsic antioxidant and anti-inflammatory properties and also able to support cell growth and proliferation.

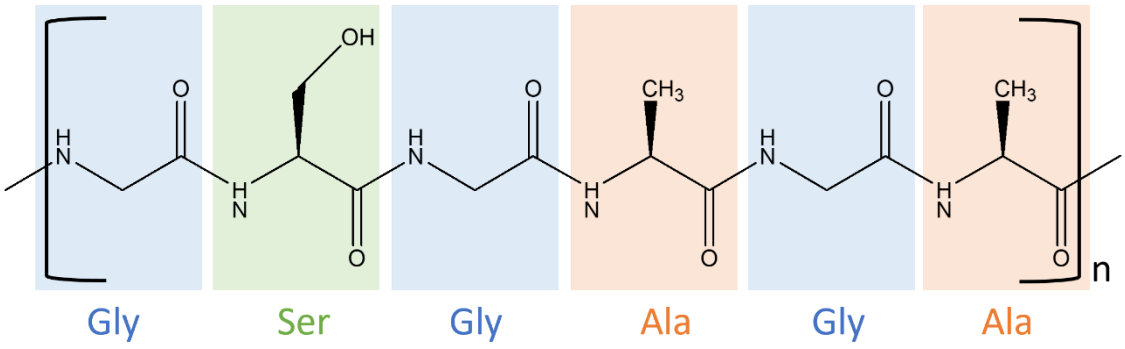


Figure II-3 - Silk fibroin primary structure.

II-1.3. Alginate (ALG)

Alginate is a natural polymer derived from brown sea algae, formed by block copolymers of β-D-mannuronic acid (M) and L-guluronic acid (G), which structure is presented in Figure II-4. The physical properties of the polymer are dependent on the proportions of the M and G blocks. Moreover, one of the key features of ALG, is its ability to form hydrogels by divalent cations chelation [18]. The formation of ALG hydrogels is carried out by ionic crosslinking of the G-blocks by divalent cations such us Ca^{2+}, Ba^{2+}, and Sr^{2}. It means that the hydrogel-forming ability and the mechanical properties of the final construct would depend on the relative amounts of M and G in the ALG molecular structure [18]. Thus, ALG has been widely used to produce hydrogels and scaffold-based cell culture materials. Allied to the fast ionic crosslinking ability, ALG is also known for its low toxicity and high toxicity biocompatibility [18,19]. The lack of alginase, the enzyme responsible to cleave ALG chains, makes it a non-degradable polymer. Though, ionically crosslinked gels are easily dissolved through the release of the divalent ions into the surrounding media due to the exchange reactions with monovalent cations, such as sodium or phosphate ions [20]. Furthermore, ALG allows blending of different molecules and growth factors [20], providing the

final constructs with the desired biological response and the ideal 3D environment for cell seeding and/or encapsulation.

Thus, in **Chapter VI** of this thesis, ALG, acemannan (ACE), and a synthesized Bio-IL (Ch[Caffeate]) were combined to produce based beads to be used as a drug delivery system. In **Chapter VII**, the ALG/ACE/Ch[Caffeate] system was also used to create hybrid inks for 3D bioprinting (printing with incorporated living cells), respectively.

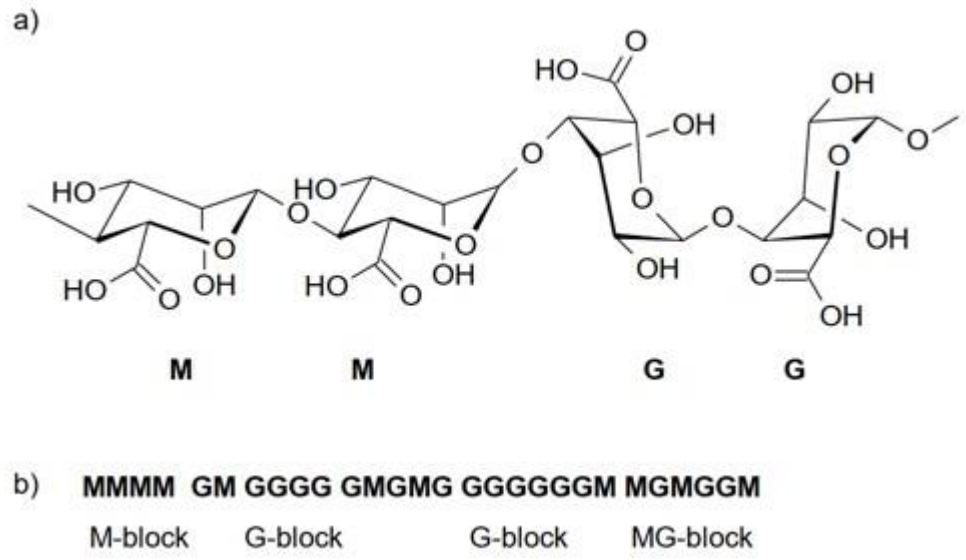


Figure II-4 – Alginate. (a) conformation of the polymer oligosaccharide chain and (b) distribution of M and G blocks in the polymer polysaccharide chain. Reprinted with permission from [18].

II-1.4. Acemannan (ACE)

Acemannan (ACE) is a β-(1,4)-acetylated soluble polymannose, and is the main bioactive polysaccharide present in the *Aloe vera* leaves [21]. Some recent studies are focused on the use of ACE for pharmacological and biological applications, reporting its effect in managing oral diseases, tumour growth, and bacterial suppression [22,23]. Besides, many works explore its immunomodulatory potential [21,24,25]. Some works even report the gel formation ability of ACE with chitosan and ALG, resulting in bioengineered films and beads, and the production of ACE-based sponges by using a methacrylation reaction [25–27]. As such, it enables its use for fabricating several bioactive tissue engineering constructs [28].

In this thesis, ACE was explored for the formation of ALG/ACE/(Ch[Caffeate]) blended formulations. In that approach, the ALG gelation ability, due to Ca^{2+} traces in the ACE composition, enables the development of different biomaterials with diverse applications. In **Chapter VI** ALG/ACE-based beads were fabricated, while in **Chapter VII** an ALG/ACE-based bioink was successful developed.

II-2. METHODS

II-2.1. Biocompatible ionic liquids (Bio-ILs) synthesis and characterization

In this section, the steps taken for the Bio-ILs synthesis and characterization will be discriminated, along with the rationale behind the cation and anion sources choice.

II-2.1.1. Bio-ILs Synthesis

All reagents were obtained and used in their commercially available forms. Herein, two phenolic-based Bio-ILs, cholinium caffeate (Ch[Caffeate]) and cholinium gallate (Ch[Gallate]), with hypothetically intrinsic antioxidant and anti-inflammatory features, were synthetized as previously described [29,30]. The presented bioactivity is owned by their anionic precursors, caffeic acid and gallic acid, respectively, which are phenolic compounds widely known for the stated features [31,32].

Briefly, cholinium hydroxide (Ch[OH]) (Sigma-Aldrich, USA) was dropwise added to either a gallic acid (Sigma-Aldrich, USA) or a caffeic acid (Sigma-Aldrich, USA) in a methanolic solution, with a molar excess of 1.1 equivalents, at 0 °C, under nitrogen atmosphere, taking place a neutralization reaction. These reaction mixtures were stirred overnight, at room temperature, protected from light, and under an inert nitrogen atmosphere, due to Ch[OH] air sensitivity. Briefly, a nitrogen flow was guaranteed into the reaction container to displace the air, keep the container atmosphere inert, and free of oxygen (Figure II-5a). The excess methanol and water resulting from the neutralization reaction were further removed using a rotary evaporator. The unreacted antioxidant acid accumulated was removed through acetone washings repeated three times, in the case of Ch[Caffeate], and methanol for Ch[Gallate], followed by filtration to recover the solid state Bio-IL. Different solvents were used to perform the washings due to the final products solubilities. The residual solvent was further removed under reduced pressure using the rotary

evaporator, and the resultant Bio-IL, either Ch[Caffeate] or Ch[Gallate] were dried under vacuum for at least 72 h, using a vacuum line, as the one depicted in Figure II-5b.

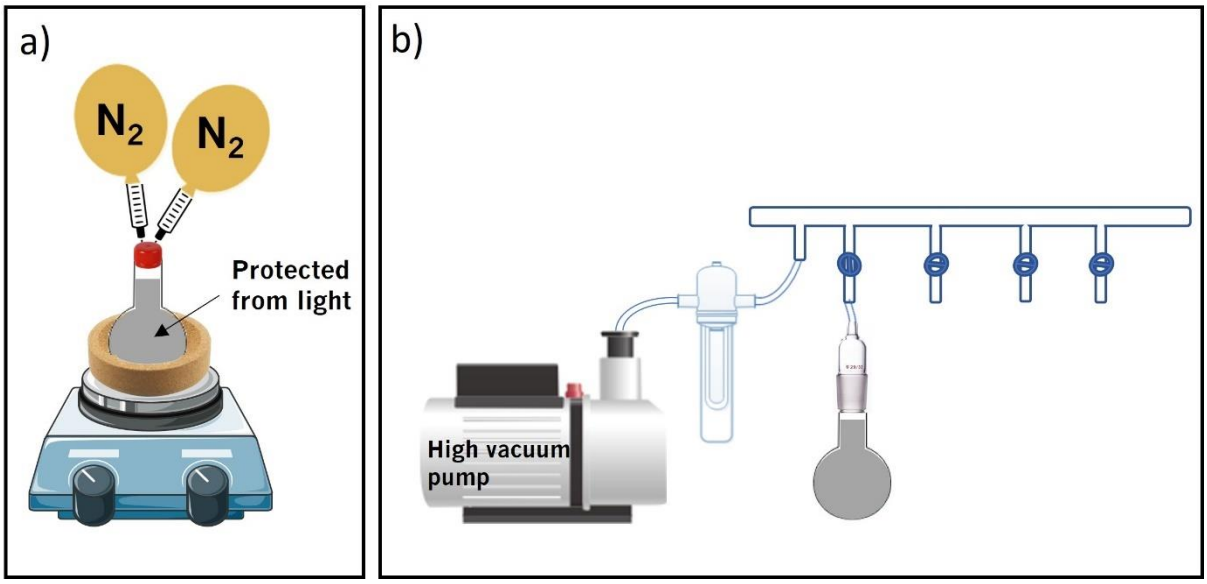


Figure II-5 – Bio-ILs synthesis experimental set-up: (a) reaction mixture in an inert atmosphere and (b) vacuum line used for drying the final reaction product.

II-2.1.2. Bio-ILs characterization

The purity and accuracy of the Bio-ILs synthesized were confirmed using ^{1}H nuclear magnetic resonance (NMR). The NMR spectra were obtained on an Avance III spectrometer (Bruker, Germany) operating at a resonance frequency of 400.13 MHz (1H). D_2O was used as a solvent and a reference for chemical shits, which are reported in ppm (parts per million).

II-2.2. Biomaterials processing

The method behind biomaterial processing plays a critical role in its final physico-chemical properties in further *in vitro* and *in vivo* behavior. In this section, the processing methodologies used for the biomaterial's fabrication in this thesis will be discriminated while detailing the suitability of the specific technique used to reach the final goal.

II-2.2.1. Preparation of silk fibroin (SF) solutions

To prepare the SF solutions used in **Chapter IV** and **Chapter V** of this thesis, *Bombyx mori* silkworm cocoons, kindly supplied by Portuguese Association of Parents and Friends of Mentally Disabled Citizens (APPACDM) (Castelo Branco, Portugal) were cut into fragments and boiled in a 0.02 M sodium carbonate (Na_2CO_3) solution, for 1 hour. This degumming process, previously described [33], allowed sericin removal from the silk fibers. Sericin is a natural protein that acts as a glue to hold the fibers together during cocoon production [34]. It is reported that sericin in SF-based biomaterials triggered inflammatory reactions [34]; therefore, its removal is needed. Further, the SF fibers were rinsed with water to remove any possible sericin residue, and the fibers were air-dried at room temperature. The dried SF fibers were dissolved by implementing a previously established protocol, using a 9.3 M lithium bromide (LiBr) solution, for 3 h, at 70 °C [35]. The SF solution was further dialyzed in a Slide A-Lyzer cassette (Pierce, 3500 Da MWCO) against distilled water for 4 days at room temperature, with water changes every 2 h. The molecular weight cut off of the membrane was 3500 Da, permeable enough to permit the exit of the LiBr salts, and to allow the water to circulate, while keeping the 25 and 390 kDa SF light and heavy chains, respectively [34]. Moreover, removing the excess of LiBr from the SF solution is mandatory since it is reported that the LiBr residues decrease the viability of fibroblasts seeded in SF films [36]. Other works show its effect in inhibiting the glycogen synthase kinase-3β, a serine/threonine kinase that controls the cell cycle progression [37].

The resultant SF solution was centrifuged for 20 min at 5000 rpm and 37 °C, and immediately used or stored at 4 °C. The final SF concentration was calculated by weighting an empty container (W1) and weighting the same boat with 1 mL of the produced SF solution (W2). The container was placed into an oven at 70 °C overnight and further weighed (W3). The concentration of the SF solution was determined using Equation II-1.

$$SF\ \%\ \left(\frac{W}{V}\right) = \left(\frac{W3-W1}{W2-W1}\right) \times 100 \qquad \text{Equation II-1}$$

II-2.2.2. Freeze-drying

In this thesis, the freeze-drying technique was used to fabricate porous polymeric architectures in **Chapter III**, **Chapter IV**, **Chapter V** and **Chapter VI**. Freeze-drying is a widespread technique that

involves three steps: the solubilization of a polymer in an appropriated solvent and its concentration; the freezing of the polymer-solvent mixture into a mold, and the gradual removal of the solvent through vacuum sublimation [38]. Moreover, the final shape of the produced biomaterial can be modulated using different types of molds. Besides, its internal structure (pore size and interconnectivity) is manageable by controlling and changing the polymer concentration and freezing method, including the freezing rate, temperature range, and time [39]. The porosity of the biomaterial is a consequence of the solvent release, which corresponds to the spaces occupied by the ice crystals. The size of ice crystals depends on the freezing rate, which ultimately depends on the freezing temperature. For instance, lower temperatures, such as – 80 °C are associated with lower freezing periods and, consequently, smaller pores [40].

II-2.2.2.1 *Chitin/Cholinium acetate-based sponges production*

First, chitin from crab shells (practical grade; Sigma-Aldrich, USA) with a degree of N-acetylation of 57.9 %, determined by elemental analysis, was ground through a Wiley Mill (model 4, Thomas), resulting in grounded α-chitin with 106 μm particle size. The potential of ILs toward the processing of natural origin polymers is well known, including the challenging α-chitin, which is often limited by its strong inter and intra-molecular bonds that difficult its solubilization. However, the use of the commonly used ILs prevents the use of the final constructs right after processing, being mandatory the removal of the solvent [41]. In **Chapter III** of this thesis, cholinium acetate (Ch[ACE]), (Iolitec-Ionic Liquids Technologies GmbH, Germany) a commercially available Bio-IL, was tested towards the dissolution of α-chitin, and its processing into 3D constructs as a sustainable and innovative strategy for the development of biomaterials using solvents with improved cytocompatibility. The complete dissolution of 1% (w/w) α-chitin was accomplished after four cycles of 2 h stirring at 90 °C, followed by a 15 min cycle of 10 seconds sonication pulses (ultrasonic processor model VCX-130PB-220). The dissolution was monitored using a Leica DM750 light microscope.

Following the dissolution, the α-chitin/Ch[ACE] mixture was molded into specific silicone molds and placed at -20° C overnight to form ionogels, since the chitin/IL mixtures cooling process leads to the formation of gels [42,43]. On the following day, the structures were stabilized by immersion in different non-solvents, namely ethanol, acetone, isopropanol, and methanol, which are known to promote the regeneration of polymeric biomatrices, including the ones containing α-chitin, as previously reported [43–46]. In other to evaluate the Bio-IL influence in further studies, two formulations were established based

on the presence (CACE-A) or absence (CACE-B) of Ch[ACE] in the final α-chitin constructs. The gels were immersed in the selected non-solvent for 2 and 24 h (with periodic changes), respectively. The immersion for 24 h allowed us to remove all the Ch[ACE] from the gels, which was monitored by conductivity measurements at each solvent change using a conductivity meter (INOLAB, Multi level 3) with a SondaWTWTetraCon 325. After, CACE-A and CACE-B gels were washed with H_2O for 2 h, and placed at -80 °C overnight to promote the ice crystal formation before freeze-drying for three days.

II-2.2.2.2 *SF and SF/Bio-IL-based sponges production*

In both **Chapter IV** and **Chapter V** of this thesis, SF and SF-based sponges were used. Firstly, and following the determination of the SF solution concentration, different SF solutions were prepared until the final concentrations of 1, 3, and 7% (w/v) were obtained, by mixing the original SF solution with H_2O. This allowed us to determine the best concentration to proceed to further studies. After, 0.5, 1, and 3 % (w/v) of the previously synthetized Ch[Gallate] were dissolved into the SF solution, frozen at -80 °C, and freeze-dried for 3 days (**Chapter IV**). This resulted in four sponges' formulations namely, SS, SChGal0.5, SChGal1 and SChGal3, containing 0, 0.5, 1 and 3 % (w/v) of Ch[Gallate], respectively in **Chapter IV.**

Moreover, SF/Ch[Caffeate] and SF/Ch[Gallate] containing 1% (w/v) of the respective Bio-IL, as well as 0.01 % (w/v) of the analgesic drug acetaminophen (ACT), only the 3% (w/v) SF solution, still following the same methodology (**Chapter V**). Herein, the SF-based sponges' formulations produced are depicted in Table II-1.

Table II-1 - Sample identification used throughout the Chapter VI

Sample	SF concentration % (w/v)	ACT % (w/v)	Ch[Gallate] % (w/v)	Ch[Caffeate] % (w/v)
SS	3	-	-	-
SS-A		0.01	-	-
SCG		-	1	-
SCC			-	1
SCG-A		0.01	1	-
SCC-A			-	1

Some studies reported the use of methanol/ethanol solutions and water-based annealing procedures [47,48], to induce the β-sheet formation. However, other work showed improved results concerning the final SF-based constructs' mechanical properties, using methanol:H_2O 4:1 solutions [17]. Considering this, after freeze-drying procedure, the β-sheet induction in the sponges was enabled by placing the samples in a desiccator containing a flask with an aqueous methanol solution:H_2O 4:1. The described system was kept under vacuum for 24 hour, to create a saturated atmosphere. The following day, the flask with the mixture was removed, and the samples were left under vacuum for an additional 24 h.

II-2.2.2.3 *Alginate(ALG)/acemannan(ACE)/ Ch[Caffeate] based beads production*

In **Chapter VI** of this thesis ALG/ACE- and ALG/ACE/ Ch[Caffeate], based beads were fabricated using the extrusion dipping method. For that, a 5 % (w/v) aqueous ALG solution and a 5 % (w/v) aqueous ACE solution were prepared. The beads were fabricated by dipping the ALG solution into the ACE bath with the support of a syringe pump (FUSION 200, Kranalytical). Based on our previous knowledge concerning the ALG gelification ability when in contact with divalent cations (**II-1.3.**), it was expected that once the 5 % (w/v) ALG solution entered in contact with the ACE, which has Ca^{2+} traces in its composition, the gelification immediately occurred, and beads were formed. The ALG extrusion was performed at 1 ml/min. For the fabrication of ALG/ACE/Ch[Caffeate]-based beads, the Ch[Caffeate]) was dissolved at different concentrations, namely 0.5, 1, and 3 % (w/v) in the ACE coagulation bath, and Bio-IL was entrapped in the beads when the gelification occurs. The beads were kept in the ACE coagulation bath overnight, aiming to maximize Bio-IL incorporation. After the beads were washed with phosphate-buffered saline to remove the unreacted ACE and immersed in a barium chloride ($BaCl_2$, Sigma-Aldrich, Portugal) coagulation bath (20 mM $BaCl_2$, 10 mM 3-(N-morpholino)propanesulfonic acid (MOPS) and 119 nM NaCl). Ba^{2+} has a significantly higher affinity towards ALG than Ca^{2+} , and has been proved to improve the stability of ALG beads [49]. Herein, and considering only Ca^{2+} traces in the ACE composition, the $BaCl_2$ coagulation bath was used to improve the beads stability. MOPS buffer was reportedly used to chelate Ba^{2+} ions from the ALG core, and to control the excess of Ba^{2+} [50,51], considering the toxicity of this ion when in excess [49]. The beads were then rinsed with phosphate buffer saline solution (PBS), frozen at -80 °C overnight, and then freeze-dried. This methodology resulted in the fabrication of different ALG/ACE-based beads formulations, containing 0, 0.5, 1, and 3 % (w/v) of Ch[Caffeate], designated as ALA, ALAC0.5, ALAC1, and ALAC3, respectively.

II-2.2.3. Three-dimensional printing

Printing technologies go back thousands of years, with Woodblock printing before 220 A.D. in China, followed by the development of the printing press in 15th century Europe [52]. In the last few decades, the revolution in this field occurred with the shifting of advanced printing technologies from two-dimensional (2D) printing to the production of three-dimensional (3D) structures. This opened new avenues towards the exploitation of the additive manufacturing process from rapid prototyping and manufacturing in a broader range of fields, including the biomedical one [52]. 3D printing was described for the first time in 1986 by Charles W. Hull, who printed thin layers of a material that was further cured with ultraviolet light, giving origin to a solid 3D structure [52]. Years later, this process was applied to the fabrication of scaffolds from biological materials, used for transplantation, with or without seeded cells [53]. Recent progress in the field naturally led to the exploitation of 3D bioprinting combining natural origin macromolecules and living cells [52]. 3D bioprinting is expected to lead to great progress in tissue engineering and biomedical fields, providing bioprinted constructs for drug screening to organ reconstruction and/or transplantation, biomolecule or cell delivery, and disease modeling. It allows to obtain tissue analogue constructs by controlling the layer-by-layer material extrusion and the 3D deposition of living cells and the supporting materials [53,54]. The latter's advantages over conventional 3D dimensional printing are obvious and include accurate cell distribution, high-resolution cell deposition, scalability, and cost-effectiveness [52]. However, some challenges remain, including the limitation of printable biomaterials, the need to improve printing scalability and speed, and the ability to produce a bioink with adequate biological features without compromising mechanical properties [52]. In **Chapter VII** of this thesis, 3D bioprinting was for the first time the used to manufacture 3D printable cell-laden ALG/ACE-based and ALG/ACE/Ch[Caffeate]-based hydrogels, with improved physical-chemical features and biological performance.

II-2.2.3.1 *ALG/ACE/Ch[Caffeate] Ink preparation*

ALG is one of the most studied polymers for fabricating of bioprinted constructs for cartilage applications by extrusion printing [55]. The critical parameters that determine the printability of this polymer are not only the bioprinter-related ones, including diameter and velocity of the nozzle, air pressure, distance, and temperature of platform and syringe, but also ALG's intrinsic properties [55]. Taking advantage of the knowledge obtained in **Chapter VI**, concerning the ALG's gelation ability in the

presence of divalent cations [18], a ink was developed by mixing ACE powder to achieve a final concentration of 5 % (w/v) in a 5 % (w/v) ALG solution (ALAC), with the help of the ultra-turrax, in ice. This mixture was processed for 10 min, at 10 000rpm, until homogeneity was reached. The process was repeated for the ALG/ACE/Ch[Caffeate] mixture (ALACaff), being additionally included 5 min stirring, in ice, at 10 000 rpm, with Ch[Caffeate] added following the processing of ALG/ACE mixtures. Additionally, a control ink was prepared using the 5 % (w/v) ALG solution and 0.35 % (w/v) $CaCl_2$ (Ctr). The prepared ALAC, ALACaff, and Ctrl mixtures were centrifuged at 9000 rpm for 5 min, to remove any air bubbles.

II-2.2.3.2 *ALG/ACE/Ch[Caffeate] printing methodology*

Each cartridge was filled with 5 ml of ink. The printing process was carried out at 13 °C using sterile material. A printing nozzle of 410 μm of inner diameter, at a printing speed of 18 mms^{-1} was used to print the 3D mesh structures: 10 x 10 x 1 mm (width x length x height) with a total of 4 layers and a pore size of 250 μm. To reinforce the stability of the structure, the 3D printed structures were ionically crosslinked for 5 min in a 5 % (w/v) $CaCl_2$ solution prepared in Dulbecco's modified Eagle's medium (DMEM)/F12.

II-2.3. Biomaterials' characterization

Herein, the techniques used for their physicochemical characterization of the developed biomaterials will be described, as well as the rationale behind their use towards a specific goal.

II-2.3.1. Fourier Transformed Infrared Spectroscopy (ATR-FTIR)

FTIR technique provides the absorption or reflectance infrared spectrum of a certain solid, liquid or gas. In the infrared region, the sample molecules selectively absorb radiation and undergo a vibrational transition, which refers to the excitation of a molecule to a higher vibrational state. Consequently, the analysis of the vibrational absorption bands in the infrared spectrum, provides the ability tp detect functional groups and identify chemical structures. In the FTIR technique, instead of irradiating the sample with a monochromatic beam of light, the beam contains many frequencies of infrared radiation at once, which allows a rapid measurement of the spectrum of the sample [56]. The attenuated total reflectance (ATR) is a sampling technique that can be coupled to the FTIR equipment. It relies on the internal reflection

of the incident IR radiation, which is attenuated by a crystal, creating an evanescent wave, part of the IR light that travels into the sample, where it can be absorbed [57]. The penetration depth of the evanescent wave into the sample is defined by the refractive index difference between the sample and the ATR crystal. The beam is then collected by a detector as it exits from the crystal. Moreover, the availability of improved equipment and software, as well as the ability to use the samples directly into their solid or liquid state, enabled a great expansion in the use of FTIR in studies of protein secondary structure and protein dynamics in the past decades [58].

An IR Prestige-21 FTIR spectrometer (Shimadzu, Japan) with the attenuated total reflectance (ATR) apparatus was used in **Chapter III**, **Chapter IV,** and **Chapter V** of this thesis, to identify different chemical structures. A transmittance spectrum was obtained by performing 32 scans in each spectrum over a range of 400-4000 cm^{-1} at a 2 cm^{-1} resolution.

II-2.3.1.1 *Determination of the deacetylation degree of chitin (DD%)*

The properties of chitin and chitosan (which is obtained by deacetylation of chitin with concentrated alkali and high-temperature treatments) strongly depend on its DD%, which concerns the deacetylated units in the polymers chains [59]. The deacetylation process mainly involves the removal of acetyl groups from the molecular chain of the polymer, leaving behind a complete amino group (-NH2). Considering that the main parameters involved in this process are temperature, reaction time, and the concentration of the reagents [59], it was mandatory to evaluate the deacetylation degree of the α-chitin after its processing with the selected Bio-IL, in the **Chapter III** of this thesis. This study was carried out using Equation II- 2.

$$DD\% = 100 \times \left[\left(\frac{A1655}{A3450}\right) \times \frac{100}{1.33}\right] \qquad \text{Equation II-2}$$

where A1655 is the absorbance at 1655 cm^{-1} (amide I band) as a measure of the N-acetyl group content, and A3430 is the absorbance at 3430 cm^{-1} (hydroxyl bands) as an internal standard. The value 1.33 represents the ratio of absorbance for a fully acetylated compound.

II-2.3.1.2 *Fourier self-deconvolution (FSD)*

FTIR is a well-established experimental technique for the analysis of secondary structure changes in polypeptides and proteins. For that, it was used in **Chapter IV** and **Chapter V** of this thesis to study the changes in the SF secondary structure after processing and β-sheet induction using methanol:H2O saturated atmosphere. For that, the Origin 9.0 Software was used to perform the FSD of the obtained infrared spectrum in the amide I region, 1595–1705 cm^{-1}. FSD spectra were a curve fitted to Gaussian line shape profiles to measure the related areas of the amide I components. After, the deconvoluted amide I spectra area was normalized, and the relative areas of the single bands were used to determine the fraction of the secondary structural elements. The band assignments used for the quantification were previously described [60].

II-2.3.2. Scanning electron microscopy (SEM)

SEM is a useful imaging technique for the characterization of the surface of the biomaterial through the acquisition of 2D high-resolution images. The principle behind this technique relies on the interactions between a beam of electrons that hits the sample, and the atoms of the sample. Briefly, when scanning a conductive material, this beam is scattered and produces signals which are detectable by the equipment, where they are transformed into a 2D image. By the position of the detected beam and the intensity of the signal, the produced image reflects the topographic details of the sample with high magnifications [61]. The success of this technique is strongly dependent on the sample preparation. Considering the need for conductivity, due to the scattering of the electron beam, SEM samples require special preparation to increase their conductivity and to stabilize them. Therefore, the samples are usually coated with a thin layer of conductive materials, such as gold, platinium or carbon. In this thesis, the morphology of the samples fabricated in **Chapter III**, **Chapter IV**, **Chapter V**, **Chapter VI** and **Chapter VII** was evaluated using a NanoSEM-FEI Nova 200 with an integrated microanalysis X-ray system (EDS – energy dispersive spectrometer). Prior to analysis, the samples were coated with gold (Fisons Instruments, Sputter Coater SC502, United Kingdom), and the micrographs were taken at different magnifications

II-2.3.3. Microcomputed tomography

Microcomputed tomography (micro-CT) analysis is a non-destructive technique that allows to analyze the microstructure of samples using a x-ray source and a stationary detector [62]. While scanning, the sample rotates, and the final result is a series of 2D cross-sections that can be processed and reconstructed in 3D images. Micro-CT gives detailed information on the sample density and microstructure information, including porosity, pore size and pore wall thickness. The microstructural features of the structures produced in **Chapters III, Chapter IV** and **Chapter VII**, namely the porosity, mean pore size, and interconnectivity, were assessed by micro-CT and using the CTanalyzer program, being previously reconstructed with the NRecon program version 1.1.3 (Skyscan). In addition, the 3D reconstructions in **Chapters III** and **Chapter IV** were obtained using the CTvox software. Samples of each formulation were scanned using a high-resolution skyscan 1072, (Skyscan, Belgium) and SkyScan 1272 (Bruker, USA). The acquisition parameters were adjusted according to the sample and are particularly detailed in each chapter.

II-2.3.4. Thermal properties – Differential scanning calorimetry (DSC)

DSC is one of the most used calorimetric techniques, being commonly used to determine the thermal properties of materials, and to establish a connection between temperature and their physical properties. DSC allows to measure how physical properties of a sample change, along with temperature, against time. During the temperature change, the apparatus measures a heat quantity radiated or absorbed by the sample based on the temperature difference between the sample and the reference material, denoting an endothermic or exothermic process [63]. Thus**,** DSC provides information regarding the enthalpies of transitions by the analysis of the resulting curve of heat flux vs. temperature.

In **Chapter III,** the DSC analysis of the produced sponges was performed, under a flowing nitrogen atmosphere between 25 and 400 °C at a heating rate of 10 °C min^{-1} using a DSC Q100 from TA Instruments instrument, allowing us to determine the influence of the Ch[ACE] presence in the final construct decomposition temperature.

II-2.3.5. Rheological studies

Rheology studies the deformation and flow of materials under an applied force. The rheological characterization of biomaterials allows to know the viscoelastic flow behavior of the developed systems, which are closely associated with their final application [64]. Polymeric and disperse systems show mechanical properties intermediate between those liquids and solids because they are composed of viscous and elastic components. The rheological analysis provides the viscosity, elasticity, and plastic behavior of materials under changes of frequency, time, or temperature. Moreover, the ratio of the G''/G' is also helpful to determine the interaction strength of the internal structure of the developed biomaterials. Samples with higher storage modulus, G' are considered elastic solids, while samples with higher loss modulus, G'', are considered as more viscous or as having a liquid behavior [65]. Meaning that the determination of these parameters allowed to study the stability of the three-dimensional network of the wet sponges produced in **Chapter III**. The oscillatory rheological measurements of the wet sponges were carried out using a Malvern Instruments Kinexus rheometer equipped with a stainless steel parallel-plate sample holder of 8 mm diameter and between 1.5 and 2.5 mm gap, which was in accordance with the height of the biomaterials.

II-2.3.6. Mechanical properties

Evaluating the mechanical properties of biomaterials is critical in biomedicine, since it allows access to the biomaterial's response to stress, its strength, and how it sustains mechanical stretching. By performing a tensile test, we can obtain a stress/strain curve that reflects the reaction of the material to the increasing stresses being applied, giving information about the point of failure, the modulus of elasticity, and the yield strength [66]. Considering the selected application towards cartilage tissue regeneration, the developed constructs must be able to support the physiologic joint loading. Moreover, when implanted *in vivo* the scaffolds are subjected to compressive forces. Thus, a 3D structure should stand the hydrostatic pressures while maintaining the spaces needed for cell growth and new matrix formation [67]. According to this, assessing the mechanical properties of the materials developed in **Chapter IV** and **Chapter V** is mandatory. Herein, the mechanical behavior of the sponges was evaluated under compression load using a Universal Mechanical Testing Equipment (Instron 5543, USA), equipped with a 50 N load cell, at room temperature.

II-2.3.7. Solid-state nuclear magnetic resonance (NMR)

Solid-state NMR has increasingly been explored for the analysis of pharmaceutical solids in the last decades since a huge number of pharmaceutical formulations are produced in a solid-state [68]. Moreover, solid-state NMR is a great tool to explore the morphology and miscibility of blended materials, being a pre-requisite to understand the structure-property relationship and, consequently, to the design of new and improved biomaterials [69,70]. Thus, in **Chapter IV** and **Chapter V** of this thesis, the solid-state NMR was performed to evaluate the possible interactions among the sponges' compounds. The spectra were measured at 298 K in a Bruker NEO-750 spectrometer (750 MHz proton frequency) equipped with a Varian T3 solid triple resonance probe 1H/X/Y that uses a zirconia rotor. The probe was adapted to the Bruker spectrometer by an A2B conversion kit (Revolution NMR, LLC). The spectrometer control software was TopSpin 4.x. All the spectra were processed with MestreNova software v14.2 (Mestrelab Research Inc.).

II-2.3.8. X-ray Photoelectron Spectroscopy (XPS)

XPS is a XPS is a surface quantitative analysis technique that provides information regarding the surface chemistry of materials, its elemental composition, and the elements' chemical and electronic state [71]. Briefly, an x‐ray source (most often AlKα or MgKα) irradiates the sample, which is in a ultrahigh vacuum, which ejects core‐level electrons from the surficial atoms. The kinetic energy of a photo‐emitted core electron is dependent on its binding energy in the atom and depends on the elements that compose the material [71]. In **Chapter VI** of this thesis, the produced beads' surface and core were subjected to XPS analysis, which allowed us to understand how the different polymers and Ch[Caffeic] were distributed in the 3D architectures in the different formulations. For that, an instrument from Kratos Axis-Supra equipped with an aluminum Kα (Al-Kα) monochromatized radiation X-ray source (1486.6 eV) and ESCApe software was used. The chemical composition of core and surface of the beads was accessed using a Constant Analyser Energy mode using an emission current of 15 mA and a 160 eV and 20 eV pass energy for survey and high-resolution spectra, respectively. The region high-resolution analysis was performed for C 1s, O 1s, Na 1s, Ca 2p, Ba 3d, and N 1s, using a linear type background to its fitting. The lower binding energy C1s photo peak, which is related to C1s hydrocarbon peak, was set at 285.0 eV for charge referencing.

II-2.3.9. Swelling

. The water uptake, or swelling ability, of an implantable biomaterial is crucial to the success of its application. The ability of a biomaterial to absorb and retain water in its structure are key features for metabolites, nutrients, and body fluids to flow throughout it [72]. Moreover, considering that 70%-85% of the cartilaginous tissue total weight is water, the ability to retain water is fundamental to promote the interaction among all cartilage's components and provide the ideal mechanical properties for this tissue to resist all the mechanical forces and stress [73]. In this thesis, the swelling percentage of the biomaterials developed in **Chapter III**, **Chapter IV**, **Chapter V** and **Chapter VI** was determined by their immersion into PBS solutions, at 37 °C, using Equation II- 3, where Ws is the weight of the swollen sample, and Wd is the weight of the dry sample.

$$Swelling = \left[\frac{Ws - Wd}{Wd}\right] \times 100 \qquad \text{Equation II-3}$$

II-2.3.10. Equilibrium water content (EWC)

Due to hydrogels great ability to absorb and retain water, they have been successfully explored toward cell encapsulation and tissue repair [74]. In the **Chapter VII** of this thesis the EWC of the biprinted hydrogels was determined by soaking them into tris-HCl-buffer (TBS) (pH 7.4) at 37 °C for 24 h. In **Chapter VII** of this thesis the EWC of the bioprinted hydrogels was determined by soaking them into tris-HCl-buffer (TBS) (pH 7.4) at 37 °C for 24 h. Previous works report the low stability of ALG-based biomaterials in the presence of phosphates and acetates present in the phosphate and acetate buffer solutions [75,76]. Therefore, TBS pH 7.4 was used as media in the further ALG-based hydrogel assays, since it reportedly increases their stability [75,76]. After, the excess of TBS in the hydrogels was gently absorbed with filter paper and weigh (Ww). TBS was used in the bioprinted hydrogels assays, instead of PBS, due to the absence of phosphate ions it its composition and Ca2+ presence, which together prevent the ALG hydrogels degradation through competition with the Ca2+ ions in the 3D structure. The hydrogels were further lyophilized for 3 days, and the weight was again recorded (Wd). The EWC (% (w/w)) was calculated using Equation II- 4.

$$EWC(\%) = \frac{w_w - w_d}{w_w} \times 100$$ Equation II-4

II-2.3.11. Biomaterials' stability

The stability/degradation of a tissue engineering constructed or drug delivery platform, should be adequate by mirroring the rate of the new tissue formation, allowing the cells to replace the biomaterial by producing extracellular matrix (ECM), or in a way that allows the controlled release of bioactive molecules [52]. In this thesis, the stability/weight loss of the fabricated sponges (**Chapter III**, **Chapter IV** and **Chapter V**) and beads (**Chapter VI**), was studied by their immersion in PBS. Furthermore, the weight loss of the 3D bioprinted constructs fabricated in **Chapter VII** was evaluated by immersion in TBS.

The weight loss was quantified using the initial weight of the sample (*wi*), and the weight of the samples after drying at 37 °C and until they reached constant weight (*wf*), using the Equation II-5. TBS is widely choose as the buffer for assays involving ALG hydrogels, instead of other buffers such as PBS, since its allows the structures to retain their original shape, due to the absence of phosphates [75,76].

$$Weight\ loss\ (\%) = \left[\frac{Wi - Wf}{Wi}\right] \times 100$$ Equation II-5

II-2.3.12. Bioactive molecules release

Herein, phenolic-based Bio-ILs were synthetized and used to produced bioactive constructs for cartilage tissue engineering purposes. To study the release of these compounds from the support polymeric matrix is mandatory to understand and target their therapeutic focus and adequate dosage [77].

In **Chapter IV** and **Chapter V** of this thesis, the Ch[Gallate] release from the sponges, was performed by their immersion in PBS, at 37 °C. At pre-determined times, 1mL of the immersion solution was collected, and the same volume of fresh PBS was added to ensure the maintenance of a constant volume. The Ch[Gallate] content was determined by UV spectroscopy using a microplate reader (Synergy HT, BIO-TEK, Winooski, VT, USA) at 259 nm. Additionally, in **Chapter V** the same procedure was carried out for the ACT cumulative release quantification, still using a different wavelength 243 nm, and

in the **Chapter VI** and **Chapter VII,** for Ch[Caffeate], at 285 nm, in the latter using TBS as the release medium, according to earlier exposed rational. The compound content at each time point was plotted as a cumulated percentage release determined using Equation II-6, where, $C_{(n-1)}$ and C_n correspond to the compound concentration at times n-1 and n, V0 is the initial volume of the release medium, V is the withdraw volume, and M is the compound mass loaded in the biomaterial.

$$Cumulative\ release\ (\%) = \frac{V_0 C_n + V C_{n-1} \times 100}{M}$$ Equation II-6

II-2.3.13. *In chemico* antioxidant activity assays

Reactive oxygen species (ROS), are known to be involved in the pathology of several cartilage-related diseases, including osteoarthritis (OA), by being harmful to chondrocytes, in a way that they may induce the apoptosis of these cells [78]. Considering the potential antioxidant activities of the synthetized Bio-ILs, its acidic precursors, the free ACT form, and ACE, it is expected to have antioxidant bioactivity on the biomaterials prepared in the **Chapter IV**, **Chapter V,** and **Chapter VI**. According to this, the *in chemico* antioxidant activities of the materials and precursors were determined using the 2,2- diphenyl-1 picrylhydrazyl (DPPH) radical scavenging assay [79]. The principle of this test is based on the color change of the DPPH solution from purple to yellow, as the radical is quenched by the antioxidant compound. This reaction was monitored by visible spectroscopy at 517 nm, using UV spectroscopy using a microplate reader (Synergy HT, BIO-TEK, Winooski, VT, USA) [29]. The DPPH radical scavenging activity, AA(%), was determined according to Equation II-7, where A_0 and A_1 are the absorbance of the control and the samples, respectively.

$$AA\ (\%) = \frac{A_0 - A_1}{A_0} \times 100$$ Equation II-7

II-2.3.14. Injection force

The injectability of a solution refers to its ability to pass through a needle easily, and it includes factors such as pressure or force required for injection [80]. This feature is also critical when using encapsulated cells (e.g., in the extrusion process) since they can only bear a certain amount of force and

remain viable. According to the literature, an injectable biomaterial can be classified as very easy to inject (injection force: 0–10 N), easy to inject (11–25 N), injectable (26–100 N), difficult to inject (100– 130 N), and very difficult to inject (>130 N) [81]. The injection force of the bioinks produced in **Chapter VII**, before cell encapsulation, was determined by performing injectability measurements (PARALAB, Porto, Portugal) with a 5 ml syringe (Termo-JPN) with a 410 μm of needle, as the one used for the bioprinting.

II-2.4. Evaluation of the antimicrobial properties of the fabricated constructs

The ability of an implantable biomaterial to have inherent antimicrobial features is currently a key aspect for the success of the implantation process [82–84]. The development of biomaterials with intrinsic antimicrobial properties has been extensively explored due to the increasingly antimicrobial resistance. Recently ILs have been explored and widely studied as a possible defense against multi-drug-resistant bacteria, with particular prominence on medicine and pharmacology [85].

In **Chapter V** of this thesis the antimicrobial activity of Ch[Gallate] and Ch[Caffeate] against *Staphylococcus aureus* (*S. aureus*), methicillin-resistant Staphylococcus aureus (MRSA), *Escherichia coli* (*E. coli),* and vancomycin-resistant *Staphylococcus aureus* (VRSA) was evaluate by the radial diffusion assay, while the antimicrobial activity of the SF/Bio-IL-based sponges was assessed against Gram$^+$ bacteria MRSA, and Gram- bacteria, *E.coli*.

The Kirby–Bauer method [86] was chosen for the radial diffusion assay but it was adapted from the original method for testing microbial resistance to antibiotic drugs. This method involves placing paper discs impregnated with the compound in the study onto the surface of agar plates, which have previously been seeded with the bacteria to be tested. Then, the antimicrobial compound diffuses into the agar where it may inhibit the bacterial growth in the surrounding disc zone [86]. In this thesis, the microbial cultures were grown in Luria–Bertani (LB) broth medium at 37 °C overnight. In the next day, the bacteria were centrifuged at 9000 rpm for 5 min at 4 °C, and then, the bacteria pellet was washed twice with sterile PBS; pH 7.4. The bacteria pellet was re-suspended in sterile PBS ; pH 7.4 adjusted to an optical density of 0.3 (λ = 610 nm) and spread onto Muller Hinton Agar (Oxoid, UK) with a sterile swab. Blank sterile disks (Oxoid, UK) were impregnated with the different concentrations of the Bio-ILs and placed on top of the inoculated agar and incubated overnight at 37 °C.

The antimicrobial properties of the SF/Bio-IL-based sponges were determined by immerging in 1 mL of LB medium inoculated with *E. coli* and MRSA, respectively, and incubated at 37°C for 24 h. The

viability, adherence, and formation of bacterial biofilms on the SS, SCG, and SCC sponges were further analyzed by Live/ Dead staining and SEM.

II-2.4.1. Bacterial viability, adherence and biofilm formation in the SF/Bio-IL-based sponges

II-2.4.1.1 *Live/Dead staining*

For the determination of the bacterial viability a Live/Dead Bacterial Viability Kit (Molecular probes, L7007, Invitrogen), was used. This is a convenient and easy-to-use kit, for monitoring the viability of bacterial populations. The rationale behind this kit performance is that bacteria with a compromised membrane, which are considered dead or to be dying will be stained with red, whereas bacteria with an intact membrane will stain green [87].

Briefly, after the incubation, each sponge was washed twice with sterile PBS, pH 7.4, and stained with 1 mL solution of the Live/Dead Bacterial Viability Kit for 15 min at room temperature, followed by washing with sterile PBS (pH 7.4) to remove excess dye. Live bacteria were stained with green using SYTO 9 and Dead bacteria were stained red using pyridinium iodide (PI) and visualized using a Confocal laser microscope (Leica TCS/SP8). The images were acquired using a digital camera (AxioCam MRm5, Zeiss) and analysed by ImageJ2 (NIH, Maryland, USA). The quantification was performed by processing the images using ImgaeJ2. Firstly, the images were transformed in a single channel 8-bit image, followed by image segmentation through converting the grey-scale image into a binary black and white image, allowing us to select the correct image threshold. After, we split the separate cells, to appear as one, by using the watershed filter. Then, the prepared image was subjected to automatic counting.

II-2.4.2. SEM sample preparation

In **Chapter V**, the SEM analysis of the sponges with fixed bacteria only differs from sub-section **II-2.3.2**. in the sample preparation methodology. Briefly, the sponges were fixed with 4 % glutaraldehyde for 60 min in the dark at room temperature. The samples were further dehydrated in a series of ethanol-water solutions with increasing ethanol concentration twice (50, 70, 80, 90, and 100%, v/v) and left to dry overnight before coating with palladium by ion sputtering.

II-2.5. Biological assessment assays

Following the biomaterials production, optimization, and characterization, it is mandatory to verify their cyto-compatibility. This section includes the methodologies used for the biological characterization of the fabricated biomaterials, including the used cell types, the cell seeding procedures and the techniques used to evaluate the cellular performance, considering our final goal as the management of cartilage related pathologies. The cell viability, proliferation, morphology, and overall performance of the cells were evaluated, and the used procedures and the rationale behind their use are herein briefly described.

II-2.5.1. Cells used in the study

Cell culture tests *in vitro* are mandatory before any *in vivo* validation. The work herein developed was carried out using different cell lines, as well as primary cells. The cells may be removed from the original tissue by enzymatic or mechanical means - being named as primary cells – or they can be chemically or virally induced to acquire the ability to divide indefinitely into a specific cell type – being named cell lines. The following sub-section includes a description of the cells that were used throughout this thesis, including their nature, origin, and the subculturing method for the following *in vitro* tests.

II-2.5.1.1 *L929*

L929 L929 is a mouse fibroblast cell line standardly used for cytotoxicity studies, the initial method used to determine the potential toxicity of developed biomaterials. L929 cell line from mouse connective tissue was used in **Chapter III** and **Chapter V** of this thesis. L929 cells, purchased from the European Collection of Authenticated Cell Culture, England (ECACC, UK) were cultured in DMEM low-glucose supplemented with 10% heat inactivated fetal bovine serum (FBS, Gibco) and a 1 % antibiotic–antimycotic (ThermoFisher) mixture. The L929 cells were incubated in 5 % CO_2 at 37 ^{o}C, and the medium changed every 2-3 days. Cells were routinely trypsinized (0.25 % trypsin–EDTA solution; Life Technologies, Carlsbad, CA, USA), centrifuged at 300 g for 5 min (Eppendorf 5810R centrifuge equipped with an A-4-62 rotor), and re-suspended at a density of 5 x 10^{5} cells in T150 cell culture flasks (BD Biosciences, Enzifarma, Porto, Portugal).

II-2.5.1.2 *Human adipose stem cells (hASCs)*

hASCs are of special interest due to its limited autoimmune response, potential *in vitro* cell expansion, high ability to differentiate into several cell lineages, including into chondrocytes [88,89]. As a first approach, the use of hASCs allowed us to evaluate and conjecture the biological behavior of the developed constructs, since these cells are more sensitive than cell lines.

hASCs were used in **Chapter III** and **Chapter IV** of this thesis and were obtained from sub-cutaneous fat tissue under protocols established with the Plastic Surgery Department of the Hospital da Prelada (Porto, Portugal), isolated (following a very well optimized protocol approved by the Ethics Committee of University of Minho) using enzymatic digestion. The isolation protocol was divided in three main steps:

i) collection of human adipose tissue by liposuction aspiration and washing in phosphate buffered saline (PBS) with 1 % antibiotic

ii) enzymatic digestion with 0.05 % (w/v) of collagenase type II (Sigma, USA) under agitation for 45 min, at 37°C

iii) the resulting stromal vascular fraction (SVF) pellet (with hASC and other cells), obtained after filtration and centrifugation (800 g, 10 min, 4 °C) was re-suspended in red blood cell lysis buffer (155 mM of ammonium chloride, 12 mM of potassium bicarbonate and 0.1 mM of ethylenediaminetetraacetic acid, all from Sigma-Aldrich, Germany) for 10 min, at RT,

iv) after centrifugation (300 g, 5 min, RT), the supernatant was discarded and the cell pellet re-suspended and cultured in MEM alpha medium (α-MEM; GibcoR, Life Technologies, Carlsbad, CA, USA), supplemented with 2.2 g/L of sodium bicarbonate, 10% (v/v) of FBS and 1% (v/v) of antibiotic/antimycotic solution (complete **α**-MEM medium) and maintained at 37 °C, in an incubator with 5% CO_2 atmosphere. Human ASCs were selected by plastic adherence and harvested (P0) 7 days after isolation at 90% confluence.

The phenotype of hASCs has been extensively characterized using tissue samples obtained from the same anatomic region (abdominal subcutaneous adipose tissue), collected using similar techniques and isolated following the same procedure. Isolated hASCs were characterized by RT-PCR for CD44, STRO-1, CD105 and CD90 markers [90,91].

hASCs were routinely cultured using **α**-MEM medium and regularly trypsinized (0.25 % trypsin–Ethylenediaminetetraacetic acid (EDTA) solution; Life Technologies, Carlsbad, CA, USA) for 5 min, at 37

°C, centrifuged at 300 g for 5 min (Eppendorf 5810R centrifuge equipped with an A-4-62 rotor), and re-suspended at a density of 5 x 10^5 cells in T150 cell culture flasks (BD Biosciences, Enzifarma, Porto, Portugal).

II-2.5.1.3 *THP-1*

Inflammation and inflammatory cytokines release are crucial for the occurrence and progression of OA, as well as other cartilage related pathologies [92]. LPS-stimulated THP-1 macrophages have been widely used as an inflammation model [93,94]. Considering the potential anti-inflammatory effect of the produced biomaterials, and their further application as solutions for OA management, this cell line was used in the **Chapter IV**, **Chapter V**, **Chapter VI** and **Chapter VII**.

Human monocytic cell line (THP-1) (SIGMA, USA) was expanded, in suspension, using RPMI 1640 Medium, GlutaMAX™ Supplement, HEPES (Thermo Fisher Scientific, USA), supplemented with 10% FBS and 1% (v/v) antibiotic/antimycotic, under standard culture conditions (37°C in a humidified atmosphere containing 5 % CO_2).

II-2.5.1.4 *ATCD5*

The chondrogenic like ATDC 5 cell line was used in the **Chapter V**, **Chapter VI** and **Chapter VII** of this thesis. This cell line is derived from mouse teratocarcinoma cells and is characterized as a chondrogenic cell line that undergoes a sequential process analogous to chondrocyte differentiation. It was reported that during cell culture of ATDC5 cell line, cartilaginous nodules were formed through cellular condensation, with the cells exhibiting the phenotype of chondrocytes. Thus, these cells are considered as excellent *in vitro* model to study chondrocyte related pathologies, including osteoarthritis (OA) [95].

ATDC5 cell line was purchased from the European Collection of Authenticated Cell Culture (ECACC, UK), England. This cell line was expanded in DMEM/F12 medium (Dulbecco's Modified Eagle Medium: Nutrient Mixture F-12, Thermo Fisher Scientific, USA), supplemented with 10% FBS, sodium bicarbonate (Sigma-Aldrich, USA) and 1 % antibiotic/antimycotic, under standard culture conditions (at 37 °C, with 5 % CO_2, in a 95% humidified incubator). Cells were regularly trypsinized (0.25 % trypsin–Ethylenediaminetetraacetic acid (EDTA) solution; Life Technologies, Carlsbad, CA, USA) for 5 min, at 37 °C, centrifuged at 300 g for 5 min (Eppendorf 5810R centrifuge equipped with an A-4-62 rotor), and re-

suspended at a density of 5 x 10^5 cells in T150 cell culture flasks (BD Biosciences, Enzifarma, Porto, Portugal).

II-2.5.1.5 *Primary human chondrocytes (HC) and primary human osteoarthritis chondrocytes (HC-OA)*

Aiming to obtain more physiologically relevant results, human chondrogenic primary cells, previously isolated and characterized [96] (HC and HC-OA), were used in the **Chapter V** of this thesis.

Briefly, they were obtained from human cartilage during arthroscopic surgeries on male and female donors with ages between 19 and 56 years (Centro Hospitalar Póvoa do Varzim). The articular cartilage was removed from the bone and cut into small pieces. The samples were washed several times with 1 % PBS/antibiotic-antimycotic (v/v) solution, digested with 0.08 % collagenase type II (Sigma-Aldrich, USA)/DMEM/F12 medium 1:1 (v/v), and incubated at 37 °C, in a water bath overnight, with gentle agitation. The digested tissue was filtered, and cell suspension centrifuged at 500 *g* for 5 min.

HC cells were expanded and cultured in DMEM/F12 medium (Dulbecco's Modified Eagle Medium: Nutrient Mixture F-12, Thermo Fisher Scientific, USA), supplemented with 10 % of FBS, sodium bicarbonate (Sigma-Aldrich, USA) and 1 % (v/v) antibiotic-antimycotic, under standard culture conditions (at 37 °C, with 5 % CO_2, in a 95% humidified incubator). Cells were regularly trypsinized (0.25 % trypsin–Ethylenediaminetetraacetic acid (EDTA) solution; Life Technologies, Carlsbad, CA, USA) for 5 min, at 37 °C, centrifuged at 300 *g* for 5 min (Eppendorf 5810R centrifuge equipped with an A-4-62 rotor), and re-suspended at a density of 5 x 10^5 cells in T150 cell culture flasks (BD Biosciences, Enzifarma, Porto, Portugal).

II-2.5.2. Cryopreservation

The cryopreservation of the cells used in this thesis was carried out using a Statebourne Biosystem 24 cryogenic tank (Statebourne Cryogenics Ltd., UK). The cell suspensions of 1x10^6 cells/mL were prepared in 10% (v/v) DMSO (N182, VWR, Radnor, PA, USA) in FBS, and transferred into 1.5 mL cryovials (479-6841, VWR, Radnor, PA, USA). Then, cell suspensions were transfered to Mr. Frosty containers and kepf at -80 °C freezer for a minimum period of 12 h. The cryovials were subsequently stored at -176 °C in the cryogenic tank.

II-2.5.3. Seeding strategies

The seeding strategy must be adjusted depending on the area the substrate and on whether it is a 2D or 3D seeding, prior to the *in vitro* validation assays.

II-2.5.3.1 *2D cell culture assays*

In **Chapter VI**, confluent ATDC5 were harvested and seeded at a density of 2×10^6 cells/cm^2, in a 24-well plate. After 24 h, the ALG/ACE beads, containing the bioactive Ch[Caffeic], were added to the culture medium. After each of the selected times of culture, the cells' metabolic activity, viability and proliferations were accessed, aiming to evaluate the performance of the developed drug delivery system when in contact with ATDC5 chondrocyte-like cells. The cells were kept in culture for 30 days with specific time points (1, 7, 14 and 21 days) to evaluate the evolution of the cellular performance.

In **Chapter V** of this thesis the ATDC5 and the L929 cell line were seeded at a density of 1×10^6 cells/cm^2, in 48 well plates, and incubated for 24 h in a CO_2 incubator, prior to the extract's addition (II-2.4.4.2. MEM extract assay). The cells were kept in culture for 3 days, and the cell viability was evaluated after 1, 2 and 3 days.

HC and HC-OA were also cultured in **Chapter V** of this thesis, in DMEM/12 at a density of 1×10^6 cells/cm^2 in a 96 well plate, aiming to further evaluate the influence of the fabricated sponges in the intracellular ROS scavenging. The HC were kept in culture for 48 h, time after which the intracellular ROS were evaluated.

II-2.5.3.2 *THP-1 monocytes*

In **Chapter IV**, **Chapter V**, **Chapter VI** and **Chapter VII** of this thesis, THP-1 cell line was expanded in suspension in DMEM/F12 until the ideal cell density was reached. Afterwards, the cells were centrifuged at 300 *g* for 5 min, and seeded at a density of 5×10^5 cells/cm^2, in 24 well plates. The cells were seeded in RPMI medium with 100 nM Phorbol 12-myristate-13 acetate (PMA) (Sigma-Aldrich, St. Louis, MO, USA) for 24 h, aiming to induce the differentiation into adherent macrophage-like cells. After incubation, an additional volume of RPMI medium was added to the wells without PMA and incubated for additional 48 h. Then, THP-1 cells were incubated with 100 ng.mL^{-1} of LPS in RPMI medium and

incubated for 5 h, to induce the inflammatory response. After the 5 h incubation, the respective biomaterials were added to the cell culture. The cells were kept in culture for 7 days, without media changes, with a 500 µl RPMI addition after 3 days of culture, in **Chapter IV**, **Chapter V** and **Chapter VI**. In **Chapter VII** the cells were kept in culture for 3 days.

II-2.5.3.3 *3D cell culture assays*

In **Chapter III** and **Chapter IV** of this thesis, aiming to assess the biological behavior of the produced constructs, hASCs were harvested and seeded at a density of 3×10^5 cells/cm^3 and 2×10^5 cells/cm^3 (respectively, in **Chapters III** and **IV**), on the top of SF sponges using the droplet method. In this seeding methodology the total amount of cells per structure was resuspended in 20 µL of α-MEM (concentrated droplet), and left for 3 h to promote cell attachment, before addition of medium (1 ml). The cells were kept in culture for 7 days to evaluate the cellular behavior.

In the **Chapter V** the same technique was used to seed HC and HC-OA into the fabricated SF sponges, at a density of 1×10^6 cells/cm^3 per sponge. This assay was carried out in order to evaluate 3D architectures' ability to support HC adhesion and proliferation. The cells were kept in culture for 21 days, with specific cell culture time points after 1, 7, 14 and 21 days.

II-2.5.3.4 *Bioink cell encapsulation*

The cell-laden bioinks, prepared in the **Chapter VII** of this thesis, were prepared by encapsulating 8×10^6 cells/ml of ATDC5 chondrocyte-like cells. Briefly, 300 µl of culture medium containing the respective number of cells, were transferred by pipetting into the middle of 5 ml of each bioink blends, and carefully manually stirred to create a homogenous distribution of the cells. The printing procedure was carried out as described in II-2.2.3.1 and II-2.2.3.1, and the cell-laden constructs were kept in culture using DMEM/F12, for 14 days, with specific time points after 1, 7 and 14 days.

II-2.5.3.5 *Co-culture studies*

In the **Chapter VII** of this thesis the human monocyte cell line THP-1 was selected to investigate the crosstalk between macrophages and encapsulated ATDC5 cells, using co-culture systems. Cell lines offer an easy, inexpensive and stable platform, which allows consistent and reproducible results. This co-

culture system was employed to investigate how the inflammation scenario, characteristic of early-stage OA, interferes with the encapsulated ATDC5 viability, adhesion and proliferation. For that, THP-1 cells were seed as described in the subsection II-2.4.3.2. Following the 5 h of LPS incubation, the bioprinted constructs (II-2.2.3.1 and II-2.2.3.1) were included in the cell culture system using cell culture inserts, as depicted in Figure II-6, for 7 days, with specific time points after 1 and 7 days.

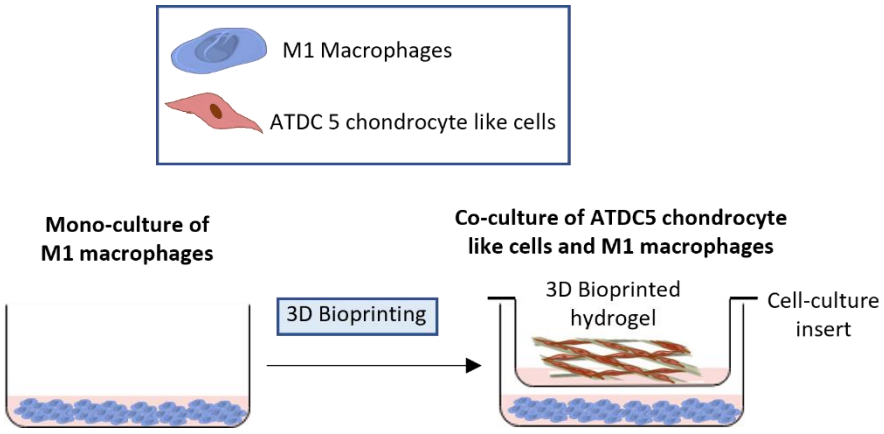


Figure II-6 – Schematic representation of the 3D bioprinted constructs and THP-1 co-culture systems

II-2.5.4. Biological performance tests

It is mandatory to evaluate how the microenvironment in which the cells are cultured affects their behavior, whether their cultured in 2D or 3D culture systems. At a first approach the cytotoxicity of the developed biomaterials must be assessed. After, the cell adhesion and proliferation, the cell morphology and distribution throughout the biomaterial, in 3D cultures, as well as the overall biological performance of the constructs must be determined. The assays used to study the cells biological behavior are herein briefly described.

II-2.5.4.1 *Cell viability assay*

The cell viability assays allow to determine if the studied molecules and/or biomaterials display direct cytotoxic effects that eventually lead to the cell death [97]. These effects are a direct consequence of contacting with certain molecules or with compounds that are released from the biomaterials, during the culture time.

Herein, the 3-(4,5-dimethylthiazol-2-yl)-5-(3-carboxyme-thoxyphenyl)-2-(4 sulfophenyl)-2H tetrazolium (MTS) assay was used to quantitatively evaluate the cellular metabolic activity, in **Chapter III**, **Chapter**

IV, **Chapter V**, **Chapter VI** and **Chapter VII.** Briefly, the metabolic activity of cells seeded in the sponges (**Chapter III**, **Chapter IV and Chapter V**), in contact with the beads **(Chapter VI)** or encapsulated into the bioprinted hydrogels (**Chapter VII)** was evaluated using the CellTiter 96 AQueous One Solution Cell Proliferation Assay (MTS, Promega). The constructs with the seeded/encapsulated cells or the cells seeded in the bottom of the plates, were placed in a mixture containing serum-free cell culture medium and MTS reagent at a 5:1 ratio, and incubated for 3 h, at the end of which the optical density was read (OD 490 nm) using a microplate reader (Synergy HT, BIO-TEK, Winooski, VT, USA).

II-2.5.4.2 *MEM extract assay*

The MEM extract assay is a cytotoxicity test which provides the rate of cytotoxicity of leachable released from biomaterials. To obtain the extracts, the materials are incubated in culture medium for 24 h at 37°C, with agitation. After the incubation, the extracts are filtered and added to a monolayer of cells. The effect of exposition of cells to the extract is measured after 1, 2 and 3 days by MTS, and cell morphology. The MEM extract assay was used in the **Chapter V** of this thesis to establish the rate of cytotoxicity of leachable from the developed sponges and their effect in the intracellular ROS production. Moreover, it was also carried out to evaluate the cytotoxicity of different ACT concentrations prepared in cell culture medium, to stablish de values for further studies. Briefly, if the extract contains toxic leachable from the biomaterials, the cells will react with cell growth inhibition, decrease/increase metabolism, intracellular granulation, cell death, or a change in the cell morphology. To further evaluate the cytotoxicity the MTS assay was performed.

II-2.5.4.3 *Live/Dead assay*

The live/dead assay is carried out using two fluorescent molecules that differentially label live and dead cells. The Live cell dye – calcein-AM – labels intact, viable cells green, the dead cell dye – propidium iodide (PI) – labels cells with compromised plasma membranes red. Calcein-AM is a highly lipophilic acetomethoxy form of calcein, being a cell membrane permeable dye. It requires the presence of intracellular esterases for the desterification of calcein AM and also plasma membrane integrity for the retention of the fluorescent calcein product [98]. On the other, PI is cell membrane impermeable and thus it binds to the cytoplasmic DNA when the cellular membrane of dead cells is disrupted. cells. When bound to DNA, the fluorescence produced by PI is enhanced 40-fold, allowing its detection by fluorescence

microscopy. The live/dead assay was herein used as a qualitative measurement of the viability, being used as a complement for the quantitative assays.

Briefly, in the **Chapter III**, **Chapter IV**, **Chapter V** and **Chapter VI** of this thesis the fluorescent dyes, PI and Calcein-AM were incubated with the constructs in PBS for 15 min, at 37 °C. After this time, the constructs were analyzed using a confocal microscope (TCS/SP8, Leica, Wetzlar, Germany). Images were recorded digitally and further processed using LASX software (Leica) and ImageJ2. The same procedure was carried out in **Chapter VII** but using TBS instead of PBS to prepare the dye solution.

II-2.5.4.4 *Cell proliferation quantification*

It is mandatory to quantify the cell proliferation in order to understand the effect of the produced biomaterials in the mitotic activity of the cells in culture. There are several methods available to quantify the cell proliferation but the most popular are based on nucleic acid binding dyes, which are also the most sensitive ones [99].

In **Chapter III**, **Chapter IV**, **Chapter V**, **Chapter VI** and **Chapter VII** of this thesis the commercially available kit Quant-iT™ PicoGreen™ dsDNA Assay (ThermoFisher) was used to evaluate cellular proliferation. When bound to dsDNA, PicoGreen has a maximum fluorescence enhancement, with little or no interference by ECM proteins produced by the cells. Briefly, the constructs with the seeded cells, or the cells seeded in the bottom of the plates, were washed with PBS, immersed in Milli-Q water, incubated 1 h at 37°C, and frozen at -80 °C, until further use. This process allows the cells to be lysed by osmotic shock and the resulting supernatant (containing the DNA) was used for the assay. The fluorescence of each specimen was measured by incubating samples with Picogreen for 10 min, according to manufacturer instructions. Fluorescence was measured using a microplate reader (Synergy HT, BIO-TEK, Winooski, VT, USA) at an excitation wavelength of 485 nm, and an emission wavelength of 528 nm. Standard curves of DNA were also prepared according to manufacturer instructions.

II-2.5.4.5 *Cell morphology and distribution*

The morphology adopted by cells after contact with the different biomaterials or culture environments is a key feature to validate the biological performance of the fabricated constructs, as well as to evaluate their phenotypic impact [100]. Cell morphology and distribution after seeding/encapsulation was

evaluated in the **Chapter III**, **Chapter IV**, **Chapter V**, **Chapter VI** and **Chapter VII** of this thesis using DAPI (4′,6-diamidino-2-phenylindole)/Phalloidin-TRITC (Ph) staining. Ph is a bicyclic peptide that when conjugated to fluorescent dyes, binds to actin filaments in fixed and permeabilized cells. Cell cytoskeleton has critical functions in the intracellular organelle transport, cell division, motility, and signaling, thus providing vital information about the cytoskeleton dynamics, namely orientation and colonization. On the other hand, DAPI is a blue-fluorescent stain with high affinity for DNA, being frequently used as a nuclear counterstain [101].

Briefly, the cells were fixed with 10% formalin buffered solution and kept at 4 °C. In a different way, in **Chapter VII** the samples were fixed using paraformaldehyde. For permeabilization, 0.2% (v/v) Triton X-100 in PBS was added for 5 min and DAPI (1:1000)/Ph (1:100) were used for nuclei and cytoplasm staining, respectively, for 20 min. The images were further acquired by using a laser scanning confocal microscopy imaging system (TCS SP8, Leica, Wetzlar, Germany) using an excitation wavelength of 405 nm for DAPI, and 561 nm for Ph.

II-2.5.4.6 *Intracellular ROS detection*

ROS are usually produced in low levels in articular chondrocytes, and they are vital in the control of the intracellular signaling mechanisms that contribute to homeostasis of the cartilage. ROS are able to modulate chondrocyte apoptosis, the gene expression, the ECM synthesis/breakdown, and also the cytokine production. However, in pathological scenarios, such in patients in OA, it was reported an overproduction of ROS which ultimately ends in cartilage degradation. Hence, it is clear the role of the oxidative stress in cartilage related diseases [102]. In the **Chapter V** of this thesis, HC seeded at a density of 4×10^3 cells/well, in a 96 well plate, contacted with the leachable of the produced sponges, in DMEM-F12 for 24 h. In the following day, after removing the medium and washing the cells, twice, with Hank's Balanced Salt Solution, without phenol red (HBSS, Cytiva - GE Healthcare Europe GmbH), the oxidative stress was induced by adding 100μM and 500 μM of hydrogen peroxide (H_2O_2), in DMEM-F12, for 3 h [103]. After 3 h, the cells were rinsed with HBSS (twice), and incubated with 5 μM of 2′,7′-Dichlorofluorescin diacetate (H_2DCFA, Sigma Aldrich), in HBSS, for 30 minute at 37 °C, in the dark. After incubation, the fluorescence intensity was measured using a microplate reader (Synergy HT, BIO-TEK, Winooski, VT, USA; Ex: 495nm, Em. 529 nm), and the metabolic activity of the cells determined using CellTiter 96® AQueous One Solution Cell Proliferation Assay (MTS, Promega), by reading the optical density 490 nm, also in a microplate reader (Synergy HT, BIO-TEK, Winooski, VT, USA).

II-2.5.4.7 *Real-time polymerase chain reaction (RT-PCR)*

Polymerase chain reaction (PCR) is a widely used technique in molecular biology that provides the amplification of a small amount of DNA, in several cycles, enabling detailed studies of gene expression. To evaluate transcripts expression, in the first step the total RNA needs to be isolated and transcribed to cDNA by using reverse transcription. The cDNA enters a series of temperature cycles which enable its denaturation, and subsequently the annealing of the selected primers and amplification, by the DNA polymerase enzyme. By using real-time PCR, the accumulation of amplification product is measured as the reaction progresses, in real time, with product quantification after each cycle. We have used SYBR® Green as intercalating DNA dye. The intensity of the dye's fluorescence increases with each successive PCR cycle and can be used to quantify DNA in the reaction [104]. Herein, RT-PCR was carried out to evaluate the effect of the sponges produced in the **Chapter V** in HC and HC-OA gene expression seeded onto them.

Total RNA isolation was performed using the Trizol reagent, which is a ready-to-use reagent for the isolation of high-quality total RNA, DNA and protein from biological samples. After each experimental time, the samples were washed with PBS, immersed in Tri reagent (TermoFisher Scientific), and kept at -80 °C for later RNA extraction. The RNA extraction was performed using the Direct-zol kit (Zymo) according to manufacturer's instructions. Briefly, samples were defrosted on ice and homogeneized by vortex, to guarantee the lysis and removal of cells within the scaffolds. After precipitation with 100% ethanol, the mRNA was washed, and then resuspended in DNAse/RNAse-free water. To quantify total RNA, a Nanodrop ND-1000 spectrophotometer (ThermoFisher, USA) was used. One microgram of total RNA was reverse transcribed to obtain a pool of cDNA that was then used for real-time PCR with specific primers. Real-time PCR was used in all experimental conditions to detect the gene expression of inflammation and cartilaginous related genes. cDNA synthesis was carried out using the commercial kit qScript cDNA Synthesis kit (Quanta BioSciences, USA). The cDNA was further used as a template for the amplification of the genes of interest. Herein SYBR Green was used for the detection of amplification in real-time PCR. SYBR Green is a nonspecific fluorescent dyes that intercalate with any double-stranded DNA [104]. The primers were designed using the Primer3 software and synthesized by MWG Biotech and the sequences are presented in Table I-1. Human Beta-2 microglobulin (hB2M) was used as reference gene, and the expression of all target genes was normalized to the expression of this gene for the same sample. The

gene expression quantification was performed according to the Livak method ($2^{-\Delta\Delta_{Ct}}$ method) [105], according to Equation II-8, considering the negative control as calibrator.

$$Fold\ expression\ (FE) = 2^{-\Delta\Delta Ct} \qquad \text{Equation II-8}$$

Table II-2 – Sequence of the primers used for real-time quantitative RT-PCR analysis

	Primer sequence	Accession number
Human Beta-2 microglobulin (hB2M)	F – TGGAGGCTATCCAGCGTACT R – CGGATGGATGAAACCCAGACA	NM_004048.2
Human tumor necrosis factor (TNF-α)	F – ATGTTGTAGCAAACCCTCAAGC R – TGATGGCAGAGAGGAGGTTG	NM_000594.4
Human interleukin 6 (IL-6)	F – AGGAGACTTGCCTGGTGAAA R – GCATTTGTGGTTGGGTCAG	NM_000600.5
Human nitric oxide synthase 2 (NOS2)	F – GGACATCGCGTGGGTGAA R – TTTATCGCTCGGAGCCTGC	NM_000625.4
Human cyclooxygenese-2 (COX-2)	F – ATGGGGTGATGAGCAGTTGT R – GAAAGGTGTCAGGCAGAAGG	NM_000963.3
Human transforming growth factor β (TGF-β)	F – AACAAAAAGGTACATGGCCCC R – CCACCAATGGAACATCGTCG	NM_000660.7
Collagen, Type II, apha 1 (COL2A1)	F – CGGTGAGAAGGGAGAAGTTG R – GACCGGTCACTCCAGTAGGA	NM_001844.5

II-2.5.4.8 *Glycosaminoglycans (GAGs) quantification assays*

GAGs are cartilage-specific extracellular matrix components which play a crucial role in the regulation and expression of the chondrocyte-like phenotype, and support chondrogenesis both *in vitro* and *in vivo* [106]. This means that the fabricated biomaterials should be able to provide the adequate cues for GAGs production and accumulation, along the culture time.

II-2.5.4.8.1 Dimethylmethylene blue (DMB) assay

The dye 1,9-dimethylmethylene is a thiazine chromotrope agent that presents a change in the absorption spectrum due to the induction of metachromasia when bound to sulfated GAGs enabling rapid

detection of GAGs in solution [107]. As a first approach, in the **Chapter VI** of this thesis, the chondrogenic ECM formation was assessed using the DMB assay as a GAGs quantification method.

Briefly, the GAG standards were obtained by preparing a chondroitin sulfate solution that ranged from 0 to 50 μg/ml. To each well of a 96-well plate were added samples or standards in triplicate, and then the dimethyl methylene blue reagent (DMB, Sigma-Aldrich) was added. The OD was immediately measured at 525 nm, on a microplate reader (Synergy HT, BIO-TEK, Winooski, VT, USA). A standard curve was created, and GAG sample values were read from the standard graph.

II-2.5.4.8.1 Alcian Blue staining

Alcian Blue (Sigma, USA) staining is primarily used to stain acid mucopolysaccharides. It is a positively charged, very large, molecule that binds to the negatively charged low density mucin found in biological tissues [107]. In the **Chapter VI** of this thesis the alcian blue staining was used to visualize the glycosaminoglycans (GAGs) content produced by ATDC5 cells [108], after contact with the ALG/ACE and ALG/ACE beads. Cells were fixed in 1% w/v acetic acid solution, for a few seconds and stained with 1% Alcian blue 8GX in 0.1 M HCl, for 1 hour. Cells were washed in H_20, and images were captured using a Leica DM750 microscope.

II-2.5.4.9 *Hemolytic properties*

The hemolytic properties test allows to evaluate how the produced biomaterials interact with the blood components, which is crucial for a successful implantation. The most abundant blood cells are the erythrocytes, which are responsible for oxygen and carbon dioxide exchanges [109]. The hemolytic properties of the SF-based sponges, produced in the **Chapter IV** of this thesis, were assessed using erythrocytes from whole human blood. The blood was continually mixed and further centrifuged at 200 *g*, for 20 min(Centrifuge Eppendorf, 5810 R), followed by removing the top layer, which contains the red blood cells concentrated (RBC). The RBC was washed three times with PBS, and centrifuged at 3700 rpm for 5 min, to remove the supernatant. This process was performed three times. The RBC was diluted in PBS to a final concentration of 5% (w/v). Each sponge was seeded with 400μL of the RBC solution and incubated for 60 min, at 37 °C. After that, the samples were subjected to centrifugation, at 3700 rpm for 5 min, and the supernatant was collected. PBS and 1% SDS solution were used as negative and

positive controls, respectively. The absorbance of the collected supernatant was read at 540 nm of wavelength in a microplate reader (Synergy HT, BIO-TEK, Winooski, VT, USA). The hemolytic rate was determined using Equation II-9.

$$\text{Hemolytic rate } (\%) = \frac{Abs_{sample} - Abs_{PBS}}{Abs_{Triton} - Abs_{PBS}} \times 100 \qquad \text{Equation II-9}$$

II-2.5.4.10 *Cytokines release quantification in THP-1 differentiated macrophages*

The cartilage degeneration, particularly in OA scenarios, is strongly associated with inflammation, being characterized by the overproduction of pro-inflammatory cytokines in the synovium [110]. In the **Chapter IV**, **Chapter V**, **Chapter VI** and **Chapter VII** of this thesis, the cytokines secreted by THP-1 activated macrophages, in contact with the produced biomaterials, were evaluated, aiming to assess their potential towards the control of the inflammatory process in the cartilaginous tissue.

II-2.5.4.10.1 Enzyme-linked Immunosorbent Assay (ELISA)

ELISA is an analytical biochemistry assay used to detect and measure soluble ligands, such as antibodies, antigens, proteins or peptides in biological samples. In **Chapter IV**, **Chapter V** and **Chapter VI** of this thesis, ELISA was used to quantify the products secreted by THP-1 macrophages after contacting with the biomaterials in study. The ELISA procedure relies on antigen-antibody binding, in which the antigen is quantified using a solid-phase enzyme immunoassay. It is a highly specific and sensitive methodology because of this antigen-antibody reaction [111].

Firstly, the culture medium was collected, and frozen at -80 °C, until analysis. The ELISA assays were performed using several commercial ELISA kits namely IL-10 (900-K21, Peprotech), as an anti-inflammatory cytokine quantification kit, and TNF-α (EK0525, Tebu-Bio) and IL-6 (900-K16, Peprotech), as pro-inflammatory cytokine quantification kits.

In the **Chapter VII** of this thesis, the cytokines secreted by the THP-1 macrophages co-cultured with ATDC5, encapsulated in the bioprinted hydrogels, were quantified using the Luminex. The Luminex uses magnetic bead sets marked with differing ratios of two different fluorophores, conjugated with

monoclonal antibodies specific for different cytokines or chemokines. Once the cytokine of interest has bound, a secondary detection antibody specific for the interest molecule is added [112]. The beads were further read on a Luminex machine (Bioplex-100, Bio-Rad) which has two lasers, one that identifies the bead, and consequently the specific cytokine or chemokine, and another that can detect the amount of the detection agent on the bead. Altogether this data is used to quantify the molecule of interest. The quantification of the human cytokines in the supernatants previously collected, and frozen at -80 °C, was assessed using a Cytokine 10-Plex Human Panel (Fisher Scientific, Austria), using Luminex™, and the assay was performed according to the manufacturer instructions.

II-2.6. Statistical Analysis

All quantitative data are presented as mean ± standard deviation (SD). Statistical analyses were performed using a GraphPad Prism 8.0 software (GraphPad Software, USA). The different sets of samples were initially tested for Gaussian distribution (Normality). In case of a positive result, samples were analyzed by Ordinary 1-way ANOVA followed by Dunnett's Multiple Comparison test. If the data did not follow a normal distribution, the Mann–Whitney U test was used when two groups were compared, and the Kruskal-Wallis test followed by Dunn's multiple comparison test, when more than two groups were compared.

II-3. References

[1] S.S. Silva, J.M. Gomes, L.C. Rodrigues, R.L. Reis, Chitin and Its Derivatives, in: Polysaccharides Microb. Orig., Springer International Publishing, Cham, 2022: pp. 205–228. https://doi.org/10.1007/978-3-030-42215-8_13.

[2] S.S. Silva, J.F. Mano, R.L. Reis, Potential applications of natural origin polymer-based systems in soft tissue regeneration., Crit. Rev. Biotechnol. 30 (2010) 200–21. https://doi.org/10.3109/07388551.2010.505561.

[3] S.S. Silva, J.F. Mano, R.L. Reis, Ionic liquids in the processing and chemical modification of chitin and chitosan for biomedical applications, Green Chem. 19 (2017) 1208–1220. https://doi.org/10.1039/C6GC02827F.

[4] J.L. Shamshina, P. Berton, R.D. Rogers, Advances in Functional Chitin Materials: A Review, ACS Sustain. Chem. Eng. 7 (2019) 6444–6457. https://doi.org/10.1021/acssuschemeng.8b06372.

[5] S.S. Silva, J.M. Gomes, L.C. Rodrigues, R.L. Reis, Marine - Derived Polymers in Ionic Liquids : Architectures Development and Biomedical Applications, Mar. Drugs. 18 (2020) 346. https://doi.org/10.3390/md18070346.

[6] A. Takada, J.I. Kadokawa, Fabrication and characterization of polysaccharide ion gels with ionic liquids and their further conversion into value-added sustainable materials, Biomolecules. 5 (2015) 244–262. https://doi.org/10.3390/biom5010244.

[7] A. Takegawa, M. aki Murakami, Y. Kaneko, J. ichi Kadokawa, Preparation of chitin/cellulose composite gels and films with ionic liquids, Carbohydr. Polym. 79 (2010) 85–90. https://doi.org/10.1016/j.carbpol.2009.07.030.

[8] Y. Qin, X. Lu, N. Sun, R.D. Rogers, Dissolution or extraction of crustacean shells using ionic liquids to obtain high molecular weight purified chitin and direct production of chitin films and fibers, Green Chem. 12 (2010) 968. https://doi.org/10.1039/c003583a.

[9] P.S. Barber, C.S. Griggs, J.R. Bonner, R.D. Rogers, Electrospinning of chitin nanofibers directly from an ionic liquid extract of shrimp shells, Green Chem. 15 (2013) 601–607. https://doi.org/10.1039/c2gc36582k.

[10] N. Kasoju, U. Bora, Silk fibroin in tissue engineering, Adv. Healthc. Mater. 1 (2012) 393–412. https://doi.org/10.1002/adhm.201200097.

[11] Z. Zhou, J. Cui, S. Wu, Z. Geng, J. Su, Silk fibroin-based biomaterials for cartilage/osteochondral repair, Theranostics. 12 (2022) 5103–5124. https://doi.org/10.7150/thno.74548.

[12] C. Vepari, D.L. Kaplan, Silk as a biomaterial, Prog. Polym. Sci. 32 (2007) 991–1007. https://doi.org/10.1016/j.progpolymsci.2007.05.013.

[13] M.S. Zafar, D.J. Belton, B. Hanby, D.L. Kaplan, C.C. Perry, Functional material features of Bombyx mori silk light versus heavy chain proteins, Biomacromolecules. 16 (2015) 606–614. https://doi.org/10.1021/bm501667j.

[14] C.Z. Zhou, F. Confalonieri, M. Jacquet, R. Perasso, Z.G. Li, J. Janin, Silk fibroin: Structural implications of a remarkable amino acid sequence, Proteins Struct. Funct. Genet. 44 (2001) 119–122. https://doi.org/10.1002/prot.1078.

[15] L.D. Koh, Y. Cheng, C.P. Teng, Y.W. Khin, X.J. Loh, S.Y. Tee, M. Low, E. Ye, H.D. Yu, Y.W. Zhang, M.Y. Han, Structures, mechanical properties and applications of silk fibroin materials, Prog. Polym. Sci. 46 (2015) 86–110. https://doi.org/10.1016/j.progpolymsci.2015.02.001.

[16] F. Zhang, Q. Lu, X. Yue, B. Zuo, M. Qin, F. Li, D.L. Kaplan, X. Zhang, Regeneration of high-quality silk fibroin fiber by wet spinning from CaCl2-formic acid solvent, Acta Biomater. 12 (2015) 139–145. https://doi.org/10.1016/j.actbio.2014.09.045.

[17] S.S. Silva, J.M. Gomes, A.C. Vale, S. Lu, R.L. Reis, S.C. Kundu, Green Pathway for Processing Non-mulberry Antheraea pernyi Silk Fibroin/Chitin-Based Sponges: Biophysical and Biochemical Characterization, Front. Mater. 7 (2020) 135. https://doi.org/10.3389/fmats.2020.00135.

[18] P. Rosiak, I. Latanska, P. Paul, W. Sujka, B. Kolesinska, Modification of alginates to modulate their physic-chemical properties and obtain biomaterials with different functional properties, Molecules. 26 (2021). https://doi.org/10.3390/molecules26237264.

[19] M. Dalheim, J. Vanacker, M.A. Najmi, F.L. Aachmann, B.L. Strand, B.E. Christensen, Efficient functionalization of alginate biomaterials, Biomaterials. 80 (2016) 146–156. https://doi.org/10.1016/j.biomaterials.2015.11.043.

[20] K.Y. Lee, D.J. Mooney, Alginate: Properties and biomedical applications, Prog. Polym. Sci. 37 (2012) 106–126. https://doi.org/10.1016/j.progpolymsci.2011.06.003.

[21] C. Liu, Y. Cui, F. Pi, Y. Cheng, Y. Guo, H. Qian, Extraction, Purification, Structural Characteristics, Biological Activities and Pharmacological Applications of Acemannan, a Polysaccharide from Aloe vera: A Review, Molecules. 24 (2019) 1554. https://doi.org/10.3390/molecules24081554.

[22] N.J. Sadgrove, M.S.J. Simmonds, Pharmacodynamics of Aloe vera and acemannan in therapeutic applications for skin, digestion, and immunomodulation, Phyther. Res. 35 (2021) 6572–6584. https://doi.org/10.1002/ptr.7242.

[23] F. Salah, Y. El Ghoul, A. Mahdhi, H. Majdoub, N. Jarroux, F. Sakli, Effect of the deacetylation degree on the antibacterial and antibiofilm activity of acemannan from Aloe vera, Ind. Crops Prod. 103 (2017) 13–18. https://doi.org/10.1016/j.indcrop.2017.03.031.

[24] S. Kumar, A.B. Tiku, Immunomodulatory potential of acemannan (polysaccharide from Aloe vera) against radiation induced mortality in Swiss albino mice, Food Agric. Immunol. 27 (2016) 72–86. https://doi.org/10.1080/09540105.2015.1079594.

[25] S.S. Silva, L.C. Rodrigues, R.L. Reis, An alternative approach to prepare alginate/acemannan 3D architectures, SN Appl. Sci. 1 (2019) 1–10. https://doi.org/10.1007/s42452-019-0690-2.

[26] A.Y. Escobedo-Lozano, A. Domard, C.A. Vel??zquez, F.M. Goycoolea, W.M. Arg??elles-Monal, Physical properties and antibacterial activity of chitosan/acemannan mixed systems, Carbohydr. Polym. 115 (2015) 707–714. https://doi.org/10.1016/j.carbpol.2014.07.064.

[27] L.C. Rodrigues, S.S. Silva, R.L. Reis, Acemannan-based films: an improved approach envisioning biomedical applications, Mater. Res. Express. 6 (2019) 095406. https://doi.org/10.1088/2053-1591/ab2f66.

[28] S. Rahman, P. Carter, N. Bhattarai, Aloe Vera for Tissue Engineering Applications, J. Funct. Biomater. 8 (2017) 6. https://doi.org/10.3390/jfb8010006.

[29] E.S. Morais, N.H.C.S. Silva, T.E. Sintra, S.A.O. Santos, B. Miguel, I.F. Almeida, P.C. Costa, I. Correia-sá, S.P.M. Ventura, A.J.D. Silvestre, M.G. Freire, C.S.R. Freire, Anti-inflammatory and antioxidant nanostructured cellulose membranes loaded with phenolic-based ionic liquids for cutaneous application, Carbohydr. Polym. 206 (2019) 187–197. https://doi.org/10.1016/j.carbpol.2018.10.051.

[30] T.E. Sintra, A. Luís, S.N. Rocha, A.I.M.C.L. Ferreira, F. Gonçalves, L.M.N.B.F. Santos, B.M. Neves, M.G. Freire, S.P.M. Ventura, J.A.P. Coutinho, Enhancing the antioxidant characteristics of phenolic acids by their conversion into cholinium salts, ACS Sustain. Chem. Eng. 3 (2015) 2558–2565. https://doi.org/10.1021/acssuschemeng.5b00751.

[31] B. Cizmarova, B. Hubkova, B. Bolerazska, M. Marekova, A. Birkova, Caffeic acid: A brief overview of its presence, metabolism, and bioactivity, Bioact. Compd. Heal. Dis. 3 (2020) 74–81. https://doi.org/10.31989/bchd.v3i4.692.

[32] B. Badhani, N. Sharma, R. Kakkar, Gallic acid: A versatile antioxidant with promising therapeutic and industrial applications, RSC Adv. 5 (2015) 27540–27557. https://doi.org/10.1039/c5ra01911g.

[33] S.S. Silva, E.G. Popa, M.E. Gomes, M.B. Oliveira, S. Nayak, B. Subia, J.F. Mano, S.C. Kundu, R.L. Reis, Silk hydrogels from non-mulberry and mulberry silkworm cocoons processed with ionic liquids, Acta Biomater. 9 (2013) 8972–8982. https://doi.org/10.1016/j.actbio.2013.06.044.

[34] B.D. Lawrence, Processing of Bombyx mori for biomedical applications, Woodhead Publishing Limited, 2014. https://doi.org/10.1533/9780857097064.1.78.

[35] S.S. Silva, A. Motta, M.T. Rodrigues, A.F.M. Pinheiro, M.E. Gomes, J.F. Mano, R.L. Reis, C. Migliaresi, Novel genipin-cross-linked chitosan/silk fibroin sponges for cartilage engineering strategies, Biomacromolecules. 9 (2008) 2764–2774. https://doi.org/10.1021/bm800874q.

[36] Y. Yang, H.W. Kwak, K.H. Lee, Effect of Residual Lithium Ions on the Structure and Cytotoxicity of Silk Fibroin Film, Int. J. Ind. Entomol. 27 (2013) 265–270. https://doi.org/10.7852/ijie.2013.27.2.265.

[37] C.D. Mao, P. Hoang, P.E. DiCorleto, Lithium Inhibits Cell Cycle Progression and Induces Stabilization of p53 in Bovine Aortic Endothelial Cells, J. Biol. Chem. 276 (2001) 26180–26188. https://doi.org/10.1074/jbc.M101188200.

[38] R.S. Ambekar, B. Kandasubramanian, Progress in the Advancement of Porous Biopolymer Scaffold: Tissue Engineering Application, Ind. Eng. Chem. Res. 58 (2019) 6163–6194. https://doi.org/10.1021/acs.iecr.8b05334.

[39] A. Haider, S. Haider, M. Rao Kummara, T. Kamal, A.A.A. Alghyamah, F. Jan Iftikhar, B. Bano, N. Khan, M. Amjid Afridi, S. Soo Han, A. Alrahlah, R. Khan, Advances in the scaffolds fabrication techniques using biocompatible polymers and their biomedical application: A technical and statistical review, J. Saudi Chem. Soc. 24 (2020) 186–215. https://doi.org/10.1016/j.jscs.2020.01.002.

[40] I.N. Savina, G.C. Ingavle, A.B. Cundy, S. V. Mikhalovsky, A simple method for the production of large volume 3D macroporous hydrogels for advanced biotechnological, medical and environmental applications, Sci. Rep. 6 (2016) 1–9. https://doi.org/10.1038/srep21154.

[41] J.M. Gomes, S.S. Silva, R.L. Reis, Biocompatible ionic liquids: Fundamental behaviours and applications, Chem. Soc. Rev. 48 (2019) 4317–4335. https://doi.org/10.1039/c9cs00016j.

[42] Y. Wu, T. Sasaki, S. Irie, K. Sakurai, A novel biomass-ionic liquid platform for the utilization of native chitin, Polymer (Guildf). 49 (2008) 2321–2327. https://doi.org/10.1016/j.polymer.2008.03.027.

[43] J. ichi Kadokawa, Dissolution, derivatization, and functionalization of chitin in ionic liquid, Int. J. Biol. Macromol. 123 (2019) 732–737. https://doi.org/10.1016/j.ijbiomac.2018.11.165.

[44] S.S. Silva, A. Rita, C. Duarte, A. Paula, J.F. Mano, R.L. Reis, Green processing of porous chitin structures for biomedical applications combining ionic liquids and supercritical fluid technology, Acta Biomater. 7 (2011) 1166–1172. https://doi.org/10.1016/j.actbio.2010.09.041.

[45] S.S. Silva, A.R.C. Duarte, J.M. Oliveira, J.F. Mano, R.L. Reis, Alternative methodology for chitin-hydroxyapatite composites using ionic liquids and supercritical fluid technology, J. Bioact. Compat. Polym. 28 (2013) 481–491. https://doi.org/10.1177/0883911513501595.

[46] M.M. Jaworska, T. Kozlecki, A. Gorak, Review of the application of ionic liquids as solvents for chitin, J. Polym. Eng. 32 (2012) 67–69. https://doi.org/10.1515/polyeng-2011-0145.

[47] S.S. Silva, N.M. Oliveira, M.B. Oliveira, D.P.S. Da Costa, D. Naskar, J.F. Mano, S.C. Kundu, R.L. Reis, Fabrication and characterization of Eri silk fibers-based sponges for biomedical application, Acta Biomater. 32 (2016) 178–189. https://doi.org/10.1016/j.actbio.2016.01.003.

[48] Q. Lu, X. Hu, X. Wang, J.A. Kluge, S. Lu, P. Cebe, D.L. Kaplan, Water-insoluble silk films with silk I structure, Acta Biomater. 6 (2010) 1380–1387. https://doi.org/10.1016/j.actbio.2009.10.041.

[49] Ý.A. Mørch, I. Donati, B.L. Strand, G. Skjåk-Bræk, Effect of Ca 2+ , Ba 2+ , and Sr 2+ on Alginate Microbeads, Biomacromolecules. 7 (2006) 1471–1480. https://doi.org/10.1021/bm060010d.

[50] K.M. Gattás-Asfura, M. Valdes, E. Celik, C.L. Stabler, Covalent layer-by-layer assembly of hyperbranched polymers on alginate microcapsules to impart stability and permselectivity, J. Mater. Chem. B. 2 (2014) 8208–8219. https://doi.org/10.1039/C4TB01241K.

[51] H. Kristina K., G.-A. Kerim M., S. Cherie L., Microencapsulation of islets within alginate/poly(ethyleneglycol) gels cross-linked via Staudinger ligation, Acta Biomater. 7 (2011) 614–624. https://doi.org/10.1016/j.actbio.2010.07.016.Microencapsulation.

[52] Z. Xie, M. Gao, A.O. Lobo, T.J. Webster, 3D bioprinting in tissue engineering for medical applications: The classic and the hybrid, Polymers (Basel). 12 (2020). https://doi.org/10.3390/POLYM12081717.

[53] S. V. Murphy, A. Atala, 3D bioprinting of tissues and organs, Nat. Biotechnol. 32 (2014) 773–785. https://doi.org/10.1038/nbt.2958.

[54] C. Antich, J. de Vicente, G. Jiménez, C. Chocarro, E. Carrillo, E. Montañez, P. Gálvez-Martín, J.A. Marchal, Bio-inspired hydrogel composed of hyaluronic acid and alginate as a potential bioink for 3D bioprinting of articular cartilage engineering constructs, Acta Biomater. 106 (2020) 114–123. https://doi.org/10.1016/j.actbio.2020.01.046.

[55] I. Gorroñogoitia, U. Urtaza, A. Zubiarrain-Laserna, A. Alonso-Varona, A.M. Zaldua, A Study of the Printability of Alginate-Based Bioinks by 3D Bioprinting for Articular Cartilage Tissue Engineering, Polymers (Basel). 14 (2022) 1–17. https://doi.org/10.3390/polym14020354.

[56] M. Schneider, P. Demoulin, R. Sussmann, J. Notholt, Fourier transform infrared spectrometry, Monit. Atmos. Water Vap. Ground-Based Remote Sens. In-Situ Methods. 10 (2013) 95–111. https://doi.org/10.1007/978-1-4614-3909-7_6.

[57] K.A. Oberg, A.L. Fink, A new attenuated total reflectance fourier transform infrared spectroscopy method for the study of proteins in solution, Anal. Biochem. 256 (1998) 92–106. https://doi.org/10.1006/abio.1997.2486.

[58] J. Kong, S. Yu, Fourier Transform Infrared Spectroscopic Analysis of Protein Secondary Structures Protein FTIR Data Analysis and Band Assignment, Acta Biochim. Biophys. Sin. (Shanghai). 39 (2007) 549–559. https://doi.org/10.1111/j.1745-7270.2007.00320.x.

[59] F. Boukhlifi, Quantitative Analysis by IR: Determination of Chitin/ Chitosan DD, in: Mod. Spectrosc. Tech. Appl., 2020: pp. 1–24. https://doi.org/10.1016/j.colsurfa.2011.12.014.

[60] X. Hu, D. Kaplan, P. Cebe, Determining beta-sheet crystallinity in fibrous proteins by thermal analysis and infrared spectroscopy, Macromolecules. 39 (2006) 6161–6170. https://doi.org/10.1021/ma0610109.

[61] T. Dokland, D.W. Hutmacher, M.M.-L. Ng, J.-T. Schantz, Techniques in Microscopy for Biomedical Applications, WORLD SCIENTIFIC, 2006. https://doi.org/10.1142/5911.

[62] I.F. Cengiz, J.M. Oliveira, R.L. Reis, Micro-CT – a digital 3D microstructural voyage into scaffolds: a systematic review of the reported methods and results, Biomater. Res. 22 (2018) 1–11. https://doi.org/10.1186/s40824-018-0136-8.

[63] P. Gill, T.T. Moghadam, B. Ranjbar, Differential scanning calorimetry techniques: applications in biology and nanoscience, J. Biomol. Tech. 21 (2010) 167–93. https://www.ncbi.nlm.nih.gov/pmc/articles/PMC2977967/.

[64] A. Borzacchiello, F. Della Sala, L.A. Ambrosio, Rheometry of polymeric biomaterials, Elsevier Ltd., 2017. https://doi.org/10.1016/B978-0-08-100737-2.00010-8.

[65] C. Gonçalves, S.S. Silva, J.M. Gomes, I.M. Oliveira, R.F. Canadas, F.R. Maia, H. Radhouani, R.L. Reis, J.M. Oliveira, Ionic Liquid-Mediated Processing of SAIB-Chitin Scaffolds, ACS Sustain. Chem. Eng. 8 (2020) 3986–3994. https://doi.org/10.1021/acssuschemeng.0c00385.

[66] J. Davis, Tensile testing., 2nd ed., ASM international., 2004.

[67] A.R. Armiento, L.P. Hatt, G. Sanchez Rosenberg, K. Thompson, M.J. Stoddart, Functional Biomaterials for Bone Regeneration: A Lesson in Complex Biology, Adv. Funct. Mater. 30 (2020) 1909874. https://doi.org/10.1002/adfm.201909874.

[68] P.A. Tishmack, D.E. Bugay, S.R. Byrn, Solid-state nuclear magnetic resonance spectroscopy - Pharmaceutical applications, J. Pharm. Sci. 92 (2003) 441–474. https://doi.org/10.1002/jps.10307.

[69] C.T. Nakazawa, A. Higuchi, A. Asano, T. Kameda, D. Aytemiz, Y. Nakazawa, Solid-state NMR studies for the development of non-woven biomaterials based on silk fibroin and polyurethane, Polym. J. 49 (2017) 583–586. https://doi.org/10.1038/pj.2017.16.

[70] S.E. Ashbrook, J.M. Griffin, K.E. Johnston, Recent Advances in Solid-State Nuclear Magnetic Resonance Spectroscopy, Annu. Rev. Anal. Chem. 11 (2018) 485–508. https://doi.org/10.1146/annurev-anchem-061417-125852.

[71] J. Lefebvre, F. Galli, C.L. Bianchi, G.S. Patience, D.C. Boffito, Experimental methods in chemical engineering: X-ray photoelectron spectroscopy-XPS, Can. J. Chem. Eng. 97 (2019) 2588–2593. https://doi.org/10.1002/cjce.23530.

[72] L. Zhang, X. Liu, G. Li, P. Wang, Y. Yang, Tailoring degradation rates of silk fibroin scaffolds for tissue engineering, J. Biomed. Mater. Res. - Part A. 107 (2019) 104–113. https://doi.org/10.1002/jbm.a.36537.

[73] C.J. Little, N.K. Bawolin, X. Chen, Mechanical Properties of Natural Cartilage and Tissue-Engineered Constructs, TISSUE Eng. Part B. 17 (2011) 213–227. https://doi.org//10.1089/ten.teb.2010.0572.

[74] W. Wei, J. Li, X. Qi, Y. Zhong, G. Zuo, X. Pan, T. Su, J. Zhang, W. Dong, Synthesis and characterization of a multi-sensitive polysaccharide hydrogel for drug delivery, Elsevier Ltd., 2017. https://doi.org/10.1016/j.carbpol.2017.08.133.

[75] L.R. Bogdanova, P. V. Zelenikhin, A.O. Makarova, O.S. Zueva, V. V. Salnikov, Y.F. Zuev, O.N. Ilinskaya, Alginate-Based Hydrogel as Delivery System for Therapeutic Bacterial RNase, Polymers (Basel). 14 (2022) 2461. https://doi.org/10.3390/polym14122461.

[76] T. Ito, M. Saito, T. Uchino, M. Senna, M. Iafisco, M. Prat, L. Rimondini, M. Otsuka, Preparation of injectable auto-forming alginate gel containing simvastatin with amorphous calcium phosphate as a controlled release medium and their therapeutic effect in osteoporosis model rat, J. Mater. Sci. Mater. Med. 23 (2012) 1291–1297. https://doi.org/10.1007/s10856-012-4597-3.

[77] A.R. Chandrasekaran, C.Y. Jia, C.S. Theng, T. Muniandy, S. Muralidharan, S. Arumugam, Invitro studies and evaluation of metformin marketed tablets-Malaysia, 01 (2011) 214–217.

[78] W. Zhang, W.B. Robertson, J. Zhao, W. Chen, J. Xu, Emerging Trend in the Pharmacotherapy of Osteoarthritis, Front. Endocrinol. (Lausanne). 10 (2019) 431. https://doi.org/10.3389/fendo.2019.00431.

[79] S.B. Kedare, R.P. Singh, Genesis and development of DPPH method of antioxidant assay, J. Food Sci. Technol. 48 (2011) 412–422. https://doi.org/10.1007/s13197-011-0251-1.

[80] F. Cilurzo, F. Selmin, P. Minghetti, M. Adami, E. Bertoni, S. Lauria, L. Montanari, Injectability evaluation: An open issue, AAPS PharmSciTech. 12 (2011) 604–609. https://doi.org/10.1208/s12249-011-9625-y.

[81] K. Song, A.M. Compaan, W. Chai, Y. Huang, Injectable Gelatin Microgel-Based Composite Ink for 3D Bioprinting in Air, ACS Appl. Mater. Interfaces. 12 (2020) 22453–22466. https://doi.org/10.1021/acsami.0c01497.

[82] M. Samie, A.F. Khan, J.G. Hardy, M.A. Yameen, Electrospun Antibacterial Composites for Cartilage Tissue Engineering, Macromol. Biosci. 22 (2022) 2200219. https://doi.org/10.1002/mabi.202200219.

[83] D. Bicho, S. Ajami, C. Liu, R.L. Reis, J.M. Oliveira, Peptide-biofunctionalization of biomaterials for osteochondral tissue regeneration in early stage osteoarthritis: Challenges and opportunities, J. Mater. Chem. B. 7 (2019) 1027–1044. https://doi.org/10.1039/c8tb03173h.

[84] A.R. Franco, E. Palma Kimmerling, C. Silva, F.J. Rodrigues, I.B. Leonor, R.L. Reis, D.L. Kaplan, Silk-Based Antimicrobial Polymers as a New Platform to Design Drug-Free Materials to Impede Microbial Infections, Macromol. Biosci. 18 (2018) 1–15. https://doi.org/10.1002/mabi.201800262.

[85] A. Miskiewicz, P. Ceranowicz, M. Szymczak, K. Bartuś, P. Kowalczyk, The use of liquids ionic fluids as pharmaceutically active substances helpful in combating nosocomial infections induced by Klebsiella Pneumoniae new delhi strain, Acinetobacter Baumannii and Enterococcus species, Int. J. Mol. Sci. 19 (2018). https://doi.org/10.3390/ijms19092779.

[86] J.J. Biemer, Antimicrobial Susceptibility Testing by the Kirby-Bauer Disc Diffusion Method, Ann Clin Lab Sci. 3 (n.d.) 135–140. http://www.annclinlabsci.org/content/3/2/135.short#cited-by.

[87] L. Netuschil, T.M. Auschill, A. Sculean, N.B. Arweiler, Confusion over live / dead stainings for the detection of vital microorganisms in oral biofilms - which stain is suitable ?, (2014) 1–12.

[88] J.R. Mauney, T. Nguyen, K. Gillen, C. Kirker-Head, J.M. Gimble, D.L. Kaplan, Engineering adipose-like tissue *In vitro* and *in vivo* utilizing human bone marrow and adipose-derived mesenchymal stem cells with silk fibroin 3D scaffolds, Biomaterials. 28 (2007) 5280–5290. https://doi.org/10.1016/j.biomaterials.2007.08.017.

[89] M.E. Gomes, T. Rada, R.L. Reis, Adipose tissue-derived stem cells and their application in bone and cartilage tissue engineering, Tissue Eng. - Part B Rev. 15 (2009) 113–125. https://doi.org/10.1089/ten.teb.2008.0423.

[90] T. Rada, R.L. Reis, M.E. Gomes, Novel method for the isolation of adipose stem cells (ASCs), J Tissue Eng Regen Med. 12 (2009) 158–159. https://doi.org/10.1002/term.

[91] A.I. Gonçalves, M.T. Rodrigues, S.J. Lee, A. Atala, J.J. Yoo, R.L. Reis, M.E. Gomes, Understanding the role of growth factors in modulating stem cell tenogenesis, PLoS One. 8 (2013). https://doi.org/10.1371/journal.pone.0083734.

[92] S. Liu, Z. Deng, K. Chen, S. Jian, F. Zhou, Y. Yang, Z. Fu, H. Xie, J. Xiong, W. Zhu, Cartilage tissue engineering: From proinflammatory and anti-inflammatory cytokines to osteoarthritis treatments (Review), Mol. Med. Rep. 25 (2022) 99. https://doi.org/10.3892/mmr.2022.12615.

[93] L. Kou, S. Xiao, R. Sun, S. Bao, Q. Yao, R. Chen, Biomaterial-engineered intra-articular drug delivery systems for osteoarthritis therapy, Drug Deliv. 26 (2019) 870–885. https://doi.org/10.1080/10717544.2019.1660434.

[94] I.M. Oliveira, C. Gonçalves, E.P. Oliveira, R. Simón-Vázquez, A. da Silva Morais, Á. González-Fernández, R.L. Reis, J.M. Oliveira, PAMAM dendrimers functionalised with an anti-TNF α antibody and chondroitin sulphate for treatment of rheumatoid arthritis, Mater. Sci. Eng. C. 121 (2021) 111845. https://doi.org/10.1016/j.msec.2020.111845.

[95] Y. Yao, Y. Wang, ATDC5: An excellent *in vitro* model cell line for skeletal development, J. Cell. Biochem. 114 (2013) 1223–1229. https://doi.org/10.1002/jcb.24467.

[96] G. Jiménez, S. Venkateswaran, E. López-Ruiz, M. Perán, S. Pernagallo, J.J. Díaz-Monchón, R.F. Canadas, C. Antich, J.M. Oliveira, A. Callanan, R. Walllace, R.L. Reis, E. Montañez, E. Carrillo, M. Bradley, J.A. Marchal, A soft 3D polyacrylate hydrogel recapitulates the cartilage niche and allows growth-factor free tissue engineering of human articular cartilage, Acta Biomater. 90 (2019) 146–156. https://doi.org/10.1016/j.actbio.2019.03.040.

[97] T.L. Riss, R.A. Moravec, A.L. Niles, S. Duellman, H.A. Benink, T.J. Worzella, L. Minor, Cell Viability Assays, Assay Guid. Man. (2004) 1–25. http://www.ncbi.nlm.nih.gov/pubmed/23805433.

[98] T. Riss, A. Niles, R. Moravec, N. Karassina, J. Vidugiriene, Cytotoxicity Assays : *In vitro* Methods to Measure Dead Cells Dyes That Selectively Penetrate Dead Cells Trypan blue Fluorescent DNA Binding Dyes That Penetrate Dead Cells, Assay Guid. Manual. (2019) 1–15. https://www.ncbi.nlm.nih.gov/books/NBK540958/pdf/Bookshelf_NBK540958.pdf.

[99] V.M.C. Quent, D. Loessner, T. Friis, J.C. Reichert, Discrepancies between metabolic activity and DNA content as tool to assess cell proliferation in cancer research, J. Cell. Mol. Med. 14 (2010) 1003–1013. https://doi.org/10.1111/j.1582-4934.2010.01013.x.

[100] I. Nassiri, M.N. Mccall, Systematic exploration of cell morphological phenotypes associated with a transcriptomic query, Nucleic Acids Res. 46 (2018) 1–9. https://doi.org/10.1093/nar/gky626.

[101] D. Soares Da Costa, M.D.C. Márquez-Posadas, A.R. Araujo, Y. Yang, S. Merino, T. Groth, R.L. Reis, I. Pashkuleva, Adhesion of adipose-derived mesenchymal stem cells to glycosaminoglycan surfaces with different protein patterns, ACS Appl. Mater. Interfaces. 7 (2015) 10034–10043. https://doi.org/10.1021/acsami.5b02479.

[102] P. Lepetsos, A.G. Papavassiliou, ROS/oxidative stress signaling in osteoarthritis, Biochim. Biophys. Acta - Mol. Basis Dis. 1862 (2016) 576–591. https://doi.org/10.1016/j.bbadis.2016.01.003.

[103] P. Le Thi, Y. Lee, D.L. Tran, T.T.H. Thi, J. Il Kang, K.M. Park, K.D. Park, In situ forming and reactive oxygen species-scavenging gelatin hydrogels for enhancing wound healing efficacy, Acta Biomater. 103 (2020) 142–152. https://doi.org/10.1016/j.actbio.2019.12.009.

[104] M. Kubista, J.M. Andrade, M. Bengtsson, A. Forootan, J. Jonák, K. Lind, R. Sindelka, R. Sjoback, B. Sjogreen, L. Strombom, A. Stahlberg, N. Zoric, The real-time polymerase chain reaction, Mol. Aspects Med. 27 (2006) 95–125. https://doi.org/10.1016/j.mam.2005.12.007.

[105] K.J. Livak, T.D. Schmittgen, Analysis of relative gene expression data using real-time quantitative PCR and the 2-ΔΔCT method, Methods. 25 (2001) 402–408. https://doi.org/10.1006/meth.2001.1262.

[106] R.A.A. Muzzarelli, F. Greco, A. Busilacchi, V. Sollazzo, A. Gigante, Chitosan, hyaluronan and chondroitin sulfate in tissue engineering for cartilage regeneration: A review, Carbohydr. Polym. 89 (2012) 723–739. https://doi.org/10.1016/j.carbpol.2012.04.057.

[107] U. Schumacher, E. Adam, Standardization of Staining in Glycosaminoglycan Histochemistry : Alcian Blue , its Analogues , and Diamine Methods, Biotech Histochem. (1988) 18–24. https://doi.org/10.3109/10520299409106256.

[108] P.T. Newton, K.A. Staines, L. Spevak, A.L. Boskey, C.C. Teixeira, V.E. Macrae, A.E. Canfield, C. Farquharson, Chondrogenic ATDC5 cells: An optimised model for rapid and physiological matrix mineralisation, Int. J. Mol. Med. 30 (2012) 1187–1193. https://doi.org/10.3892/ijmm.2012.1114.

[109] M. Weber, H. Steinle, S. Golombek, L. Hann, C. Schlensak, H.P. Wendel, M. Avci-Adali, Blood-Contacting Biomaterials: *In vitro* Evaluation of the Hemocompatibility, Front. Bioeng. Biotechnol. 6 (2018) 99. https://doi.org/10.3389/fbioe.2018.00099.

[110] Y.P. Singh, J.C. Moses, N. Bhardwaj, B.B. Mandal, Overcoming the Dependence on Animal Models for Osteoarthritis Therapeutics – The Promises and Prospects of *in vitro* Models, Adv. Healthc. Mater. 10 (2021) 1–25. https://doi.org/10.1002/adhm.202100961.

[111] S. Sakamoto, W. Putalun, S. Vimolmangkang, W. Phoolcharoen, Enzyme-linked immunosorbent assay for the quantitative / qualitative analysis of plant secondary metabolites, J. Nat. Med. 72 (2018) 32–42. https://doi.org/10.1007/s11418-017-1144-z.

[112] T.K. Berthoud, M.N. Manaca, D. Quelhas, R. Aguilar, C. Guinovart, L. Puyol, A. Barbosa, P.L. Alonso, C. Dobaño, Comparison of commercial kits to measure cytokine responses to Plasmodium falciparum by multiplex microsphere suspension array technology, Malar. J. 10 (2011) 115. https://doi.org/10.1186/1475-2875-10-115.

SECTION 3

EXPERIMENTAL STUDIES

Chapter III

Exploring the use of choline acetate on sustainable development of α-chitin-based sponges

Chapter III

Exploring the use of choline acetate on sustainable development of α-chitin-based sponges [†]

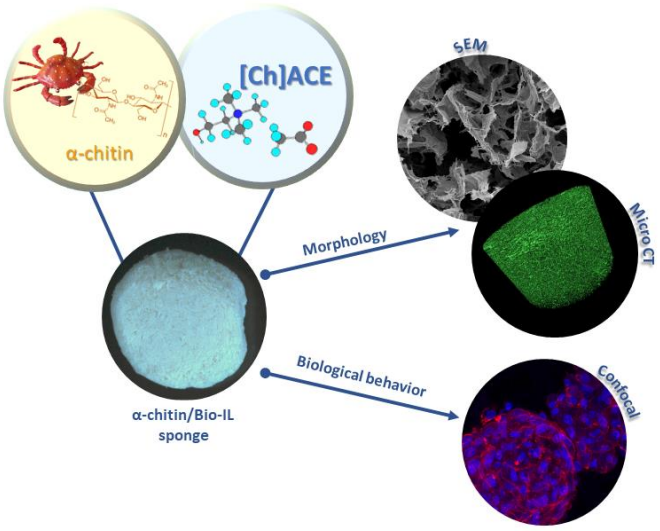
ABSTRACT

This study proposes a green and innovative methodology for the exploitation of natural polymers, namely chitin, by using solvents with reduced toxicity for the creation of porous structures with potential to be used in the biomedical field. Chitin is a promising biopolymer for the design of biodegradable constructs, and encouraging developments on its processing have been achieved using ionic liquids (ILs). However, owing to the concerns regarding ILs' toxicity, biocompatible ionic liquids (Bio-ILs) emerged as a family of ILs with enhanced toxicological features. Herein, we proposed to develop a sustainable route to produce α-chitin-based 3D structures using Bio-ILs, namely Choline Acetate (Ch[ACE]). Two chitin-based structures were produced based on the presence or absence of the Bio-IL. The characterization of the matrices demonstrated useful morphological features, including porosity (≈85%), interconnectivity (≈98.31%), and high swelling ability. Cytotoxicity assays using the L929 fibroblasts cell line proved the innocuous effect of the Bio-IL on cell metabolic activity when kept in the structures. The non-deleterious effect of Ch[ACE] onto the cells was confirmed when human adipose stem cells (hASCs) were seeded on the surface of the structures. Altogether, the present approach opens new avenues for the design of biomaterials by a sustainable pathway.

[†]This chapter is based on the following publication:

Gomes J. M., Silva S. S. and Reis R. L. "Exploring the Use of Choline Acetate on the Sustainable Development of α-Chitin-Based Sponges"; ACS Sustainable Chem. Eng. 2020, 8, 35, 13507–1351. doi: 10.1021/acssuschemeng.0c05076

III-1. GRAPHICAL ABSTRACT



III-2. INTRODUCTION

There is a worldwide demand to develop not only cheaper but also sustainable and efficient green processe s[1]. To address these requirements, the development of alternative routes using natural resources and "green solvents" has been enhanced. There has been an effort on the exploitation of renewable resources such as natural polymers for the production of multifunctional medical devices and therapeutic platforms. This interest is due to the high abundance, biocompatibility, and biodegradability of natural polymers such as alginate, silk fibroin, chitin, and chitosan [2–6]. In particular, chitin itself is a natural polymer with very striking characteristics, including the ability to accelerate wound healing and the tumour cell growth suppression, besides its nontoxicity and biocompatibility [6,7]. However, the processability of this material is probably compromised due to the strong inter- and intramolecular hydrogen bonding between its polymer chains. Nevertheless, many studies described the use of ILs, mostly containing the pyridinium or the imidazolium ring as the cationic moiety in their structure, for either the extraction, modification or dissolution of chitin [8–11].

Ionic liquids (ILs), as organic salts, possess remarkable characteristics that include low vapor pressure, high chemical and thermal stabilities, nonflammability, and intrinsic conductivity [12]. Moreover, it is possible to tailor a wide range of ILs, through the manipulation of the different cations and anions in their synthesis [13]. Nevertheless, the toxicological issues related to the use of these ILs, mainly

in biomedical applications, imply its removal before the analysis of the biomedical material performance [2,14]. To overcome these drawbacks, biocompatible ILs (Bio-ILs) arise as an alternative family of ILs, with enhanced toxicological profile and biodegradable features. The synthesis of these compounds is done by using both anionic and cationic counterparts derived from biocompatible materials such as sugar, amino acids, and carboxylic acids, which contribute to their harmless nature [12]. The Bio-ILs inherent biocompatibility, as well as their ability to disrupt hydrogen bonds and to interact with hydroxyl groups, has been attracting their use with weakly soluble polymers, facilitating their processing and enabling their wide use [15,16]. Some Bio-ILs have been used for the successful selective processing of biomass from different sources [17–20] as well as plasticizers for some polymers [21,22]. In pharmaceutics Bio-ILs have been showing their potential as biomolecules stabilizers, as solvents and as drug carrier systems for poorly soluble drugs, constituting active pharmaceutical ingredient-IL systems (API-IL) [23–27]. Several works report the use of these compounds for the development of cholinium-based bio-ion gels with low toxicity, produced based on the formation of a poly-bio-IL networks, in which the free bio-IL will be integrated, producing biomaterials with potential application as electrodes in the biomedical field [28,29]. Despite the promising reports, only a few studies can be found about the use of Bio-ILs in the tissue engineering field [12,30].

Herein, we hypothesized that a commercial Bio-IL, Choline Acetate (Ch[ACE]), could promote the dissolution and processing of α-chitin into 3D porous structures. The structures of both the Bio-IL and chitin are presented in Figure III-1. As known, chitin's solubility is affected by its crystalline structure, and α-chitin is formed by strong intermolecular hydrogen bonding, which implies a lack of solubility, resulting in lower reactivity and affinity for solvents when compared to β-chitin[6]. Based on previous studies [6,14], the dissolution of chitin can be achieved using 1-butyl-3-methylimidazolium acetate or 1-allyl-3-methylimizalium bromide at high temperature (90–95 °C), and chitin/IL gels can be formed. However, owing to these ILs toxicity, their removal from the final construct is mandatory when envisioning their application in the biomedical or tissue engineering filds. In the present work, the dissolution of α-chitin in Ch[ACE] was evaluated using sonication and stirring cycles at 90 °C. Besides, we also evaluated the effect of different solvents, namely, ethanol, acetone, isopropanol, and methanol, to tune the properties of the resulting materials. Further, two chitin-based structures were produced based on the presence or absence of the Bio-IL into the polymeric structure. With that, it is intended to evaluate the Bio-IL effect on the cytotoxicity, as well as on the *in vitro* cellular behaviour of the L929 fibroblast cell line and human adipose stem cells (hASCs), respectively.

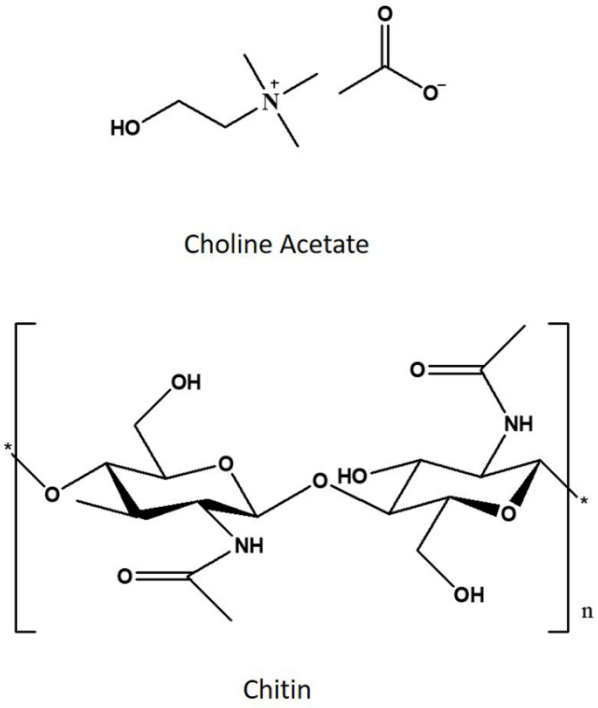


Figure III-1 - Structural representation of the choline acetate (Ch[ACE]) and the polymer chitin.

III-3. MATERIALS AND METHODS

III-3.1. Materials

The biocompatible ionic liquid choline acetate, 98% (Ch[ACE]), was purchased from Iolitec-Ionic Liquids Technologies GmbH and was used as a solvent without further purification. Chitin from crab shells (Ch; practical grade; Sigma Aldrich) with a degree of N-acetylation of 57.9%, determined by elemental analysis, were ground through a Wiley Mill (model 4, Thomas) and stored in plastic bottles. Ground α-chitin (106 μm) was used throughout the experiments to obtain reproducible results. All other chemicals were reagent grade and were used as received.

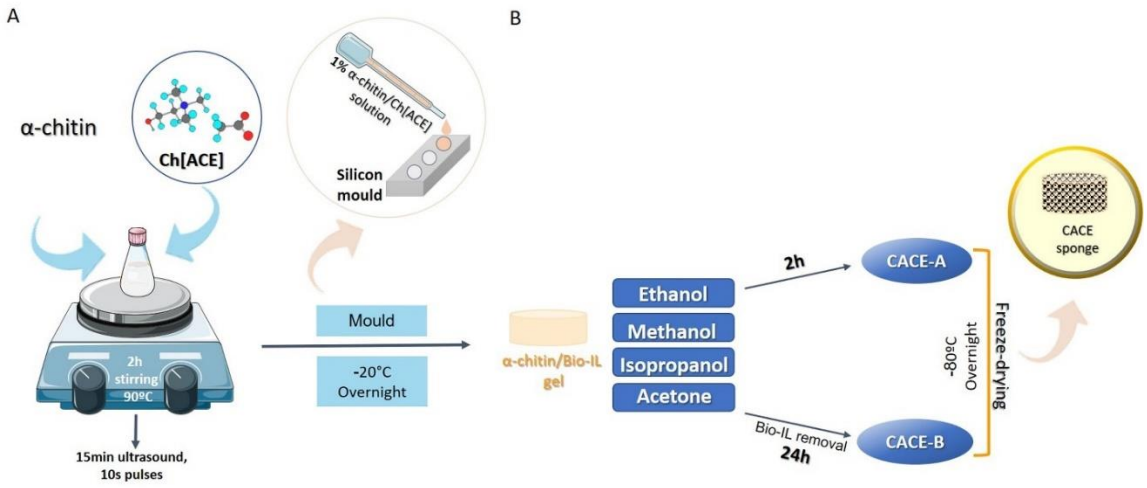
III-3.2. Preparation on the α-chitin/Bio-IL -based structures

α-Chitin was dissolved in Ch[ACE] using 4 cycles of 2 h stirring at 90 °C, followed by 15 min of 10 s sonication pulses (ultrasonic processor model VCX-130PB-220) (see scheme in Scheme III-1 A). After the dissolution step, the α-chitin/Bio-IL solution was molded into specific silicone molds and placed at -20 °C overnight. The resulting α-chitin/Bio-IL gels were immersed in different solvents, namely: ethanol,

acetone, isopropanol, and methanol. After washing with H_2O for 2h, the samples were frozen at -80 °C overnight and freeze-dried for three days, resulting in α-chitin/Ch[ACE] based structures (identified as CACE).

III-3.3. Preparation of CACE-A and CACE-B based sponges.

To prepare two formulations based on the presence (CACE-A) or absence (CACE-B) of the Bio-IL in the structure, the gels were further immersed in methanol for 2 h and 24 h (with periodic solvent changes), respectively Scheme III- 1A and Scheme III-1B. The immersion in methanol for 24 h allowed to remove all the Bio-ILs from the gels. After both CACE-A and CACE-B gels were washed with H_2O for 2 h, the samples were frozen at -80 °C overnight and freeze-dried for three days. The presence or removal of the Bio-IL was monitored through conductivity measurements of the solvent aliquots, which was made using a conductivimeter (INOLAB, Multi level 3) with a SondaWTWTetraCon 325.



Scheme III-1 - Scheme used for the production of the CACE sponges

III-3.4. Physico-chemical characterization

III-3.4.1. Light microscopy

The monitoring of the dissolution of α-chitin in Ch[ACE] was done using a Leica DM750 Leica DM750 microscope.

III-3.4.2. Stereo microscope observation

To observe and evaluate the macroscopic aspect of the CACE gels and sponges a Stereo Microscope + Lamp (Schott KL 200) Stemi 1000, ZEISS used.

III-3.4.3. Fourier transform infrared spectroscopy (FTIR)

The infrared spectra were recorded using a Shimadzu-IR, Prestige 21 spectrometer, in the spectral region of 4000-650 cm-1, with a resolution of 2 cm^{-1} at 32 scans. The data was acquired using the KBr mode and, to this end, the samples were powdered, mixed with KBr, and processed into pellets.

III-3.4.4. Determination of the degree of deacetylation (DD%) of chitin

The DD% of chitin was determined using a infrared spectroscopy adapted method [31] the following formula:

$$DD\% = 100 * \left[\left(\frac{A1655}{A3450}\right) * \frac{100}{1.33}\right] \quad \text{Equation III-1}$$

where A1655 is the absorbance at 1655 cm^{-1}(amide I band) as a measure of the N-acetyl group content, and A3430 is the absorbance at 3430 cm^{-1} (hydroxyl bands) as an internal standard. The value 1.33 represents the ratio of absorbance for a fully acetylated compound.

III-3.4.5. Stability assay

A stability assay was performed by emerging the CACE sponges in H2O and PBS. At the end of each assay time point (2h and 24h), the structures were evaluated in terms of macroscopic appearance and resistance to manipulation using forceps.

III-3.4.6. Scanning electron microscopy (SEM)

The different materials were fixed using mutual carbon adhesive tape on aluminum stubs and coated with a conductive gold layer. Their morphology was observed using a NanoSEM-FEI Nova 200 with an integrated microanalysis X-ray system (EDS – energy dispersive spectrometer).

III-3.4.7. Micro-computed tomography (micro-CT)

The morphological structure and the calculation of the morphometric parameters that characterize the samples were evaluated by micro-computed tomography (micro-CT). Samples were acquired with a SkyScan 1272 scanner (v1.1.3, Bruker, Boston, USA), with a pixel size of 10 μm. Approximately 300 projections were acquired over a rotation range of 360°, with a rotation step of 0.6°. Data sets were reconstructed using the reconstruction software (NRecon 1.6.10.2 Bruker), and the output format for each sample was bitmap images. The binary images were used for morphometric analysis (CT Analyser, v1.13, Bruker) and to build the 3D models.

III-3.4.8. Swelling

The swelling tests were performed by immersing the sponges in phosphate buffer solution (PBS) up to 24 h, at 37 °C. The weight of the dry samples was measured (WD), and after submerging them in PBS and removing the excess moisture, the samples' wet weight (WS) was obtained. The samples were afterward rehydrated up to equilibrium. The Swelling Degree (SD) was then calculated by using the following equation:

$$SD = ((WS-WD)/WD)x100 \qquad \text{Equation III-2}$$

Each experiment was repeated three times.

III-3.4.9. Differential scanning calorimetry (DSC)

A DSC analysis of the sponges was performed under a flowing nitrogen atmosphere between 25 and 400 °C at a heating rate of 10 °C min−1 using a DSC Q100 from T. A. INSTRUMENTS instrument. Both temperature and enthalpy were calibrated with an indium standard at the same experimental conditions used for the studied materials. All samples were presented, with a weight between 3 and 5 mg, in 40 μL aluminum pans, which were covered with a suitable aluminum cover.

III-3.4.10. Rheological assays

A Malvern Instruments Kinexus rheometer equipped with a stainless steel parallel-plate sample holder of 8 mm in diameter and between 1.5 and 2.5 mm gap (according to hydrogel height), was used to perform the oscillatory rheological measurements. A fixed temperature of 25°C was used into the experiments. Oscillatory experiments were preceded by strain sweep curves to determine the linear viscoelastic region (LVER) of the samples. Strain sweeps were then performed to each different sample, acquiring 10 points per decade, from 0.01 % to 100 % at a fixed frequency of 1 Hz. Mechanical spectra were achieved, and the elastic and viscous modulus (respectively G' and G'') as a function of frequency, ranging from 0.01 Hz to 100 Hz and a constant 0.1 % strain. All the tests were performed at least in triplicate.

III-3.5. Cell culture studies

III-3.5.1. Cytotoxicity

Before cell culture studies, the structures were sterilized using ethylene oxide. *In vitro* cytotoxicity tests of the produced structures were performed using the L929 mouse fibroblast-like cell line (European Collection of Cell Cultures, UK), at passage P15-P19. Cells were cultured in basic medium: Dulbecco's modified Eagle's medium (DMEM; Sigma–Aldrich, USA) with phenol red, with 10 % fetal bovine serum (Life Technologies, USA) and 1% antibiotic/antimycotic (A/A, Gibco, UK) solution. L929 cells were incubated at 37 °C in an atmosphere containing 5% of CO_2 until 90% confluence was achieved. L929 cells were seeded at a density of 3 x 10^5 cells cm^{-3} onto the CACE -based structures (CACE-A and CACE-B), following the cytotoxicity assay according to the ANSI/AAMI/ISO-10993-5 guidelines for 3 days[32]. The constructs were cultured for 1, 2, and 3 days in DMEM, 10% FBS, 1 vol.% A/A and incubated at 37 °C in a 5% CO_2 atmosphere. Controls consisted of CACE-based structures without cells, which were maintained in culture for the same periods under the same cell maintenance conditions. Tissue culture polystyrene (TCP) as a positive control was used. At the end of each culture time point, the samples were retrieved, rinsed with PBS, and evaluated in terms of cellular behavior, by MTS (3-(4,5-dimethylthiazol-2-yl)-5-(3-carboxymethoxyphenyl)-2-(4 sulfophenyl)-2H tetrazolium) assay.

III-3.5.2. Human adipose stem cell isolation and expansion

Human adipose stem cells (hASCs) were obtained from subcutaneous fat tissue, under protocols established with the Plastic Surgery Department of the Hospital da Prelada (Porto, Portugal) and isolated by enzymatic digestion as previously described. 30 Briefly, the adipose tissue samples were digested with 0.075 % collagenase type II (Col II) (C6885, Sigma) in PBS (21600-044, Invitrogen) for 45 min at 37 °C under gentle stirring. Digested tissue was filtered with a 100 μm filter mesh and centrifuged at 1000 g for 10 min at 5 °C. Afterward, the cell suspension was washed for 10 min with lysis buffer (155 mM NH4Cl, 10 mM KHCO3, 0.1 mM ED- TA = 14.61 mg, pH 7.3), to remove erythrocytes, and centrifuged at 800 g at 5 °C for 10 min. The adherent hASCs were expanded in basal medium with minimum essential medium (α-MEM) (Life Technologies, USA) with 10 vol.% FBS and 1 vol.% A/A with medium changes every 3–4 days.

III-3.5.3. Direct contact assay

For all experiments, hASCs at passages 2-3 were used and seeded at a density of 3 x 10^5 cells cm-3 onto the CACE-based structures (CACE-A and CACE-B). Controls consisted of CACE-based structures without cells maintained in culture for the same periods under the same cell maintenance conditions, and TCP was used as a positive control. The seeded structures were cultured for 1, 3 and 7 days in α-MEM with 10 vol.% FBS, 1 vol.% A/A and incubated at 37 °C in a 5% CO_2 atmosphere. At the end of each culture time point, the samples were retrieved, rinsed with PBS, and evaluated in terms of cellular behavior, by confocal analysis, MTS test, and DNA quantification.

III-3.5.4. Cell viability

The metabolic activity of cells seeded on the CACE-based structures was evaluated using the CellTiter 96® AQueous One Solution Cell Proliferation Assay (MTS, Promega). Briefly, cell–scaffold constructs were placed in a mixture containing serum-free cell culture medium and MTS reagent at a 5:1 ratio and incubated for 3 h, at the end of which the optical density was read (OD 490 nm).

The cell viability was also evaluated by fluorescence labeling using a live/dead assay. For this purpose, the CACE-based sponges were removed from the culture medium and washed with sterile PBS. Subsequently, all samples were incubated with 1 mg/mL calcein acetoxymethyl (Invitrogen, 1:500) and

1.5 mM propidium iodide (PI, Invitrogen, 1:1000) solution in PBS for 15 min, at 37 °C and washed with sterile PBS. After that, the samples were visualized under a transmitted and reflected light microscope with apotome 2 (Axio Imager Z1 m; Zeiss, Jena, Germany), showing viable cells green (Calcein AM) and non-viable cells red (PI). The laser settings were 488 nm and 543 nm for Calcein AM and PI, respectively. The software Zen was used to analyze the images.

III-3.5.5. Cell proliferation

The proliferation of the cells was evaluated using the fluorimetric PicoGreen double-stranded DNA (dsDNA) assay according to the manufacturer's instructions (Quant-iT™ PicoGreen™ dsDNA Kit, P7589, Invitrogen). Briefly, cell–scaffold constructs, collected after each period, were rinsed with PBS, placed in microtubes containing 1 ml of ultra-pure water, and stored at -80 °C until analysed. The fluorescence was measured with a microplate reader (Synergy HT, BIO-TEK, Winooski, VT, USA) at 480 and 520 nm, and the DNA concentration was calculated using a standard curve (0–2 μg ml^{-1}) relating the amount of dsDNA to the fluorescence.

III-3.5.6. Cell morphology

The cell distribution and attachment of L929 and hASCs cells on the CACE-based structures were analysed using confocal microscopy (CLSM). The matrices were fixed with 10% formalin for 30 min, and then the samples were incubated with 1 % bovine serum albumin (BSA) for 30 min. The constructs were permeabilized using 0.1% Triton X-100 for 5 min, then incubated with rhodamine-phalloidin at room temperature (RT) for 20 min, followed by washing with PBS and staining with 5 μg ml^{-1} 4',6-Diamidine-2'-phenylindole dihydrochloride (DAPI) for 30 min. Fluorescence images from the stained constructs were obtained using a confocal laser scanning microscope (Olympus FV1000).

III-3.6. Statistical analysis

All quantitative experiments were made in triplicate, and the results are expressed as means ± standard deviation for n = 3. The statistical analysis was conducted using GraphPadPrism v. 8.0 for Windows (GraphPad Software, San Diego, http://www.graphpad.com). After the evaluation of the normality of the results through the Shapiro-Wilk test, the nonparametric Mann-Whitney was applied. The

statistical significance of the swelling degree was determined using a multiple t-test, with the Holm-Sidak method. Differences between the groups at $p \leq 0.05$ were statistically significant.

III-4. RESULTS AND DISCUSSION

III-4.1. Processing of α-chitin using Ch[ACE] and morphological features of the resultant structures

The applications of Bio-ILs in polymer science is a new research field. To our knowledge, there are no previous studies regarding the use of Bio-ILs, namely choline acetate (Ch[ACE]), in the development of chitin-based 3D structures. So, in this study, several attempts were made towards the dissolution and processing of α-chitin (chitin from crab shell) using the Bio-IL Ch[ACE], including the testing of multiple stirring time intervals (30 min to 2 h) and temperatures (70 to 90 °C). All the dissolution tests were analysed by optical microscopy which proved that neither of them were effective in promoting the complete dissolution of α-chitin. In the literature, some works described that not only heat but also microwave and/or sonication cycles can promote the dissolution of insoluble natural materials[33–35]. Then, based on these findings, we decided to test the use of sonication cycles; and the complete dissolution of 1% wt of α-chitin in Ch[ACE] was reached using 10 s sonication pulses for 15 min, and stirring cycles at 90 °C. This process was monitored by light electron microscopy and in Figure III- 2a, and Figure III- 2b is demonstrated the total dissolution of 1% α-chitin in the Bio-IL Ch[ACE] at the end of the 4th cycle. Previous works have shown that ILs containing carboxylic acid anions have strong coordination ability or hydrogen-bond (H-bond) acceptability [6,36]. The acetate anion is a strong hydrogen bonding acceptor, which proved to be better than others such as the chlorinate and formate anions, in dissolving various chitin materials, being more effective in cracking the hydrogen bonds formed in the chitin structure [36]. The amide groups of chitin form strong inter- and intra-molecular H-bond networks that stabilize their three-dimensional structures, and its dissolution involves mainly the solvation of those parts. The acetate anion, present in the Bio-IL structure, strongly interacts with the H-bond network or hydroxyl groups forming very stable associations. These associations result in the cleavage of the chitin structure, leading to the dissolution of the polysaccharide.

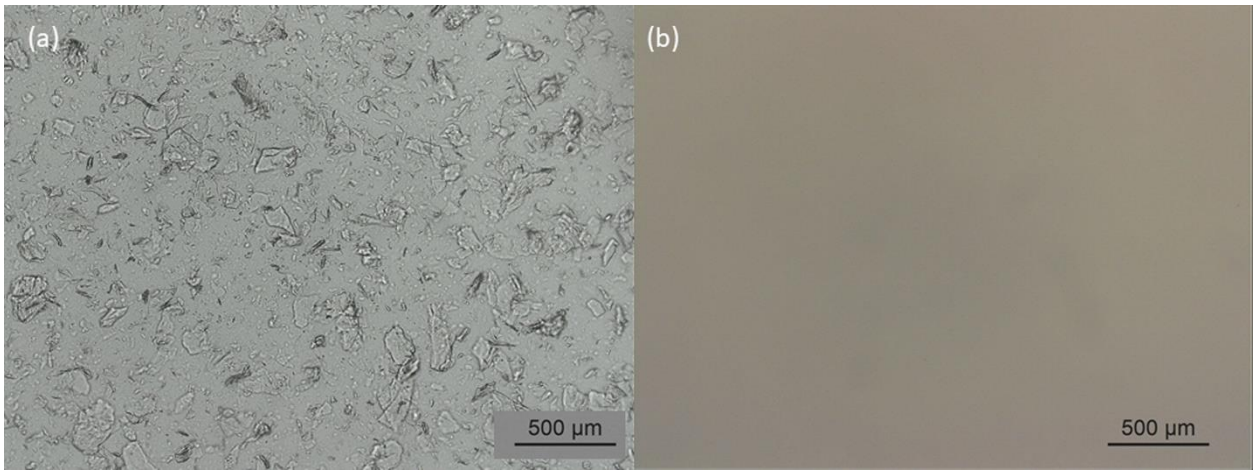


Figure III-2 - Light microscope images of the 1 % wt chitin in Ch[ACE] after (A) one dissolution cycle and (B) at the end of the 4th cycle.

After dissolution, the α-chitin/Ch[ACE] solution was molded into a cylindrical shape and cooled at -20 °C, to promote the formation chitin gels (ionogels). It is well known that the cooling process upon the chitin/IL solutions results in the correspondent chitin/IL gels, through curing [36,37]. Moreover, as a consequence of the excellent miscibility of the ILs in organic solvents, the addition of anti-solvents including water, acetone, methanol, isopropanol, and ethanol, promotes the regeneration of biomatrices [38]. Subsequently, in this work, the resultant α-chitin/Ch[ACE] gels were immersed in different solvents/coagulants, to provide materials with various features Figure III- 3a), reinforcing the gelation process. In our work, we tested the use of ethanol, methanol, isopropanol and acetone and the aspect of the structures was quite similar. The best results were obtained when using ethanol and methanol, which are widely used as successful coagulants for chitin and chitosan-based materials [37,39–41]. We hypothesise that the use of ethanol and methanol promoted the best results due to their effect in the coagulation of the polymer, as previously stated [39,41]. So, as expected some variances were observed in the formulations in which isopropanol and acetone were used. Isopropanol and acetone provided great gelation outcomes when used in other polymers/ILs gels [42,43].

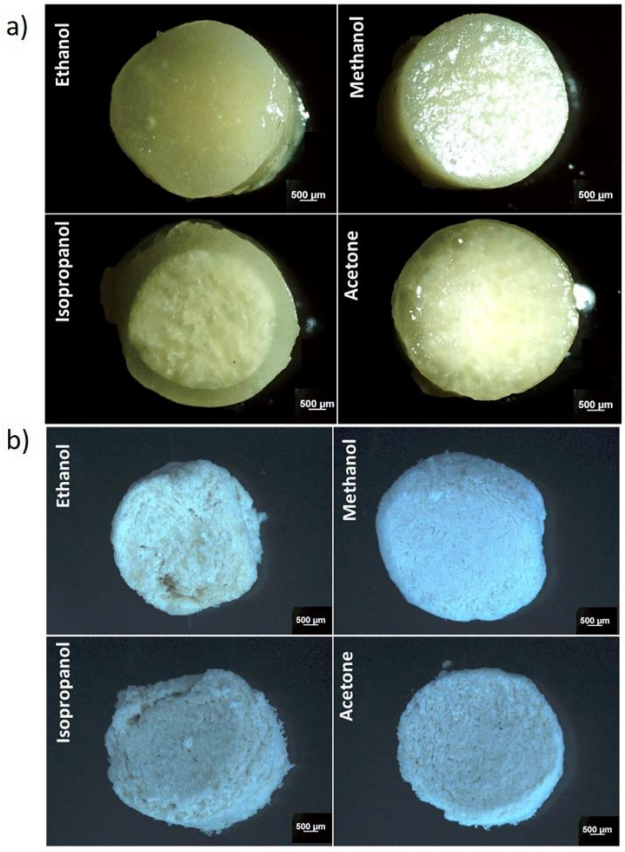


Figure III-3 - Stereomicroscope photos of the gels after (a) immersion in the solvents for 3 h and (b) freeze-drying.

After gelation and immersion in the stated solvents all samples were immersed in water, to remove the solvent, and freezed at -80 °C at least for 12 h, to promote the formation of the water crystal, before freeze-drying. All α-chitin/Ch[ACE] gels were freeze-dried and resulted in the sponges depicted in Figure III- 3b. The chitin sponges are characterized by a rough surface, with protuberances and a porous interior structure, which was evaluated by SEM. The SEM images of the cross-sections of the samples revealed that all of them have a uniform open structure with pore sizes between 15 and 45 µm, as presented in Figure III- 4.. Envisioning the application of the developed architectures for tissue engineering, stability tests of the samples in H_2O and PBS were performed. The outcomes of the stability test (Table III- 1) indicated that the structures prepared in methanol presented the best stability and firmness. In contrast, the other matrices were too fragile, collapsing when removed from H_2O or PBS, or when handled by touch or with tweezers.

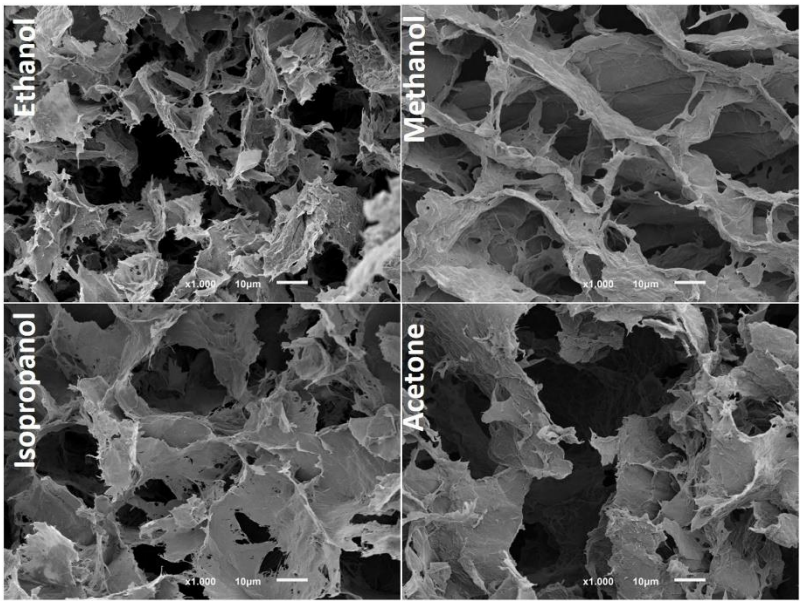


Figure III-4 **-** SEM cross-section images of the CACE-based sponges.

Table III-1 - Observations obtained from the stability assay.

	PBS		**H_2O**	
	2 h	24 h	2 h	24 h
Methanol	Stable	Stable	Stable	Stable
Acetone	Nonstable	Nonstable	Nonstable	Nonstable
Isopropanol	Nonstable	Nonstable	Nonstable	Nonstable
Ethanol	Nonstable	Nonstable	Nonstable	Nonstable

Considering the biocompatibility of Bio-IL (Ch[ACE]), we decided to establish two formulations based on the presence (CACE-A) and absence (CACE-B) of the solvent into the structure. Since Bio-ILs have excellent conductivity [12], the conductivity of the solvent aliquots collected after immersion of the gels for 2 h (CACE-A) or 24 h (CACE-B) was monitored. We observed that the consistency and firmness of the chitin gel formation were better after 2 h in contact with methanol, and then identified it as CACE-A. In sample CACE-B, the progressive decrease in conductivity during the multiple solvent changes, for one day, has confirmed the efficiency of the Bio-IL removal Figure III- 5b. As evidenced in previous studies, it was assumed that the samples with a conductivity below 1.5 μS/cm were free of Ch[ACE][2].

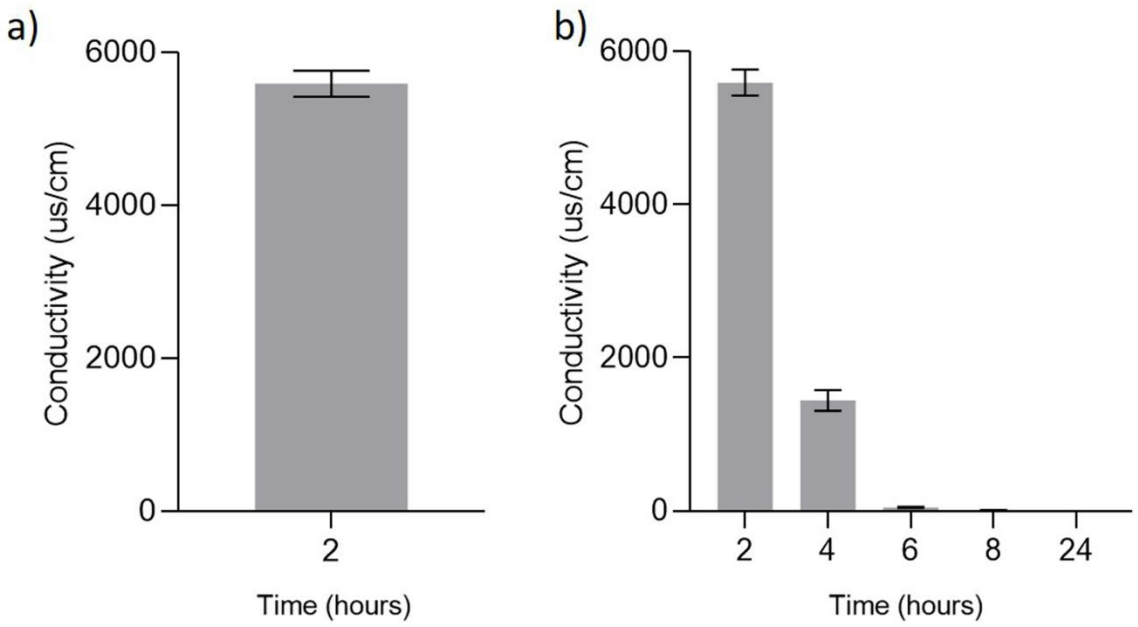


Figure III-5 - Conductivity measurements on the aliquots of methanol obtained after immersion of the structures for (a) 2 h for the preparation of formulation A and (b) up to 24 h, for the preparation of formulation B.

III-4.2. Effect of the presence/absence of Bio-IL into the architectures

After choosing the best solvent (methanol), following the strategy described above, the two established formulations (CACE-A and CACE-B) were defined, and further studies were conducted on them. The main objective was to evaluate if the presence of the Bio-IL in the CACE-based sponges influenced their morphology, cytotoxicity, and biological behavior.

III-4.2.1. Morphological features

A quantitative analysis of the 3D morphometric parameters that characterize the CACE sponges was performed by micro-CT analysis. The 3D images of the CACE sponges, as well as the mean thickness, porosity, mean pore sizes, and interconnectivity, are presented Figure III-6 and Table III-2. The findings indicated that the presence/absence of the Bio-IL in the structure does not significantly affect the interconnectivity. However, it is noticeable a slight increase both in the porosity (72.33±1.15 to 85.77±1.93 %) and pore size (173.43±28.54 to 176.70±44.48 μm) from CACE-A to CACE-B respectively, which may be a consequence of the absence of the Bio-IL in the matrix of the CACE-B formulation. Both

developed matrices exhibit porosity and pore interconnectivity that could allow not only cell penetration and nutrient diffusion, but also their proliferation into the structure [44].

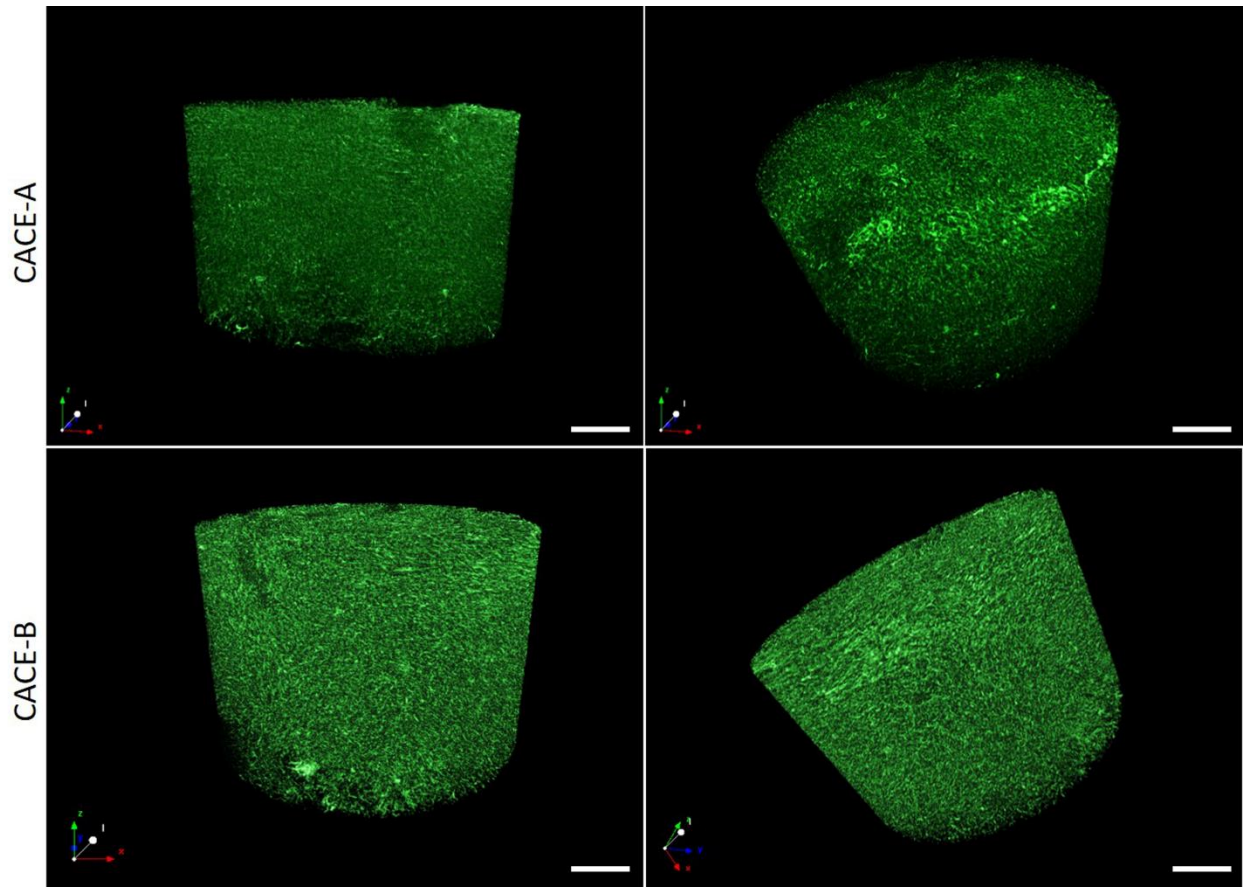


Figure III-6 - micro-CT images of the CACE-based sponges (scale bar 500µm)

Table III-2 **-** Values of interconnectivity, pore size, and porosity for CACE-based sponges obtained using micro-CT analysis.

Sample	Mean thickness (µm)	Mean pore size (µm)	Porosity (%)	Interconnectivity (%)
CACE-A	36.50±6.59	173.43±28.54	72.33±1.15	98.11±0.74
CACE-B	38.60±2.03	176.70±44.48	85.77±1.93	98.31±0.61

III-4.2.2. Rheology assay

The mechanical spectra of the CACE-A and CACE-B based sponges were acquired throughout rheological experiments (Figure III-7). The magnitude ratio of the G''/G' allows measuring the interaction strength of the internal structure of the material. Samples with higher storage modulus (G', gel character, elastic sample) are elastic solids, while samples with higher loss storage (G'', liquid character, viscous sample) are viscous liquids [42]. By the analysis of the spectra, it was observed that both samples present different behaviours throughout the frequencies being the modulus values significantly higher for higher frequency values. The higher G' of both samples may be representative of the stability of the three-dimensional network in the wet sponges. Comparatively, from a general point of view, the sample CACE-B presents low values for both G' and G'', meaning that the Bio-IL presence in the samples improves its mechanical properties.

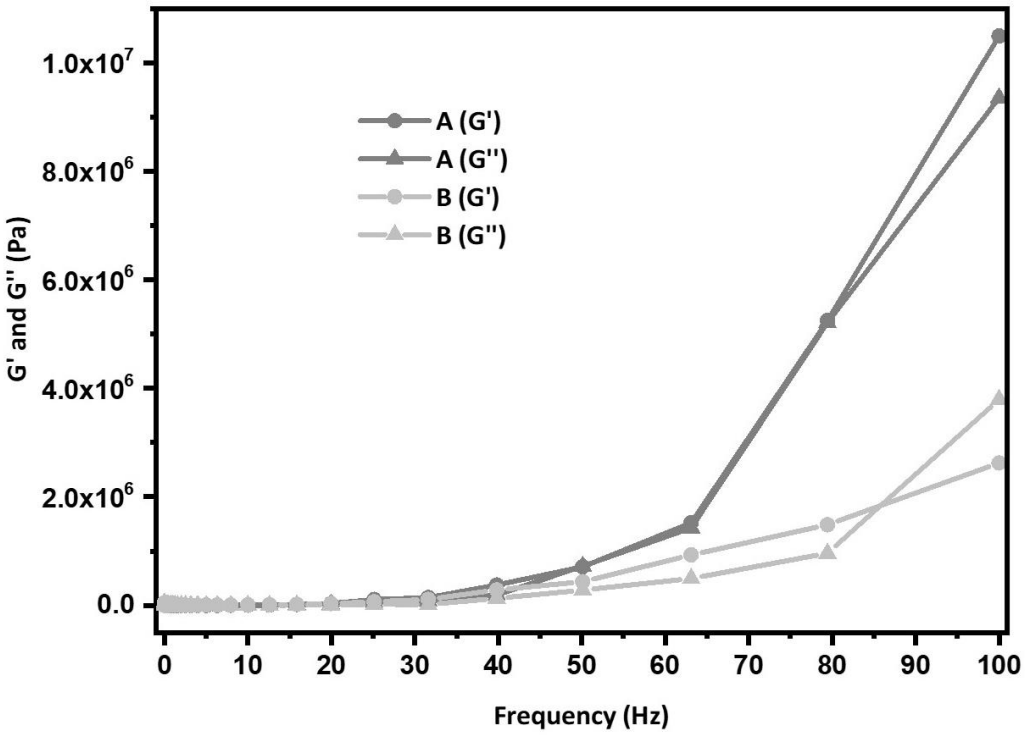


Figure III-7 - Storage modulus (G') and loss modulus (G'') of the CACE based sponges.

III-4.2.3. Degree of deacetylation (DD%) of chitin after processing

The DD% of the processed α-chitin was determined by Fourier to transform infrared spectroscopy (FTIR), since it is a relatively quick technique for the qualitative and quantitative evaluation of the DD%

[45]. The FTIR spectra, with the assignment of the relevant bands used for the DD% calculations, are presented in Supplementary Figure III-1 By using Eq. 1 we determined that the DD% of chitin in CACE-A and CACE-B sponges after processing is 27.1 and 28.6 % respectively. The DD% is a vital feature for some natural polymers, including chitin and chitosan (obtained by deacetylation of chitin with concentrated alkali and high-temperature treatments), determining their behaviour including the reactivity and solubility [46]. For instance, opposed to chitin, which is extremely insoluble in common solvents, chitosan is soluble in diluted acidic solutions, which was found to be a practical advantage. Some deacetylation procedures allow obtaining chitosan with DD% ranging between 80 to 90% [47]. The DD% of native α-chitin used in this work is 29.0%. These findings suggest that the innovative processing methodology herein presented does not significantly influence the DD% of chitin, despite the sonication and temperature cycles used for its processing.

III-4.2.4. Swelling

The swelling degree of the CACE sponges immersed in PBS for 24 h is presented in Figure III-8. It was observed a considerable swelling degree, around 3800%, in both formulations. In fact, it was observed an instant expansion of the structures immediately after the immersion of the sponges into the PBS solution. It is noticeable a slightly higher value in the swelling % in the structures in which the Bio-IL is present (CACE-A). Considering the solubility of the Bio-IL in PBS we hypothesize that the immersion of the sponges will lead to its removal from the structures. As previously shown, the Ch[ACE] removal induces an increase in the matrix porosity and consequently conducting to a higher PBS absorption. Although CACE-B has higher porosity than CACE.A, no significant statistical differences were observed between both formulations in different time points. Moreover, over time, it is clear the tendency to stabilize the swelling degree values. The developed sponges have a super absorbent-like behavior, being able to absorb and retain aqueous solutions, in this case, PBS, up to several hundred times their weight [48]. This characteristic may be appealing when considering the use of the produced structures as drug delivery systems. The high water retaining ability, in association with the high porosity of the CACE-sponges, suggests that a load of specific drugs into its structure and the further controlled release through, for instance, diffusion or swelling control, can be effectively attained [49,50]. Moreover, CACE sponges also have potential use in wound healing, allowing to keep a moist atmosphere at the site of application and adequate wound management, by absorbing the excess exudate and toxins [49–51].

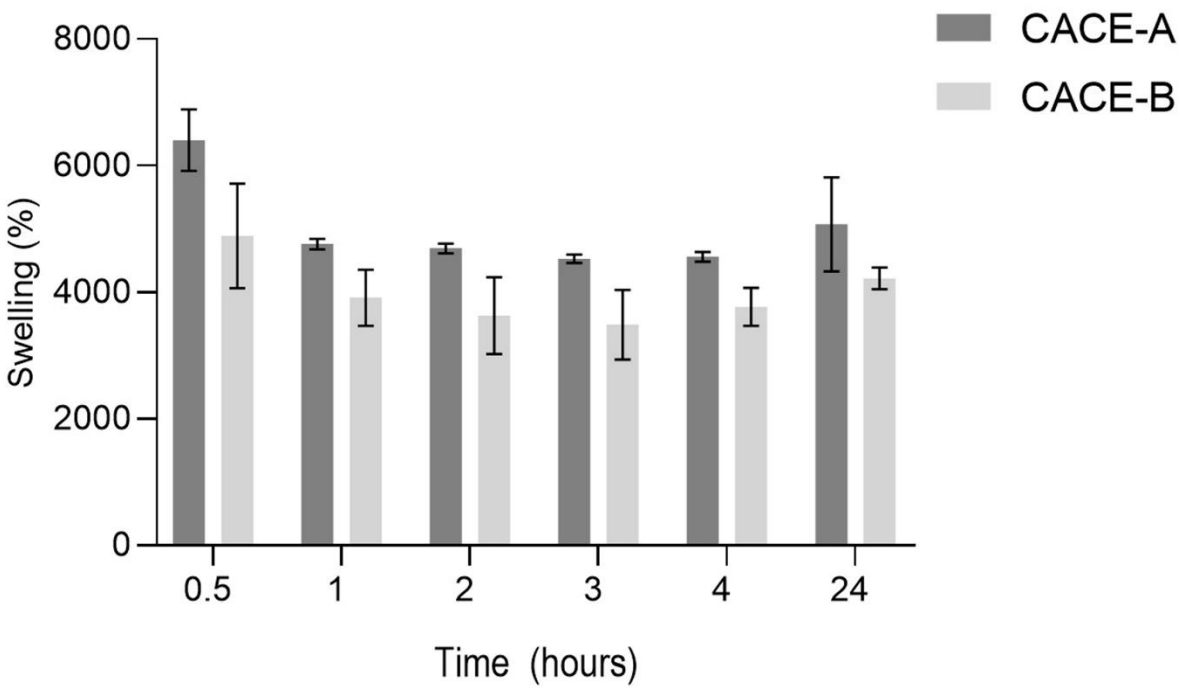


Figure III-8 **-** Swelling profile for CACE sponges immersed in PBS.

III-4.2.5. Thermal properties

The thermal properties of the CACE sponges were obtained by performing a DSC analysis on both CACE-A and CACE-B. The DSC thermograms for the sponges are shown in Supplementary Figure III- 2. The first endothermic peaks at 62.3 °C and 55.8 °C, for CACE-A and CACE-B respectively, suggest a dehydration process. CACE-A shows an endothermic curve around 230.7 °C, which may be attributed to the Ch[ACE] decomposition. The reported decomposition temperature of Ch[ACE] is 189 °C [52]. However, its interaction with chitin may lead to an increase in its resistance to degradation. In addition, the absence of this peak in the DSC thermogram of the CACE-B sample corroborates that Ch[ACE] is not present in this formulation, how was verified by the conductivity measurements. The exothermic peaks at 396.6 °C and 386.9 °C, for CACE-A and CACE-B respectively, are associated with the polymer degradation. Chitin's decomposition usually occurs around 400 °C, which is related to the decomposition of N-acetylglucosamine (GlcNAc) units that predominates in this structure [53]. The difference between these values in the different samples suggests once again that the effect of the Bio-IL in the structure, as well as its interaction with the polymer, can increase the resistance of the material to degradation.

III-4.3. Cell culture studies

III-4.3.1. Cytotoxicity

Cytotoxicity studies are a useful initial method to determine the potential toxicity of a developed biomaterial. To evaluate the cytotoxicity of CACE sponges, L929 cells were used in this study, following standard protocols[32]. The results showed that there is an increase in the metabolic activity after 72 h of culture Figure III-9; nevertheless, statistical analysis showed no significant differences in the metabolic activity between the different conditions at the same time point. Therefore, those findings mean that the presence of the Bio-IL Ch[ACE] in the structures results in sponges with no cytotoxicity. Even though ILs are considered green solvents, several studies have proved that the commonly used ones have some level of toxicity [12]. In a previous work from our group, in which an IL from the imidazolium family (1-butyl-3-imidazolium acetate ([bmim][Ac]) was used to process chitin into porous structures, it was proved to be critical to remove the IL from the polymeric matrix to have good cytotoxicity results, using the L929 cell line [39]. Considering that, our results are exciting since the maintenance of the Bio-IL in the CACE-based structures does not have a negative impact on the cell viability after 72 hours of culture. These results prove that the herein presented processing pathway contributes to the production of biomaterials using Bio-ILs without their removal is needed.

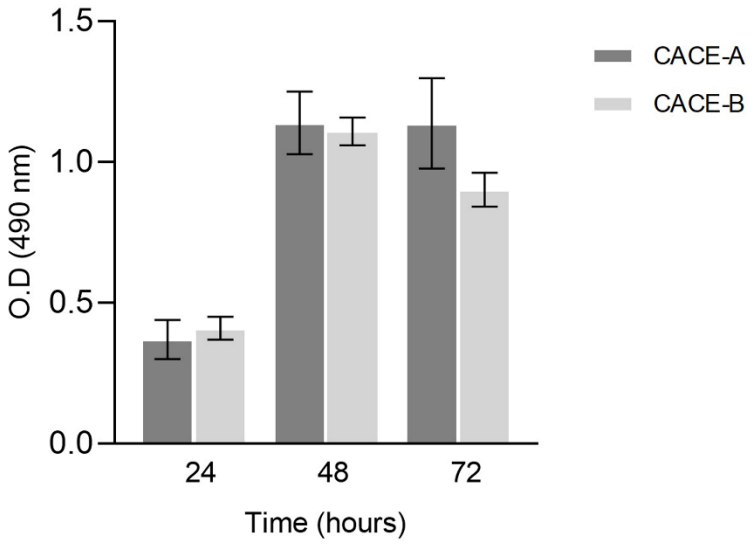


Figure III-9 - MTS results of L929 seeded both on the CACE-A and CACE-B structures cultured up to 72 h.

III-4.3.2. Biological behaviour

To evaluate the biological behavior of the developed biomaterials, a direct contact assay with hASCs was performed up to 7 days. hASCs were chosen due to their sensibility and ability to differentiate into the desired tissue. The MTS results revealed that cells could keep good metabolic activity up to 7 days of culture in both structures, revealing good cell growth (CACE-A and CACE-B, Figure III-10a. Regarding the statistical analysis, significant differences in the metabolic activity between the cells seeded in the different structures (CACE-A and CACE-B) at the same time point were observed. Higher cell growth was observed when the cells were seeded in the CACE-A, which proves that the presence of the Bio-IL in the matrix of the produced sponges does not negatively affect the cells by reducing their metabolic activity.

Furthermore, the results of DNA quantification showed that hASCs were able to proliferate from the initial time point to 7 days in both structures. However, a slight decrease in cell proliferation was seen in the CACE-A between 3 and 7 days (Figure III-10b). Statistical analysis showed significant differences in the dsDNA content between the different conditions, namely between the cells seeded in the different structures (CACE-A and CACE-B) at the same time points.

After 24h of culture, the cells were completely adapted to the CACE structures since no significant differences were observed between the cell growth and profanation after 72h of contact. However, both cells' metabolic activity and proliferation are higher in the CACE-A samples than in the CACE-B, in all time points, indicating that the cell viability in not affected by the Bio-IL presence and suggesting a positive effect of the Bio-IL on the hASCs behavior, which should be further studied. Moreover, the live dead assay results (Supplementary Figure III-3) are according to those obtained in the MTS and dsDNA quantification assays. Upon the presence of the Ch[ACE] in the structures, no detectable/negligibly cell death can be seen, indicating that Ch[ACE] did not induce any deleterious effect on cell viability. This behavior could be a consequence of better cell adhesion and spreading through the porous structure upon the presence of the Bio-IL.

The herein presented results, regarding either the cell viability and proliferation, are encouraging, since in a previous study, in which the authors produced chitin-hydroxyapatite composites aiming bone regeneration using the IL [bmim][Ac], it is reported the mandatory removal of the IL, in order to maintain a good cellular behavior, using an osteoblast-like cell line [54]. Moreover, other works using different polymers such as silk fibroin and chitosan processed with common ILs, obtained good biological behaviour results succeeding the IL removal [2,13,42,55].

Confocal laser scanning microscopy (CLSM) confirmed cell attachment and spreading on the surface of the sponges (Figure III-10c). Independently of the sponge, the cells attached to their surfaces. F-actin staining (in red) and the nuclei (in blue) showed that the culturing of cells directly with each formulation (CACE-A or CACE-B) did not promote any visible cell damage and that the cells kept their morphology, presenting intact actin filaments and round nuclei confirming the previously observed [56,57]. It is also possible to observe that in the CACE-A a cell organization around their structure from day 3 to day 7, while in the CACE-B, the cells were randomly distributed, which once again suggests the advantageous effect for the cells of the Bio-IL presence in the polymeric matrix.

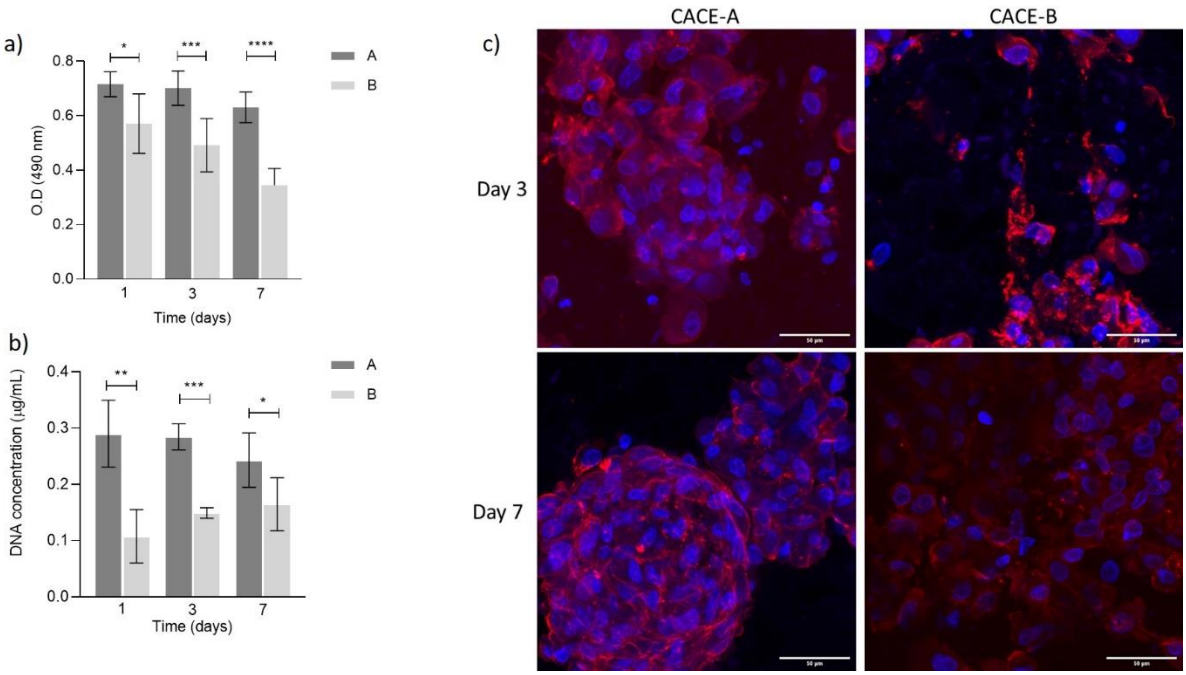


Figure III-10 - MTS results (a) and dsDNA content, (b) of hASCS seeded both on the CACE-A and CACE-B structures up to 7 days of culture. Data represents ±SD (*$p < 0.05$, nonparametric Mann-Whitney); (c) Confocal laser micrographs of hASCs cultured on CACE-A and CACE-B structures after 3 and 7 days. The cells were stained with rhodamine-phalloidin for actin filaments (red) and Hoechst 33342 for nuclei (blue).

III-5. CONCLUSION

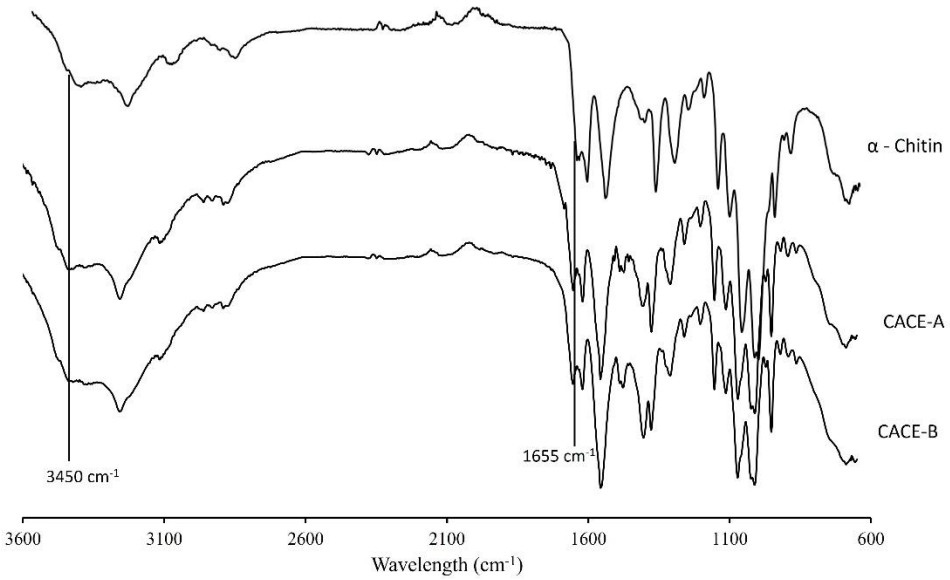
This work has proposed an alternative and innovative route to explore the use of biocompatible ionic liquid (Ch[ACE]) in the processing of chitin to enlarge its applications. The evaluation of the presence and absence of (Ch[ACE]) in chitin-based structures demonstrated that it does not affect their morphological

features. Besides, the non-cytotoxic profile of both developed structures, as well as the positive biological performance of them using hASCs, suggested that those sponges can sustain good cell viability and proliferation without any deleterious effect of Ch[ACE] onto cells. It contrasts with most previous works in which ILs were used to process the natural polymer chitin since the removal of the IL was mandatory to promote good biological behavior. Although the exploitation of Bio-ILs in the biomedical area is recent, the outcomes demonstrated herein open new avenues to the development of biomaterials using Bio-ILs with potential applications into the biomedical and tissue engineering fields.

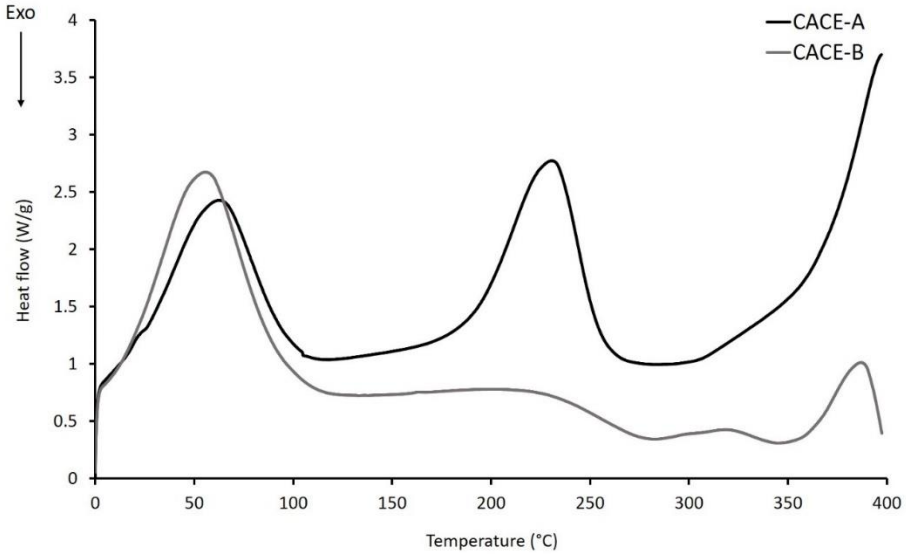
ACKNOWLEDGMENTS

The authors especially acknowledge financial support from Portuguese FCT (PD/BD/135247/2017). This work is also financially supported by PhD programme in Advanced Therapies for Health (PATH) (PD/00169/2013), FCT R&D&I projects with references PTDC/BII-BIO/31570/2017, and R&D&I Structured Projects with reference NORTE-01-0145-FDER-000021.

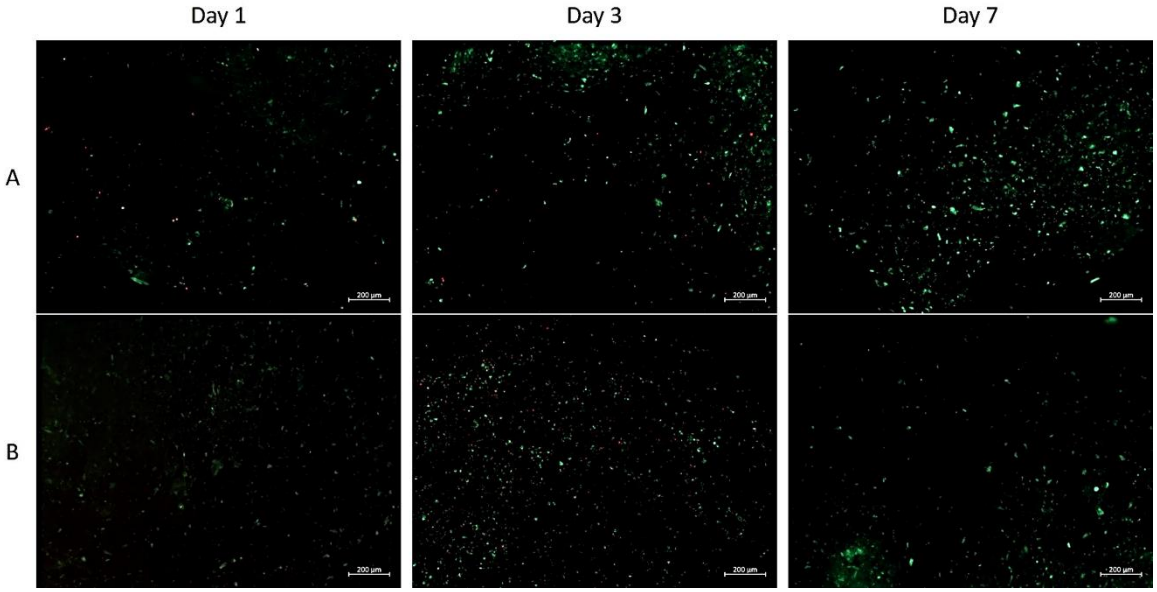
III-6. SUPPLEMENTARY MATERIAL



Supplementary Figure III-1 – FTIR spectra of the CACE-based sponges and α-chitin.



Supplementary Figure III-2- DSC thermograms of the CACE sponges.



Supplementary Figure III-3 – Representative live/dead images from hASCs seeded both on the A and B structures up to 7 days of culture.

III-7. REFERENCES

[1] R.A. Sheldon, Green and sustainable manufacture of chemicals from biomass: state of the art, Green Chem. 16 (2014) 950–963. https://doi.org/10.1039/C3GC41935E.

[2] S.S. Silva, N.M. Oliveira, M.B. Oliveira, D.P.S. Da Costa, D. Naskar, J.F. Mano, S.C. Kundu, R.L. Reis, Fabrication and characterization of Eri silk fibers-based sponges for biomedical application, Acta Biomater. 32 (2016) 178–189. https://doi.org/10.1016/j.actbio.2016.01.003.

[3] S.S. Silva, T.C. Santos, M.T. Cerqueira, A.P. Marques, L.L. Reys, T.H. Silva, S.G. Caridade, J.F. Mano, R.L. Reis, The use of ionic liquids in the processing of chitosan/silk hydrogels for biomedical applications, Green Chem. 14 (2012) 1463–1470. https://doi.org/10.1039/c2gc16535j.

[4] L. Yang, Z. Zheng, C. Qian, J. Wu, Y. Liu, S. Guo, G. Li, M. Liu, X. Wang, D.L. Kaplan, Curcumin-functionalized silk biomaterials for anti-aging utility, J. Colloid Interface Sci. 496 (2017) 66–77. https://doi.org/10.1016/j.jcis.2017.01.115.

[5] L.A. Lucia, A. Ayoub, Polysaccharide-based fibers and composites: Chemical and engineering fundamentals and industrial applications, Springer International Publishing, 2018. https://doi.org/10.1007/978-3-319-56596-5.

[6] S.S. Silva, J.F. Mano, R.L. Reis, Ionic liquids in the processing and chemical modification of chitin and chitosan for biomedical applications, Green Chem. 19 (2017) 1208–1220. https://doi.org/10.1039/C6GC02827F.

[7] J.L. Shamshina, P. Berton, R.D. Rogers, Advances in Functional Chitin Materials: A Review, ACS Sustain. Chem. Eng. 7 (2019) 6444–6457. https://doi.org/10.1021/acssuschemeng.8b06372.

[8] A. Takada, J.I. Kadokawa, Fabrication and characterization of polysaccharide ion gels with ionic liquids and their further conversion into value-added sustainable materials, Biomolecules. 5 (2015) 244–262. https://doi.org/10.3390/biom5010244.

[9] A. Takegawa, M. aki Murakami, Y. Kaneko, J. ichi Kadokawa, Preparation of chitin/cellulose composite gels and films with ionic liquids, Carbohydr. Polym. 79 (2010) 85–90. https://doi.org/10.1016/j.carbpol.2009.07.030.

[10] Y. Qin, X. Lu, N. Sun, R.D. Rogers, Dissolution or extraction of crustacean shells using ionic liquids to obtain high molecular weight purified chitin and direct production of chitin films and fibers, Green Chem. 12 (2010) 968. https://doi.org/10.1039/c003583a.

[11] P.S. Barber, C.S. Griggs, J.R. Bonner, R.D. Rogers, Electrospinning of chitin nanofibers directly from an ionic liquid extract of shrimp shells, Green Chem. 15 (2013) 601–607. https://doi.org/10.1039/c2gc36582k.

[12] J.M. Gomes, S.S. Silva, R.L. Reis, Biocompatible ionic liquids: fundamental behaviours and applications, Chem. Soc. Rev. (2019) 135247. https://doi.org/10.1039/C9CS00016J.

[13] S.S. Silva, T.C. Santos, M.T. Cerqueira, A.P. Marques, L.L. Reys, The use of ionic liquids in the processing of chitosan / silk hydrogels for biomedical applications, Green Chem. 14 (2012) 1463–1470. https://doi.org/10.1039/c2gc16535j.

[14] S.S. Silva, A.R.C. Duarte, J.F. Mano, R.L. Reis, Design and functionalization of chitin-based microsphere scaffolds, Green Chem. 15 (2013) 3252–3258. https://doi.org/10.1039/c3gc41060a.

[15] A. Idris, R. Vijayaraghavan, U.A. Rana, D. Fredericks, A.F. Patti, D.R. Macfarlane, Dissolution of feather keratin in ionic liquids†, Green Chem. 15 (2013) 525–534. https://doi.org/10.1039/c2gc36556a.

[16] H. Garcia, R. Ferreira, M. Petkovic, J.L. Ferguson, M.C. Leitão, H.Q.N. Gunaratne, K.R. Seddon, L.P.N. Rebelo, C. Silva Pereira, Dissolution of cork biopolymers in biocompatible ionic liquids, Green Chem. 12 (2010) 367–369. https://doi.org/10.1039/b922553f.

[17] Q. Liu, X.-D. Hou, M. Zong, Ionic liquids from renewable biomaterials : synthesis , characterization and application in the pretreatment of biomass †, Green Chem. 14 (2012) 304–307. https://doi.org/10.1039/c2gc16128a.

[18] X.-D. Hou, T.J. Smith, N. Li, M. Zong, Novel Renewable Ionic Liquids as Highly Effective Solvents for Pretreatment of Rice Straw Biomass by Selective Removal of Lignin, Biotechnol. Bioeng. 109 (2012) 2484–2493. https://doi.org/10.1002/bit.24522.

[19] F. Liu, Q. Liu, A. Wang, T. Zhang, Direct Catalytic Hydrogenolysis of Kraft Lignin to Phenols in Choline- Derived Ionic Liquids, ACS Sustain. Chem. Eng. 4 (2016) 3850–3856. https://doi.org/10.1021/acssuschemeng.6b00620.

[20] D. Outeiriño, I. Costa-trigo, A. Paz, F.J. Deive, A. Rodríguez, J. Manuel, Biorefining brewery spent grain polysaccharides through biotuning of ionic liquids, Carbohydr. Polym. 203 (2019) 265–274. https://doi.org/10.1016/j.carbpol.2018.09.042.

[21] G. Colomines, P. Decaen, D. Lourdin, E. Leroy, Biofriendly ionic liquids for starch plasticization: a screening approach, RSC Adv. 6 (2016) 90331–90337. https://doi.org/10.1039/C6RA16573G.

[22] S. Guilois, V. Jury, N. Allanic, E. Leroy, P. Decaen, A. Rolland-sabaté, S. Guilois, V. Jury, N. Allanic, E. Leroy, Choline Chloride vs Choline Ionic liquids for starch thermoplasticization, Carbohydr. Polym. 117 (2017) 424–432. https://doi.org/10.1016/j.carbpol.2017.09.012.

[23] A. Banerjee, K. Ibsen, T. Brown, R. Chen, C. Agatemor, S. Mitragotri, Ionic liquids for oral insulin delivery, 115 (2018) 1–6. https://doi.org/10.1073/pnas.1722338115.

[24] E.E.L. Tanner, K.N. Ibsen, S. Mitragotri, Transdermal insulin delivery using choline-based ionic liquids (CAGE), J. Control. Release. 286 (2018) 137–144. https://doi.org/10.1016/j.jconrel.2018.07.029.

[25] C. Florindo, A.B. Pereiro, N.S.M. Vieira, A.A. Matias, C.M.M. Duarte, P.N. Rebelo, I.M. Marrucho, Cholinium-based ionic liquids with pharmaceutically active anions †, RSC Adv. 4 (2014) 28126–28132. https://doi.org/10.1039/c3ra47615d.

[26] R. Moshikur, R. Chowdhury, R. Wakabayashi, Y. Tahara, Ionic liquids with methotrexate moieties as a potential anticancer prodrug : Synthesis , characterization and solubility evaluation, J. Mol. Liq. 278 (2019) 226–233. https://doi.org/10.1016/j.molliq.2019.01.063.

[27] S.S.D. Kumar, M. Surianarayanan, R. Vijayaraghavan, A.B. Mandal, D.R. Macfarlane, Curcumin loaded poly(2-hydroxyethyl methacrylate) nanoparticles from gelled ionic liquid - *In vitro* cytotoxicity and anti-cancer activity in SKOV-3 cells, Eur. J. Pharm. Sci. 51 (2014) 34–44. https://doi.org/10.1016/j.ejps.2013.08.036.

[28] M. Isik, T. Lonjaret, H. Sardon, R. Marcilla, T. Herve, G.G. Malliaras, E. Ismailova, D. Mecerreyes, Cholinium-based ion gels as solid electrolytes for long-term cutaneous electrophysiology, J. Mater. Chem. C. 3 (2015) 8942–8948. https://doi.org/10.1039/c5tc01888a.

[29] E. Bihar, T. Roberts, E. Ismailova, M. Saadaoui, M. Isik, A. Sanchez-Sanchez, D. Mecerreyes, T. Hervé, J.B. De Graaf, G.G. Malliaras, Fully Printed Electrodes on Stretchable Textiles for Long-Term Electrophysiology, Adv. Mater. Technol. 2 (2017). https://doi.org/10.1002/admt.201600251.

[30] I. Noshadi, B.W. Walker, R. Portillo-lara, E.S. Sani, Engineering Biodegradable and Biocompatible Bio-ionic Liquid Conjugated Hydrogels with Tunable Conductivity and Mechanical Properties, Nature. 7 (2017) 1–18. https://doi.org/10.1038/s41598-017-04280-w.

[31] F. Boukhlifi, Quantitative Analysis by IR: Determination of Chitin/ Chitosan DD, in: Mod. Spectrosc. Tech. Appl., 2020: pp. 1–24. https://doi.org/10.1016/j.colsurfa.2011.12.014.

[32] ISO 2009 Biological evaluation of medical devices:part 5. Test for *In vitro* cytotoxicity ISO 10993-5, n.d.

[33] F. Cheng, H. Wang, G. Chatel, G. Gurau, R.D. Rogers, Facile pulping of lignocellulosic biomass using choline acetate, Bioresour. Technol. 164 (2014) 394–401. https://doi.org/10.1016/j.biortech.2014.05.016.

[34] M. Sharma, C. Muskesh, D. Mondal, K. Prasad, Dissolution of α-chitin in deep eutectic solvents, RCS Adv. 3 (2013) 18149–18155. https://doi.org/10.1039/c3ra43404d.

[35] R.P. Swatloski, S.K. Spear, J.D. Holbrey, R.D. Rogers, Dissolution of cellose with ionic liquids, J. Am. Chem. Soc. 124 (2002) 4974–4975. https://doi.org/10.1021/ja025790m.

[36] Y. Wu, T. Sasaki, S. Irie, K. Sakurai, A novel biomass-ionic liquid platform for the utilization of native chitin, Polymer (Guildf). 49 (2008) 2321–2327. https://doi.org/10.1016/j.polymer.2008.03.027.

[37] J. ichi Kadokawa, Dissolution, derivatization, and functionalization of chitin in ionic liquid, Int. J. Biol. Macromol. 123 (2019) 732–737. https://doi.org/10.1016/j.ijbiomac.2018.11.165.

[38] J. Chen, F. Xie, X. Li, L. Chen, Ionic liquids for the preparation of biopolymer materials for drug/gene delivery: A review, Green Chem. 20 (2018) 4169–4200. https://doi.org/10.1039/c8gc01120f.

[39] S.S. Silva, A. Rita, C. Duarte, A. Paula, J.F. Mano, R.L. Reis, Green processing of porous chitin structures for biomedical applications combining ionic liquids and supercritical fluid technology, Acta Biomater. 7 (2011) 1166–1172. https://doi.org/10.1016/j.actbio.2010.09.041.

[40] S.S. Silva, A.R.C. Duarte, J.M. Oliveira, J.F. Mano, R.L. Reis, Alternative methodology for chitin-hydroxyapatite composites using ionic liquids and supercritical fluid technology, J. Bioact. Compat. Polym. 28 (2013) 481–491. https://doi.org/10.1177/0883911513501595.

[41] M.M. Jaworska, T. Kozlecki, A. Gorak, Review of the application of ionic liquids as solvents for chitin, J. Polym. Eng. 32 (2012) 67–69. https://doi.org/10.1515/polyeng-2011-0145.

[42] C. Gonçalves, S.S. Silva, J.M. Gomes, I.M. Oliveira, R.F. Canadas, F.R. Maia, H. Radhouani, R.L. Reis, J.M. Oliveira, Ionic Liquid-Mediated Processing of SAIB-Chitin Scaffolds, ACS Sustain. Chem. Eng. 8 (2020) 3986–3994. https://doi.org/10.1021/acssuschemeng.0c00385.

[43] K. Prasad, D. Mondal, M. Sharma, M.G. Freire, C. Mukesh, J. Bhatt, Stimuli responsive ion gels based on polysaccharides and other polymers prepared using ionic liquids and deep eutectic solvents, Carbohydr. Polym. 180 (2018) 328–336. https://doi.org/10.1016/j.carbpol.2017.10.020.

[44] S. V. Madihally, H.W.T. Matthew, Porous chitosan scaffolds for tissue engineering, Biomaterials. 20 (1999) 1133–1142. https://doi.org/10.1016/S0142-9612(99)00011-3.

[45] M.R. Kasaai, A review of several reported procedures to determine the degree of N-acetylation for chitin and chitosan using infrared spectroscopy, Carbohydr. Polym. 71 (2008) 497–508. https://doi.org/10.1016/j.carbpol.2007.07.009.

[46] M.L. Duarte, M.C. Ferreira, M.R. Marvão, J. Rocha, An optimised method to determine the degree of acetylation of chitin and chitosan by FTIR spectroscopy, Int. J. Biol. Macromol. 31 (2002) 1–8. https://doi.org/10.1016/S0141-8130(02)00039-9.

[47] M.B. Kaczmarek, K. Struszczyk-Swita, X. Li, M. Szczęsna-Antczak, M. Daroch, Enzymatic modifications of chitin, chitosan, and chitooligosaccharides, Front. Bioeng. Biotechnol. 7 (2019). https://doi.org/10.3389/fbioe.2019.00243.

[48] A. Mignon, N. De Belie, P. Dubruel, S. Van Vlierberghe, Superabsorbent polymers: A review on the characteristics and applications of synthetic, polysaccharide-based, semi-synthetic and 'smart' derivatives, Eur. Polym. J. 117 (2019) 165–178. https://doi.org/10.1016/j.eurpolymj.2019.04.054.

[49] E. Caló, V. V. Khutoryanskiy, Biomedical applications of hydrogels: A review of patents and commercial products, Eur. Polym. J. 65 (2015) 252–267. https://doi.org/10.1016/j.eurpolymj.2014.11.024.

[50] M. Sadeghi, H. Hosseinzadeh, Synthesis of starch-poly(sodium acrylate-co-acrylamide) superabsorbent hydrogel with salt and pH-responsiveness properties as a drug delivery system, J. Bioact. Compat. Polym. 23 (2008) 381–404. https://doi.org/10.1177/0883911508093504.

[51] S. Dey, D. Kenneally, M. Odio, I. Hatzopoulos, Modern diaper performance: construction, materials, and safety review, Int. J. Dermatol. 55 (2016) 18–20. https://doi.org/10.1111/ijd.13333.

[52] Y. Fukaya, Y. Iizuka, K. Sekikawa, H. Ohno, Bio ionic liquids : room temperature ionic liquids composed wholly of biomaterials, Green Chem. 9 (2007) 1155–1157. https://doi.org/10.1039/b706571j.

[53] L.S. Guinesi, The use of DSC curves to determine the acetylation degree of chitin / chitosan samples, 444 (2006) 128–133. https://doi.org/10.1016/j.tca.2006.03.003.

[54] S.S. Silva, A.R.C. Duarte, J.M. Oliveira, J.F. Mano, R.L. Reis, Alternative methodology for chitin – hydroxyapatite composites using ionic liquids and supercritical fluid technology, J. Bioact. Compat. Polym. (2013) 5. https://doi.org/10.1177/0883911513501595.

[55] S.S. Silva, E.G. Popa, M.E. Gomes, M.B. Oliveira, S. Nayak, B. Subia, J.F. Mano, S.C. Kundu, R.L. Reis, Silk hydrogels from non-mulberry and mulberry silkworm cocoons processed with ionic liquids, Acta Biomater. 9 (2013) 8972–8982. https://doi.org/10.1016/j.actbio.2013.06.044.

[56] S. Ahrens, S. Zelenay, D. Sancho, P. Hanč, S. Kjær, C. Feest, G. Fletcher, C. Durkin, A. Postigo, M. Skehel, F. Batista, B. Thompson, M. Way, C. Reis e Sousa, O. Schulz, F-Actin Is an Evolutionarily Conserved Damage-Associated Molecular Pattern Recognized by DNGR-1, a Receptor for Dead Cells, Immunity. 36 (2012) 635–645. https://doi.org/10.1016/j.immuni.2012.03.008.

[57] L.C. Crowley, B.J. Marfell, N.J. Waterhouse, Analyzing cell death by nuclear staining with Hoechst 33342, Cold Spring Harb. Protoc. 2016 (2016) 778–781. https://doi.org/10.1101/pdb.prot087205.

Chapter IV

Silk fibroin/cholinium gallate-based architectures as therapeutic tools

Chapter IV

Silk fibroin/cholinium gallate-based architectures as therapeutic tools ‡

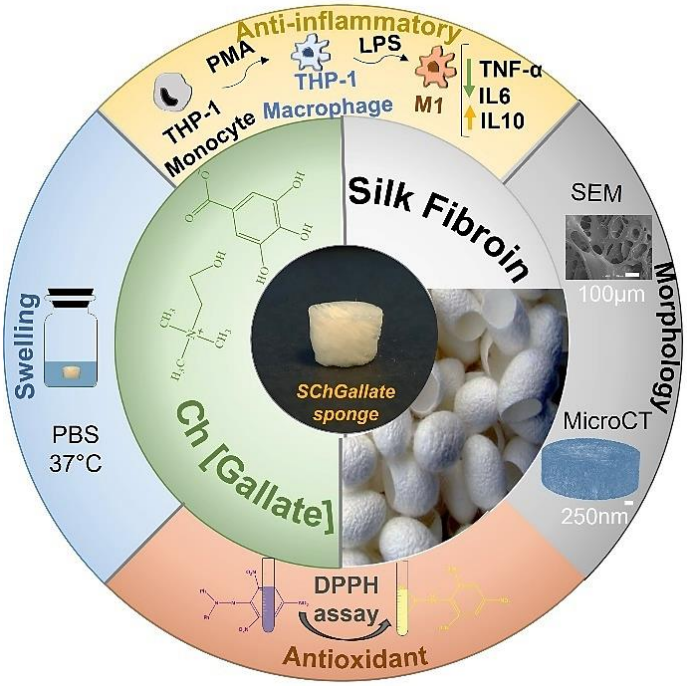
ABSTRACT

The combination of natural resources with biologically active biocompatible ionic liquids (Bio-IL) is presented as a combinatorial approach for developing tools to manage inflammatory diseases. Innovative biomedical solutions were constructed by combining silk fibroin (SF) and Ch[Gallate], a Bio-IL with antioxidant and anti-inflammatory features, as freeze-dried 3D-based sponges. An evaluation of the effect of the Ch[Gallate] concentration (≤3% w/v) on the SF/Ch[Gallate] sponges was studied. Structural changes observed on the sponges revealed that the Ch[Gallate] presence positively affected the β-sheet formation while not influencing the silk native structure, which was suggested by the FTIR and solid-state NMR results, respectively. Also, it was possible to modulate their mechanical properties, antioxidant activity, and stability/degradation in an aqueous environment, by changing the Ch[Gallate] concentration. The architectures showed high water uptake ability and a weight loss that follows the controlled Ch[Gallate] release rate studied for 7 days. Furthermore, the sponges supported human adipose stem cells adhesion and proliferation, up to 7 days. TNF-α, IL-6 (pro-inflammatory) and IL-10 (anti-inflammatory) release quantification from a human monocyte cell line revealed a decrease in the concentrations of the pro-inflammatory cytokine in samples containing Ch[Gallate]. These outcomes encourage the use of the developed architectures as tissue engineering solutions, potentially targeting inflammation processes.

‡ This chapter is based on the following publication:

Gomes J. M., Silva S. S., Fernandes E. M., Lobo F. C. M. and Reis R. L "Silk fibroin/cholinium gallate-based architectures: bio-based tools for inflammatory diseases treatment"; Acta Biomaterialia 2022, 147, 168-184, doi: /10.1016/j.actbio.2022.05.020.

IV-1. GRAPHICAL ABSTRACT



IV-2. INTRODUCTION

The inflammatory process associated with chronic diseases, such as osteoarthritis, rheumatoid arthritis, and even cancer, frequently prevents pathology management and treatment [1–4]. Tissue engineering strategies promote regeneration and healing processes, allowing the design architectures that combine key factors, including growth factors and biochemical cues, to fulfill a specific treatment requirement [3,5,6]. Nonetheless, the successful combination of cells, materials, and bioactive agents persists as one of the major challenges faced in tissue engineering [6]. Using natural polymers, in combination with ionic liquids (IL), particularly those with biocompatible and bioactive features, allows to extend their use to the biomedical field and develop effective and sustainable biomedical solutions [7]. Biocompatible ionic liquids (Bio-ILs) are organic salts, mostly synthesized using anionic and cationic counterparts derived from biocompatible materials. These compounds have proven their potential as polymer plasticizers [8,9], as solvents for the selective extraction of compounds from biomass [10,11], and for enhancing the polymer processability and consequent applicability, which is limited due to the poor dissolution ability [12]. In addition, many advantages are brought by using active pharmaceutical ingredients (APIs) as Bio-ILs moieties, including the increase of the bioactive compounds' stability,

solubility, and bioavailability [13–15]. For instance, the use of phenolic compounds, such as gallic acid, which are known for their antioxidant and anti-inflammatory properties [16], as anionic counterparts in the synthesis of cholinium-based ILs allows to overcome their limited water solubility, extending their applicability [17]. Therefore, Bio-ILs' association with natural polymers such as cellulose, chitosan, gelatin, and silk fibroin (SF), has been successfully attempted for the development of innovative solutions which include implantable power sources and next-generation medical bionics, which take advantage not only on the Bio-ILs biocompatibility but also their conductivity [18–23]. SF, derived from silkworm cocoons is particularly attractive due to its good biocompatibility, lack of toxicity, and mechanical strength [23]. Sericin, a natural macromolecular protein derived from silkworm cocoons, has also been exploited to develop biomaterials, such as films, hydrogels, and sponges as tissue engineering and biomedical solutions [24–27]. Recently, ILs have been used to process SF from silk cocoons from mulberry silkworms, bombyx mori, non-mulberry Eri, and *Antheraea pernyi* into films nanofibers, nanoparticles, hydrogels, and 3D scaffolds [28–33]. In most of those studies, IL removal is mandatory to minimize the potential cytotoxicity of the resulting matrices. However, only a few studies report its use in combination with Bio-ILs, with the few available being focused on developing actuator devices and medical bionics [19,23]. Recently, we have shown that cholinium acetate, a commercial Bio-IL, was helpful in processing α-chitin into 3D structures and could be kept in the matrices [12]. The biological performance of the α-chitin/cholinium acetate architectures using human adipose stem cells (hASCs) demonstrated that the hASCs were viable and proliferated onto them, indicating the solvent's harmless effect on the cultured cells. However, by comparing the number of studies on the biomedical potential between ILs and Bio-ILs is possible to conclude that the use of Bio-ILs in the biomedical field is still in its early-stage.

Herein, we hypothesized the development of 3D-based sponges through the association of SF and Ch[Gallate]. The proposed SF/Ch[Gallate]-based sponges would have antioxidant and anti-inflammatory activities due to the intrinsic features of Ch[Gallate], while taking advantage of the SF's recognized biocompatibility [34]. Therefore, is expected that the developed architectures would have an adequate biological performance to act as biomedical materials for managing the inflammation phase, which is frequently associated with diseases such as cancer, degenerative cartilage, and age-related pathologies, including osteoarthritis and Alzheimer's, respectively [2,35,36]. The present study investigates the effect of different concentrations of the Ch[Gallate] (up to 3% w/v) on the antioxidant capacity, structural changes, and morphological features of the SF/Ch[Gallate] sponges. Also, the swelling ability and Ch[Gallate] release was studied in phosphate-buffered saline (PBS) medium. Furthermore, the biological

behavior of the sponges was studied by culturing hASCs into them, and their therapeutic effect was assessed using the human monocyte cell line, THP-1, both up to 7 days of culture.

IV-3. MATERIALS AND METHODS

IV-3.1. Materials

Silk fibroin from cocoons of Bombyx mori was kindly supplied by the APPACDM (Castelo Branco, Portugal). Cholinium hydroxide (Ch[OH]) 45% in methanol solution and Gallic acid, both used in the synthesis, were purchased from Sigma-Aldrich, St. Louis, MO, USA. 2,2-diphenyl-1-picrylhydrazyl (DPPH) was also purchased from Sigma-Aldrich, St. Louis, MO, USA. All other chemicals were reagent grade, and they were used as received. Human blood samples were obtained from Serviço de Imuno-Hemoterapia - Centro Hospitalar de São João (Portugal) under an approved institutional board protocol (ethical commission of CHSJ/FMUP approved at 18/13/2018). The samples were collected in sterile BD Vacutainer® coagulation tubes (BD-Plymouth, UK), which contained 3.8 % sodium citrate.

IV-3.2. Synthesis of Choline-Gallate (Ch[Gallate])

Ch[Gallate] was synthesized as previously reported [16]. Briefly, Cholinium hydroxide (Ch[OH]) was dropwise added to the gallic acid solution in methanol, 1.1 equivalent, at 0 °C, and under a nitrogen atmosphere. The reaction mixture was stirred under a nitrogen atmosphere overnight at room temperature. The methanol and water were removed under reduced pressure on the following day, and the unreacted acid was washed with methanol at least 3 times. The residual solvent was removed under reduced pressure, and the resultant Ch[Gallate], which chemical structure is present in Scheme 1, was dried under a high vacuum for at least 72h. The high purity of the produced Ch[Gallate] was confirmed by ^{1}H nuclear magnetic resonance (NMR). NMR spectra were obtained on an Avance III spectrometer (Bruker, Germany) operating at a resonance frequency of 400.13 MHz (1H). Deuterium oxide (D_2O) was used as a solvent and used as a reference for chemical shifts which are reported in ppm (parts per million).

IV-3.3. Preparation of the SF/Ch[Gallate] sponges

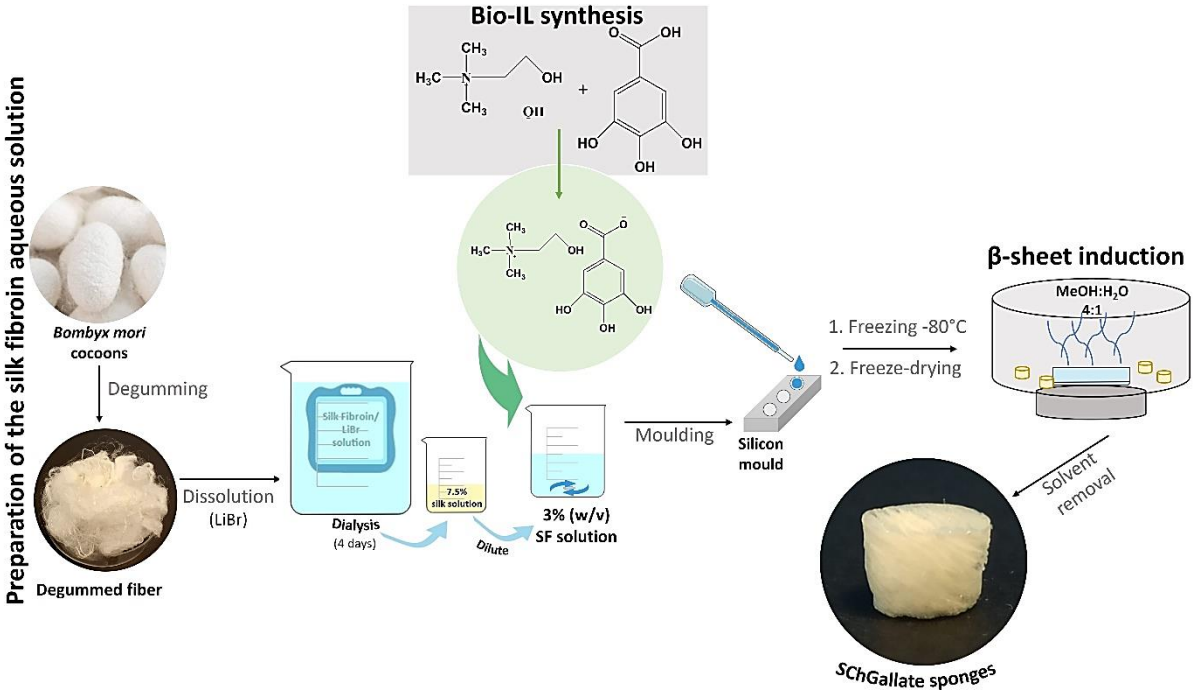
IV-3.3.1. SF preparation

Firstly, SF was isolated from *Bombyx mori* cocoons following a previously described protocol [37]. Briefly, the cocoons were cut into small pieces and boiled for 1h in an aqueous solution of 2.12 mg/mL of Na_2CO_3 (degumming process). The resultant fibroin filaments were rinsed in boiling distilled water and air-dried at room temperature. The SF fibers were further dissolved in 9.3M LiBr, for 3h, at 70 °C, by optimizing a previously developed protocol [28]. Then, the SF was dialyzed in a Slide A-Lyzer cassette (Pierce, 3500 Da MWCO) against distilled water for 4 days at RT. The water was changed every 2h. The resultant SF solution was centrifuged for 20 min., at 5000 rpm, 7 °C, and immediately used or stored at 4 °C. The final SF concentration was calculated by weighting an empty boat (W1), followed by weighting the same boat with 1mL of the produced SF solution (*W2*). The boat was placed into an oven at 70 °C overnight and weighed the next day (*W3*). The concentration of the SF solution was determined using Equation IV-1:

$$SF\ \%\ \left(\frac{W}{V}\right) = \left(\frac{W3-W1}{W2-W1}\right) \times 100 \qquad \text{Equation IV-1}$$

IV-3.3.2. SF/Ch[Gallate] loaded sponges preparation

SF/Ch[Gallate] solutions were prepared by mixing Ch[Gallate], in a range from 0.5 to 3% (w/v), into the previously prepared SF solutions. Further, the SF/Ch[Gallate] mixtures were molded into silicone molds (diameter 4mm), frozen at -80 °C overnight, and freeze-dried for at least 3 days, and the different sponge formulations were obtained (Scheme IV-1). Following the freeze-drying, the samples were placed in a desiccator containing a flask with an aqueous solution of methanol:H_2O 4:1. The system was kept under vacuum for 24 h to create a saturated atmosphere in methanol/H_2O, aiming to induce the β-sheet formation. After 24h, the flask with the methanol:H_2O aqueous solution was removed, and the samples were left under vacuum for 24h, to remove the solvent excess. SF sponges (SS) without Bio-IL were prepared using the same procedure, still without the Bio-IL addition step, and they are used as a control. Throughout the paper, SChGal0.5, SChGal1, and SChGal3 formulations correspond to sponges containing 0.5, 1, and 3% (w/v) of Ch[Gallate], respectively (see details in Table IV-1, and SChGallate sponges will be used as the designation to denote the architectures containing Ch[Gallate].



Scheme IV-1 - Schematic representation for the preparation of the SChGallate sponges.

Table IV-1 - Sample identification used throughout the paper

Sample identification	SF concentration % (w/v)	Ch[Gallate] concentration % (w/v)
SS	3	-
SChGal0.5		0.5
SChGal1		1
SChGal3		3

IV-3.3.3. Stereo microscope observation

To evaluate the macroscopic aspect of the developed SChGallate sponges a Stereo Microscope + Lamp (Schott KL 200) Stemi 1000, ZEISS, was used.

IV-3.4. Physico-chemical and morphological characterization of the *SS and SChGallate sponges*

IV-3.4.1. Antioxidant activity of Gallic acid, Ch[Gallate], SS and SChGallate sponges

The antioxidant activities of the samples were determined using the 2,2- diphenyl-1 picrylhydrazyl (DPPH) radical scavenging assay [38]. The principle of this test is based on the color change of the DPPH solution from purple to yellow, as the radical is quenched by the antioxidant. This reaction was monitored by visible spectroscopy at 517 nm [16]. Briefly, a volume of 1mM DPPH solution in methanol was mixed with 50 mL of methanol with the sponges immersed. Samples were kept in the dark for 1h, 4h, and 24h at room temperature, and the absorbance at 517 nm was determined at the end of each time point. A blank control was made with DPPH solution in methanol, and sponges without the Bio-IL were also used as an assay control. Moreover, for comparison purposes, the same process was applied to the precursor acid (Gallic acid), and measurements were carried out using pure Ch[Gallate] in a methanol solution. The DPPH radical scavenging activity, AA(%), was determined according to Equantion IV-2:

$$AA\ (\%) = \frac{A_0 - A_1}{A_0} \times 100 \qquad \text{Equation IV-2}$$

where A_0 and A_1 are the absorbance of the control and the samples, respectively.

IV-3.4.2. Fourier Transform Infrared spectroscopy

The FTIR-ATR spectra of the SF and SChGallate-based sponges were obtained using a Shimadzu-IR, Prestige 21 spectrometer equipped with a single horizontal ATR cell. The spectra were recorded in the spectral region of 4000-400 cm^{-1}, with a resolution of 2 cm^{-1} and 32 scans. The quantification of the secondary structure was based on the analysis of the amide I and amide II regions (1700–1450 cm^{-1}). The previously collected spectra were linear baseline corrected, normalized, and subsequently deconvoluted by fitting with a Lorentzian function using PeakFit v4.12 software (Systat Software Inc., California, USA). Next, the average percentage for the secondary structures, mainly β–sheet, random-coil/α-helix, and turns, were calculated by integrating the area of each deconvoluted peak curve, normalizing the obtained value to the total area of the amide I and amide II regions [39].

IV-3.4.3. Solid-State NMR study

Solid NMR spectra were measured at 298 K in a Bruker NEO-750 spectrometer (750 MHz proton frequency) equipped with a Varian T3 solid triple resonance probe ^{1}H/X/Y that uses zirconia rotor of an outer diameter of 3.2 mm with an effective sample capacity of 22 µL which corresponds to approximately 30 mg of the powder sample. The probe was adapted to the Bruker spectrometer by a A2B conversion kit (*Revolution NMR, LLC*). The spectrometer control software was TopSpin 4.x. All the spectra were processed with MestreNova software v14.2 (*Mestrelab Research Inc.).* Carbon-13 chemical shifts were referenced externally to the methylene signal of crystalline α-form of glycine at 43.5 ppm.

^{13}C CP-MAS spectra (sequence "hC.cp" of the Bruker library) were measured with an inter-scan delay (d_1) of 2 s, the minimum number of scans was 500 and the MAS rate was 20 kHz. Cross-polarization was applied during 2 ms with a constant carbon field strength of 63.1 kHz, and the power on the 1H nucleus was linearly ramped from 70% to 100% with a peak field strength of 59.0 kHz. Heteronuclear decoupling during the FID acquisition was performed with Spinal-64 with a proton field strength of 79.4 kHz.

IV-3.4.4. Scanning electron microscopy (SEM)

The different matrices were fixed using mutual carbon adhesive tape on aluminum stubs and coated with a conductive gold layer. Their morphology was observed using a NanoSEM-FEI Nova 200 with an integrated microanalysis X-ray system (EDS – energy dispersive spectrometer).

IV-3.4.5. Micro-computed tomography (micro-CT)

The morphological structure and the calculation of the morphometric parameters that characterize the samples were evaluated by micro-computed tomography (micro-CT). Samples were acquired with a SkyScan 1272 scanner (v1.1.3, Bruker, Boston, USA), with a pixel size of 10 µm. Approximately 300 projections were acquired over a rotation range of 360°, with a rotation step of 0.6°. Data sets were reconstructed using the reconstruction software (NRecon 1.6.10.2 Bruker), and the output format for each sample was bitmap images. The binary images were used for morphometric analysis (CT Analyser, v1.13, Bruker) and to build the 3D models.

IV-3.4.6. Mechanical properties

The mechanical behavior of the sponges was performed under compression load using a Universal Mechanical Testing Equipment (Instron 5543, USA), equipped with a 50 N load cell at room temperature. The crosshead speed was set as 1 mm·min^{-1}, and at least 6 specimens with cylindrical shapes were tested for each sponge composition. The determination of the elastic modulus was used as the initial slope in the stress-strain curve. The yield strength, or the yield point, is generally used to describe the stress at the transition from elastic to plastic deformation and it was determined by using the intersection of a parallel line to the modulus at an offset strain of 0.2 %. The immediate recovery of the samples was determined after reaching 50 % of strain.

IV-3.4.7. Swelling

The swelling tests were performed by immersing the SS and SChGallate sponges in PBS, pH 7.4, up to 7 days, at 37 °C, in triplicate. The weight of the swollen samples was determined after removing the excess surface water by gently tapping the surface with filter paper. The percentage of water uptake was determined using Equation IV-3, where *Ws* is the weight of the swollen sample, and *Wd* is the weight of the dry sample.

$$Swelling = \left[\frac{Ws - Wd}{Wd}\right] \times 100 \qquad \text{Equation IV-3}$$

IV-3.4.8. Weight loss

The weight loss of the SS and SChGallate sponges was evaluated after immersion into phosphate buffer saline (PBS) solution at pH 7.4 for periods up to 7 days. The experiment was conducted at 37 °C in triplicate. After each time of immersion, the samples were dried at 37°C until they reached constant weight (W_i), and the percentage of weight loss was calculated using Equation IV-4

$$Weight\ loss\ (\%) = \left[\frac{Wi - Wf}{Wi}\right] \times 100 \qquad \text{Equation IV-4}$$

where, W_i corresponds to the weight of the sponges before the immersion.

IV-3.4.9. Ch[Gallate] release

The study of the Ch[Gallate] release from the SChGallate sponges (medium dry weights of 6.83 ± 1.64 mg, 8.18 ± 1.51 mg, 9.62 ± 1.80 mg for SS, SChGal1 and SChGal3, respectively) was performed following a previously reported procedure [16]. Briefly, the dried sponges were placed in vessels containing 4mL of PBS solution, pH 7.4, at 37 °C, under stirring, and protected from light due to the solvent's light sensibility. At pre-determined times, 1mL of the PBS solution was collected, and the same volume of fresh PBS was added to ensure the maintenance of a constant volume. The Ch[Gallate] content was determined by UV spectroscopy, using a microplate reader (Synergy HT, BIO-TEK, Winooski, VT, USA) at 259 nm. The Bio-IL content at each time point was plotted as a cumulated percentage release determined using Equation IV-6

$$Cumulative\ release\ (\%) = \frac{1}{4} \times C(t-1) + C(t) \qquad \text{Equation IV-5}$$

where, *C(t-1)* and *C(t)* correspond to the Bio-IL concentration at times n-1 and n. The volume of sample withdrawn, and the bath volume is 1mL and 4mL, respectively. Calibration curves were established, and PBS was used as a reference for the baseline correction of the values.

IV-3.5. Cell Culture Studies

IV-3.5.1. Human adipose stem cell isolation and expansion

Human adipose stem cells (hASCs) were obtained from subcutaneous fat tissue under protocols established with the Plastic Surgery Department of the Hospital da Prelada (Porto, Portugal), isolated by enzymatic digestion and characterized by RT-PCR for CD44, STRO-1, CD105 and CD90 markers, as previously described [40,41]. Briefly, the adipose tissue samples were rinsed with PBS containing 10% of an antibiotic-antimycotic solution (A/A, Gibco, UK) and digested with 0.075% collagenase type II (Col II) (C6885, Sigma) in PBS for 45 min at 37 °C under gentle stirring. Digested tissue was filtered with a 100 µm filter mesh, followed by a centrifugation step at 1000 g, for 10 min, at 5 °C. Afterward, the cell

suspension was washed for 10 min with lysis buffer (155 mM NH_4Cl, 10 mM $KHCO_3$, 0.1 mM EDTA = 14.61 mg, pH 7.3), to remove erythrocytes, and centrifuged at 800g at 5 °C for 10 min. The adherent hASCs were expanded in basal medium with minimum essential medium (α-MEM) (Life Technologies, USA) with 10 vol.% FBS and 1 vol.% A/A with medium changes every 3–4 days.

IV-3.5.2. Cell seeding

For all experiments, hASCs at passages 2-3 were used and seeded at a density of 2 x 10^5 cells/cm^3 onto SS and SChGallate sponges (SChGa1 and SChGal3) with ± 4mm of height. Controls consisted of SChGallate sponges without cells maintained in culture for the same periods and under the same cell maintenance conditions. TCP was used as a positive control. Before cell culture studies, all the structures were sterilized using ethylene oxide. The seeded structures were cultured for 1, 3, and 7 days in α-MEM with 10 % (v/v) fetal bovine serum (FBS) (Life Technologies, USA) and 1% (v/v) A/A solution and incubated at 37 °C in 5% CO_2 atmosphere. After each culture time point, the samples were retrieved, rinsed with PBS, and evaluated in terms of cellular behavior by MTS and live/dead test, DNA quantification, and confocal analysis.

IV-3.5.3. Cell viability

The metabolic activity of cells seeded on the SS sponge and SChGallate sponges were evaluated using the CellTiter 96® AQueous One Solution Cell Proliferation Assay (MTS, Promega). Briefly, the cell–scaffold constructs were placed in a mixture containing serum-free cell culture medium and MTS reagent at a 5:1 ratio and incubated for 3 h. The optical density was read (OD 490 nm).

In addition, cell viability was also assessed by fluorescence labeling using a live/dead assay. For this, the sponges were removed from the culture medium and washed with sterile PBS. After, all samples were incubated with 1 mg/mL calcein acetoxymethyl (Invitrogen, 1:500) and 1.5 mM propidium iodide (PI, Invitrogen, 1:1000) solution in PBS for 15 min, at 37 °C and washed with sterile PBS. Further, the samples were visualized using a confocal laser scanning microscope (Leica TCS/SP8). The software Zen was used to analyze the images.

IV-3.5.4. Cell proliferation

The proliferation of the cells throughout the sponges was evaluated using the fluorometric PicoGreen double-stranded DNA assay, according to the manufacturer's instructions (Quant-iT™ PicoGreen™ dsDNA Kit, P7589, Invitrogen). Briefly, after each time-point, the cell–scaffold constructs were rinsed with PBS, placed in microtubes containing 1 ml of ultra-pure water, and stored at -80 °C until analysed. The fluorescence was measured with a microplate reader (Synergy HT, BIO-TEK, Winooski, VT, USA) at 480 and 520 nm. The DNA concentration was calculated using a standard curve (0–2 μg ml^{-1}) relating the amount of dsDNA to the fluorescence.

IV-3.5.5. Cell morphology

The cell distribution and attachment on the structures were analyzed using a confocal laser scanning microscope (CLSM). The matrices were fixed with 10% formalin for 30 min, and then the samples were incubated with 1 % bovine serum albumin (BSA) for 30 min. The constructs were permeabilized using 0.1 % Triton X-100 for 5 min, then incubated with rhodamine-phalloidin at room temperature (RT) for 20 min, followed by washing with PBS and staining with 5 μg ml-1 4',6-Diamidine-2'-phenylindole dihydrochloride (DAPI) for 30 min. Fluorescence images from the stained constructs were obtained using a confocal laser scanning microscope (Olympus FV1000).

IV-3.5.6. Measurement of reactive oxygen species (ROS) in live-cell system

To evaluate the correct energetic balance of the cells, ROS production was analyzed by CLSM. After each time point, the hASCs were washed with Hank's balanced salt solution (HBSS, Cytiva life sciences) three times and incubated with 10 μM of 2′,7′-Dichlorofluorescin diacetate (DCF, Sigma Aldrich) and 0.5 μg ml^{-1} Hoechst (Thermo Scientific) in HBSS, for 45min at 37 °C in the dark. After incubation, the cells were washed three times with HBSS and analyzed using a CLSM. A SS sample, without cells, was analyzed using the 488 nm laser corresponding to the green channel, to evaluate the autofluorescence of the material.

IV-3.5.7. Therapeutic efficacy of the SChGallate sponges

To evaluate the anti-inflammatory potential of the developed sponges, an *in vitro* model was used consisting of a THP-1 cell line stimulated with lipopolysaccharide (LPS) (Sigma-Aldrich, St. Louis, MO, USA), as previously reported [42]. THP-1 cells were seeded at a density of 1×10^6 cells/mL using RPMI medium with 100 nM Phorbol 12-myristate-13 acetate (PMA) (Sigma-Aldrich, St. Louis, MO, USA) for 24 h. After incubation time, an additional volume of RPMI medium was added to the wells without PMA and incubated for 48 h. THP-1 cells were incubated with 100 ng mL−1 of LPS in RPMI medium and incubated for 5 h, to induce the inflammatory response. After this period, the SChGallate sponges were added to the cells, which were cultured up to 7 days, and after each time point 1, 3 and 7 days, the culture medium was removed and stored at −80 ◦C for further analysis.

The concentration of the pro-inflammatory cytokines tumor necrosis factor (TNF-α) and interleukin 6 (IL-6) in the medium after THP-1 being in contact with the sponges were also evaluated. For that, Human TNF-alpha DuoSET ELISA (R&D Systems, Minneapolis, MN, USA) and Human IL-6 DuoSET ELISA (R&D Systems, Minneapolis, MN, USA) kits were used. The determination of the concentration of the anti-inflammatory cytokine interleukin 10 (IL-10) was performed using a Human IL-10 DuoSET ELISA (R&D Systems, Minneapolis, MN, USA). The optical density at 450 nm was read in a microplate reader (Synergy HT, BIO-TEK, Winooski, VT, USA).

IV-3.6. Hemolytic properties

The hemolytic properties of the SS and SChGallate sponges were tested using erythrocytes from whole human blood. The blood was continually mixed and centrifuged at 200 g for 20min, followed by removing the top layer, which contains the red blood cells concentrated (RBC). The RBC was washed three times with PBS, centrifuged (Centrifuge Eppendorf,5810 r) at 3700 rpm for 5 min and the supernatant removed. This process was performed three times. The RBC was diluted in PBS, 5% (w/v). Each sponge was seeded with 400 µL of the RBC solution and incubated for 60 min at 37 °C. After that, the samples were subjected to centrifugation, at 3700 rpm for 5 min, and the supernatant was collected. PBS and 1% SDS solution were used as negative and positive controls, respectively. The absorbance of the collected supernatant was read at 540 nm of wavelength in a microplate reader (Synergy HT, BIO-TEK, Winooski, VT, USA).

$$\text{Hemolytic rate (\%)} = \frac{Abs_{sample} - Abs_{PBS}}{Abs_{SDS} - Abs_{PBS}} \times 100 \qquad \text{Equation IV-6}$$

IV-3.7. Statistical analysis

All quantitative experiments were run in triplicate, and the results are expressed as means ± standard deviation for n = 3. Statistical analysis of the data was conducted using GraphPadPrism v. 8.0 for Windows (GraphPad Software, San Diego, http://www.graphpad.com). After the evaluation of the normality of the results through the Shapiro-Wilk test, the data were analyzed using One-way ANOVA and Tukey's multiple comparisons test, when presenting a normal distribution, and a nonparametric Krustal-wallis test was performed, when data did not follow a normal distribution. Differences between the groups at $p \leq 0.05$ were considered to be statistically significant.

IV-4. RESULTS AND DISCUSSION

IV-4.1. SCh[Gallate] loaded sponges production and physico-chemical characterization

The developed combinatorial approach using natural compounds, namely biomacromolecules and Bio-ILs, presents an innovative solution to build therapeutical tools for biomedical purposes. The association of phenolic compounds with the cholinium cation to form Bio-ILs is an alternative strategy to overcome the stability and poor solubility of phenolic compounds [17,18]. Then, combining the easy processability, biocompatibility, and outstanding mechanical properties of SF [34] with Ch[Gallate], a phenolic-based Bio-IL with known antioxidant and anti-inflammatory properties[17], would be advantageous for developing SChGallate sponges with improved features. To achieve these objectives, herein the phenolic-based Bio-IL, Ch[Gallate], was synthesized by conjugating the anion gallate, derived from gallic acid, with the cholinium (2-hydroxyethyl)trimethylammonium) cation, from a cholinium hydroxide solution, in an acid-base reaction (see Scheme 1) [16]. Ch[Gallate] was obtained as a white powder, and its purity was confirmed by NMR analysis (Supplementary Figure IV-1). By its analysis, it was possible to confirm the success in the Ch[Gallate] synthesis and its purity by the presence of the peaks corresponding to the $N(CH_3)_3$ group in the cholinium cation, as a singlet; two multiplets matching the 2H in the NCH_2CH_2OH group and a singlet which corresponds to the H-2 and H-6 in the Ch[Gallate] aromatic ring.[16] In parallel, an aqueous solution of SF from *bombyx mori* was obtained using optimized

standard protocols [28]. Further, the prepared SF solution at different concentrations (1, 3, and 7% w/v) was used to produce SF-based sponges using the freeze-drying technique to determine the best SF concentration to be further used in combination with Ch[Gallate]. Many avenues are available to produce porous SF sponges, including gas foaming, salt leaching, and freeze-drying [43–45]. The last technique was selected since all processing steps occur under aqueous conditions, as well as in the absence of harmful solvents. Previous studies demonstrated that scaffolds produced using freeze-drying presented satisfactory *in vitro* results with good cell attachment, proliferation, and viability [46]. Moreover, the findings revealed that developed samples with lower SF concentrations (1% w/v) were fragile and showed low resistance to handling. These results were similar to those previously reported data that revealed that sponges prepared with low SF concentrations (0.5% and 1% (w/v)) were more fragile and difficult to handle than others prepared with higher concentrations [47,48]. The sponges prepared with SF 7% (w/v) and 3% (w/v) were by far more resistant to handling. Moreover, the micro-CT data of these SF constructs (Supplementary Figure IV-2), revealed that SF 1%, SF 3%, and SF 7% presented 78.4 μm and 78.01 %, 70.3 μm and 76.6%, 30.7 μm and 45.3% of mean pore size and porosity percentages, respectively. The results indicated that SF 7% presented smaller pore sizes, and porosity values compared to the others. Accordingly to the literature, matrices with small pore size values may further prevent cell infiltration and nutrient diffusion through the structures [49]. Considering the handling difficulties associated with the SF 1%, and the difficulty of these sponges to retain their shape, the SF 3% (w/v) was the selected condition to proceed with the production of SChGallate sponges. As the synthesized Ch[Gallate] is soluble in water, its solubilization at 0.5%,1%, and 3% (w/v) was made directly into the SF 3% (w/v) aqueous solution. The resulting SF/Ch[Gallate] aqueous solutions were molded, frozen at -80°C, and freeze-dried. Soft white sponges were produced from all conditions as presented in Scheme IV-1.

The antioxidant activity of the synthesized Ch[Gallate], its precursor compound (gallic acid), and the developed SChGallate sponges was evaluated using the DPPH radical scavenging assay.[38] Gallic acid, used as the anionic moiety in Ch[Gallate] synthesis, and was also used as a positive control. Gallic acid is a naturally occurring polyphenol with strong antioxidant and free radical scavenging ability.[50] The results depicted in Figure IV-1 showed that the synthetized Bio-IL, Ch[Gallate] has similar antioxidant activity compared with its precursor, gallic acid, and this trend was maintained for up to 24h. Considering the SS and SChGallate sponges, the antioxidant activity is higher in the SChGal1 and SChGal3 formulations compared with SS and SChGal0.5, which presented very similar antioxidant activities, below 60%, and increasing after 24h for the SChGal0.5. Statistical analysis revealed significant differences

between SS and SChGal0.5 and the other conditions, SChGal1 and SChGal3, in all the studied time points. Those findings suggested that incorporating Ch[Gallate] improved the antioxidant activity of the developed SChGallate sponges compared to SS. Published data suggests that the inherent antioxidant activity of SF is associated with the presence of tyrosine and tryptophan amino acids, which contain phenolic side chains, justifying the herein obtained lower, but existent, SF antioxidant activity [51]. Based on these findings, both SChGal1 and SChGal3 sponges were selected to further characterization. Some previously published reports presented approaches involving the incorporation of plant extracts (e.g., fenugreek seed extract) or pigments (e.g. melanin) into SF to produce potential antioxidant SF-based matrices [51,52]. Some studies also suggested the use of cholinium-based salts (e.g., Ch[Gallate]) to improve the activities of the polymeric matrices due to their outstanding properties, namely antioxidant and anti-inflammatory features [16,17]. Bacterial nanocellulose membranes were soaked in a 10mg/ml aqueous Ch[Gallate] solution, resulting in a material with antioxidant activity of over 80% [16]. The present work obtained comparable antioxidant properties using substantially lower amounts of Ch[Gallate] in SF architectures. Our results suggested that SChGallate sponges could be promising and effective antioxidant matrices to regulate the overproduction and accumulation of free radicals, which are known as leading causes of several diseases such as atherosclerosis, osteoarthritis, cancer, aging, and diabetes [2,50,53,54].

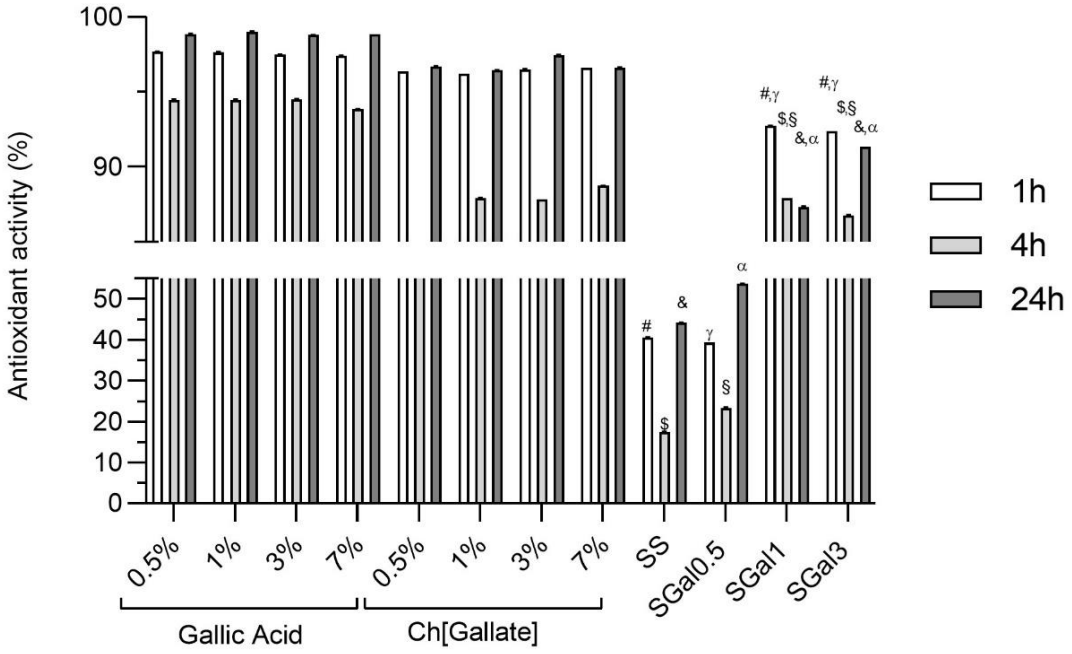


Figure IV-1 - Antioxidant activity of gallic acid, Ch[Gallate] ,SS, SChGal1 and SChGal3 in a solution of DPPH in Metanol. Symbols and letters denote statistically significant differences with different degrees of confidence. Symbol # denotes statistical differences for $p < 0.0001$ between SS and SChGal1 and SChGal3 at 1h; $ denotes statistical differences for $p < 0.0001$ between SS and SChGal1 and SChGal3 at 4h; & denotes statistical differences for $p < 0.0001$ between SS and SChGal1 and SChGal3 at 24h; γ denotes statistical differences for $p < 0.0001$ between SChGal0.5 and SChGal1 and SChGal3 at 1h; § denotes statistical differences for $p < 0.0001$ between SChGal0.5 and SChGal1 and SChGal3 at 4h and α SChGal0.5; and α denotes statistical differences for $p < 0.0001$ between SChGal0.5 and SChGal1 and SChGal3 at 24h .

The infrared spectra of the pure Ch[Gallate], SS, and SChGallate sponges were obtained to confirm the presence of Ch[Gallate] into the sponges (Figure IV-2A), as well as to investigate their structural changes, mainly those related to the rearrangement into β-sheet conformation. By the analysis of the spectra, it was possible to observe peaks in the region between 1200-1300 cm^{-1}, which were attributed to the C-OH stretching bond vibrations typical of phenol functional groups in the Ch[Gallate] structure, while the peak corresponding to the CN vibration in the cholinium was noted at 1185 cm^{-1} [16]. It was observed that both SS and Ch[Gallate] present a peak around 1600 cm^{-1}, corresponding to C=O stretching vibrations [32]. This peak was not clear in SChGal1, which presents a lower amount of Ch[Gallate] in its structure; thus, we hypnotized that it was merged with the ones corresponding to the amide III present in SF (1230 cm^{-1}). Between 1100 and 750 cm^{-1}, the peaks correspond to the CH out-of-plane bending vibration of the aromatic rings of Ch[Gallate] [16]. Some peaks, such as 795 cm^{-1}, 953 cm^{-1} and 1037 cm^{-1}, present in this area were absent in the SS spectrum, confirming the Bio-IL presence in the SChGal1 and SChGal3 samples. However, the 953 cm^{-1} and 1037 cm^{-1} peaks were slightly shifted for 954 cm^{-1} and 1047 cm^{-1}, respectively, suggesting some interactions between SF and Ch[Gallate]. The spectra of the

SChGallate sponges present higher similarities to the SS than to the Ch[Gallate] since the amount of SF in the sponges is superior to Ch[Gallate]. The β-sheet formation was confirmed in both formulations (SChGal1 and SChGal3) by the presence of peaks at 1620-1647 cm^{-1} (amide I), 1514-1537 cm^{-1} (amide II), and 1227-1192 cm^{-1} (amide III).[55] It was possible to observe small shift changes in the peaks corresponding to the amides. In the amide I region SS presented a peak at 1647 cm^{-1} which shifts to 1645 cm^{-1} in SChGal1 and SChGal3. Similarly, a shift in the amide III bands was noticeable from 1232 cm^{-1}, which is present in the SS, to 1228 cm^{-1} in the SChGal1 and SChGal3 samples. These changes are likely to occur due to the interactions between the Ch[Gallate] and the SF structure since it is known that ILs may induce a small shift in the stretching frequency of amides [56,57]. SF contains a vast range of amino acids with functional groups including alcohols, amine, phenols, thiols, and carboxyl groups [58] that could interact with small molecules, such as Ch[Gallate]. Therefore, we speculate that amino acid chains in SF can entrap Ch[Gallate] in their structure through interactions via non-covalent forces such as hydrogen bonding, hydrophobic bonding, and van der Waals forces [59].

The amide I and II spectral deconvolutions were assessed to determine changes to the β-sheet conformation on the SF and SChGallate-based sponges (Figure IV-2B). The β-sheet content in the sponges was 25.2% (SS), 30.2% (SChGal1), and 29.3% (SChGal3), whereas the α-helix/random coil conformations were 7.8% (SS), 11.0% (SChGal 1), and 8.0% (SChGal3), with the statistical analysis revealing significative differences between the β-sheet and the other secondary structure elements, in all formulations. The higher β-sheet conformations on both SChGal sponges confirmed that the presence of Ch[Gallate] in the structure positively affects the β-sheet formation. This is in accordance with other studies, which shown that the introduction of ILs and Bio-ILs in the silk matrices induced an increase in the β-sheet conformation content [23]. Also, the higher β-sheet conformation in the SChGal1 and SChGal3 suggested that these formulations could have better structural stability and water insolubility.

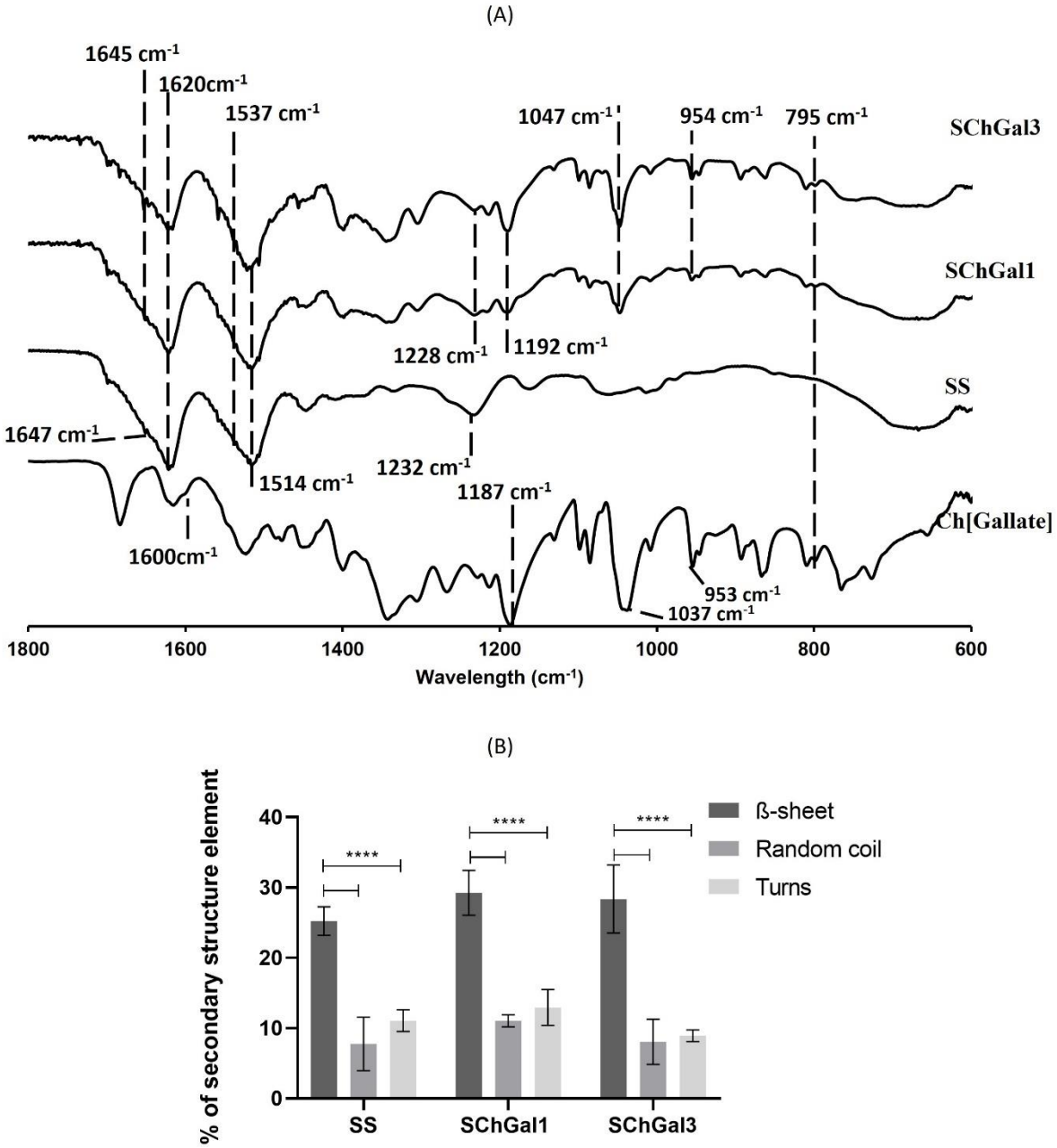


Figure IV-2 - (A) FTIR spectra of SS, SChGal, and Ch[Gallate]; (B) Percentage of β-sheet, random coil, and turn conformations after amide I and II spectra deconvolution of SS, SChGal1, and SChGal3. Data represent ±SD (*$p < 0.05$, ordinary 2wayANOVA).

The ^{13}C-CPMAS spectrum of the original SS, Ch[Gallate], and the sponges SChGal1 and SChGal3 are shown in Figure IV-3 including the signal assignment to the components. The spectrum of SS (Figure IV-3A) shows the expected pattern of signals for a protein in the solid state [60]. Signals of choline and gallic acid in the spectrum of ChGallate (Figure IV-3B) were identified based on the agreement with the predicted chemical shifts calculated with Mestrenova software for these two molecules. Using the mentioned assignments of SS and Ch[Gallate] as a reference, it was straightforward to assign the peaks in the spectra of SChGal1 (Figure 3C) and SChGal3 (Figure 3D) since the signal patterns and chemical shifts of the peaks were essentially unaltered. The higher intensity of the signals of Ch[Gallate] relative to SS in the spectrum of SChGal3 (Figure 3D) respect to SChGal1 is also consistent with the concentration of Ch[Gallate] used for the preparation of these samples which is 3% and 1% (w/v), respectively.

Regarding the structure of SS protein in these samples, it is well established that chemical shifts in both solution and solid state NMR are reporters of the secondary structure hints of proteins even at the amino acid level [61]. Interestingly, it can be appreciated in Figure IV-3 that the signals of the SS protein appear with very similar intensity patterns, and essentially the geometrical center of the peaks remains at the same chemical shift for the three SS, SChGal1 and SChGal3 samples, as depicted by the vertical stripped lines. This result strongly suggests that the secondary structure elements of SS remain very similar or unaltered in these samples, and it is in agreement with the rather similar β-sheet content of the sponges obtained herein by FTIR analysis (i.e. 25.2% (SS), 30.2% (SChGal1), and 29.3% (SChGal3)).

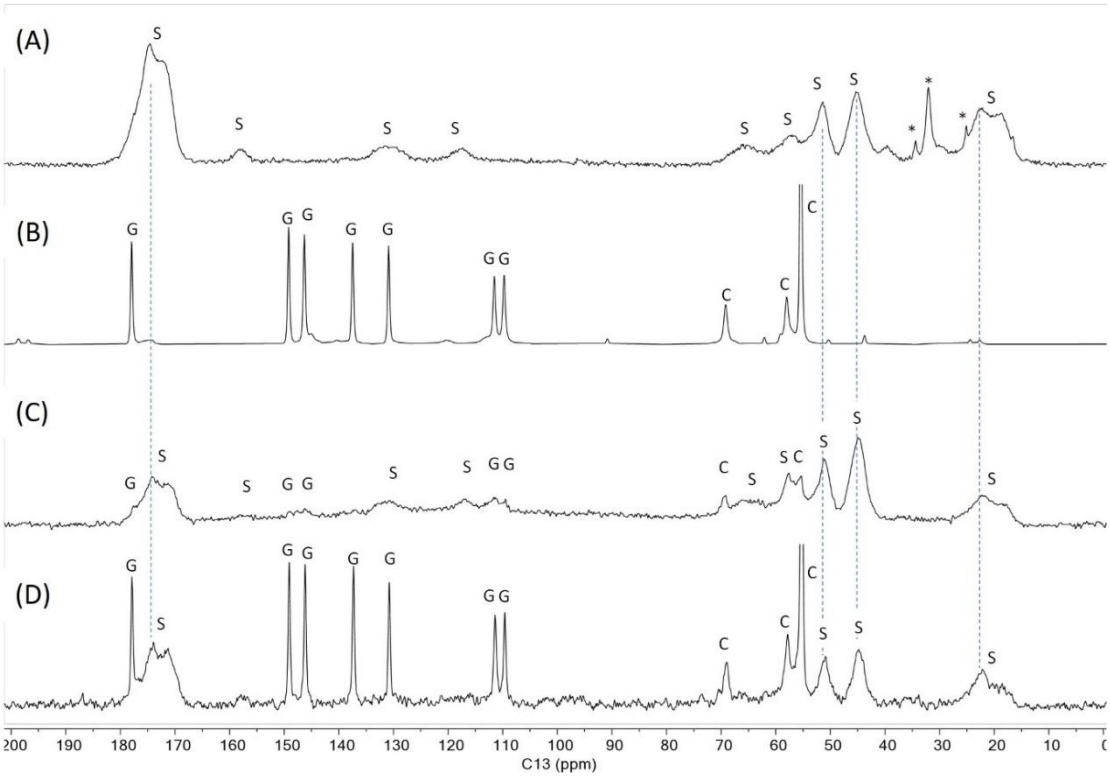
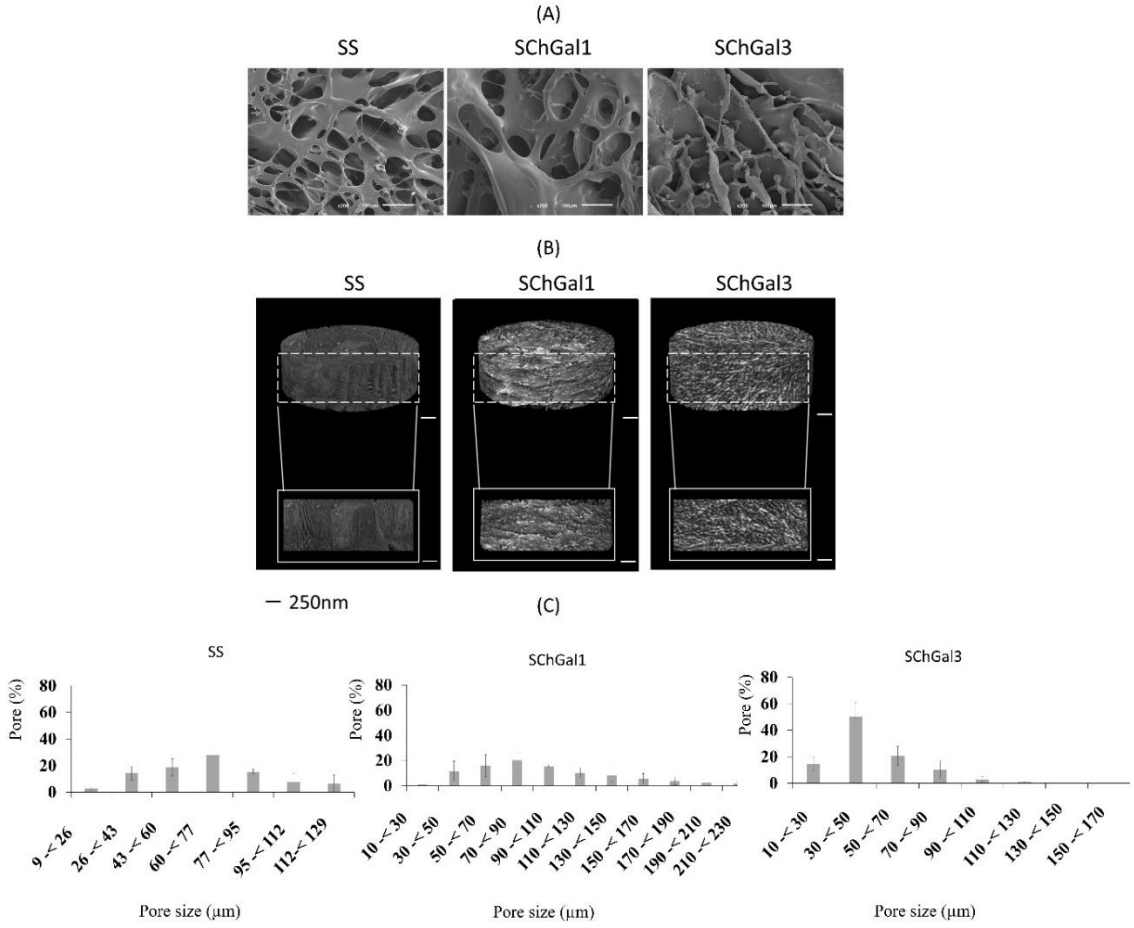


Figure IV-3- ^{13}C-CPMAS spectra of solid samples A) SS, B) Ch[Gallate], C) SChGal1 and D) SChGal3. The letter used for the assignment of the components is choline (C), gallate (G) and silk sponge protein (S). The asterisks in a) denote some impurities. Vertical striped lines are drawn to guide the eye for certain signals of the protein S that are discussed in the text.

Figure IV-4A presents the SEM images of the sponges' surfaces, showing that all sponges presented a non-uniform and randomly arranged pore structure. As expected, by using the freeze-drying technique to produce SF scaffolds, the freezing step encouraged the formation of uniform ice crystals, which originated highly interconnected porous constructs by lyophilization [62]. In addition, a quantitative analysis of the morphometric parameters of the sponges was carried out by micro-CT. The 3D images of the sponges, obtained from digital geometry processing from a series of 2D x-ray images, are shown in Figure IV-3B. The 3D morphometric parameters, Figure IV-3D, (mean thickness, pore size, porosity, and pore size distribution) were obtained through these images. Concerning the pore sizes, the mean values obtained were 70.3 ± 0.1, 64.5 ± 5.8, and 49.9 ± 8.2 μm for SS, SChGal1, and SChGal3, respectively. The porosity values were higher for SS, 76.6 ± 6.2%, while SChGal1 presented 75.4 ± 1.3% and SChGal3 46.1 ± 12.2%. The results support that all formulations presented an interconnected porous structure, as assumed by the SEM images, with interconnectivity percentage values of 81.76 ± 3.58% for SS, 91.10 ± 5.75% for SChGal1, and 73.26 ± 3.6% for SChGal3. Both porosity and mean pore size values decreased with the increase of Ch[Gallate] concentration in the sponges, meaning that it is possible to modulate these parameters by changing their final concentration. Our results are in accordance with previously

published data since earlier studies showed that the presence of the Bio-IL, cholinium acetate, in chitin-based sponges led to a decrease in both the porosity and mean pore sizes of the final constructs, namely 85.8 ± 1.9 to 72.33 ± 1.15 (porosity) and 176.70 ± 44.48 to 173.43 ± 28.54 μm (pore size) for the structures prepared without and with cholinium acetate, respectively [12]. Moreover, another report also showed that by changing the ratio of gelatin methacryloyl to Bio-IL from 100/0 to 20/80 the pore size decreased from 86.4 ± 20.3 μm to 39.0 ± 7.9 μm [21]. In the present study, despite the clear differences between all samples, especially SChGal1 and SChGal3, we proceeded to further studies with the three established formulations (SS, SChGal1, and SChGal3) to investigate the effect of different Ch[Gallate] concentrations on the constructs' swelling, stability, biological behavior, and therapeutic efficacy.



(D)

Sample	Mean thickness (μm)	Mean pore size (μm)	Porosity (%)	Interconnectivity (%)
SS	29.1 ± 3.6	70.3 ± 0.1	6.6 ± 6.3	81.8 ± 3.6
SChGal1	24.9 ± 0.6	64.5 ± 5.8	75.4 ± 1.3	91.1 ± 5.8
SChGal3	49.1 ± 7.8	49.9 ± 8.2	46.1 ± 12.2	73.3 ± 3.7

Figure IV-4 – SEM images of the SS and SChGallate-based sponges' cross sections, scale bar 100μm (A); and (B) micro-CT 3D images, scale bar 250nm; (C) pore size distribution of the SS, SChGal1 and SChGal3-based sponges, and (D) morphometric parameters.

It is expected that three-dimensional (3D) sponges should possess appropriate mechanical properties for physical support during tissue development, despite their highly interconnected porous structure. The effect of the Ch[Gallate] concentration on the mechanical properties under compression load of the SF/Ch[Gallate]-based sponges was evaluated by measuring its elastic modulus, yield strength, and the immediate recovery of the sponges after 50 % of strain, as shown in Figure IV-5**.** The

representative curves of the mechanical behavior are presented in Figure 5D revealing the soft behavior of the sponges with an elastic modulus around 88 KPa for SS, when compared with the higher elastic modulus of the sponges containing silk fibroin and Ch[Gallate], Figure IV-5A. It was observed that the mean value of compressive modulus of the sponges increases with the increase of Ch[Gallate] concentration, being of 1278 KPa for 1 % of Ch[Gallate] and 1467 KPa and for 3 % of Ch[Gallate], respectively. Thus, the presence and the increase of Ch[Gallate] concentration lead to a stiffer sponge. Similar trend was observed for the results of yield strength, which corresponds to the transition point between the elastic to plastic behavior of the stress-strain curve (see Figure 5D) and the results shown in Figure IV-5B. The compression yield strength increased from 8.21 KPa for SS to 56 KPa up to 57 KPa for SChGal1 and SChGal3 respectively, representing a reinforcement almost seven times higher than the SS sponges. Similarly, in other studies, the use of cholinium-based ILs improves the properties of the final architectures, hypothetically due to the hydrogen bond capability of the cholinium anion with available acceptor and donor sites, enhancing the binding between the polymer molecules itself, as well as the Bio-IL [19]. With the increase of the mechanical properties of the sponges, it was observed an expected decrease on the recovery of the original shape after the compression test at 50 % of strain. The sponges with Ch[Gallate] present a considerable immediate recovery after the test between 60 % and 70 % of the initial size, while SS recover around 92 %. The improvement in the mechanical properties of the sponges is also beneficial for the stress transfer during the compression process. Those findings also reinforce the positive influence of the Bio-IL presence into SF structure, due to the increase of β-sheet in the presence of Ch[Gallate] as previously discussed by FTIR and NMR analysis.

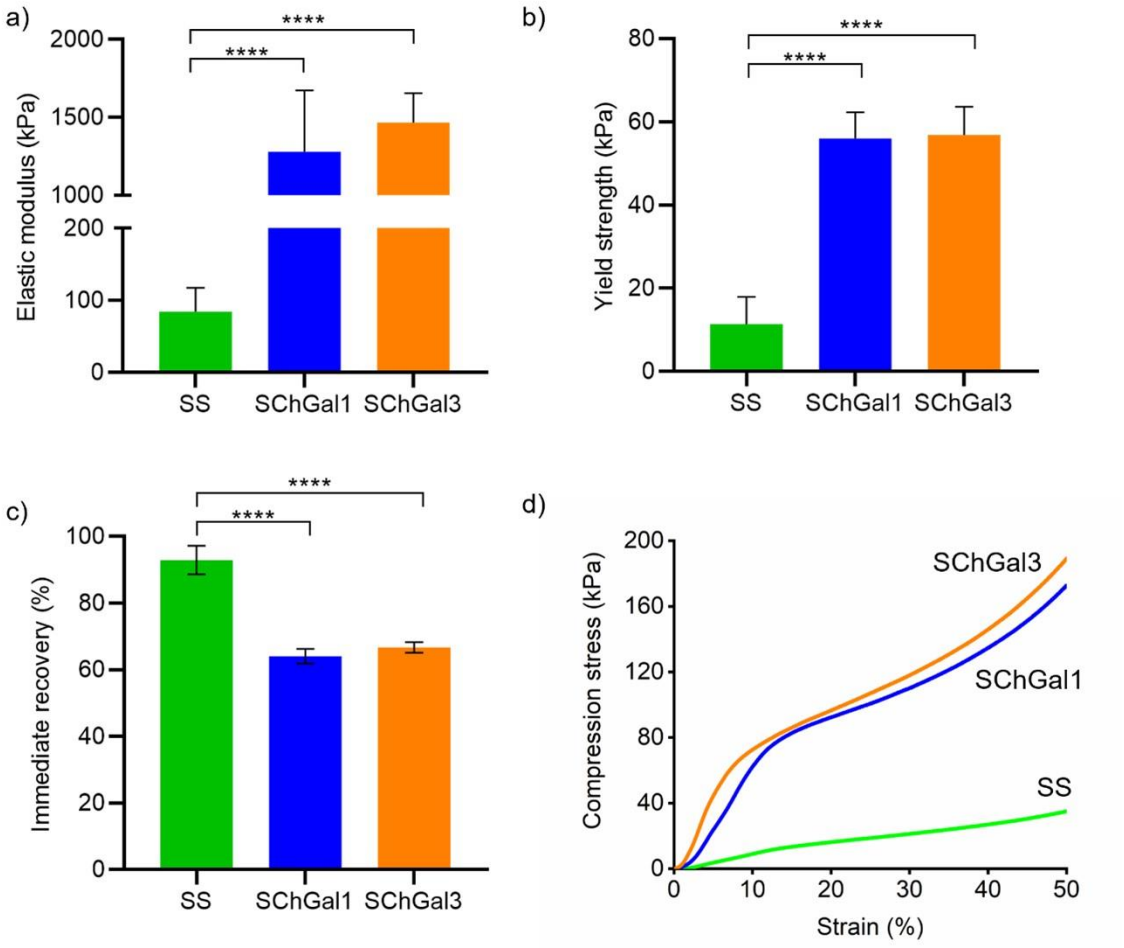


Figure IV-5 - Mechanical behavior of the sponge materials under compression load. (A) Compressive modulus. Data represent ± SD (*p < 0.05, one-way ANOVA); (B) Compressive strength at yield. Data represent ± SD (*p < 0.05, one-way ANOVA); (C) Immediate recovery of the samples after the compression at 50 % of strain; and d) Representative compression stress-strain curves. Data represent ± SD (*p < 0.05, one-way ANOVA).

The ability of a biomaterial to uptake and preserve water into its structure is vital for its use as tissue engineering solutions, since the nutrients, metabolites, and body fluids passage through the biomaterial are directly associated with these features [43]. The water uptake of the developed sponges was evaluated after immersion into PBS for up to 24h. In all samples, it was noticeable stabilization of the water uptake potential immediately after 30min of immersion (Figure IV-6A). The SS samples presented a significantly higher water uptake ability that increased along time (from 972% up to 1947%) compared to the other formulations that presented maximum swelling values up to 969% to SChGal1, and 294% to SChGal3. Also, the statistical analysis indicated that the water uptake percentages follow the order SS> SChGal1> SChGal3, revealing a reduction of the water uptake ability with the increase of the Ch[Gallate] content in

the architecture. The swelling behavior of the sponges suggested a hydrogel-like behavior, being considered a three-dimensional polymer network rich in water [63]. Moreover, the high water uptake ability percentage values obtained for all conditions suggest efficacy in the transference of nutrients, metabolites, and body fluids through the scaffold, constituting a benefit when envisioning its further body implantation [43,64]. Moreover, it was observed that the water uptake ability of the SChGallate sponges was much more pronounced for samples prepared with lower Bio-IL content (SChGal1, 1% (w/v) Bio-IL), while a significant decrease was observed following an increase in the Bio-IL content (SChGal3, 3% (w/v) Bio-IL). As discussed before, specific SF-Ch[Gallate] interactions could occur; therefore, at low Ch[Gallate] concentration, those interactions, together with high porosity (75%) and respectable β-sheet content (60%), may explain the higher water uptake ability of SChGal1. The achieved data are in accordance with previous reports showing that SF-based scaffolds with higher porosity, present higher water uptake ability percentages [12,65]. On the other hand, when the Ch[Gallate] concentration increases (SChGal3), the effect of the interactions would be superimposed, and other factors such as low porosity (46%) and high beta-sheet content (65%) are more pronounced.

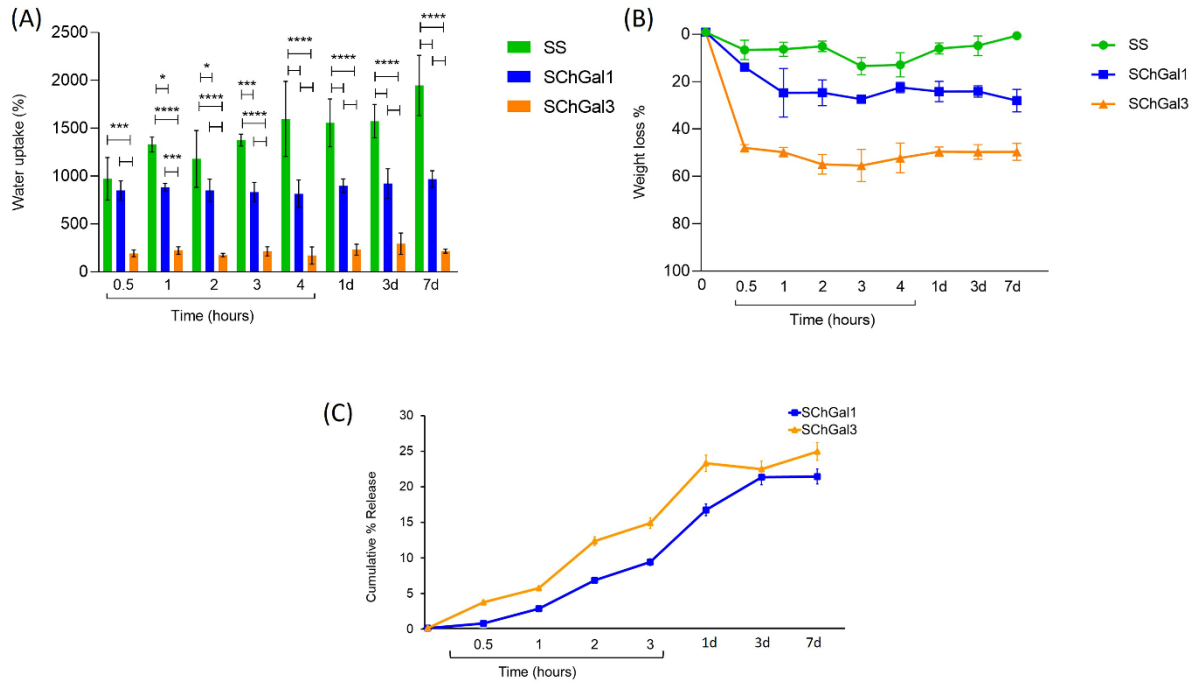


Figure IV-6 – Water uptake (A), weight loss (B) of the SS, SChGal1, and SChGal3 in PBS. Data represent ±SD (*$p < 0.05$, 2way ANOVA) and cumulative percentage release of Ch[Gallate] from the SChGallate-based sponges into PBS, up to 7 days (C).

The analysis of the stability of the sponges in PBS (Figure IV-6B) indicated that SS samples present non-significant weight loss values when immersed in PBS (up to 9%). This result is also in agreement with previous studies, which show reduced weight loss by immersing SF sponges in PBS, even up to 16 days [43]. SChGal1 and SChGal3 presented a weight loss maximum of 25% and 55%, respectively, up to 7 days. These findings suggested the possibility to tune the stability of the final constructs by changing the Ch[Gallate] concentration on the structure, a promising result since the next generation of implantable scaffolds ideally will present controlled biodegradation [43].

Considering the solubility of Ch[Gallate] in PBS, we hypothesized that the immersion of the sponges would lead to its release from the structures, which could explain the observed reduction of the stability and the differences in weight loss percentages. To support this hypothesis, the cumulative release of Ch[Gallate] from the sponges was studied by their immersion in PBS solution, at pH 7.4, up to 7 days, corresponding to the time points used for further cell culture studies. The findings indicated that both SChGal1 and SChGal3 allow a controlled release of Ch[Gallate] (Figure IV-6C). As expected, and even though a similar release profile was evident between SChGal1 and SChGal3, it was always higher in the latter, considering the different and higher concentration of Ch[Gallate] into SChGal3. Therefore, these findings support the hypothesis that the weight loss profile observed for SChGal3 was related to Ch[Gallate] release. Altogether, these results proved that the Ch[Gallate] concentration in the matrices could be used to modulate their stability/degradation in an aqueous environment, which as mentioned, remains a critical element in the tissue engineering field [43,66].

IV-4.2. Cell Culture Studies

To evaluate the biological behavior of the developed sponges, a cellular study using hASCs was conducted, up to 7 days. hASCs were selected due to their availability in the body, being easy to isolate, and having the sensibility and ability to differentiate into the required tissues, which are desirable features for tissue repair [12]. Several natural polymers have already been explored to culture hASCs in 3D architectures envisioning tissue engineering applications, including SF [67,68]. However, studies involving the use of Bio-IL and hASCS are scarce [12]. The metabolic activity (MTS assay), cell proliferation (DNA quantification), and cell morphology (CLSM) of the hASCs seeded on the SChGallate sponges were assessed up to 7 days of culture. The MTS revealed that hASCs were metabolically active when seeded on the SS, SChGal1, and SChGal3 (Figure IV-7A). The statistical analysis showed significant differences on the first day of culture, mainly between the SS and SChGallate-based sponges, suggesting the

importance of the presence of Ch[Gallate] as a boost at a primary phase in the cell metabolic activity. Moreover, the live-dead analysis indicated that most hASCs were viable in all samples after 7 days of culture (Supplementary Figure IV-3). Similarly, previously published data showed that using cellulose-based biomaterials in combination with Bio-ILs, namely those derived from phenolic salts, in contact with either macrophages and keratinocytes is not harmful to the cells, not having any cytotoxic effect after 24h [18]. Our previous study also showed that hASCs could adhere, grow, and proliferate by keeping the Bio-IL in the structure, up to 7 days [12]. Interestingly, one could observe that in the present study, the hASCs cells became metabolically more active from day 3 to day 7, which may be a consequence of the change of the culture medium at day 3, leading to a decrease in the Ch[Gallate] concentration in the medium which theoretically interfers with the cellular ROS balance. Nevertheless, a continuous Ch[Gallate] release over time is expected, as suggested by the data concerning the Bio-IL release in PBS (Figure IV-7C), which could explain the differences in metabolic activity of the SChGallate sponges at day 3. After 7 days, the metabolic activity on the SS condition was kept, while it increased on the SChGal1 and SChGal3. The enhancement of metabolic activity was significantly higher for the cells seeded on the SChGal1. In addition, the results from the DNA quantification (Figure IV-7B), corroborated the ability of the cells to proliferate throughout the structures from 3 days onwards, being clearer in the SChGal1. The confocal laser scanning microscopy (CLSM) analysis (Figure IV-7C) confirmed the hASCs cell attachment and spread on the developed sponges' surface, by F-actin staining (in red) and the nuclei (in blue). Stress fibers are tension-generating, load-bearing mechanosensitive structures, whose formation reflects ASCs response to the external environment: the presence of stress fibers is often correlated with strong cell adhesion to the substrate [69]. The hASCs seeded on the SChGallate sponges presented the expected morphology of adherent hASCs, presenting a cytoskeleton with well-structured actin fibers and extended lamellipodia [70]. Moreover, cell-to-cell interactions were clear after 7 days of culture, particularly in the SChGal1 condition.

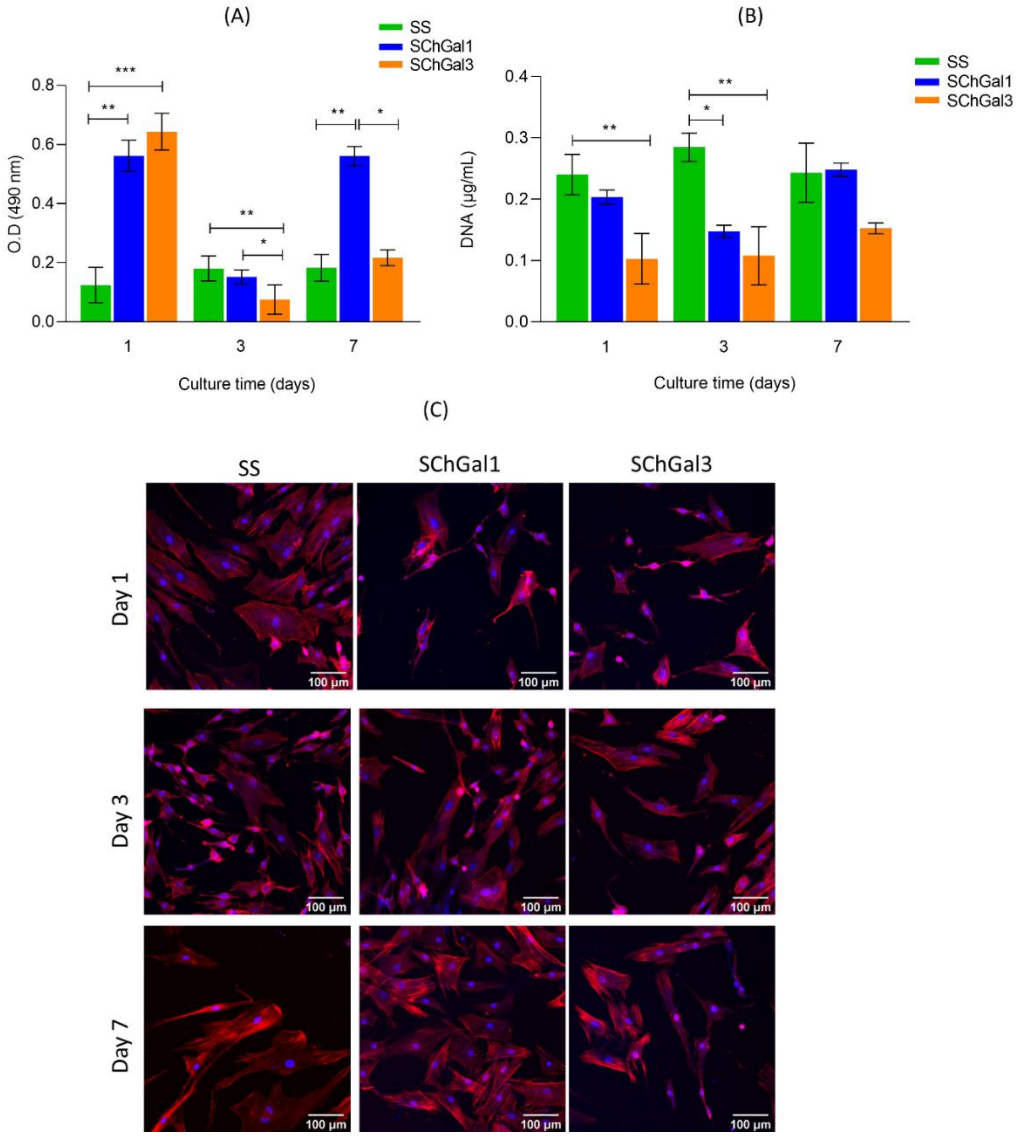


Figure IV-7 - (A) Metabolic activity and (B) DNA content of hASCs seeded on the SS, SChGal1, and SChGal3 sponges up to 7 days of culture; Data represent ±SD (*p < 0.05, nonparametric Krustal-wallis test). (C) confocal laser micrographs of hASCs cultured on sponge structures after 1, 3, and 7 days. The cells were stained with rhodamine-phalloidin for actin filaments (red) and DAPI for nuclei (blue). Scale bar: 100 µm

The excess of intracellular ROS is involved in the apoptosis process, while low and moderate levels act as signal transducers that activate hASCs [71]. It is known that H_2O_2-induced ROS production in hASCs may effectively promote their proliferation, migration, and regeneration [72]. Considering the antioxidant properties of the developed SChGallate sponges, a measurement of ROS in the hASCs cultured on sponges at each time point was carried out using fluorescence quantification, facing the reduction in the metabolic activity of cells on day 3 (Figure IV-8). A SS sample, without cells, was also observed using the green laser, aiming to evaluate the influence of the possible autofluorescence of the SF in the analysis, which was proved to be vestigial and non-significant (see CLMS image Supplementary Figure IV-4).

Although the statistical differences in fluorescence intensity were not significant among the different samples at the different culture time points, the data suggested a slight increase in the ROS production in the SChGal1 and SChGal3 conditions mostly at day 7. At day 3 a decrease in the metabolic activity is observed that can be associated with the high amount of Ch[Gallate] in the culture medium, which is progressively released and uptaken by the cells. The high amount of this compound, with proved antioxidant activity, in the medium would contribute to the ROS production reduction and, therefore, decrease the cellular metabolic activity. The change of the culture medium at day 3 leads to the reduction of this compound in the culture medium and, consequently, to an increase in the ROS production, as it is depicted in Figure IV-8. Following this rationale, we hypothesized that from 7 days of culture, a ROS balance is achieved, allowing a recovery of the cell metabolic activity [71,72]. The increase in cell metabolic activity in both sponges was previously observed at 7 days, particularly for SChGal1 (Figure IV-7A).

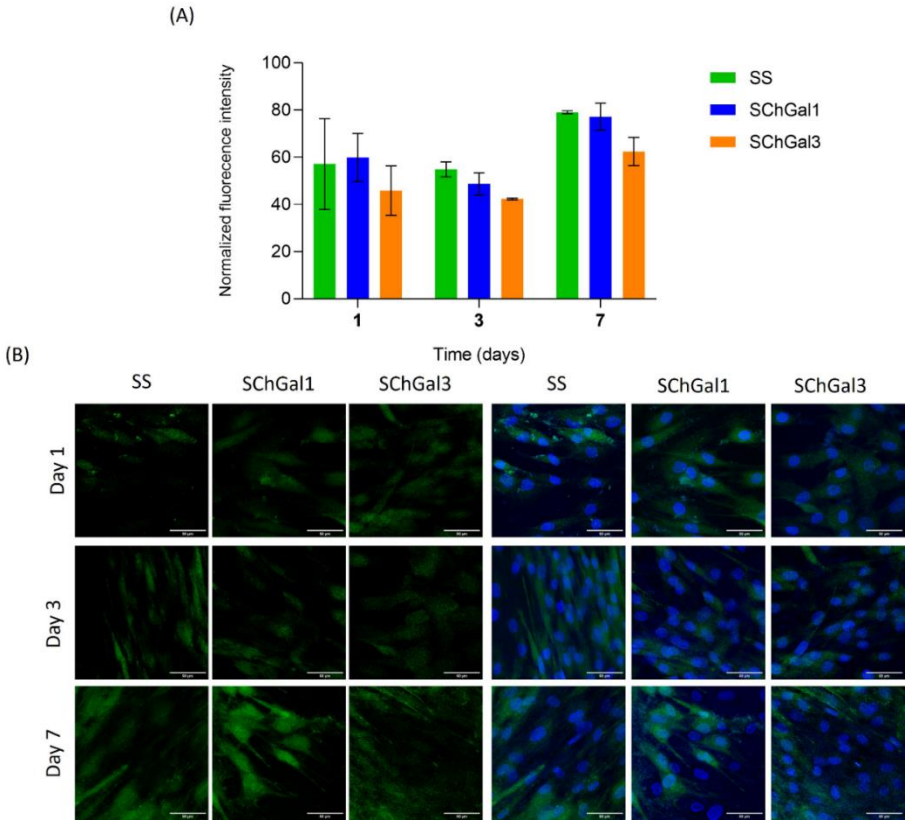


Figure IV-8 - *In vitro* ROS measurement using DCF-DA fluorescence assay (A) quantification graph by fluorescence intensity, normalized by the number of cells and (B) the CFLM images of ROS in hASCs. H2DCFDA probe (in green) was used to stain ROS, and Hoechst (blue) was used to stain the cell's nucleus. Scale bar: 50 μm

The therapeutic efficacy of the sponges was evaluated by quantifying the tumor necrosis factor (TNF-α), interleukin-6 (IL-6) and interleukin-10 (IL-10) in differentiated and LPS-stimulated THP-1 cells. The cell

differentiation of THP-1 monocytes to macrophages was confirmed by observing the transition from a suspension cell phenotype to an attached cell phenotype [73]. The main goal was to evaluate the efficacy of the SChGallate sponges to decrease TNF-α and IL-6, which are cytokines released as a pathophysiologic response to many chronic autoimmune and inflammatory diseases, such as rheumatoid arthritis and osteoarthritis [74,75]. In addition, IL-10, which is an anti-inflammatory cytokine, is known to inhibit the production of pro-inflammatory cytokines by activated monocytes/macrophages, including some of the most important cytokines driving chronic inflammation, such as TNF-α and IL-6, and for this purpose was also quantified [76]. Dexamethasone was used as a model anti-inflammatory drug since it is one of the strongest and most used corticosteroids. This agent is approved to treat pathologies including osteoarthritis, tendonitis, rheumatoid arthritis, bursitis, and tenosynovitis [77]. Herein, it was used in a concentration of 5mg/ml, since several works reported it as the average value to have a therapeutic effect when injected [4,42,77]. In THP-1 cells, LPS has been proven to induce the production of pro-inflammatory cytokines, including TNF-α and IL-6 [76,78].

We demonstrated that both SS and LPS-stimulated cells showed increasing amounts of TNF-α and IL-6, thereby indicating that the stimulation of cells was achieved (Figure IV-9). The obtained data revealed a decrease in the TNF-α concentration in the samples containing the Ch[Gallate] in their matrix. After 1 day of treatment, the SChGallate sponges showed a greater potential to reduce the TNF-α concentration than the used model drug, with significant differences between SChGal1 and the dexamethasone-treated cells. On days 3 and 7, the reduction was more accentuated in the SChGal3. The statistical analysis of the data revealed significant differences between SChGal1, SChGal3, and dexamethasone after 3 and 7 days of culture. The differences in the TNF-α release amount in the cells cultured with SChGallate sponges can be related to Ch[Gallate] concentration in each formulation, and its sustainable release over culture time. The porosity and water uptake data (Figure IV-6D and Figure IV-6A, respectively), revealed significantly higher values for SChGal1 in both cases, which may be related to the immediate release of Ch[Gallate] from the sponges, justifying its instant effect on the TNF-α blockage at day 1. On the other hand, SChGal3 presented lower porosity values and lower water uptake ability, resulting in a more sustained and prolonged Ch[Gallate] release, which supports the data presented in Figure IV-9. Similar to what we have seen in the present work, previous studies on *in vitro* inflammation models with loaded betamethasone/tyramine-modified gellan gum/SF hydrogels, [42] showed that the entrapment of a therapeutic compound promoted its sustainable release up to 7 days, extending the therapeutic effect compared to the free drug. Those matrices were suggested to target rheumatoid arthritis treatment. TNF-

α, which is vital in the regulation of innate immune response, is an appealing target in chronic inflammatory diseases. Its blockage was proved to be significant in treating several diseases, including arthritis, Crohn's disease, psoriasis, ulcerative colitis, and juvenile idiopathic arthritis [1]. In addition, the control of the immune response when implanting a biomaterial is vital to improve its integration and promote tissue regeneration [79]. Concerning the IL-6 quantification, no significant statistical differences were observed between SChGal1 and SChGal3, both conditions, along with the control drug, dexamethasone, the ones that presented the lower IL-6 values (Figure IV-9B). Significant statistical differences were observed between SS and SChGallate sponges and between the LPS-stimulated cells and the treated conditions (SChGal1, SChGal3, and Dexamethasone). Furthermore, the SChGallate sponges induced an increase of the anti-inflammatory IL-10 levels compared to the LPS control, SS, and dexamethasone, with statistical differences between SS and SChGallate sponges at all studied time points (Figure IV-9C). IL-10 secretion by LPS-activated macrophages is superior to expected. However, these values may be explained as an immune system attempt to balance pro- and anti-inflammatory signals, increasing the IL-10 secretion, when facing the super expression of the pro-inflammatory factors [80]. This balance between pro-and anti-inflammatory factors allows to avoid excessive inflammation and control the tissue damage [80].

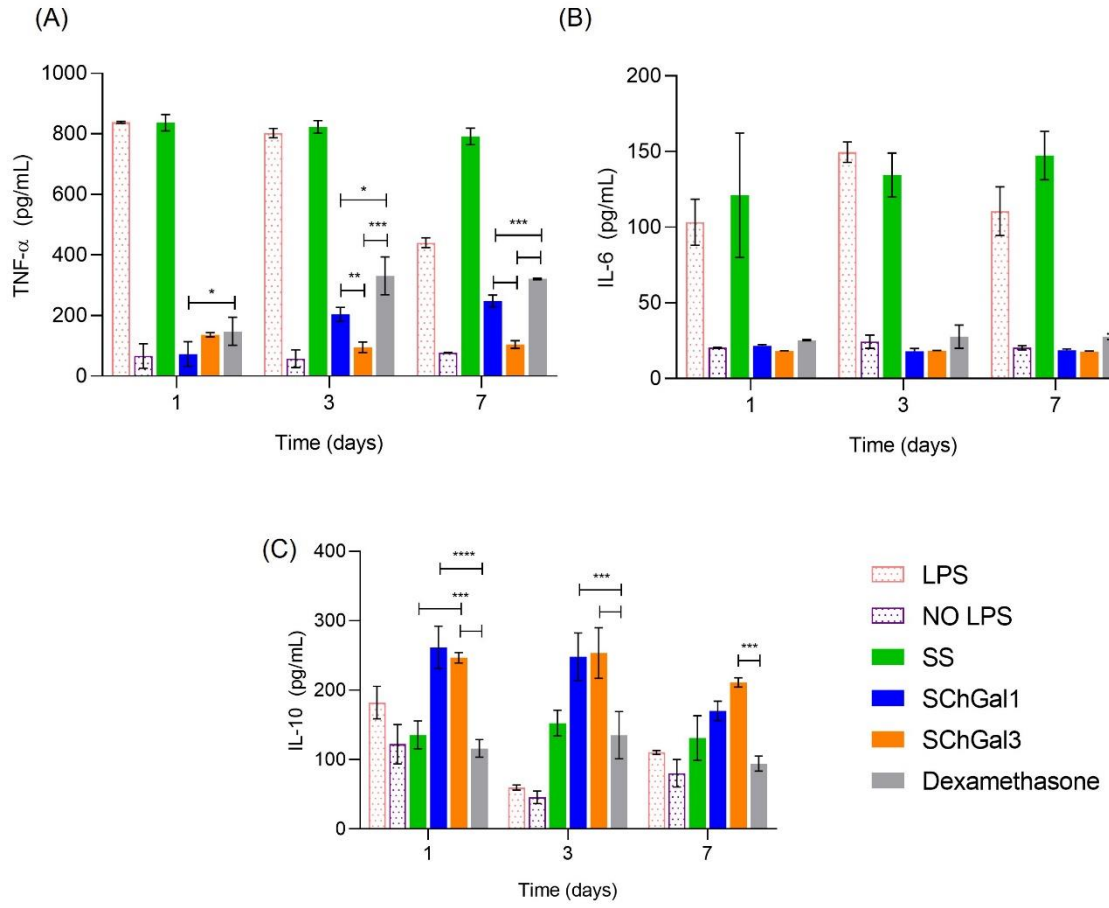


Figure IV-9 - (A) TNF-α, (B) IL-6 and (C) IL-10 amounts in the different conditions. Data represent ±SD (*p < 0.05, nonparametric Krustal-wallis test).

Pro-inflammatory cytokines targeting is often used as a therapeutic strategy for treating inflammatory diseases [76]. In addition, the TNF-α/IL-10 ratio is considered a parameter of chronic inflammation [81]. On the other hand, a balanced IL-6/IL-10 ratio is clinically relevant since it is known to decrease the risk of chronic inflammation and consequential metabolic disorders [81]. Considering this, we calculated the cytokine production ratio which is presented in Table IV-2. By analyzing the data, we concluded that both TNF-α/IL-10 and IL-6/IL-10 ratios are considerably decreased in the SChGallate conditions. Those findings are in agreement with the published data, where RAW 264.7 cell lines response to polysaccharides treatment was studied. The obtained results may indicate that SChGallate sponges can be potential tools to suppress chronic inflammation and that these sponges may reduce inflammation by balancing the IL-6/IL-10 ratio in the immune system [81]. Overall, SChGallate sponges inhibited the production of TNF-α and IL-6, and increased the secretion of IL-10, when compared to the controls (LPS-stimulated cells) suggesting its successful application, despite the need for further complementary studies.

Table IV-2 - The ratio of cytokines in THP-1 activated macrophages.

	Cytokine production ratio					
	TNF-α/IL-10			IL-6/IL-10		
Time (days)	**1**	**3**	**7**	**1**	**3**	**7**
LPS	5.9 ± 1.1	20.1 ± 2.2	4.8 ± 0.8	0.7 ± 0.2	3.7 ± 0.4	1.1 ± 0.4
SS	7.2 ± 0.9	5.9 ± 0.4	4.1 ± 1.3	0.8 ± 0.12	1.03 ± 0.1	0.9 ± 0.3
SChGal1	0.4 ± 0.1	0.7 ± 0.1	0.3 ± 0.1	0.1 ± 0.01	0.1 ± 0.01	0.1 ± 0.01
SChGal3	0.5 ± 0.01	1.5 ± 0.02	0.5 ± 0.03	0.1 ± 0.01	0.11 ± 0.01	0.1 ± 0.00

IV-4.3. Hemocompatibility

Hemocompatibility is an important criterion that limits the clinical applicability of blood-contacting materials, one of the most critical features for *in vivo* applicability. The most abundant blood cells are the erythrocytes, responsible for oxygen and carbon dioxide exchanges. These cells are prone to rupture and hemolysis due to shear stress and changes in osmotic pressure [82]. Considering the further *in vivo* applicability of the developed SChGallate sponges, their hemocompatibility was accurately studied by direct contact with fresh human blood. The results depicted in Figure IV-10 showed that either SS or SChGallate sponges present a hemolysis percentage inferior to 2%, which according to the standard hemolytic index (ASTM F756-00(2000)) allows to consider them as non-hemolytic. In previous work on SF:SAIB scaffolds, the results showed hemolytic rates below 2% [83]. However, other studies show hemolytic percentages varying from 3.1 to 4.5% when using poly L-lactic acid/SF-gelatin scaffolds [84], and percentages of 3 %, when testing the hemolytic rate of mulberry SF scaffolds [85].

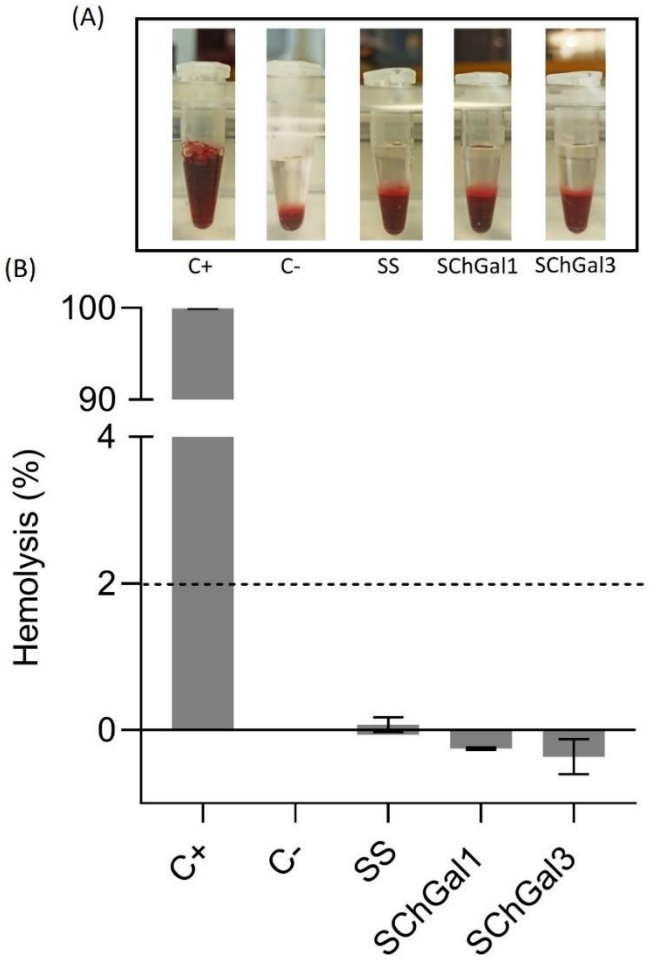


Figure IV-10 - (A) Representative images of the hemolysis assay and (B) Percentage of hemolysis induced by the controls (C+, positive control and C-, negative control), SS and the SChGallate sponges in contact with blood cells. Error bars are indicating the standard error of the mean.

IV-5. CONCLUSIONS

In this work, SChGallate sponges with high antioxidant activity were successfully produced combining SF from *bombyx mori* cocoons and Ch[Gallate], a Bio-IL. The presence of Ch[Gallate] at different concentrations in the SChGallate positively influenced the β-sheet content, while significantly improving the mechanical properties of the final constructs, when compared to the SS sponges. Moreover, the solid-state NMR and FTIR studies revealed that the silk native structure was not affected by Ch[Gallate] presence in the samples, independently of its concentration, being that the peaks intensity proportional to the Ch[Gallate] concentration on the sponges. Furthermore, also suggests that β-sheet formation was positively influenced by its presence. The sponges had a hydrogel-like behavior and a weight loss profile

that were associated with the Ch[Gallate] sustained release over time. Therefore, it seems that the Ch[Gallate] concentration into the matrix could be helpful to modulate the physico-chemical properties of the architectures in aqueous media. The *in vitro* studies using hASCs showed that the developed biomaterials supported cell growth and proliferation up to 7 days of culture, while the qualitative ROS analysis suggested that a low or moderate intracellular amount of these compounds may increase the hASCs metabolic activity and proliferation. Furthermore, the developed SChGallate sponges showed greater therapeutic potential than the SS, with some results suggesting their ability to control the balance between pro- and anti-inflammatory cytokines. Lastly, the hemolysis assay proved that SS and SChGallate sponges had hemolytic rates lower than 2%, indicating good blood biocompatibility. Considering the obtained results we would be able to point out that the SChGal1 as the most attractive and sustainable formulation to be used as a therapeutic strategy for inflammatory disease treatment.

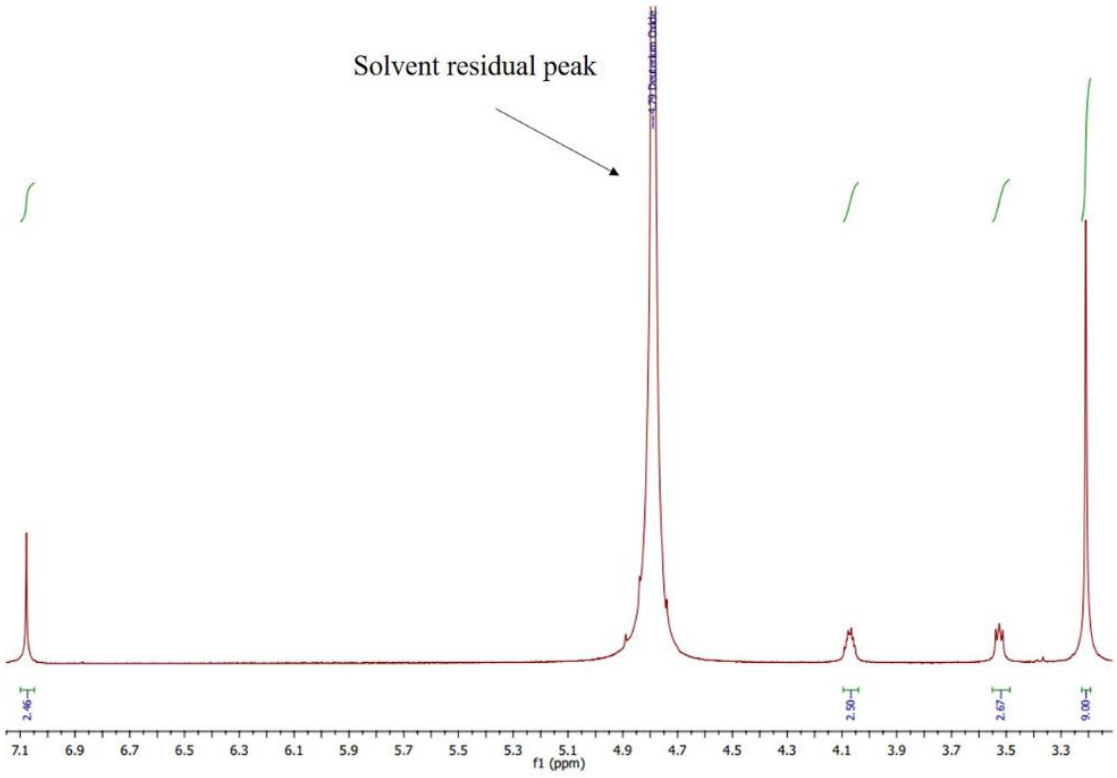
Overall, the bioactive SChGallate sponges provided paths towards accurately targeting pathologies with associated inflammatory processes, constituting innovative tools to be applied in tissue engineering strategies.

ACKNOWLEDGMENTS

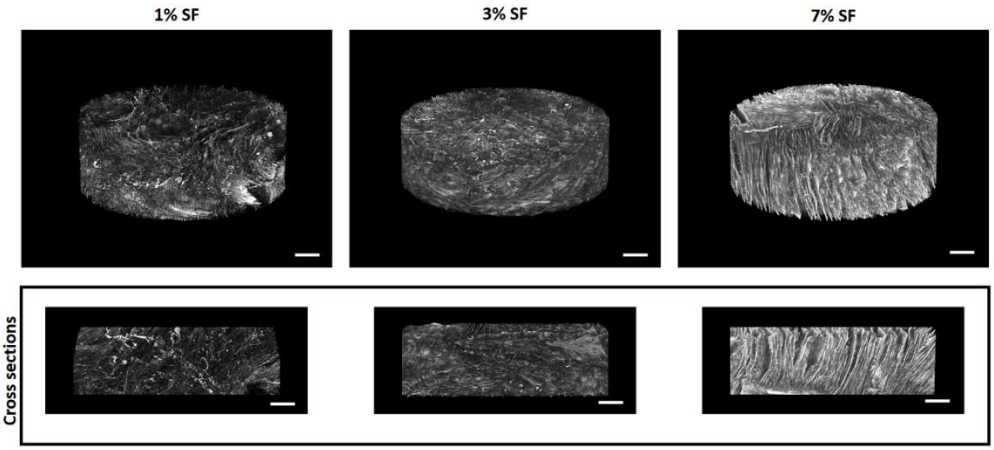
The authors want to acknowledge the financial support obtained by the European Regional Development Fund (ERDF) on the project FROnTHERA (NORTE-01-0145-FEDER-000023) and the FCT PhD Grant on the Doctoral Program on Advanced Therapies for Health (PATH) (PD/BD/128102/2016).

IV-6. SUPPLEMENTARY MATERIAL

^{1}H of pure Ch[Gallate] – Ch[Gallate] was obtained as a white solid (89% yield). ^{1}H NMR (D_2O, 300 MHz, [ppm]): δ 6.87 (s, 2H, H-2 and H-6), 3.79-3.67 (m, 2H, NCH_2CH_2OH), 3.18-309 (m, 2H, NCH_2CH_2OH), 2.84 (s, 9H, $N(CH_3)_3$).



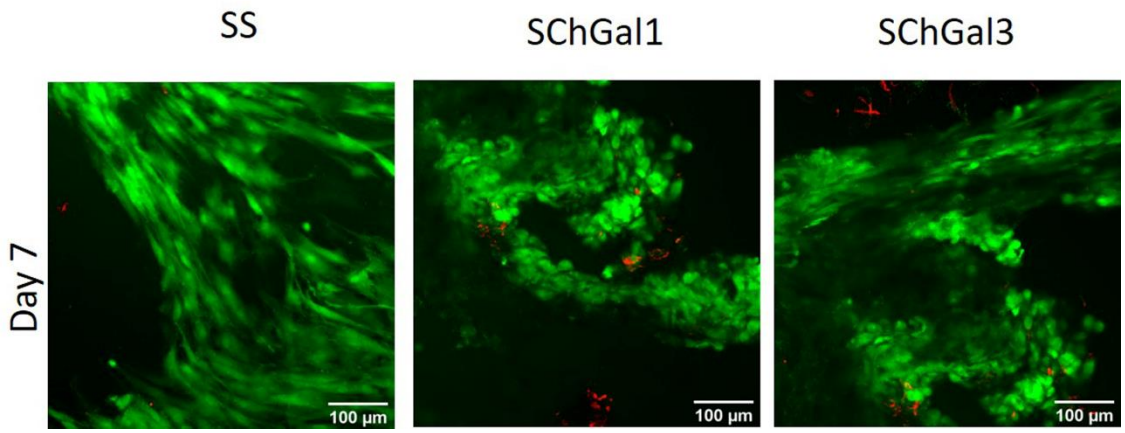
Supplementary Figure IV-1 - ^{1}H of pure Ch[Gallate].



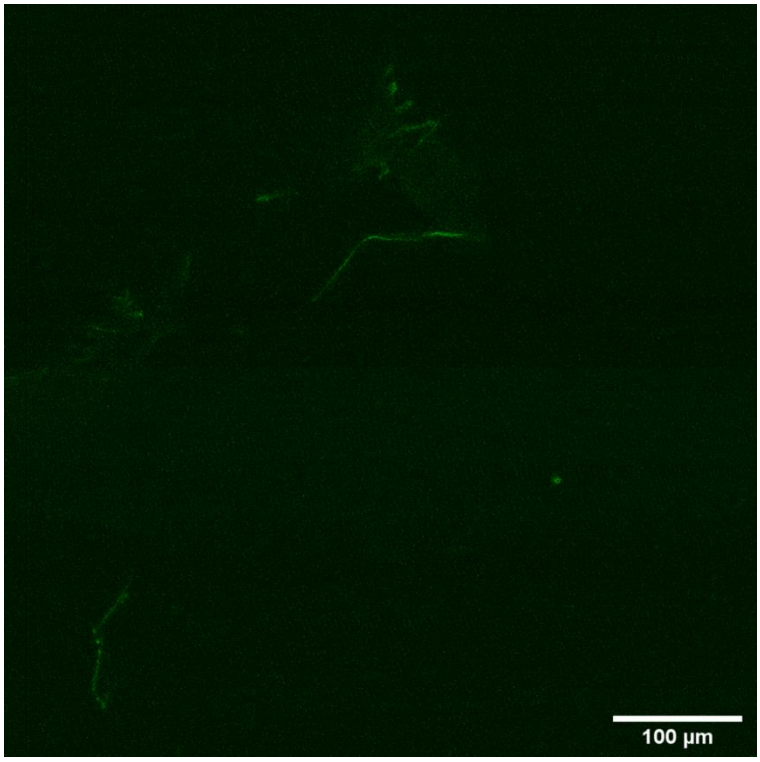
MORPHOMETRIC PARAMETERS

Sample	Mean pore size (μm)	Porosity (%)	Interconnectivity (%)
1% SF	80 ± 0.03	80 ± 2	79 ± 1
3% SF	70 ± 0.1	77 ± 6	82 ± 4
7% sf	31 ± 0.1	45 ± 3	51 ± 3

Supplementary Figure IV-2 - Micro-CT data of silk sponges at different % (w/v) - micro-CT 3D images and morphometric parameters. Scale bar 250nm.



Supplementary Figure IV-3 - Confocal microscope projection image of the live/dead assay after 7 days of culture.



Supplementary Figure IV-4 - Confocal microscope image of the SS – Green channel (488nm).

IV-7. REFERENCES

[1] C. Brightling, L. Chachi, D. Desai, Y. Amrani, Chapter 18: Tumor necrosis factor alpha, in: Inflmmation Allergy Drug Des., Blackwell Publishing Ltd, 2011: pp. 225–235.

[2] N. Khansari, Y. Shakiba, M. Mahmoudi, Chronic Inflammation and Oxidative Stress as a Major Cause of Age- Related Diseases and Cancer, Recent Pat. Inflamm. Allergy Drug Discov. 3 (2009) 73–80. https://doi.org/10.2174/187221309787158371.

[3] J.L. Escobar Ivirico, M. Bhattacharjee, E. Kuyinu, L.S. Nair, C.T. Laurencin, Regenerative Engineering for Knee Osteoarthritis Treatment: Biomaterials and Cell-Based Technologies, Engineering. 3 (2017) 16–27. https://doi.org/10.1016/J.ENG.2017.01.003.

[4] I.M. Oliveira, C. Gonçalves, M.E. Shin, S. Lee, R.L. Reis, G. Khang, J.M. Oliveira, Enzymatically crosslinked tyramine-gellan gum hydrogels as drug delivery system for rheumatoid arthritis treatment, Drug Deliv. Transl. Res. 11 (2021) 1288–1300. https://doi.org/10.1007/s13346-020-00855-9.

[5] J. Ringe, M. Sittinger, Tissue engineering in the rheumatic diseases, Arthritis Res. Ther. 11 (2009) 1–11. https://doi.org/10.1186/ar2572.

[6] J. Litowczenko, M.J. Woźniak-Budych, K. Staszak, K. Wieszczycka, S. Jurga, B. Tylkowski, Milestones and current achievements in development of multifunctional bioscaffolds for medical application, Bioact. Mater. 6 (2021) 2412–2438. https://doi.org/10.1016/j.bioactmat.2021.01.007.

[7] J.M. Gomes, S.S. Silva, R.L. Reis, Biocompatible ionic liquids: Fundamental behaviours and applications, Chem. Soc. Rev. 48 (2019) 4317–4335. https://doi.org/10.1039/c9cs00016j.

[8] G. Colomines, P. Decaen, D. Lourdin, E. Leroy, Biofriendly ionic liquids for starch plasticization: a screening approach, RSC Adv. 6 (2016) 90331–90337. https://doi.org/10.1039/C6RA16573G.

[9] S. Guilois, V. Jury, N. Allanic, E. Leroy, Choline Chloride vs Choline Ionic liquids for starch thermoplasticization, Carbohydr. Polym. 117 (2017) 424–432. https://doi.org/10.1016/j.carbpol.2017.09.012.

[10] H. Garcia, R. Ferreira, M. Petkovic, J.L. Ferguson, M.C. Leitão, H.Q.N. Gunaratne, K.R. Seddon, L.P.N. Rebelo, C. Silva Pereira, Dissolution of cork biopolymers in biocompatible ionic liquids, Green Chem. 12 (2010) 367–369. https://doi.org/10.1039/b922553f.

[11] F. Cheng, H. Wang, G. Chatel, G. Gurau, R.D. Rogers, Facile pulping of lignocellulosic biomass using choline acetate, Bioresour. Technol. 164 (2014) 394–401. https://doi.org/10.1016/j.biortech.2014.05.016.

[12] J.M. Gomes, S.S. Silva, R.L. Reis, Exploring the Use of Choline Acetate on the Sustainable Development of α-Chitin-Based Sponges, ACS Sustain. Chem. Eng. 8 (2020) 13507–13516. https://doi.org/10.1021/acssuschemeng.0c05076.

[13] I.M. Marrucho, L.C. Branco, L.P.N. Rebelo, Ionic Liquids in Pharmaceutical Applications, Annu. Rev. Chem. Biomol. Eng. 5 (2014) 527–546. https://doi.org/10.1146/annurev-chembioeng-060713-040024.

[14] K. Peng, Y. Gao, P. Angsantikul, A. LaBarbiera, M. Goetz, A.M. Curreri, D. Rodrigues, E.E.L. Tanner, S. Mitragotri, Modulation of Gastrointestinal Mucus Properties with Ionic Liquids for Drug Delivery, Adv. Healthc. Mater. 10 (2021) 1–14. https://doi.org/10.1002/adhm.202002192.

[15] T. Zhang, B. Sun, J. Guo, M. Wang, H. Cui, H. Mao, B. Wang, F. Yan, Active pharmaceutical ingredient poly(ionic liquid)-based microneedles for the treatment of skin acne infection, Acta Biomater. 115 (2020) 136–147. https://doi.org/10.1016/j.actbio.2020.08.023.

[16] E.S. Morais, N.H.C.S. Silva, T.E. Sintra, S.A.O. Santos, B. Miguel, I.F. Almeida, P.C. Costa, I. Correia-sá, S.P.M. Ventura, A.J.D. Silvestre, M.G. Freire, C.S.R. Freire, Anti-inflammatory and antioxidant nanostructured cellulose membranes loaded with phenolic-based ionic liquids for cutaneous application, Carbohydr. Polym. 206 (2019) 187–197. https://doi.org/10.1016/j.carbpol.2018.10.051.

[17] T.E. Sintra, A. Luís, S.N. Rocha, A.I.M.C.L. Ferreira, F. Gonçalves, L.M.N.B.F. Santos, B.M. Neves, M.G. Freire, S.P.M. Ventura, J.A.P. Coutinho, Enhancing the antioxidant characteristics of phenolic acids by their conversion into cholinium salts, ACS Sustain. Chem. Eng. 3 (2015) 2558–2565. https://doi.org/10.1021/acssuschemeng.5b00751.

[18] E.S. Morais, N.H.C.S. Silva, T.E. Sintra, S.A.O. Santos, B. Miguel, I.F. Almeida, P.C. Costa, I. Correia-sá, S.P.M. Ventura, A.J.D. Silvestre, M.G. Freire, C.S.R. Freire, Anti-inflammatory and antioxidant nanostructured cellulose membranes loaded with phenolic-based ionic liquids for cutaneous application, Carbohydr. Polym. 206 (2019) 187–197. https://doi.org/10.1016/j.carbpol.2018.10.051.

[19] X. Jia, C. Wang, V. Ranganathan, B. Napier, C. Yu, Y. Chao, M. Forsyth, F.G. Omenetto, D.R. MacFarlane, G.G. Wallace, A Biodegradable Thin-Film Magnesium Primary Battery Using Silk Fibroin–Ionic Liquid Polymer Electrolyte, ACS Energy Lett. 2 (2017) 831–836. https://doi.org/10.1021/acsenergylett.7b00012.

[20] X. Jia, Y. Yang, C. Wang, C. Zhao, V. Ranganathan, D.R. MacFarlane, M. Forsyth, G.G. Wallace, Biocompatible ionic liquid-biopolymer electrolyte enabled thin and compact magnesium air batteries, ACS Appl. Mater. Interfaces. 6 (2014) 21110–21117. https://doi.org/10.1021/am505985z.

[21] I. Noshadi, B.W. Walker, R. Portillo-lara, E.S. Sani, Engineering Biodegradable and Biocompatible Bio-ionic Liquid Conjugated Hydrogels with Tunable Conductivity and Mechanical Properties, Nature. 7 (2017) 1–18. https://doi.org/10.1038/s41598-017-04280-w.

[22] P. Leleux, C. Johnson, X. Strakosas, J. Rivnay, T. Hervé, R.M. Owens, G.G. Malliaras, Ionic liquid gel-assisted electrodes for long-term cutaneous recordings, Adv. Healthc. Mater. 3 (2014) 1377–1380. https://doi.org/10.1002/adhm.201300614.

[23] A. Reizabal, D.M. Correia, C.M. Costa, L. Perez-Alvarez, J.L. Vilas-Vilela, S. Lanceros-Méndez, Silk Fibroin Bending Actuators as an Approach Toward Natural Polymer Based Active Materials, ACS Appl. Mater. Interfaces. 11 (2019) 30197–30206. https://doi.org/10.1021/acsami.9b07533.

[24] P. Wang, H. He, R. Cai, G. Tao, M. Yang, H. Zuo, A. Umar, Y. Wang, Cross-linking of dialdehyde carboxymethyl cellulose with silk sericin to reinforce sericin film for potential biomedical application, Carbohydr. Polym. 212 (2019) 403–411. https://doi.org/10.1016/j.carbpol.2019.02.069.

[25] G. Tao, Y. Wang, R. Cai, H. Chang, K. Song, H. Zuo, P. Zhao, Q. Xia, H. He, Design and performance of sericin/poly(vinyl alcohol) hydrogel as a drug delivery carrier for potential wound dressing application, Mater. Sci. Eng. C. 101 (2019) 341–351. https://doi.org/10.1016/j.msec.2019.03.111.

[26] G. Tao, R. Cai, Y. Wang, H. Zuo, H. He, Fabrication of antibacterial sericin based hydrogel as an injectable and mouldable wound dressing, Mater. Sci. Eng. C. 119 (2021) 111597. https://doi.org/10.1016/j.msec.2020.111597.

[27] G. Tao, R. Cai, Y. Wang, L. Liu, H. Zuo, P. Zhao, A. Umar, C. Mao, Q. Xia, H. He, Bioinspired design of AgNPs embedded silk sericin-based sponges for efficiently combating bacteria and promoting wound healing, Mater. Des. 180 (2019) 107940. https://doi.org/10.1016/j.matdes.2019.107940.

[28] S.S. Silva, A. Motta, M.T. Rodrigues, A.F.M. Pinheiro, M.E. Gomes, J.F. Mano, R.L. Reis, C. Migliaresi, Novel genipin-cross-linked chitosan/silk fibroin sponges for cartilage engineering strategies, Biomacromolecules. 9 (2008) 2764–2774. https://doi.org/10.1021/bm800874q.

[29] S.S. Silva, N.M. Oliveira, M.B. Oliveira, D.P.S. Da Costa, D. Naskar, J.F. Mano, S.C. Kundu, R.L. Reis, Fabrication and characterization of Eri silk fibers-based sponges for biomedical application, Acta Biomater. 32 (2016) 178–189. https://doi.org/10.1016/j.actbio.2016.01.003.

[30] D.N. Rockwood, R.C. Preda, T. Yücel, X. Wang, M.L. Lovett, D.L. Kaplan, Materials fabrication from Bombyx mori silk fibroin, Nat. Protoc. 6 (2011) 1612–1631. https://doi.org/10.1038/nprot.2011.379.

[31] S.S. Silva, T.C. Santos, M.T. Cerqueira, A.P. Marques, L.L. Reys, T.H. Silva, S.G. Caridade, J.F. Mano, R.L. Reis, The use of ionic liquids in the processing of chitosan / silk hydrogels for biomedical applications, Green Chem. 14 (2012) 1463–1470. https://doi.org/10.1039/c2gc16535j.

[32] S.S. Silva, J.M. Gomes, A.C. Vale, S. Lu, R.L. Reis, S.C. Kundu, Green Pathway for Processing Non-mulberry *Antheraea pernyi* Silk Fibroin/Chitin-Based Sponges: Biophysical and Biochemical Characterization, Front. Mater. 7 (2020) 135. https://doi.org/10.3389/fmats.2020.00135.

[33] C. Gonçalves, S.S. Silva, J.M. Gomes, I.M. Oliveira, R.F. Canadas, F.R. Maia, H. Radhouani, R.L. Reis, J.M. Oliveira, Ionic Liquid-Mediated Processing of SAIB-Chitin Scaffolds, ACS Sustain. Chem. Eng. 8 (2020) 3986–3994. https://doi.org/10.1021/acssuschemeng.0c00385.

[34] N. Kasoju, U. Bora, Silk fibroin in tissue engineering, Adv. Healthc. Mater. 1 (2012) 393–412. https://doi.org/10.1002/adhm.201200097.

[35] J.W. Kinney, S.M. Bemiller, A.S. Murtishaw, A.M. Leisgang, A.M. Salazar, B.T. Lamb, Inflammation as a central mechanism in Alzheimer's disease, Alzheimer's Dement. Transl. Res. Clin. Interv. 4 (2018) 575–590. https://doi.org/10.1016/j.trci.2018.06.014.

[36] R. Liu-Bryan, R. Terkeltaub, Emerging regulators of the inflammatory process in osteoarthritis, Nat. Rev. Rheumatol. 11 (2015) 35–44. https://doi.org/10.1038/nrrheum.2014.162.

[37] S.S. Silva, E.G. Popa, M.E. Gomes, M.B. Oliveira, S. Nayak, B. Subia, J.F. Mano, S.C. Kundu, R.L. Reis, Silk hydrogels from non-mulberry and mulberry silkworm cocoons processed with ionic liquids, Acta Biomater. 9 (2013) 8972–8982. https://doi.org/10.1016/j.actbio.2013.06.044.

[38] S.B. Kedare, R.P. Singh, Genesis and development of DPPH method of antioxidant assay, J. Food Sci. Technol. 48 (2011) 412–422. https://doi.org/10.1007/s13197-011-0251-1.

[39] A.R. Franco, E. Palma Kimmerling, C. Silva, F.J. Rodrigues, I.B. Leonor, R.L. Reis, D.L. Kaplan, Silk-Based Antimicrobial Polymers as a New Platform to Design Drug-Free Materials to Impede Microbial Infections, Macromol. Biosci. 18 (2018) 1–15. https://doi.org/10.1002/mabi.201800262.

[40] T. Rada, R.L. Reis, M.E. Gomes, Novel method for the isolation of adipose stem cells (ASCs), J Tissue Eng Regen Med. 12 (2009) 158–159. https://doi.org/10.1002/term.

[41] A.I. Gonçalves, M.T. Rodrigues, S.J. Lee, A. Atala, J.J. Yoo, R.L. Reis, M.E. Gomes, Understanding the role of growth factors in modulating stem cell tenogenesis, PLoS One. 8 (2013). https://doi.org/10.1371/journal.pone.0083734.

[42] I.M. Oliveira, C. Gonçalves, M.E. Shin, S. Lee, R.L. Reis, G. Khang, J.M. Oliveira, Anti-Inflammatory Properties of Injectable Betamethasone-Loaded Tyramine-Modified Gellan Gum/Silk Fibroin Hydrogels, Biomolecules. 10 (2020) 1456. https://doi.org/10.3390/biom10101456.

[43] L. Zhang, X. Liu, G. Li, P. Wang, Y. Yang, Tailoring degradation rates of silk fibroin scaffolds for tissue engineering, J. Biomed. Mater. Res. - Part A. 107 (2019) 104–113. https://doi.org/10.1002/jbm.a.36537.

[44] L.P. Yan, J. Silva-Correia, M.B. Oliveira, C. Vilela, H. Pereira, R.A. Sousa, J.F. Mano, A.L. Oliveira, J.M. Oliveira, R.L. Reis, Bilayered silk/silk-nanoCaP scaffolds for osteochondral tissue engineering: *in vitro* and *in vivo* assessment of biological performance, Acta Biomater. 12 (2015) 227–241. https://doi.org/10.1016/j.actbio.2014.10.021.

[45] D. Maniglio, W. Bonani, C. Migliaresi, A. Motta, Silk fibroin porous scaffolds by N2O foaming, J. Biomater. Sci. Polym. Ed. 29 (2018) 491–506. https://doi.org/10.1080/09205063.2018.1423811.

[46] V.P. Ribeiro, S. Pina, J.M. Oliveira, R.L. Reis, Silk Fibroin-Based Hydrogels and Scaffolds for Osteochondral Repair and Regeneration, Adv. Exp. Med. Biol. 1058 (2018) 305–325. https://doi.org/10.1007/978-3-319-76711-6_14.

[47] J. Rnjak-Kovacina, L.S. Wray, K.A. Burke, T. Torregrosa, J.M. Golinski, W. Huang, D.L. Kaplan, Lyophilized Silk Sponges: A Versatile Biomaterial Platform for Soft Tissue Engineering, ACS Biomater. Sci. Eng. 1 (2015) 260–270. https://doi.org/10.1021/ab500149p.

[48] H.J. Park, J.S. Lee, O.J. Lee, F.A. Sheikh, B.M. Moon, H.W. Ju, J.H. Kim, D.K. Kim, C.H. Park, Fabrication of microporous three-dimensional scaffolds from silk fibroin for tissue engineering, Macromol. Res. 22 (2014) 592–599. https://doi.org/10.1007/s13233-014-2083-0.

[49] S. V. Madihally, H.W.T. Matthew, Porous chitosan scaffolds for tissue engineering, Biomaterials. 20 (1999) 1133–1142. https://doi.org/10.1016/S0142-9612(99)00011-3.

[50] B. Badhani, N. Sharma, R. Kakkar, Gallic acid: A versatile antioxidant with promising therapeutic and industrial applications, RSC Adv. 5 (2015) 27540–27557. https://doi.org/10.1039/c5ra01911g.

[51] M. Nune, S. Manchineella, T. Govindaraju, K.S. Narayan, Melanin incorporated electroactive and antioxidant silk fibroin nanofibrous scaffolds for nerve tissue engineering, Mater. Sci. Eng. C. 94 (2019) 17–25. https://doi.org/10.1016/j.msec.2018.09.014.

[52] S. Selvaraj, N.N. Fathima, Fenugreek Incorporated Silk Fibroin Nanofibers - A Potential Antioxidant Scaffold for Enhanced Wound Healing, ACS Appl. Mater. Interfaces. 9 (2017) 5916–5926. https://doi.org/10.1021/acsami.6b16306.

[53] M.F. El-Refaei, S.H. Abduljawad, A.H. Alghamdi, Alternative Medicine in Diabetes - Role of Angiogenesis, Oxidative Stress, and Chronic Inflammation, Rev. Diabet. Stud. 11 (2014) 231–244. https://doi.org/10.1900/RDS.2014.11.231.

[54] A.S. Marchev, P.A. Dimitrova, A.J. Burns, R. V. Kostov, A.T. Dinkova-Kostova, M.I. Georgiev, Oxidative stress and chronic inflammation in osteoarthritis: can NRF2 counteract these partners in crime?, Ann. N. Y. Acad. Sci. 1401 (2017) 114–135. https://doi.org/10.1111/nyas.13407.

[55] J. Kong, S. Yu, Fourier Transform Infrared Spectroscopic Analysis of Protein Secondary Structures Protein FTIR Data Analysis and Band Assign- ment, Acta Biochim. Biophys. Sin. (Shanghai). 39 (2007) 549–559. https://doi.org/10.1111/j.1745-7270.2007.00320.x.

[56] R. Yadav, N.K. Kahlon, S. Kumar, N. Devunuri, P. Venkatesu, Biophysical study on the phase transition behaviour of biocompatible thermoresponsive polymer influenced by tryptophan-based amino acid ionic liquids, Polymer (Guildf). 228 (2021) 123871. https://doi.org/10.1016/j.polymer.2021.123871.

[57] D.U. Lee, J.Y. Jeong, J.W. Han, G.C. Kwon, P. Attri, I.T. Kim, Effect of ionic liquids on the physical properties of the newly synthesized conducting polymer, Int. J. Polym. Sci. 2018 (2018) 1–8. https://doi.org/10.1155/2018/8275985.

[58] C. Vepari, D.L. Kaplan, Silk as a biomaterial, Prog. Polym. Sci. 32 (2007) 991–1007. https://doi.org/10.1016/j.progpolymsci.2007.05.013.

[59] T. Ozdal, E. Capanoglu, F. Altay, A review on protein-phenolic interactions and associated changes, Food Res. Int. 51 (2013) 954–970. https://doi.org/10.1016/j.foodres.2013.02.009.

[60] N. Tiwari, S. Wegner, A. Hassan, N. Dwivedi, R.N. Rai, N. Sinha, Probing short and long-range interactions in native collagen inside the bone matrix by BioSolids CryoProbe, Magn. Reson. Chem. 59 (2021) 99–107. https://doi.org/10.1002/mrc.5084.

[61] Y. Shen, F. Delaglio, G. Cornilescu, A. Bax, TALOS+: A hybrid method for predicting protein backbone torsion angles from NMR chemical shifts, J. Biomol. NMR. 44 (2009) 213–223. https://doi.org/10.1007/s10858-009-9333-z.

[62] B.B. Mandal, S.C. Kundu, Non-bioengineered silk fibroin protein 3D scaffolds for potential biotechnological and tissue engineering applications, Macromol. Biosci. 8 (2008) 807–818. https://doi.org/10.1002/mabi.200800113.

[63] H. Zheng, B. Zuo, Functional silk fibroin hydrogels: preparation, properties and applications, J. Mater. Chem. B. 9 (2021) 1238–1258. https://doi.org/10.1039/d0tb02099k.

[64] A. Teimouri, M. Azadi, R. Emadi, J. Lari, A.N. Chermahini, Preparation, characterization, degradation and biocompatibility of different silk fibroin based composite scaffolds prepared by freeze-drying method for tissue engineering application, Polym. Degrad. Stab. 121 (2015) 18–29. https://doi.org/10.1016/j.polymdegradstab.2015.08.004.

[65] N. Kasoju, N. Hawkins, O. Pop-Georgievski, D. Kubies, F. Vollrath, Silk fibroin gelation via non-solvent induced phase separation, Biomater. Sci. 4 (2016) 460–473. https://doi.org/10.1039/c5bm00471c.

[66] Y. Wang, U.J. Kim, D.J. Blasioli, H.J. Kim, D.L. Kaplan, *In vitro* cartilage tissue engineering with 3D porous aqueous-derived silk scaffolds and mesenchymal stem cells, Biomaterials. 26 (2005) 7082–7094. https://doi.org/10.1016/j.biomaterials.2005.05.022.

[67] J.R. Mauney, T. Nguyen, K. Gillen, C. Kirker-Head, J.M. Gimble, D.L. Kaplan, Engineering adipose-like tissue *in vitro* and *in vivo* utilizing human bone marrow and adipose-derived mesenchymal stem cells with silk fibroin 3D scaffolds, Biomaterials. 28 (2007) 5280–5290. https://doi.org/10.1016/j.biomaterials.2007.08.017.

[68] M.E. Gomes, T. Rada, R.L. Reis, Adipose tissue-derived stem cells and their application in bone and cartilage tissue engineering, Tissue Eng. - Part B Rev. 15 (2009) 113–125. https://doi.org/10.1089/ten.teb.2008.0423.

[69] K. Burridge, E.S. Wittchen, The tension mounts: Stress fibers as force-generating mechanotransducers, J. Cell Biol. 200 (2013) 9–19. https://doi.org/10.1083/jcb.201210090.

[70] D. Soares Da Costa, M.D.C. Márquez-Posadas, A.R. Araujo, Y. Yang, S. Merino, T. Groth, R.L. Reis, I. Pashkuleva, Adhesion of adipose-derived mesenchymal stem cells to glycosaminoglycan surfaces with different protein patterns, ACS Appl. Mater. Interfaces. 7 (2015) 10034–10043. https://doi.org/10.1021/acsami.5b02479.

[71] S.G. Park, J.H. Kim, Y. Xia, J.H. Sung, Generation of reactive oxygen species in adipose-derived stem cells: Friend or foe?, Expert Opin. Ther. Targets. 15 (2011) 1297–1306. https://doi.org/10.1517/14728222.2011.628315.

[72] A.K. Machado, S.G. Homrich, C.C.R. Rodrigues, V.F. Azzolin, M.M.M.F. Duarte, D.M. Pillar, L.S. Lenz, T.C. Unfer, D.V. de Souza, I.B.M. Da Cruz, Human adipose-derived stem cells obtained from lipoaspirates are highly susceptible to hydrogen peroxide mediated cytogenotoxicity, Arch. Biosci. Heal. 1 (2019) 11–28. https://doi.org/10.18593/abh.17060.

[73] N.V. Montoya, R. Peterson, K.J. Ornell, D.R. Albrecht, J.M. Coburn, Silk particle production based on silk/PVA phase separation using a microfabricated co-flow device, Molecules. 25 (2020) 1–19. https://doi.org/10.3390/molecules25040890.

[74] E. Chisari, K.M. Yaghmour, W.S. Khan, The effects of TNF-alpha inhibition on cartilage: a systematic review of preclinical studies, Osteoarthr. Cartil. 28 (2020) 708–718. https://doi.org/10.1016/j.joca.2019.09.008.

[75] C.S. Bonnet, D.A. Walsh, Osteoarthritis, angiogenesis and inflammation, Rheumatology. 44 (2005) 7–16. https://doi.org/10.1093/rheumatology/keh344.

[76] M. Amoroso, M. Rossol, H. Heine, U. Meusch, D. Quandt, C. Klein, M.J. Sweet, S. Hauschildt, LPS-induced cytokine production in human monocytes and macrophages, Crit. Rev. Immunol. 31 (2012) 379–446. http://www.ncbi.nlm.nih.gov/pubmed/22142165.

[77] S.J. Dreyer, W.J. Beckworth, Commonly Used Medications in Procedures, Pain Proced. Clin. Pract. (2011) 5–12. https://doi.org/10.1016/B978-1-4160-3779-8.10002-8.

[78] P. Ubanako, N. Xelwa, M. Ntwasa, LPS induces inflammatory chemokines via TLR-4 signalling and enhances the Warburg Effect in THP-1 cells, PLoS One. 14 (2019) 1–17. https://doi.org/10.1371/journal.pone.0222614.

[79] Y. Wang, D. Yao, L. Li, L. Li, Z. Qian, W. He, R. Ding, H. Liu, H. Liu, Y. Fan, Y. Fan, Y. Fan, Effect of Electrospun Silk Fibroin-Silk Sericin Films on Macrophage Polarization and Vascularization, ACS Biomater. Sci. Eng. 6 (2020) 3502–3512. https://doi.org/10.1021/acsbiomaterials.0c00175.

[80] J.M. Cicchese, S. Evans, C. Hult, L.R. Joslyn, T. Wessler, J.A. Millar, S. Marino, N.A. Cilfone, J.T. Mattila, J.J. Linderman, D.E. Kirschner, Dynamic balance of pro- and anti-inflammatory signals controls disease and limits pathology, Immunol. Rev. 285 (2018) 147–167. https://doi.org/10.1111/imr.12671.

[81] P. Suabjakyong, K. Nishimura, T. Toida, L.J.L.D. Van Griensven, Structural characterization and immunomodulatory effects of polysaccharides from Phellinus linteus and Phellinus igniarius on the IL-6/IL-10 cytokine balance of the mouse macrophage cell lines (RAW 264.7), Food Funct. 6 (2015) 2834–2844. https://doi.org/10.1039/c5fo00491h.

[82] M. Weber, H. Steinle, S. Golombek, L. Hann, C. Schlensak, H.P. Wendel, M. Avci-Adali, Blood-Contacting Biomaterials: *In vitro* Evaluation of the Hemocompatibility, Front. Bioeng. Biotechnol. 6 (2018) 99. https://doi.org/10.3389/fbioe.2018.00099.

[83] C. Gonçalves, J.M. Gomes, F.R. Maia, H. Radhouani, S.S. Silva, R.L. Reis, J.M. Oliveira, Fabrication of biocompatible porous SAIB/silk fibroin scaffolds using ionic liquids, Mater. Chem. Front. 5 (2021) 6582–6591. https://doi.org/10.1039/d1qm00583a.

[84] G.B. Yin, Y.Z. Zhang, S.D. Wang, D.B. Shi, Z.H. Dong, W.G. Fu, Study of the electrospun PLA/silk fibroin-gelatin composite nanofibrous scaffold for tissue engineering, J. Biomed. Mater. Res. - Part A. 93 (2010) 158–163. https://doi.org/10.1002/jbm.a.32496.

[85] A. Muthumanickkam, S. Subramanian, M. Goweri, W. Sofi Beaula, V. Ganesh, Comparative study on eri silk and mulberry silk fibroin scaffolds for biomedical applications, Iran. Polym. J. (English Ed. 22 (2013) 143–154. https://doi.org/10.1007/s13726-012-0113-3.

Chapter V

Unraveling the potential of biocompatible ionic liquid-based sponges for osteoarthritis therapy by reducing inflammation and oxidative stress

Chapter V

Unraveling the potential of biocompatible ionic liquid-based sponges for osteoarthritis therapy by reducing inflammation and oxidative stress [§]

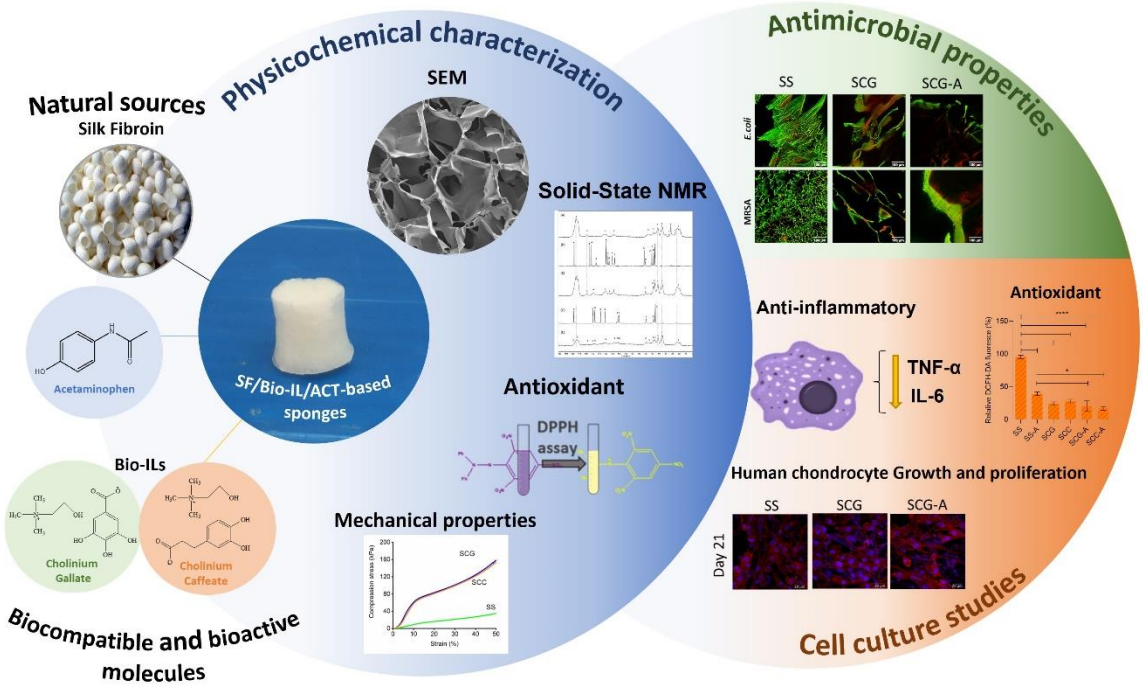
ABSTRACT

Chronic inflammatory osteoarthritis (OA) is one of the leading causes of morbidity worldwide. Current therapeutic approaches target oxidative stress and inflammation, but they frequently fail to prevent disease progression or cartilage regeneration. Herein, biocompatible ionic liquid-based sponges with anti-inflammatory, antioxidant, and analgesic activities were designed as bioactive systems. To achieve this goal, we assessed the potential of 3D sponge-like structures made of silk fibroin (SF) loaded with two phenolic-based anti-inflammatory and antioxidant biocompatible ionic liquids (Bio-IL; Cholinium gallate and Cholinium caffeate), as well as an analgesic drug, acetaminophen (ACT), as a novel therapeutic approach. Both Bio-ILs and impregnated sponges demonstrated antibacterial activity against Methicillin-resistant *Staphylococcus aureus* and *Escherichia coli*. Furthermore, the constructs reduced ROS generation in primary human chondrocytes (HC), whereas activated macrophages derived from THP-1, produced fewer proinflammatory mediators, such as TNF-α and IL-6, after contact with the constructs. Moreover, the architectures supported the decrease of pro-inflammatory gene expression in osteoarthritic human chondrocytes (HC-OA), where an increase in COL2A1 expression was found after 21 days of culture in both HC and HC-OA. Overall, our findings support that Bio-IL-based sponges can be an innovative solution for OA therapy, reducing inflammation and oxidative stress while promoting cartilage regeneration.

[§] This chapter is based on the following publication:

Gomes J. M., Silva S. S, Rodrigues L. C., Franco, A. R., Fernandes E. M., Soares da Costa, D., Lobo F. C. M. Martín-Pasto M., Taboada and Reis L. R. "Unraveling the potential of biocompatible ionic liquid-based sponges for osteoarthritis therapy by reducing inflammation and oxidative stress"; 2022, Submitted

V-1. GRAPHICAL ABSTRACT



V-2. INTRODUCTION

Age-related articular cartilage damage often results in pain and impairment due to the loss of cartilage mechanical function and osteoarthritic (OA) degeneration [1]. The regeneration of articular cartilage remains one of the most difficult clinical challenges in the treatment of OA. Currently available medical treatments rely on symptom-relieving nonpharmacological approaches, such as physical therapy, exercise, and pharmacological strategies using analgesics, non-selective/selective inhibitors, or other nonsteroidal anti-inflammatory drugs [2]. However, the efficacy of these approaches in treating OA is limited due to patient age and other related health conditions. Autologous cell-based cartilage tissue engineering has emerged as an innovative and promising strategy for repairing severely damaged cartilage [3,4]. The development of biomaterials capable of providing a suitable environment for chondrogenic cell growth is, therefore critical, despite their unclear role in OA treatment [1,2].

Scaffolds, hydrogels, and nanoparticles for OA treatment have been created using materials from different sources [5,6]. Natural polymers, like alginate, fibrin, chitosan, and silk fibroin (SF), are widely used in developing biomaterials for OA, whether as drug carriers, 3D culture constructs, or disease

modeling [2,7,8]. SF is one of the most used nature-derived materials for tissue regeneration because of its unique mechanical properties, excellent biocompatibility, and controlled stability [9,10]. As such, SF-based biomaterials have been extensively investigated to be used for cartilage regeneration either as micro or nanocarriers for the local delivery of drugs of interest, thus providing a good local environment, supporting the adhesion and proliferation or as support for chondrocytes [7,8,11].

On the other hand, several drugs have been tested for OA treatment; however, their therapeutic potential can be hampered due to loss of drug activity or disease progress [12]. At the same time, the use of certain drugs with low solubility limits their *in vivo* bioavailability due to a fast metabolism and bloodstream clearance [7,13]. Biocompatible ionic liquids (Bio-ILs), an innovative class of compounds, have recently emerged in response to the demand for environmentally friendly solvents for different fields[14]. Combinations of cations and anions are used in the design and fabrication of Bio-ILs, enabling tuning their bioactivity and biocompatibility [14–17]. Therefore, Bio-ILs can act as solvents for poorly soluble and unstable drugs, increasing the active pharmaceutical ingredient (API) stability, bioavailability, and activity [14–17]. On the other hand, an ideal implantable biomaterial should prevent microbial colonization of multidrug-resistant organisms, which is prone to happen following a joint replacement surgery, namely in patients with degenerative joint diseases, such as OA [18,19]. To meet these needs, the design of Bio-ILs with antibacterial properties can be achieved using cholinium as a cation and amoxicillin/ penicillin as an anionic counterpart. As a result, these Bio-ILs inhibit the growth of clinically significant pathogens like Methicilin-resistant *Staphylococcus aureus* (MRSA), *Pseudomonas aeruginosa* ATCC15692, *Salmonella enterica serovar*, and *Escherichia coli* (*E. coli*) [20–24]. The Bio-ILs act like a detergent disrupting the bacteria's lipid cell membrane because of the amphiphilic nature of these compounds [25]. Therefore, there is an increasing interest in using Bio-ILs as an innovative approach to engineer biomaterials that can sustain tissue regeneration owing to their relevant activity, biological performance, and inherent antibacterial properties [19,23].

According to our previous work, the morphological features, swelling, and stability of the SF/Ch[Gallate] sponges can be controlled by their Bio-IL content (≤3% w/v) [26]. Herein, the influence of two distinct Bio-ILs, namely cholinium gallate (Ch[Gallate]) and cholinium caffeate (Ch[Caffeate]), on the production of SF/Bio-ILs systems was evaluated. Furthermore, beyond the antioxidant and anti-inflammatory action expected from these systems, the incorporation of analgesic drugs, such as acetaminophen (ACT), will provide a system with an additional effect. From the large analgesic drug list, ACT was selected because it is considered the first-line treatment for patients with mild to moderate OA

[27]. We hypothesized that the bioactive Bio-ILs would have a longer-lasting action on the free radicals productions, the activation of the signaling cascades, and the release of inflammatory mediators and cytokines when the constructs are implanted. In addition, local pain management will be made by the ACT's effect. In these systems, SF is a backbone structure to support the Bio-ILs and ACT. To evaluate these hypotheses, the physico-chemical and morphological features of the developed architectures were assessed. Furthermore, anti-inflammatory, and cellular antioxidant activities were investigated using a human monocyte cell line (THP-1) and human chondrocytes (HC). The antibacterial potential of the SF/Bio-ILs-based sponges against Methicilin-resistant *Staphylococcus aureus* (MRSA), and *Escherichia coli (E. coli)* was also evaluated. In addition, HC and osteoarthritic human chondrocytes (HC-OA) were cultured within the constructs for up to 21 days, and the biological behaviour and therapeutic impact of the constructs were examined analyzing the expression of chondrocyte-related genes by RT-PCR.

V-3. MATERIALS AND METHODS

V-3.1. Materials

Silk fibroin (SF) from cocoons of *Bombyx mori* was kindly supplied by the APPACDM (Castelo Branco, Portugal). Cholinium hydroxide (Ch[OH]) 45% in methanol solution, gallic acid, and caffeic acid, used in the synthesis, were bought from Sigma-Aldrich, St. Louis, MO, USA. 2,2-diphenyl-1-picrylhydrazyl (DPPH) was also purchased from Sigma-Aldrich, St. Louis, MO, USA. All other chemicals were reagent grade, and they were used as received. Human blood samples were obtained from Serviço de Imunohemoterapia - Centro Hospitalar de São João (Portugal) under an approved institutional board protocol (ethical commission of CHSJ/FMUP approved on 18/13/2018). The samples were collected in sterile BD Vacutainer® coagulation tubes (BD-Plymouth, UK) containing 3.8% sodium citrate.

V-3.2. Synthesis of Cholinium-Gallate (Ch[Gallate]) and Cholinium-Caffeate (Ch[Caffeate])

Both Bio-ILs were synthesized as previously reported [15]. Briefly, cholinium hydroxide (Ch[OH]) was dropwise added to the gallic acid or caffeic acid solution in methanol, 1.1 equivalent, at 0°C, and under a nitrogen atmosphere. The mixture was stirred under a nitrogen atmosphere, over night at room temperature. The methanol and water were removed under reduced pressure on the following day, and

the unreacted acid was washed with methanol at least 3 times in the case of Ch[Gallate], and with acetone when producing Ch[Caffeate]. The residual solvent was removed under reduced pressure, and the resultant Bio-IL, in which chemical structures are present in Scheme 1, was dried under a high vacuum for at least 72h. The high purity of the produced compounds was confirmed by ^{1}H nuclear magnetic resonance (NMR). NMR spectra were obtained on an Avance III spectrometer (Bruker, Germany) operating at a resonance frequency of 400.13 MHz (1H). D_2O was used as a solvent and a reference for chemical shifts reported in ppm (parts per million).

V-3.3. Preparation of the SF/Bio-IL sponges

V-3.3.1. SF preparation

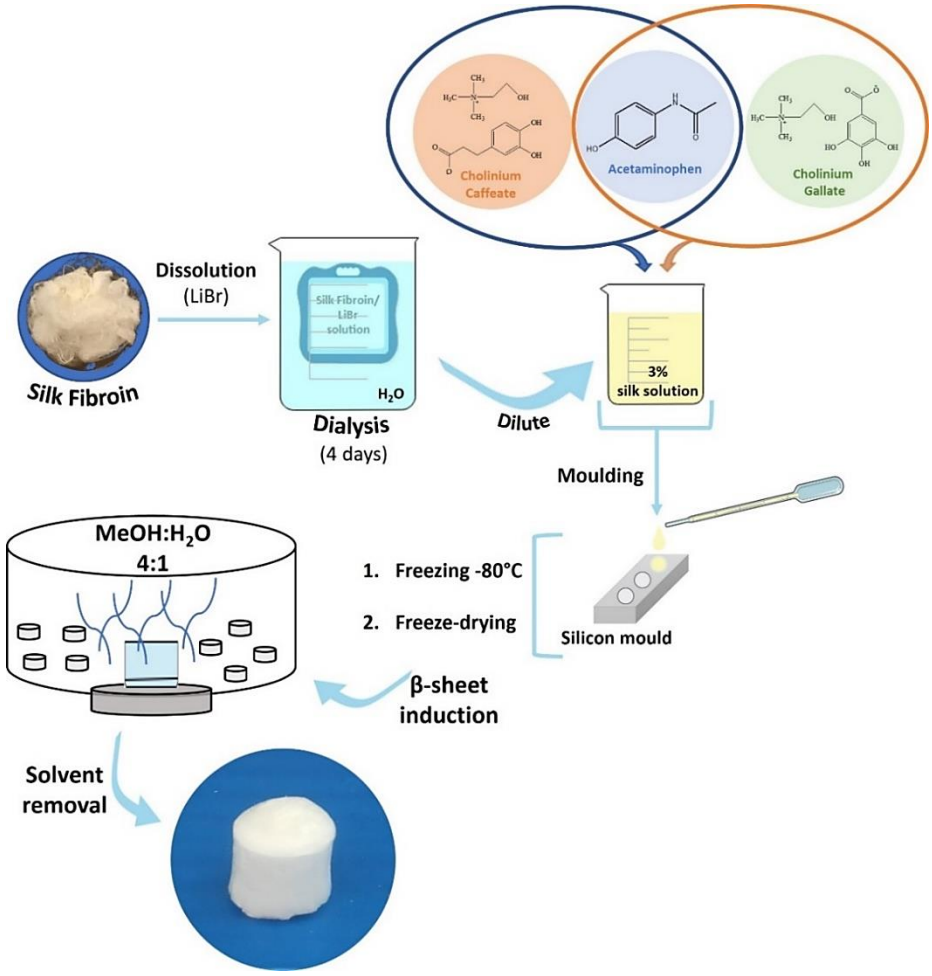
Firstly, SF was isolated from *Bombyx mori* cocoons following a previously described protocol [28]. After cutting them into small pieces, the cocoons were boiled for 1h in an aqueous solution of 2.12 mg/mL of Na_2CO_3 (degumming process). The resultant fibroin filaments were rinsed in distilled water and air-dried at room temperature. The SF fibers were further dissolved in 9.3M LiBr, for 3h, at 70 °C, by optimizing a previously developed protocol [29]. Then, the SF was dialyzed in a Slide A-Lyzer cassette (Pierce, 3500 Da MWCO) against distilled water for 4 days at room temperature. The water was changed every 2h. The resultant SF solution was centrifuged for 20 min at 5000 rpm, 7 °C, and immediately used or stored at 4 °C. The final SF concentration was calculated by adding 1 ml of the SF solution to an empty container (W1), followed by weighing the container with the SF solution (W2). The SF solution in the container was dried in an oven at 70°C overnight and weighed the next day (W3). The concentration of the SF solution was determined using Equation V-1.

$$SF\ \%\ \left(\frac{W}{V}\right) = \left(\frac{W3-W1}{W2-W1}\right) \times 100 \qquad \text{Equation V-1}$$

V-3.3.2. Preparation of SF/Bio-IL/Acetaminophen (ACT) loaded sponges

The different systems (detailed in Table VI-1) were prepared by incorporating 1% (w/v) of Ch[Gallate] or Ch[Caffeate], 0.01% (w/v) of ACT into 3% (w/v) of SF solution and manually stirred, at room temperature, until complete dissolution. The SF/Bio-IL and SF/Bio-IL/ACT mixtures were molded into

silicone molds (diameter 8mm), frozen at -80 °C overnight, and freeze-dried for at least 3 days, as represented in Scheme V-1. Following the freeze-drying, the samples were placed in a desiccator for 24h, under vacuum. Further, the samples were exposed to a methanol/H_2O saturated atmosphere (created by placing a flask of an aqueous solution of methanol:H_2O, 4:1 inside the desiccator) to induce the β-sheet formation. After 24h, the flask with the methanol:H_2O aqueous solution was removed, and the samples were left under vacuum for 24h to remove the solvent excess. The same procedure was utilized to create SF sponges (SS) without either the Bio-IL or ACT, which were then used as a control. Throughout the paper, SS-A, SCG, SCC, SCG-A and SCC-A formulations correspond to sponges containing 0.01 % (w/v) of ACT, 1% (w/v) Ch[Gallate], 1% (w/v) Ch[Caffeate], 1% (w/v) Ch[Gallate] + 0.01% (w/v) of ACT and 1% (w/v) Ch[Caffeate] + 0.01% (w/v) of ACT, respectively (see details in Table VI-1).



Scheme V-1 - Schematic representation of the SS-A, SCG. SCC, SCG-A and SCC-A sponges' preparation

Table V-1 - Sample identification used throughout the paper.

Sample	SF concentration % (w/v)	ACT % (w/v)	Ch[Gallate] % (w/v)	Ch[Caffeate] % (w/v)
SS	3	-	-	-
SS-A		0.01	-	-
SCG		-	1	-
SCC			-	1
SCG-A		0.01	1	-
SCC-A			-	1

V-3.4. Physico-chemical characterization

V-3.4.1. Solid-State NMR study

Solid NMR spectra were measured at 298 K in a Bruker NEO-750 spectrometer (750 MHz proton frequency) equipped with a Varian T3 solid triple resonance probe 1H/X/Y that uses a zirconia rotor of an outer diameter of 3.2 mm with an effective sample capacity of 22 μL, which corresponds to approximately 30 mg of the powder sample. The probe was adapted to the Bruker spectrometer by a A2B conversion kit (Revolution NMR, LLC). The spectrometer control software was TopSpin 4.x. All the spectra were processed with MestreNova software v14.2 (Mestrelab Research Inc.). Carbon-13 chemical shifts were referenced externally to the methylene signal of crystalline α-form of glycine at 43.5 ppm.

The ^{13}C CP-MAS spectra (sequence "hC.cp" of the Bruker library) were measured with an inter-scan delay (d_1) of 2 s, the minimum number of scans was 500, and the MAS rate was 20 kHz. Cross-polarization was applied for 2 ms with a constant carbon field strength of 63.1 kHz; the power on the ^{1}H nucleus was linearly ramped from 70% to 100% with a peak field strength of 59.0 kHz. Heteronuclear decoupling during the FID acquisition was performed with Spinal-64 with a proton field strength of 79.4 kHz.

V-3.4.2. Mechanical properties

The mechanical behavior of the sponges was assessed under uniaxial compression load using Universal Mechanical Testing Equipment (Instron 5543, USA), equipped with a 50 N load cell at room temperature. The crosshead speed was set as 1 mm·min^{-1}, and at least 6 specimens with cylindrical shapes were tested for each sponge composition. The determination of the elastic modulus was used as the initial slope in the stress-strain curve. The yield strength, or the yield point, was used to describe the stress at the transition from elastic to plastic deformation. It was determined by the intersection of a parallel line to the modulus at an offset strain of 0.2%. The immediate recovery of the samples was determined after reaching 50% of the strain by using a digital caliper (Mitutoyo, Japan).

V-3.4.3. Fourier Transform Infrared spectroscopy

The FTIR-ATR spectra of the sponges were obtained using a Shimadzu-IR, Prestige 21 spectrometer equipped with a single horizontal ATR cell. The spectra were recorded in the spectral region of 4000-400 cm^{-1}, with a resolution of 2 cm^{-1} and 32 scans. The quantification of the secondary structure was based on the analysis of the amide I and amide II regions (1700–1450 cm^{-1}). The previously collected spectra were linear baseline corrected, normalized, and subsequently deconvoluted by fitting with a Lorentzian function using PeakFit v4.12 software (Systat Software Inc., California, USA). Next, the average percentage for the secondary structures, mainly β–sheet, random-coil/α-helix, and turns, were calculated by integrating the area of each deconvoluted peak curve, normalizing the obtained value to the total area of the amide I and amide II regions [30].

V-3.4.4. Scanning electron microscopy (SEM)

The different constructs were fixed using mutual carbon adhesive tape on aluminum stubs and coated with a conductive gold layer. The morphology of the sponges was observed using a NanoSEM-FEI Nova 200 with an integrated microanalysis X-ray system (EDS – energy dispersive spectrometer).

V-3.4.5. Swelling

The swelling tests were carried out by immersing the SS, SS-A, SCG, SCC, SCG-A, and SCC-A sponges in phosphate buffer solution (PBS), pH 7.4, up to 7 days, at 37 °C, in triplicate. The excess surface water was removed before the determination of the weight of the swollen samples by gently tapping the surface with filter paper. Then, the percentage of water uptake was determined using Equation V-2 where *Ws* is the weight of the swollen sample, and *Wd* is the weight of the dry sample.

$$Swelling = \left[\frac{Ws-Wd}{Wd}\right] \times 100 \qquad \text{Equation V-2}$$

V-3.4.6. Stability

The weight loss of the developed sponges was evaluated after immersion into phosphate buffer saline (PBS) solution at pH 7.4, up to 7 days. The experiment was conducted at 37 °C in triplicate. After each time of immersion, the samples were dried at 37 °C until they reached constant weight (W_f), and the percentage of weight loss was calculated using Equation V-3, where W_i corresponds to the weight of the sponges before the immersion.

$$Weight\ loss\ (\%) = \left[\frac{Wi-Wf}{Wi}\right] \times 100 \qquad \text{Equation V-3}$$

V-3.4.7. Bio-active compounds *release*

The release of the Bio-IL Ch[Gallate] and Ch[Caffeate], and ACT from the SF sponges were performed following previously reported protocol [26]. Briefly, the dried sponges were placed in vessels containing 5ml of a PBS solution (pH 7.4) at 37 °C and protected from light due to the solvent's light sensitivity. After 30min, 1h, 2h, 4h, 24h, 3d, and 7d, 1mL of the PBS solution was collected, and the same volume of PBS was added to maintain a constant volume. The Ch[Gallate], Ch[Caffeate], and ACT content was determined by UV spectroscopy using a microplate reader (Synergy HT, BIO-TEK, Winooski, VT, USA) at 259, 285, and 243nm. The compound content at each time point was plotted as a cumulated percentage release determined using Equation V-4

$$Cumulative\ release\ (\%) = \frac{V_0 C_n + V C_{n-1} \times 100}{M}$$ Equation V-4

Where, C_{n-1} and C_n correspond to each compound concentration at times n-1 and n, V_0 is the initial volume of the drug release medium, V is the withdraw volume, and M is the compound mass loaded into one sponge. Calibration curves were established, and PBS was used as a reference for the baseline correction of the values.

V-3.4.8. Antioxidant activity assays

The antioxidant activity of the Bio-ILs and the developed sponges were determined using the 2,2-diphenyl-1 picrylhydrazyl (DPPH) radical scavenging assay [31]. The principle of this test is based on the color change of the DPPH solution from purple to yellow, as the radical is quenched by the antioxidant. This reaction was monitored by visible spectroscopy at 517 nm. [15] Briefly, a volume of 1mM DPPH solution in methanol was mixed with 4 mL of methanol, and the sponges were immersed. Samples were kept in the dark for 1h, 4h, and 24h at room temperature, and the absorbance at 517nm was determined at the end of each time point. A blank was made with DPPH solution in methanol and Gallic acid, the precursor of one of the Bio-ILs (Ch[Gallate]), and was used as the positive control. The antioxidant activity of ACT at different concentrations was also evaluated. The DPPH radical scavenging activity, AA(%), was determined according to Equation V-5

$$AA\ (\%) = \frac{A_0 - A_1}{A_0} \times 100$$ Equation V-5

Where A_0 and A_1 are the absorbance of the control and the samples, respectively.

V-3.5. Antimicrobial properties

V-3.5.1. Radial diffusion assay

The antimicrobial activity of the Bio-ILs ([Ch]Gallate and Ch[Caffeate]) was evaluated by radial diffusion assay against well-known pathogens Gram-negative bacteria (*Pseudomonas aeruginosa, Escherichia coli*) and Gram-positive bacteria (Methicillin-resistant *S. aureus-MRSA,* Vancomycin-resistant *S. aureus-VRSA, Enterococcus feacalis, Bacillus pumillus*). Luria–Bertani (LB) broth medium was used to grow the bacterial cultures at 37 °C overnight with stirring (140 rpm). Then, cells were centrifuged at 9000 rpm (Eppendorf 5810R, S-4-104) for 5 min at 4 °C, and the cell pellet was washed twice with sterile PBS (pH 7.4). The cell pellet was re-suspended in sterile PBS (pH 7.4), adjusted to an optical density of 0.1 (λ = 610 nm), and spread onto Muller Hinton Agar (Oxoid, UK) with a sterile swab. Blank sterile disks (Oxoid, UK) were impregnated with 30 µL of different concentrations of the Bio-ILs (0.05, 1, and 3 % (w/v), placed on top of the inoculated agar and incubated overnight at 37 °C. Experiments were carried out in triplicates. Antibiotic-impregnated disks (Kanamycin 50 µg/ml; Oxoid, UK) were used as the positive control, and PBS-impregnated disks were used as a negative control. The diameter of the zone formed around the disks was measured to calculate the area of growth inhibition.

V-3.5.2. Evaluation of the antimicrobial properties of the produced SF/Bio-IL-based sponges

The antibacterial properties of SS, SCG, and SCC sponges were assessed against Methicilin-resistant *Staphylococcus aureus* (MRSA), and *Escherichia coli (E. Coli).* Before the antibacterial tests, the sponges were sterilized under an ethylene oxide atmosphere (42°C, for 3h). Bacterial cultures were grown in LB broth overnight at 37°C, as described above. Then, the SS, SCG, and SCC sponges were immersed in 1 mL of LB medium inoculated with 3.1×10^6 or 2.1×10^6 of *E. coli* and MRSA, respectively, and incubated at 37 °C with agitation (150 rpm) for 24 h. The viability of the bacteria in the SS, SCG, and SCC sponges was analyzed by Live/ Dead staining, while bacteria adherence and formation of biofilms on the sponges was assessed by SEM [30]. Briefly, after each growth time, the sponges were washed twice with sterile PBS (pH 7.4) and stained with 1 mL of the solution of Live/Dead Bacterial Viability Kit (Molecular probes, L7007, Invitrogen) for 15 min at room temperature. Then, the samples were washed three times with sterile PBS (pH 7.4) to remove excess dye. Live bacteria were stained green using SYTO 9, and dead

bacteria were stained red using PI and visualized using a Confocal laser scanning microscope (Leica TCS/SP8), under 20x magnification. Four images were acquired using a digital camera (AxioCam MRm5, Zeiss) and analyzed by ImageJ (NIH, Maryland, USA). For SEM analysis, samples were fixed with 4% glutaraldehyde for 60 min in the dark at room temperature. Sponges and control materials were dehydrated in a series of ethanol-water solutions with increasing ethanol concentration twice (50, 70, 80, 90, and 100%, v/v) and left to dry overnight before coating with palladium by ion sputtering.

V-3.6. *In vitro* studies

V-3.6.1. Human chondrocytes (HC) and Human chondrocytes Osteoarthritis (HC-OA) isolation and expansion

The human chondrogenic primary cells from healthy and osteoarthritic tissues, HC and HC-OA, respectively, were collected from human cartilage during arthroscopic surgeries on both male and female donors aged between 19 and 56 years (Centro Hospitalar Póvoa do Varzim) as previously described [32]. Firstly, the articular cartilage tissue was detached from the bone and cut into small fragments. The samples were washed several times with 1% PBS/antibiotic-antimycotic (v/v) solution and digested with 0.08% collagenase type II (Sigma-Aldrich, USA)/DMEM-F12 medium 1:1 (v/v). After digestion, the samples were incubated overnight at 37 °C in a water bath with mild agitation. The digested tissue was filtered to obtain a cell suspension, which was further centrifuged at 500 g for 5 min. HC and HC-OA cells were expanded in DMEM/F12 medium (Dulbecco's Modified Eagle Medium: Nutrient Mixture F-12, Thermo Fisher Scientific, USA), supplemented with 10% of Heat Inactivated Fetal Bovine Serum (FBS) (Alfagene, Portugal), sodium bicarbonate (Sigma-Aldrich, USA) and 1% (v/v) antibiotic-antimycotic (Alfagene, Portugal), at 37 °C in a 5% CO_2 incubator, until confluency was reached.

V-3.6.2. Cell culture

HC and HC-OA cells were cultured in DMEM/F12 medium (Dulbecco's Modified Eagle Medium: Nutrient Mixture F-12, Thermo Fisher Scientific, USA), supplemented with 10% FBS (Alfagene, Portugal), sodium bicarbonate (Sigma-Aldrich, USA) and 1% (v/v) antibiotic–antimycotic (Alfagene, Portugal), at 37 °C in a 5% CO_2 incubator.

THP-1 cells (SIGMA, USA) were cultured in RPMI 1640 Medium, GlutaMAXt Supplement, HEPES (Thermo Fisher Scientific, USA), supplemented with 10% of FBS and 1% of antibiotic–antimycotic, at 37°C in a humidified atmosphere containing 5% CO_2, until confluency.

V-3.6.3. Measurement of intracellular ROS

HC cells were seeded at a density of 4 × 10^3 cells/well, in a 96-well plate, using DMEM-F12, for 24h. At the same time, SS, SS-A, SCG, SCC, SCG-A, and SCC-A sponges were incubated with DMEM-F12 for 24h, at 37°C. Afterwards, the culture medium was removed, and the medium in contact with sponges was added to the previously seeded cells for 24h. The next day, after removing the medium and washing the cells twice with HBSS, the oxidative stress was induced by adding 100µM and 500 µM of H_2O_2 in DMEM-F12, for 3h, following a previously reported protocol.[33] After 3h, the cells were rinsed with HBSS (twice) and incubated with 5µM of 2′,7′-Dichlorofluorescin diacetate (H_2DCFA, Sigma Aldrich), in HBSS, for 1min at 37 °C, in the dark. After incubation, the fluorescence intensity was measured using a microplate reader (Synergy HT, BIO-TEK, Winooski, VT, USA) (Ex: 495nm, Em. 529 nm), and the metabolic activity of the cells was determined using CellTiter 96® AQueous One Solution Cell Proliferation Assay (MTS, Promega), by reading the optical density 490 nm, also in a microplate reader.

V-3.6.4. Assessment of the anti-inflammatory potential of the developed SF/Bio-IL/ACT-based sponges

To evaluate the anti-inflammatory potential of the developed sponges, an *in vitro* model was used consisting of a THP-1 cell line stimulated with lipopolysaccharide (LPS) (Sigma-Aldrich, St. Louis, MO, USA), as previously reported.[34] THP-1 cells were seeded at a density of 1 × 10^6 cells/mL in RPMI medium with 100 nM Phorbol 12-myristate-13 acetate (PMA) (Sigma-Aldrich, St. Louis, MO, USA) for 24 h. After incubation time, a 1ml volume of RPMI medium was added to the wells without PMA and incubated for 48 h. THP-1 cells were incubated with 100 ng mL−1 of LPS in RPMI medium and incubated for 5 h, to induce the inflammatory response. After this period, the sponges were added to the cells and cultured for up to 7 days. After each time point (1, 3, and 7 days), the culture medium was removed and stored at −80 ◦C for further analysis.

The concentration of the proinflammatory cytokines TNF-α and IL-6 and anti-inflammatory IL-1, in the medium were evaluated after THP-1 cells were in contact with the sponges. For that, Human TNF-alpha DuoSET ELISA (R&D Systems, Minneapolis, MN, USA) and Human IL-6 DuoSET ELISA (R&D Systems, Minneapolis, MN, USA) kits were used. In addition, the determination of the concentration of the anti-inflammatory cytokine IL-10 was performed using a Human IL-10 DuoSET ELISA (R&D Systems, Minneapolis, MN, USA). The optical density at 450 nm was read in a microplate reader (Synergy HT, BIO-TEK, Winooski, VT, USA).

V-3.6.5. Cell viability

HC were seeded at a density of 100 × 10^3 cells/sponge, in a 24-well plate, using DMEM-F12 for up to 21 days. After each of the defined time points (1, 7, 14, and 21 days), the metabolic activity of cells seeded on the sponges was evaluated using the CellTiter 96® AQueous One Solution Cell Proliferation Assay (MTS, Promega). Briefly, the cell–scaffold constructs were placed in a mixture containing serum-free cell culture medium and MTS reagent at a 5:1 ratio and incubated for 3 h. The optical density was read (OD 490 nm).

In addition, cell viability was also assessed by fluorescence labeling using a live/dead assay. The sponges were removed from the culture medium and washed with sterile PBS. After, all samples were incubated with 1 mg/mL calcein acetoxymethyl (Invitrogen, 1:500) and 1.5 mM propidium iodide (PI, Invitrogen, 1:1000) solution in PBS for 15 min, at 37 °C and washed with sterile PBS. Further, the samples were visualized using a confocal laser scanning microscope (Leica, TCS/SP8). The software Fiji was used to analyze the images.

V-3.6.6. Cell proliferation

The proliferation of the cells throughout the sponges was evaluated using the fluorometric PicoGreen double-stranded DNA assay, according to the manufacturer's instructions (Quant-iT™ PicoGreen™ dsDNA Kit, P7589, Invitrogen). Briefly, after each time-point, the cell–scaffold constructs were rinsed with PBS, placed in microtubes containing 1 ml of ultra-pure water, and stored at -80 °C until analyzed. A microplate reader was used to measure the fluorescence (Bio-Tek Instruments, USA) at Ex. 480 and Em. 520 nm.

A standard curve (0–2 µg ml-1) was used to calculate the DNA concentration, relating the amount of dsDNA to the fluorescence.

V-3.6.7. Cell morphology

The cell distribution and attachment on the structures were analyzed using a confocal laser scanning microscope (CLSM). The constructs were fixed with 10% formalin for 30 min, and then the samples were incubated with 1% bovine serum albumin (BSA) for 30 min. The constructs were permeabilized using 0.1 % Triton X-100 in PBS for 5 min, washed with PBS and incubated with rhodamine-phalloidin at room temperature (RT) for 20 min. Following another washing with PBS, staining with 5 µg ml-1 of 4',6-Diamidine-2'-phenylindole dihydrochloride (DAPI) was performed for 30 min. Fluorescence images from the stained constructs were obtained using a confocal laser scanning microscope (Leica TCS/SP8).

V-3.6.8. Therapeutic effect of the produced SF/Bio-IL/ACT-based sponges over HC-OA

HC and HC-OA (cell passage=2/3), previously isolated and characterized, were used for this assay. Briefly, the HC and HC-OA were seeded at a density of 100 × 10^3 cells/sponge in a 24-well plate, using DMEM-F12, for 1 and 21 days, as previously described.

V-3.6.9. RNA isolation and gene expression analysis

At each time point, total RNA was extracted from HC, and HC-OA seeded in the sponges (SS, SCG, and SCG-A) from two independent assays, using the DirectzolTM RNA MiniPrep kit (Zymo Research, USA), following the manufacturer's instructions. Briefly, after 1 and 21 days of culture, the constructs were washed with PBS, immersed in Tri reagent (Sigma-Aldrich, USA), and stored at – 80 °C until further use.

The expression of tumor necrosis factor (TNF-α), interleukin-6 (IL-6), cyclooxygenase-2 (COX-2), inducible nitric oxide synthase (iNOS), transforming growth factor (TGF-β) and collagen type II alpha 1 chain (COL2A1), were assessed by real-time RT-PCR. Samples were thawed and vortexed to ensure the lysis and removal of cells within the sponges. After precipitation with 100% ethanol, the mRNA was washed with Directzol Prewash and wash buffers and then resuspended in DNAse/RNAse-free water. To quantify total RNA, a Nanodrop ND-1000 spectrophotometer (Nano-Drop Technologies, USA) was used. The

complementary DNA (cDNA) synthesis was carried out according to qScript cDNA Synthesis kit (Quanta BioSciences, USA). The cDNA was further used as a template for the amplification of TEC-related genes (Supplementary Table V-1) using PerfeCta SYBR Green FastMix kit (Quanta Biosciences, USA), following manufacturer's instructions. The transcripts expression of each sample was normalized to the housekeeping gene hB2M and calculated according to the Livak method ($2-\Delta\Delta CT$) where cultures in the bottom of the well of HC and HC-OA were used as calibrators.

V-3.7. Statistical analysis

All experiments were run in triplicate. The results are expressed as means ± standard deviation for n = 3. The statistical analysis was conducted using GraphPadPrism v. 8.0 for Windows (GraphPad Software, San Diego, http://www.graphpad.com). Normality of the data was evaluated by the Shapiro-Wilk test. When data followed a normal distribution, One-way ANOVA and Tukey's multiple comparisons test was employed. For data that did not follow a normal distribution, a nonparametric Krustal-wallis test was performed. Differences between the groups at $p \leq 0.05$ were considered statistically significant.

V-4. RESULTS AND DISCUSSION

V-4.1. SF/Bio-IL-based sponges' preparation and characterization

We successfully fabricated SF/Bio-IL/ACT-based sponges as solutions for OA cartilage degeneration using a biocompatible and green methodology. The sponges were prepared by incorporating the phenolic Bio-ILs, Ch[Gallate] or Ch[Caffeate] at 1% (w/v) into an SF solution (3% (w/v)). Figure V-1 depicts the ^{13}C-CPMAS spectrum of the original pure SS, Ch[Caffeate], Ch[Gallate], and the sponges SCC and SCG, as well as the signal assignment of the components. The SS sponge spectrum demonstrates the expected pattern of signals for a protein in the solid state, as described in the literature [35]. The signals of choline and caffeic acid in the spectrum of Ch[Caffeate], and choline and gallic acid in the spectrum of Ch[Gallate] (Figure V-1B and Figure V-1D, respectively) were identified using the predicted chemical shifts of these molecules calculated with Mestrenova. In the spectrum of Ch[Caffeate] (Figure V-1B), there are six carbon peaks, whereas only three should be expected for this molecule. This indicates the presence of two choline species in different environments, with an approximate proportion of 70:30 based on their NMR intensities. Caffeic acid only shows the expected nine signals in the same spectrum. This suggests that

choline and caffeic acid are forming a complex that is the dominant specie in the sample due to their opposite polarity. Also, the minoritarian specie may correspond to excess free choline in this sample, and an unidentified anion may compensate its positive charge (e.g. an inorganic anion) that does not generate peak in the ^{13}C-CPMAS spectrum (Figure V-1B) or the alternative ^{13}C-direct-polarization spectrum (data not shown). The peaks in the spectrum of SCC (Figure V-1C) were easily assigned using the assignments of SS and Ch[Caffeate] as references because the signal patterns and chemical shifts of the peaks were unchanged. The intensity of the signals of Ch[Caffeate] relative to SS in the spectrum (Figure V-1C) is consistent with the 1% (w/v) concentration of Ch[Caffeate] used to prepare this sample. Similarly, the signal patterns and chemical shifts of the peaks assigned to SS and Ch[Gallate] remained unchanged in the SCG spectra (Figure V-1E). These results are consistent with those from our earlier research [26]. As with SCC, the intensity of the signals of Ch[Gallate] relative to SS in the SCG spectra (Figure V-1E) is consistent with the 1% (w/v) Ch[Gallate] concentration used to prepare these samples. However, the broadening of the signals relative to caffeate acid in the SCC spectrum is rather similar to that of the SS protein, implying that there are no covalent interactions (e.g., hydrogen bond, π-stacking, etc.) between [Caffeate] moiety and the SS protein rather than a simple physical entrapment. In terms of the SS protein structure in these samples, it is well established that chemical shifts in both solution and solid-state samples, achieved by NMR analysis are reporters of proteins down to the amino acid level [36]. The geometrical center of the peaks for the three samples (SS, SCC, and SCG) remained at the same chemical shift despite the low resolution and broadness of the SS protein peaks (Figure V-1A), which are shown by the vertical striped lines.

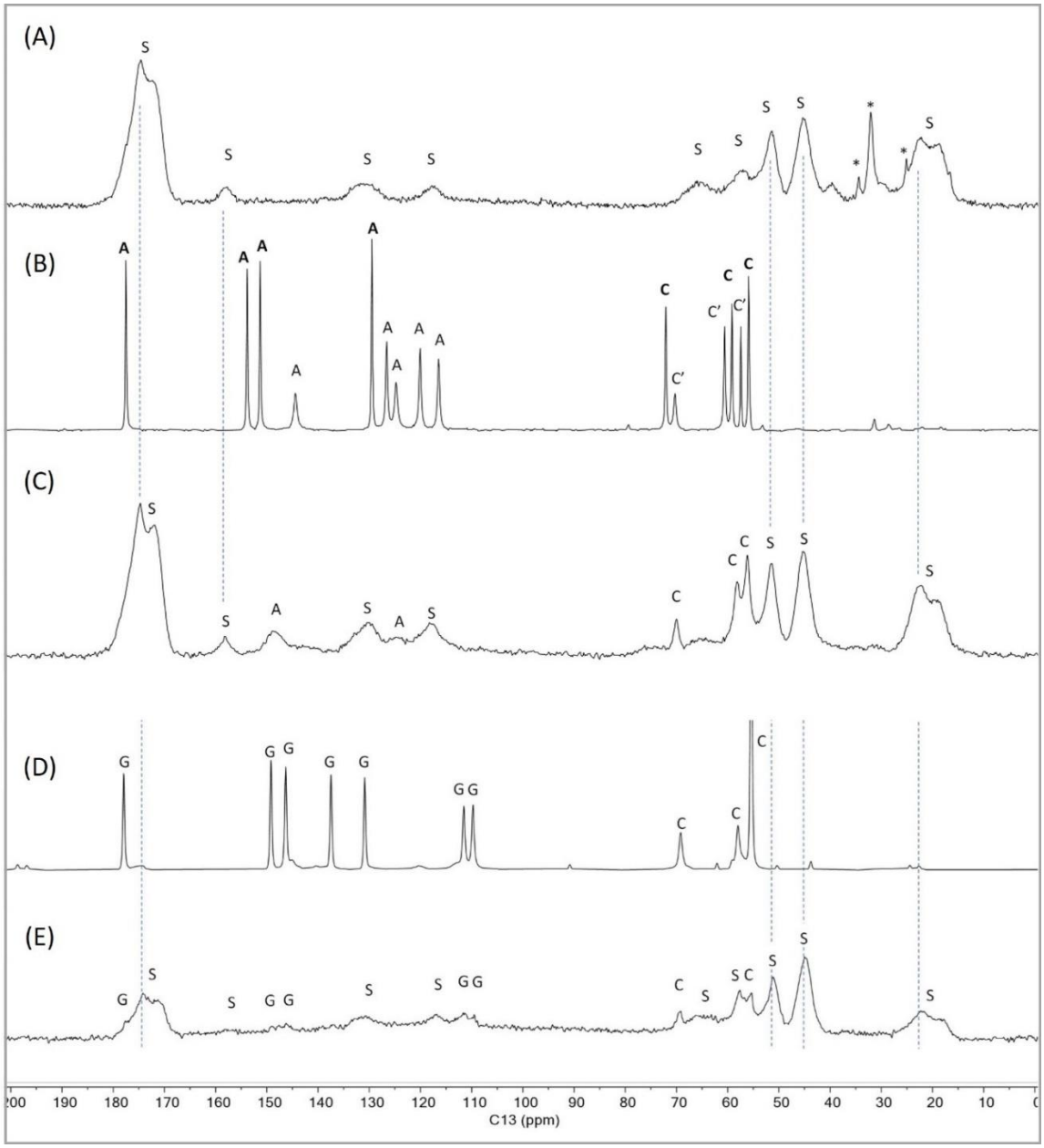


Figure V-1 - ^{13}C-CPMAS spectra of solid sponges (A) SS, (B) Ch[Caffeate], (C) SCC. (D) Ch[Gallate] and (E) SCG. The letters used for the assignment of the components are choline (C), caffeate (A), gallate (G), and silk sponge protein (S). The asterisks in a) denote the presence of some impurities. In b) the signals C' correspond to a minoritarian specie of choline. Vertical striped lines are drawn to guide the eye for certain signals of the protein S that are discussed in the text.

V-4.1.1. Mechanical properties

The ability of a construct to mimic the mechanical properties of the healthy cartilage is critical to the treatment success. Despite the porous and interconnected structure of the SS, SCG, and SCC sponges, it is expected that their mechanical properties can provide adequate physico-chemical support during tissue development [26].

The uniaxial mechanical properties under compression load of the SS, SCG, and SCC sponges were evaluated by measuring the elastic modulus and yield strength, aiming to assess the effect of adding Ch[Gallate] or Ch[Caffeate] to the sponges (Figure V-2A-B). Moreover, the immediate recovery of the sponges after reaching 50% of strain was also determined (Figure V-2C). Figure 2A shows that the elastic modulus values for SS are around 88 kPa, while the values for SCG and SCC are in the range of 1278 kPa and 1217 kPa, respectively. A similar trend was previously observed in other studies, where the cholinium-based Bio-ILs (Ch[ILs]) integration on the structure increased sponge stiffness by the obtained an increase of the compressive modulus when compared to the unloaded sponge (SS) [26]. The stress-strain curves of the SS/Bio-IL-based sponges (Figure V-2D) confirm that SS has a softer behavior when compared to the SCG and SCC sponges. When compared to the SS, the presence of either Ch[Gallate] or Ch[Caffeate] in the sponges increased their yield strength (Figure V-2B). Considering the compressive modulus assessment, for SS was approx. 8 kPa, while for the SCG and SCC sponges this value was approximately 56 kPa and 55 kPa, respectively. This significant reinforcement of the mechanical properties observed for the Bio-ILs loaded sponges, when compared to the SS, may be due to the cholinium cation's moiety hydrogen bonding capability. The available acceptor and donor sites in the cholinium structure are responsible for the interactions established between polymer molecules and Bio-ILs, already confirmed by the NMR analysis (Figure V-1). After the compression test at 50% strain (Figure 2C), there was an expected slight decrease in the recovery, SCG and SCC sponges show an immediate recovery after the test of approximately 64% and 68% of the initial size, respectively, whereas SS recovers approximately 93%. These results suggest that the presence of Bio-ILs in 3D natural polymer matrices has a positive impact on the mechanical properties of the final constructs.

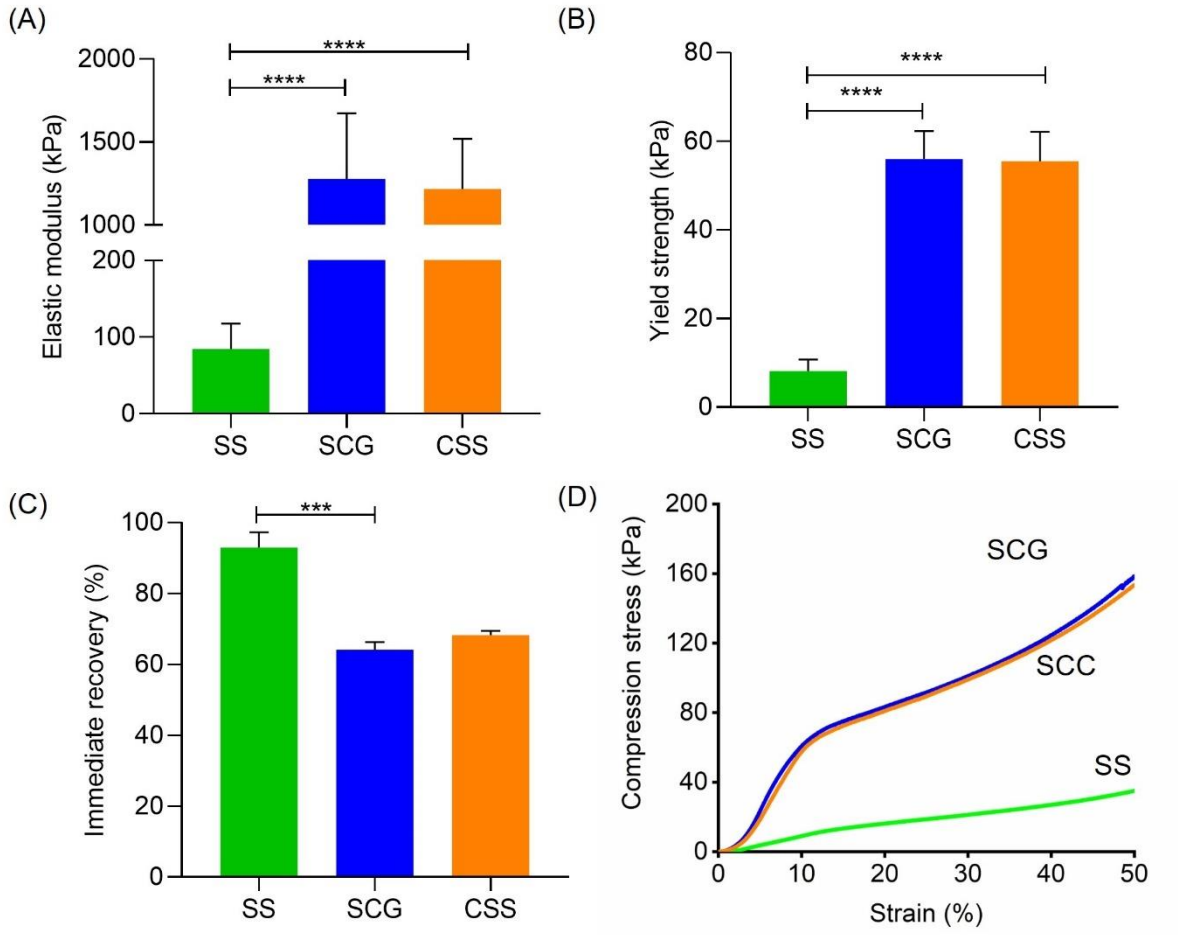


Figure V-2 - Mechanical behavior of the sponge materials under compression load. (A) Compressive modulus; (B) Compressive strength at yield; (C) Immediate recovery of the samples after the compression at 50 % of strain; and (D) Representative compression stress-strain curves. All data represent ± SD (*$p < 0.05$, one-way ANOVA).

V-4.1.2. Evaluation of the antimicrobial properties of the SF/Bio-IL-based sponges

Overcoming the antimicrobial resistance boosted the need to engineer biomaterials with inherent and improved antimicrobial features [19,30,37]. The reduction of infections and bacterial adhesiveness to implantable biomaterials are important issues in orthopedic surgery, including joint surgeries in OA patients [18]. Herein, we evaluated the antibacterial activity of the two designed Bio-ILs, Ch[Gallate] and Ch[Caffeate], against MRSA, E. coli, *S. aureus*, VRSA and *P. aeroginosa* by the radial diffusion assay (Supplementary Figure V-2).. Cholinium hydroxide does not present, by itself, reported antibacterial activity, being a non-toxic and naturally abundant derivative of choline [38]. Nonetheless, numerous studies have demonstrated the antibacterial potential of gallic and caffeic acids [39,40], suggesting the inclusion of this action through the gallate and caffeate moieties. Bio-ILs, Ch[Gallate], and Ch[Caffeate]

demonstrated high bacterial activity against all tested bacteria at concentrations of 1% (w/v) and 3% (w/v) (Supplementary Figure V-2), confirming that even after the neutralization reaction with cholinium hydroxide for the respective Bio-ILs synthesis, the antimicrobial activities were maintained. Furthermore, at the same concentration (0.5% (w/v)), Ch[Gallate] had no inhibitory effect against *E. coli* (Supplementary Figure V-2). Thus, results show that Ch[ILs] demonstrates antibacterial activity against Gram – (*E. coli*) and Gram + bacteria (MRSA, *S. aureus*, and VRSA), with no inhibition effects over *P. aeruginosa* (data not shown). Relating this with other reports in the literature [25], it is expected that the antibacterial properties of Ch[ILs] are based on electrostatic interactions between the positively charged Bio-IL and the negatively charged bacterial membranes. According to this, they disrupt the intramembranous region of the bacteria wall, allowing cytoplasmic material leakage and, consequently bacteria death [25].

Given the intrinsic properties of the SF/Bio-IL-based sponges, their antibacterial ability was assessed to evaluate their inhibitory bacterial adhesion and ability to prevent biofilm formation. The results showed that both SCG and SCC-based sponges supported lower bacteria viability than SS sponges, for both of the studied bacteria, after 24h of growth (Figure V-3A-B). Considering *E.coli*, despite the dead bacteria (±23.72%) in SS, there is a significantly higher percentage of bacteria killed for both SCG and SCC (89.59% and 62.44%, respectively). The results for MRSA showed that the percentage of living bacteria in the SS formulation is 65.12%, while all bacteria in the other conditions (SCG and SCC) are dead. Furthermore, biofilm formation was only observed in the SS sponges (Figure V-3C), indicating that the SF/Bio-IL-based sponges significantly reduced bacterial adherence and biofilm formation. According to these observations is possible to infer that the sponges' inhibitory activity is mainly due to the incorporation of Bio-ILs, which is supported by potential inhibitory evidence in disc diffusion assays (Supplementary Figure V-2).

In summary, the antimicrobial activity results revealed that both studied Bio-ILs present a high protective effect against viability and adhesion of bacteria to the sponges' surface, which would be advantageous given that the susceptibility to bacterial infection increases when biomaterials are implanted, preventing biofilm formation [18,41].

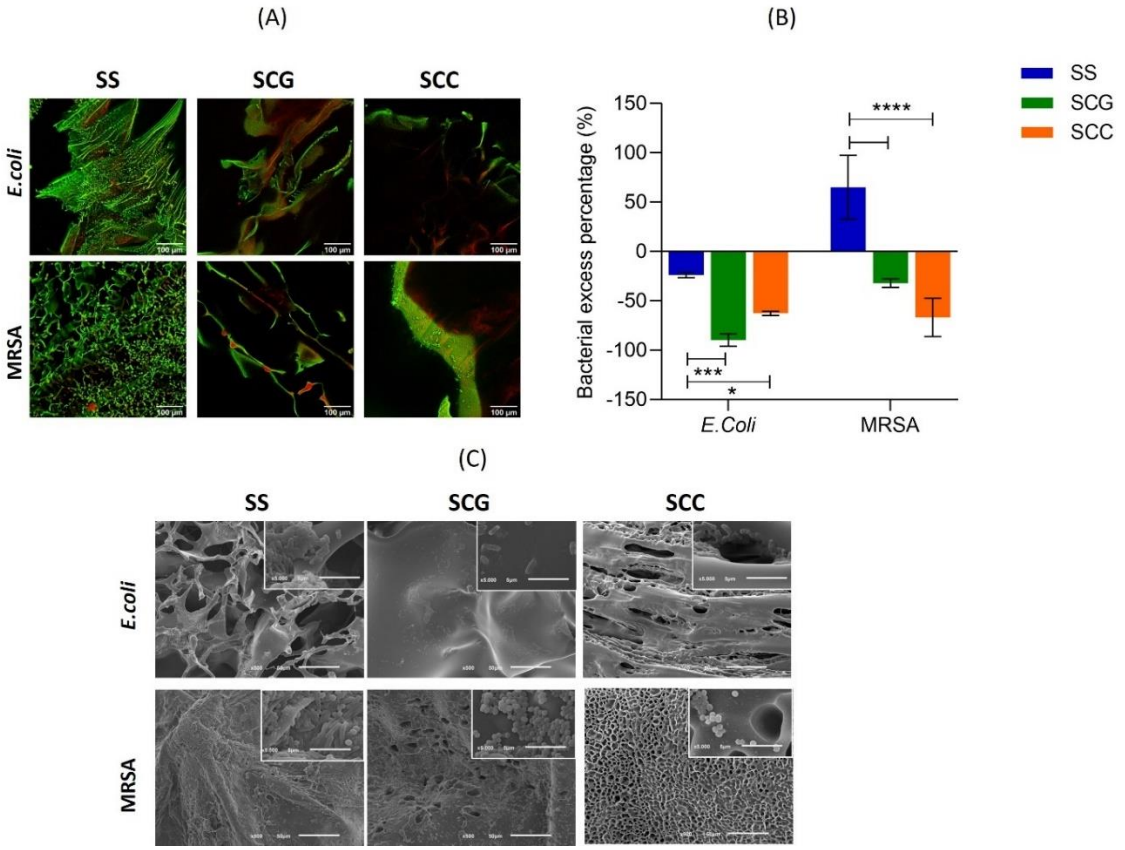


Figure V-3 - (A) Live/dead images, (B) live/dead quantification by excess bacterial percentage, and (C) SEM images of the bacteria fixed on the sponges after 24h of culture. The excess bacterial percentage ranges from -100% to 100%, for only death and live bacteria, respectively.

V-4.2. SF/Bio-IL-based/acetaminophen (ACT) loaded sponges - physico-chemical and *in vitro* assessment of the designed constructs

V-4.2.1. ACT cytotoxic assessment

Acetaminophen (ACT) was included in the SS, SCG, and SCC sponges to provide them analgesic properties, one of the main OA hallmarks, aiming to reduce patients' pain immediately after the sponges' implantation. ACT is a model analgesic drug suggested as a first-line pain treatment in OA [27]. Our preliminary cytotoxicity studies using different ACT concentrations (available in Supplementary Methods 1) indicated that ACT had no cytotoxic effect on the L929 and ATDC5 cell lines at a concentration of 0.01% (w/v) (Supplementary Figure V-1). Similar effect was previously observed on metabolic activity of human chondrocytes at a concentration of 10 g/mL (equivalent to 0.01% (w/v)) [42]. According to this, 0.01%, was the concentration selected to be incorporated in the SF/Bio-IL-based sponges' system.

V-4.2.2. FTIR analysis

FTIR-ATR spectra of the amide I (1700–1600 cm^{-1}) and amide II (1600–1500 cm^{-1}) regions of the sponge-like structures were measured after treatment with metanol:H_2O (80:20) in a saturated atmosphere to investigate the successful β-sheet induction of the SF sponge component [26]. To assess changes in the β-sheet conformation on the sponges, the spectral deconvolution of the amide I and II region was evaluated (Figure 4). After methanol treatment, the β-sheet content in the sponges was 29.87% for SS, 22.31% for SS-A, 28.63% for SCG, 30.48% for SCC, 29.36% for SCG-A, and 30.47% for SCC-A (Figure V-4).

The α-helix/random coil conformations were 7.77% for SS, 13.32% for SS-A, 6.34% for SCG, 9.83% for SCC, 9.73% for SCG-A, and 6.56% for SCC-A. Results show that the incorporation of Ch[Gallate] or Ch[Caffeate] Bio-IL and ACT in the SF sponges do not affect β-sheet conformation ((Figure V-4), indicating that the structural stability and water insolubility of the SF were maintained. These findings are consistent with earlier research reports where adding ILs and/or Bio-ILs to the SF matrices had a favorable impact on the β-sheet conformation content [26,43]. Moreover, these results are in accordance with the ones obtained for the solid-state NMR study, which strongly suggests that the secondary structure elements of SS remain essentially unchanged in the studied samples.

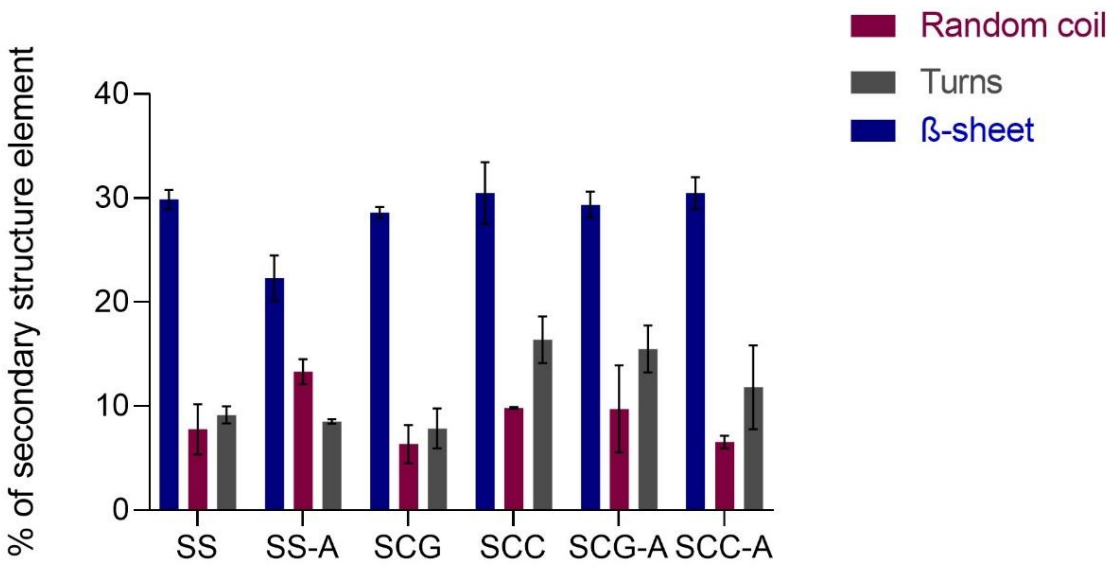


Figure V-4 - Percentage of β-sheet, random coil, and turn conformations after amide I and II spectra deconvolution of SS, SS-A, SCG, SCC, SCG-A, and SCC-A. Data represent ±SD (∗p < 0.05, ordinary 2wayANOVA).

V-4.2.3. Morphology assessment

The morphology of the SS, SS-A, SS/Bio-IL, and SS/Bio-IL/ACT-based sponges was evaluated by SEM (Figure V-5). All SF-based sponge formulations produced using the freeze-drying technique revealed a porous and interconnected structure (Figure V-5). The pore size values ranged from 100 to 122 μm, with no statistically significant differences among the samples. Furthermore, the use of Ch[Gallate] and Ch[Caffeate] at 1% (w/v) and ACT at 0.01% (w/v) concentrations in the sponge's formulations did not affect the sponge's structure.

Besides, the pore size of freeze-dried SF sponges appears to be strongly influenced by the SF solution concentration. According to the literature, the LiBr dissolution method and freeze-drying are widely used to create SF sponges, and an SF solution with 8% (w/v) yielded sponges with pore sizes of 87.1 ± 25.2 μm [44]. These smaller pore sizes obtained compared to the achieved in the present study (100 and 122 μm), maybe be due to the higher concentration (8% (w/v)) of the SF solution used for scaffold production compared to the one used in the current work (3% (w/v)). This hypothesis is in line with other reported data, where scaffolds made from 2% (w/v) SF solutions also showed higher pore sizes, being 150 ± 20 μm [45]. Thus, SF solution concentration can be used to tune sponges' porosity.

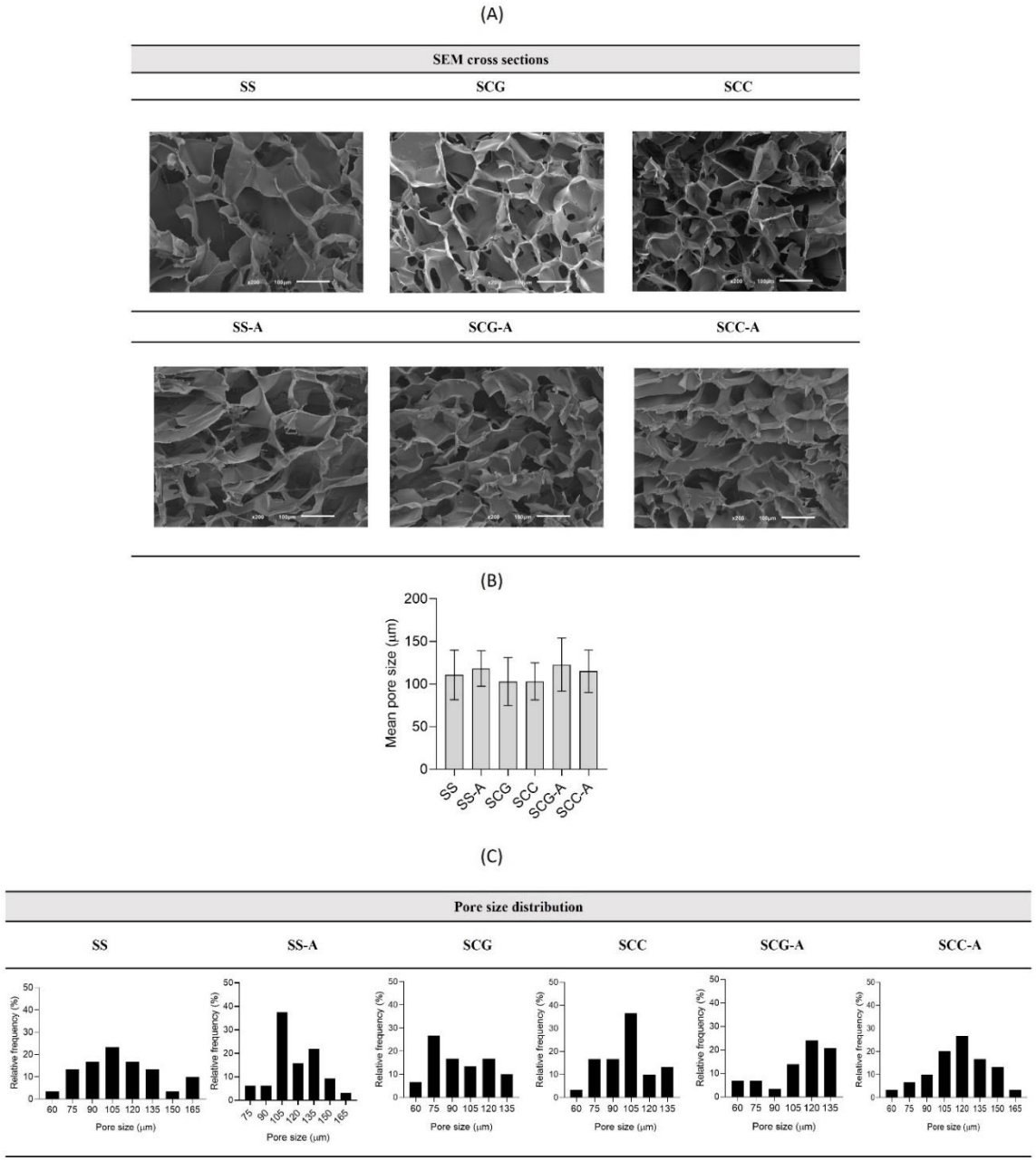


Figure V-5 - (A) SEM cross-sectional images of the developed sponges; (B) Mean pore sizes and (C) distribution.

V-4.2.4. Water uptake, stability, and bioactive compounds release

The ability of an implantable construct to absorb and retain water in its structure is critical to its success in tissue regeneration. Moreover, the passage of nutrients, metabolites, and body fluids through the biomaterial is directly related to its water absorption capacity [44]. In the cartilaginous tissue, in which water accounts for 70%-85% of its total weight, the ability to retain water is important since it allows interaction among all cartilage components and gives strength to resist all mechanical forces and stress

[46]. Considering these factors, water absorption experiments were carried out to determine the liquid absorption capacity of the SF/Bio-IL/ACT sponges. Figure V-6A shows the results of the swelling ability of sponges after immersion in PBS, for up to 7 days. All formulations showed similar swelling behavior, and water uptake was immediately stabilized after 1 hour of immersion. Despite only exhibiting significant statistical differences after 4h, 1d, and 3d with SCG, and after 7d with SCG, SCG-A, SCC, and SCC-A, the SS formulation has significantly higher water uptake % values than the others studied formulations, suggesting that the incorporation of the Bio-ILs in the sponge induces a reduction on its hydrophilic character. This is in line with previous data that indicated that SF sponges have higher water uptake values than formulations containing SF and other polymers and/or Bio-ILs [26,47].

The maximum water uptake values achieved are 1947%, 1597%, 969%, 1735%, 1403%, and 1810% for SS, SS-A, SCG, SCG-A, SCC, and SCC ACT, respectively. This profile suggests that Bio-ILs incorporation into the system lead to a reduction on the hydrophilic nature of the system that is again increased through the incorporation of ACT. The observed non-significant differences in pore sizes obtained across all studied conditions (Figure V-5), allowed us to hypothesize that the observed tendency for higher water uptake for SS is mainly modulated through the incorporation of the Bio-ILs presence and not, as earlier reported, from the ability of the water to cross through the pores [45].

The stability profile of the SF/Bio-IL/ACT-based sponges is shown in Figure V-6B. When immersed in PBS, the SS formulation exhibits non-significant weight loss values (up to 8%), similarly to those previously reported [26,44,45]. Likewise, SS-A, showed a maximum weight loss of 9%, which results from the low amount of ACT loaded in the sponge, that did not significantly affect its weight loss. Maximum weight loss values of 26%, 31%, 45%, and 36% were observed for SCG, SCC, SCG-A and SCC-A, respectively. These findings reveal a simultaneous release of ACT and the Bio-IL from the SF matrices, as the studied Bio-ILs are soluble in PBS. Our NMR results (Figure V-1) suggested that the Bio-ILs were physically entrapped and not covalently bonded to the SF network backbone, favoring its release to the media. The same trend was already reported in other published studies [48], being the release of the entrapped Bio-ILs from the polymeric matrices considered the primary contributor to the observed biomaterials' weight loss. Then, the incorporation of the Bio-ILs into the polymeric matrices can be used to tune their structural stability, which would regulate their degradation according to the targeted tissue.

Considering this, the cumulative release of the analgesic drug, ACT, as well as the bioactive Bio-ILs, Ch[Gallate] or Ch[Caffeate], from the SF/Bio-ILs/ACT-based sponges, was studied by immersing the sponges in PBS, for up to 7 days (Figure V-6C-E). The ACT release profile from the sponges (Figure V-6C)

indicated a continuous release of the ACT in all formulations during the first 4 hours of the study. Therefore, the immediate release of ACT in small doses may be effective in relieving initial pain, concerning OA treatment.

Although no specific binding is proved between the SF structure and the anion counterpart of the used Bio-ILs (Figure 1), Ch[Caffeate] cumulative % release from the sponges is significantly lower than the observed for Ch[Gallate] (Figure V-6D and Figure V-6E). Both Bio-ILs, Ch[Gallate] and Ch[Caffeate] are water soluble [45], but in our study, the sponges SCG and SCG-A have maximum Ch[Gallate] release values of 54% and 45%, respectively, when the sponges SCC and SCC-A showed maximum Ch[Caffeate] release values of 9% and 18%, respectively. These differences in the release profile could be due to the longer anion structure of the Ch[Caffeate] that can lead to a stronger entrapment in the SS sponge. This behavior can also be related to lower charge distribution on the anion counterpart, able to potentiate a higher electrostatic interaction between anion and the SS polymeric backbone donor sites, making more difficult for Ch[Caffeate] to release from the sponge.

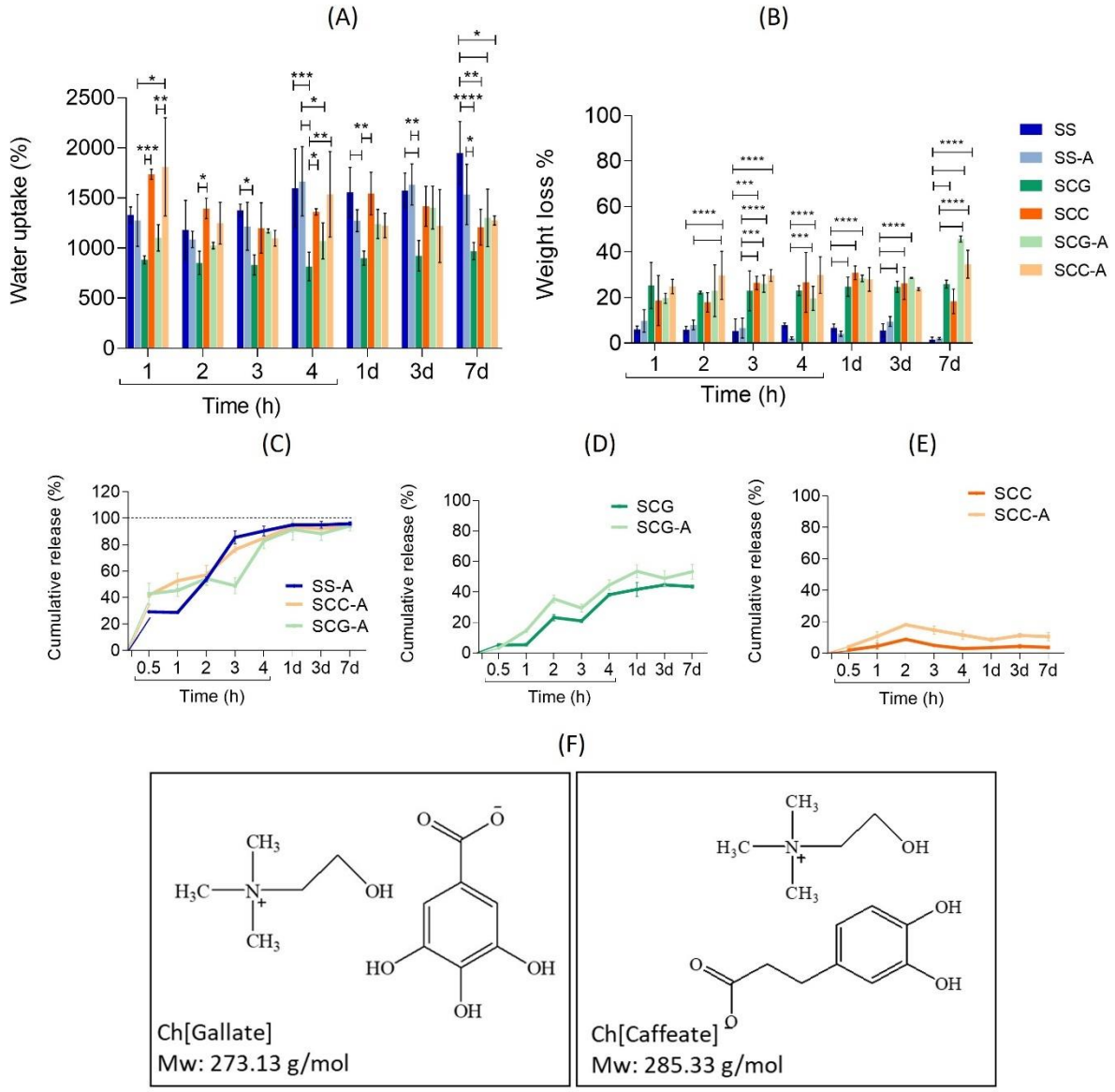


Figure V-6 - Water uptake (A) and weight loss (B) of the SS, SS-A, SCG, SCG-A, and SCC-A sponges in PBS. Data represent ±SD (*p < 0.05, 2way ANOVA). (C) Cumulative percentage release of ACT from SS-A, SCG-A, and SCC-A into PBS, up to 7 days; (D) cumulative percentage release of Ch[Gallate] from SCG and SCG-A into PBS, up to 7 days, and (E) cumulative percentage release of Ch[Caffeate] from SCC and SCCAC into PBS, up to 7 days.

V-4.2.5. Antioxidant activity

It is well-known that the increase in oxidative stress can be harmful to chondrocytes, promoting the senescence and apoptosis of these cells [49,50]. Reactive oxygen species (ROS) are involved in the pathology of OA, meaning that compounds that can lower ROS levels may hold potential for OA treatment by managing ROS levels [27]. With this in mind, the antioxidant activity of the developed sponges was evaluated by the DPPH method [31].

As expected, the sponges with SS and SS-A show very low antioxidant activity up to 24h when compared to the other formulations containing Bio-ILs (Figure V-7A). After 1h, sponges with SCG or SCC presented very similar antioxidant activity, 93.09% and 86.73%, respectively (Figure V-7A). The same tendency was observed in the other formulations, SCG-A and SCC-A. However, SCC sponges presented higher antioxidant activity up to 24h of reaction (Figure V-7B), which may be related to the amount of Bio-IL that remains in the architecture along time due to higher retention observed. For most of the formulations is possible to note that the antioxidant activity of the sponges diminished after 24h (Figure V-7B), keeping mean values of 27.56 ± 1.77 %, 75.83 ± 2.22 %, 93.86 ± 0.70 %, 80.54 ± 1.46 % and 85.38 ± 2.03 % for SS-A, SCG, SCC, SCG-A, and SCC-A respectively.

The presence of the substituent at the position relative to the hydroxyl group in the ACT phenolic structure, allows the compound to react with ROS, acting as a scavenger for these molecules [51]. Considering the increase of antioxidant activity observed in the samples containing ACT, its antioxidant potential was also evaluated (Figure V-7B). Freestanding ACT solutions were evaluated, and the results show that ACT, at a concentration of 0.01 % (w/v), has a maximum activity of 75.81% after 4h, diminishing to 60.88% after 24h (Figure V-7B). At a higher concentration (between 0.25% and 1% (w/v)), ACT antioxidant activity does not significantly vary along time (after 1h, 4h, and 24h) (Figure V-7B). These results suggest that ACT also plays an active role on the antioxidant activity of the structures, improving its performance through a synergistic action of ACT and Bio-ILs (Ch[Gallate] or Ch[Caffeate]) that lead to a more stable antioxidant performance along time.

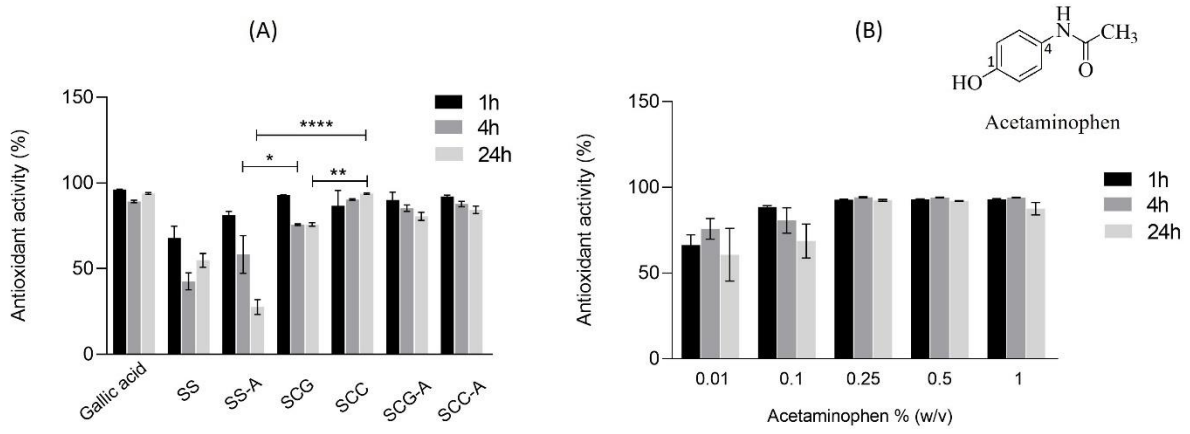


Figure V-7 - Antioxidant activity of the sponges formulations by DPPH method (A). Gallic acid at 1 % (w/v) was used as control. SS, SS-A, SCG, SCC, SCG-A, and SCC-A sponges in a solution of DPPH in metanol, up to 24h. Antioxidant activity of free ACT at different concentrations (B). Data represented as mean±SD (*p < 0.05, nonparametric Krustal-Wallis test).

V-4.3. *In vitro* studies

V-4.4. Assessment of the anti-inflammatory potential of the developed sponges

OA is characterized by an imbalance of pro- and anti-inflammatory cytokines, with proinflammatory cytokines commonly upregulated and anti-inflammatory cytokines downregulated. As a result, detecting and quantifying those cytokines can be an effective method for validating OA models or for diagnosing OA [52,53]. Proinflammatory cytokines like tumor necrosis factor (TNF- α) and interleukin-6 (IL-6) can be used as tools to induce OA and cartilage damage, allowing the replication of the disease and contributing to the inflammatory effect of the synovium in the OA model [52,54,55].

To assess the anti-inflammatory potential of the developed sponges, the proinflammatory cytokines TNF-α and IL-6 were measured in the supernatants of differentiated and LPS-stimulated THP-1 cells seeded in the sponges for up to 7 days in culture (Figure V-8). The anti-inflammatory interleukin-10 (IL-10) was also quantified in the supernatants of differentiated and LPS-stimulated THP-1 cells seeded in the sponges for up to 7 days. IL-10 is one of the main anti-inflammatory cytokines involved in OA pathogenesis, inhibiting HC apoptosis and decreasing the proinflammatory TNF-α and IL-6 [56,57]. Also, betamethasone was used as a control, since it is one of the strongest and most used corticosteroids for OA treatment [12]. The differentiation of THP-1 monocytes to macrophages was accessed by observing the transition from a suspension cell phenotype to an attached cell phenotype [26]. LPS induces the production of proinflammatory cytokines in THP-1 cells, including TNF-α and IL-6 [58,59].

Figure 8 shows that on LPS-stimulated cells and in contact with sponges SS and SS-A it produced significantly more TNF-α and IL-6 than other cytokines throughout the culture, indicating that the cells were successfully stimulated. TNF-α concentrations were lower in SCG, SCC, SCG-A, and SCC-A compared to LPS-stimulated cells, SS, SS-A, and the ACT-free form (Figure V-8A). Given the vestigial anti-inflammatory ACT properties[60], this effect could be mainly attributed to the presence of Ch[Gallate] and Ch[Caffeate]. Statistically significant differences were not observed in the production of TNF-α and IL-6 in the presence of SCG, SCC, SCG-A, and SCC-A sponges, which confirms the negligible contribution of ACT for the anti-inflammatory behaviour of the structures. Compared to the betamethasone results, the sponges containing Bio-ILs show comparable results, indicating a blockage in TNF-α secretion immediately after 1 day of culture (Figure V-8A). The same trend was observed when in culture for up to 7 days, with SCG, SCC, SCG-A, and SCC-A sponges exhibiting lower TNF- α values than the control,

betamethasone. We hypothesized that the sustained and prolonged Bio-ILs release demonstrated by matrices (Figure V-6C - D) might be responsible for this effect. The pro-inflammatory cytokine IL-6 showed a similar pattern (Figure V-8B). When compared to LPS-activated macrophages, SS and SS-A sponges, and free ACT, it is noticeable that the SCG, SCC, SCG-A, and SCC-A sponges inhibited the release of the anti-inflammatory cytokine IL-6. A similar trend was observed for the control drug, betamethasone. The results presented herein for the quantification of proinflammatory cytokines are consistent with previously published data, where biomaterials containing Ch[ILs] in their matrices showed an inhibitory effect on the release of a pro-inflammatory cytokine from THP-1 activated macrophages [26]. Other studies reported effective treatment of pathologies such as rheumatoid arthritis using the same cell line, drugs, and other bioactive molecule entrapment, such as betamethasone and anti-TNF- α antibodies [42,61].

The SCG, SCC, SCG-A, and SCC-A sponges had increased levels of IL-10 secretion compared to SS and SS-A sponges, and free ACT (Figure V-8C). After 3 and 7 days, IL-10 secretion by LPS-activated macrophages is higher than expected. This can be explained by an attempt to balance pro- and anti-inflammatory factors by increasing IL-10 secretion when proinflammatory factors are overexpressed [62]. The mechanism has previously been described as an attempt to control excessive inflammation while limiting tissue damage caused by proinflammatory cytokines [56,62,63].

High levels of TNF-α release in cartilage stimulate the production of MMPs from synovial fibroblasts, leading to cartilage tissue destruction and chondrogenesis inhibition via the nuclear factor-kB (NF-kB) pathway by downregulating SOX9 [64]. The disruption of the catabolism and anabolism processes in OA results in the development of a disease process that includes inflammation, tissue degradation, and continuous production of inflammatory factors, leading to a gradual loss of joint function and pain. In the present study, results indicated that SCG and SCC sponges block the secretion of anti-inflammatory cytokines and can be used as strategies for OA management. Although there are no significant differences between SCG and SCC sponges, as well as SCG-A and SCC-A sponges, we anticipate that the rapid and local release of ACT from the matrices (Figure V-6C) can result in effective and immediate pain relief, without compromising the anti-inflammatory action of the system. We have also shown that Ch[Caffeate] has a similar effect to Ch[Gallate] in terms of blocking proinflammatory cytokines.

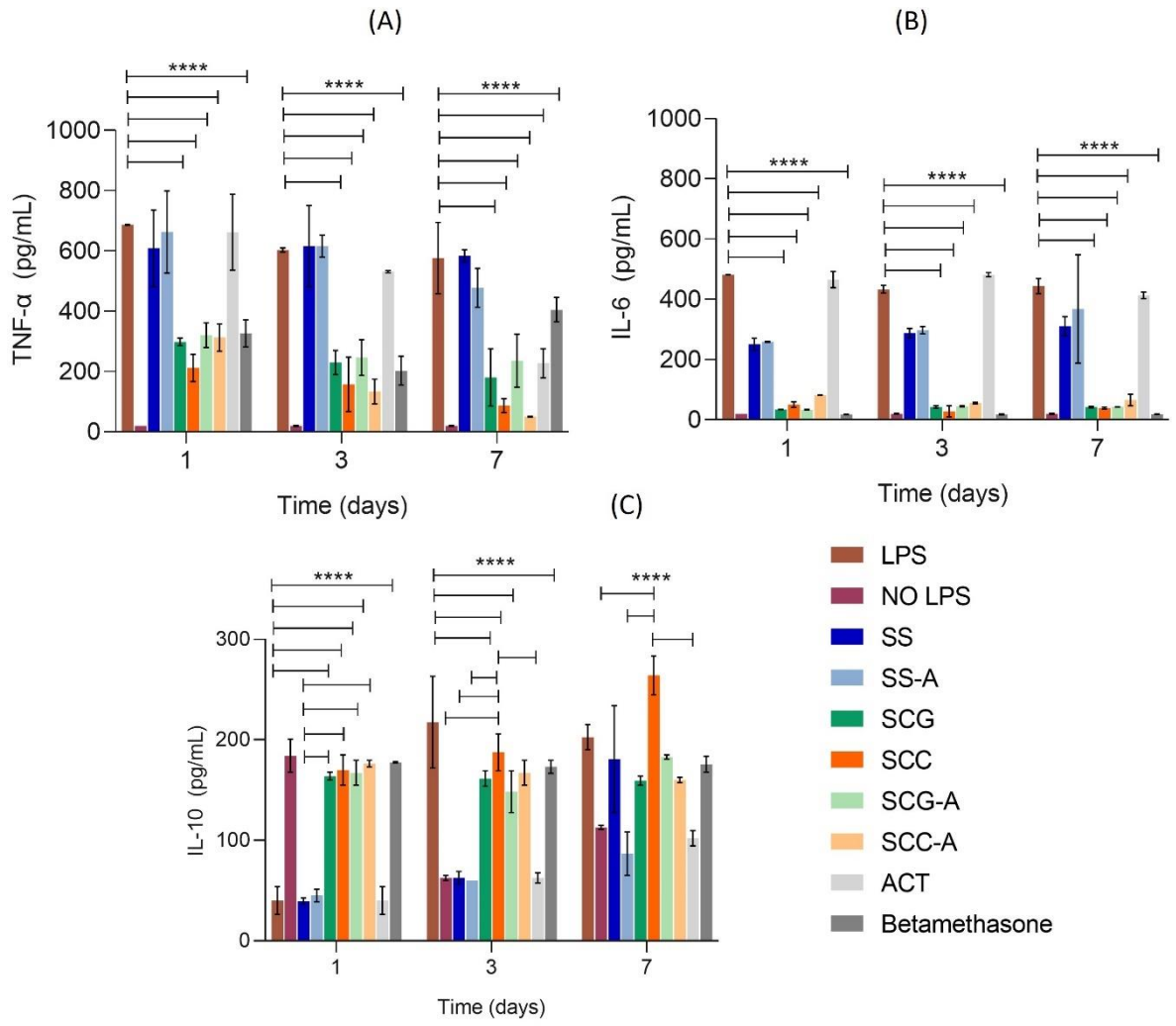


Figure V-8 - Cytokines quantification: (A) TNF-α, (B) IL-6, and (C) IL-10 amounts in the different conditions. Data represented as mean ±SD (*p < 0.05, nonparametric Krustal-wallis test).

V-4.4.1. Protective effect against ROS

The detrimental effect of ROS overproduction in chondrocytes in osteoarthritic scenarios is clear [65]. The antioxidant activity of the produced sponges was confirmed (Figure V-9). Preliminary toxicity tests were carried out (Figure V-9A), confirming the sponges' good biocompatibility profile toward HC growth. Previous studies have also reported the good biocompatibility of Ch[Gallate] and Ch[Caffeate] over primary human adipose stem cells, the macrophage cell line Raw 264.7, and the keratinocytes cell line HaCaT [15,26].

To induce ROS overproduction, two different concentrations of hydrogen peroxide (H_2O_2) were tested, 500μM and 100 μM, based on previously reported studies [66,67] (Figure V-9B). At a concentration of

500µM H_2O_2, it is possible to observe that cells in contact with the lixiviate of the SCG, SCC, SCG-A, and SCC-A sponges presented higher relative metabolic activity values, which may be mostly a consequence of the protective effect of the Bio-ILs over HC throughout the ROS scavenging effect [51]. Similar results were obtained by Lee et al. [51], when treating HC, stimulated 500 µM of H_2O_2, with delphinidin. The metabolic activity of the cells following the 100 µM treatment was not affected. Based on these results, the concentration of 100 µM H_2O_2 was chosen for the intracellular ROS quantification assay, since all samples present similar behavior to the control (SS), allowing for a better study of the scavenging effect by still generating ROS (Figure V-9C). We observed that the intracellular oxidative stress in HC cells treated with SS-A, SCG, SCC, SCG-A, and SCC-A was significantly decreased compared to SS alone. Despite the weaker antioxidant activity of SF, it can be described as a suitable carrier of antioxidants [68], which, in this case, are the Bio-ILs. Additionally, there is a tendency for decreased fluorescence intensity values in samples containing both Bio-IL (SCC and SCG) sponges and ACT (SCG-A and SCC-A) sponges, demonstrating that these samples can effectively reduce ROS levels.

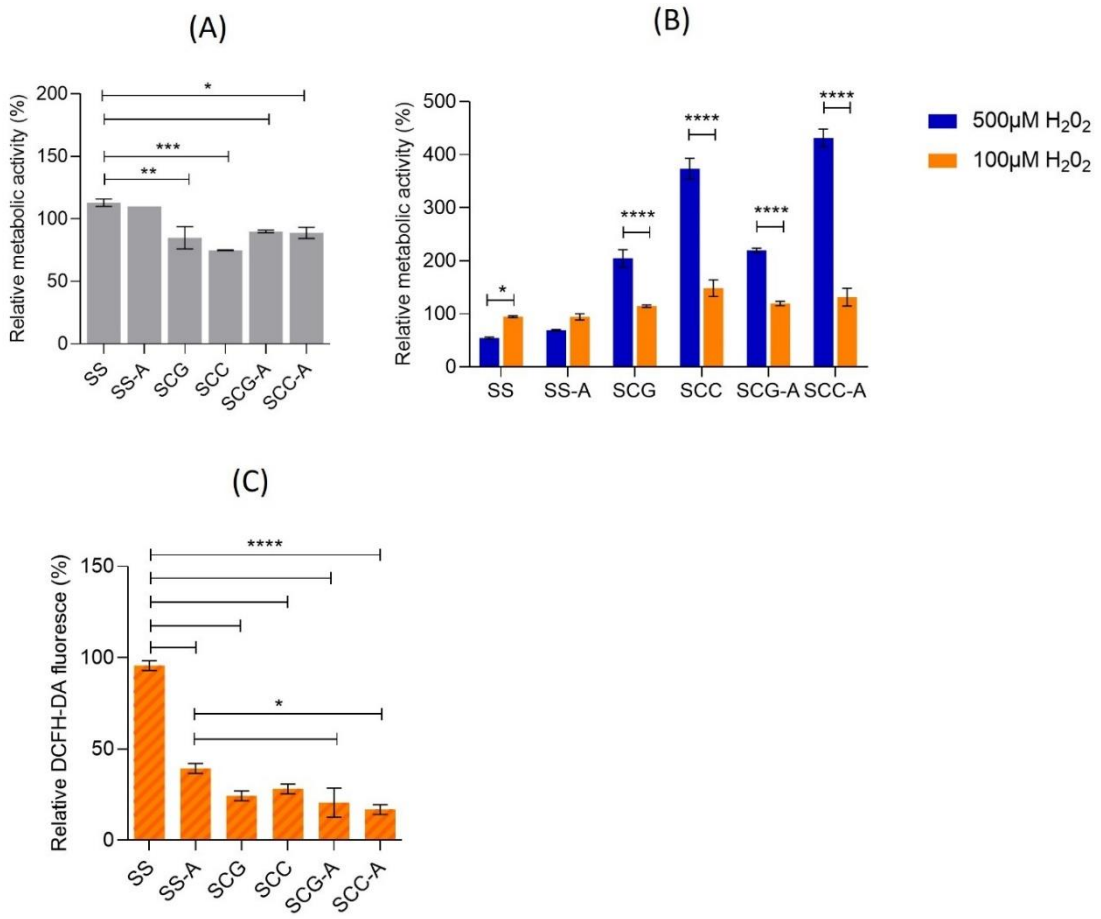


Figure V-9 - Cytocompatibility and antioxidant effect of SS, SS-A, SCG, SCC, SCG-A and SCC-A over HC stimulated with H_2O_2. (A) Cytocompatibility of the HC in DMEM-F12 and (B) cell protective effect of the SS, SS-A, SCG, SCC, SCG-A, and SCC-A

sponges after different H_2O_2 concentrations for 3h. (C) Quantification of intracellular ROS level measured by the relative fluorescence intensity of DCFH-DA after H_2O_2 stimulus at 100 µM. Data represent ±SD (*$p < 0.05$, 2way ANOVA).

V-4.4.2. HC viability and proliferation seeded on the SF/Ch[Gallate]/ACT-based sponges

Our findings so far indicated that the SCG, SCC, SCG-A, and SCC-A may have the potential for OA treatment. Previous studies reported the successful use of SF-based biomaterials for primary chondrocyte culture to develop cartilage tissue engineering solutions [69,70]. However, to our knowledge, none of them used Bio-ILs. The Ch[Gallate]-based samples were selected as a model, as according to the previous characterization, no significant differences were found in the physico-chemical and biological performances achieved between the two used Bio-ILs-based materials. For that, chondrogenic primary cells (HC) and osteoarthritic human chondrocytes (HC-OA) were seeded on the SS, SCG, and SCG-A sponges for up to 21 days. Further, cell viability, proliferation, and gene expression were evaluated.

According to the findings (Figure IV-10A-B), the cell metabolic and proliferation increased over the culture time on all conditions, with the live and dead assay results supporting it (Figure IV-10C). These results suggest that the intrinsic features of the developed architectures (SS, SCG, and SCG-A) could sustain cell growth by the adhesion of the cells to the scaffold surfaces. Furthermore, the confocal laser micrographs of the HC cells after 21days of culture, confirmed the HC cell attachment and spreading on the sponges' surface and the formation of actin stress fibers (Figure IV-10D), which are often correlated with strong cell adhesion to the substrate [71]. Overall, the developed constructs may be valuable therapeutic tools for studying OA treatment.

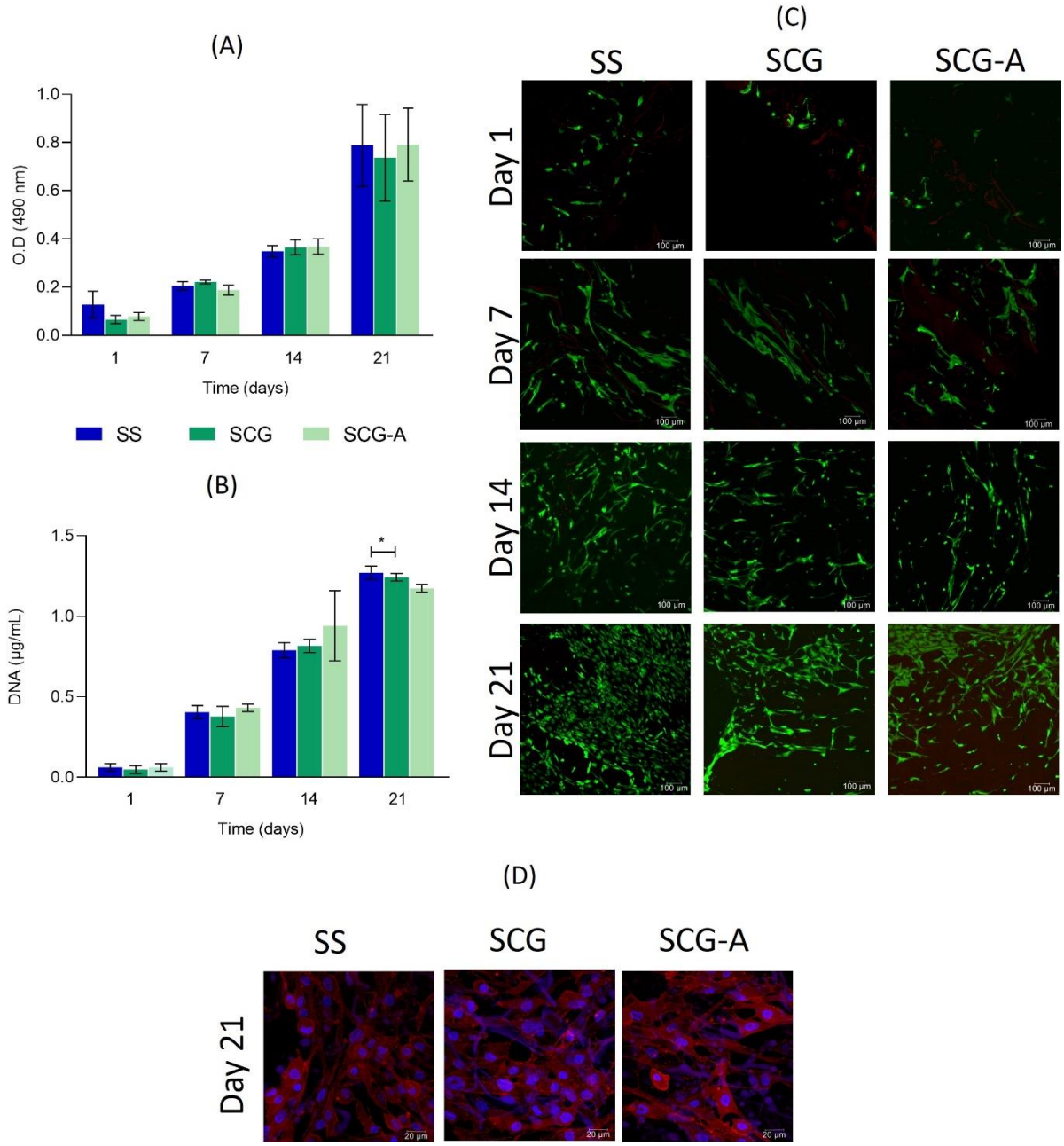


Figure V-10 - (A) Metabolic activity, (B) and DNA content, (C) Microscope projection image of the live/dead assay of HC seeded in the SS, SCG, and SCG-A sponges, up to 21 days. (D) confocal laser scanning micrographs of HC cultured on sponge structures after 14 and 21 days. The cells cytoskeleton was stained with rhodamine-phalloidin (red), and nuclei were counterstained with DAPI (blue). Scale bar: 20 µm.

V-4.4.3. Therapeutic effect of the constructs over HC-OA

Cartilage and bone deterioration are both connected with OA development and cause articular chondrocytes to release inflammatory mediators, hence preventing collagen type II deposition, which is one of the cartilage's main components [72]. In this sense, the gene response of proinflammatory cytokines TNF-α and IL-6 in healthy (HC) (Figure V-11A) and osteoarthritic chondrocytes (HC-OA) (Figure V-11B) seeded in the sponges was assessed. The results revealed that HC expresses basal levels of both TNF-α and IL-6 compared to the HC-OA seeded in the SS sponges (Figure V-11A). These findings are in accordance with prior research that found higher expression of proinflammatory proteins in human OA joint cartilage, compared to normal and healthy tissue [73]. The HC-OA cells seeded in SCG and SCG-A sponges present lower expression of TNF-α and IL-6, compared to SS, with statistical significance and similar to the ones obtained for the healthy HC. These results suggest that there is downregulation in the expression of genes encoding for proinflammatory mediators, which are stimulators of the inflammatory and degradative cascades in OA [74,75]. Some pharmaceutical therapies for OA include the use of selective cyclooxygenase (COX)-2 inhibitors because levels of IL-6 and TNF-α increase together with COX-2 in OA situations exposing the cartilage to chronic inflammatory conditions [13,74]. A similar trend was observed in our study. COX-2 expression is significantly reduced in HC-OA seeded in SCG and SCG-A sponges, compared with SS sponges. Furthermore, the levels of inducible nitric oxide synthase (iNOS) were increased in SS sponges in both cell types but are downregulated in the SCG and SCG-A sponges (Figure V-11A-B). A similar result has been described in another study using SS sponges [76]. According to our findings, Ch[Gallate] and ACT decrease the production and release of related proinflammatory cytokines, including IL6 and TNF-α, hence modulating inflammatory immunity. Moreover, lowering iNOS2 expression would result in less NO release by chondrocytes, which would theoretically postpone joint deterioration [75,76]. Some anabolic factors, including TGF-β are secreted by chondrocytes and can stimulate the synthesis of extracellular matrix, therefore cartilage repair [74,75]. In that sense, the increase in the TGF-β, observed for SCG and SCG-A sponges (Figure V-11B), would protect cartilage from chronic inflammatory conditions [74]. Following the TGF-β effect on the extracellular matrix, we have evaluated the expression of collagen type II (COL2A1). COL2A1 represents the most abundant collagen in the cartilage matrix [76]. After 21 days, the expression of COL2A1 is up-regulated in the HC-OA seeded in the SCG and SCG-A sponges, despite non-significant statistical differences observed (Figure V-11C).

Moreover, the upregulation of COL2A1 genes, strongly indicates that HC were kept in a matrix-producing phenotype, when seeded in the sponges for up to 21 days, as previously described [76].

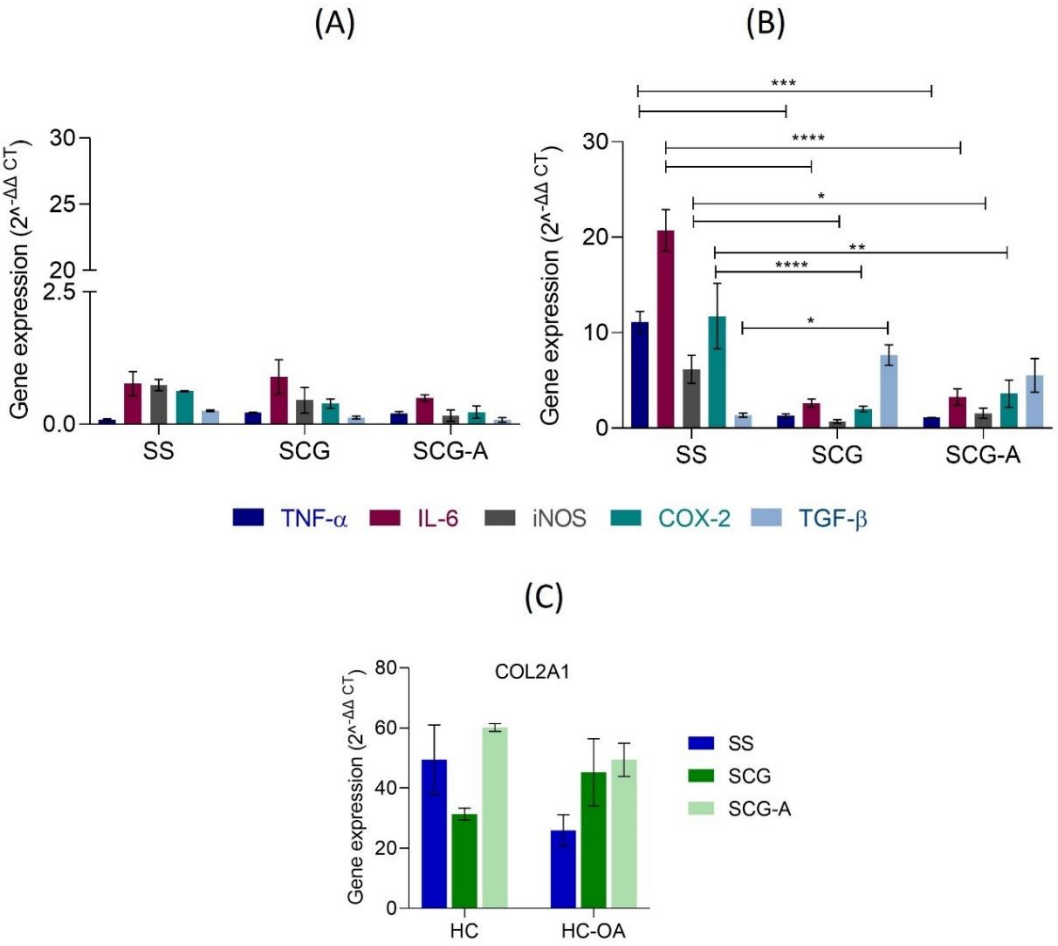


Figure V-11 - Gene expression of TNF-α, IL-6, iNOS, COX-2 and TGF-β of (A) HCs and (B) HC-OA seeded into SS, SCG and SCG-A after 24h of culture; and (C) COL2A1 expression of HCs and HCs-OA seeded into SS, SCG and SCG-A after 21 days of culture. Data represented as mean ±SEM (*p < 0.05, 2way ANOVA).

V-5. CONCLUSIONS

In the present work, a tissue engineering strategy comprising natural biomacromolecules including SF, the phenolic-based Bio-ILs, Ch[Gallate] and Ch[Caffeate], and the analgesic drug ACT was developed. The biomaterials created exhibit reinforced stiffness and adequate functional properties, including antibacterial activity against therapeutically relevant bacteria and anti-inflammatory properties, as demonstrated by the inhibition of pro-inflammatory cytokine release from THP-1-derived macrophages. In

addition, the constructs exhibited potent antioxidant activity, which significantly alleviated oxidative stress. Beyond that, the sponges have the potential to enable cartilaginous tissue regeneration, as evidenced by their capacity to increase the primary human chondrocyte growth and proliferation for up to 21 days. Furthermore, after 21 days of culture, the gene expression data indicates that SCG and SCG-A sponges efficiently protect cartilage from chronic inflammatory conditions by downregulating proinflammatory TNF-α and IL-6, iNOS, and COX-2, as well as upregulating TGF-β and overexpression of COL2A1. Our study provides new insights into the use of 3D architectures based on Bio-ILs combined with biopolymers as potential therapeutic solutions for cartilaginous tissue regeneration, further expanding the present knowledge in future OA therapies.

Acknowledgements

The authors especially acknowledge financial support from Portuguese FCT (PD/BD/135247/2017,CEECIND/01306/2018, SFRH/BPD/93697/2013, SFRH/BPD/85790/2012, SFRH/BPD/100760/2014 and 2021.07421.BD). In addition, this work is financially supported by PhD Programme in Advanced Therapies for Health (PATH) (PD/00169/2013), FCT R&D&I projects with references PTDC/BII-BIO/31570/2017, and R&D&I Structured Projects with reference NORTE-01-0145-FEDER-02219015.

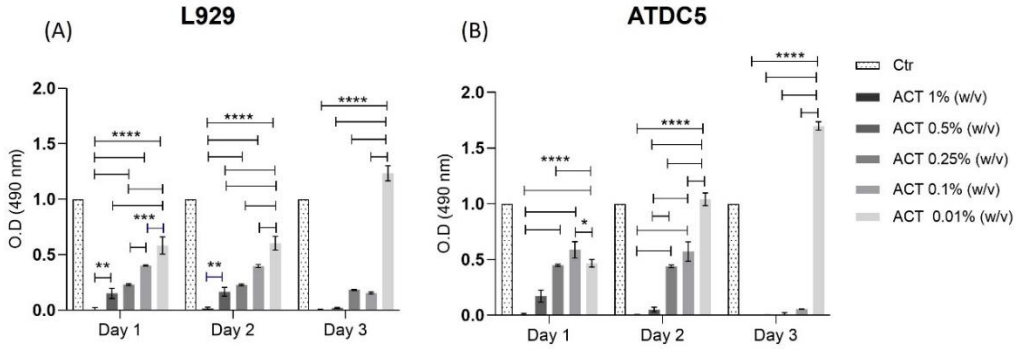
V-6. SUPPLEMENTARY MATERIAL

V-6.1. Supplementary methods

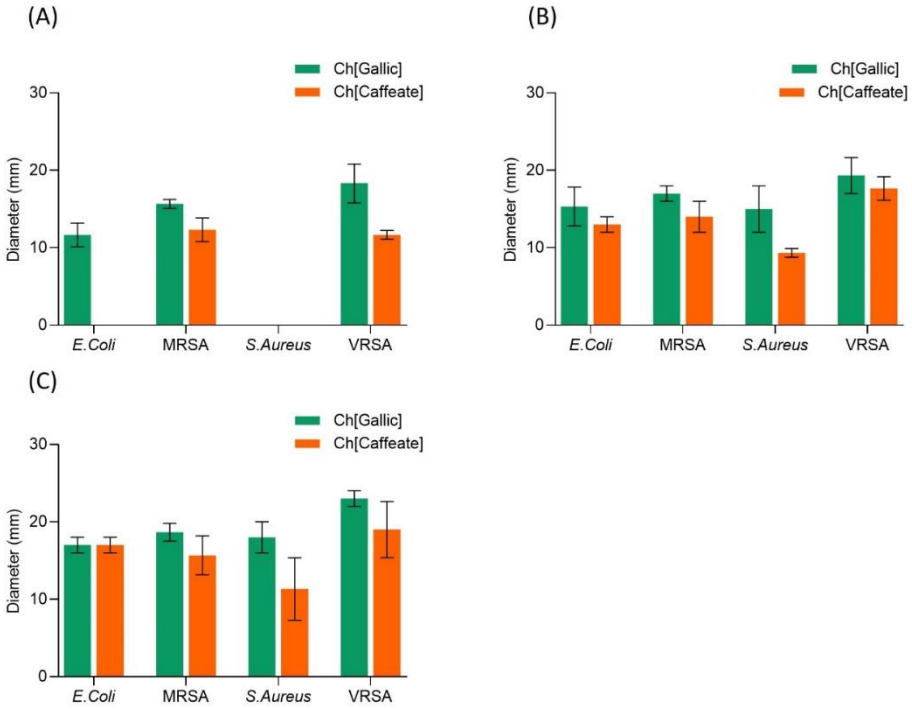
V-6.1.1. Acetaminophen cytotoxicity

The cytotoxicity of the acetaminophen (ACT) was evaluated using the L929 mouse fibroblast-like cell line (European Collection of Cell Cultures, UK) and the ATDC5 chondrocyte-like cell line (European Collection of Authenticated Cell Culture, England). L929 were cultured in basic medium: Dulbecco's modified Eagle's medium (DMEM; Sigma-Aldrich, USA) with phenol red, with 10% fetal bovine serum (Life Technologies, USA) and 1% antibiotic/antimycotic (A/A, Gibco, UK) solution. L929 cells were incubated at 37 °C in an atmosphere containing 5% of CO_2, until 90% confluence was achieved. ATDC 5 cell line was cultured in DMEM medium (Dulbecco's Modified Eagle Medium: Nutrient Mixture F-12, Alfagene, Portugal), with 10% fetal bovine serum and 1% A/A solution, under standard culture conditions (37 ◦C in a humidified atmosphere, containing 5 v/v CO_2), until 90% confluence was achieved. L929 and ATDC5 cells were seeded at a density of 1×10^6 cells/cm^2 in a 48well plate and incubated for 24h in a CO2 incubator, before the extract's addition. At the same time, solutions of 1, 0.5, 0.25, 0.1 and 0.01% (w/v) of ACT in DMEM low glucose and DMEM-F12 were prepared and placed in the water bath at 37°C and 60 rpm, for 24 hours. In the following day the ACT solutions were filtered using a 0.45 Fm membrane filter and added to the cells. After 24, 48, and 72 hours the cell cultures' metabolic activities were evaluated.

V-6.2. Supplementary figures and tables



Supplementary Figure V-1 - Metabolic activity of L929 and ATDC5 cell line after 24, 48 and 72h of culture with ACT extracts.



Supplementary Figure V-2 - Disc diffusion assay results with A) 0.5% (w/v), B) 1% (w/v) and C) B) 3% (w/v) Bio-IL solution.

Supplementary Table V-1 - Primers used for real-time quantitative RT-PCR analysis

	Primer sequence	Accession number
Human Beta-2 microglobulin (hB2M)	F – TGGAGGCTATCCAGCGTACT R – CGGATGGATGAAACCCAGACA	NM_004048.2
Human tumor necrosis factor (TNF-α)	F – ATGTTGTAGCAAACCCTCAAGC R – TGATGGCAGAGAGGAGGTTG	NM_000594.4
Human interleukin 6 (IL-6)	F – AGGAGACTTGCCTGGTGAAA R – GCATTTGTGGTTGGGTCAG	NM_000600.5
Human nitric oxide synthase 2 (NOS2)	F – GGACATCGCGTGGGTGAA R – TTTATCGCTCGGAGCCTGC	NM_000625.4
Human cyclooxygenese-2 (COX-2)	F – ATGGGGTGATGAGCAGTTGT R – GAAAGGTGTCAGGCAGAAGG	NM_000963.3
Human transforming growth factor β (TGF-β)	F – AACAAAAAGGTACATGGCCCC R – CCACCAATGGAACATCGTCG	NM_000660.7
Collagen, Type II, apha 1 (COL2A1)	F – CGGTGAGAAGGGAGAAGTTG R – GACCGGTCACTCCAGTAGGA	NM_001844.5

V-7. REFERENCES

[1] Y. Wang, D.J. Blasioli, H.J. Kim, H.S. Kim, D.L. Kaplan, Cartilage tissue engineering with silk scaffolds and human articular chondrocytes, Biomaterials. 27 (2006) 4434–4442. https://doi.org/10.1016/j.biomaterials.2006.03.050.

[2] Y.P. Singh, J.C. Moses, N. Bhardwaj, B.B. Mandal, Overcoming the Dependence on Animal Models for Osteoarthritis Therapeutics – The Promises and Prospects of *in vitro* Models, Adv. Healthc. Mater. 10 (2021) 1–25. https://doi.org/10.1002/adhm.202100961.

[3] V. Rai, M.F. Dilisio, N.E. Dietz, D.K. Agrawal, Recent strategies in cartilage repair: A systemic review of the scaffold development and tissue engineering, J. Biomed. Mater. Res. - Part A. 105 (2017) 2343–2354. https://doi.org/10.1002/jbm.a.36087.

[4] J. Radhakrishnan, A. Subramanian, U.M. Krishnan, S. Sethuraman, Injectable and 3D Bioprinted Polysaccharide Hydrogels: From Cartilage to Osteochondral Tissue Engineering, Biomacromolecules. 18 (2017) 1–26. https://doi.org/10.1021/acs.biomac.6b01619.

[5] Y. Wu, S. Zhu, C. Wu, P. Lu, C. Hu, S. Xiong, J. Chang, B.C. Heng, Y. Xiao, H.W. Ouyang, A Bi-lineage conducive scaffold for osteochondral defect regeneration, Adv. Funct. Mater. 24 (2014) 4473–4483. https://doi.org/10.1002/adfm.201304304.

[6] Y. Yan, T. Sun, H. Zhang, X. Ji, Y. Sun, X. Zhao, L. Deng, J. Qi, W. Cui, H.A. Santos, H. Zhang, Euryale Ferox Seed-Inspired Superlubricated Nanoparticles for Treatment of Osteoarthritis, Adv. Funct. Mater. 29 (2019) 1–14. https://doi.org/10.1002/adfm.201807559.

[7] B. Crivelli, E. Bari, S. Perteghella, L. Catenacci, M. Sorrenti, M. Mocchi, S. Faragò, G. Tripodo, A. Prina-Mello, M.L. Torre, Silk fibroin nanoparticles for celecoxib and curcumin delivery: ROS-scavenging and anti-inflammatory activities in an *in vitro* model of osteoarthritis, Eur. J. Pharm. Biopharm. 137 (2019) 37–45. https://doi.org/10.1016/j.ejpb.2019.02.008.

[8] K. Panjapheree, S. Kamonmattayakul, J. Meesane, Biphasic scaffolds of silk fibroin film affixed to silk fibroin/chitosan sponge based on surgical design for cartilage defect in osteoarthritis, Mater. Des. 141 (2018) 323–332. https://doi.org/10.1016/j.matdes.2018.01.006.

[9] H. Miao, R. Shen, W. Zhang, Z. Lin, H. Wang, L. Yang, X.Y. Liu, N. Lin, Near-Infrared Light Triggered Silk Fibroin Scaffold for Photothermal Therapy and Tissue Repair of Bone Tumors, Adv. Funct. Mater. 31 (2021) 1–9. https://doi.org/10.1002/adfm.202007188.

[10] V.P. Ribeiro, J. Silva-Correia, C. Gonçalves, S. Pina, H. Radhouani, T. Montonen, J. Hyttinen, A. Roy, A.L. Oliveira, R.L. Reis, J.M. Oliveira, Rapidly responsive silk fibroin hydrogels as an artificial matrix for the programmed tumor cells death, PLoS One. 13 (2018) 1–21. https://doi.org/10.1371/journal.pone.0194441.

[11] T.K. Mwangi, R.D. Bowles, D.M. Tainter, R.D. Bell, D.L. Kaplan, L.A. Setton, Synthesis and characterization of silk fibroin microparticles for intra-articular drug delivery, Int. J. Pharm. 485 (2015) 7–14. https://doi.org/10.1016/j.ijpharm.2015.02.059.

[12] D. Primorac, V. Molnar, V. Matišić, D. Hudetz, Ž. Jeleč, E. Rod, F. Čukelj, D. Vidović, T. Vrdoljak, B. Dobričić, D. Antičević, M. Smolić, M. Miškulin, D. Ćaćić, I. Borić, Comprehensive review of knee osteoarthritis pharmacological treatment and the latest professional societies' guidelines, Pharmaceuticals. 14 (2021) 1–20. https://doi.org/10.3390/ph14030205.

[13] L. Kou, S. Xiao, R. Sun, S. Bao, Q. Yao, R. Chen, Biomaterial-engineered intra-articular drug delivery systems for osteoarthritis therapy, Drug Deliv. 26 (2019) 870–885. https://doi.org/10.1080/10717544.2019.1660434.

[14] J.M. Gomes, S.S. Silva, R.L. Reis, Biocompatible ionic liquids: Fundamental behaviours and applications, Chem. Soc. Rev. 48 (2019) 4317–4335. https://doi.org/10.1039/c9cs00016j.

[15] E.S. Morais, N.H.C.S. Silva, T.E. Sintra, S.A.O. Santos, B. Miguel, I.F. Almeida, P.C. Costa, I. Correia-sá, S.P.M. Ventura, A.J.D. Silvestre, M.G. Freire, C.S.R. Freire, Anti-inflammatory and antioxidant nanostructured cellulose membranes loaded with phenolic-based ionic liquids for cutaneous application, Carbohydr. Polym. 206 (2019) 187–197. https://doi.org/10.1016/j.carbpol.2018.10.051.

[16] W. Huang, X. Wu, J. Qi, Q. Zhu, W. Wu, Y. Lu, Z. Chen, Ionic liquids: green and tailor-made solvents in drug delivery, Drug Discov. Today. 25 (2020) 901–908. https://doi.org/10.1016/j.drudis.2019.09.018.

[17] Z. Sidat, T. Marimuthu, P. Kumar, L.C. du Toit, P.P.D. Kondiah, Y.E. Choonara, V. Pillay, Ionic liquids as potential and synergistic permeation enhancers for transdermal drug delivery, Pharmaceutics. 11 (2019) 96. https://doi.org/10.3390/pharmaceutics11020096.

[18] V. Allizond, S. Comini, A.M. Cuffini, G. Banche, Current Knowledge on Biomaterials for Orthopedic Applications Modified to Reduce Bacterial Adhesive Ability, Antibiotics. 11 (2022) 529. https://doi.org/10.3390/antibiotics11040529.

[19] D. Bicho, S. Ajami, C. Liu, R.L. Reis, J.M. Oliveira, Peptide-biofunctionalization of biomaterials for osteochondral tissue regeneration in early stage osteoarthritis: Challenges and opportunities, J. Mater. Chem. B. 7 (2019) 1027–1044. https://doi.org/10.1039/c8tb03173h.

[20] M. Zakrewsky, K.S. Lovejoy, T.L. Kern, T.E. Miller, V. Le, A. Nagy, Ionic liquids as a class of materials for transdermal delivery and pathogen neutralization, PNAS. 111 (2014) 13313–13318. https://doi.org/10.1073/pnas.1403995111.

[21] R. Ferraz, V. Teixeira, D. Rodrigues, R. Fernandes, C. Prudêncio, J.P. Noronha, Ž. Petrovski, L.C. Branco, Antibacterial activity of Ionic Liquids based on ampicillin against resistant bacteria, RSC Adv. 4 (2014) 4301–4307. https://doi.org/10.1039/c3ra44286a.

[22] R. Md Moshikur, M.R. Chowdhury, M. Moniruzzaman, M. Goto, Biocompatible ionic liquids and their applications in pharmaceutics, Green Chem. 22 (2020) 8116–8139. https://doi.org/10.1039/D0GC02387F.

[23] R. Ferraz, D. Silva, A.R. Dias, V. Dias, M.M. Santos, L. Pinheiro, C. Prudêncio, J.P. Noronha, Ž. Petrovski, L.C. Branco, Synthesis and antibacterial activity of ionic liquids and organic salts based on penicillin g and amoxicillin hydrolysate derivatives against resistant bacteria, Pharmaceutics. 12 (2020) 221. https://doi.org/10.3390/pharmaceutics12030221.

[24] R. Bielas, A. Mielańczyk, M. Skonieczna, Ł. Mielańczyk, D. Neugebauer, Choline supported poly(ionic liquid) graft copolymers as novel delivery systems of anionic pharmaceuticals for anti-inflammatory and anti-coagulant therapy, Sci. Rep. 9 (2019) 14410. https://doi.org/10.1038/s41598-019-50896-5.

[25] F. Siopa, T. Figueiredo, R.F.M. Frade, I. Neto, A. Meirinhos, C.P. Reis, R.G. Sobral, C.A.M. Afonso, P. Rijo, Choline-Based Ionic Liquids: Improvement of Antimicrobial Activity, ChemistrySelect. 1 (2016) 5909–5916. https://doi.org/10.1002/slct.201600864.

[26] J.M. Gomes, S.S. Silva, E.M. Fernandes, F.C.M. Lobo, M. Martín-Pastor, P. Taboada, R.L. Reis, Silk fibroin/cholinium gallate-based architectures as therapeutic tools, Acta Biomater. 147 (2022) 168–184. https://doi.org/10.1016/j.actbio.2022.05.020.

[27] W. Zhang, W.B. Robertson, J. Zhao, W. Chen, J. Xu, Emerging Trend in the Pharmacotherapy of Osteoarthritis, Front. Endocrinol. (Lausanne). 10 (2019) 431. https://doi.org/10.3389/fendo.2019.00431.

[28] S.S. Silva, E.G. Popa, M.E. Gomes, M.B. Oliveira, S. Nayak, B. Subia, J.F. Mano, S.C. Kundu, R.L. Reis, Silk hydrogels from non-mulberry and mulberry silkworm cocoons processed with ionic liquids, Acta Biomater. 9 (2013) 8972–8982. https://doi.org/10.1016/j.actbio.2013.06.044.

[29] S.S. Silva, A. Motta, M.T. Rodrigues, A.F.M. Pinheiro, M.E. Gomes, J.F. Mano, R.L. Reis, C. Migliaresi, Novel genipin-cross-linked chitosan/silk fibroin sponges for cartilage engineering strategies, Biomacromolecules. 9 (2008) 2764–2774. https://doi.org/10.1021/bm800874q.

[30] A.R. Franco, E. Palma Kimmerling, C. Silva, F.J. Rodrigues, I.B. Leonor, R.L. Reis, D.L. Kaplan, Silk-Based Antimicrobial Polymers as a New Platform to Design Drug-Free Materials to Impede Microbial Infections, Macromol. Biosci. 18 (2018) 1–15. https://doi.org/10.1002/mabi.201800262.

[31] S.B. Kedare, R.P. Singh, Genesis and development of DPPH method of antioxidant assay, J. Food Sci. Technol. 48 (2011) 412–422. https://doi.org/10.1007/s13197-011-0251-1.

[32] G. Jiménez, S. Venkateswaran, E. López-Ruiz, M. Perán, S. Pernagallo, J.J. Díaz-Monchón, R.F. Canadas, C. Antich, J.M. Oliveira, A. Callanan, R. Walllace, R.L. Reis, E. Montañez, E. Carrillo, M. Bradley, J.A. Marchal, A soft 3D polyacrylate hydrogel recapitulates the cartilage niche and allows growth-factor free tissue engineering of human articular cartilage, Acta Biomater. 90 (2019) 146–156. https://doi.org/10.1016/j.actbio.2019.03.040.

[33] P. Le Thi, Y. Lee, D.L. Tran, T.T.H. Thi, J. Il Kang, K.M. Park, K.D. Park, In situ forming and reactive oxygen species-scavenging gelatin hydrogels for enhancing wound healing efficacy, Acta Biomater. 103 (2020) 142–152. https://doi.org/10.1016/j.actbio.2019.12.009.

[34] I.M. Oliveira, C. Gonçalves, M.E. Shin, S. Lee, R.L. Reis, G. Khang, J.M. Oliveira, Anti-Inflammatory Properties of Injectable Betamethasone-Loaded Tyramine-Modified Gellan Gum/Silk Fibroin Hydrogels, Biomolecules. 10 (2020) 1456. https://doi.org/10.3390/biom10101456.

[35] N. Tiwari, S. Wegner, A. Hassan, N. Dwivedi, R.N. Rai, N. Sinha, Probing short and long-range interactions in native collagen inside the bone matrix by BioSolids CryoProbe, Magn. Reson. Chem. 59 (2021) 99–107. https://doi.org/10.1002/mrc.5084.

[36] Y. Shen, F. Delaglio, G. Cornilescu, A. Bax, TALOS+: A hybrid method for predicting protein backbone torsion angles from NMR chemical shifts, J. Biomol. NMR. 44 (2009) 213–223. https://doi.org/10.1007/s10858-009-9333-z.

[37] M. Samie, A.F. Khan, J.G. Hardy, M.A. Yameen, Electrospun Antibacterial Composites for Cartilage Tissue Engineering, Macromol. Biosci. 22 (2022) 2200219. https://doi.org/10.1002/mabi.202200219.

[38] A. Zhu, S. Bai, L. Li, M. Wang, J. Wang, Choline Hydroxide: An Efficient and Biocompatible Basic Catalyst for the Synthesis of Biscoumarins Under Mild Conditions, Catal. Letters. 145 (2015) 1089–1093. https://doi.org/10.1007/s10562-015-1487-6.

[39] B. Badhani, N. Sharma, R. Kakkar, Gallic acid: A versatile antioxidant with promising therapeutic and industrial applications, RSC Adv. 5 (2015) 27540–27557. https://doi.org/10.1039/c5ra01911g.

[40] B. Cizmarova, B. Hubkova, B. Bolerazska, M. Marekova, A. Birkova, Caffeic acid: A brief overview of its presence, metabolism, and bioactivity, Bioact. Compd. Heal. Dis. 3 (2020) 74–81. https://doi.org/10.31989/bchd.v3i4.692.

[41] J.D. Caplin, A.J. García, Implantable antimicrobial biomaterials for local drug delivery in bone infection models, Acta Biomater. 93 (2019) 2–11. https://doi.org/10.1016/j.actbio.2019.01.015.

[42] I.M. Oliveira, C. Gonçalves, E.P. Oliveira, R. Simón-Vázquez, A. da Silva Morais, Á. González-Fernández, R.L. Reis, J.M. Oliveira, PAMAM dendrimers functionalised with an anti-TNF α antibody and chondroitin sulphate for treatment of rheumatoid arthritis, Mater. Sci. Eng. C. 121 (2021) 111845. https://doi.org/10.1016/j.msec.2020.111845.

[43] A. Reizabal, D.M. Correia, C.M. Costa, L. Perez-Alvarez, J.L. Vilas-Vilela, S. Lanceros-Méndez, Silk Fibroin Bending Actuators as an Approach Toward Natural Polymer Based Active Materials, ACS Appl. Mater. Interfaces. 11 (2019) 30197–30206. https://doi.org/10.1021/acsami.9b07533.

[44] L. Zhang, X. Liu, G. Li, P. Wang, Y. Yang, Tailoring degradation rates of silk fibroin scaffolds for tissue engineering, J. Biomed. Mater. Res. - Part A. 107 (2019) 104–113. https://doi.org/10.1002/jbm.a.36537.

[45] B.B. Mandal, S.C. Kundu, Non-bioengineered silk fibroin protein 3D scaffolds for potential biotechnological and tissue engineering applications, Macromol. Biosci. 8 (2008) 807–818. https://doi.org/10.1002/mabi.200800113.

[46] C.J. Little, N.K. Bawolin, X. Chen, Mechanical Properties of Natural Cartilage and Tissue-Engineered Constructs, TISSUE Eng. Part B. 17 (2011) 213–227. https://doi.org//10.1089/ten.teb.2010.0572.

[47] N. Kasoju, N. Hawkins, O. Pop-Georgievski, D. Kubies, F. Vollrath, Silk fibroin gelation via non-solvent induced phase separation, Biomater. Sci. 4 (2016) 460–473. https://doi.org/10.1039/c5bm00471c.

[48] T.E. Sintra, A. Luís, S.N. Rocha, A.I.M.C.L. Ferreira, F. Gonçalves, L.M.N.B.F. Santos, B.M. Neves, M.G. Freire, S.P.M. Ventura, J.A.P. Coutinho, Enhancing the antioxidant characteristics of phenolic acids by their conversion into cholinium salts, ACS Sustain. Chem. Eng. 3 (2015) 2558–2565. https://doi.org/10.1021/acssuschemeng.5b00751.

[49] P. Lepetsos, A.G. Papavassiliou, ROS/oxidative stress signaling in osteoarthritis, Biochim. Biophys. Acta - Mol. Basis Dis. 1862 (2016) 576–591. https://doi.org/10.1016/j.bbadis.2016.01.003.

[50] O.M. Zahan, O. Serban, C. Gherman, D. Fodor, The evaluation of oxidative stress in osteoarthritis, Med. Pharm. Reports. 93 (2020) 12–22. https://doi.org/10.15386/mpr-1422.

[51] E.R. Blough, M. Wu, Acetaminophen : beyond pain and fever-relieving, Front. Pharmacol. 2 (2011) 1–6. https://doi.org/10.3389/fphar.2011.00072.

[52] C.S. Bonnet, D.A. Walsh, Osteoarthritis, angiogenesis and inflammation, Rheumatology. 44 (2005) 7–16. https://doi.org/10.1093/rheumatology/keh344.

[53] C.M. Dancevic, D.R. McCulloch, Current and emerging therapeutic strategies for preventing inflammation and aggrecanase-mediated cartilage destruction in arthritis, Arthritis Res. Ther. 16 (2014) 429. https://doi.org/10.1186/s13075-014-0429-9.

[54] P.J. Cope, K. Ourradi, Y. Li, M. Sharif, Models of osteoarthritis: the good, the bad and the promising, Osteoarthr. Cartil. 27 (2019) 230–239. https://doi.org/10.1016/j.joca.2018.09.016.

[55] M. Laavola, T. Leppänen, M. Hämäläinen, K. Vuolteenaho, T. Moilanen, R. Nieminen, E. Moilanen, IL-6 in osteoarthritis: Effects of pine stilbenoids, Molecules. 24 (2019) 109. https://doi.org/10.3390/molecules24010109.

[56] A. Schuerwegh, E. Dombrecht, W. Stevens, J. Van Offel, C. Bridts, L. De Clerck, Influence of pro-inflammatory (IL-1α, IL-6, TNF-α, IFN-γ) and anti-inflammatory (IL-4) cytokines on chondrocyte function, Osteoarthr. Cartil. 11 (2003) 681–687. https://doi.org/10.1016/S1063-4584(03)00156-0.

[57] M.E.R. van Meegeren, G. Roosendaal, N.W.D. Jansen, M.J.G. Wenting, A.C.W. van Wesel, J.A.G. van Roon, F.P.J.G. Lafeber, IL-4 alone and in combination with IL-10 protects against blood-induced cartilage damage, Osteoarthr. Cartil. 20 (2012) 764–772. https://doi.org/10.1016/j.joca.2012.04.002.

[58] P. Ubanako, N. Xelwa, M. Ntwasa, LPS induces inflammatory chemokines via TLR-4 signalling and enhances the Warburg Effect in THP-1 cells, PLoS One. 14 (2019) e0222614. https://doi.org/10.1371/journal.pone.0222614.

[59] A.C. Lima, R.L. Reis, H. Ferreira, N.M. Neves, Glutathione reductase-sensitive polymeric micelles for controlled drug delivery on arthritic diseases, ACS Biomater. Sci. Eng. 7 (2021) 3229–3241. https://doi.org/10.1021/acsbiomaterials.1c00412.

[60] T. Chen, S. Ehnert, G. Tendulkar, S. Zhu, C. Arnscheidt, R.H. Aspera-Werz, A.K. Nussler, Primary human chondrocytes affected by cigarette smoke—therapeutic challenges, Int. J. Mol. Sci. 21 (2020) 1901. https://doi.org/10.3390/ijms21051901.

[61] I.M. Oliveira, C. Gonçalves, M.E. Shin, S. Lee, R.L. Reis, G. Khang, J.M. Oliveira, Enzymatically crosslinked tyramine-gellan gum hydrogels as drug delivery system for rheumatoid arthritis treatment, Drug Deliv. Transl. Res. 11 (2021) 1288–1300. https://doi.org/10.1007/s13346-020-00855-9.

[62] J.M. Cicchese, S. Evans, C. Hult, L.R. Joslyn, T. Wessler, J.A. Millar, S. Marino, N.A. Cilfone, J.T. Mattila, J.J. Linderman, D.E. Kirschner, Dynamic balance of pro- and anti-inflammatory signals controls disease and limits pathology, Immunol. Rev. 285 (2018) 147–167. https://doi.org/10.1111/imr.12671.

[63] P. Wojdasiewicz, Ł.A. Poniatowski, D. Szukiewicz, The Role of Inflammatory and Anti-Inflammatory Cytokines in the Pathogenesis of Osteoarthritis, Mediators Inflamm. 2014 (2014) 1–19. https://doi.org/10.1155/2014/561459.

[64] E. Chisari, K.M. Yaghmour, W.S. Khan, The effects of TNF-alpha inhibition on cartilage: a systematic review of preclinical studies, Osteoarthr. Cartil. 28 (2020) 708–718. https://doi.org/10.1016/j.joca.2019.09.008.

[65] S. Xue, X. Zhou, W. Sang, C. Wang, H. Lu, Y. Xu, Y. Zhong, L. Zhu, C. He, J. Ma, Cartilage-targeting peptide-modified dual-drug delivery nanoplatform with NIR laser response for osteoarthritis therapy, Bioact. Mater. 6 (2021) 2372–2389. https://doi.org/10.1016/j.bioactmat.2021.01.017.

[66] D.Y. Lee, Y.J. Park, M.G. Song, D.R. Kim, S. Zada, D.H. Kim, Cytoprotective effects of delphinidin for human chondrocytes against oxidative stress through activation of autophagy, Antioxidants. 9 (2020) 1–17. https://doi.org/10.3390/antiox9010083.

[67] A. Chierchia, N. Chirico, L. Boeri, I. Raimondi, G.A. Riva, M.T. Raimondi, M. Tunesi, C. Giordano, G. Forloni, D. Albani, Secretome released from hydrogel-embedded adipose mesenchymal stem cells protects against the Parkinson's disease related toxin 6-hydroxydopamine, Eur. J. Pharm. Biopharm. 121 (2017) 113–120. https://doi.org/10.1016/j.ejpb.2017.09.014.

[68] M. Nune, S. Manchineella, T. Govindaraju, K.S. Narayan, Melanin incorporated electroactive and antioxidant silk fibroin nanofibrous scaffolds for nerve tissue engineering, Mater. Sci. Eng. C. 94 (2019) 17–25. https://doi.org/10.1016/j.msec.2018.09.014.

[69] H.J. Park, J.S. Lee, O.J. Lee, F.A. Sheikh, B.M. Moon, H.W. Ju, J.H. Kim, D.K. Kim, C.H. Park, Fabrication of microporous three-dimensional scaffolds from silk fibroin for tissue engineering, Macromol. Res. 22 (2014) 592–599. https://doi.org/10.1007/s13233-014-2083-0.

[70] C. Vepari, D.L. Kaplan, Silk as a biomaterial, Prog. Polym. Sci. 32 (2007) 991–1007. https://doi.org/10.1016/j.progpolymsci.2007.05.013.

[71] D. Soares Da Costa, M.D.C. Márquez-Posadas, A.R. Araujo, Y. Yang, S. Merino, T. Groth, R.L. Reis, I. Pashkuleva, Adhesion of adipose-derived mesenchymal stem cells to glycosaminoglycan surfaces with different protein patterns, ACS Appl. Mater. Interfaces. 7 (2015) 10034–10043. https://doi.org/10.1021/acsami.5b02479.

[72] M. Rahimi, G. Charmi, K. Matyjaszewski, X. Banquy, J. Pietrasik, Recent developments in natural and synthetic polymeric drug delivery systems used for the treatment of osteoarthritis, Acta Biomater. 123 (2021) 31–50. https://doi.org/10.1016/j.actbio.2021.01.003.

[73] R. Vernal, E. Velásquez, J. Gamonal, J.A. Garcia-Sanz, A. Silva, M. Sanz, Expression of proinflammatory cytokines in osteoarthritis of the temporomandibular joint, Arch. Oral Biol. 53 (2008) 910–915. https://doi.org/10.1016/j.archoralbio.2008.04.004.

[74] M. Moussa, D. Lajeunesse, G. Hilal, O. El Atat, G. Haykal, R. Serhal, A. Chalhoub, C. Khalil, N. Alaaeddine, Platelet rich plasma (PRP) induces chondroprotection via increasing autophagy, anti-inflammatory markers, and decreasing apoptosis in human osteoarthritic cartilage, Exp. Cell Res. 352 (2017) 146–156. https://doi.org/10.1016/j.yexcr.2017.02.012.

[75] S. Liu, Z. Deng, K. Chen, S. Jian, F. Zhou, Y. Yang, Z. Fu, H. Xie, J. Xiong, W. Zhu, Cartilage tissue engineering: From proinflammatory and anti-inflammatory cytokines to osteoarthritis treatments, Mol. Med. Rep. 25 (2022) 1–15. https://doi.org/10.3892/MMR.2022.12615.

[76] F. Zhou, X. Zhang, D. Cai, J. Li, Q. Mu, W. Zhang, S. Zhu, Y. Jiang, W. Shen, S. Zhang, H.W. Ouyang, Silk fibroin-chondroitin sulfate scaffold with immuno-inhibition property for articular cartilage

Chapter VI

Alginate/acemannan derived beads loaded with a biocompatible ionic liquid as a bioactive delivery system

Chapter VI

Alginate/acemannan derived beads loaded with a biocompatible ionic liquid as a bioactive delivery system ¨

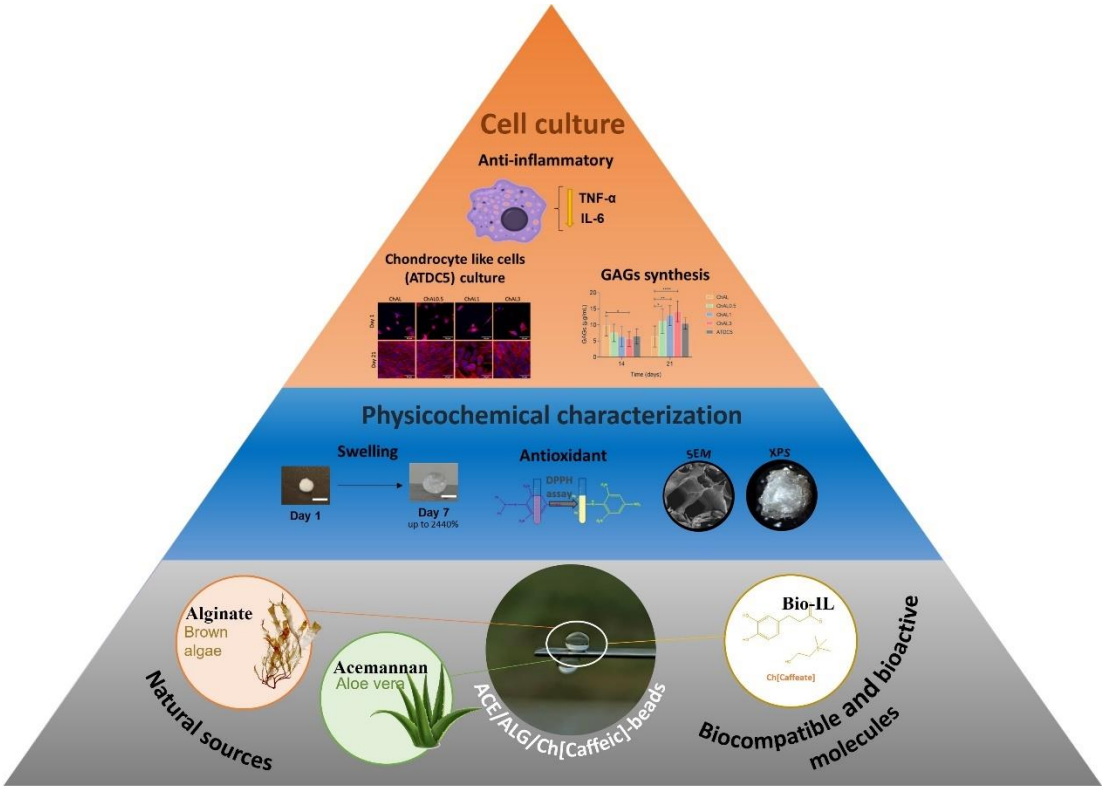
ABSTRACT

Combining biomacromolecules with green chemistry principles and clean technologies has proven to be an effective approach for developing drug delivery systems, providing a prolonged and sustained release of the encapsulated material. The current study investigates the potential of cholinium caffeate (Ch[Caffeate]), a phenolic-based biocompatible ionic liquid (Bio-IL) entrapped in alginate/acemannan beads, as a drug delivery system able to reduce local joint inflammation on osteoarthritis (OA) treatment. The synthesized Bio-IL has antioxidant and anti-inflammatory actions that, combined with biopolymers as 3D architectures, promote the entrapment and sustainable release of the bioactive molecules over time. The physico-chemical and morphological characterization of the beads showed that they have a porous and interconnected structure, with a high swelling ability (up 2400%), and proved the successful encapsulation of Ch[Caffeate], which significantly improved the antioxidant activities of the constructs. Besides, the structures provide the environment for ATDC5 cell proliferation and cartilage-like ECM formation. Further, the ability to block the release of pro-inflammatory cytokines (TNF-α and IL-6) from differentiated macrophages was evidenced by ChAL-Ch[Caffeate] beads. These outcomes suggest that the established strategy based on using natural and bioactive macromolecules to develop 3D constructs has great potential to be used as therapeutic tools for patients with OA.

¨ This chapter is based on the following publication:

Gomes J. M., Silva S. S., Rodrigues L. C and Reis R. L "Alginate/acemannan derived beads loaded with a biocompatible ionic liquid as a bioactive delivery system"; 2022 (Submitted).

VI-1. GRAPHICAL ABSTRACT



VI-2. INTRODUCTION

Special attention has been given to the development of sustainable strategies with reduced environmental impacts involving biodegradable and biocompatible molecules, mostly if biomedical applications are envisaged [1–3]. Building advanced materials based on biocompatible ionic liquids (Bio-ILs) combined with natural molecules able to act as enhanced key therapeutics and drug delivery vehicles constitutes an effective strategy [4,5]. Bio-ILs have been raised as a research topic for the pharmaceutical and biomedical fields as active pharmaceutical ingredients (APIs) systems. They are tunable compounds, and their synthesis is a straightforward scaled-up acid-base neutralization reaction. By choosing cationic or anionic moieties and their substituents from compounds with intrinsic bioactivity, it is possible to produce APIs-Bio-ILs systems [6]. Drug delivery systems involving Bio-ILs are a promising pathway to enhance the solubility and permeability of the interest compound since they can enhance the drug bioavailability and delivery, relieving the polymorphic problems associated with crystalline active pharmaceutical ingredients [4,7]. For instance, Bio-ILs were used to develop API-poly(ionic liquid) (API

PIL)-based microneedle patches containing salicylic acid, creating an effective transport pathway in the epidermis. These compounds were also used for transdermal[8] and oral delivery[9] of insulin. The oral formulations allowed insulin transport effectively and, at the same time, protecting the molecule from enzymatic degradation [9].

As the biomedical and technological fields develop, attention has shifted toward using biomaterials for cartilage regeneration, including osteoarthritis (OA) treatment [10]. OA is the most prevalent degenerative cartilage disease, is mainly characterized by the articular surface's softening, fibrillation, and erosion [11]. Despite the challenges associated with cartilage regeneration, mainly due to its avascular and aneural nature and scarce cell population, drug delivery systems are a promising strategy for OA therapy since they significantly reduce the side effects and improve the treatment efficacy [12–14]. Natural polymers are renewable resources widely used to design several architectures while fulfilling the green chemistry principles [1,2]. Natural and synthetic macromolecules, such as chitosan, hyaluronic acid, alginate, and poly(lactic-co-glycolic) acid (PLGA), have been used to prepare matrices as therapeutic delivery agents for OA [15–17]. From those polymers, micro-scaled particles, such as microspheres, microgels, and beads, have been widely investigated due to their sustained drug release profile, protection of the loaded drug from rapid clearance from the body, increase of its half-life period, and extended effect [18–21].

Herein, we report the potential of cholinium Caffeate (Ch[Caffeate]), a phenolic-based biocompatible ionic liquid (Bio-IL) entrapped in beads composed by alginate (ALG), a marine origin polymer, and acemannan (ACE), the most abundant polysaccharide of aloe vera leaves, as a bioactive delivery system able to reduce local joint inflammation on osteoarthritis treatment. For that purpose, the Bio-IL was synthesized using Caffeate acid, the source of the cationic moiety, with antioxidant and inflammatory action [22]. The resultant Bio-IL is expected to have higher water-solubility and similar toxicity, enhancing its biological performance by increasing its antioxidant and anti-inflammatory properties compared with the precursors. Further, ACE and ALG were used in a combinatorial approach where the ACE/ALG/Bio-IL-based architectures were produced using an extrusion dipping method. Previous studies demonstrated that ACE and ALG combination improved matrices' properties [23]. In those systems, the ALG jellification occurs when in contact with ACE since it possesses Ca^{+2}. Herein, Ch[Caffeate] was added at different concentrations to the ACE bath to evaluate their effect on the final properties of the beads. The developed architectures were characterized to assess their morphological aspects, structural features, swelling ability, stability, and antioxidant properties. Furthermore, the ability of the produced architectures to

induce chondrocyte adhesion and proliferation was studied using the ATDC5, a chondrogenic cell line, for up to 21 days. Glycosaminoglycans (GAGs) quantification was also performed to detect the cartilage-like ECM formation after cell contact with beads. Moreover, we hypothesized that the intrinsic features of each component of the ACE/ALG/Bio-IL beads may act synergistically, reducing the reactive oxygen species (ROS) production and decreasing the secretion of pro-inflammatory cytokines, such as TNF-α and IL-6 in THP-1 activated macrophages.

VI-3. MATERIALS AND METHODS

VI-3.1. Materials

For the Bio-IL synthesis, Cholinium hydroxide (Ch[OH]) 45% in methanol solution and Caffeate acid were purchased from Sigma-Aldrich, St. Louis, MO, USA. Also, 2,2-diphenyl-1-picrylhydrazyl (DPPH) was purchased from Sigma-Aldrich, St. Louis, MO, USA. Acemannan in powder (ACE; BiAloe®Mwaverage 200kPa) was purchased from Lorand Laboratories (Texas, USA). According to the manufacturer, the molecular weight of low-viscosity alginate (Sigma-Aldrich (USA)), was 58.9 kg/mol, the mannuronate/guluronate ratio is 2.65, and its viscosity is 12.8 cps, measured in 1% water, at 25 °C. All other chemicals were reagent grade, and they were used as received.

VI-3.2. Synthesis of Cholinium Caffeate (Ch[Caffeate])

Ch[Caffeate] was synthesized as previously reported [5]. A methanolic solution of caffeic acid was mixed with cholinium hydroxide (Ch[OH]) solution in a 1:1 proportion under a nitrogen atmosphere, and the temperature was maintained at 0°C. The mixture was kept stirring overnight at room temperature under a nitrogen atmosphere. On the following day, the methanol and water were removed, under reduced pressure, and the unreacted acid was washed with acetone. After removing the residual acetone, using the rotary evaporator, the resultant Ch[Caffeate] (Figure VI-1) was dried under a high vacuum for 72h, at least. ^{1}H NMR was performed to validate the purity of the synthesized Ch[Caffeate], and the NMR spectra were obtained on an Avance III spectrometer (Bruker, Germany) operating at a resonance frequency of 400.13 MHz (1H). The samples were prepared using DMSO-D6 solvent, also used as a reference for chemical shits reported in ppm (parts per million).

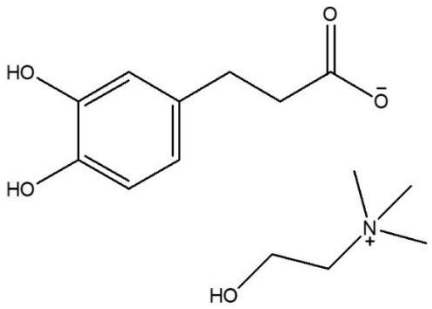


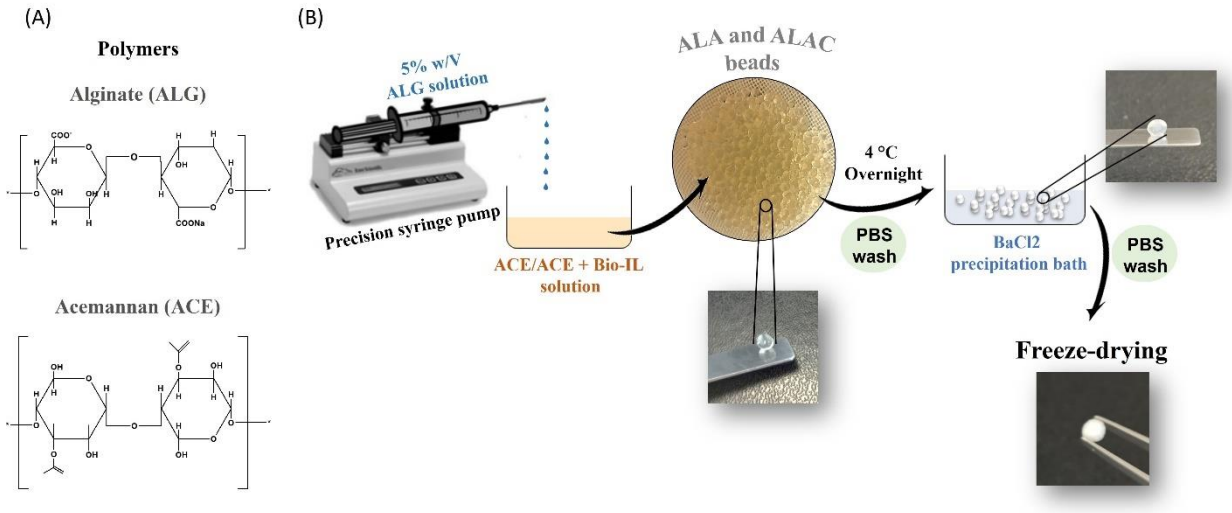
Figure VI-1 - Cholinium Caffeate (Ch[Caffeate]) chemical structure.

VI-3.3. Preparation of the ALG/ACE-Ch[Caffeate] beads

Beads of ALG and ACE were produced following a reported protocol [24]. Briefly, aqueous solutions of ALG (5% w/v) and ACE (5% w/v) were prepared. The architectures were prepared by dipping the ALG solutions (1ml/min) into the ACE bath. For the formulations containing the Bio-IL, Ch[Caffeate], in its composition, the desired amount of the compound was added to the 5% w/v ACE solution. Solutions of Bio-IL/5%ACE were prepared at 0.5, 1, and 3% w/v, following the specifications depicted in Table 1. The identification of the different formulations is detailed in Table VI-1. To ensure the maximization of the incorporation of the compound into the beads system, they were maintained in the Ch[Caffeate]/5% ACE solution overnight, at -4 °C. Further, the beads were rinsed with phosphate-buffered saline (PBS) solution and immersed in a $BaCl_2$ (20 mM $BaCl_2$, 10 mM 3-(N-morpholino)propanesulfonic acid (MOPS) and 119 nM NaCl) for 4 min, to improve the stability of the produced constructs [25]. The beads were washed with PBS, frozen at -80 °C overnight, and then freeze-dried. A schematic representation of the biomaterials preparation is depicted in Scheme VI-1. Throughout the manuscript, ALA and ALAC will be used to identify the conditions without and with Ch[Caffeate] in the matrix, respectively.

Table VI-1 - Identification of the samples

Condition	[ALG] % (w/V)	[ACE] % (w/V)	Ch[Caffeate] % (w/V)
ALA	5	5	NA
ALAC0.5			0.5
ALAC1			1
ALAC3			3



Scheme VI-1 - (A) Alginate and acemannan chemical structure and (B) Schematic representation the ALA and ALAC-based beads preparation.

VI-3.4. Physico-chemical and morphological characterization of the ALG/ACE-Ch[Caffeate] beads

VI-3.4.1. Scanning electron microscopy (SEM)

ALA and ALAC-based structures, and the correspondent cross-section, were fixed with carbon adhesive tape on aluminum stubs and coated with a gold conductive layer. A NanoSEM-FEI Nova 200 with an integrated EDS – energy dispersive spectrometer was used to observe the constructs' morphology. Pore size analysis and pore size distribution were performed using ImageJ software and GraphPadPrism v. 8.0 for Windows (GraphPad Software, San Diego, http://www.graphpad.com) on SEM images displaying the beads cross-sections.

VI-3.4.2. Nuclear magnetic resonance (NMR)

The interactions among the different components of the beads were evaluated by ^{1}H NMR spectroscopy. The ^{1}H RMN spectra of ALG, ACE, and the ACE/Ch[Caffeate] solutions were collected in DMSO-d6 being recorded on a Burker Avance III.

VI-3.4.3. XPS

An instrument from Kratos Axis-Supra equipped with an aluminum Kα (Al-Kα) monochromatized radiation X-ray source (1486.6 eV) and ESCApe software was used to perform, at the core and shell, the ALA and ALAC beads analysis. All measurements were performed in a vacuum at 10^{-8} Pa and a 90° take-off angle. Chemical composition of core and shell of the ALA and ALAC beads was accessed using a Constant Analyser Energy mode using an emission current of 15mA and a 160 eV and 20 eV pass energy for survey and high-resolution spectra, respectively. The regions high-resolution analyses were performed for C 1s, O 1s, Na 1s, Ca 2p, Ba 3d and N 1s, using a linear type background to its fitting. In addition, the lower binding energy C1s photo peak, which is related to C1s hydrocarbon peak, was set at 285.0 eV for charge referencing.

VI-3.4.4. Antioxidant of the ALA and ALAC beads

The antioxidant activity of the beads was assessed using the 2,2- diphenyl-1 picrylhydrazyl (DPPH) radical scavenging assay [26]. The rationale behind this method is the color change of the DPPH solution from purple to yellow, as the antioxidant quenches the radical [26]. The stated reaction was monitored using visible spectroscopy at 517 nm, using a protocol previously described [27]. Briefly, the ALA and ALAC-based beads were immersed in a 1mM DPPH solution in methanol and kept in the dark for 1 h, 4 h, and 24 h at room temperature. After each of the defined time points, the absorbance at 517nm was assessed. A DPPH solution in methanol was used as blank and as a control for the beads without the Bio-IL. The same method was applied to Caffeate acid, the Bio-IL precursor. AA(%) (DPPH radical scavenging activity) was determined following Equation VI -1:

$$AA\ (\%) = \frac{A_0 - A_1}{A_0} \times 100 \qquad \text{Equation VI-1}$$

where A_0 and A_1 are the absorbance of the control and the samples, respectively.

VI-3.4.5. Swelling and stability.

The ALA and ALAC-based beads' swelling ability was assessed by immersing the beads in PBS for up to 7 days at 37 °C. The swollen beads' weight was accessed after the excess surface water removal.

The percentage of water uptake was determined using Equation VI-2, where *Ws* is the weight of the swollen sample, and *Wd* is the weight of the dry sample.

$$Water\ uptake = \left[\frac{Ws-Wd}{Wd}\right] \times 100 \qquad \text{Equation VI-2}$$

VI-3.4.6. Ch[Caffeate] release

The release of Ch[Caffeate] from the beads was evaluated following a previously described procedure [5]. Briefly, the dried ALA and ALAC beads were emerged in PBS pH 7.4, at 37 °C, in the dark. After 30min, 1h, 2h, 3h, 4h, 1 day, 3 days, and 7 days, 1mL of the PBS solution was collected, and its absorbance was read in a microplate reader (Synergy HT, BIO-TEK, Winooski, VT, USA) at 285 nm. The same volume of fresh PBS was added to the vessels. The cumulated percentage of Ch[Caffeate] released from the samples was determined according to Equation VI-3

$$Cumulative\ release\ (\%) = \frac{V_0 C_n + V C_{n-1} \times 100}{M} \qquad \text{Equation VI-3}$$

where, C_{n-1} and C_n is the Ch[Caffeate] concentration at times n-1 and n, V0 is the initial volume of the Bio-IL release medium, V is the withdraw volume, and M is the Ch[Caffeate] mass loaded in the 10mg of beads, the amount used for each condition in the assay. Calibration curves were established with concentrations from 0.01% (w/v) to 5% (w/v) and from 0.025% (w/v) to 5% (w/v), for Ch[Caffeate] and ACE, respectively.

VI-3.5. Cell Culture Studies

Chondrogenic ATDC5, a mouse chondrocyte teratocarcinoma-derived cell line, was cultured in Dulbecco's Modified Eagle Medium: Nutrient Mixture F-12 (DMEM/F12, Thermo Fisher Scientific, USA) supplemented with 10% fetal bovine serum (FBS; Alfagene, Portugal) and 1% antibiotic/antimycotic solution (final concentration of penicillin 100 units/mL and streptomycin 100 mg/mL; Alfagene, Portugal). ATDC5 cells were cultured in a 5% CO_2 incubator at 37 °C, until confluency was reached. Confluent ATDC5 were harvested and seeded at a density of 4 000 cells per well in a 24-well plate. ALA

and ALAC-based beads were added to the culture medium 24h later. Triplicates of each condition were collected after 1, 7, 14, and 21 days to perform the following biochemical assays.

VI-3.5.1. Cell viability

The viability of the ATDC5 cells was determined using a CellTiter 96® AQueous One Solution Cell Proliferation Assay (MTS, Promega). Following the contact with the ALA and ALAC-based beads during the stated time points, a mixture containing serum-free cell culture medium and MTS reagent at a 5:1 ratio was added to the cells and incubated for 3 h. The optical density was read (OD 490 nm).

The cell viability was also evaluated by fluorescence labeling using a live/dead assay. The ALA and ALAC-based beads were removed from the culture medium, and the cells were washed with sterile PBS. ATDC5 cells were further incubated with 1 mg/mL calcein acetoxymethyl (Invitrogen, 1:500) and 1.5 mM propidium iodide (PI, Invitrogen, 1:1000) solution in PBS for 15 min at 37 °C and washed with sterile PBS. Further, the samples were visualized using a confocal laser scanning microscope (Olympus FV1000). The Zen software was used to evaluate the obtained images.

VI-3.5.2. Cell proliferation

A fluorimetric PicoGreen double-stranded DNA assay was used to access ATDC5 cell proliferation, following the manufacturer's instructions (Quant-iT™ PicoGreen™ dsDNA Kit, P7589, Invitrogen). After each defined time-point, the cells were rinsed with PBS. Afterward, 1 ml of ultra-pure water was added to each well, and the plates were stored at -80 °C until analyses. The fluorescence was measured with a microplate reader (Synergy HT, BIO-TEK, Winooski, VT, USA) at 480 and 520 nm. The concentration of DNA was calculated using a standard curve ranging from 0–2 $\mu g\ ml^{-1}$, which correlates the dsDNA amount to the fluorescence values.

VI-3.5.3. Cell morphology

The morphology of the ATDC5 cells after contacting with the beads was evaluated using confocal microscopy (CLSM). Firstly, the cells were fixed with 10 % formalin for 30 min. The fixed cells were formerly incubated with 1 % bovine serum albumin (BSA) for 30 min, followed by permeabilization using 0.1 % Triton X-100 for 5 min. After, the cells were incubated with rhodamine-phalloidin at room

temperature (RT) for 20 min, followed by washing with PBS and staining with 5 µg ml-1 4',6-Diamidine-2'-phenylindole dihydrochloride (DAPI), for 30 min. The fluorescence images from the stained cells were obtained using a confocal laser scanning microscope (Olympus FV1000), and the Zen software was used to evaluate the acquired images.

VI-3.5.4. GAGs formation evaluation

VI-3.5.4.1 *Dimethyl methylene blue (DMB) assay*

The chondrogenic ECM formation was detected after 14 and 24 days of culture using a GAGs quantification assay [28]. The GAG standards were obtained by preparing a chondroitin sulfate solution that ranged from 0 to 50µg/ml. To each well of a 96-well plate were added samples or standards in triplicate, and then the dimethyl methylene blue reagent (DMB, Sigma-Aldrich) was added. The OD was immediately measured at 525 nm on a microplate reader (Synergy HT, BIO-TEK, Winooski, VT, USA). A standard curve was created, and GAG sample values were read from the standard graph.

VI-3.5.4.2 *Alcian blue staining*

Proteoglycan synthesis was evaluated by staining the ATDC5 cells with Alcian blue (Sigma-Aldrich). Cells were fixed in 1% w/v acetic acid solution for a few seconds and stained with 1% Alcian blue 8GX in 0.1 M HCl for 1 h. Finally, cells were washed in dH_20, and images were captured using a Leica DM750 Leica DM750 microscope.

VI-3.5.5. Therapeutic efficacy

The anti-inflammatory potential of the developed ALA and ALAC-based beads was assessed using an *in vitro* model consisting of a THP-1 cell line stimulated with lipopolysaccharide (LPS) (Sigma-Aldrich, St. Louis, MO, USA) [29]. As previously reported [27], THP-1 cells were seeded at a density of 1×10^6 cells/mL using RPMI medium with 100 nM phorbol 12-myristate-13 acetate (PMA) (Sigma-Aldrich, St. Louis, MO, USA) for 24 h. On the following day, the RPMI + PMA medium was removed, the cells were rinsed twice with fresh RPMI, and 500ml of RPMI medium was added to the differentiated cells (without PMA) and incubated for 48 h. After, and aiming to induce the inflammatory response, THP-1 cells were

incubated for 5 h with 100 ng mL^{-1} of LPS in RPMI. The cells were then cultured up to 7 days, and after 1, 3 and 7 days, the culture medium was removed and stored at −80 ◦C for further analysis.

The TNF-α and IL-6 concentration in the RPMI after contacting with the beads was further evaluated using a Human TNF-alpha DuoSET ELISA (R&D Systems, Minneapolis, MN, USA) kit, Human IL-6 DuoSET ELISA (R&D Systems, Minneapolis, MN, USA) kits and DuoSet Ancillary Reagent Kit 2 (R&D Systems, Minneapolis, MN, USA). The analysis was performed according to the manufacturers' indications. A microplate reader (Synergy HT, BIO-TEK, Winooski, VT, USA) was used to access the optical density (450 nm) of the solutions.

VI-3.6. Statistical analysis

Triplicate assessments were performed for all quantitative experiments, with the results expressed as means ± standard deviation. Data statistical analysis was conducted on GraphPadPrism v.8.0 (GraphPad Software, San Diego, http://www.graphpad.com). Differences between the groups at $p \leq 0.05$ were considered to be statistically significant.

VI-4. RESULTS AND DISCUSSION

ALAC-based architectures were developed using sustainable procedures which involved the combination of natural polymers (ALG and ACE), Bio-ILs (Ch[Caffeate]), and green processing methods, including extrusion deeping and freeze-drying. ALG is a water-soluble marine polymer, highly stable and with controllable gelation in the presence of di- or polyvalent cations, usually described by the egg-box model [23,24,30]. The presence of Ca^{2+} traces in ACE composition, the main polysaccharide in aloe vera leaves, and its cytocompatibility led to the exploration of its gel formation potential with ALG, as reported in previous work from our group, aiming different biomedical applications [24]. Herein, a Bio-IL with anti-oxidant and anti-inflammatory properties, Ch[Caffeate], was synthesized and included in the beads at different concentrations, as described in Table VI-1 [5].

VI-4.1. Physico-chemical and morphological characterization of the ALG/ACE-Ch[Caffeate] beads

Firstly, the purity of the synthesized Bio-IL, Ch[Caffeate], obtained as a white solid, was confirmed by NMR (Supplementary Figure VI-1). By its analysis, it was possible to ensure the success in the Ch[Caffeate] synthesis and its purity by the presence of the peaks corresponding to the $N(CH_3)_3$ group in the cholinium cation, as a singlet at 3.11 ppm; two multiplets corresponding to 2H between 3.53-3.51 and 4.04-4.08, corresponding to $NC\underline{H}_2CH_2OH$ and $NCH_2C\underline{H}_2OH$, respectively. Moreover, the peaks corresponding to the aromatic ring on the Caffeate acid structure are duplets at 6.35 ppm, 6.94 ppm, 7.19 ppm, and 7.09 ppm and as a doublet, representing the equivalent hydrogens in the structure at 6.74 ppm [5]. The NMR spectra of ACE and the different ACE/Ch[Caffeate] solutions, further used in the beads production, are also presented in Figure VI-2. By its analysis, we confirmed the presence of both components, Ch[Caffeate] and ACE, in the mixtures. No significant changes were observed in the Ch[Caffeate] peaks in the mixtures compared to its pure form, indicating the absence of aggregates or chemical bonds, as schematized in Scheme VI-2. A similar observation was observed in other NMR studies involving the IL 1-butyl-3-methylimidazolium chloride and the natural polymer cellulose to produce ion gels [31]. In that study, no splitting of the resonance lines due to the chemical shift of different aggregates was observed, suggesting that aggregates were not formed in the mixtures [31]. In another study, the authors reported the use of ILs (1-(3-aminopropyl)-imidazole) to modify sodium alginate magnetic nanoparticles, aiming lipase immobilization, and the NMR of the final gel confirmed, once again, the presence of both components [32]. Moreover, the magnitude/intensity of the signals corresponding to the Bio-IL, Ch[Caffeate], increases with the Bio-IL concentration in the mixtures. This result was expected since the intensity of NMR resonance signals should be proportional to the molar concentration of the compound in the sample [33].

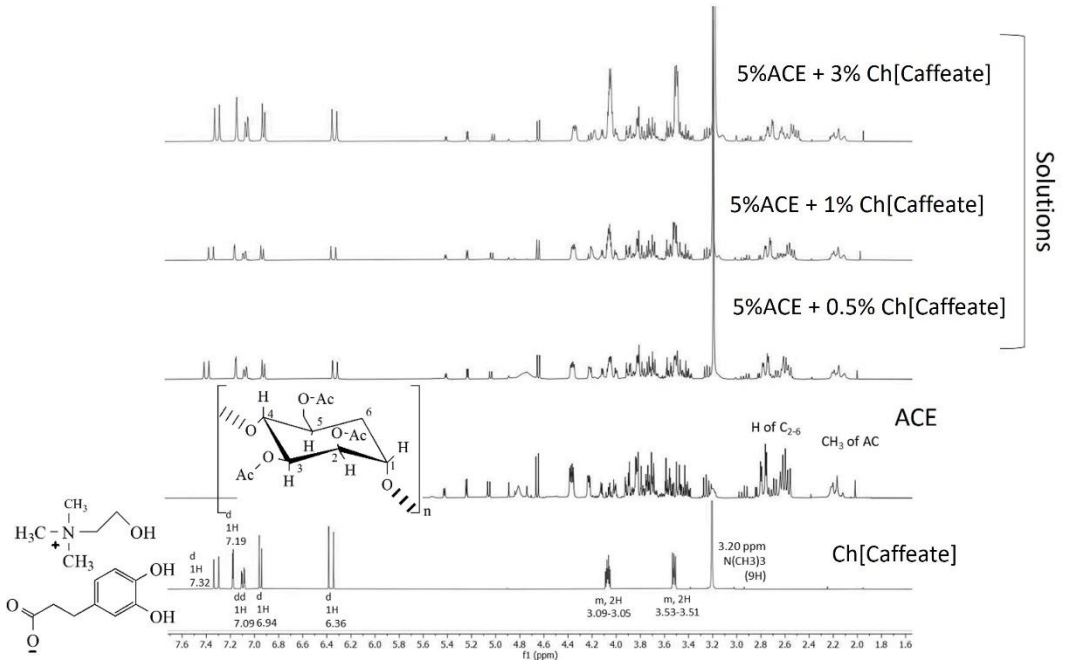


Figure VI-2 - NMR spectra of Ch[Caffeate], ACE, and the different ACE/Ch[Caffeate] mixtures, used for the beads preparation. Chemical shift in parts per million (ppm).

Following the extrusion dipping, the beads were immersed in a $BaCl_2$ bath, as depicted in Scheme VI-1, to form a more stable ALG/ACE system. ACE presents traces of Ca^{2+}, consequently leading to the formation of fragile beads. Further, the samples were rinsed with PBS, frozen at -80 °C, and freeze-dried. Scheme 2 are depicted the interactions expected between the Ba^{2+} and the remaining free COO^- groups in ALG. Previous studies have used the Ba^{2+} anion to form ALG gels instead of the traditional Ca^{2+} [25,34]. The results have shown that Ba^{2+} has an extreme effect on ALG gel strength, significantly increasing their stability [34].

The morphology of the surfaces and cross-sections of the developed ALA and ALAC beads was evaluated by SEM (Figure VI-3). The surface of the beads presents considerable roughness, while their cross-sections show the expected porous and open structure since alginates are known to form gels with interconnected pores by ionotropic gelation in the presence of di- cations [35]. The mean pore size values achieved were 209.46 µm, 209.16 µm, 221.30 µm, and 217.56 µm for ALA, ALAC0.5, ALAC1, and ALAC3, respectively, with no significant differences among the samples. According to these results, we conclude that the different Ch[Caffeate] concentrations incorporated in the beads did not significantly influence their porosity, suggesting that the cohesion of the structure is mainly driven by the ionic cross-linking of ALG in the presence of calcium ions. In this case, the addition of di- cations, Ca^{2+} from the ACE, as cross-linker to the ALG solution induces the alignment of the G-blocks, being the calcium ions bound between the two chains like eggs in an egg box. Therefore, the reactivity of Ca^{2+} to ALG is a consequence

of the dimer association of the G-block regions, and the pore size depends on the amount of Ca^{2+} in the system [35,36]. Herein, the ACE concentration (5% (w/v)) is kept throughout the experiment. Consequently, no significant differences were observed in the pore size values.

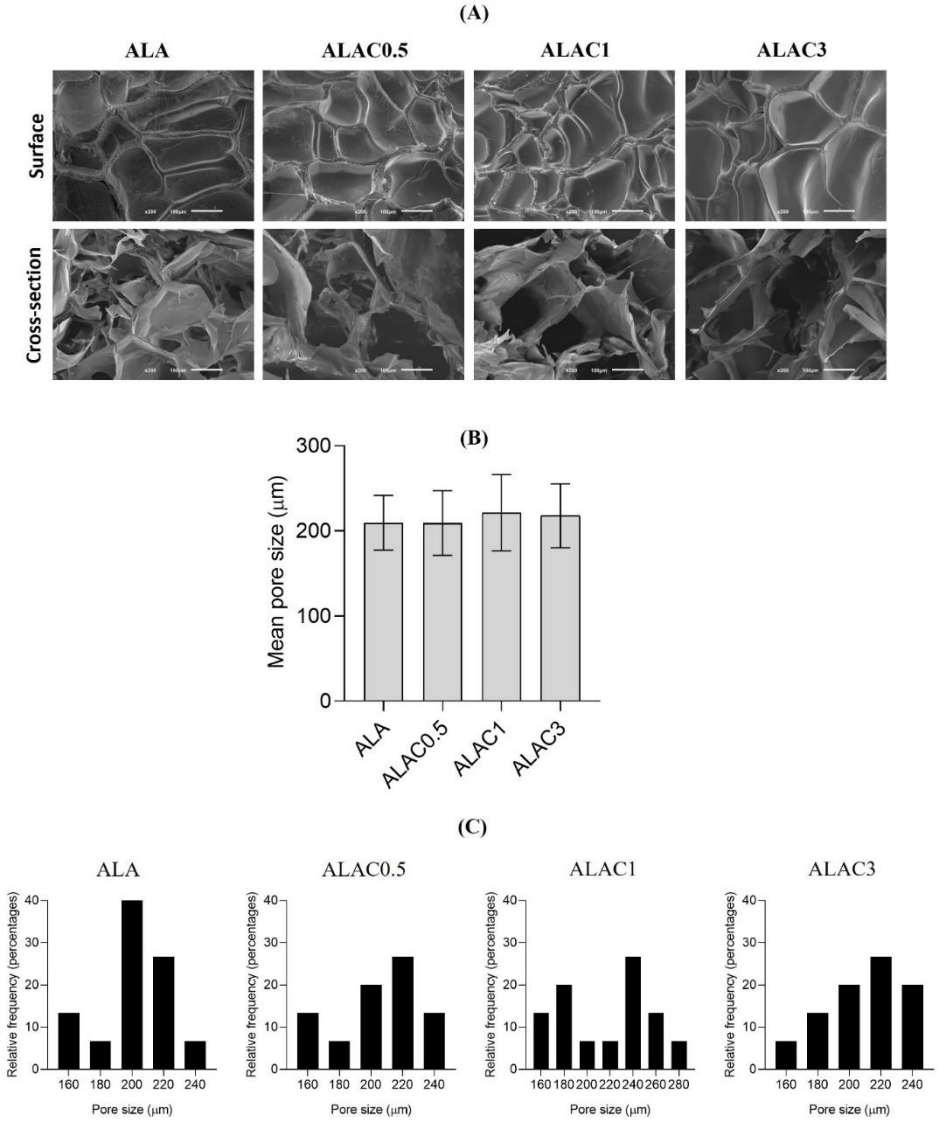
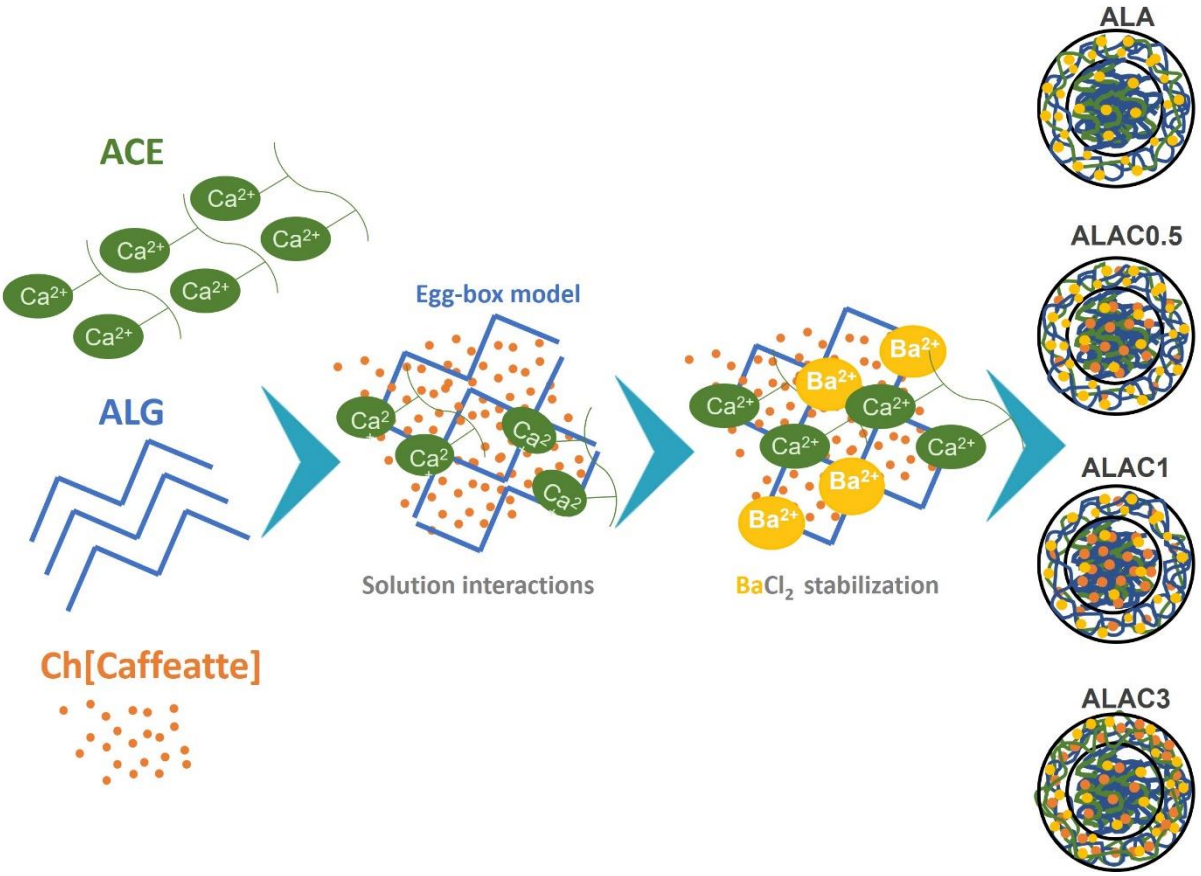


Figure VI-3 (A) SEM images of the ALA and ALAC beads surfaces and cross-sections; (B) mean pore sizes; data represent ±SD (*$p < 0.05$, one-way ANOVA) and (C) pore size distribution.



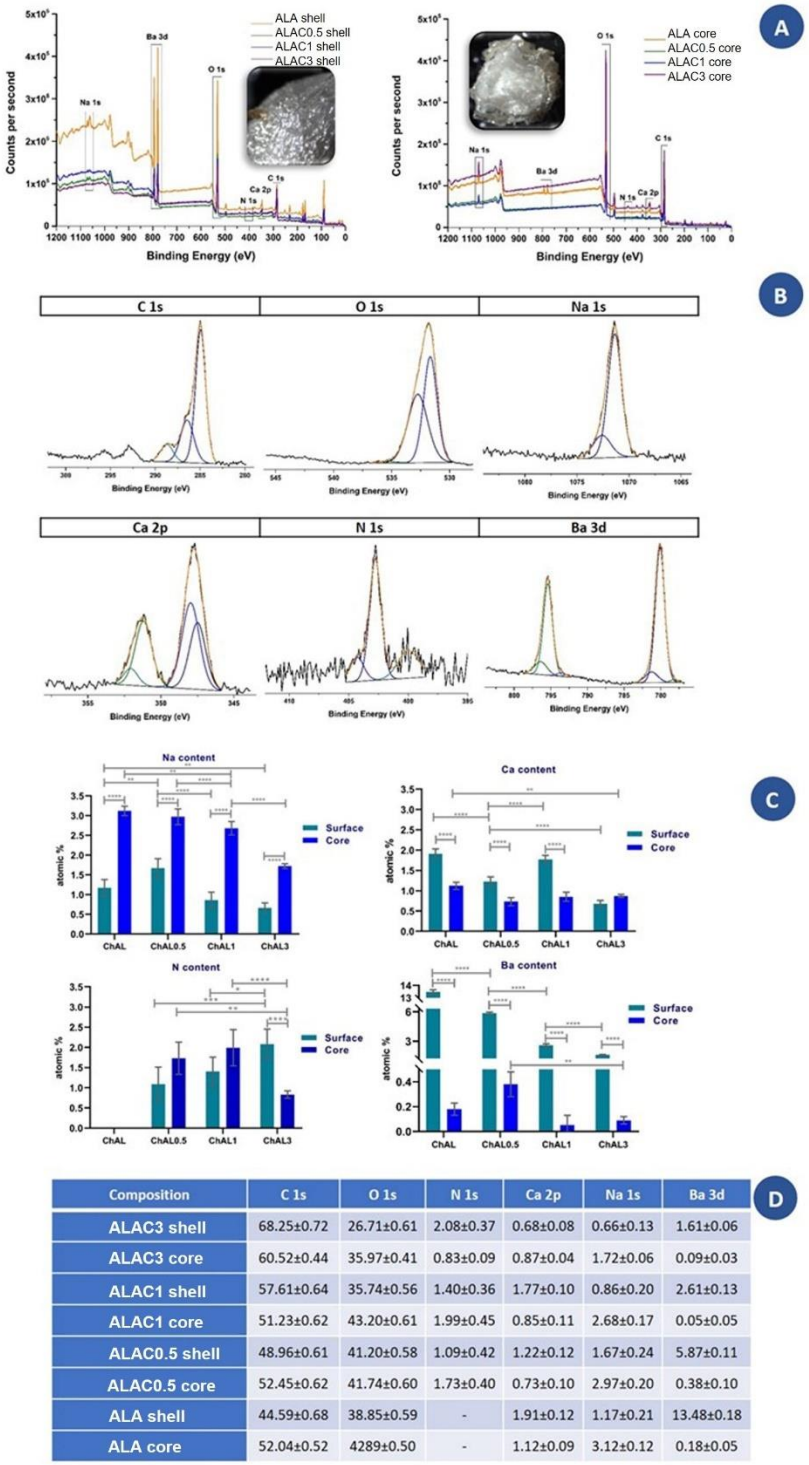
Scheme VI-2 - Schematic representation of the beads components in the mixture and their distribution over the structure of the beads following immersion in the $BaCl_2$ bath and freeze-drying process.

The XPS analysis performed on the shells and cores of the designed beads allowed us to construct a hypothesis of the distribution of the polymer into the 3D architectures. The survey spectra, Figure VI-4A, confirmed the presence of the characteristic components present in each formulation, particularly carbon, oxygen, calcium, sodium, and barium, for all samples and nitrogen only for the ALAC formulations. Their distribution was analysed by high-resolution analysis. The achieved data is depicted in Figure VI-4B to Figure VI-4D. The schematic representation of the interactions and the distribution of the beads components is depicted in Scheme VI-2. As expected, the Ba ion present in the stabilization bath is preferentially localized at the beads' surface, reducing the amount of the compound detected at the core of the beads. This difference is more pronounced for the ALA sample, where the barium amount at the surface is significantly higher than in the ALAC beads surfaces, with a tendency to decrease with the increase of the Ch[Caffeate] content.

It is also noted a homogeneous distribution of the Ch[Caffeate] into the structures for ALAC0.5 and ALAC 1; still, for ALAC 3 the Ch[Caffeate] is preferentially located at the bead surface, which may influence its release profile. Considering the composition of the beads along the structure is possible to hypothesize

that the increase of Ch[Caffeate] in the structure promotes a change in the polymer's network organization. For the ALA, ALAC0.5, and ALAC1 formulations, ACE is predominantly at the surface and ALG at the core, similar to the earlier reported for ACAL2 structure [24]. On the other hand, the increase of Ch[Caffeate] on the formulation to 3% (ALAC3) promoted a more homogeneous ACE distribution along the architecture, remaining the core of the bead mostly composed of ALG.

According to this hypothesized model of polymer organization, the reduction of the ALG amount at the beads' surface may justify the reduction of the barium ions required for the stabilization of the structure and consequently detected at the surface of the beads. The exposed hypothesis is coherent with the expected as the ALG solution is extruded into an ACE bath, inducing the formation of a shell. This also agrees with the microscopical images of the beads (insert in Figure VI-4A), where a white core is observed covered by a slightly yellow shell, due to the presence of ACE.



Composition	C 1s	O 1s	N 1s	Ca 2p	Na 1s	Ba 3d
ALAC3 shell	68.25±0.72	26.71±0.61	2.08±0.37	0.68±0.08	0.66±0.13	1.61±0.06
ALAC3 core	60.52±0.44	35.97±0.41	0.83±0.09	0.87±0.04	1.72±0.06	0.09±0.03
ALAC1 shell	57.61±0.64	35.74±0.56	1.40±0.36	1.77±0.10	0.86±0.20	2.61±0.13
ALAC1 core	51.23±0.62	43.20±0.61	1.99±0.45	0.85±0.11	2.68±0.17	0.05±0.05
ALAC0.5 shell	48.96±0.61	41.20±0.58	1.09±0.42	1.22±0.12	1.67±0.24	5.87±0.11
ALAC0.5 core	52.45±0.62	41.74±0.60	1.73±0.40	0.73±0.10	2.97±0.20	0.38±0.10
ALA shell	44.59±0.68	38.85±0.59	-	1.91±0.12	1.17±0.21	13.48±0.18
ALA core	52.04±0.52	4289±0.50	-	1.12±0.09	3.12±0.12	0.18±0.05

Figure VI-4 - Summary of XPS results A) Survey XPS scans of the core and shell of ALA and ALAC beads with inserted representative microscopical images of the beads' surface and core; B) Regions high-resolution representative spectra of ALA and ALAC beads for the interest elements regions; C) Relevant elements content in the structures; and D) Table containing the composition of the shell and core of the ALA and ALAC beads.

The local inflammatory response sideways with aging and/or mechanical load strongly contributes to increased oxidative stress in OA [37,38]. The detrimental effect of oxidative stress on cells and its association with the disease progression led some authors to propose the regulation of oxidative stress as a potential new target for disease therapy [39]. Envisioning this approach, the antioxidant activity of Caffeate acid, Ch[Caffeate], and the developed matrices was evaluated using the DPPH radical scavenging assay. The results are depicted in Figure VI-5, and show that the antioxidant activity of the samples was maintained up to 24h either in the precursor, Caffeate acid, and the synthesized Bio-IL, Ch[Caffeate]. Caffeate acid was used as the anionic moiety for the Ch[Caffeate] synthesis and as a positive control for the DPPH radical scavenging assay. Caffeate acid is widely known for its antioxidant properties owned by the presence of two hydroxyl groups on its aromatic ring [40]. ALA and ALAC0.5 present similar antioxidant activity behaviors, reaching their maximum (98.7 % and 97.9 %, respectively) after 24h. According to this, the antioxidant activity in these formulations is not directly associated with the Ch[Caffeate], but to the ACE present in both formulations [41]. Several studies have reported the antioxidant properties of ACE, and its benefits in pharmacological and biological applications, namely wound healing management, neuroprotective effects, and other pathologies, where the reduction of the damage caused by reactive oxygen species (ROS) is vital [41,42]. In our study, the intrinsic features of ACE, such as antioxidant activity, would reinforce the overall activity of the developed structures. Still, the antioxidant activity of the beads was higher in the ALAC1 and ALAC3 formulations, the ones containing higher amounts of Ch[Caffeate]. We expected that the ALG and ACE interactions would be stronger than those between the Ch[Caffeate] and these compounds, mostly due to the Ca^{2+} traces in the ACE composition [24]. Moreover, this theory is also supported by the NMR assay performed on the Ch[Caffeate]/ACE mixtures (Figure VI-2), which demonstrated that no specific interactions occur between ACE and Ch[Caffeate]. Following the rationale, the Ch[Caffeate] release from the beads would be more immediate than the ACE. Therefore, the formulations containing higher amounts of Ch[Caffeate] revealed higher antioxidant activity values at the initial time points (1h and 4h). After 24h, the antioxidant activity was similar in all formulations, with ALAC1 and ALAC3 revealing a gradual increase in the antioxidant activity over time, reaching the maximum values after 24h (97.2% and 97.8%, respectively).

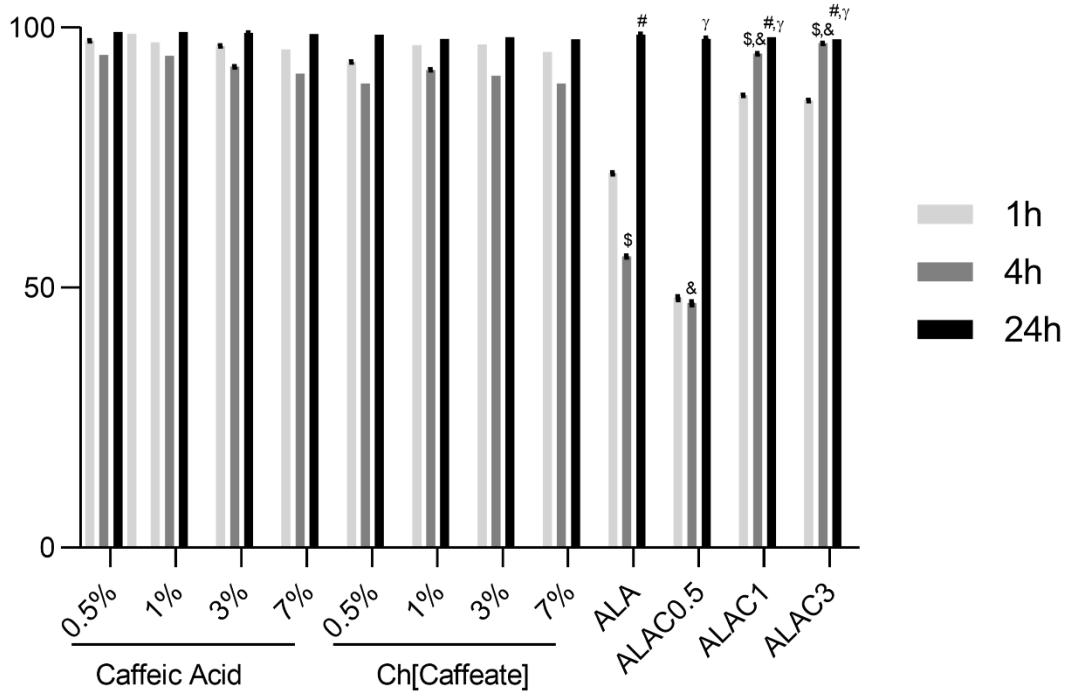


Figure VI-5 - Antioxidant activity of Caffeate acid, Ch[Cafeic], and the developed ALA and ALAC beads. Symbols and letters denote statistically significant differences with different degrees of confidence. Symbol $ denotes statistical differences for $p < 0.001$ between ALA and ALAC1 and ALAC3 at 4h; & denotes statistical differences for $p < 0.0001$ between ALAC0.5 and ALAC1 and ALAC3 at 4h; # denotes statistical differences for $p < 0.0001$ between ALA and ALAC1 and ALAC3 at 24h; γ denotes statistical differences for $p < 0.0001$ between ALAC0.5 and ALAC1 and ALAC3 at 24h. Data represent ±SD (*$p < 0.05$, 2way ANOVA).

The water uptake of the beads was evaluated after immersion into a PBS solution for up to 7 days (Figure VI-6A). In tissue engineering, it is well known that the ability to take up fluids from the surrounding medium plays a vital role in their applicability [43]. The water uptake profile is similar among all formulations and increases over time. All samples present considerably high swelling ability, and the maximum values are obtained after 7 days (2443 %, 2168 %, 1885 % and 2048 % for ALA, ALAC0.5, ALAC1 and ALAC3, respectively). The statistical analysis showed only significant differences between ALAC0.5 and ALAC3 after 1 day and, ALA and ALAC3, after 7 days. After immersion in the PBS solution, the freeze-dried beads became hydrated and revealed a gel-like appearance (Figure VI-6A). Previous studies reported that the swelling of ion-crosslinked sodium alginate beads mostly occurs by ion-exchange processes, particularly by the Ca^{2+} release from the beads [30]. In our study, we can hypothesize that when the ALA and ALAC beads are immersed in the PBS solution, the Na^{+} anions from the PBS exchange with the Ca^{2+} binding with the COO^{-} in the ALG structure [30]. This phenomenon results in the electrostatic repulsion among negatively charged $–COO^{-}$ groups, resulting in the chain relaxation and increasing the

beads swelling along the experiment time (up to 7 days). Previous studies have also shown that the use of Ba^{2+} in the ALG hydrogel beads formation increases their swelling potential [34]. In Figure VI-4C, the amount of Ba^{2+} in the different formulations follows the order ALA > ALAC0.5 > ALAC1 > ALAC3, which corresponds to the tendency observed for the swelling ability of the constructs. Meaning that, our results are in accordance with the ones previously published [34].

The stability of the beads in PBS was evaluated through weight loss quantification (Figure VI-6B). The maximum values achieved were 19%, 27%, 33%, and 39% obtained for ALA, ALAC0.5, ALAC1 and ALAC3, respectively, for up to 7 days. Besides, no significative differences were observed, a clear tendency was noted, an increase in the weight loss following the increase of Ch[Caffeate] in the matrices (0, 0.5, 1, and 3%(w/v), respectively), that is possibly a consequence of its release from the structure, along time. In all studied time points, except for 1 and 2 days, statistical differences were observed between ALA and ALAC3, which corresponds to the formulation without Ch[Caffeate] in its matrix and the one containing the higher amount of this compound. The chain relaxation, a consequence of the electrostatic repulsion among negatively charged $–COO^-$ groups referred to above, may contribute to the Ch[Caffeate] release, which is thought to be trapped in the network previously formed in the presence of divalent anion. Besides, Ch[Caffeate] was previously proved to be water soluble [22]; therefore, we hypothesized that these weight loss values might correspond to the dissolution of Ch[Caffeate] into PBS.

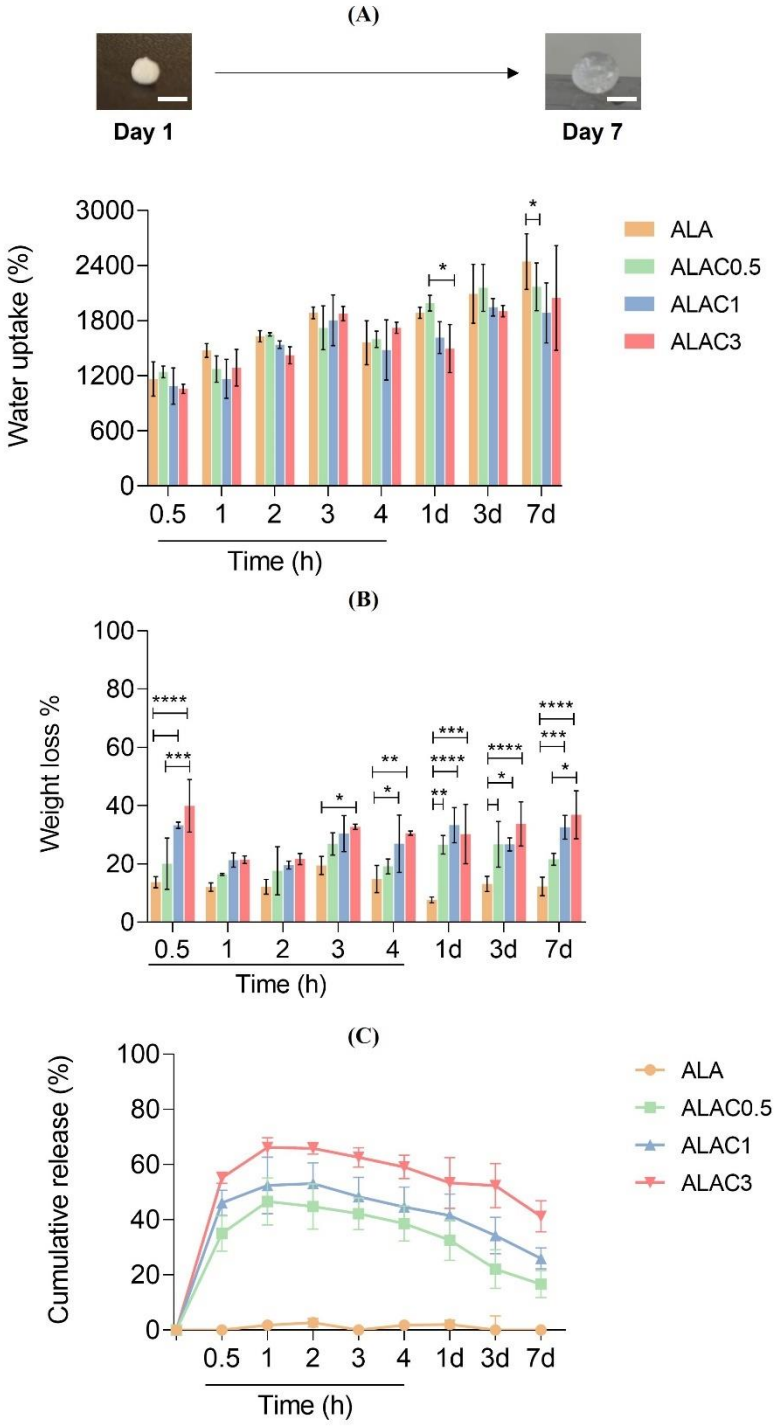


Figure VI-6 - (A) Water uptake, (B) stability in PBS of the developed ALA and ALAC beads. Scale bar 2mm. Data represent ±SD (*p < 0.05, 2way ANOVA) and (C) Cumulative percentage release of Ch[Caffeate] from the ALAC beads into PBS, up to 7 days.

The cumulative release of Ch[Caffeate] from the developed ALA and ALAC beads was studied by their immersion in a PBS solution, at pH 7.4, for up to 7 days. The data (Figure VI-6C.) showed that the cumulative release percentage from the beads is proportional to the Ch[Caffeate] concentration in the matrices, meaning that a higher Ch[Caffeate] content leads to a higher cumulative release percent value.

It is clear an initial burst release phase that, in some cases, may be effective in treating disease [44], followed by a prolonged release, up to 7 days. These findings support the hypothesis that the weight loss profile observed for the ALA and ALAC beads (Figure VI-6B) was related to Ch[Caffeate] release. In addition, considering the XPS data (Figure VI-4), and the fact that the N element, associated with the cholinium cation in the Ch[Caffeate] structure, is predominantly present in the ALAC3 surface, rather than the core, contrarily to what is verified for ALAC0.5 and ALAC1. We hypothesize that its surficial location on the structure of the bead promoted its faster release, contributing to higher weight loss % at lower time points. Moreover, and considering the proximity of the Ch[Caffeate] (285 nm) and ACE (300 nm) [23] maximum absorbance peaks, we supposed that the ACE release might cumulatively contribute to the absorbance values herein observed.

VI-4.2. Cell culture studies

VI-4.2.1. Biological beahvior

The cartilage structure and function is controlled by chondrocytes that regulate extracellular matrix (ECM) turnover of components such as collagen, glycoproteins, proteoglycans, and hyaluronan. These components are responsible for maintaining tissue homeostasis [13,45]. The imbalance in the metabolic activity of these cells, which happens mostly due to proinflammatory cytokines and growth factors that have anabolic and catabolic effects, leads to degenerative diseases like OA [45]. Considering these facts, the influence of ALA and ALAC beads on ATDC5 chondrocyte-like cells was studied. ATDC5 chondrocyte-like cells were chosen since they are an excellent *in vitro* cell model for chondrocyte research [46–48]. The ATDC5 cell viability and proliferation were evaluated by MTS, and DNA quantification assays (Figure VI-7A and Figure VI-7B). Although there were some significant differences between ALA and ALAC beads, the cell viability increased over time in all conditions, seeming to stabilize after 14 days, which is also corroborated by the CLSM images, which show very similar cell density between 14 and 21 days (Figure VI-7C). The same trend was observed for the DNA quantification results, indicating only significant differences after 21 days and between ALA and ALAC3. These results suggest that the increased metabolic activity over the culture time can probably be attributed to cell proliferation. The developed beads had no harmful effects on cell viability and proliferation in the ATDC5 cell line and promoted their growth and proliferation for up to 21 days. Moreover, the live-dead analysis indicated that ATDC5 cells were viable in all samples after 21 days of culture (Supplementary Figure VI-2). The images obtained by

CLSM (Figure VI-7C) confirmed that the cells kept their morphology and integrity following the culture time by F-actin staining (in red) and the nuclei (in blue). After 21 days of culture, ATDC5 cells show a flat morphology with an organized cytoskeleton in all studied conditions. Several works reported the successful use of ALG as a sustainable delivery system or as a hydrogel to support chondrocyte-like cell growth and proliferation, supporting its ability to restore cartilage [13,49]. Although, to our knowledge, there are no studies involving the use of ATDC5 cells in the presence of Bio-ILs. However, a positive biological response was observed when culturing human adipose stem cells in chitin and silk fibroin sponges containing cholinium acetate and cholinium gallate, respectively [27,50]. The same was verified for ACE, with some recent studies reporting its effects on cancer therapeutics, diabetes and skin disease management, and its immunomodulatory potential [51,52]. The presented results demonstrated that the bioactive Bio-IL, Ch[Caffeate], has no harmful effects on the ATDC5 chondrocyte-like cells' metabolic activity, proliferation, and structure up to 21 days of culture.

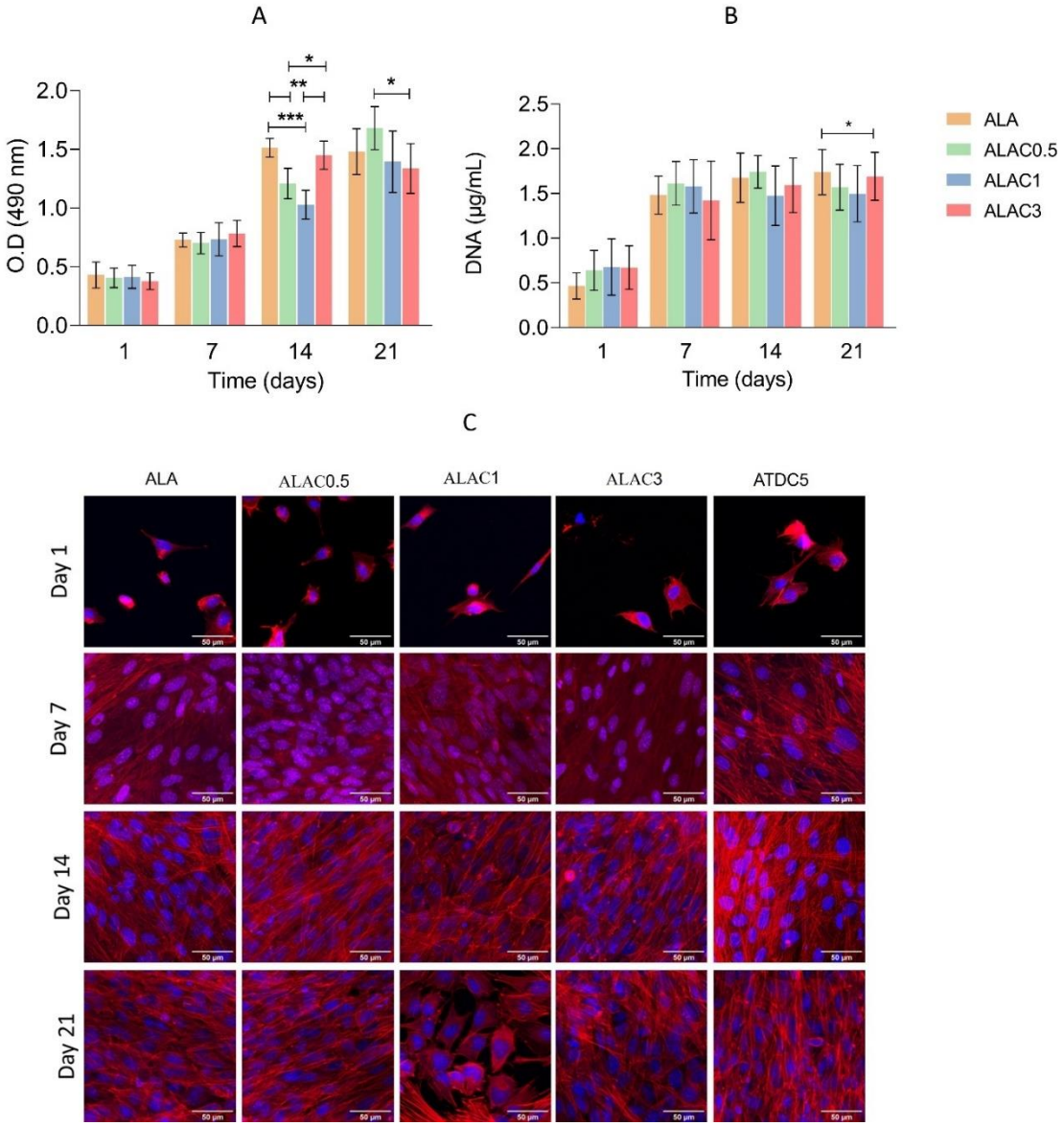


Figure VI-7 (A) Metabolic activity and (B) DNA content of ATDC5 cells after contacting with ALA and ALAC beads, up to 21 days; Data represent ±SD (*p < 0.05, **p < 0.005 and ***p < 0.0005, nonparametric Krustal-wallis test). (C) confocal laser micrographs of ATDC5 cells after contacting with ALA and ALAC beads, for up to 21 days. The cells were stained with rhodamine-phalloidin for actin filaments (red) and DAPI for nuclei (blue). Scale bar: 100 µm

VI-4.2.2. GAGs formation evaluation

GAGs are a typical component of cartilaginous ECM, and the breakdown of these proteoglycans leads to a reduction in the compressive stiffness of the tissue, which accelerates the rate of collagen loss [45]. The GAGs production in the ECM is vital for chondrocyte function and is involved in regulating the chondrocyte phenotype [28]. Herein, we observed the synthesis of GAGs after 14 days of culture, with a propensity to increase over the culture time (Figure VI-8A). Significant differences were observed after 21

days between ALA and the ALAC beads (ALAC0.5, ALAC1, and ALAC3), with ALAC3 revealing the higher GAGs content. These data suggested that the Ch[Caffeate] influences the GAGs production, which after 21 days increases proportionally to the Bio-IL content in the matrices. After 14 and 21 days, the cells were fixed and stained for GAGs using Alcian blue (Figure VI-8B) [46]. From the analysis of these images, we could observe that a large proportion of each ATDC5 monolayer was Alcian blue-positive, either after 14 and 21 days, demonstrating that ATDC5 cells produced a glycosaminoglycan (GAG)-rich ECM. Future studies involving the use of mesenchymal stem cells and the analysis of common chondrocyte molecular markers may confirm the chondrogenic lineage prevalence.

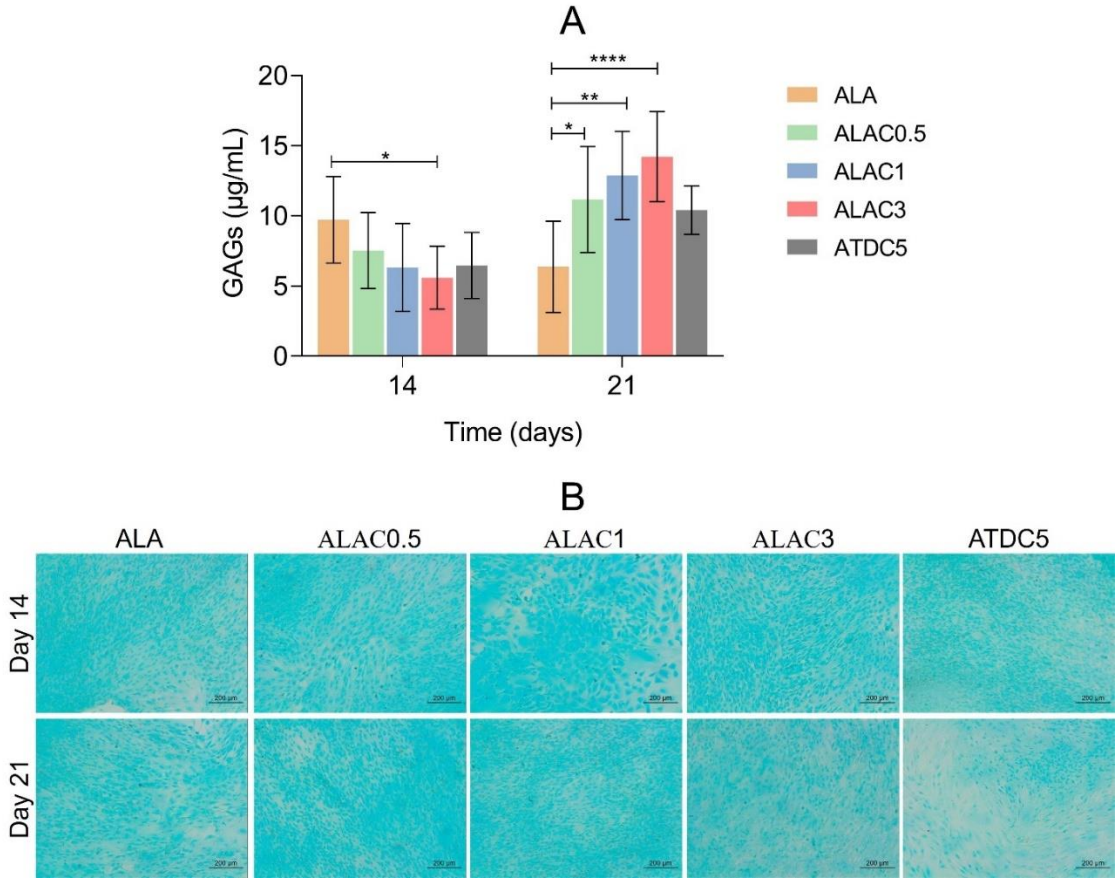


Figure VI-8 -. (A) GAGs quantification assay of ATDC5 cells (data represent ±SD (*p < 0.05, 2way ANOVA); and (B) Chondrocyte marker analysis on ATDC5 cells by histochemical staining of the proteoglycan's synthesis.

VI-4.2.3. Therapeutic efficacy

The secretion and detection of pro-inflammatory cytokines in the synovial fluid is common in patients with OA.[53,54] Tumour necrosis factor-alpha (TNF-α) release in the cartilage leads to the release of matrix metalloproteinases (MMPs) from synovial fibroblasts resulting in its destruction, inhibiting chondrogenesis through the nuclear factor-kB (NF-kB) pathway by downregulating the SOX9 production [55]. In some studies, cytokines such as TNF-α and IL-6 are used as tools for inducing OA and cartilage damage, since their effect in tissues makes it closely replicate the natural disease, contributing to the inflammatory effect of the synovium in the model [53,56,57].

Herein, the ALA and ALAC beads' capacity to decrease the levels of TNF-α and IL-6 present in the medium was evaluated using differentiated THP-1 cells, stimulated with LPS, to simulate the inflammatory condition in arthritis. Following the establishment of the inflammation, 7 conditions were tested: 1) cells without treatment, 2) cells differentiated with PMA but without LPS stimulation, used as control, 3) cells treated with betamethasone, 4) ALA, 5) ALAC0.5, 6) ALAC1 and 7) ALAC3. The established dosage of betamethasone, one of the corticosteroids of choice for the OA treatment, is 6mg/ml, the selected concentration to be used as a control [58]. Figure VI-9 shows the amount of free TNF-α and IL-6 over time of incubation with the ALA and ALAC beads. LPS has been proven to induce the production of pro-inflammatory cytokines in THP-1 cells, including TNF-α and IL-6 [59,60]. Both LPS-stimulated cells and ALA showed significant amounts of TNF-α and IL-6 over the culture time, indicating that the stimulation of cells was successfully achieved. In all studied time points, significant differences were observed between these and the ALAC beads (ALAC0.5, ALAC1, and ALAC3). The data presented in Figure VI-9 also shows a decrease in the TNF-α and IL-6 amounts in the samples containing Ch[Caffeate] in their matrices (ALAC0.5, ALAC1, and ALAC3). However, no significant differences were obtained among the three conditions (ALAC0.5, ALAC1, and ALAC3) containing Ch[Caffeate] in all studied culture times. Still, a trend was visible as the free TNF-α decreased over time. The blockage of TNF-α at early time points may be a consequence of the initial burst release of Ch[Caffeate] (Figure VI-6A.). A decrease in IL-6 was also observed over time, as the differences are more noteworthy between day 1 and day 3/day 7 than between the latter. Reducing these pro-inflammatory cytokines secretion is beneficial considering that their release from various cell types is responsible for OA progression, inducing synovial inflammation and cartilage degradation.[61–63] In addition to that, the observed prolonged release mechanism was able to maintain the therapeutic dose for more extended periods.

Overall, the findings concerning the TNF-α and IL-6 blockage by the developed ALAC beads suggested that all the loaded formulations (ALAC0.5, ALAC1, and ALAC3) can effectively reduce the secretion of these pro-inflammatory cytokines. As shown in previous studies, the *in vitro* inhibition of TNF-α and IL-6 is beneficial by improving osteochondral viability, proliferation, and chondrogenesis, enhancing the natural repair of chondral lesions, which occur in OA. [55]. Moreover, detecting these molecules in synovial fluid in osteoarthritic cartilage makes their inhibition an appealing potential target in disease treatment [54,57]. Far along, the inflammatory microenvironment and its regulations must be considered in cartilage management and replacement therapy as a path to improve the chances of effective joint mobility restoration [12].

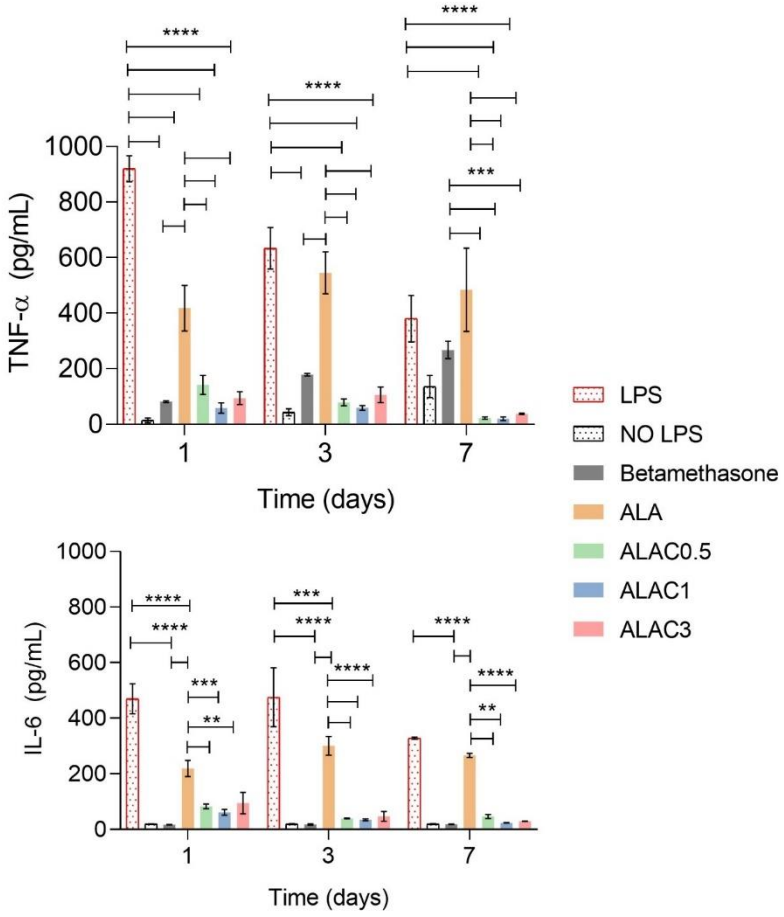


Figure VI-9 - Quantification of the TNF-α and IL-6 content in the medium in LPS and non-LPS stimulated cells, betamethasone treated cells, and in contact with the different ALA and ALAC beads. Data represent ±SD (*p < 0.05, 2way ANOVA).

VI-5. Conclusion

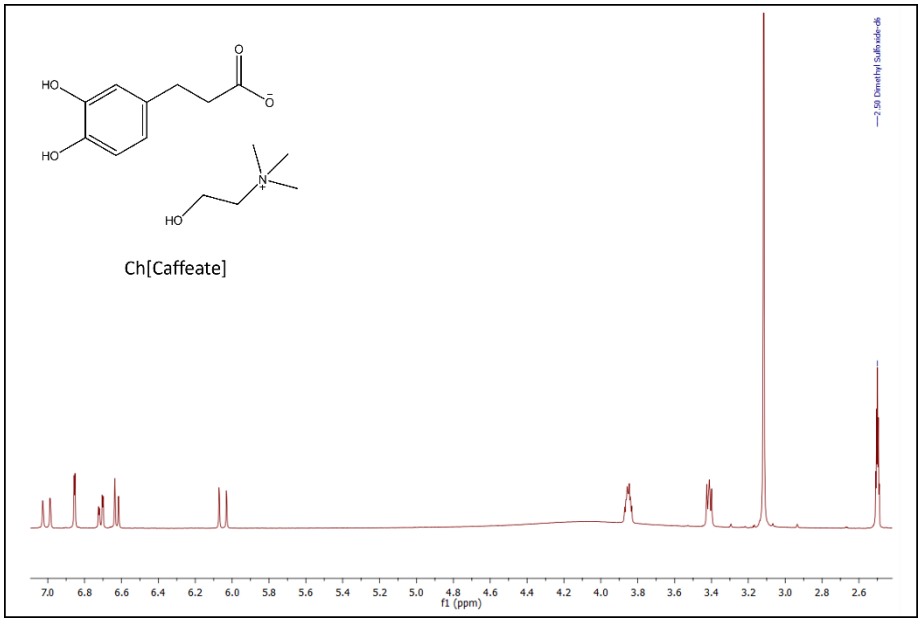
In summary, a sustainable, easily scaled-up, and physiologically relevant drug delivery system, with the potential to be explored for the delivery of sensitive drugs and biologically active molecules, was developed in mild conditions.

The fabricated porous and interconnected ALA and ALAC beads presented high swelling ability and a gel-like behavior, which are ideal for promoting greater drug encapsulation efficiencies, allowing the sustainable release of bioactive molecules, such as Ch[Caffeate]. Additionally, the produced beads could promote ROS scavenging while allowing ATDC5 chondrocyte-like cells to grow and proliferate, for up to 21 days, with ALAC3 outperforming the other tested conditions, due to the increased GAGs production, after 21 days of culture. ALAC beads also showed the ability to block the secretion of pro-inflammatory cytokines (TNF-α and IL-6) from differentiated THP-1 macrophages. Overall, the proposed strategy supports the great potential of green chemistry for health applications, including degenerative cartilage diseases, such as OA, based on the use of appropriate biological molecules and biodegradable materials.

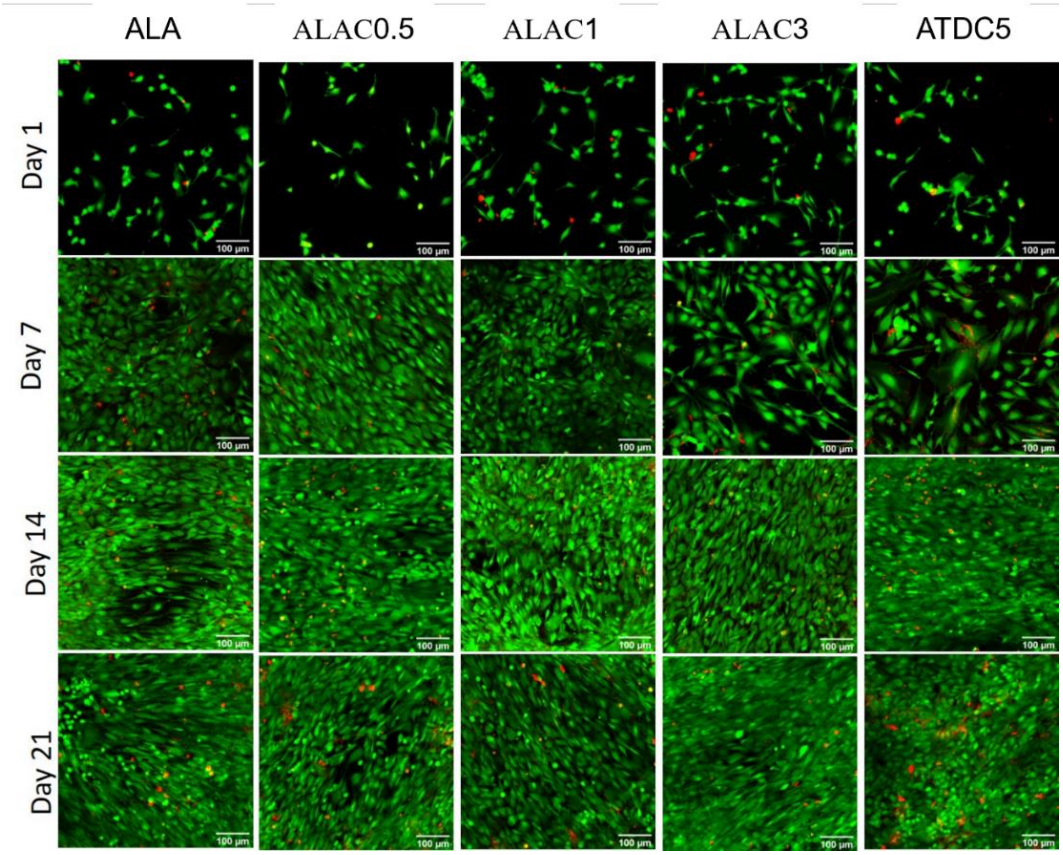
Acknowledgements

The authors especially acknowledge financial support from Portuguese FCT (PD/BD/135247/2017, SFRH/BPD/93697/2013 and CEECIND/01306/2018). This work is also financially supported by PhD programme in Advanced Therapies for Health (PATH) (PD/00169/2013), FCT R&D&I projects with references PTDC/BII-BIO/31570/2017, PTDC/CTM-CTM/29813/2017, and R&D&I Structured Projects with reference NORTE-01-0145-FDER-000021.

VI-6. SUPPLEMENTARY MATERIAL



Supplementary Figure VI-1 ^{1}H of pure Ch[Caffeate].



Supplementary Figure VI-2 - Confocal microscope projection image of the live/dead assay of ATDC 5 cells after contact with ChAL and ChAL-Ch[Caffeate] beads, up to 21 days.

VI-7. REFERENCES

[1] S.S. Silva, A.R.C. Duarte, J.F. Mano, R.L. Reis, Design and functionalization of chitin-based microsphere scaffolds, Green Chem. 15 (2013) 3252–3258. https://doi.org/10.1039/c3gc41060a.

[2] S.S. Silva, T.C. Santos, M.T. Cerqueira, A.P. Marques, L.L. Reys, The use of ionic liquids in the processing of chitosan / silk hydrogels for biomedical applications, Green Chem. 14 (2012) 1463–1470. https://doi.org/10.1039/c2gc16535j.

[3] A. Benedetto, P. Ballone, Room Temperature Ionic Liquids Meet Biomolecules: A Microscopic View of Structure and Dynamics, ACS Sustain. Chem. Eng. 4 (2016) 392–412. https://doi.org/10.1021/acssuschemeng.5b01385.

[4] J.M. Gomes, S.S. Silva, R.L. Reis, Biocompatible ionic liquids: Fundamental behaviours and applications, Chem. Soc. Rev. 48 (2019) 4317–4335. https://doi.org/10.1039/c9cs00016j.

[5] E.S. Morais, N.H.C.S. Silva, T.E. Sintra, S.A.O. Santos, B. Miguel, I.F. Almeida, P.C. Costa, I. Correia-sá, S.P.M. Ventura, A.J.D. Silvestre, M.G. Freire, C.S.R. Freire, Anti-inflammatory and antioxidant nanostructured cellulose membranes loaded with phenolic-based ionic liquids for cutaneous application, Carbohydr. Polym. 206 (2019) 187–197. https://doi.org/10.1016/j.carbpol.2018.10.051.

[6] W. Huang, X. Wu, J. Qi, Q. Zhu, W. Wu, Y. Lu, Z. Chen, Ionic liquids: green and tailor-made solvents in drug delivery, Drug Discov. Today. 25 (2020) 901–908. https://doi.org/10.1016/j.drudis.2019.09.018.

[7] K. Peng, Y. Gao, P. Angsantikul, A. LaBarbiera, M. Goetz, A.M. Curreri, D. Rodrigues, E.E.L. Tanner, S. Mitragotri, Modulation of Gastrointestinal Mucus Properties with Ionic Liquids for Drug Delivery, Adv. Healthc. Mater. 10 (2021) 1–14. https://doi.org/10.1002/adhm.202002192.

[8] E.E.L. Tanner, K.N. Ibsen, S. Mitragotri, Transdermal insulin delivery using choline-based ionic liquids (CAGE), J. Control. Release. 286 (2018) 137–144. https://doi.org/10.1016/j.jconrel.2018.07.029.

[9] A. Banerjee, K. Ibsen, T. Brown, R. Chen, C. Agatemor, S. Mitragotri, Ionic liquids for oral insulin delivery, 115 (2018) 1–6. https://doi.org/10.1073/pnas.1722338115.

[10] J.L. Escobar Ivirico, M. Bhattacharjee, E. Kuyinu, L.S. Nair, C.T. Laurencin, Regenerative Engineering for Knee Osteoarthritis Treatment: Biomaterials and Cell-Based Technologies, Engineering. 3 (2017) 16–27. https://doi.org/10.1016/J.ENG.2017.01.003.

[11] A. Kakkar, A. Singh, S.K. Saraswat, S. Srivastava, N. Khatri, R.K. Nagar, M. Kumar, P. Meena, R. Datt, S. Pandey, Cartilage repair using stem cells & biomaterials: advancement from bench to bedside, Mol. Biol. Rep. 47 (2020) 8007–8021. https://doi.org/10.1007/s11033-020-05748-1.

[12] X. Li, X. Wang, Q. Liu, J. Yan, D. Pan, L. Wang, Y. Xu, F. Wang, Y. Liu, X. Li, M. Yang, ROS-Responsive Boronate-Stabilized Polyphenol–Poloxamer 188 Assembled Dexamethasone Nanodrug for Macrophage Repolarization in Osteoarthritis Treatment, Adv. Healthc. Mater. 10 (2021) 1–11. https://doi.org/10.1002/adhm.202100883.

[13] L. Kou, S. Xiao, R. Sun, S. Bao, Q. Yao, R. Chen, Biomaterial-engineered intra-articular drug delivery systems for osteoarthritis therapy, Drug Deliv. 26 (2019) 870–885. https://doi.org/10.1080/10717544.2019.1660434.

[14] Y.P. Singh, J.C. Moses, N. Bhardwaj, B.B. Mandal, Overcoming the Dependence on Animal Models for Osteoarthritis Therapeutics – The Promises and Prospects of *In vitro* Models, Adv. Healthc. Mater. 10 (2021) 1–25. https://doi.org/10.1002/adhm.202100961.

[15] M. Rahimi, G. Charmi, K. Matyjaszewski, X. Banquy, J. Pietrasik, Recent developments in natural and synthetic polymeric drug delivery systems used for the treatment of osteoarthritis, Acta Biomater. 123 (2021) 31–50. https://doi.org/10.1016/j.actbio.2021.01.003.

[16] C. Antich, J. de Vicente, G. Jiménez, C. Chocarro, E. Carrillo, E. Montañez, P. Gálvez-Martín, J.A. Marchal, Bio-inspired hydrogel composed of hyaluronic acid and alginate as a potential bioink for 3D bioprinting of articular cartilage engineering constructs, Acta Biomater. 106 (2020) 114–123. https://doi.org/10.1016/j.actbio.2020.01.046.

[17] F. Comblain, G. Rocasalbas, S. Gauthier, Y. Henrotin, Chitosan: A promising polymer for cartilage repair and viscosupplementation, Biomed. Mater. Eng. 28 (2017) S209–S215. https://doi.org/10.3233/BME-171643.

[18] N. Goto, K. Okazaki, Y. Akasaki, K. Ishihara, K. Murakami, K. Koyano, Y. Ayukawa, N. Yasunami, T. Masuzaki, Y. Nakashima, Single intra-articular injection of fluvastatin-PLGA microspheres reduces cartilage degradation in rabbits with experimental osteoarthritis, J. Orthop. Res. 35 (2017) 2465–2475. https://doi.org/10.1002/jor.23562.

[19] Z. Zhang, G. Huang, Intra-articular lornoxicam loaded PLGA microspheres: Enhanced therapeutic efficiency and decreased systemic toxicity in the treatment of osteoarthritis, Drug Deliv. 19 (2012) 255–263. https://doi.org/10.3109/10717544.2012.700962.

[20] P. Arunkumar, S. Indulekha, S. Vijayalakshmi, R. Srivastava, Synthesis, characterizations, *in vitro* and *in vivo* evaluation of Etoricoxib-loaded Poly (Caprolactone) microparticles-a potential Intra-articular drug delivery system for the treatment of Osteoarthritis, J. Biomater. Sci. Polym. Ed. 27 (2016) 303–316. https://doi.org/10.1080/09205063.2015.1125564.

[21] A. Sulistio, F.M. Mansfeld, F. Reyes-Ortega, A.M. D'Souza, S.M.Y. Ng, S. Birkett, A. Blencowe, G.G. Qiao, C.B. Little, C.C. Shu, A.M. Bendele, D. Valade, A.C. Donohue, J.F. Quinn, M.R. Whittaker, T.P. Davis, R.J. Tait, Intra-articular Treatment of Osteoarthritis with Diclofenac-Conjugated Polymer Reduces Inflammation and Pain, ACS Appl. Bio Mater. 2 (2019) 2822–2832. https://doi.org/10.1021/acsabm.9b00232.

[22] T.E. Sintra, A. Luís, S.N. Rocha, A.I.M.C.L. Ferreira, F. Gonçalves, L.M.N.B.F. Santos, B.M. Neves, M.G. Freire, S.P.M. Ventura, J.A.P. Coutinho, Enhancing the antioxidant characteristics of phenolic acids by their conversion into cholinium salts, ACS Sustain. Chem. Eng. 3 (2015) 2558–2565. https://doi.org/10.1021/acssuschemeng.5b00751.

[23] L.C. Rodrigues, S.S. Silva, R.L. Reis, Acemannan-based films: an improved approach envisioning biomedical applications, Mater. Res. Express. 6 (2019) 095406. https://doi.org/10.1088/2053-1591/ab2f66.

[24] S.S. Silva, L.C. Rodrigues, R.L. Reis, An alternative approach to prepare alginate/acemannan 3D architectures, SN Appl. Sci. 1 (2019) 1–10. https://doi.org/10.1007/s42452-019-0690-2.

[25] L.L. Reys, V. Vaithilingam, M.M.J.P.E. Sthijns, E. Soares, T. Rademakers, R. Vries, S.G. Mohammed, D. Bont, M.J. Jetten, C. Hermanns, O.P. da S. Filho, A. Stell, N.I. Mourad, P. Gianello, V.L.S. LaPointe, S.S. Silva, R.L. Reis, T.H. Silva, A.A. Apeldoorn, Fucoidan Hydrogels Significantly Alleviate Oxidative Stress and Enhance the Endocrine Function of Encapsulated Beta Cells, Adv. Funct. Mater. 31 (2021) 1–16. https://doi.org/10.1002/adfm.202011205.

[26] S.B. Kedare, R.P. Singh, Genesis and development of DPPH method of antioxidant assay, J. Food Sci. Technol. 48 (2011) 412–422. https://doi.org/10.1007/s13197-011-0251-1.

[27] J.M. Gomes, S.S. Silva, E.M. Fernandes, F.C.M. Lobo, M. Martín-Pastor, P. Taboada, R.L. Reis, Silk fibroin/cholinium gallate-based architectures as therapeutic tools, Acta Biomater. 147 (2022) 168–184. https://doi.org/10.1016/j.actbio.2022.05.020.

[28] S.S. Silva, A. Motta, M.T. Rodrigues, A.F.M. Pinheiro, M.E. Gomes, J.F. Mano, R.L. Reis, C. Migliaresi, Novel genipin-cross-linked chitosan/silk fibroin sponges for cartilage engineering strategies, Biomacromolecules. 9 (2008) 2764–2774. https://doi.org/10.1021/bm800874q.

[29] I.M. Oliveira, C. Gonçalves, M.E. Shin, S. Lee, R.L. Reis, G. Khang, J.M. Oliveira, Anti-Inflammatory Properties of Injectable Betamethasone-Loaded Tyramine-Modified Gellan Gum/Silk Fibroin Hydrogels, Biomolecules. 10 (2020) 1456. https://doi.org/10.3390/biom10101456.

[30] S.K. Bajpai, S. Sharma, Investigation of swelling/degradation behaviour of alginate beads crosslinked with Ca2+ and Ba2+ ions, React. Funct. Polym. 59 (2004) 129–140. https://doi.org/10.1016/j.reactfunctpolym.2004.01.002.

[31] J. Kaszyńska, A. Rachocki, M. Bielejewski, J. Tritt-Goc, Influence of cellulose gel matrix on BMIMCl ionic liquid dynamics and conductivity, Cellulose. 24 (2017) 1641 – 1655. https://doi.org/10.1007/s10570-017-1223-z.

[32] H. Suo, L. Xu, C. Xu, X. Qiu, H. Huang, Y. Hu, Enhanced catalytic performance of lipase covalently bonded on ionic liquids modified magnetic alginate composites, J. Colloid Interface Sci. 553 (2019) 494–502. https://doi.org/10.1016/j.jcis.2019.06.049.

[33] S.K. Bharti, R. Roy, Quantitative 1H NMR spectroscopy, TrAC - Trends Anal. Chem. 35 (2012) 5–26. https://doi.org/10.1016/j.trac.2012.02.007.

[34] Ý.A. Mørch, I. Donati, B.L. Strand, G. Skjåk-Bræk, Effect of Ca 2+ , Ba 2+ , and Sr 2+ on Alginate Microbeads, Biomacromolecules. 7 (2006) 1471–1480. https://doi.org/10.1021/bm060010d.

[35] E.G. Deze, S.K. Papageorgiou, E.P. Favvas, F.K. Katsaros, Porous alginate aerogel beads for effective and rapid heavy metal sorption from aqueous solutions: Effect of porosity in Cu2+ and Cd2+ ion sorption, Chem. Eng. J. 209 (2012) 537–546. https://doi.org/10.1016/j.cej.2012.07.133.

[36] S. Peretz, M. Florea-Spiroiu, D.-F. Anghel, D. Bala, C. Stoian, G. Zgherea, Preparation of Porous Calcium Alginate Beads and Their Use for Adsorption of O-Nitrophenol from Aqueous Solutions, Micro Nanoeng. 22 (2013) 123–136.

[37] A.S. Marchev, P.A. Dimitrova, A.J. Burns, R. V. Kostov, A.T. Dinkova-Kostova, M.I. Georgiev, Oxidative stress and chronic inflammation in osteoarthritis: can NRF2 counteract these partners in crime?, Ann. N. Y. Acad. Sci. 1401 (2017) 114–135. https://doi.org/10.1111/nyas.13407.

[38] S. Xue, X. Zhou, W. Sang, C. Wang, H. Lu, Y. Xu, Y. Zhong, L. Zhu, C. He, J. Ma, Cartilage-targeting peptide-modified dual-drug delivery nanoplatform with NIR laser response for osteoarthritis therapy, Bioact. Mater. 6 (2021) 2372–2389. https://doi.org/10.1016/j.bioactmat.2021.01.017.

[39] B. Poulet, F. Beier, Targeting oxidative stress to reduce osteoarthritis, Arthritis Res. Ther. 18 (2016) 15–16. https://doi.org/10.1186/s13075-015-0908-7.

[40] B. Cizmarova, B. Hubkova, B. Bolerazska, M. Marekova, A. Birkova, Caffeate acid: A brief overview of its presence, metabolism, and bioactivity, Bioact. Compd. Heal. Dis. 3 (2020) 74–81. https://doi.org/10.31989/bchd.v3i4.692.

[41] C. Liu, Y. Cui, F. Pi, Y. Cheng, Y. Guo, H. Qian, Extraction, Purification, Structural Characteristics, Biological Activities and Pharmacological Applications of Acemannan, a Polysaccharide from Aloe vera: A Review, Molecules. 24 (2019) 1554. https://doi.org/10.3390/molecules24081554.

[42] T. Best, P. Howe, J. Bryan, J. Buckley, A. Scholey, Acute effects of a dietary non-starch polysaccharide supplement on cognitive performance in healthy middle-aged adults, Nutr. Neurosci. 18 (2015) 76–86. https://doi.org/10.1179/1476830513Y.0000000101.

[43] L.P. Yan, J.M. Oliveira, A.L. Oliveira, S.G. Caridade, J.F. Mano, R.L. Reis, Macro/microporous silk fibroin scaffolds with potential for articular cartilage and meniscus tissue engineering applications, Acta Biomater. 8 (2012) 289–301. https://doi.org/10.1016/j.actbio.2011.09.037.

[44] N. Kamaly, B. Yameen, J. Wu, O.C. Farokhzad, Degradable Controlled-Release Polymers and Polymeric Nanoparticles : Mechanisms of Controlling Drug Release, ACS Chem. Rev. 116 (2016) 2602–2663. https://doi.org/10.1021/acs.chemrev.5b00346.

[45] H. Akkiraju, A. Nohe, Role of chondrocytes in cartilage formation, progression of osteoarthritis and cartilage regeneration, J. Dev. Biol. 3 (2015) 177–192. https://doi.org/10.3390/jdb3040177.

[46] P.T. Newton, K.A. Staines, L. Spevak, A.L. Boskey, C.C. Teixeira, V.E. Macrae, A.E. Canfield, C. Farquharson, Chondrogenic ATDC5 cells: An optimised model for rapid and physiological

matrix mineralisation, Int. J. Mol. Med. 30 (2012) 1187–1193. https://doi.org/10.3892/ijmm.2012.1114.

[47] S.S. Silva, N.M. Oliveira, M.B. Oliveira, D.P.S. Da Costa, D. Naskar, J.F. Mano, S.C. Kundu, R.L. Reis, Fabrication and characterization of Eri silk fibers-based sponges for biomedical application, Acta Biomater. 32 (2016) 178–189. https://doi.org/10.1016/j.actbio.2016.01.003.

[48] I.M. Oliveira, C. Gonçalves, E.P. Oliveira, R. Simón-Vázquez, A. da Silva Morais, Á. González-Fernández, R.L. Reis, J.M. Oliveira, PAMAM dendrimers functionalised with an anti-TNF α antibody and chondroitin sulphate for treatment of rheumatoid arthritis, Mater. Sci. Eng. C. 121 (2021) 111845. https://doi.org/10.1016/j.msec.2020.111845.

[49] L. Zeng, Y. Yao, D.A. Wang, X. Chen, Effect of microcavitary alginate hydrogel with different pore sizes on chondrocyte culture for cartilage tissue engineering, Mater. Sci. Eng. C. 34 (2014) 168–175. https://doi.org/10.1016/j.msec.2013.09.003.

[50] J.M. Gomes, S.S. Silva, R.L. Reis, Exploring the Use of Choline Acetate on the Sustainable Development of α-Chitin-Based Sponges, ACS Sustain. Chem. Eng. 8 (2020) 13507–13516. https://doi.org/10.1021/acssuschemeng.0c05076.

[51] N.J. Sadgrove, M.S.J. Simmonds, Pharmacodynamics of Aloe vera and acemannan in therapeutic applications for skin, digestion, and immunomodulation, Phyther. Res. 35 (2021) 6572–6584. https://doi.org/10.1002/ptr.7242.

[52] S. Boonyagul, W. Banlunara, P. Sangvanich, P. Thunyakitpisal, Effect of acemannan, an extracted polysaccharide from Aloe vera, on BMSCs proliferation, differentiation, extracellular matrix synthesis, mineralization, and bone formation in a tooth extraction model, Odontology. 102 (2014) 310–317. https://doi.org/10.1007/s10266-012-0101-2.

[53] C.S. Bonnet, D.A. Walsh, Osteoarthritis, angiogenesis and inflammation, Rheumatology. 44 (2005) 7–16. https://doi.org/10.1093/rheumatology/keh344.

[54] C.M. Dancevic, D.R. McCulloch, Current and emerging therapeutic strategies for preventing inflammation and aggrecanase-mediated cartilage destruction in arthritis, Arthritis Res. Ther. 16 (2014) 429. https://doi.org/10.1186/s13075-014-0429-9.

[55] E. Chisari, K.M. Yaghmour, W.S. Khan, The effects of TNF-alpha inhibition on cartilage: a systematic review of preclinical studies, Osteoarthr. Cartil. 28 (2020) 708–718. https://doi.org/10.1016/j.joca.2019.09.008.

[56] P.J. Cope, K. Ourradi, Y. Li, M. Sharif, Models of osteoarthritis: the good, the bad and the promising, Osteoarthr. Cartil. 27 (2019) 230–239. https://doi.org/10.1016/j.joca.2018.09.016.

[57] M. Laavola, T. Leppänen, M. Hämäläinen, K. Vuolteenaho, T. Moilanen, R. Nieminen, E. Moilanen, IL-6 in osteoarthritis: Effects of pine stilbenoids, Molecules. 24 (2019) 1–11. https://doi.org/10.3390/molecules24010109.

[58] R.J. Douglas, Corticosteroid injection into the osteoarthritic knee: Drug selection, dose, and injection frequency, Int. J. Clin. Pract. 66 (2012) 699–704. https://doi.org/10.1111/j.1742-1241.2012.02963.x.

[59] P. Ubanako, N. Xelwa, M. Ntwasa, LPS induces inflammatory chemokines via TLR-4 signalling and enhances the Warburg Effect in THP-1 cells, PLoS One. 14 (2019) 1–17. https://doi.org/10.1371/journal.pone.0222614.

[60] A.C. Lima, R.L. Reis, H. Ferreira, N.M. Neves, Glutathione reductase-sensitive polymeric micelles for controlled drug delivery on arthritic diseases, ACS Biomater. Sci. Eng. 7 (2021) 3229–3241. https://doi.org/10.1021/acsbiomaterials.1c00412.

[61] R. Liu-Bryan, R. Terkeltaub, Emerging regulators of the inflammatory process in osteoarthritis, Nat. Rev. Rheumatol. 11 (2015) 35–44. https://doi.org/10.1038/nrrheum.2014.162.

[62] T. Liang, T. Chen, J. Qiu, W. Gao, X. Qiu, Y. Zhu, X. Wang, Y. Chen, H. Zhou, Z. Deng, P. Li, C. Xu, Y. Peng, A. Liang, P. Su, B. Gao, D. Huang, Inhibition of nuclear receptor RORα attenuates cartilage damage in osteoarthritis by modulating IL-6/STAT3 pathway, Cell Death Dis. 12 (2021) 886. https://doi.org/10.1038/s41419-021-04170-0.

[63] S. Nasi, H.-K. Ea, A. So, N. Busso, Revisiting the Role of Interleukin-1 Pathway in Osteoarthritis: Interleukin-1α and -1β, and NLRP3 Inflammasome Are Not Involved in the Pathological Features of the Murine Menisectomy Model of Osteoarthritis, Front. Pharmacol. 8 (2017) 1–12. https://doi.org/10.3389/fphar.2017.00282

Chapter VII

3D bioactive ionic liquid-based constructs: An anti-inflammatory approach for early-stage osteoarthritis

Chapter VII

3D bioactive ionic liquid-based constructs: An anti-inflammatory approach for early-stage osteoarthritis ††

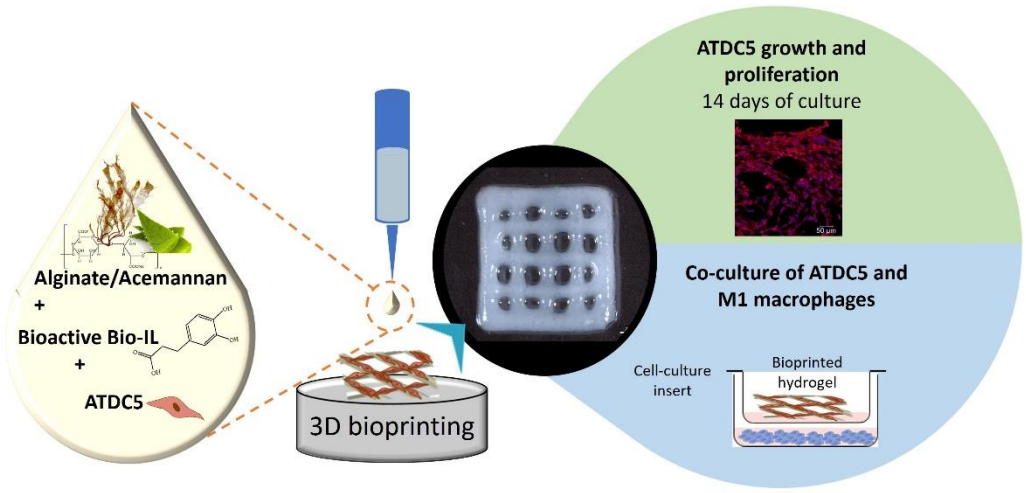
ABSTRACT

3D bioprinting enables the fabrication of biomimetic cell-laden constructs for cartilage regeneration, offering exclusive strategies for precise pharmacological screenings in osteoarthritis (OA). Synovial inflammation plays a crucial role in OA's early-stage and progression, being characterized by an increase of synovial pro-inflammatory mediators and cytokines, and chondrocyte apoptosis. Hence, it is urgent to develop disease models, including inflammatory cells, aiming to screen drugs targeting those events. To address these issues, a phenolic-based biocompatible ionic liquid approach, combining alginate (ALG), acemannan (ACE), and cholinium caffeate (Ch[Caffeate], were used to produce easily printable bioinks. This strategy was highly effective to obtain 3D constructs with good printing resolution and high structural integrity. The encapsulation of chondrocytes like ATDC5 cells provided structures with good cell distribution, viability, and growth, for up to 14 days. The co-culture of the constructs with THP-1 macrophages proved their ability to block pro-inflammatory cytokines (TNF-α and IL-6) and mediators (GM-CSF), released by the cultured cells. Moreover, the incorporation of the biocompatible ionic liquid into the system significantly improved its bioactive performance without compromising its physico-chemical features. Overall, these findings demonstrate that ALG/ACE/Ch[Caffeate] bioinks have great potential for bioengineering cartilage tissue analogs. Besides, the developed ALG/ACE/Ch[Caffeate] bioinks protected encapsulated chondrocyte-like cells from the effect of the inflammation, assessed by a co-culture system with THP-1 macrophages. Altogether, these results support the increasing use of Bio-ILs in the biomedical field, particularly for the development of 3D bioprinting-based models for inflammatory-based changes in OA.

†† This chapter is based on the following publication:

Gomes J. M., Marques, L. F., Rodrigues L. C, Silva, T. H., Silva S. S., and Reis R. L "3D bioactive ionic liquid-based constructs as an anti-inflammatory approach for early-stage osteoarthritis", 2022 (Submitted).

VII-1. GRAPHICAL ABSTRACT



VII-2. INTRODUCTION

The progressive degeneration of osteochondral and cartilaginous tissues, together with the complex and multifactorial etiology of osteoarthritis (OA) makes disease prevention and treatment a challenge [1]. OA clinical symptoms include thinning of cartilage, inflammation, pain, and impaired movement [1,2]. Current medical treatments are restricted to symptom-relieving strategies, including nonpharmacological solutions, namely physical therapy and exercise, and pharmacological approaches, such as analgesics, non-selective/selective inhibitors, and nonsteroidal anti-inflammatory drugs [1,3]. Tissue engineering alternative strategies, based on the use of autologous cell-based cartilage constructs, promise to play an effective role in the repair of complex cartilage damage. In that sense, some efforts have been made towards developing biomaterials capable of providing a favorable environment for chondrogenic cell growth [1,4]. Moreover, developing therapeutic avenues is vital to understand the disease mechanisms, its progression, and the cellular and molecular contributors to the pathology [1]. Different processing strategies were already used to develop OA models (e.g., scaffold fabrication, freeze-drying, electrospinning, and solvent casting), still with associated drawbacks, able to be overcome by the 3D printing technology, such as longer processing time, small-scale production, insufficient mechanical integrity and reproducibility [5]. In addition, 3D bioprinting allows overcoming the challenge associated with cell seeding in the conventionally formed scaffold by maintaining similar cell densities throughout the constructs [5]. Scaffold-based 3D bioprinted cultures present many advantages, including mimicking the *in vivo* microenvironment, allowing cell-cell interactions, providing structural support to sensitive cells,

and offering natural environmental cues to the cells [1,6]. The 3D bioprinted constructs may be produced using natural-origin polymers, such as collagen, hyaluronic acid, gelatin, agarose, chitosan, silk fibroin, and alginate (ALG) [5,7–10]. These constructs have many advantages, such as the cost-effectiveness of the method, biocompatibility, and bioactivity [1,11–13].

Previous studies indicated that active biocompatible ionic liquids (Bio-ILs) processed with natural biomacromolecules have led to matrices with tailorable sizes, morphologies, and functionalities, improving their potential application as tissue engineering solutions [11,14]. In addition, Bio-ILs are stable organic salts synthesized using both counterparts derived from biocompatible materials [15]. Bio-ILs use in active pharmaceutical ingredients (APIs) systems is accomplished by using either the anionic or cationic moiety from compounds with the properties of interest, often promoting an increase in the compounds' bioactivity, stability, solubility and bioavailability [11,14]. Several APIs have been used to produce APIs/Bio-ILs systems, including analgesic drugs [16], APIs with anti-inflammatory and antipyretic activity [16,17], as well as phenolic acids with proven anti-inflammatory and antioxidant features (e.g., gallic acid, caffeic acid, and ellagic acid) [14]. Despite the successful findings of these studies, only a few works reported the use of ILs in 3D printing to develop wearable electronic devices, still not envisioning tissue engineering solutions [13,18].

In this work, we propose a cost-effective 3D bioprinted construct with intrinsic bioactivity and good biological performance, combining natural polymers and cholinium caffeate (Ch[Caffeate], a phenolic-based Bio-IL). From our knowledge, for the first time, 3D cell-laden constructs were fabricated incorporating a Bio-IL. Previous works have reported the use of ILs for biomacromolecules dissolution before the printing, or poly(ionic liquid)s for developing 3D polymeric-based constructs but never encapsulating cells [46–48]. Several works reported the use of ALG-based hydrogels for encapsulation of chondrocytes, in combination or not with other natural polymers for cartilage repair and as bioink in 3D bioprinting [7–9,19]. However, some issues are associated with the calcium chloride concentration used for alginate ionic crosslinking since the cytocompatibility is concentration-dependent [20–22]. Instead, recent studies propose that acemannan (ACE), the main polysaccharide in the aloe vera leaves, can promote cell proliferation and differentiation *in vitro*, and also possesses Ca^{2+} traces in its structure, able to interact with ALG [23,24]. Other studies have focused on the ACE anti-inflammatory effects, which are thought to be owed to the interaction of the mannose sections on the ACE molecule with the mannose receptor of white blood cells [25]. In this sense, this work aimed to prepare a bioink combining a synthesized cholinium caffeate, ALG, and ACE and their further characterization. Furthermore, the ability

of the developed 3D bioprinted constructs to support ATDC5 chondrocyte-like cell viability, growth, and proliferation was performed for up to 14 days. Beyond that, to study the behaviour of the encapsulated cells in an inflammatory environment, a co-culture system was developed where THP-1 differentiated macrophages were in contact with the constructs to simulate the synovial fluid OA scenarios.

VII-3. MATERIALS AND METHODS

VII-3.1. Materials

Cholinium hydroxide (Ch[OH]) 45% in methanol solution and Caffeic acid, both used in the Bio-ILS synthesis, were purchased from Sigma-Aldrich, St. Louis, MO, USA. 2,2-diphenyl-1-picrylhydrazyl (DPPH) was also purchased from Sigma-Aldrich, St. Louis, MO, USA. Acemannan (ACE, BiAloe® Mw average 200 kPa) powder obtained from aloe vera extracts, was purchased from Lorand Laboratories (Texas, USA). Sodium alginate (ALG, ~ 250 cP) from brown algae was supplied by Sigma-Aldrich (USA). All other reagents were of analytical grade and used as received.

VII-3.2. Synthesis of Choline-Caffeate (Ch[Caffeate])

Ch[Caffeate] was synthesized as previously reported [14]. Briefly, Cholinium hydroxide (Ch[OH]) was dropwise added to the caffeic acid solution in methanol, 1.1 equivalent, at 0 °C, and under a nitrogen atmosphere. The mixture was stirred under a nitrogen atmosphere overnight at room temperature. The methanol and water were removed under reduced pressure on the following day, and the unreacted acid was washed with acetone at least 3 times. The residual solvent was removed under reduced pressure, and the resultant Ch[Caffeate], whose chemical structure is present in Figure VII-1, dried under a high vacuum for at least 72 h. The high purity of the produced Ch[Caffeate] was confirmed by ^{1}H nuclear magnetic resonance (NMR). NMR spectra were collected on an Avance III spectrometer (Bruker, Germany) operating at a resonance frequency of 400.13 MHz (1H). D_2O was used as a solvent and a reference for chemical shifts reported in ppm (parts per million).

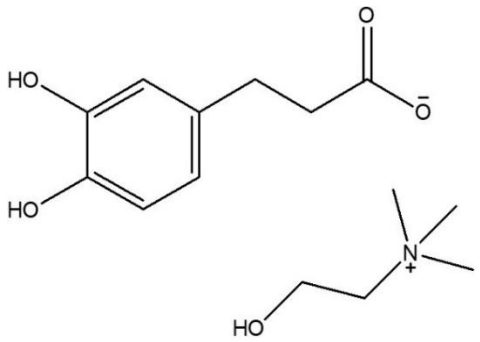


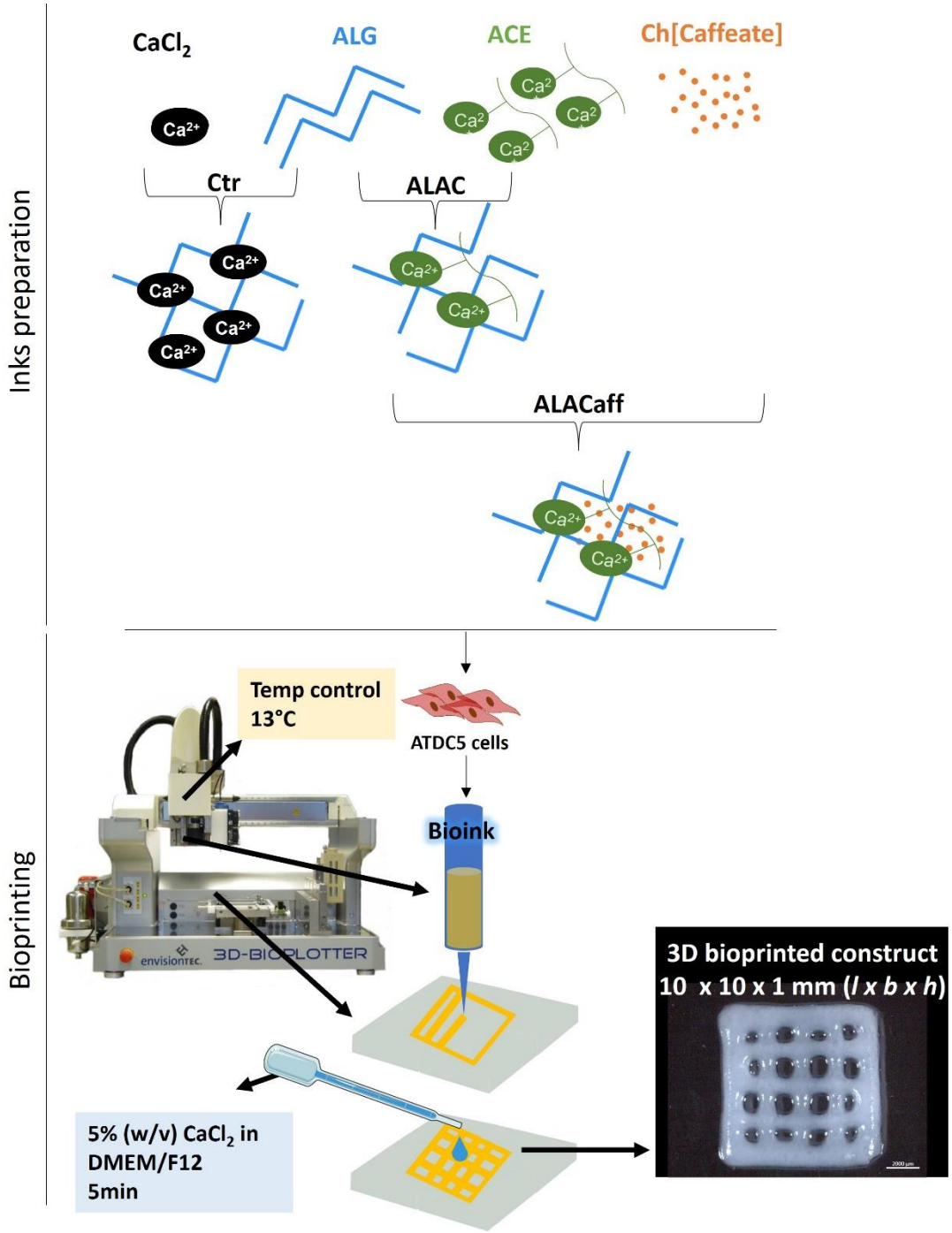
Figure VII-1 - Cholinium Caffeate (Ch[Caffeate]) chemical structure.

VII-3.3. ALG/ACE/Ch[Caffeate]ink preparation and characterization

For the inks preparation, a 5% (w/v) sodium alginate (ALG) solution was prepared, and ACE was added to obtain a 5% (w/v) concentration. The ALG/ACE mixture was stirred using the ultra-turrax (T 18 digital ULTRA-TURRAX® - IKA), at 10000g for 10 min, in an ice bath. For the formulation containing 1% (w/v) Ch[Caffeate], the Bio-IL was added to a ALG/ACE mixture previously prepared, and stirred for 5 min. A control was prepared using the same methodology, mixing calcium chloride ($CaCl_2$) in the prepared ALG solution to promote ionic gelation (the final concentration of calcium chloride was 0.35% (w/v). The schematic representation of the inks preparation process is illustrated in Scheme VII-1. The sample identification used throughout the manuscript is detailed in Table VII-1.

Table VII-1 - Sample identification used throughout the paper

Sample identification	ALG %(w/v)	ACE %(w/v)	Ch[Caffeate] %(w/v)	$CaCl_2$%(w/v)
Ctrl	5	0	0	0.35
ALAC		5	0	0
ALACaff		5	1	0



Scheme VII-1 - Schematic representation of the 3D bioprinting process and macroscopic image of the printed constructs.

VII-3.3.1. Injection force

To assess the injection force needed to extrude the ink (before encapsulating the ATDC5 cells) from the syringe, injectability measurements (PARALAB, Porto, Portugal) with a 5 ml syringe (Termo-JPN) with 410 μm of needle size were performed.

VII-3.4. 3D printing methodology

The bioprinting process is schematically represented in Scheme VII-1**.** For bioprinting, a 3D-Bioplotter (4thGeneration, EnvisionTEC, Germany) dispensing system was used. Squares 10 mm in length and 1 mm in height (4 layers), with 250 μm of pore size (considered the hole itself, excluding the thickness of the filament) were printed with 90° orientation between adjacent layers, at 18 $mm \cdot s^{-1}$ with a printing nozzle of 410 μm of inner diameter, as illustrated in Scheme VII-1. The ink (2.5 ml) was printed, and the used compositions are depicted in Table VII-1. Following the printing, the inks were crosslinked using a drop of 5% (w/v) $CaCl_2$ solution in TBS for approximately 5 min. The printing was carried out at 13 °C, and the resulting 3D structures were characterized.

VII-3.5. 3D Printed hydrogels characterization

VII-3.5.1. SEM

The different matrices were fixed using mutual carbon adhesive tape on aluminum stubs and coated with a conductive gold layer. A NanoSEM-FEI Nova 200 with an integrated microanalysis X-ray system (EDS – energy dispersive spectrometer) was used to observe the morphology of the constructs.

VII-3.5.2. Micro-CT

The microstructure and architecture of the 3D printed hydrogels were evaluated through a microcomputed tomography (micro-CT) technique. The samples were lyophilized and scanned using a high-resolution micro-CT (SkyScan 1272, Bruker, USA) with a pixel size of 10 μm, the voltage range of 50 kV, and current source of 200 μA (version 1.1.3). Approximately 250 projections were acquired over a rotation angle of 360°, with a rotation step of 0.3°. Data sets were reconstructed using a standardized cone-beam reconstruction software (NRecon 1.6.10.2, Bruker). Representative data set of the slices was segmented into binary images with a dynamic threshold between 50 and 255. After that, the binary images were used for morphometric analysis (CT Analyser, v1.15.4.0, Bruker, USA). Quantitative information of total porosity (%), pore size (μm), pore distribution (%), and interconnectivity (%) was assessed for the structures' filaments. The results are presented as the mean of the measurements on three hydrogel samples.

VII-3.5.3. Equilibrium water content (EWC) of the printed hydrogels

To determine the equilibrium water content, the printed hydrogels (Ctrl, ALAC, and ALACaff) were soaked using tris-HCl-buffer (TBS) (pH 7.4) at 37 °C for 24 h. Then, the hydrogels were gently blotted with filter paper to remove the superficial water and weighed (Ww). Then, the hydrogels were lyophilized for 3 days, and the weight was again recorded (Wd). The EWC (% (w/w)) was calculated as described in Equation VII-1. The measurements were performed in triplicate.

$$EWC(\%) = \frac{w_w - w_d}{w_w} \times 100 \qquad \text{Equation VII-1}$$

VII-3.5.4. Ch[Caffeate] release

The study of the Ch[Caffeate] release from the hydrogels was performed following a previously reported procedure [14]. Briefly, the dried Ctrl, ALAC, and ALACaff hydrogels were placed in vessels containing a TBS pH 7.4, at 37 °C, and protected from light due to the Bio-IL light sensibility. At pre-determined times, 1 ml of the TBS solution was collected, and the same volume of fresh TBS was added to maintain a constant volume. The Ch[Caffeate] content was determined by UV spectroscopy using a microplate reader (Synergy HT, BIO-TEK, Winooski, VT, USA) at 285 nm. The IL content at each time point was plotted as a cumulated percentage release determined using Equation VII-2.

$$Cumulative\ release\ (\%) = \frac{V_0 C_n + V C_{n-1}}{M} \times 100 \qquad \text{Equation VII-2}$$

where, $C_{(n-1)}$ and C_n correspond to the Bio-IL concentration at times n-1 and n, V_0 is the initial volume of the drug release medium, V is the withdraw volume, and m is the Ch[Caffeate] mass loaded in the 10 mg of beads, amount used for each condition in the assay. Calibration curves were established with concentrations from 0.01% (w/v) to 5% (w/v) and from 0.025% (w/v) to 5% (w/v), for Ch[Caffeate] and ACE, respectively. PBS was used as a reference for the baseline correction of the values.

VII-3.6. Cyto-compatibility and *in vitro* assessment of the 3D bioprinted constructs

VII-3.6.1. Preparation of the ALG/ACE/ATDC5 Bio-Ink

The ATDC5 chondrocyte-like cell line was used for cell culture. Before encapsulation, cells at passages between 9 and 12 were cultured using Dulbecco's Modified Eagle Medium: Nutrient Mixture F-12 (DMEM/F12, Thermo Fisher Scientific, USA) supplemented with 10% fetal bovine serum (FBS; Alfagene, Portugal) and 1% antibiotic/antimycotic solution (final concentration of penicillin 100 units/mL and streptomycin 100 mg/mL; Alfagene, Portugal). A 5% CO_2 controlled atmosphere, at 37 °C, was used to culture the cells, until confluency was reached. Confluent ATDC5 cells were trypsinized and encapsulated in the Ctrl, ALAC, and ALACaff bioinks at a density of 8×10^6 cells·ml^{-1}. Briefly, 300 µl of cell suspension was transferred into the bioink-containing syringe and carefully stirred to create a homogenous distribution of the cells. The bioink (2.5 ml) was printed, and the used compositions are depicted in Table 1. Following the bioprinting, the bioinks were crosslinked using a drop of 5% (w/v) $CaCl_2$ solution in Dulbecco's Modified Eagle Medium: Nutrient Mixture F-12 (DMEM/F12, Thermo Fisher Scientific, USA), for approximately 5 min. The printing was carried out at 13 °C, and the resulting 3D structures were characterized. The resulting 3D printed hydrogels were maintained in DMEM/F12 condition for 14 days with medium changes every three days.

VII-3.6.2. Live dead and metabolic activity

The metabolic activity of cells encapsulated in the bioinks was evaluated using the CellTiter 96® AQueous One Solution Cell Proliferation Assay (MTS, Promega). Briefly, the 3D bioprinted hydrogels were placed in a mixture containing serum-free cell culture medium and MTS reagent at a 5:1 ratio and incubated for 3 h. The optical density was read (OD 490 nm).

In addition, cell viability was also assessed by fluorescence labeling using a live/dead assay. The 3D bioprinted hydrogels were removed from the culture medium and washed with sterile TBS. After, all samples were incubated with 1 mg/mL calcein acetoxymethyl (Invitrogen, 1:500) and 1.5 mM propidium iodide (PI, Invitrogen, 1:1000) solution in DMEM/F12 for 15 min, at 37 °C and washed with sterile PBS. Further, the samples were visualized using a confocal laser scanning microscope (Olympus FV1000). The software Zen was used to analyze the images.

VII-3.6.3. Cell proliferation

The proliferation of the cells throughout the hydrogels was evaluated using the fluorometric PicoGreen double-stranded DNA assay, according to the manufacturer's instructions (Quant-iT™ PicoGreen™ dsDNA Kit, P7589, Invitrogen). Briefly, after each time-point, the 3D bioprinted hydrogels were rinsed with TBS, placed in microtubes containing 1 ml of ultra-pure water, and stored at -80 °C until being analysed. A microplate reader (Synergy HT, BIO-TEK, Winooski, VT, USA) was used to measure the fluorescence at 480 and 520 nm. A standard curve (0–2 $\mu g.ml^{-1}$) was used to calculate the DNA concentration, relating the amount of dsDNA to the fluorescence.

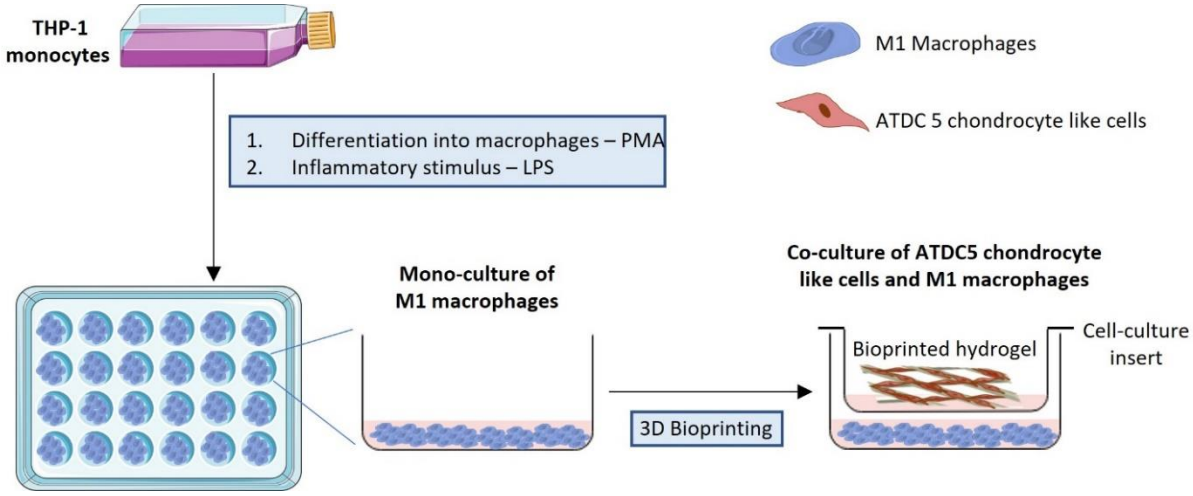
VII-3.6.4. Cell morphology

The ATDC5 cell distribution and morphology of the structures were analyzed using a confocal laser scanning microscope (CLSM). The samples were fixed with 10 % formalin for 30 min, and then incubated with 1 % bovine serum albumin (BSA) for 30 min. The constructs were permeabilized using 0.1 % Triton X-100 for 5 min, then incubated with rhodamine-phalloidin at room temperature (RT) for 20 min, followed by washing with PBS and finally stained with 5 $\mu g.ml^{-1}$ 4',6-Diamidine-2'-phenylindole dihydrochloride (DAPI) for 30 min. Fluorescence images from the stained constructs were obtained using a CLSM (Olympus FV1000).

VII-3.6.5. 3D printed cell-laden hydrogels co-cultured with macrophages

A co-culture system was used to assess the potential anti-inflammatory and biological effects of the 3D-printed hydrogels. ATDC5 cells were encapsulated in the hydrogels, as previously described, and THP-1 cell line was seeded as reported [11]. A representation of the co-culture system used is depicted in Scheme VII-2 Briefly, THP-1 cells were seeded at a density of 1×10^6 cells/mL using RPMI medium with 100 nM Phorbol 12-myristate-13 acetate (PMA) (Sigma-Aldrich, St. Louis, MO, USA) for 24 h. After incubation, an additional volume of RPMI medium was added to the wells without PMA and incubated for 48 h. THP-1 cells were incubated with 100 ng mL^{-1} of LPS in RPMI medium and incubated for 5 h, to induce the inflammatory response. After this period, the printed hydrogels were put in contact with the cells, using a cell culture insert with a pore size membrane of 0.4 μm, and cultured for up to 7 days.

After each time point, 1 and 7 days, the culture medium was collected and stored at −80 °C for further analysis.



Scheme VII-2 - Schematic representation of the experimental culture conditions of the developed direct transmembrane co-culture system

VII-3.6.5.1 *ATDC5 metabolic activity and proliferation*

To evaluate the effect of the inflammatory environment in the ATDC5 chondrocyte-like cells encapsulated in the different 3D bioprinted hydrogels, their metabolic activity was evaluated. For that purpose, a CellTiter 96® AQueous One Solution Cell Proliferation Assay (MTS, Promega) was used, as described above, after 1 and 7 days of culture. In addition, the cell proliferation throughout the hydrogels was evaluated in the same culture times using the fluorometric PicoGreen double-stranded DNA assay, according to the manufacturer's instructions (Quant-iT™ PicoGreen™ dsDNA Kit, P7589, Invitrogen).

VII-3.6.5.2 *Cytokine Quantification*

For the cytokine quantification, a Luminex system was used. The magnetic bead sets, included in the systems, were marked with differing ratios of two different fluorophores, which were conjugated with monoclonal antibodies specific for different cytokines or chemokines. A secondary detection antibody specific to the interested molecule was added, once the cytokine of interest had bounded [26]. The beads were further read on a Luminex machine (Bioplex-100, Bio-Rad) which has two lasers, one that identifies

the bead, and, consequently the cytokine or chemokine it is specific for, and one that can detect the amount of the detection agent on the bead. Altogether this data is used to quantify the molecule of interest. The quantification of the human cytokines in the supernatants was evaluated using a Cytokine 10-Plex Human Panel (Fisher Scientific, Austria), using Luminex™ , and the assay was performed according to the manufacturer's instructions.

VII-3.7. Statistical analysis

The experiments were run in triplicate, and the results are expressed as means ± standard deviation for n = 3. The statistical analysis was carried out using GraphPadPrism v. 8.0 for Windows (GraphPad Software, San Diego, http://www.graphpad.com). After the evaluation of the normality of the results through the Shapiro-Wilk test, when presenting a normal distribution, the data were analyzed using One-way ANOVA and Tukey's multiple comparisons test; when not presenting a normal distribution, a nonparametric Krustal-wallis test was performed. Differences at $p \leq 0.05$ were considered to be significant.

VII-4. RESULTS AND DISCUSSION

VII-4.1. Bioink production and physico-chemical characterization of the produced 3D constructs

3D bioprinting is a revolutionary tool in the healthcare field, which promoted the recent boost in the effort to create novel bioinks [27]. In the present work, a bioink with intrinsic bioactivity was developed by combining 5% (w/v) ALG, 5% (w/v) ACE, and 1% (w/v) Ch[Caffeate], a Bio-IL, being the concentration of the bioink compounds chosen based on our previous knowledge [23]. Firstly, the Bio-IL, Ch[Caffeate] was synthesized and characterized by ^{1}H NMR (Supplementary Figure VII-1). By the analysis of the ^{1}H NMR spectrum, it was possible to confirm the successful Ch[Caffeate] synthesis, as well as the purity of the final product, by the presence of the peaks corresponding to the $N(CH_3)_3$ group in the cholinium cation, as a singlet at 3.11 ppm; two multiplets corresponding to 2H between 3.53-3.51 and 4.04-4.08, corresponding to $NC\underline{H}_2CH_2OH$ and $NCH_2C\underline{H}_2OH$, respectively. The peaks corresponding to the aromatic ring on the Caffeate acid structure are duplets at 6.35 ppm, 6.94 ppm, 7.19 ppm, and 7.09 ppm and as a doublet, representing the equivalent hydrogens in the structure at 6.74 ppm [14]. Bio-ILs synthesis, by associating phenolic compounds with the cholinium cation, is an alternative and superior strategy to

overcome phenolic compounds' lack of stability and poor solubility [11,14,31]. Ch[Caffeate] is a Bio-IL with anti-oxidant and anti-inflammatory features, which is expected to improve the bioactivity of the final bioprinted construct, by managing the critical features of OA microenvironment [32]. As a first approach, for the bioink formation, ACE and Ch[Caffeate] were added to the 5% (w/v) ALG solution simultaneously. However, we were unable to print continuously due to its elastic-like behavior. This behavior could be related to the Bio-IL hydrogen bonding ability and, consequently, to the formation of intramolecular hydrogen bonds, which was previously observed for Caffeate acid derivatives [33]. In another approach, Ch[Caffeate] (1% w/v) was added to an ALG/ACE previously formed gel. It is well known that ALG is a highly stable polymer with controllable gelation in the presence of di- cations, resulting in a structure described as the egg-box model [26,34,35]. In ALG/ACE system, the presence of Ca^{2+} traces in the ACE would promote the reaction with the (COO–) groups in the ALG structure, forming a gel, as observed in previous work from our group [26]. This bioink formation strategy resulted in an ALG/ACE/Bio-IL smooth and uniform gel. In parallel, a bioink (control) composed of ALG solution (5% w/v), was developed using $CaCl_2$ (Table VII-1) [32].

The injectability is a very important property of a hydrogel-based material when aiming for its applicability in tissue engineering [33]. This feature is related to the ability of the hydrogel-based materials to be extruded through a syringe-cannulated needle combination when a certain force or pressure is applied [33]. The injection force of the produced inks was evaluated, and the results are presented in Figure VII-2A. The values of injection force used were 13N, 12N, and 12N, for Ctrl, ALAC, and ALACaff inks, respectively, being considered easy to inject inks (11–25 N), according to literature references [33]. Similar injectability values were reported in studies involving inks formed by ALG in mixtures with other polymers, namely collagen [34,35]. The printability of the developed inks and their ability to produce tissue grafts with a defined architecture were confirmed through the 3D printing of geometrically defined constructs (Figure VII-2B). The macroscopic appearance of the printed models is presented in Figure VII-2C, and a representative video of the 3D constructs printing process can be found in the supplementary material (Supplementary Video-VII-1). As seen in the video, the ink deposition is performed layer-by-layer.

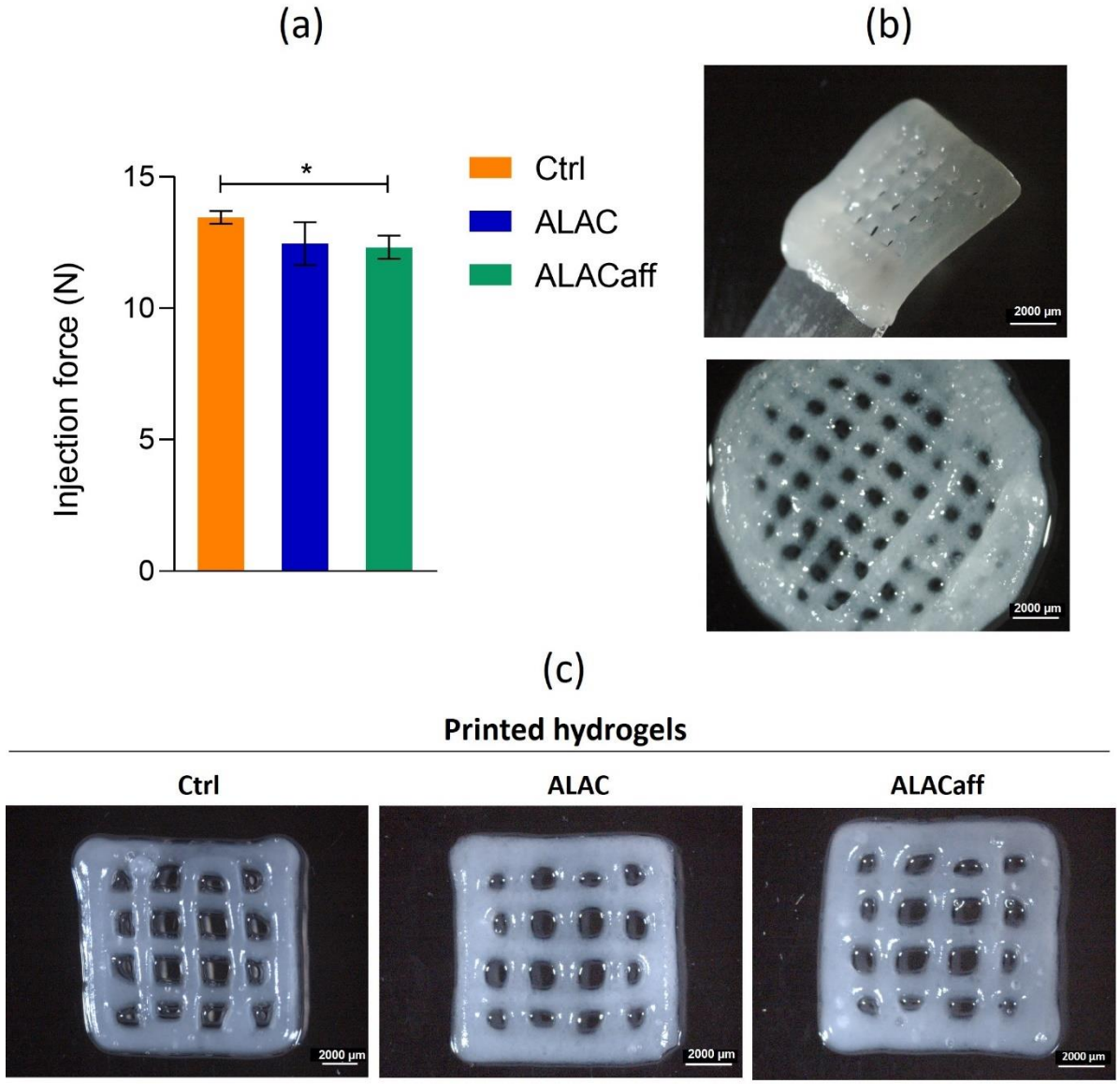
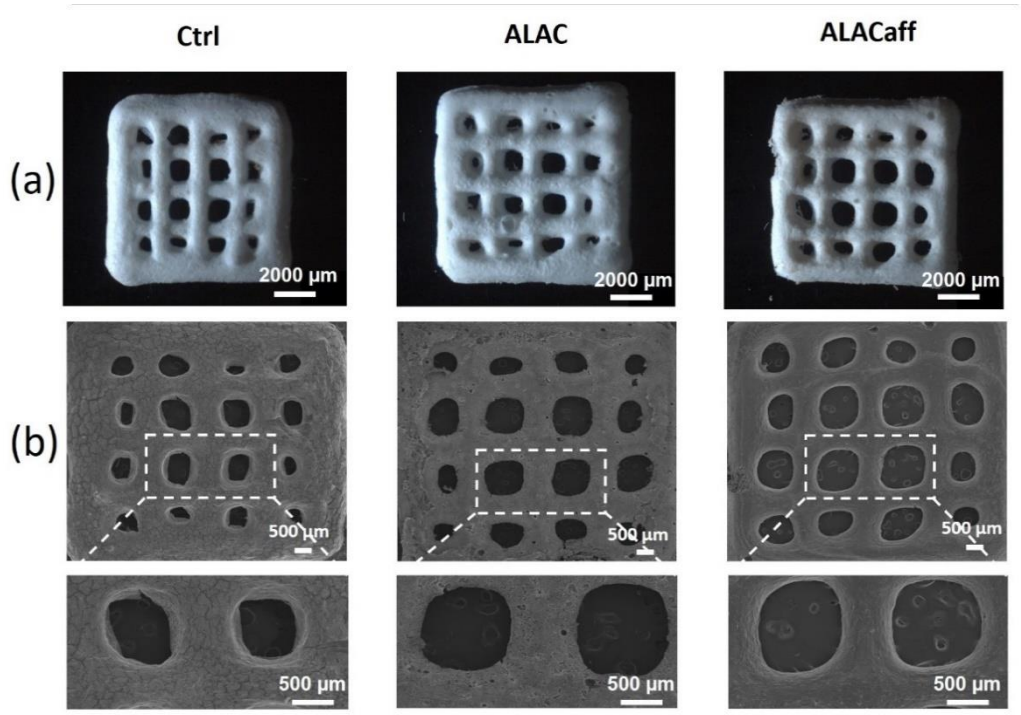


Figure VII-2 - (a) Injection force profile of the prepared inks; (b) macroscopic printability evaluation using different 3D models, and (c) photos of the hydrogels right after the printing process.

The hydrogels were frozen with liquid nitrogen (-196°C) and freeze-dried following the printing process. This freezing temperature was carried out on printed hydrogels to allow a faster freezing process than -80°C, or even -20°C, allowing to obtain structures with similar features to the printed hydrogels. Figure VII-3A depicts the macroscopic appearance of the constructs after freeze-drying. In addition, SEM analysis and micro-CT was carried out on the architectures to investigate the printing accuracy of the manufacturing process. The top view images of the produced 3D constructs (Figure VII-3B) show a homogeneous distribution of the pores with a well-defined shape in all the formulations. The herein-used printing conditions (15 °C) and the use of biocompatible materials allow us to conjugate printing fidelity with incorporated living cells, which leaves room for the use of Bio-ILs in 3D bioprinting.

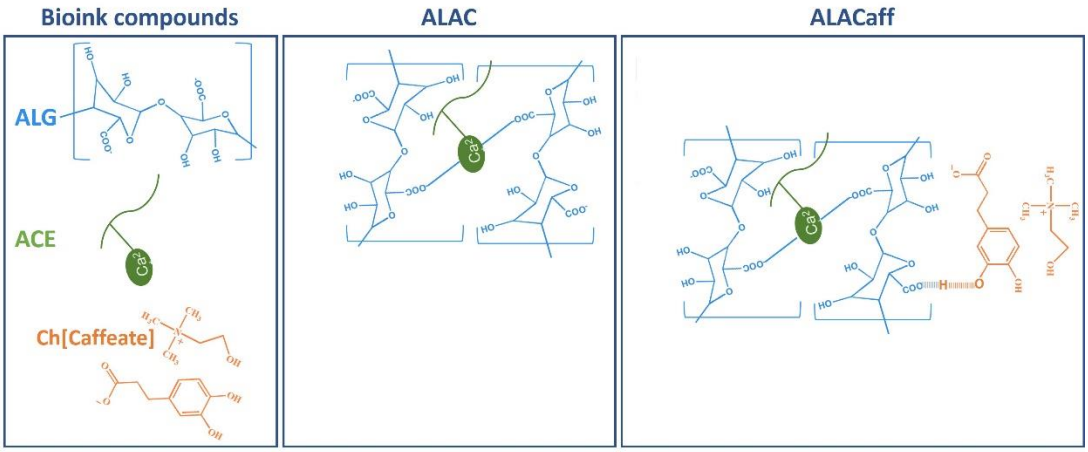
Moreover, by the analysis of the morphometric parameters (Figure VII-3C) obtained by μ-CT, we were able to study the internal structure of the printed filaments, which is crucial to understand the potential success in further cell culture assays. The porosities values for the Ctrl, ALAC and ALACaff filaments were 22.32 ± 0.07 %, 29.47 ± 0.49 %, and 49.92 ± 0.01 %, respectively, with the correspondent mean pore sizes of 47.23 ± 1.24 μm, 35.18 ± 5.01 μm and 56.62 ± 13.24 μm. The filament microporosities were proved to be well-interconnected, showing interconnectivity values of 46.08 ± 7.58 %, 77.34 ± 5.09 % and 70.21 ± 4.64 % for Ctrl, ALAC and ALACaff, respectively. Ctrl presented lower porosity, mean pore size, and interconnectivity values compared to ALAC and ALACaff. This may result from the use of $CaCl_2$ for the chemical crosslinking of the Ctrl ink, offering a higher amount of the Ca^{2+} ions to link to ALG guluronic blocks than ACE, which according to the literature, present only traces of Ca^{2+}, resulting from its extraction [23,36]. This would provide Ctrl a more compact 3D network, with reduced porosity and interconnectivity, compared to the other formulations. ALACaff architectures presented significantly higher porosity and pore size values (49.92 ± 0.01 % and 56.62 ± 13.24 μm, respectively) than ALAC (29.47 ± 0.49 % and 35.18 ± 5.01 μm). In our previous work [37] the porosity of ALG/ACE/Ch[Caffeate] beads was not affected by the Bio-IL concentrations, meaning that the cohesion of the structures was mainly driven by the ionic cross-linking of ALG in the presence of Ca^{2+}. Also, it was hypothesized that the ultra-turrax processing could help the formation of the interactions between the ink compounds, mainly considering the strong hydrogen bonding ability of the caffeic acid derivatives [30], including Ch[Caffeate]. Notwithstanding the addition of the water-soluble Ch[Caffeate] [28] after the ACE mixing, as described before, would promote its interaction with the ALG structure due to the strong hydrogen bonding ability of this compound, thus interfering with the ionic crosslinking ability of the system, and consequently the final construct porosity. The interaction of the Ch[Caffeate] with the ALG structure most probably occurs through the -OH groups in the Ch[Caffeate] aromatic ring. The probable interactions between the different compounds of the ALAC and ALACaff ink are represented in Scheme VII-3**.**



(c)

Sample	Mean pore size (µm)	Porosity (%)	Interconnectivity (%)
Ctrl	47.23 ± 1.24	22.32 ± 0.07	46.08 ± 7.58
ALAC	35.18 ± 5.01	29.47 ± 0.49	77.34 ± 5.09
ALACaff	56.62 ± 13.24	49.92 ± 0.01	70.21 ± 4.64

Figure VII-3 - (a) Macroscopic appearance of the 3D printed constructs after freeze drying; (b) SEM images of the printed hydrogels and (c) values of mean thickness, pore size, porosity, and interconnectivity obtained using µ-CT analysis.



Scheme VII-3 - Interactions between the bioink components

The equilibrium water content (EWC) of the printed hydrogels was evaluated using TBS and the results demonstrated that all formulations, Ctrl, ALAC and ALACaff, presented high EWC values, 92.01%, 91.64% and 92.57%, respectively, with no significant statistical differences among the formulations (Figure VII-4A). Previous works report the low stability of ALG-based biomaterials in the presence of phosphates and acetates present in the phosphate and acetate buffer solutions [38,39]. Therefore, TBS pH 7.4 was used as the medium to the EWC and for further stability and release assays since it was reported to provide a pronounced increase in the stability of ALG-based microcapsules and hydrogels [38,39]. Previous works, in which 3D composites were printed using ALG/Agarose and ALG/Collagen inks, demonstrated that the EWC values significantly decreased when compared to the ALG-based structures [9]. This behavior is due to the water uptake ability of ALG, which is strongly related to the presence of its hydrophilic functional groups [36], that may be reduced through the interactions established in the composite formation, increasing its resistance to water load and consequently degradation. In our case, the reduction of the hydrophilic groups' availability in the Ctrl, ALAC, and ALACaff would occur during ink formation and processing due to the ionic crosslinking and hydrogen bonding, decreasing the hydrophilicity of the final construct. The water content of a hydrogel is a vital feature that strongly affects its purpose [40]. Low EWC values are not ideal for biomaterials capable of bearing strong load and keeping flexibility, as for soft tissue applications, including cartilage, since they become hard and brittle as these values decrease, losing the mechanical advantages. Thereby, the herein obtained EWC values for Ctrl, ALAC, and ALACaff architectures are satisfactory when envisioning cartilage regeneration approaches.

The stability of the printed constructs was also evaluated through weight loss quantification, and the maximum values achieved were 7%, 31%, and 34% for Ctrl, ALAC, and ALACaff, respectively, for up to 14

days (Figure VII-4B). Additionally, the 3D-printed constructs were able to keep their original shape up to 14 days of immersion in TBS, which is in accordance with some previously published results [38,39]. Moreover, ALACaff presents significantly higher weight loss values when compared to Ctrl, owned to the water solubility of Ch[Caffeate], already reported in previously published works [14,28], which favors the Bio-IL release over time (Figure VII-4C).

According to the achieved profile, after 4h of immersion, Ch[Caffeate] reaches its maximum cumulative % release (approximately 40%), reaching a plateau up to 14 days. The suggested prolonged drug release is an advantage considering the rapid clearance of the NSAIDs, as well as other smaller molecules and proteins, which present a half-life of around 5 h [41]. Moreover, this is in agreement with the expected interactions in the ink composite, where besides Ch[Caffeate] being linked by hydrogen bonding (Scheme VII-3), it is thought that it may also be trapped in the network of the ink composite network. The entrapped Ch[Caffeate] release is favored by the polymer-based chain relaxation, a consequence of the electrostatic repulsion among negatively charged $–COO^-$ groups that occur in solution. As already reported, when immersed in TBS solution, ALG-derived architectures suffer an exchange of the Ca^{2+} binding divalent cations responsible for the ALG egg-box structure by Na^+ cations from solution [32], which reduces the strength of interactions favouring the release of the matrix content.

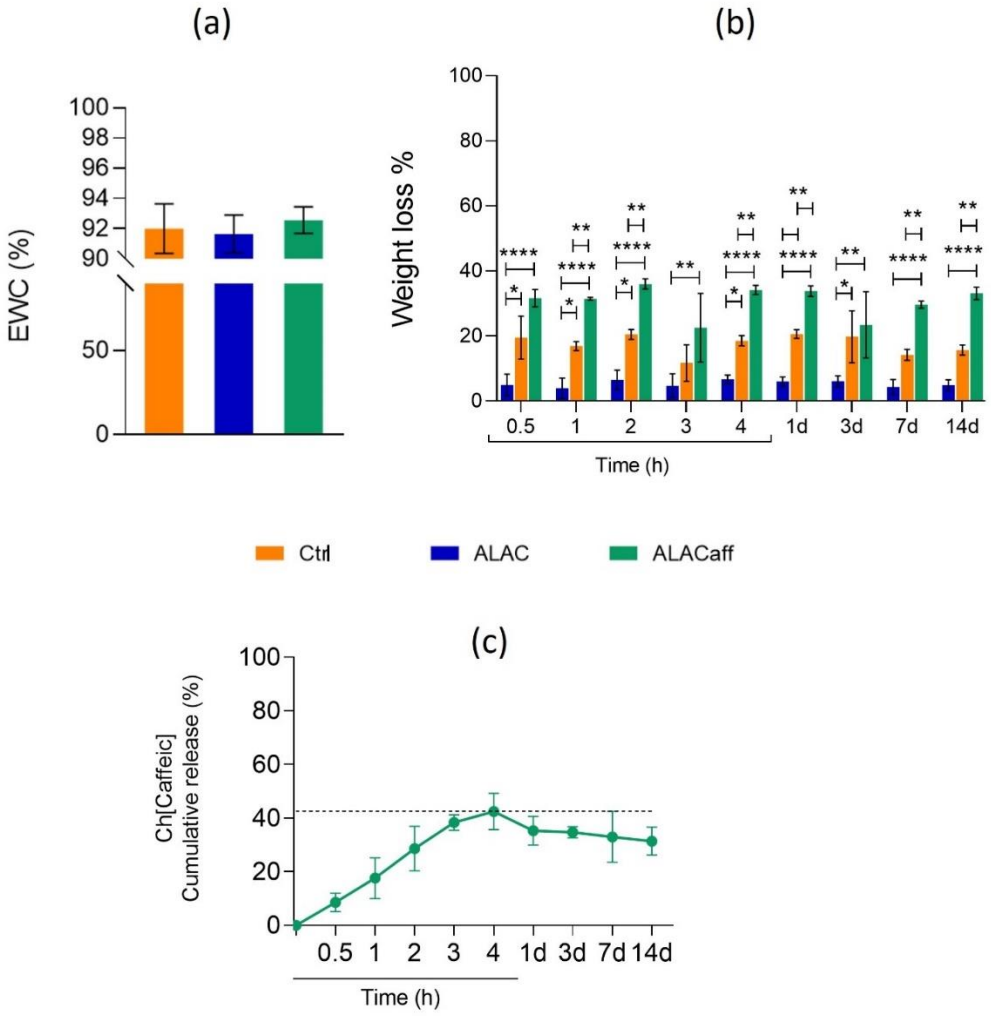


Figure VII-4 - (a) equilibrium water content, (b) weight loss and (c) cumulative Ch[Caffeate] release of the hydrogels in TBS, up to 14 days.

VII-4.2. Cyto-compatibility and *in vitro* assessment the 3D bioprinted constructs

For a successful bioink development and its clinical and biomedical application, it is crucial to determine its cytocompatibility and biocompatibility [35]. Considering this, bioactive inks that retain the capacity to be extruded with minimal forces, as for the ones herein developed, are thus preferred. The biological behavior of the developed 3D bioprinting system was tested by incorporating ATDC5 cells. ATDC5 chondrocyte-like cells were chosen since they are well established as an excellent *in vitro* cell model for chondrocyte research [42–44]. Besides, the cell density should be adjusted according to the tissue of interest, providing an adequate cell distribution within the printed filaments, and resulting in the required cell-to-cell interactions [35]. Thus, a cell density of 8×10^{6} cells·ml^{-1} was chosen based on previous works from our group [35]. After day 1, all three conditions (Ctrl, ALAC, and ALACaff) presented similar

cell metabolic activity profiles with no statistically significant differences (Figure VII-5A). These findings indicate that the ATCD5 cell metabolic activity seems not to be affected by the bioprinting process. After 7 days of culture, the cell metabolic activity and proliferation in the Ctrl group decreased compared to ALAC and ALACaff, with significant statistical differences. Similar results were observed on the influence of $CaCl_2$ on cell viability of ALG-based hydrogel with encapsulated chondrocytes [20], with the data showing that the formulations with 0.1% $CaCl_2$ had higher cell viability than the ones with 0.25% $CaCl_2$ and 0.5% $CaCl_2$. After 7 days of culture, the cell metabolic activity and proliferation of the incorporated chondrocytes seemed to stabilize. This behavior is commonly seen in 3D chondrocyte cultures in ALG constructs, which reportedly go through a mechanism comparable to the contact inhibition process in monolayer chondrocyte cultures, where cell proliferation ceases after a plateau level [20–22]. Furthermore, the calcein-AM results (Figure VII-5C) are in agreement with the findings obtained for cell metabolic viability, confirming that the cell viability was not affected by the bioprinting process, and the encapsulated cells in the different bioink were homogeneously distributed through all constructs. During the culture time, it is recognizable that the inner cellular density was increasing and that cells were changing from a round shape to an elongated morphology. After 14 days of culture, increased cell proliferation and attachment in ALAC and ALACaff are evident when compared to Ctrl (Figure VII-5). These results agree with previously published data that noted that cell viability and proliferation of chondrocytes incorporated in ALG-based hydrogels is favored by its blending with other macromolecules (such as collagen), rather than when encapsulated in hydrogels composed only by ALG [9,45]. The herein presented results also demonstrate that incorporating Ch[Caffeate] in the bioink composite does not negatively affect the biological performance of the construct, remaining comparable to the achieved for ALAC. We proved that cellular fate depends on the bioink in which the cells are cultured. Moreover, the qualitative assessment of ATDC5 morphological behavior after 14 days of culture was performed by acquiring and analyzing DAPI and phalloidin-stained confocal laser microscopy images (Figure VII-5D). It is possible to observe a clear increase in cell spreading in the ALAC and ALACaff, compared to Ctrl. Moreover, in contrast with Ctrl, intensively polymerized actin is observed in ALAC and ALACaff, with clear actin chains. Similar results were observed on ALG-based constructs, where relatively weak actin fluorescence was observed [9,45]. The difference in the cell morphology from a round (Ctrl) to an elongated shape (ALAC and ALACaff) corroborate the observation of the live/dead assay. There is also unquestionable cell-cell communication within the constructs after 14 days of culture.

The structural stability of the constructs after 14 days of culture was also analyzed. Although the constructs were bioprinted with high porosity, to allow the nutrient and cell waste exchange, it was

possible to observe their high structural integrity over 14 days of culture (Figure VII-5E). These results reveal that ALAC and ALACaff are highly cytocompatible and have adequate properties to maintain the structural integrity of the 3D bioprinted constructs while providing a stable environment for the encapsulated cells to remain viable and organized. Moreover, ALAC and ALACaff offer an appropriate environment for the growth, spreading, and cell-cell communication of chondrocyte-like cells, with the formation of a highly intrinsic matrix network, after 14 days of culture.

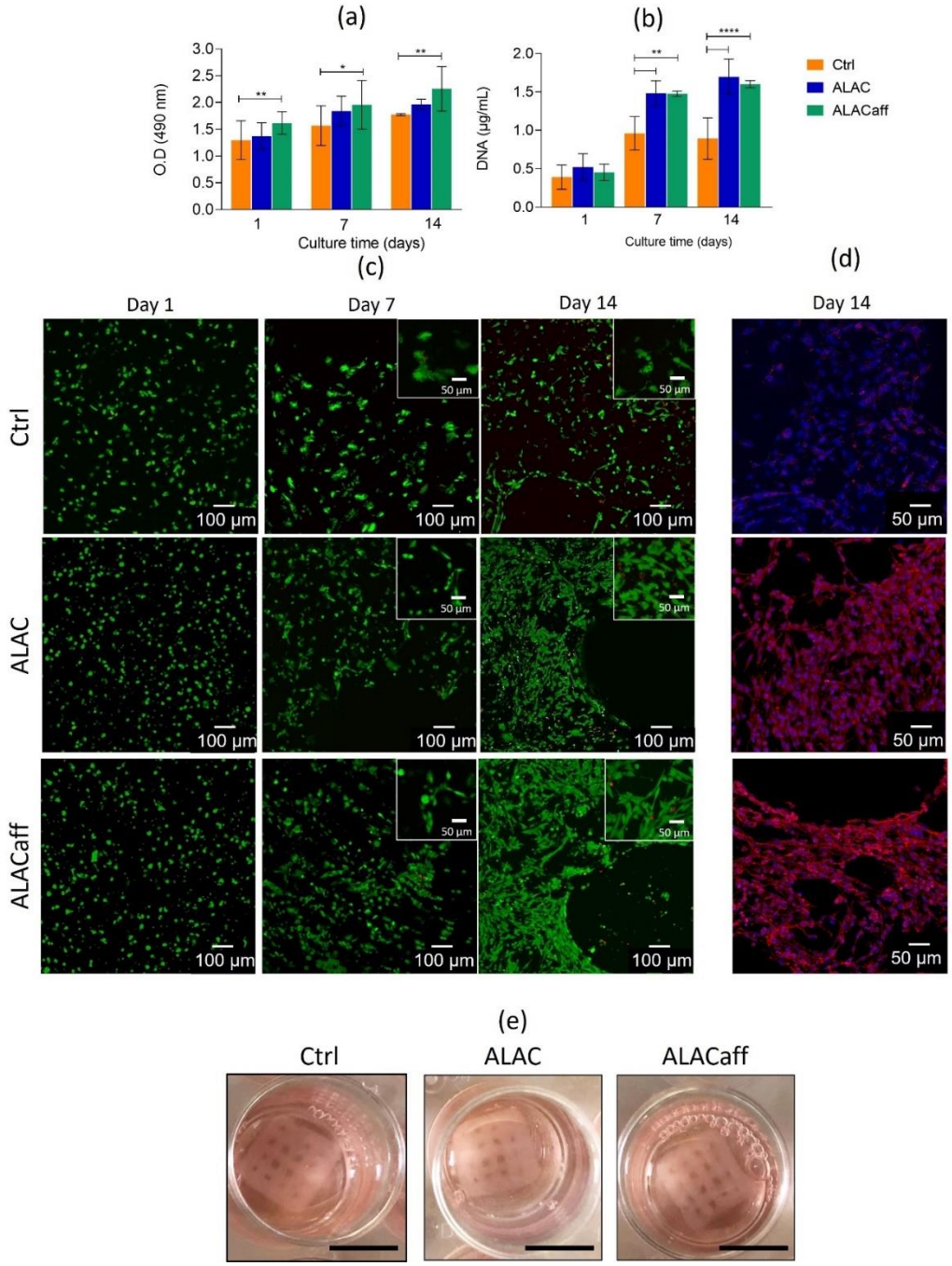


Figure VII-5 - Biological performance of the bioprinted hydrogels. (a) Cell's metabolic activity and (b) dsDNA content after 1, 7 and 14 days of cell culture. (c) live (green)/dead (red) assay after 1, 7 and 14 days of cell culture and (d) DAPI (nuclei)/phalloidin (cytoskeleton) images of ATDC5 cells incorporated at 8×10^{6} after 14 after culture. (e) Representative images of the constructs after 14 days of cell culture. Scale bar: 10 mm.

VII-4.3. Early-stage OA mimicking and therapeutic effect

Once the cytocompatibility of the produced 3D bioprinted constructs was confirmed, they were exposed to OA-like conditions using a co-culture system with THP-1 activated macrophages, as illustrated

in Scheme 2. A co-culture system is the culture of multiple cell types in a shared environment, in which the cell-cell interaction occurs via the secreted factors into the medium [1]. The ability of the ALAC and ALACaff to attenuate some specific disease conditions was further evaluated (the studies were carried out using the Ctrl as the experimental control). There is strong evidence that inflammation plays a significant role in early-stage OA pathogenesis, with both the innate and adaptive immune systems, activating the inflammatory cascade [5,49]. Aiming to study the immunomodulatory effects and protection of the ACE and Ch[Caffeate] over the encapsulated ATDC5 cells, the 3D bioprinted constructs (Ctrl, ALAC and ALACaff) were co-cultured with LPS stimulated THP-1 cells. As previously reported, the differentiation of THP-1 monocytes to macrophages was confirmed by observing the transition from a suspension cell phenotype to an attached cell phenotype [11].

The metabolic activity of encapsulated ATDC5 cells exposed to THP-activated macrophages was superior in ALAC and ALACaff, compared to Ctrl, after 1 and 7 days of culture (Figure VII-6A). These results suggest a protective effect provided by ACE and Ch[Caffeate] over the ATDC5 cells, which are affected by the THP-1 secreted cytokines. These outcomes are corroborated by the DNA quantification results presented in Figure VII-6B. After 7 days of culture, a higher proliferation of ATDC5 cells encapsulated in ALAC and ALACaff, compared to Ctrl, was also observed.

To better understand these results, and knowing that there is a secretion of proinflammatory cytokines in LPS stimulated THP-1 cells [11], which is also common in the synovial fluid of patients with OA[50,51], the cytokine profile of the conditioned media was evaluated (Figure VII-6C). The tumor necrosis factor-alpha (TNF-α) release is known to be responsible for the release of other anti-inflammatory cytokines (such as interleukine-6 (IL-6)), which affects chondrocyte differentiation, function, and viability [29]. In some studies, these pro-inflammatory cytokines, are used as tools for inducing OA and cartilage damage, since their effect in tissues makes it closely replicate the natural disease, contributing to the inflammatory effect of the synovium in the model [2,50,52]. By analyzing the results presented in Figure 6C we can confirm that the LPS-stimulated cells and Ctrl showed significant amounts of TNF-α and IL-6 over the culture time, indicating that the stimulation of cells was successfully achieved. Moreover, after 7 days of culture, a decrease in the TNF-α secretion to the cell culture medium by the THP-1 was observed in the ALAC and ALACaff systems. Significant statistical differences obtained between Ctrl and ALAC, confirming the synergistic anti-inflammatory effect of Ch[Caffeate] and ACE release to the media. Despite no significant statistical differences, the IL-6 quantification data (Figure VII-6C) shows a tendency to decrease from Ctrl > ALAC > ALACaff. However, the high amount of IL-6 in the conditioned medium may

result from the high TNF-α amounts after 1 day of culture. This is in agreement with the increase in the ATDC5 cell viability and DNA quantification (Figure VII-6A and Figure VII-6B, respectively), for ALAC and ALACaff, after 7 days of culture. In addition, an obvious anti-inflammatory effect of ACE is observed by the decrease in both TNF-α and IL-6, after 7 days of culture. Previous studies suggest that ACE can modulate macrophage activation and cytokine production in M1 macrophages, having a potential anti-inflammatory effect [25,53], which is in line with our results. A similar co-culture system and *in vitro* inflammation model was used by Lima *et al.*, to study the biological effect of micelles encapsulating a drug, dexamethasone [54], one of the most widely prescribed corticosteroids for OA treatment that, to mitigate disease symptoms and minimize unwanted effects, should be combined with other agents [55]. Nonetheless, the model similarity, herein different bioactive compounds (ACE and Ch[Caffeate]) were evaluated. Likewise, the results showed that the encapsulated molecules were able to promote a reduction of the negative effect of the inflammation over the normal cells, in their case, primary human articular chondrocytes.

IL-10 belongs to the anti-inflammatory cytokine list involved in inhibiting the main proinflammatory cytokines responsible for the development and progression of OA, TNF-α and IL-6 [56]. In all the studied conditions, significantly increased values for ALACaff after 1 day of culture. Also, IL-10 secretion by LPS-activated macrophages is higher than expected after 1 and 7 days. This phenomenon can be explained by the immune system attempt to balance the pro- and anti-inflammatory factors, by increasing the IL-10 secretion when the pro-inflammatory factors are overexpressed, as mentioned above [57]. Previous studies also described this mechanism as an effort to control the inflammation and, consequently, the tissue damage caused by the pro-inflammatory mediators involved [29,57,58]. In parallel, granulocyte-macrophage colony-stimulating factor (GM-CSF) depletion can strongly affect the severity and progression of numerous inflammatory arthritis models, such as OA [49]. Previous studies done in the immune cells of mice with collagen-induced arthritis corroborated that this proinflammatory mediator is able to restore the balance between the secretion of proinflammatory and anti-inflammatory factors, being a key pain mediator [29,49,59]. In the present work, there is an obvious decrease in the GM-CSF levels in the ALACaff supernatants, which suggests that this formulation may have satisfactory effects not only in the control of early-stage OA inflammation, but also in the disease pain management. Based on the presented results, we consider that the control of synovitis, which is the joint infiltrate composed mostly by macrophages and proinflammatory mediators, must be considered in OA management as a strategy to improve the associated symptoms, including pain, and as a chance of effectively restore joint mobility. Knowing that the inflammatory mediators are known to play a major role in the early-stage OA [32,60],

the herein presented approach constitutes a physiologically relevant strategy to study this disease stage. Further work must be carried out to create more robust and reliable disease models.

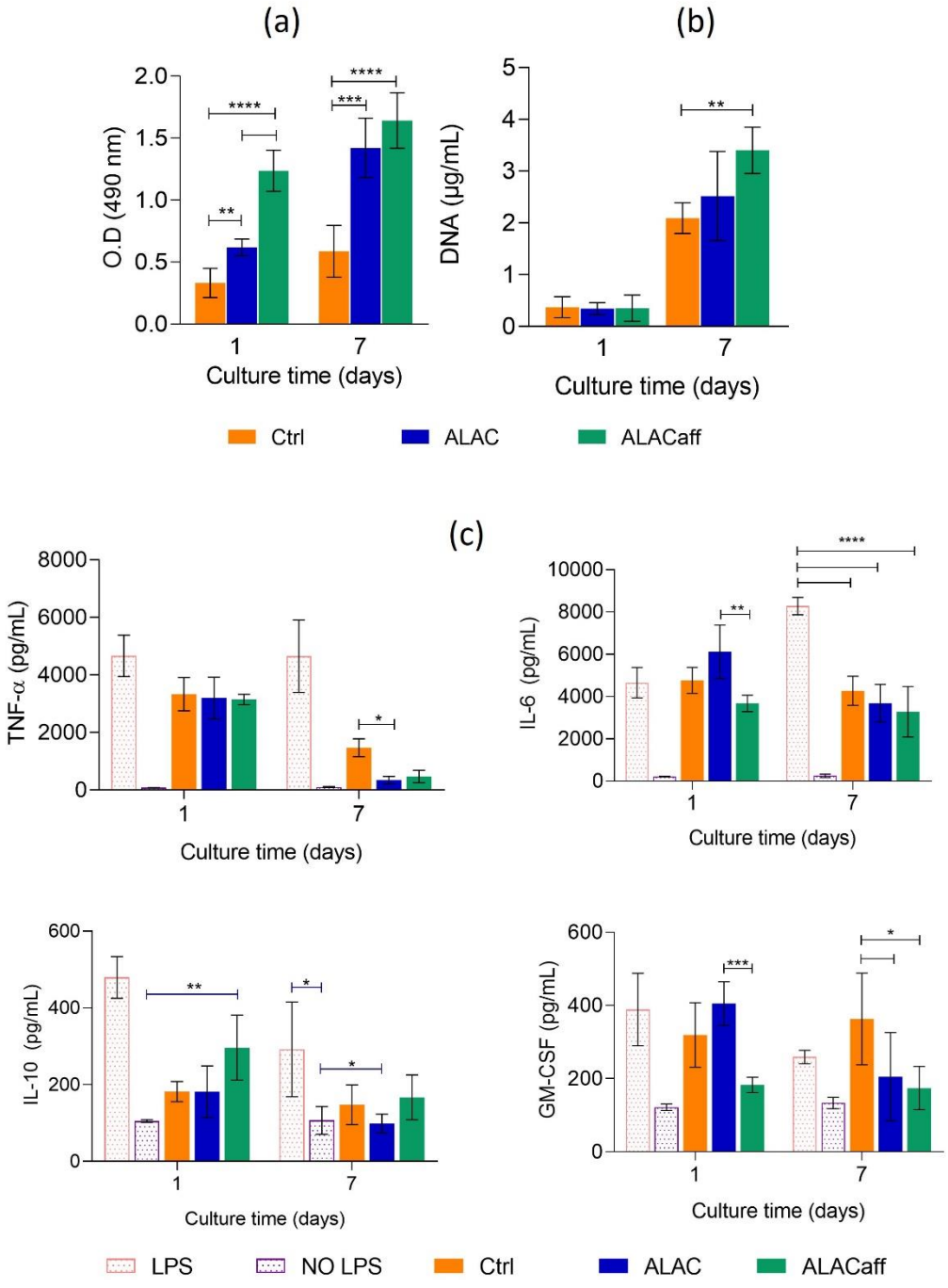


Figure VII-6 - (a) Metabolic activity and (b) dsDNA content of the ATDC5 cells encapsulated in the 3D bioprinted hydrogels in an inflammatory environment after 1 and 7 days of culture.

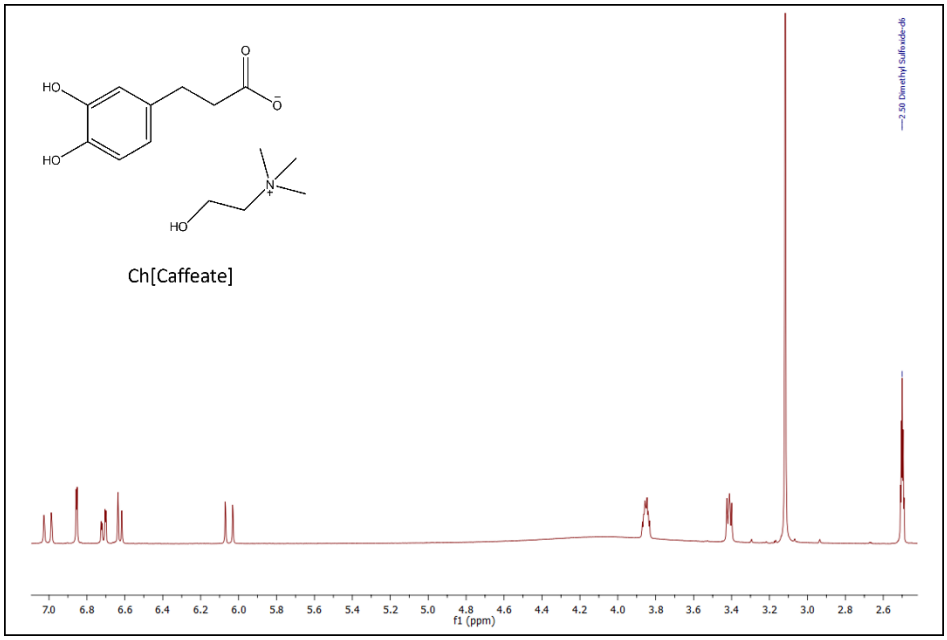
VII-5. Conclusions

3D bioprinted constructs composed of ALG, ACE, and a phenolic-based Bio-IL, Ch[Caffeate] with encapsulated ATDC5 chondrocyte-like cells were successfully produced. The developed inks were easy to inject, and the bioprinted ALAC and ALACaff constructs presented adequate porosities, equilibrium water content, and degradation rates. The cell encapsulation and controlled 3D deposition were successfully achieved with high cell viability, up to 14 days of culture for ALAC and ALACaff. These formulations were able to promote a reduction of the negative effect of the inflammation over the normal cells, mostly due to the synergistic anti-inflammatory action of ACE and Ch[Caffeate]. Moreover, ALACaff provided exciting results concerning the blockage of OA pro-inflammatory mediators, particularly GM-CSF, which is highly associated with arthritic pain, mostly due to Ch[Caffeate] release to the media. There are still some challenges concerning the clinical translation of 3D bioprinted-based models, and deeper studies on ALACaff should be performed, including the use of primary human chondrocytes and multiple cell types to better mimic the disease. Moreover, the developed strategy opens new avenues for exploring Bio-ILs combined with natural polymers envisioning 3D bioprinting-based models for inflammatory-based changes in OA, confirming the growing relevance of the Bio-ILs in the biomedical scenario.

Acknowledgments

The authors especially acknowledge financial support from Portuguese FCT (PD/BD/135247/2017, CEECIND/01306/2018 and CEECIND/04687/2017). This work is also financially supported by PhD programme in Advanced Therapies for Health (PATH) (PD/00169/2013), FCT R&D&I project with reference PTDC/BII-BIO/31570/2017, and R&D&I Structured Project with reference NORTE-01-0145-FEDER-000021.

VII-6. SUPPLEMENTARY MATERIAL



Supplementary Figure VII-1 - ^{1}H of pure Ch[Caffeate].

VII-7. REFERENCES

[1] Y.P. Singh, J.C. Moses, N. Bhardwaj, B.B. Mandal, Overcoming the Dependence on Animal Models for Osteoarthritis Therapeutics – The Promises and Prospects of *in vitro* Models, Adv. Healthc. Mater. 10 (2021) 1–25. https://doi.org/10.1002/adhm.202100961.

[2] P.J. Cope, K. Ourradi, Y. Li, M. Sharif, Models of osteoarthritis: the good, the bad and the promising, Osteoarthr. Cartil. 27 (2019) 230–239. https://doi.org/10.1016/j.joca.2018.09.016.

[3] B.B. Seo, Y. Kwon, J. Kim, K.H. Hong, S.E. Kim, H.R. Song, Y.M. Kim, S.C. Song, Injectable polymeric nanoparticle hydrogel system for long-term anti-inflammatory effect to treat osteoarthritis, Bioact. Mater. 7 (2022) 14–25. https://doi.org/10.1016/j.bioactmat.2021.05.028.

[4] Y. Wang, D.J. Blasioli, H.J. Kim, H.S. Kim, D.L. Kaplan, Cartilage tissue engineering with silk scaffolds and human articular chondrocytes, Biomaterials. 27 (2006) 4434–4442. https://doi.org/10.1016/j.biomaterials.2006.03.050.

[5] Y.P. Singh, J.C. Moses, A. Bandyopadhyay, B.B. Mandal, 3D Bioprinted Silk-Based *in vitro* Osteochondral Model for Osteoarthritis Therapeutics, Adv. Healthc. Mater. 2200209 (2022) 1–15. https://doi.org/10.1002/adhm.202200209.

[6] Y. Zhang, H. Chen, X. Long, T. Xu, Three-dimensional-engineered bioprinted *in vitro* human neural stem cell self-assembling culture model constructs of Alzheimer's disease, Bioact. Mater. 11 (2022) 192–205. https://doi.org/10.1016/j.bioactmat.2021.09.023.

[7] M. Müller, E. Öztürk, Ø. Arlov, P. Gatenholm, M. Zenobi-Wong, Alginate Sulfate–Nanocellulose Bioinks for Cartilage Bioprinting Applications, Ann. Biomed. Eng. 45 (2017) 210–223. https://doi.org/10.1007/s10439-016-1704-5.

[8] K. Markstedt, A. Mantas, I. Tournier, H. Martínez Ávila, D. Hägg, P. Gatenholm, 3D bioprinting human chondrocytes with nanocellulose-alginate bioink for cartilage tissue engineering applications, Biomacromolecules. 16 (2015) 1489–1496. https://doi.org/10.1021/acs.biomac.5b00188.

[9] X. Yang, Z. Lu, H. Wu, W. Li, L. Zheng, J. Zhao, Collagen-alginate as bioink for three-dimensional (3D) cell printing based cartilage tissue engineering, Mater. Sci. Eng. C. 83 (2018) 195–201. https://doi.org/10.1016/j.msec.2017.09.002.

[10] K.S. Hwang, E.U. Seo, N. Choi, J. Kim, H.N. Kim, 3D engineered tissue models for studying human-specific infectious viral diseases, Bioact. Mater. 21 (2023) 576–594. https://doi.org/10.1016/j.bioactmat.2022.09.010.

[11] J.M. Gomes, S.S. Silva, E.M. Fernandes, F.C.M. Lobo, M. Martín-Pastor, P. Taboada, R.L. Reis, Silk fibroin/cholinium gallate-based architectures as therapeutic tools, Acta Biomater. 147 (2022) 168–184. https://doi.org/10.1016/j.actbio.2022.05.020.

[12] I.C. Liao, F.T. Moutos, B.T. Estes, X. Zhao, F. Guilak, Composite three-dimensional woven scaffolds with interpenetrating network hydrogels to create functional synthetic articular cartilage, Adv. Funct. Mater. 23 (2013) 5833–5839. https://doi.org/10.1002/adfm.201300483.

[13] G.C. Luque, M.L. Picchio, A.P.S. Martins, A. Dominguez-Alfaro, N. Ramos, I. del Agua, B. Marchiori, D. Mecerreyes, R.J. Minari, L.C. Tomé, 3D Printable and Biocompatible Iongels for Body Sensor Applications, Adv. EleCtrlon. Mater. 7 (2021). https://doi.org/10.1002/aelm.202100178.

[14] E.S. Morais, N.H.C.S. Silva, T.E. Sintra, S.A.O. Santos, B. Miguel, I.F. Almeida, P.C. Costa, I. Correia-sá, S.P.M. Ventura, A.J.D. Silvestre, M.G. Freire, C.S.R. Freire, Anti-inflammatory and antioxidant nanostructured cellulose membranes loaded with phenolic-based ionic liquids for cutaneous application, Carbohydr. Polym. 206 (2019) 187–197. https://doi.org/10.1016/j.carbpol.2018.10.051.

[15] J.M. Gomes, S.S. Silva, R.L. Reis, Biocompatible ionic liquids: Fundamental behaviours and applications, Chem. Soc. Rev. 48 (2019) 4317–4335. https://doi.org/10.1039/c9cs00016j.

[16] G. Chantereau, M. Sharma, A. Abednejad, B.M. Neves, G. Sèbe, V. Coma, M.G. Freire, C.S.R. Freire, A.J.D. Silvestre, Design of Nonsteroidal Anti-Inflammatory Drug-Based Ionic Liquids with Improved Water Solubility and Drug Delivery, ACS Sustain. Chem. Eng. 7 (2019) 14126–14134. https://doi.org/10.1021/acssuschemeng.9b02797.

[17] A.M.O. Azevedo, S.P.F. Costa, A.F.V. Dias, A.H.O. Marques, P.C.A.G. Pinto, K. Bica, A.K. Ressmann, M.L.C. Passos, A.R.T.S. Araújo, S. Reis, M.L.M.F.S. Saraiva, Anti-inflammatory choline based ionic liquids: Insights into their lipophilicity , solubility and toxicity parameters, J. Mol. Liq. 232 (2017) 20–26. https://doi.org/10.1016/j.molliq.2017.02.027.

[18] M.A. Smirnov, V.S. Fedotova, M.P. Sokolova, A.L. Nikolaeva, V.Y. Elokhovsky, M. Karttunen, Polymerizable choline-and imidazolium-based ionic liquids reinforced with bacterial cellulose for 3d-printing, Polymers (Basel). 13 (2021). https://doi.org/10.3390/polym13183044.

[19] C. Antich, J. de Vicente, G. Jiménez, C. Chocarro, E. Carrillo, E. Montañez, P. Gálvez-Martín, J.A. Marchal, Bio-inspired hydrogel composed of hyaluronic acid and alginate as a potential bioink for 3D bioprinting of articular cartilage engineering constructs, Acta Biomater. 106 (2020) 114–123. https://doi.org/10.1016/j.actbio.2020.01.046.

[20] E. Çelik, C. Bayram, R. Akçapinar, M. Türk, E.B. Denkbaş, The effect of calcium chloride concentration on alginate/Fmoc-diphenylalanine hydrogel networks, Mater. Sci. Eng. C. 66 (2016) 221–229. https://doi.org/10.1016/j.msec.2016.04.084.

[21] B. Beekman, N. Verzijl, R.A. Bank, K. Von Der Mark, J.M. TeKoppele, Synthesis of collagen by bovine chondrocytes cultured in alginate; posttranslational modifications and cell-matrix interaction, Exp. Cell Res. 237 (1997) 135–141. https://doi.org/10.1006/excr.1997.3771.

[22] J. Guo, G.W. Jourdian, D.K. Maccallum, Culture and growth characteristics of chondrocytes encapsulated in alginate beads, Connect. Tissue Res. 19 (1989) 277–297. https://doi.org/10.3109/03008208909043901.

[23] S.S. Silva, L.C. Rodrigues, R.L. Reis, An alternative approach to prepare alginate/acemannan 3D architectures, SN Appl. Sci. 1 (2019) 1–10. https://doi.org/10.1007/s42452-019-0690-2.

[24] F. Pahlevanzadeh, H. Mokhtari, H.R. Bakhsheshi-Rad, R. Emadi, M. Kharaziha, A. Valiani, S.A. Poursamar, A.F. Ismail, S. RamaKrishna, F. Berto, Recent trends in three-dimensional bioinks based on alginate for biomedical applications, 2020. https://doi.org/10.3390/ma13183980.

[25] N.J. Sadgrove, M.S.J. Simmonds, Pharmacodynamics of Aloe vera and acemannan in therapeutic applications for skin, digestion, and immunomodulation, Phyther. Res. 35 (2021) 6572–6584. https://doi.org/10.1002/ptr.7242.

[26] T.K. Berthoud, M.N. Manaca, D. Quelhas, R. Aguilar, C. Guinovart, L. Puyol, A. Barbosa, P.L. Alonso, C. Dobaño, Comparison of commercial kits to measure cytokine responses to Plasmodium falciparum by multiplex microsphere suspension array technology, Malar. J. 10 (2011) 115. https://doi.org/10.1186/1475-2875-10-115.

[27] M.L. Bedell, A.J. Melchiorri, J. Aleman, A. Skardal, A.G. Mikos, A high-throughput approach to compare the biocompatibility of candidate bioink formulations, Bioprinting. 17 (2020) e00068. https://doi.org/10.1016/j.bprint.2019.e00068.

[28] T.E. Sintra, A. Luís, S.N. Rocha, A.I.M.C.L. Ferreira, F. Gonçalves, L.M.N.B.F. Santos, B.M. Neves, M.G. Freire, S.P.M. Ventura, J.A.P. Coutinho, Enhancing the antioxidant characteristics of phenolic acids by their conversion into cholinium salts, ACS Sustain. Chem. Eng. 3 (2015) 2558–2565. https://doi.org/10.1021/acssuschemeng.5b00751.

[29] P. Wojdasiewicz, Ł.A. Poniatowski, D. Szukiewicz, The Role of Inflammatory and Anti-Inflammatory Cytokines in the Pathogenesis of Osteoarthritis, Mediators Inflamm. 2014 (2014) 1–19. https://doi.org/10.1155/2014/561459.

[30] M. Demurtas, V. Onnis, P. Zucca, A. Rescigno, J.I. Lachowicz, L. De Villiers Engelbrecht, M. Nieddu, G. Ennas, A. Scano, F. Mocci, F. Cesare Marincola, Cholinium-Based Ionic Liquids from Hydroxycinnamic Acids as New Promising Bioactive Agents: A Combined Experimental and Theoretical Investigation, ACS Sustain. Chem. Eng. 9 (2021) 2975–2986. https://doi.org/10.1021/acssuschemeng.1c00090.

[31] L.C. Rodrigues, S.S. Silva, R.L. Reis, Acemannan-based films: an improved approach envisioning biomedical applications, Mater. Res. Express. 6 (2019) 095406. https://doi.org/10.1088/2053-1591/ab2f66.

[32] S.K. Bajpai, S. Sharma, Investigation of swelling/degradation behaviour of alginate beads crosslinked with Ca2+ and Ba2+ ions, React. Funct. Polym. 59 (2004) 129–140. https://doi.org/10.1016/j.reactfunctpolym.2004.01.002.

[33] K. Song, A.M. Compaan, W. Chai, Y. Huang, Injectable Gelatin Microgel-Based Composite Ink for 3D Bioprinting in Air, ACS Appl. Mater. Interfaces. 12 (2020) 22453–22466. https://doi.org/10.1021/acsami.0c01497.

[34] Y. Chen, X. Xiong, X. Liu, R. Cui, C. Wang, G. Zhao, W. Zhi, M. Lu, K. Duan, J. Weng, S. Qu, J. Ge, 3D Bioprinting of shear-thinning hybrid bioinks with excellent bioactivity derived from gellan/alginate and thixotropic magnesium phosphate-based gels, J. Mater. Chem. B. 8 (2020) 5500–5514. https://doi.org/10.1039/d0tb00060d.

[35] G.S. Diogo, C.F. Marques, S. Freitas-Ribeiro, C.G. Sotelo, R.I. Pérez-Martin, R.P. Pirraco, R.L. Reis, T.H. Silva, Mineralized collagen as a bioactive ink to support encapsulation of human adipose stem cells: A step towards the future of bone regeneration, Mater. Sci. Eng. C. (2021) 112600. https://doi.org/10.1016/j.msec.2021.112600.

[36] L. Aguero, S. Alpdagtas, E. Ilhan, D. Zaldivar-Silva, O. Gunduz, Functional role of crosslinking in alginate scaffold for drug delivery and tissue engineering: A review, Eur. Polym. J. 160 (2021) 110807. https://doi.org/10.1016/j.eurpolymj.2021.110807.

[37] J.M. Gomes, S.S. Silva, L.C. Rodrigues, R.L. Reis, Alginate/acemannan derived beads loaded with a biocompatible ionic liquid as a bioactive delivery system, Carbohydr. Polym. Submitted (2022).

[38] L.R. Bogdanova, P. V. Zelenikhin, A.O. Makarova, O.S. Zueva, V. V. Salnikov, Y.F. Zuev, O.N. Ilinskaya, Alginate-Based Hydrogel as Delivery System for Therapeutic Bacterial RNase, Polymers (Basel). 14 (2022) 2461. https://doi.org/10.3390/polym14122461.

[39] T. Ito, M. Saito, T. Uchino, M. Senna, M. Iafisco, M. Prat, L. Rimondini, M. Otsuka, Preparation of injectable auto-forming alginate gel containing simvastatin with amorphous calcium phosphate as a controlled release medium and their therapeutic effect in osteoporosis model rat, J. Mater. Sci. Mater. Med. 23 (2012) 1291–1297. https://doi.org/10.1007/s10856-012-4597-3.

[40] X. Zhao, Y. Xia, X. Zhang, X. Lin, L. Wang, International Journal of Biological Macromolecules Design of mechanically strong and tough alginate hydrogels based on a soft-brittle transition, 139 (2019) 850–857. https://doi.org/10.1016/j.ijbiomac.2019.08.057.

[41] A. Sulistio, F.M. Mansfeld, F. Reyes-Ortega, A.M. D'Souza, S.M.Y. Ng, S. Birkett, A. Blencowe, G.G. Qiao, C.B. Little, C.C. Shu, A.M. Bendele, D. Valade, A.C. Donohue, J.F. Quinn, M.R. Whittaker, T.P. Davis, R.J. Tait, Intra-articular Treatment of Osteoarthritis with Diclofenac-Conjugated Polymer Reduces Inflammation and Pain, ACS Appl. Bio Mater. 2 (2019) 2822–2832. https://doi.org/10.1021/acsabm.9b00232.

[42] P.T. Newton, K.A. Staines, L. Spevak, A.L. Boskey, C.C. Teixeira, V.E. Macrae, A.E. Canfield, C. Farquharson, Chondrogenic ATDC5 cells: An optimised model for rapid and physiological matrix mineralisation, Int. J. Mol. Med. 30 (2012) 1187–1193. https://doi.org/10.3892/ijmm.2012.1114.

[43] S.S. Silva, N.M. Oliveira, M.B. Oliveira, D.P.S. Da Costa, D. Naskar, J.F. Mano, S.C. Kundu, R.L. Reis, Fabrication and characterization of Eri silk fibers-based sponges for biomedical application, Acta Biomater. 32 (2016) 178–189. https://doi.org/10.1016/j.actbio.2016.01.003.

[44] I.M. Oliveira, C. Gonçalves, E.P. Oliveira, R. Simón-Vázquez, A. da Silva Morais, Á. González-Fernández, R.L. Reis, J.M. Oliveira, PAMAM dendrimers functionalised with an anti-TNF α antibody and chondroitin sulphate for treatment of rheumatoid arthritis, Mater. Sci. Eng. C. 121 (2021) 111845. https://doi.org/10.1016/j.msec.2020.111845.

[45] G.S. Diogo, C.F. Marques, C.G. Sotelo, R.I. Pérez-Martín, R.P. Pirraco, R.L. Reis, T.H. Silva, Cell-Laden Biomimetically Mineralized Shark-Skin-Collagen-Based 3D Printed Hydrogels for the Engineering of Hard Tissues, ACS Biomater. Sci. Eng. 6 (2020) 3664–3672. https://doi.org/10.1021/acsbiomaterials.0c00436.

[46] H. Nulwala, A. Mirjafari, X. Zhou, Ionic liquids and poly(ionic liquid)s for 3D printing – A focused mini-review, Eur. Polym. J. 108 (2018) 390–398. https://doi.org/10.1016/j.eurpolymj.2018.09.023.

[47] D.H.A.T. Gunasekera, S. Kuek, D. Hasanaj, Y. He, C. Tuck, A.K. Croft, R.D. Wildman, Three dimensional ink-jet printing of biomaterials using ionic liquids and co-solvents †, Faraday Discuss. 190 (2016) 509–523. https://doi.org/10.1039/c5fd00219b.

[48] K. Ahmed, M. Kawakami, A. Khosla, H. Furukawa, Soft, conductive nanocomposites based on ionic liquids/carbon nanotubes for 3D printing of flexible eleCtrlonic devices, Polym. J. 51 (2019) 511–521. https://doi.org/10.1038/s41428-018-0166-z.

[49] A.D. Cook, J. Pobjoy, S. Steidl, M. Dürr, E.L. Braine, A.L. Turner, D.C. Lacey, J.A. Hamilton, Granulocyte-macrophage colony-stimulating factor is a key mediator in experimental osteoarthritis pain and disease development, Arthritis Res. Ther. 14 (2012) 1–9. https://doi.org/10.1186/ar4037.

[50] C.S. Bonnet, D.A. Walsh, Osteoarthritis, angiogenesis and inflammation, Rheumatology. 44 (2005) 7–16. https://doi.org/10.1093/rheumatology/keh344.

[51] C.M. Dancevic, D.R. McCulloch, Current and emerging therapeutic strategies for preventing inflammation and aggrecanase-mediated cartilage destruction in arthritis, Arthritis Res. Ther. 16 (2014) 429. https://doi.org/10.1186/s13075-014-0429-9.

[52] M. Laavola, T. Leppänen, M. Hämäläinen, K. Vuolteenaho, T. Moilanen, R. Nieminen, E. Moilanen, IL-6 in osteoarthritis: Effects of pine stilbenoids, Molecules. 24 (2019) 1–11. https://doi.org/10.3390/molecules24010109.

[53] A. Farid, A. Tawfik, B. Elsioufy, G. Safwat, *in vitro* and *in vivo* anti-Cryptosporidium and anti-inflammatory effects of Aloe vera gel in dexamethasone immunosuppressed mice, Int. J. Parasitol. Drugs Drug Resist. 17 (2021) 156–167. https://doi.org/10.1016/j.ijpddr.2021.09.002.

[54] A.C. Lima, R.L. Reis, H. Ferreira, N.M. Neves, Glutathione reductase-sensitive polymeric micelles for controlled drug delivery on arthritic diseases, ACS Biomater. Sci. Eng. 7 (2021) 3229–3241. https://doi.org/10.1021/acsbiomaterials.1c00412.

[55] X. Li, D.C. Dubois, D. Song, R.R. Almon, W.J. Jusko, X. Chen, Modeling combined immunosuppressive and anti-inflammatory effects of dexamethasone and naproxen in rats predicts the steroid-sparing potential of naproxens, Drug Metab. Dispos. 45 (2017) 834–845. https://doi.org/10.1124/dmd.117.075614.

[56] S. Liu, Z. Deng, K. Chen, S. Jian, F. Zhou, Y. Yang, Z. Fu, H. Xie, J. Xiong, W. Zhu, Cartilage tissue engineering: From proinflammatory and anti-inflammatory cytokines to osteoarthritis treatments, Mol. Med. Rep. 25 (2022) 1–15. https://doi.org/10.3892/MMR.2022.12615.

[57] J.M. Cicchese, S. Evans, C. Hult, L.R. Joslyn, T. Wessler, J.A. Millar, S. Marino, N.A. Cilfone, J.T. Mattila, J.J. Linderman, D.E. Kirschner, Dynamic balance of pro- and anti-inflammatory signals controls disease and limits pathology, Immunol. Rev. 285 (2018) 147–167. https://doi.org/10.1111/imr.12671.

[58] A.. Schuerwegh, E.. Dombrecht, W.. Stevens, J.. Van Offel, C.. Bridts, L.. De Clerck, Influence of pro-inflammatory (IL-1α, IL-6, TNF-α, IFN-γ) and anti-inflammatory (IL-4) cytokines on chondrocyte function, Osteoarthr. Cartil. 11 (2003) 681–687. https://doi.org/10.1016/S1063-4584(03)00156-0.

[59] K.M.C. Lee, V. Prasad, A. Achuthan, A.J. Fleetwood, J.A. Hamilton, A.D. Cook, Targeting GM-CSF for collagenase-induced osteoarthritis pain and disease in mice, Osteoarthr. Cartil. 28 (2020) 486–491. https://doi.org/10.1016/j.joca.2020.01.012.

SECTION 5

GENERAL CONCLUSIONS

Chapter VIII

General Conclusions and Future Perspectives

Chapter VIII

General Conclusions and Future Perspectives

VIII-1. GENERAL CONCLUSIONS

Biocompatible ionic liquids (Bio-ILs) emerged as a response to the need to develop compounds with improved environmental and biological features. The tunability of these solvents, brought by the possibility of different cation and anion combinations, allows to produce Bio-ILs that meet specific requirements, namely biodegradability, low toxicity, biocompatibility, bioactivity and antimicrobial features. Thus, the relevance of Bio-IL in biomaterials development, and their role in different fields, such as synthesis, electrochemistry, and extraction, is clear. Actually, Bio-ILs exploitation in the biomedical and tissue engineering fields is still in its early stage, being a niche requiring further research and investment. The work performed under the scope of this thesis aimed to explore the use of Bio-ILs as new solutions for developing innovative therapeutic platforms and advanced therapies. The versatility of the Bio-ILs, along with their intrinsic bioactivity, allowed the fabrication of various architectures, including sponges, beads, and 3D-bioprinted hydrogels.

Chapter III of this thesis used a sustainable Bio-IL-based strategy to produce 3D-based chitin constructs. The findings indicated that the presence of Bio-IL in the matrices improved their mechanical properties and thermal stability. Moreover, their ability to support human adipose stem cell growth and proliferation confirmed the harmless biological effect of the Bio-ILs presence, confirming that it can be maintained into the matrices without any harmful effect on the cells. The replacement of ionic liquids (IL) for the proposed Bio-ILs avoided the usually mandatory removal of the IL following the biomaterials fabrication, when considering its use in the biomedical field. Therefore, the outcomes of this chapter provided us with important insights that significantly contributed to the further works of this thesis, mostly concerning the biological and physico-chemical benefits underlying the maintenance of the Bio-IL in the polymeric matrices.

In **Chapter IV**, an approach based on the Bio-ILs tunability was developed, in which a phenolic-based Bio-IL, cholinium gallate (Ch[Gallate]), was synthesized by pairing the cholinium cation with an

anion from a compound with intrinsic bioactivity (gallic acid). Ultimately, this approach improved the bioactivity of the precursor compound (gallic acid), since its Bio-IL-based form is more soluble and thus more bioavailable. Furthermore, the SF was employed as the polymeric support in this approach because of its recognized biocompatibility, which would ensure that the effects achieved can be mainly attributed to the presence of Bio-IL. The Ch[Gallate] was further dissolved, in different concentrations, into the silk fibroin (SF)-based solution that were further molded and lyophilized to produce sponges, granting them the bioactive features of the Bio-IL, anti-inflammatory, and anti-oxidant, and also acting as a tool to modulate the physico-chemical properties of the architectures. Beyond that, the constructs supported the growth and proliferation of adipose stem cells. Therefore, the strategy herein explored, allowed us to produce bioactive SF-based sponges, owned to the Ch[Gallate] presence, which opened new avenues for the exploitation of Bio-ILs for the development of tissue engineering strategies, specifically toward the management of pathologies with associated inflammatory scenarios.

The outcomes of **Chapter IV**, together with the challenging hallmarks of osteoarthritis (OA), which include the synovium inflammation, associated oxidative stress, and the consequent degradation of the extracellular matrix (ECM), help us to envisage the further works developed under the scope of this thesis (**Chapter V to Chapter VII**). Different architectures (sponges, beads, hydrogels) were developed in these works to address the stated OA typical events.

In **Chapter V**, the knowledge obtained on the ability to fabricate Bio-IL/biopolymer systems with intrinsic bioactivity led us to synthesize an additional phenolic-based Bio-IL derived from phenolic acid (caffeic acid). At the same time, we explored the influence of both Bio-ILs, namely cholinium gallate (Ch[Gallate]) and cholinium caffeate (Ch[Caffeate]), on the physico-chemical and biological performance of the systems. Our findings confirmed the successful dissolution of both Ch[Caffeate] and Ch[Gallate], into SF solutions, which allowed the engineering of bioactive Bio-IL/SF-based constructs. In addition, acetaminophen, a model analgesic drug, was included in the Bio-IL/SF-based sponges, targeting the first stage managing of patients' pain. With this combination, we intended to build an "ideal" system to target cartilage regeneration in OA scenarios. Despite the differences in the Bio-ILs structures and consequent charge distribution, the architectures presented similar and satisfactory results concerning the anti-inflammatory and antioxidant features, and improved mechanical properties. Beyond that, in our strategy, an evaluation of the antimicrobial properties of the matrices against Methicillin-resistant *Staphylococcus aureus* and *Escherichia coli* demonstrated that the sponges containing either of the Bio-ILs had enhanced antimicrobial properties compared to the SF sponges. Also, the reduced bacterial adherence and biofilm

formation of the structures can help to develop effective treatment strategies, particularly appealing for tissue regeneration applications. Furthermore, the Bio-IL/SF-based constructs supported human chondrocyte cell growth and proliferation, while providing the downregulation of OA inflammatory-related genes in osteoarthritic cells. This make these biomaterials viable implantable solutions for OA therapy, reducing inflammation and oxidative stress while promoting cartilage regeneration and preventing critical biofilm formation after joint replacement surgeries.

The studies concerning Bio-ILs release from the matrices performed in **Chapter V**, suggested that Ch[Caffeate], despite no covalent interactions with the SF structure, presented stronger physical entrapment, mostly owned to its larger structure, showing a more sustained release profile. Based on these results, an alginate/acemannan/Ch[Caffeate] system was explored in **Chapter VI** as an attempt to develop a drug delivery system targeting OA's local joint inflammation. The construction of alginate/acemannan/Ch[Caffeate] beads involved the ionic crosslinking of alginate in the presence of acemannan, which contains calcium ions, and Ch[Caffeate]. Additionally, it was suggested by the analysis that the Bio-IL distribution in the structures and its concentration might influence how the polymer´s network is organized. Besides, the sustainable release of Ch[Caffeate] from the beads prevented ROS formation, while blocking the release of the proinflammatory cytokine from macrophages, resulting from the Bio-ILs' antioxidant and anti-inflammatory features. Additionally, Ch[Caffeate] release from the beads resulted in good ATDC5 chondrocyte-like cell growth and proliferation, with increased glycosaminoglycans (GAGs) production. Herein, the proposed strategy was established as a sustainable and physiologically relevant drug delivery system targeting degenerative cartilage pathologies.

The versatility of the alginate/acemannan/Ch[Caffeate] system led us to explore it as a substrate for developing bioinks in **Chapter VII** of this thesis. The produced bioinks were easy to inject and offered a favorable environment for ATDC5 chondrocyte-like cell growth and proliferation. Moreover, the 3D bioprinted-based constructs were co-cultured with activated macrophages, which allowed us to mimic the inflammation scenarios in OA. Also, the chondrocyte-like cells encapsulated in the alginate/acemannan/Ch[Caffeate] system were protected from the detrimental effect of the proinflammatory mediators released by the macrophages compared to the control (alginate hydrogels). This approach opened new avenues toward the exploitation of Bio-ILs into the development of 3D bioprinting constructs, to manage inflammatory alterations in OA, increasing the Bio-ILs' relevance in the biomedical context.

Overall, the cumulative data generated from the works described in this thesis demonstrated that the use of Bio-ILs could be a sustainable, cost-effective, and cytocompatible strategy, either as platforms for biomaterials processing, or as bioactive mediators for the management of degenerative disorders, like OA.

FUTURE PERSPECTIVES

Even though, the results herein presented lay essential foundations toward the use of Bio-ILs as added value compounds in the biomedical and tissue engineering fields, namely for cartilage regeneration purposes, there are still vital steps to be taken on the way to expand their use.

As the developed biomaterials showed to be promising in the tissue engineering field further studies should be performed applying the herein developed biomaterials (**Chapter V** and **Chapter VI**) in osteoarthritic animal models, since *in vivo* studies will confirm the safety and translational potential of advanced systems. Studies resourcing to pre-clinical models should also be performed to validate the predictability of the cellular responses, and consequently their potential clinical relevance. The use of animal models to assess the safety and efficacy of novel treatments continues to be mandatory before clinal studies.

In addition, and considering the intrinsic Bio-ILs conductivity, the herein synthetized Bio-ILs, as well as the developed technologies, may be explored for the fabrication of advanced functional materials envisioning either cardiac or neuronal applications, tissues that present responsiveness to electrical stimulation. Therefore, the use of electroconductive biomaterials, besides promoting cellular adhesion, proliferation, differentiation, and growth, would allow the modulation of different cell types, including neurons, cardiomyocytes, and cardiac fibroblasts.

In **Chapter VII** of this thesis, anti-inflammatory 3D bioprinted Bio-IL-based constructs were successfully developed. However, future work would involve human chondrocytes in optimized 3D printed architectures and the attempt to print different cell types, closely mimicking the joint tissue. For that, other approaches could be studied, such as the bioprinting of multiple cell types (e.g., chondrocytes and osteoblasts); or the use of stem cells in the developed bioink (e.g., adipose-derived mesenchymal stem cells), previously primmed into the osteogenic lineage (in bone ink) or in the chondrogenic lineage (in cartilage ink). Therefore, these further investigations would allow the creation of more reliable and robust bioprinted constructs.

The work developed on the scope of this thesis evidences the tremendous benefits of Bio-IL-based biomaterials, resulting in constructs with enhanced biocompatibility and bioactivity, while involving sustainable methodologies. The herein developed Bio-IL-based platforms demonstrated potential to be used toward the treatment and regeneration of specific tissues, as scaffold-based approaches that provide physical support and biological cues for the growth of cells in a 3D environment, providing improved cell-cell communication. Likewise, they can be used as drug delivery systems or biologically active substances in developing 3D bioprinted architectures. Furthermore, the biomaterial systems showed the potential to be used as personalized medicine approachs to obtain better therapeutic outcomes. Iin the near future, it is expected that the herein acquired knowledge could have a translation into the clinical field. Thus, deeper studies using improved *in vitro* and *in vivo* osteoarthritic models, should be performed to validate the data obtained in this thesis. In summary, significant steps have been taken toward the study of the potential of using Bio-ILs in the tissue engineering field, representing a starting point for their wider exploitation.